EFFECT OF HYPOXIA ON INSULIN SECRETION AND VIABILITY OF PANCREATIC ISLET TISSUE

by

KEITH EVAN DIONNE

B.S. Chemical Engineering
Brigham Young University, 1982

M.S. Chemical Engineering
Technology and Policy Program
Massachusetts Institute of Technology, 1988

Submitted to the Department of Chemical Engineering
in partial fulfillment of the requirements for the degree of

DOCTOR OF PHILOSOPHY

at the

MASSACHUSETTS INSTITUTE OF TECHNOLOGY

December 8, 1989

Signature of Author _____
Department of Chemical Engineering
December 8, 1989

Certified by _____
Clark K. Colton
Thesis Supervisor

Certified by _____
Martin L. Yarmush
Thesis Supervisor

Accepted by _____
William M. Deen
Chairman, Committee for Graduate Students

EFFECT OF HYPOXIA ON INSULIN SECRETION AND VIABILITY OF PANCREATIC ISLET TISSUE

by

KEITH EVAN DIONNE

Submitted to the Department of Chemical Engineering
on December 8, 1989 in partial fulfillment of the
requirements for the degree of Doctor of Philosophy in
Chemical Engineering

ABSTRACT

Diabetes affects over ten million people in the United States and with its complications is the third leading cause of death. In its most basic form, diabetes is the result of the inability of the diabetic's β-cells in the pancreatic islets of Langerhans to secrete sufficient insulin in response to a rise in blood metabolites such as glucose. Conventional insulin injection therapy is unable to adequately regulate rapidly fluctuating blood glucose levels suggesting the need for minute by minute feedback controlled insulin release. One approach to insulin replacement therapy is transplantation of islets of Langerhans immuno-isolated from tissue by a semipermeable membrane. In contrast to vascularized in vivo tissue, encapsulated islets depend on diffusion of nutrients and wastes to and from the β-cells to provide a suitable environment for survival and secretion. The response of islet cells in terms of insulin secretion and viability to this potentially hypoxic environment is presently unknown.

A perifusion system was constructed to test glucose-stimulated insulin secretion from whole islets (average diameter = 210 μm) and small reaggregated islet cell clusters (average diameter = 37 μm) under controlled pO_2. Second phase insulin secretion rate from adult rat islets decreased with bulk perfusate pO_2 below 60 mm Hg, reached one-half of maximum (P_{50}) at 27 mm Hg, and was less than two percent at 5 mm Hg. The secretion rate of small islet cell aggregates was unaffected above about 15 mm Hg and was reduced to one-half of maximum at pO_2 = 5.0 mm Hg in the bulk perfusate. Hypoxia induced reductions in insulin secretion rate were reversible and were not a result of decreased cell viability as ascertained by vital staining and by the post-hypoxia induction of glucose-stimulated insulin secretion. Long-term (1 to 5 weeks) exposure to hypoxia in static culture resulted both in decreased insulin secretion rate and in the development of central necrotic cores. The fraction of the islet core that was necrotic was correlated to islet size and to the pO_2 in the culture medium. Despite the development of large necrotic regions, after ten days of hypoxic culture, the insulin secretion rate of islets cultured at 15 mm Hg returned to normal when the pO_2 was raised to either 30 or 142 mm Hg, indicating that the effect of hypoxia on cells in the viable rim was reversible even after extended periods of oxygen deprivation.

Oxygen consumption of intact islets and small islet cell aggregates was experimentally measured as a function of the bulk medium oxygen concentration, $[O_2]$, in a stirred tank oxygen uptake chamber. The medium $[O_2]$ was monitored (50 sec^{-1}) by measuring the oxygen-quenched phosphorescence of palladium coproporphyrin. From these experiments, values of Vmax, the maximum oxygen uptake rate, and P_x, the fraction of maximum tissue uptake at a bulk medium pO_2 equal to x, were calculated. The intra-tissue oxygen diffusivity was calculated from values of P_x. These parameters were then used in a theoretical reaction/diffusion model to predict intra-islet pO_2 profiles and oxygen consumption as a function of bulk medium pO_2, islet size, and metabolic stimulation. Theoretical predictions

of islet oxygen consumption overlapped experimental oxygen uptake curves. Intra-islet pO_2 profiles, together with insulin secretion data described above, were used to extract the coefficients for a Michaelis-Menten type kinetic expression for the dependence of second phase insulin secretion on pO_2. Use of this expression permitted the prediction of oxygen-limited insulin secretion from islets to within ± 10% of experimental data and may be extended to predict secretion from encapsulated devices.

It is hypothesized that the mechanism by which hypoxia limits insulin secretion is via decreasing the rate of oxidative phosphorylation leading to a reduction in the intra-cellular ratio of [ATP]/[ADP]. Decreased [ATP] is believed to directly affect the rate of exocytotic release of insulin by a variety of pathways including slowing the ATP dependent transport of insulin secretion vesicles to the cell membrane and by opening ATP gated K^+ channels thus preventing cell depolarization. Evidence is presented in support of both of these pathways.

Experimental and theoretical results both indicate that a specific cell function (the insulin secretion rate of β-cells) is detrimentally influenced by hypoxic environments at pO_2 levels that are higher than those required to compromise cell viability. This suggests the possibility that important cell functions in other systems may be similarly affected in medical and biotechnological applications which involve culture of mammalian cell aggregates.

Thesis Supervisors: Clark K. Colton, Ph.D.
Professor of Chemical Engineering
Massachusetts Institute of Technology

Martin L. Yarmush, M.D., Ph.D.
Professor of Chemical and Biochemical Engineering
Rutgers University

ACKNOWLEDGEMENTS

Thanks

Mom	Glen
P.G.	Ardy
Ruth	Dan
Frank	John
Jared	Jesse
Ty	Scott
Bill	Regina
Norma	Sally
Joe	Jim
Clark	Maish
Alan	Gordon
Dan	Terese
Wendy	Gary

The members of the University Ward.

All the people at the National Science Foundation,

and all the people at the Hertz Foundation ... for picking up the tab.

Thanks Again.

TABLE OF CONTENTS

TABLE OF CONTENTS (cont.)

APPENDICES

CHAPTER 1:

BACKGROUND, OBJECTIVES, AND OVERVIEW

BACKGROUND

Diabetes Mellitus is a heterogeneous group of disorders characterized by high blood glucose levels and caused by insulin insufficiency. Of the estimated 8 to 12 million people in the United States that suffer from diabetes, between five and ten percent require daily insulin injections (US Pharmacopeia, 1980; Diabetes Research and Education Foundation, 1985), the remainder achieve blood glucose control through diet alone or in combination with oral hypoglycemic drugs. Although conventional insulin therapy has reduced the incidence of acute diabetic coma in the population requiring insulin, the life expectancy of diabetics is still well below that of the general population, and diabetic patients experience an extraordinarily high incidence of heart attacks, strokes, kidney failure, blindness, and other complications (See Table 1) (Matas et al., 1976; Ganda, 1983). The total health costs due to diabetes related morbidity have been estimated at over $15 billion per year in the United States (National Diabetes Advisory Board, 1981).

Recent research has indicated that many of these complications can be avoided or significantly reduced by precise and continuous control of blood glucose levels (Porte et al, 1981; Steno, 1982; Landgraf et al, 1989). However, despite intensive work on several insulin delivery systems, there is at present no treatment available which provides continuous control of blood glucose levels in ambulatory diabetics. Mechanical pumps are limited in that an implantable glucose sensor to control the insulin infusion rate has yet to be perfected (Soeldner, 1981; Shichire et al, 1984). Whole pancreas transplantation still has numerous problems associated with surgical complications, immunosuppressive therapy, and human organ procurement (Southerland et al, 1989A). The transplantation of isolated islets, although promising, is hindered by problems of human procurement, isolation and purification of islets, immune rejection, and *in vivo* function (Bonheim, 1984; Scharp, 1984; Scharp et al,

1984; Burghen and Murrell, 1989). In addition, the increasing evidence of the autoimmune nature of diabetes indicates that unprotected transplants may be destroyed by the same sequence of events that destroyed the original pancreas (Sutherland et al, 1989B).

One promising insulin delivery system that incorporates glucose feedback involves a cell-based approach consisting of insulin-producing pancreatic cells enclosed within a semipermeable membrane device. Glucose passes through the membrane to the cells where it triggers the secretion of insulin. The insulin in turn builds up in the chamber and passes back through the membrane to the body. The membrane prohibits the passage of the larger molecules and cells of the immune system thus preventing the rejection of the foreign pancreatic cells due to either histocompatibility or autoimmune causes (Scharp et al, 1984; Prowse et al, 1986).

Immuno-isolation systems have several potential advantages over other insulin delivery systems. First, since β-cells in isolated islets of Langerhans maintain most of their normal response to glucose and other secretagogues (Malaisse, 1972; Gerich et al, 1976; Unger et al, 1978), insulin (and other pancreatic hormone) release from immuno-isolation devices should be controlled by glucose feedback as well as being responsive to changes in the concentrations of non-glucose stimuli such as amino acids, fats, gastric inhibitory polypeptide, and to fluctuations in endocrine hormone concentrations which reflect changing physiologic states of the host. Second, the isolation membrane should prevent immune rejection of transplanted tissue, therefore allowing for an unlimited supply of transplant tissue through the use of xenogeneic (non-human) islets of Langerhans without immunosuppression (Scharp et al, 1984; Iwata et al, 1989; Hering et al, 1989). Finally, immuno-isolation should protect transplanted tissue from the same sequence of diabetic autoimmune rejection which destroyed the original pancreas (Scharp et al, 1984; Prowse et al, 1986; Sutherland et al, 1989B).

The work of several investigative teams has established the validity of the principles upon which immuno-isolation is based. Immune protection via membrane separation has been shown to be a viable concept in general (Algire et al, 1954), and with islets in particular (Archer et al, 1980; Darquy and Reach, 1985). Islets have been shown to maintain insulin

release during culture on hollow fibers (Chick et al, 1975; Araki et al, 1985) and in microcapsules (O'Shea et al, 1984). Extravascular devices have remained viable in vivo for grater than 250 days (Archer et al, 1980; Altman et al, 1982). Intravascular shell and tube devices have remained patent for up to five weeks provided they were equipped with large internal diameters (3 to 4 mm) and had high blood flowrates (greater than 140 ml/min) (Galletti et al, 1981). Normalized fasting blood glucose has been achieved with extravascular diffusion devices (Archer et al, 1980; O'Shea et al, 1982; Iwata et al, 1989). Intravascular devices have regulated blood glucose in both rats (Chick et al, 1975) and dogs (Naber et al, 1979; Colton et al, 1980) over a period of hours.

Despite these promising results, there are nor reports of glucose normalization of the post prandial period where rapid and sufficient insulin response is most critical. A potential explanation for this failure is that the environment, especially the pO_2, inside immuno-isolation chambers may be such that either the viability or functionality of insulin secreting β-cells is threatened.

Islets of Langerhans in vivo are highly vascularized by a glomerular-like network of capillaries that delivers arterial blood throughout the islet (Bonner-Weir and Orci, 1982; Bonner-Weir, 1984). This capillary network, combined with a very high islet blood flowrate (Lifson et al, 1980), ensures that β-cells throughout the islet receive oxygen and other nutrients at or near their arterial levels. However, when islets are isolated from the pancreas for in vitro studies or for use in transplantation (Scharp, 1984; Southerland et al, 1989A; Andersson, Korsgren, and Jansson, 1989) or immuno-isolation devices (Scharp et al, 1984), their vascular access is destroyed, and the entire islet must be supplied with oxygen and other metabolic nutrients by diffusion through the islet periphery from the surrounding tissue or medium. In the non-vascularized state, the consumption of oxygen by the cells leads to the establishment of oxygen concentration gradients both inside and outside of the islets. Consequently, the oxygen partial pressure (pO_2) in the β-cell rich islet core will be lower than that at the islet surface which, in turn, will be lower than the pO_2 in the surrounding medium or tissue.

It has been reported that short-term incubation of pieces of rabbit pancreas in static culture under an oxygen-free, 5% CO_2, 95% N_2 environment abolished their insulin secretion in response to glucose, leucine, and tolbutamide stimulation (Coore and Randle, 1964; Coore et al, 1967; Milner and Hales, 1969). Normal secretory responses were restored following 30 min of non-stimulated, normoxic culture. These results led us to hypothesize that exposure of islets to hypoxic pO_2 conditions above complete anoxia but below normal in vivo physiological levels might also affect insulin secretory response.

OBJECTIVES

The primary objectives of this research effort were to:

1) Measure the effect of intermediate levels of pO_2 on isolated islet tissue insulin secretion and viability;
2) Explore the mechanism by which hypoxia affects insulin secretion;
3) Assess the limitations that oxygen requirements impose on immuno-isolation devices.

PROJECT OVERVIEW

An overview of the project strategy is shown in Figure 1. Methods were developed for isolating and/or working with both intact islets and small cell aggregates from canine and rat pancreata. A micro-perifusion system was designed and constructed in order to test the effect of reduced oxygen tension and other metabolic factors on glucose stimulated insulin secretion from intact islets and small cell aggregates. Tissue oxygen consumption rates as a function of the surrounding medium oxygen concentration was measured for intact islets and cell aggregates. Based on these measurements, an estimate of the intra-tissue oxygen diffusivity was calculated and the pO_2 profile within perifused islets was mathematically modeled. Based on the intra-islet pO_2 profiles, an oxygen dependent model of insulin secretion was formulated. This model was fit to experimental secretion data, which provided a means by which the effect of reduced oxygen on islet insulin secretion could be summarized

by a single constant, Km_I. Insulin secretion as a function of oxygen was mathematically modelled using Km_I and a model of pO_2 profiles based on measured tissue oxygen uptake and diffusivity data.

The effect of long-term hypoxia on cell viability and insulin secretion was measured in a static culture system with environmental control. The mechanism by which hypoxia reduces insulin secretion was explored by perifusing islets with different metabolic inhibitors and measuring their effect on insulin secretion; by studying temporal response of insulin secretion following rapid changes in perfusate pO_2, and by measuring normoxic and hypoxic rates of ^{14}C-leucine uptake. From these studies, it was proposed that hypoxia reduces insulin secretion via a metabolic pathway.

The results of these research studies have been written in manuscript form. Each chapter of this document is therefore a complete manuscript in an of itself. Material that is relevant but inappropriate for inclusion in a manuscript is contained in Appendices.

REFERENCES

Algire GH, Weaver JM, and Prehn RT. (1954). Growth of cells in vivo in diffusion chambers. I. Survival of homografts in immunized mice. J Ntl Cancer Inst 15:493.

Altman JJ, Houlbart D, Bruzzo F, Desplanque N, Manoux A, Galletti PM. (1982) Implantation of semipermeable hollow fibers to prevent immune rejection of tansplanted pancreatic islets. in Islet-Pancreas-Transplantations and Artificial Pancreas. (Federlin K., Pfeiffer E, and Raptio S. eds.), Theime-Stratton, NY, pp. 43-44.

Andersson A, Korsgren O, and Jansson L. (1989) Intraportally transplanted pancreatic islets revascularized from hepatic arterial system. Diabetes 38 (Suppl. 1):192-195.

Araki Y, Solomon BA, Basile RB, Chick WL. (1985). Diabetes 34:850-54.

Archer J, Kaye R, and Mutter G. (1980). Control of streptozotocin diabetes in chinese hamsters by cultured mouse islet cells without immunosuppression. J Surg Res 28:77.

Bonheim R. (1984). Transplants: the hope and the hurdles. Diabetes Forcast. Nov-Dec. pp.23.

Bonner-Weir S, and Orci S. (1982) New Perspectives on the Microvascular of the Islets of Langerhans in the Rat. Diabetes 31: 883-889.

Bonner-Weir S. (1984) Morphological Evidence for β-cell Polarity Within the Islet of Langerhans in the Rat. Diabetes 33 (Suppl. 1): 81A.

Burghen GA, and Murrell LR. (1989) Factors influencing isolation of islets of Langerhans. Diabetes 38(Suppl. 1):129-32.

Chick WL, LIke AA, Lauris V, Galletti PM, Richardson PD, Panol G, Mix TW, and Colton CK. (1975) A hybrid artificial pancreas. Trans Amer Soc Artif Int Organs 21:8-14.

Coore HG, and Randle PJ. (1964) Regulation of Insulin Secretion Studied with Peices of Rabbit Pancreas Incubated *in vitro*. Biochem J 93: 66-77.

Coore HG, Hellman B, Idahl LA, and Taljedal IB. (1967). opusc. med 7:285.

Darquy S, and Reach G. (1985) Immunoisolation of pancreatic β-cells by micro-encapsulation: An in vitro study. Diabetologia 28:776-80.

Diabetes Research and Education Foundation. (1985). Publication number 002001-885.

Ganda OP. (1983). Morbidity and mortality from diabetes mellitus: a look at preventable aspects. Am J Public Health 73:1156-58.

Gerich JE, Charles MA, and Grodsky GM. (1976) Regulation of Pancreatic Insulin and Glucagon Secretion. Ann Rev Physiol 38: 353-388.

Hering BJ, Romann D, Clarius A, Brendel M, Slijepcevic M, Bretzel RG, and Federlin K. (1989). Xenogenic islet preparation and transplantation. Bovine islets of Langerhans: potential source for transplantation? Diabetes 38(Suppl. 1):206-208.

Iwata H, Amemiya H, Matsuda T, TAkano H, Hayashi R, and Akutsu T. (1989) Evaluation of microencapsulated islets in agarose gel as bioartificial pancreas by studies of hormone secretion in culture and by xenotransplantation. Diabetes 38(Suppl. 1):224-225.

Korsgren O, Jansson L, and Andersson A. (1989) Effects of hyperglycemia on function of isolated mouse pancreatic islets transplanted under kidney capsule. Diabetes 38:510-515.

Landgraf R, Nusser J, Muller W, Langraf-Leurs MMC, Thruau S, Ulbig M, Kampik A, Lachenmayr B, Hillebrand G, Schleibner S, Illner WD, Abendroth D, and Land W. (1989) Fate of late complications in type I diabetic patients after successfull pancreas-kidney transplantation. Diabetes 38(Suppl. 1):33-37.

Lifson N, Kramlinger KG, Mayrand FF, and Lender EJ. (1980) Blood flow to the rabbit pancreas with special reference to the islets of Langerhans. Gastroenterology 79:466-73.

Malaisse WJ. (1972) Hormonal and environmental modification of islet activity. in Handbook of Physiology, Sect. 7: Endocrnology, Vol I. Endocrine Pancreas, (Greep RO, and Astwood EB, eds.), American Physiological Society, Washington, D.C., pp. 237-260.

Matas AJ, Sutherland, DER, and Najarian, JS. (1976). Current status of islet and pancreas transplantation in diabetes. Diabetes 25:785-95.

Milner RDG, and Hales CN. (1969) The Interaction of Various Inhibitors and Stimuli of Insulin Release Studied with Rabbit Pancreas *in vitro*. Biochem J 113: 473-479.

Naber SP, Takahashi C, Chick WL, Solomon BA, Galletti PM, Richardson PD, Colton CK. (1979) Progress in development of a hybrid artificial endocrine pancreas. in Diabetes: proceedings of the 10th congress of the international diabetes federation, Vienna, Austria. Sept. 9-14.

O'Shea GM, Goosen MGA, and Sun AM (1984) Prolonged survival of transplanted islets of Langerhans encapsulated in a biocompatible membrane. Biochi Biophys Acta 804:133-36.

Porte DJ, Graf RJ, Halter JB, Pfeifer MA, and Halar E. (1981). Diabetic neuropathy and plasma glucose control. Am J Med 70:195-200.

Prowse SJ, Bellgrav d, and Lafferty KJ. (1986). Islet allografts are destroyed by disease occurance in the spontaneoulsy diabetic BB rat. Diabetes 35:110-114.

Scharp DW. (1984) Isolation and Transplantation of Islet Tissue. World J Surgery 8: 143-151.

Scharp DW, Mason NS, and Sparks RE. (1984) Islet Immuno-isolation: The use of Hybrid Artificial Organs to Prevent Islet Tissue Rejection. World J Surg 8: 221-229.

Shichire M, Kawamori R, Hakui N, Yamasaki Y, Abe H. (1984) Closed-loop glycemic control with a wearable artificial endocrine pancras: variations in daily insulin requirements to glycemic response. Diabetes 33:1200-02.

Soeldner JS (1981) Treatment of diabetes mellitus by devices. Am J Med 70:183-194.

Steno Study Group (1982). Effect pof six months of strict metabolic control on eye and kidney function in insulin dependent diabetics with background retinopathy. Lancet 1:121-124.

Sutherland DER, Goetz FC, and Sibley RK. (1989A). Recurrence of disease in pancreas transplants. Diabetes 38(Suppl. 1):85-87.

Sutherland DER, Moudry KC, and Fryd DS. (1989B). Results of pancreas-transplant registry. Diabetes 38(Suppl. 1):46-54.

Unger RH, Dobbs RE, and Orci L. (1978) Insulin, glucagon, and somatostatin secretion in the regulation of metabolism. Ann Ref Physiol 40:307-43.

United States Pharmacopia / The National Formulary. Vol XX and XV.
January, 1980.

Diabetic Complications	Incidence x Normal
• Blindness Leading cause of new blindness in adults (5,000/year)	25
• Kidney Disease 2,000 new cases of ESRD / year 30% of diabetic mortality due to uremia	17
• Gangrene 20,000 lower extremity amputations/year	5
• Heart Disease/Stroke	2
• Ketoacidosis 15,000 episodes/year 42% of diabetic mortality between ages 10 - 19	
• Mortality Life expectancy 1/3 less 50% mortality by age 50 for diabetics with onset before age 20 35,000 deaths/yr directly due to diabetes	8

TABLE 1. Primary and Secondary Complications of Diabetes[7] [7] (Deckert, Pouslen, and Larsen, 1978; Ganda, 1983)

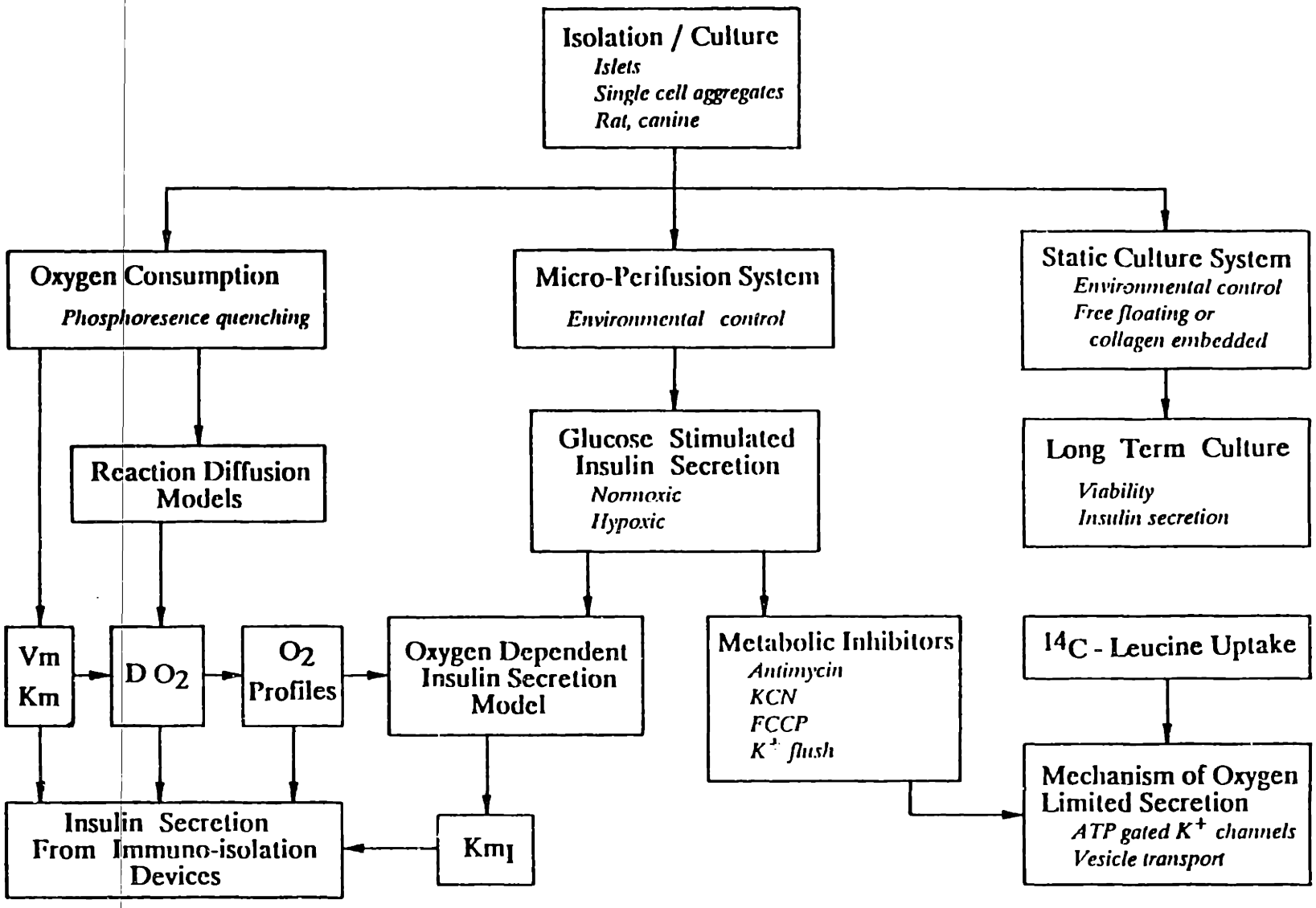

FIGURE 1. Schematic overview of the research project.

CHAPTER 2:

A MICRO-PERIFUSION SYSTEM WITH ENVIRONMENTAL CONTROL FOR ISLET INSULIN SECRETION STUDIES

SUMMARY

A continuous flow reactor (perifusion system) was fabricated and tested for measuring the kinetics of insulin secretion in response to step changes in the glucose concentration and oxygen partial pressure in the perfusate flowing around isolated pancreatic islets of Langerhans. The system was capable of mailing rapid changes in perfusate glucose concentration and pO_2, had rapid dynamic response for measuring the change in insulin secretion rate as a result of these changes in perfusate, and was suitable for studying very small volumes of tissue. Initial experiments with this system demonstrated that (1) the initial response of isolated rat islets to glucose stimulation is very fast, with the first phase peak occurring in as little as about 10 seconds, (2) bulk perfusate oxygen partial pressure levels of 30 mmHg or less reduce insulin secretion rate in graded fashion, (3) the reduction in secretion rate begins within one minute following an oxygen partial pressure decrease, and (4) the reduction in secretion rate is reversible, with a burst of insulin secretion occurring during the first minute after oxygen partial pressure is increased from low levels.

INTRODUCTION

Islets of Langerhans are spheroidal aggregates, 50 to 400 μm in diameter, that are comprised of an inner core of insulin secreting β-cells. Islets are of current interest in several applications for improved treatment of diabetes including use in an implantable hybrid immunoisolation device, in which the islets are separated from the host by a semipermeable membrane that prevents rejection by cells and antibodies (Scharp et al., 1984). In this application, the potential exists for severe oxygen limitations within the islet tissue. The same holds true for islet transplantation as a substitute for transplantation of the intact pancreas (Scharp, 1984; Southerland et al., 1989) during the period prior to islet vascularization (Andersson et al., 1989). Whereas β-cells are highly oxygenated in vivo by an extensive islet vascular system (Bonner-Weir and Orci, 1982), cells located within non-vascularized isolated islets must be supplied with nutrients and oxygen by diffusion from the surrounding environment. Oxygen consumption by the cells leads to external and internal oxygen partial pressure (pO_2) gradients which may expose a substantial fraction of the islet to hypoxic or even anoxic ($pO_2 = 0$) conditions. Previous studies in static culture (Coore and Randle, 1964; Coore et al., 1967; Milner and Hales, 1969) have demonstrated that insulin secretion is abolished during acute anoxia, but there is not data on the effect of intermediate pO_2 levels on islet insulin secretion or on the dynamic response of secretion to pO_2 changes. In addition to the effect of pO_2 on secretion rate, knowledge of the intrinsic kinetics of insulin secretion is necessary to understand its interplay with mass transfer resistances in determining the overall performance of immuno-isolation devices (Weinless and Colton, 1987).

The motivation for the study reported here is to better understand the kinetics of insulin secretion by isolated islets of Langerhans in response to glucose stimulation and, in particular, to investigate the effect of pO_2 substantially reduced from normal physiologic levels on glucose-stimulated insulin secretion rate. We have employed a continuous flow reactor in which the cells or tissue are retained by a porous barrier, and culture medium flows over or around the biological material and is then collected for analysis. Continuous flow reactors are particularly suited to studies of the dynamic response of cells to changes in

culture medium composition or environmental conditions. In an early application of this technique (Burr et al, 1969) to pancreatic tissue, the term "perifusion" was coined to distinguish the method from perfusion of culture medium through the vascular system of the intact pancreas. We employ the same term here since it is entrenched in the literature.

Islet perifusion systems have previously been described which were designed to regulate temperature, pH, and flowrate of the perfusate and to switch between perfusate streams containing different concentrations of test substances (e.g., Lacy et al., 1972; Hoshi and Shreeve, 1973; Lacy et al., 1976; Weaver et al., 1978; Gingerich et al., 1979). In addition to these capabilities, the goals of our investigation required that the system have the following characteristics: (1) regulate, monitor and rapidly change the pO_2 in the perfusate bathing the islets; (2) have a small internal volume so as to provide minimal time lag between the onset of an environmental change and sampling of the secreted insulin concentration at the outlet; and (3) function with a small volume of tissue (on the order of 10 rat islets) that could be easily obtained and accurately sized and counted.

In this paper, we describe the design of a micro-perifusion system with environmental control suitable for studies with small amounts of tissue. The dynamic response characteristics of the system are described, and the results of initial experiments on the effects of changes in glucose concentration and pO_2 on insulin secretion rate by isolated rat islets are reported. These initial results show that (1) the initial response (first phase) to glucose stimulation is virtually instantaneous, (2) intermediate levels of acute hypoxia reduce insulin secretion rate in graded fashion, and (3) the reduction in secretion rate caused by hypoxia is very rapid and reversible.

MATERIALS AND METHODS

Materials

Digestion medium: Tissue digestions were performed using Hanks balanced salt solution without Ca^{++} and Mg^{++} (H2387 Sigma Chemical Co., St. Louis, MO) to which was added 50

U/ml Penicillin, 50 μg/ml Streptomycin (600-5140AG, GIBCO, Grand Island, NY), and 0.35 g/l Hepes (H0763, Sigma Chemical Co.), pH 7.4.

Culture and perfusion medium: Islet tissue was cultured in Dulbecco's modified Eagles medium (DMEM, D5523, Sigma Chemical Co) containing 1.0 mg/ml glucose, 50 U/ml Penicillin, 50 μg/ml Streptomycin, and 10% (v/v) newborn calf serum (NBCS, 200-6010AJ, GIBCO). Perifusions were performed in the same medium with either 100 or 300 mg/dl glucose.

Insulin assay buffer: The buffer medium used for insulin assays consisted of an aqueous solution containing 6.90 g/l monobasic sodium phosphate, 7.30 g/l ethylene-diaminetetraacetic acid (EDTA, Mallinckrodt, Paris KY), 0.1 g/l thimerosal as an anti-bacterial agent (T-5125, Sigma Chemical Co), and 10.0 g/l bovine serum albumin (BSA, A-7888, Sigma Chemical Co), pH 7.4 .

Other reagents: Pancreata were digested with type IV collagenase (108 8882 Boehringer Mannheim, Indianapolis, IN). Discontinuous density gradients were prepared using dialyzed and lyophilized ficoll (Type 400-DL, F9378, Sigma Chemical Co). Reagents used for radio-immunoassay of insulin include ^{125}I-insulin (130, ^{125}I-porcine insulin, Cambridge Medical Technology, Billerica MA), guinea pig anti-rat insulin serum solution (Linco Research Inc., Eureka MO; lyophilized powder from one ml serum was hydrated with 100 ml insulin assay buffer), goat anti-guinea pig IgG serum solution (Linco Research Inc, Eureka MO; lyophilized powder from 10 ml serum was added to 100 ml insulin assay buffer containing 30 g/l polyethylene glycol (PEG) 8000, P-2139, Sigma Chemical Co. and 2 g/l BSA), and guinea pig serum (S-3634, Sigma Chemical Co.; lyophilized powder from one ml serum was added to 70 ml insulin assay buffer containing 30 g/l PEG and 2 g/l BSA). Rat insulin standard was generously donated by Dr. Konald Chance, Eli Lilly Co. (Indianapolis IN). Some perifusions and calibrations were performed with compressed gas (5.0% CO_2 and 95.0% air, supplied and calibrated by Matheson Gas Products Inc., Gloucester MA).

Islet Isolation and Culture

Rat islets of Langerhans were isolated from male Sprague Dawley rats (200 - 350 g, Charles River Laboratories, Kingston NY) using a modification of the collagenase digestion/ficoll purification technique (Lacy and Kostianovsky, 1967; Scharp et al., 1980). Each isolation batch consisted of pancreata from two or three rats whose islets were mixed together in the isolation process. Briefly, rats were anaesthetized with 0.1 ml/100 g body weight of sodium pentobarbital (65 mg/ml, J.A. Webster, N. Billerica MA) injected in the peritoneal cavity. Ice cold digestion medium (20 ml per rat) containing 1.7 mg/ml collagenase was prepared, 12-15 ml of which was used to distend the pancreas by injection via the bile duct. The distended pancreas was removed from the rat, trimmed free of extraneous tissue, and digested for 15 - 18 min at 37°C together with the remaining collagenase solution in a 50 ml T-flask (Falcon 3013, Becton Dickinson, Inc.) under mild agitation with a wrist shaker (Model 75, Burrell Co., Pittsburgh PA; setting No. 1). When microscopic examination showed that the islets were free of vascular and acinar attachments, digestion was halted by addition of ice cold culture medium. The tissue slurry was filtered through a 500 μm mesh filter (145765, Spectra macroporous filter, Spectrum Medical Ind., Los Angeles CA), rinsed twice by centrifugation and resuspension in 50 ml culture medium, and layered under a series of ficoll gradients (25%, 22%, 17.5%, and 11% ficoll, w/w) in a 50-ml centrifugation tube. The ficoll gradients were centrifuged at 1000 x g for 12 min. Viable islets, which rose to the interface between the 17.5% and 22% ficoll layers, were removed by aspiration with a one ml pipette. The purified islet fraction was rinsed in culture medium, pelleted by centrifugation, hand-picked by aspirating into a 200 μl micropipette (Pipetman, Rainin Instrument Co, Woburn MA) while viewed under a dissecting microscope, and transferred through a series of at least four petri dishes filled with culture medium in order to thoroughly remove residual ficoll and ensure islet purity. Islet preparations were visually ascertained to be 98+% pure and contained on average 300 to 500 islets (ranging from 70 to 500 μm in diameter) per rat.

Purified islets were cultured in 50 mm diameter polystyrene Petri dishes (Falcon 1007, Becton Dickinson Inc, Lincoln Park NJ). Each dish contained 100 - 300 islets in seven ml

culture medium. Dishes were placed in a 37°C incubator with a gas environment of 95% air and 5% CO_2. Islets were cultured for a minimum of 16 hr before being hand-picked for perifusion studies. (See Appendix 2A for a more detailed description of isolation and culture techniques.)

Perifusion Apparatus

Overall structure: The perifusion system (Figure 1) consisted of two incubators, one nestled inside of the other. The outer incubator (continuous gas flow incubator, model 2210, Queue Systems Inc., Parkersburg WV) provided primary temperature control at about 37°C. The inner incubator, which contained the tissue perifusion chamber and gas exchange tubing, was formed by inverting a 600 ml pyrex bowl over a 0.5-cm thick neoprene rubber mat. The interface was sealed with silicon vacuum grease. All tubing and electrical or mechanical leads entered or exited the inner incubator through small holes cut in the rubber mat using a cork borer. The temperature and gas environment (pO_2, pCO_2) of the inner chamber were rigidly controlled. Perfusion media pre-mixed with different concentrations of glucose were stored in separate reservoirs placed in the outer incubator. The perfusate was pumped through gas-permeable silicone rubber tubing coiled inside of the inner incubator where it equilibrated with the surrounding gas. The pO_2 and pH of the perfusate were monitored by in-line probes. After gas exchange, the perfusate entered a valve system which allowed switching between streams containing different concentrations of glucose. The selected medium flowed over the islets entrapped in a tissue chamber and then out of the inner and outer incubators directly into a fraction collector where it was collected for later glucose and insulin analysis.

Gas system: The control system of the Queue incubator provided a steady gas flow (0.6 l/min) consisting of pulses of CO_2, air, and N_2, which could be mixed to any desired composition ranging from 0.0 to 99.9%. The gas was humidified by bubbling it through two water-filled 250 ml erlenmeyer flasks connected in series. Mixing of the pulsed gas was achieved in a 1.0 l erlenmeyer flask. The gas then flowed into the inner incubator where it was stirred by a magnetic air fan constructed by gluing vanes onto a magnetic stirring bar.

Incoming gas flushed the inner incubator on average once every min and exited through leaks around tubing penetrating the rubber mat. All gas lines were constructed from gas impermeable tubing (Tubing 3814-1, Queue System Inc., Parkersburg WV).

To obtain a specified pO_2 in the inner incubator, the gas composition from the Queue control system was set according to the following formulas:

$$\% \text{ air} = \frac{100\ pO_2}{0.21\ (p_{atm} - pH_2O)} \quad (1)$$

$$\% N_2 = 100 - (\%CO_2 + \% \text{ air}) \quad (2)$$

The percent CO_2 was set at 5.3% in order to hold the pH of the perfusate at 7.45 . P_{atm} was monitored in the surrounding room air using a pressure transducer (type 227A, MKS Instruments, Burlington, MA) and was taken to be 760 mm Hg for use in Equation 1. The partial pressure of water, pH_2O, at 37°C was 47 mmHg (Weast, 1980). At 37°C, a fully humidified gas originally composed of 94.7% air and 5.3% CO_2 had a pO_2 of 141.8 mm Hg.

In order to decrease the time required to reach steady state following a switch to a lower gas pO_2, the change was initiated with a two-min burst of gas composed of 5.3% CO_2 and 94.7% N_2 at a flowrate of 2.0 l/min in order to flush normoxic gas out of the humidification chambers, gas mixing flask, and inner incubator. After this flush, the flowrate was decreased back to 0.6 l/min, and the composition of the gas flowing from the Queue controller was set at the specified level.

Liquid system: Each perfusion medium was stored in a 250 ml sterile flask (Falcon 3024, Becton Dickinson, Lincoln Park NJ) in the outer incubator. Serum was included in the perfusion media in order to adsorb serum proteins on the perfusion tubing surface so as to prevent the adsorption of secreted insulin (Cecil and Robinson, 1975). For most perifusions, perfusates containing 100 mg/dl (basal) and 300 mg/dl (stimulated) glucose were employed.

Perfusate was pumped from the reservoirs by a variable speed, four-channel, eight-roller peristaltic pump (model NJ-7624, Cole-Parmer, Chicago IL) which could provide a flowrate between 0.4-3.0 ml/min per channel using silicone rubber pump tubing (NJ-7624-24, Cole-Parmer). The four-channel pump could be used to pump up to four perfusion

streams through the system; normally, only two lines were used, one containing medium with 100 mg/dl glucose and the other with 300 mg/dl glucose. Teflon tubing was used to carry perfusate across the rubber mat into the inner incubator. All tubing connections were formed either by inserting the ends of teflon tubing into abutting silicone rubber tubing or by using 1/16-in id polypropylene barbed connectors (T-6365-11, Cole-Parmer, Chicago IL) to connect silicone rubber to silicone rubber tubing.

After entering the inner incubator, each perfusion medium flowed through 20 cm of thin walled silicone rubber tubing (0.058-in id, 0.077-in od, Dow Corning Silastic, Greene Rubber Co, Cambridge MA) which provided initial gas exchange and temperature equilibration of the perfusate. Gas bubbles formed in the perfusate as a result of pumping, gas exchange, and temperature change were caught with in-line bubble traps formed by connecting syringe tip filters (0.45 μm Millex-HA, Millipore, Bedford MA) to the perfusate tubing lines. After the bubble traps, each perfusate line was split into two parallel strands of narrow bore, thin walled silicone rubber tubing (0.025-in id, 0.47-in od, Dow Corning Silastic, Greene Rubber Co), each 210 cm long, in order to provide sufficient residence time and surface area for gas exchange between the perfusate and the surrounding gas. The total length of gas exchange tubing was calculated (Colton and Drake, 1971; Kim and Stroeve, 1987) to provide more than 99.9% of the approach to equilibrium at a perfusate flowrate of 0.5 ml/min.

After gas equilibration, perfusate tubing led into a switching system used to select the perfusate stream which flowed through the tissue chamber. For perifusions not involving changes in the pO_2, the perfusate switch consisted of a small four-way valve with a teflon core (Hamilton 8600 series, VWR Scientific, Boston MA), the valve stem of which extended through the rubber mat to provide access. For perifusions that involved a change in pO_2, the teflon valve core, with its high oxygen solubility, functioned as an oxygen source or sink which slowed the dynamic response of the perfusate pO_2. To avoid this problem, a simple pinch clamp system was constructed using five-in stainless steel hemostats inserted through the rubber mat. The arrangement of the pinch clamps is shown in the upper right corner of

Figure 1. The tubing employed was 0.031-in id, 0.094-in od silicone rubber (T-6411-60, Cole-Parmer, Chicago IL). Three way connections were made with 1/16-in id barbed polypropylene T-connectors (T-6365-77, Cole-Parmer). With pinch sites A opened and B closed perfusate containing 100 mg/dl glucose flowed through the tissue chamber, and perfusate containing 300 mg/dl glucose was either sent to waste or recycled to the 300 mg/dl glucose reservoir. With A closed and B opened, the situation was reversed. The hemostat clamps were actuated through the rubber mat without disturbing the environment of the inner incubator. In one early version of the apparatus, remotely activated solenoid pinch valves (443 Angar solenoid pinch valves, ASCO Boston, MA) were employed. Heat generated by the solenoid motors generated temperature oscillations in the inner incubator, and the solenoid valves were replaced by the manually-operated pinch clamps.

The selected perfusate stream flowed through the tissue chamber (lower right corner of Figure 1). As in the case of nonmetallic valves, tissue chambers employed in preliminary experiments (Swinnex filter holder, Millipore, Bedford, MA; Millex-HA filters, Millipore; 1105-000 Cell chamber, Endotronics, Coon Rapids, MN; custom-fabricated polycarbonate holder) contained potential sources or sinks of oxygen because of the high oxygen solubility of their plastic casings and/or seals. To minimize the possibility of oxygen contamination from these sources, the tissue chamber was formed by inserting a small wad of wet cotton into a four-cm long section of 0.058-in id silicone rubber tubing. The cotton plug was inserted by disconnecting the silicone rubber tubing from the polypropylene T-connecter which housed the oxygen probe. Air bubbles trapped in the perfusate tubing during insertion of the cotton plug were squeezed through the cotton and washed out of the system.

Tissue was loaded into the tissue chamber through the islet loading port formed by inserting a two-cm long lead piece of 0.031-in id, 0.094-in od silicone rubber tubing inside the slightly larger 0.058-in id silicone rubber tubing which formed the tissue chamber. The lead tubing was connected to the perfusate switch by a two-cm long section of 0.036-in od teflon tubing which was removed in order to allow insertion of a micropipette tip through

which islet tissue was introduced. The cotton plug successfully entrapped both whole islets (200 μm average diameter) and single cells (14 μm average diameter).

The perfusate pH was monitored with an in-line pH probe having 30 μl internal volume (model 19-8305-01, Pharmacia, Piscataway NJ) connected to a Beckman 31pH monitor (VWR Scientific, Boston MA). The probe was placed in the common perfusate recycle line.

The perfusate pO_2 was monitored using a prototype fluorescent pO_2 sensor (Bentley OM-100, generously donated by Dr. Hal Heitzemann of Bentley Division, Baxter Healthcare Corp, Irvine CA). The probe tip was mounted in a 1/16-in id polypropylene T-connector which was connected into the perfusate line. The volume added by insertion of the flow-through pO_2 probe was about 0.03 ml. The pO_2 sensor was based on the ability of oxygen to quench specific chromophore fluorescence (Kautsky, 1939). The sensor probe consisted of an O_2 permeable sheath filled with a fluorescent dye. The probe was connected to the sensor body by a split fiber optic cable which carried light from an illumination source in the sensor body to the probe and fluorescence from the probe to the sensor body. Fluorescence from the probe was amplified and converted to pO_2 in mm Hg using the Stern-Volmer quenching constant of the dye. The sensor was similar in concept and design to another prototype device previously described in the literature (Peterson, Fitzgerald, and Buckhold, 1984). The oxygen sensor required calibration at only a single known pO_2, was stable over long periods of time, and provided a digital measurement of pO_2 with a resolution of one mmHg and a precision of ± 0.7 mmHg. The time to achieve steady state response of the sensor was approximately 30 sec for a gas-phase pO_2 step from 142 to 0 mm Hg.

After passing through the pO_2 probe, perfusate exited both incubators via 50 cm of 0.018-in id, 0.036-in od teflon tubing (26SW, Zeus Industrial Products Inc.) and dripped into polypropylene collection tubes (55.526, Sarstedt, Princeton NJ) in a fraction collector (Isco Retriever II, Cole-Parmer, Chicago IL). Sample tubes were stored at 4°C until assayed. Glucose concentration was measured using a Beckman glucose analyzer (Glucose Analyzer II, Beckman Instruments Inc, Fullerton CA). Insulin concentration was measured by radioimmunoassay (described below).

Temperature Control: Gross temperature control was maintained by the outer incubator. Heating tape powered by a variable voltage source (Powerstat, Superior Electric Co, Bristol CN) was coiled inside of the outer incubator and was used to supply extra heat whenever the outer incubator door was opened. A six-in diameter air fan was placed inside the outer incubator in order to distribute heat emitted from the heating tape, peristaltic pump, and magnetic air stirrer. The temperature in the outer incubator was monitored by the built-in thermocouple of the Queue incubator. The temperature in the outer incubator was set at 37°C but was varied ± 3°C as required in order to maintain the temperature within the inner incubator at 37.0 ± 0.3 °C.

The temperature inside the inner incubator was monitored using a thermoresistor (YSI 511, VWR Scientific, Boston MA) connected to a digital display (Digital thermometer 500, VWR Scientific, Boston MA). This temperature was corroborated by measurements made with thermocompensators connected to the pO_2 and pH probes.

Rapid gas switching system: A variation of the normal perifusion system described above was used when it was desired to achieve very rapid changes in the pO_2 of the medium perifusing the tissue chamber (Figure 2). A second set of humidification and gas mixing chambers was connected to a compressed gas tank containing 5% CO_2 and 95% air (Matheson Gas Products Inc., Gloucester MA) which provided normoxic (pO_2 = 142 mm Hg) gas at a flowrate of 0.6 l/min. One set of perfusate gas exchange tubing was placed inside of the 1.0 l erlenmeyer flask of this system. The equilibrated perfusate was carried from the gas exchange flask to the perfusate switch in the inner incubator by 0.031-in id, 0.062-in od stainless steel tubing. In this rapid gas switching system, the tissue chamber was initially perfused with medium which was equilibrated with gas at pO_2 142 mm Hg in the second gas mixing flask, while the perfusate flowing through the gas exchange tubing in the inner incubator was pre-equilibrated at a hypoxic test level. The pO_2 of the medium flowing through the tissue chamber was then rapidly changed by switching from the normoxic to the hypoxic perfusate or vice versa.

The volume of perfusate contained in components of the liquid system, beginning with the gas exchange tubing, and the average residence time at a perfusate flowrate of 0.5 ml/min, are summarized in Table 1. The total volume after the perfusate switch and the average residence time were 0.20 ml and 24 sec, respectively, in the perifusion system with pO_2 switching capability and 0.14 ml and 17 sec, respectively, in the system not designed for pO_2 change. The normal operating parameters of the perifusion system and the range over which they could be regulated are listed in Table 2.

Insulin Radioimmunoassay (RIA)

Insulin concentration was assayed using a competitive double antibody RIA (Soeldner and Slone, 1965). Using an automatic pipette (Gilson diluter 401, Gilson Medical Electronics, Middletown WI), 100 μl of unknown sample was mixed with 300 μl of assay buffer containing 3.0 μU/ml (0.12 ng/ml) ^{125}I-insulin and 100 μl of guinea pig anti-rat insulin serum in a 2.5 ml glass test tube (60825-902, VWR Scientific, Boston MA). The mixture was incubated overnight at 4°C, during which time the anti-insulin antibody competitively bound to the labeled and unlabeled insulin in proportion to their respective concentrations. The higher the concentration of unknown insulin, the less ^{125}I-insulin was bound.

After 12 hr, total bound insulin was precipitated out of solution by adding to each tube 100 μl goat anti guinea pig IgG solution, 100 μl guinea pig serum solution to provide a source of complement, and 1000 μl assay buffer (containing 30 g/l PEG and 2 g/l BSA) to dilute the unbound ^{125}I-insulin.

The test tubes were incubated for two hr at room temperature in order to allow time for the goat anti-guinea pig IgG to bind to the guinea pig anti-insulin antibodies. The precipitate, which consisted of complexes of insulin and anti-insulin antibody crosslinked by the anti-guinea pig IgG, guinea pig complement, and PEG chains, was separated from the supernatant by centrifugation at 1000 x g for 15 min. The tubes were immediately inverted to remove the supernatant, leaving only the pellet at the bottom of the tube. The bound ^{125}I-insulin was measured using a gamma counter (Packard Auto Gamma 500, Packard, Sterling

VI), and the ratio of bound to free ^{125}I-insulin (B/F) was calculated for each tube according to: B/F = [B/(T-B)], where B, F, and T represent the radioactivity (counts/min, corrected for background) of bound and free ^{125}I-insulin and of the total ^{125}I-insulin added to each tube, respectively. For each set of assays, the total ^{125}I-insulin radioactivity added to each tube was counted in six replicate tubes from which the supernatant was not decanted.

A calibration curve was prepared with each set of assays using known concentrations of rat insulin standard prepared in an identical manner as described for unknown samples. Each calibration curve was fitted to a polynomial function of the form,

$$[I] = A + BX + CX^2 + \frac{D}{X} + \frac{E}{X^2} \qquad (3)$$

by nonlinear least squares regression, where [I] is the insulin concentration in μU/ml and X is the B/F ratio. The insulin concentration of each unknown sample was calculated by inserting the measured B/F ratio into Equation (3). Each unknown sample was assayed in duplicate and each standard in triplicate or quadruplicate. A representative calibration curve is shown in Figure 3 with the insulin concentration of the standards plotted versus the ratio of bound to free ^{125}I-Insulin. The standard deviation (n=4) in the B/F ratios are shown as horizontal error bars. Where not shown, error bars are contained within the plotted symbols. The standard deviation in measured insulin concentration (vertical error bars) was obtained by applying the fitted parameters of Equation (3) to each B/F replicate. For only one standard sample (200 μU/ml) was the error bar larger than the plotted symbol. Eight replicates with individual samples yielded coefficients of variations of about 5% (range 1.5 to 6.2%) for [I] between 25 and 200 μU/ml; about 15% (range 13 to 19%) from 1.0 to 25 μU/ml. The standard deviation below 10 μU/ml was about ± 1.3 μU/ml. The insulin secretion rate, S, per unit volume of tissue, V_t, was calculated from the measured insulin concentration [I] in each sample according to

$$S = \frac{Q\,[I]}{V_t} \qquad (4)$$

where Q is the perfusate flowrate. (See Appendix 2B for a more information on the RIA.)

Perifusion Protocol

The night before a perifusion, pre-mixed perfusate was put into sterile reservoir flasks and placed in a 37°C incubator to equilibrate with 5% CO_2 and 95% air. This incubation reduced the amount of bubbles formed during the subsequent perifusion.

Two hr before a perifusion, 10 to 15 isolated spheroidal rat islets of Langerhans approximately 200 μm in diameter were hand-picked under a dissecting microscope using a 20 μl micropipette and placed in a petri dish (Falcon 1007, Becton Dickinson) containing 10 ml of warmed (37°C) basal perfusion medium. The islets were photographed under a microscope with a calibrated reticule for later sizing.

One hr before the start of a perifusion, the peristaltic pump was started, the bubble traps were connected into the tubing lines, and the cotton plug was inserted into the tissue chamber. Gas bubbles were flushed downstream by shaking the tubing harness and squeezing them through the cotton plug. The inner incubator was sealed with silicone vacuum grease, and the system was brought to temperature (37°C) and gas (pO_2 142 mm Hg) equilibrium for at least 15 min before the islets were loaded, during which time the pO_2 probe was calibrated.

Islets were loaded into the tissue chamber by first aspirating them into the bottom third of a 200 μl pipette tip (RT20, Rainin Instrument Co, Woburn MA) using a 200 μl micropipette. Both incubators were opened to access the tissue chamber. The lead silicone rubber tubing above the tissue chamber (Figure 1) was pinched shut immediately downstream of the teflon connector, which was then removed and the 200 μl pipet tip inserted in its place. The islet suspension was gently expelled from the pipette and flowed downstream where the islets were entrapped in the cotton plug. Transfer of islets from the micropipette tip into the silicone rubber tubing was verified visually. The silicone rubber tubing was again pinched shut, the pipette tip removed, and the teflon connector reinserted. The pump was left running throughout the procedure. It was critical that no air bubbles be introduced into the perfusate tubing during islet loading because the presence of gas bubbles in contact with islets in the tissue chamber caused erratic bursts of insulin secretion in addition to slowing the

dynamic response to pO_2 changes. Once the inner incubator was resealed and the outer incubator closed, the temperature, pH, and pO_2 restabilized within about 5 min, and the system was left for another 25 min to allow the islets to adjust to the basal perifusion conditions before collecting fractions for measurement of basal insulin secretion. At time t=0, perfusate was switched from 100 to 300 mg/dl glucose.

Islet Sizing

The micrograph of the islet sample was projected onto a screen, and the external dimensions of each islet were measured using the reticule grid. Slight deviations from a spherical shape were accounted for by measuring both the largest diameter and the diameter normal to it, assuming each islet could be represented by a prolate ellipsoid, and calculating its volume, v, from $v = \pi a^2 b/6$, where a and b are the smaller and larger axes, respectively. The equivalent spherical diameter, d, for each islet was calculated as that of a sphere of equal volume, $v = \pi d^3/6$; thus, $d = (a^2 b)^{1/3}$. A representative sample of 12 rat islets of Langerhans used in a perifusion experiment is shown in Figure 4. The total volume of all islets was 0.058 mm^3, and the number-average equivalent spherical diameter of the islets was 210 ± 15 μm.

RESULTS

System Performance Characterization

Experiments were carried out to investigate the dynamic response of the perifusion system following changes in glucose and insulin concentrations and pO_2. The residence time distributions of the exit concentration following step changes in glucose from 100 to 300 mg/dl and insulin from 6 to 18 μU/ml with different internal fluid volumes and perfusate flowrates are shown in Figure 5. The fractional approach to steady state of the exit concentration, $\phi = (C-C_\infty)/(C_o-C_\infty)$, is plotted versus the dimensionless residence time, $\tau=Qt/V$, where C is the concentration at the outlet, and C_o and C_∞ are the initial and final concentrations respectively, t is time after changing the perfusate switch, and V is the perfusate volume from the switch to the outlet. The value of t for glucose and insulin data is

taken as the midpoint of the time interval over which the data is collected. Also plotted in Figure 5 is the theoretical curve for residence time distribution in parabolic laminar flow (Smith, 1970)

$$\tau \leq 0.5 \qquad \phi = 0$$
$$\tau > 0.5 \qquad \phi = 1 - \frac{1}{4}\left(\frac{1}{\tau}\right)^2 \tag{5}$$

The residence time distributions for both glucose and insulin at all flowrates and volumes investigated closely approximate that expected for laminar flow with no dispersion. Response times for 50% (t_{50}) and 90% (t_{90}) approach to steady state are summarized in Table 3. The fastest responding system (without oxygen switching capability) displayed a t_{50} and t_{90} of 8 and 14 sec, respectively, with Q = 1.0 ml/min and V = 0.14 ml. With Q = 0.5 ml/min and V = 0.2 ml in the system with oxygen switching capability (the standard setup for most experiments), t_{50} and t_{90} were 22 and 37-39 sec, respectively, for both glucose and insulin. The close similarity between the insulin and glucose responses indicates that with 10% NBCS added to the perfusion medium, insulin is neither delayed nor blunted as a result of insulin adsorption to the tubing or tissue chamber material. Identical results were obtained when one percent (w/v) BSA was substituted for the 10% NBCS.

The dynamic response following a change in pO_2 is plotted in Figure 6 for both the normal and rapid oxygen switching systems, and response times are summarized in Table 3. Each data point is plotted at the actual time of measurement. The response to the normal switch is delayed compared to that for the rapid switch because of the time required to flush the residual gas out of the humidification chambers, gas mixing flask, and inner incubator following a change in the gas composition settings and because of the time required for perfusate to equilibrate in the gas exchange tubing with the changed gas pO_2. The approach to steady state is faster following a downward step in pO_2 in both the normal and rapid switching systems. In the normal system, the more rapid downward step is made possible by the initial burst of O_2-free gas used to flush out most of the residual normoxic gas in the

entire gas system before the hypoxic gas composition is set. In contrast, the normal step up in pO_2 is made by directly setting the gas composition to the normoxic level.

With the rapid switching system, the hysteresis between down and up steps is caused by the fact that the hypoxic perfusate is equilibrated in the inner incubator and the normoxic perfusate is equilibrated in the second gas mixing flask and transported to the perfusate switch via stainless steel tubing. For an upward pO_2 switch, tubing between the perfusate switch and the pO_2 probe is initially exposed to the hypoxic gas environment of the inner incubator. Limited gas exchange over this short section of tubing slows the approach to steady state until the inner incubator gas is flushed out with normoxic gas. The response to a downward pO_2 step should most closely approximate that for laminar flow. In fact, the downward step is initially faster than predicted by laminar flow (Figure 5), possibly because the probe tip is mounted in the center of the flowstream and senses the fluid with the highest velocity. The late stages of the measured approach to steady state for both upward and downward steps in the rapid oxygen switching system are slowed compared to that expected for laminar flow because of the buffering effect of the oxygen dissolved in the silicone rubber tubing and because of delay associated with sensing by the pO_2 probe which may be caused, in part, by oxygen diffusing out of the epoxy body of the probe tip. Thus, the actual approach to steady state seen by the islets may be faster than that measured and may approximate that expected for laminar flow (Figure 5).

Effect of Changes in Perfusate pO_2 on Insulin Secretion

Initial tests of the effect of hypoxia on the insulin secretion of perifused islets were made using a perifusion system which lacked certain features of that described above. Results of these experiments established an affect of pO_2 on perifused islet insulin secretion but also demonstrated the substantial increase in pO_2 response time associated with use of plastic components having high oxygen solubility and capacity. Figure 7 illustrates the oxygen partial pressure and insulin secretion profiles of two preparations of rat islets from the same isolation batch. The perfusate switch was a Hamilton valve with a teflon core

(described above). The tissue chamber consisted of islets retained on a microporous membrane within a polycarbonate holder, the two halves of which were sealed with a teflon O-ring and silicon vacuum grease. The pO_2 probe was mounted in a polycarbonate block. At t = 0, the glucose concentration in the perfusate was raised from 100 to 300 mg/dl, and the islets rapidly responded with a burst of insulin characteristic of a normal first phase secretion response (Grodsky et al., 1969). Thereafter, the second phase insulin secretion rate rose steadily over the next 35 min, reaching approximately 700 $\mu U/min\text{-}mm^3$ islets. At t=35 min, the pO_2 of the in-flowing gas from the Queue controller was switched from 142 to 5 mmHg. The pO_2 of the perfusate fell at a moderate rate, with t_{50} and t_{90} equal to 10 and 21 min, respectively. However, the perfusate pO_2 continued to fall slowly and did not reach steady state until about one hr after the gas composition was changed. After the pO_2 change was initiated, secretion rate began to decrease almost immediately with one preparation and after about 15 min with the other. Secretion continued to drop with falling perfusate pO_2, reaching a steady basal level approximately one hr after the onset of hypoxia. At t=112 min, the gas composition was raised back to 142 mmHg oxygen. The insulin secretion rate began to rise after about 5 min when the pO_2 was about 20 mm Hg. Although the perfusate pO_2 never returned to its full normoxic level before termination of the experiment, insulin secretion returned to about 90% of its pre-hypoxic rate. The long time required to reach steady state and the inability to study the dynamics of insulin secretion in response to pO_2 changes motivated the apparatus improvements described in Materials and Methods.

The results shown in Figure 8 are from a perifusion run with the final apparatus configuration using the normal oxygen switching system which eliminated the oxygen sources and sinks associated with the perifusion shown in Figure 7. The timing of the first and second phase insulin secretion rates were similar to that shown in Figure 7. At t=45 min, pO_2 was switched to 30 mmHg. The perfusate pO_2 decreased rapidly: t_{90} was about 4 min, and a stable value of 30 ± 1 mm Hg was attained seven min after the switch. Insulin secretion rate fell rapidly and reached a steady level by the time the first sample was collected for assay over the period from 4 to 8 min after initiation of the pO_2 drop. Secretion remained at the

reduced level throughout the period of hypoxia and released a burst of insulin during the 4 min period following the initiation of the pO_2 step up. After this initial burst, the secretory rate returned to its pre-hypoxic level.

The full oxygen and insulin profiles measured in a perifusion using the rapid oxygen switching system are shown in Figure 9. The periods covering the first phase, pO_2 drop, and pO_2 rise are shown with an expanded time scale in Figure 10. First phase secretion began within the first min following a step change in glucose concentration (t=0). Second phase secretion reached a steady rate after about 10 min. At t=15 min, the gas from the Queue controller which ultimately flowed into the inner incubator was changed to 15 mm Hg oxygen. This resulted in a drop in the perifusate pO_2 (which was equilibrated with 142 mmHg oxygen in the gas mixing flask and transported to the perfusate valve via stainless steel tubing) to 100 mm Hg at t=30 min as a result of limited gas exchange through the silicone tubing between the perfusate switch and the tissue chamber. No decrease was observed in second phase insulin secretion as a result of this drop in perfusate pO_2. At t=44 min, the perfusate pO_2 was rapidly dropped to 15 mmHg by switching to the perfusate that was equilibrated with the hypoxic gas inside the inner incubator. A decrease in insulin secretion rate was observed in the perfusate sample collected during the first min following the pO_2 drop. After a dip during the three min following the pO_2 change, secretion attained a steady rate that was lower than that observed under normoxic conditions. At t=86 min, the perfusate was switched back to the normoxic stream, resulting in a rapid rise in perfusate pO_2 ($t_{50} \approx 50$ sec). The islets released a burst of insulin which peaked in the first sample collected over the one-min period immediately following initiation of the pO_2 change. The secretion rate remained elevated until the glucose concentration was switched back to 100 mg/dl at 112 min, at which time the secretion rate began to decrease.

Figure 11 illustrates the effect of multiple sequential drops in pO_2 on the insulin secretion rate of rat islets cultured for 2 weeks after isolation. The pO_2 was progressively decreased from 142 to 45, 20, 10, and 2 mm Hg using the normal oxygen switching system. The second phase insulin secretion rate was unchanged at 45 mm Hg but progressively

decreased at 20, 10 and 2 mm Hg of oxygen partial pressure. Upon reoxygenation after exposure to 2 mm Hg, the islets released a burst of insulin similar to that seen in single-step hypoxic perifusions.

Rapid First Phase Secretion

The fastest response of the perifusion system was obtained by eliminating the oxygen switching and sensing capability of the system, thereby decreasing internal volume (Table 1), and by increasing the perfusate flowrate. Figure 12 illustrates the first phase insulin spike from perifused rat islets in response to a step change in glucose at a perfusate flowrate of 0.95 ml/min which provided t_{50} and t_{90} of 8 and 14 sec for glucose, respectively (Table 3). Islets used in the perifusion shown in the upper panel were hand-picked immediately following collagenase digestion, whereas those in the lower panel were hand-picked after isolation on a ficoll gradient. Sample fractions were collected over 18 sec intervals. Following the change at t = 0, the glucose concentration at the sample outlet rose rapidly, reaching over 90% of its steady value in the first 18 sec sample collected. In the middle panel, first phase insulin from handpicked islets was observed in the first sample collected following the glucose switch. The first phase release peaked in the 3rd to 5th fractions (36-90 sec). Secretion rate slowly dropped back to its basal level over the next three min, followed by initiation of second phase secretion. In the lower panel, first phase secretion from islets purified on ficoll gradients represented a much larger burst of insulin that peaked within the first 18 sec following the glucose step change. Since the average residence time in the post-perfusate switch tubing was about nine sec at a perfusate flowrate of 0.95 ml/min, the maximal insulin secretion rate was attained in about 10 sec or less. The differences in magnitude and rapidity of first phase secretion between islets isolated by ficoll gradients or by hand-picking alone werae observed with four different isolation batches. It is not known whether these differences were caused by hypersensitivity of islets exposed to ficoll or to enzymatic damage to hand-picked islets during their relatively longer exposure to pancreatic acinar secretions.

DISCUSSION

In order to measure the intrinsic kinetics of insulin secretion in response to step changes in the glucose concentration and the oxygen partial pressure in the perfusate flowing around isolated islets of Langerhans, a micro-perifusion system was designed, built, and tested. The system was designed to both produce and monitor rapid changes in the pO_2 of the medium perfusing the tissue chamber. A small internal volume was required in order to minimize the time lag between a change in the composition of the perfusate and measurement of its effect on insulin secretion rate in samples collected at the perfusate outlet. Finally, the system had to function with small numbers of islets that could be individually sized.

Regulation of the tissue chamber pO_2 was achieved by pumping perfusate through gas permeable silicone rubber tubing where it equilibrated with the surrounding gas pO_2. The most rapid changes in the tissue chamber pO_2 were achieved by separately equilibrating two perfusate lines with gas at different pO_2 (but the same glucose concentration) so that the pO_2 in the tissue chamber could be changed by simply switching from one perfusate to the other. Great care was taken to remove potential oxygen sources or sinks with which the perfusate was in contact and which could otherwise delay or blunt the dynamic response to pO_2 changes. Perfusate pO_2 was monitored using a prototype oxygen-quenched fluorescence probe which directly measured the pO_2 of the perfusate as it flowed out of the tissue chamber. Perfusate pO_2 could be set and monitored at any level from 2 to 142 ± 1 mm Hg.

Minimal time lag between a change in perfusate composition and outlet sampling was achieved by minimizing the internal volume from the perfusate switch to the sampling port. In the non-oxygen regulating system, this volume was 0.14 ml, whereas in the oxygen regulating system it was 0.20 ml. A perfusate flowrate of 0.5 ml/min was chosen in oxygen regulated perifusions as a tradeoff between the conflicting demands for low and high perfusate flowrates. A low perfusate flowrate facilitates complete gas equilibration of the perfusate and decreases the number of islets required to provide a sufficiently high insulin concentration to be measured by RIA. A high perfusate flowrate facilitates rapid switching, good islet perifusion, and provides sufficient perfusate volume to sample over short collection

periods which allows for the measurement of more rapid dynamic responses. For flowrates of 0.5 and 1.0 ml/min, the close fit of glucose and insulin residence time distributions (Figure 5) to that predicted for parabolic laminar flow without dispersion indicates that the system does not contain significant regions of flow stagnation or back-mixing. The time required for 90% approach to steady state in perfusate pO_2 with the rapid oxygen switching system is larger than that associated with glucose and insulin step changes (Table 3) because of the additional time lag of the pO_2 probe (approximately 30 sec to reach steady state) and because of the buffer created by oxygen dissolved in the silicon rubber tubing of the tissue chamber and other post-perfusate switch tubing. The upward step of oxygen is further slowed by gas exchange in the short section of tubing from the perfusate switch to the pO_2 probe which arises from the pO_2 difference between the normoxic perfusate and hypoxic gas initially present in the inner incubator. For experiments in which only the steady-state insulin secretion rate is of interest, the slower normal oxygen switching system is adequate.

The third design objective was the capability to perifuse small numbers of islets that could be easily isolated and counted and sized on an individual basis. This objective required a handling system wherein individual islets could be accurately loaded into the islet chamber, a low perifusion flowrate, and a sensitive insulin RIA. Islets were individually hand-picked with a 20 μl micropipette, placed in groups of 10 - 15 islets for each perifusion, and photographed under a microscope for later sizing using a calibrated reticule to measure the external dimensions of each islet. Using the loading method described in Materials and Methods, each islet was visually verified to be transferred to the tissue chamber, thus preventing against the inadvertent loss of islet mass. Ten to fifteen 200-μm diameter rat islets (0.042 - 0.063 mm^3 tissue) normally secreted from 2 - 10 μU/ml insulin under basal conditions and 20 -150 μU/ml insulin with 300 mg/dl glucose stimulation, which was within the range of the insulin RIA.

Using the micro-perifusion system, we investigated the effect of varying degrees of hypoxia on insulin secretion by isolated rat islets. In these experiments, glucose concentration was increased from 100 to 300 mg/dl at t=0. After second phase insulin secretion was

established, perfusate pO_2 was reduced from its normoxic state (142 mm Hg) to a lower value. Moderate levels of hypoxia (Figures 7-11) caused a reduction in insulin secretion rate which, after an initial dip, attained a steady but lower magnitude than before the pO_2 change. In one experiment with multiple sequential pO_2 drops over the range of 45 to 2 mm Hg (Figure 11), corresponding decreases in insulin secretion rate were observed. In all cases, increase of perfusate pO_2 back to its original level resulted in a burst of insulin secretion, followed by a return to a rate comparable to its original normoxic level.

Secretion rate quickly responded to a change in pO_2. With the rapid oxygen switching system, a reduction of secretion rate was observed within the first minute following a reduction of pO_2 to 15 mm Hg (Figure 10). The burst of insulin secretion following return to normoxia was similarly rapid.

These results demonstrate a substantial effect of hypoxia in modulating insulin secretion rate of isolated rat islets in response to elevated glucose concentration. Further work is required to quantitatively characterize this phenomenon, to analyze the results in terms of physical processes which include the boundary layer and intra-islet pO_2 gradients, and to elucidate the mechanism responsible for this effect, including the remarkably rapid response to pO_2 changes.

The micro-perifusion system in its most rapidly responding configuration was also used to study the dynamics of the initial response to a step change in glucose concentration under normoxic conditions. First phase secretion was virtually instantaneous with ficoll-purified islets (Figure 12). Insulin secretion rate peaked in the first sample collected 18 sec following a change in perfusate glucose concentration from 100 to 300 mg/dl. This first phase spike subsequently decayed over a period of about two min. The duration of this spike may result, at least in part, from the time required for secreted insulin to diffuse out of the islet core into the perfusate.

Our initial studies show that the micro-perifusion system described in this paper can be used to study the effect of perfusate composition and environmental variables on secretion rate. We have employed the system with isolated rat islets of Langerhans to study the effects

of varying glucose concentration and pO_2 on the dynamics and steady state levels of insulin secretion. This system can also be applied to study other variables, such as pH, temperature, and the concentration of different substrates and drugs on the release of insulin or other hormones from a variety of secretory cells and tissues.

ACKNOWLEDGEMENTS

This work was supported in part by fellowships to Keith E. Dionne by the National Science Foundation and the John and Fannie Hertz Corporation and by grants from the Juvenile Diabetes Foundation and from Baxter Healthcare Corporation. Martin L. Yarmush is a Markey Scholar.

REFERENCES

Andersson, A., Korsgren, O., and Jansson, L. (1989). Intraportally Transplanted Pancreatic Islets Revascularized from Hepatic Arterial System. Diabetes 38(Suppl. 1):192-195.

Bonner-Weir, S., and Orci, S. (1982). New Perspectives on the Microvascular of the Islets of Langerhans in the Rat. Diabetes 31:883-889.

Burr, I.M., Stauffacher, W., Balant, L., Renold, A.E., and Grodsky, G. (1969). Dynamic Aspect of Proinsulin Release from a Perifused Rat Pancreas. The Lancet, October 25; p. 882-883.

Cecil, R., and Robertson, G.B. (1975). The Specific Binding of Insulin to Polythene and Other Materials. Biochim Biophys Acta 404:164-168.

Colton, C.K., and Drake, R.F. (1971). Effect of Boundary Conditions on Oxygen Transport to Blood Flowing in a Tube. Chem Engr Symp Ser 67:88-95.

Colton, C.K., and Weinless, N.L. (1987). A Theoretical Model for Insulin Secretion Rate in a Hybrid Artificial Pancreas. From Andrade et al. (eds), Artificial Organs, Proceedings of the International Symposium on Artificial Organs, Biomedical Engineering, and Transplantation, Salt Lake City, Utah, January 20-23, 1986, VCH Publishers, New York.

Coore, H.G, and Randle, P.J. (1964). Regulation of Insulin Secretion Studied with Pieces of Rabbit Pancreas Incubated *in vitro*. Biochem J 93:66-77.

Coore, H.G, Hellman, B., Idahl, L-A, and Taljedal, I-B. (1967). Diabetes Research at the Histological Department in Umea. Opuscula Medica 12:285-295.

Gingerich, R.L., Aronoff, S.L., Kipnis, D.M., and Lacy, P.E. (1979). Insulin and Glucagon Secretion from Rat Islets Maintained in a Tissue Culture-Perifusion System. Diabetes 28:276-281.

Grodsky, G.M., Curry, D., Idahl, H., and Bennett, L. (1969). Further Studies on the Dynamic Aspects of Insulin Release In Vitro with Evidence for a Two-Compartmental Storage System. Acta Diabet. Lat 6(Suppl. 1):554-79.

Hoshi, M., and Shreeve, W.W. (1973). Release and Production of Insulin by Isolated, Perifused Rat Pancreatic Islets: Control by Glucose. Diabetes 22:16-24.

Kautsky, H. (1939). Quenching of Luminescence by Oxygen. Trans Faraday Soc 35:216-219.

Kim, J.-I., and Stroeve, P. (1988). Mass Transfer in Separation Devices with Reactive Hollow Fibers. Chem Eng Sci 43:247-257.

Lacy, P.E., and Kostianovsky, M. (1967). Method for the Isolation of Intact Islets of Langerhans from the Rat Pancreas. Diabetes 16:35-39.

Lacy, P.E., Walker, M.W., and Fink, C.J. (1972). Perifusion of Isolated Rat Islets in Vitro: Participation of the MIcrotubular System in the Biphasic Release of Insulin. Diabetes 21:987-998.

Lacy, P.E., Finke, E.H., Conant, S., and Naber, S. (1976). Long-term Perifusion of Isolated Rat Islets *in vitro*. Diabetes 25:484-493.

Milner, R.D.G., and Hales, C.N. (1969). The Interaction of Various Inhibitors and Stimuli of Insulin Release Studied with Rabbit Pancreas *in vitro*. Biochem J 113:473-479.

Peterson, J.I., Fitzgerald, R.V., and Buckhold, D.K. (1984). Fiber-Optic Probe for *in vivo* Measurement of Oxygen Partial Pressure. Anal Chem 56:62-67.

Scharp, D.W., Downing, R., Merrel, R.C., and Greider, M. (1980). Isolating the Elusive Islet. Diabetes 29(Suppl.1):19-30.

Scharp, D.W. (1984). Isolation and Transplantation of Islet Tissue. World J Surg 8:143-151.

Scharp, D.W., Mason, N.S., and Sparks, R.E. (1984) Islet Immuno-isolation: The use of Hybrid Artificial Organs to Prevent Islet Tissue Rejection. World J Surg 8:221-229.

Smith, J.M. (1970). Chemical Engineering Kinetics. McGraw Hill, NY, p 254.

Soeldner, J.S., and Slone, D. (1965). Critical Variables in the Radioimmunoassay of Serum Insulin Using the Double Antibody Technique. Diabetes 14:771.

Southerland, D.E.R., Mondry, K.C., and Fry, D.S. (1989). Results of Pancreas-Transplant Registry. Diabetes 38(Suppl. 1):46-54.

Weast, R.C. (ed) (1980). *CRC Handbook of Chemistry and Physics*, CRC Press, Boca Raton, Florida: pp. D-196.

Weaver, D.C., McDaniel, M.L., Naber, S.P., Barry, C.D., and Lacy, P.E. (1978). Alloxan Stimulation and Inhibition of Insulin Release from Isolated Rat Islets of Langerhans. Diabetes 27:1205-14.

Table 1. Tubing Volume (V) and Average Perfusate Residence Time ($\bar{t}$)*

	With Oxygen Sensor**		Without Oxygen Sensor***	
	V (ml)	$\bar{t}$ (sec)	V (ml)	$\bar{t}$ (sec)
Gas exchange tubing	1.76	210	1.76	210
Post-Perfusate Switch				
Switch and pre-tissue chamber tubing	0.04	4.8	0.03	3.6
Tissue chamber	0.04	4.8	0.04	4.8
pO_2 probe	0.03	3.6	---	---
Post-tissue chamber and exit tubing	0.09	10.8	0.07	8.4
Total Post-Perfusate Switch Tubing	0.20	24	0.14	17

* Average residence time calculated from $\bar{t} = V/Q$, where V is the internal perfusate volume, and Q is the perfusate flowrate. Tabulated values of $\bar{t}$ correspond to Q = 0.5 ml/min.

** Perifusion system with pO_2 switching capability; includes pinch clamp perfusate switch and pO_2 probe.

*** Perifusion system without pO_2 switching capability; includes Hamilton valve and no pO_2 probe.

Table 2. Perifusion System Operating Parameters

Operating Parameter	Normal Value	Range
Temperature	37 ± 0.2°C	24 - 40 °C
Perfusate flowrate	0.50 ± .02 ml/min	0.40 - 3.0 ml/min
Perfusate velocity in tissue chamber	0.50 ± .02 cm /sec	0.40 - 3.0 cm/sec
Gas flowrate	0.60 ± .02 l/min	0.2 - 2.4 l/min
pO_2	142 ± 1 mmHg	2.0 - 675 mmHg
pH	7.45 ± .10	
Glucose	100 ± 3 mg/dl 300 ± 5 mg/dl	
No. of islets (200 μm ave. diam.)	12 islets	
Total islet volume	0.06 mm^3	
Perfusate insulin concentration:		
basal	2 - 10 μU/ml	
stimulated	20 - 150 μU/ml	

TABLE 3. Response Time of Perifusion System

	Response Time (sec) Without Oxygen Switching Capability (Vol = 0.14 ml)	Response Time (sec) With Oxygen Switching Capability (Vol = 0.20 ml)
Glucose		
Q = 1.0 ml/min		
t_{50}	8	--
t_{90}	14	--
Q = 0.5 ml/min		
t_{50}	15	22
t_{90}	27	37
Insulin		
Q = 0.5 ml/min		
t_{50}	--	22
t_{90}	--	39

	Normal Oxygen Switching (V = 0.20 ml)	Rapid Oxygen Switching (V = 0.20 ml)
Oxygen		
Q = 0.5 ml/min		
t_{50} down	130	9
up	220	51
t_{90} down	245	71
up	420	90

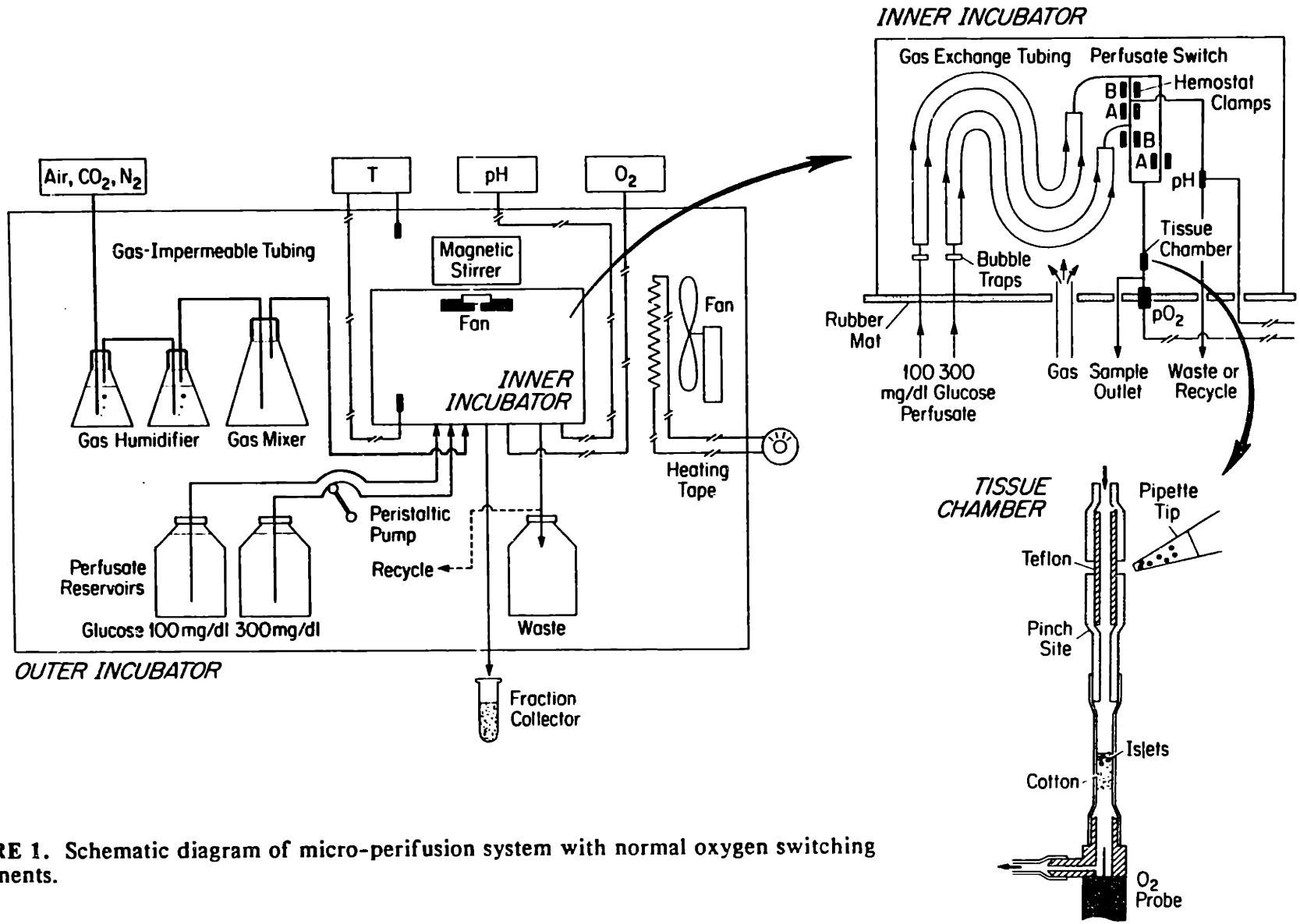

FIGURE 1. Schematic diagram of micro-perifusion system with normal oxygen switching components.

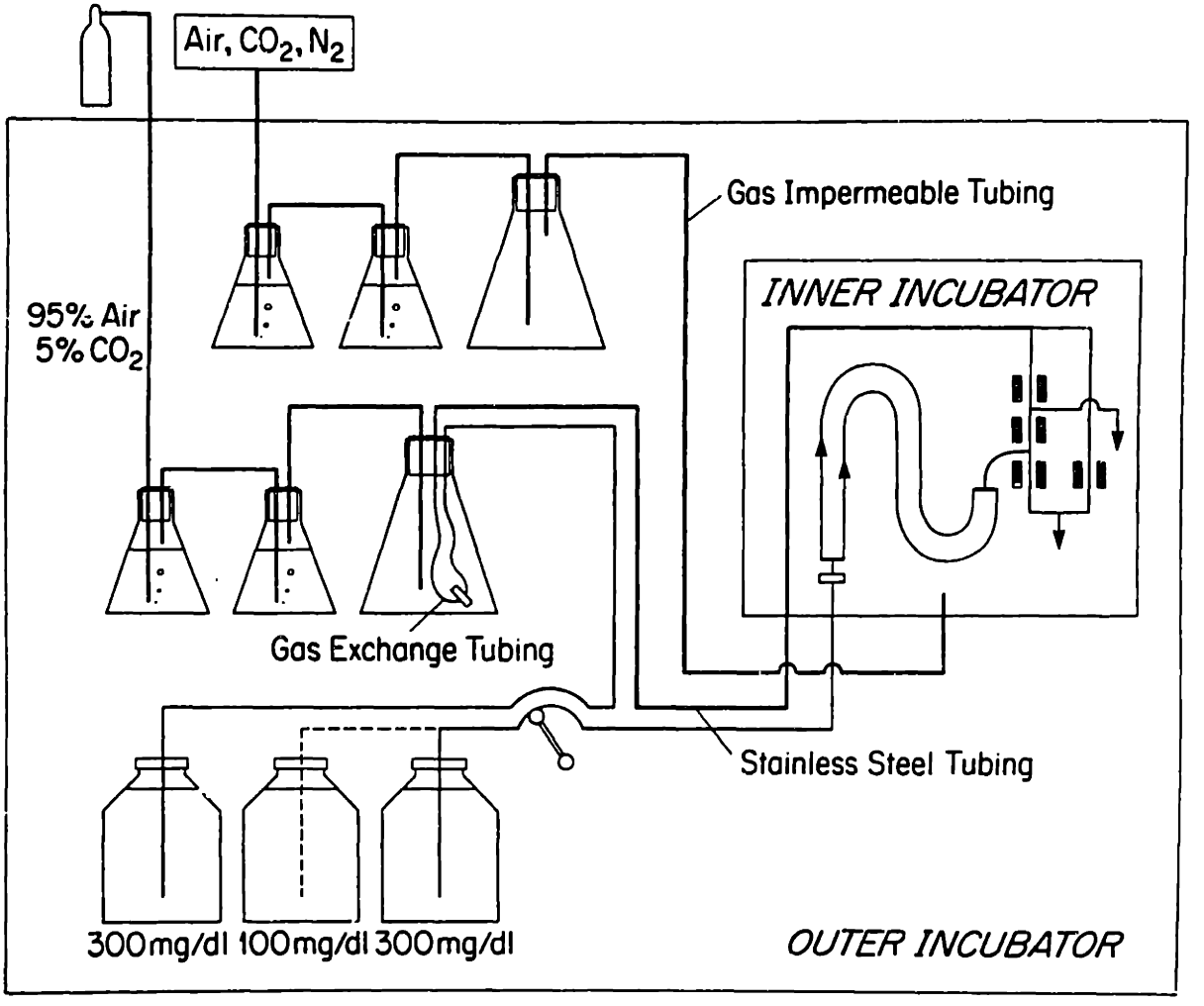

FIGURE 2. Schematic of diagram micro-perifusion system showing alterations made for rapid oxygen switching system. Components not shown are the same as in Figure 1.

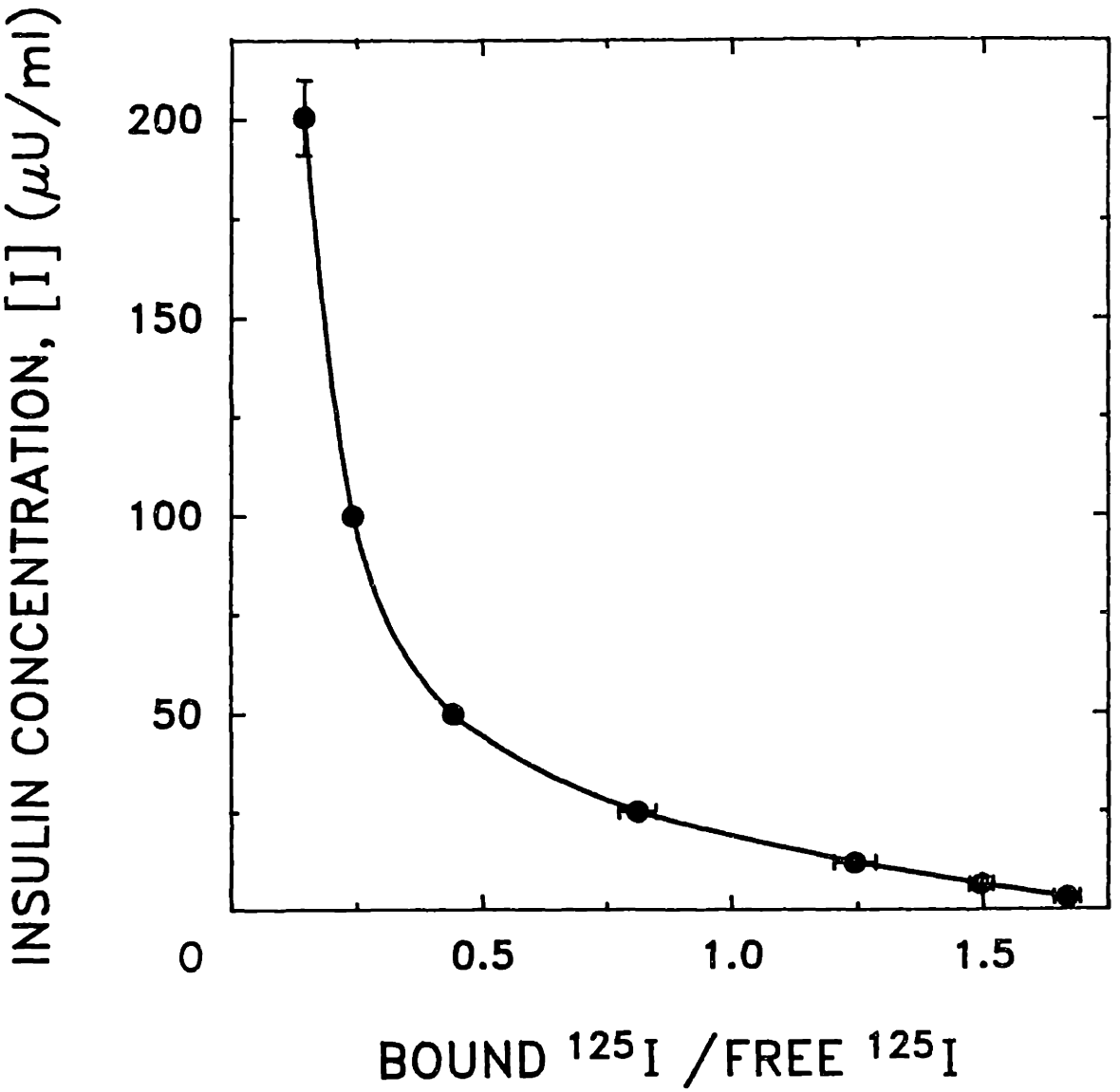

FIGURE 3. Calibration curve for insulin radioimmunoassay. The B/F ratio of standards of known insulin concentration [I] were measured in quadruplicate. Error bars represent standard deviations; where not shown, they are contained within the plotted symbols. The data were fitted to a polynomial curve (see text) from which [I] in unknown samples was calculated using measured B/F ratios.

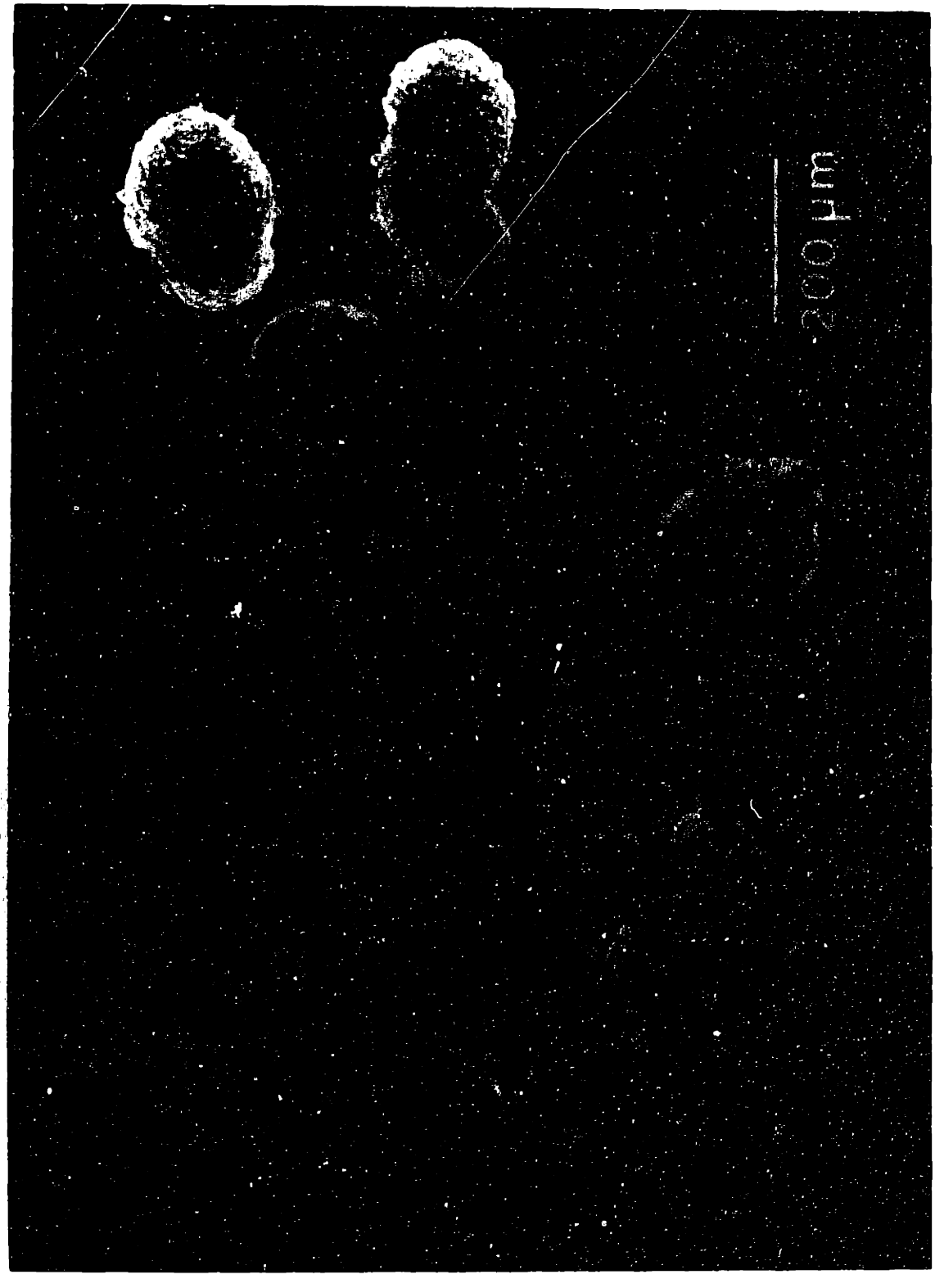
200 µm

FIGURE 4. Photomicrograph taken through a dissecting microscope of twelve rat islets of Langerhans selected for perifusion. Spheroidal islets were handpicked for uniform shape and size. The number average equivalent spherical diameter of these islets was 210 ± 15 μm. The total islet volume of the perifusion batch was 0.058 mm^3.

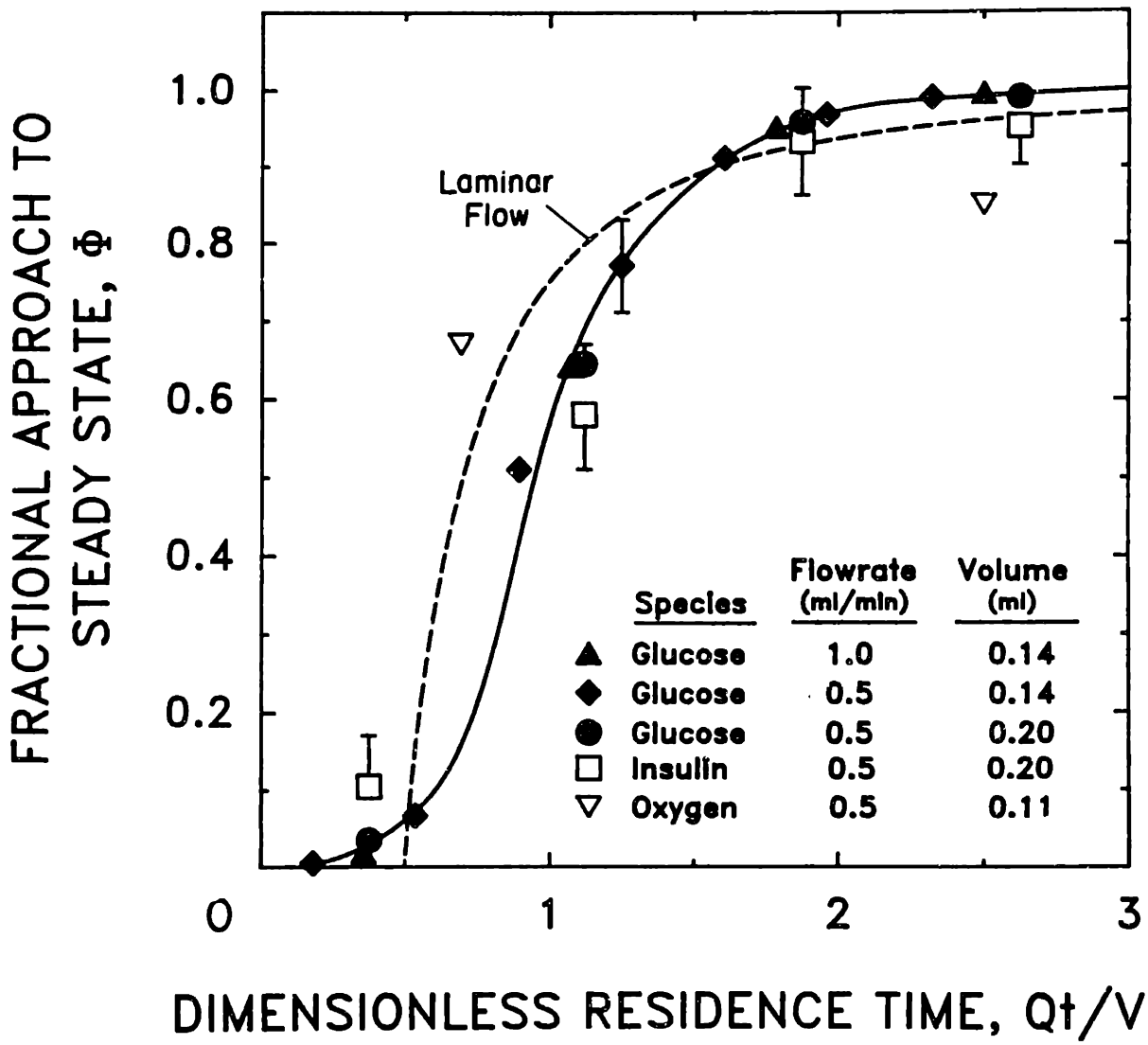

FIGURE 5. Residence time distribution of the exit concentration following a step change in perfusate composition. The fractional approach to steady state of the exit concentration, ϕ, is plotted versus the dimensionless residence time for perfusate flowrates, Q, of 0.5 and 1.0 ml/min. Internal volume, V, from the perfusate switch to the sampling port was 0.14 or 0.20 ml, depending on the absence or presence of oxygen switching capability (Table 1). For oxygen, V is the internal volume up to the pO_2 probe where oxygen was sensed. The time, t, of glucose and insulin data was taken as the midpoint of the time interval (6 and 18 sec, respectively) during which each sample was collected. For oxygen (step down), t was taken at the time of measurement. The dotted line is the theoretical residence time distribution for parabolic laminar flow. Glucose and insulin data include step changes up and down.

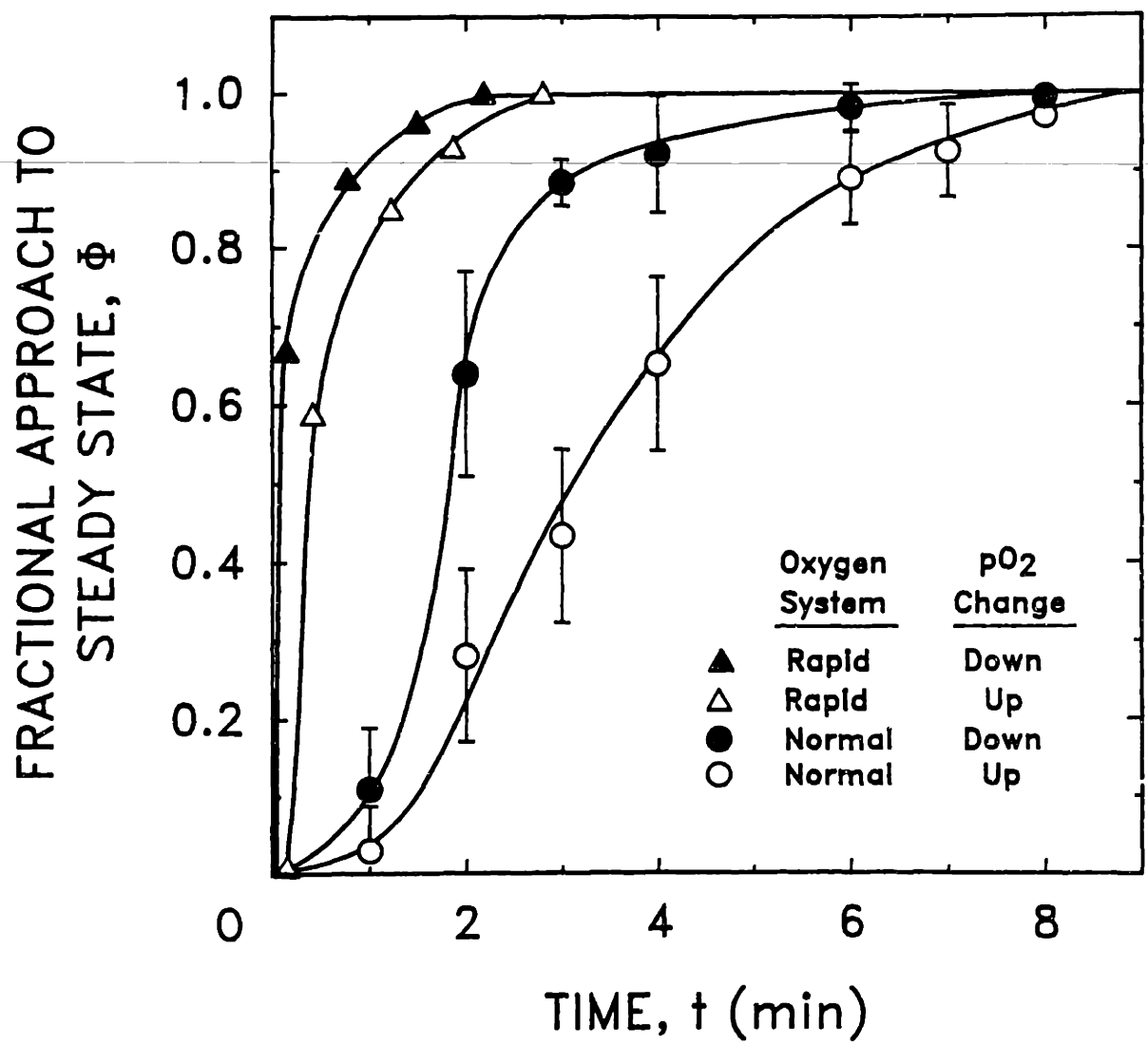

FIGURE 6. The fractional approach to steady state of perfusate pO_2 sensed by the oxygen probe following step changes up or down in perfusate pO_2 using the normal or rapid oxygen switching system is plotted versus the time at which the reading was taken. See text for explanation of the hysteresis between steps down and up. The response times for each step are listed in Table 3.

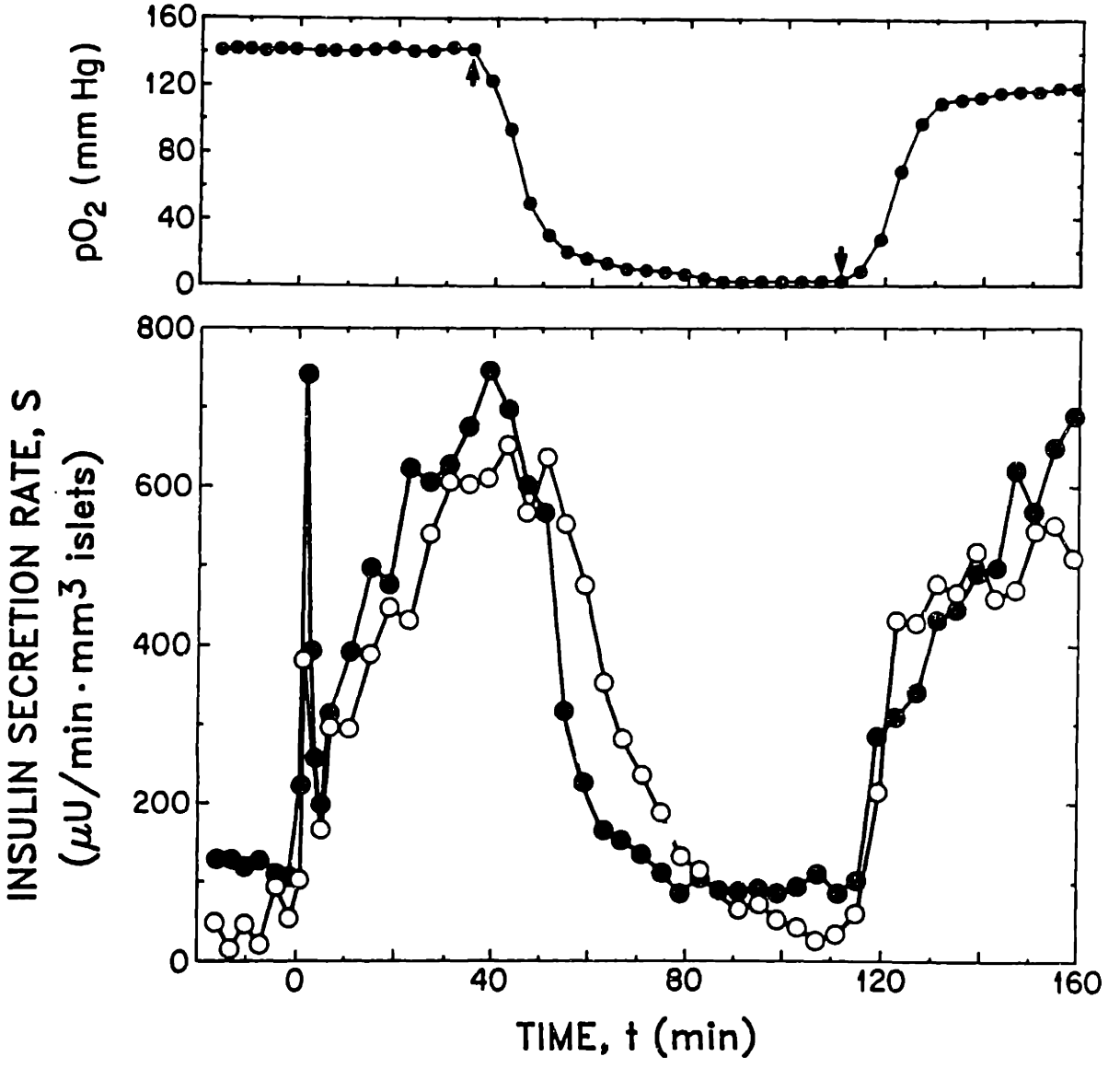

FIGURE 7. The effect of hypoxic pO_2 on second phase, glucose-stimulated insulin secretion rate of isolated rat islets of Langerhans. Measurements were made with a preliminary version of the perifusion system (see text). Perfusate flowrate was 0.7 ml/min. At t=0, glucose concentration was raised from 100 to 300 mg/dl. Perfusate samples were collected over one min intervals from 0 to 5 min and over four min intervals thereafter. Insulin secretion rate is plotted at the midpoint of the time interval over which it was collected. Arrows in the upper panel indicate the time at which step changes in the pO_2 of the gas flowing into the system were initiated. The approach to steady state pO_2 is delayed because of leaching of dissolved oxygen from plastic components in contact with the perfusate.

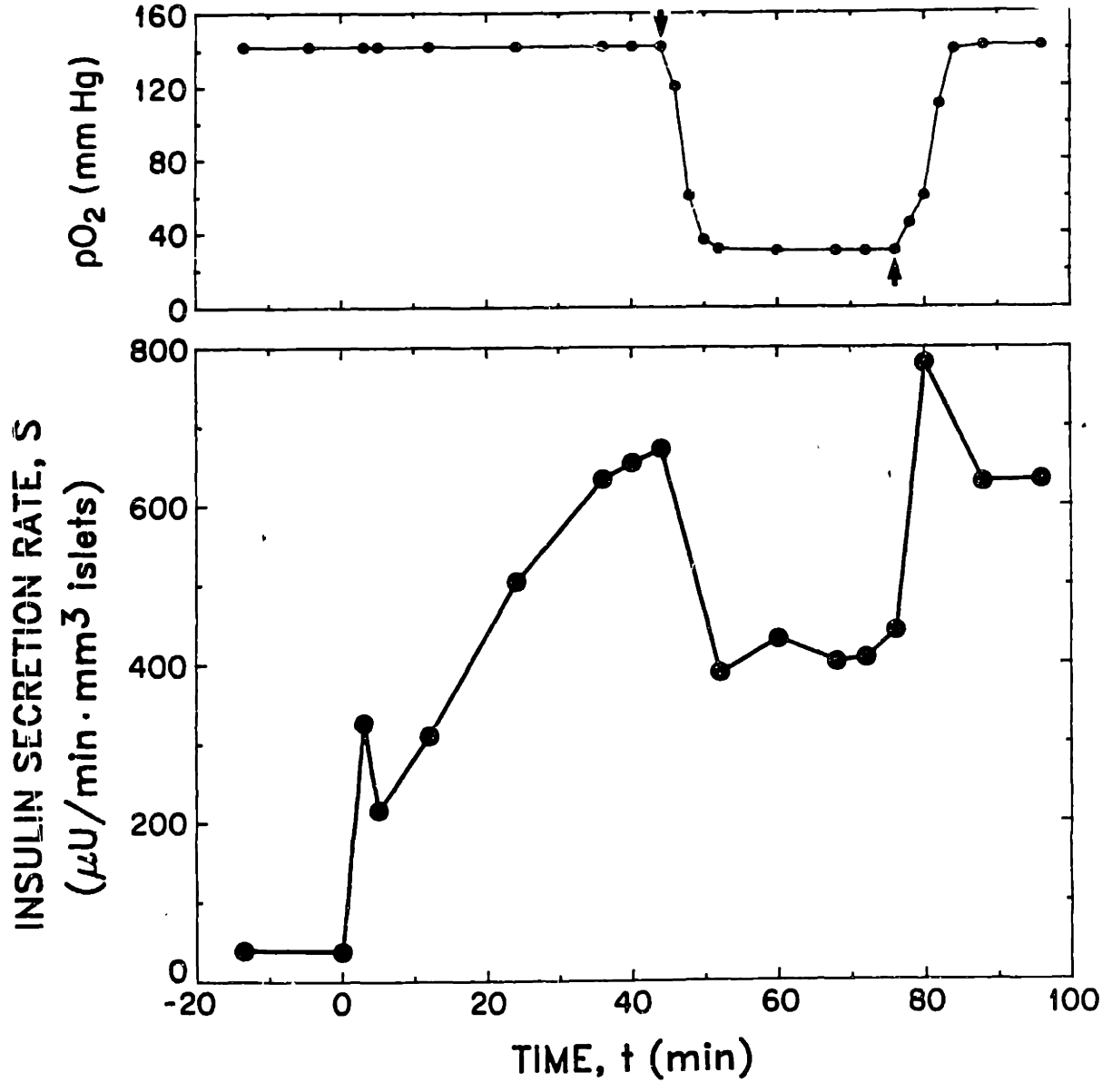

FIGURE 8. The effect of hypoxia (pO_2 = 30 mm Hg) on second phase insulin secretion rate following step changes in perfusate pO_2 using the normal oxygen switching system. Islets used in this perifusion are shown in Figure 4. Perfusate flowrate was 0.5 ml/min. Glucose concentration was increased from 100 to 300 mg/dl at t=0. Perfusate samples were collected over two min intervals from 0 to 6 min and over four min intervals thereafter. Not all samples collected were assayed for insulin. Arrows indicate the time at which pO_2 steps were initiated.

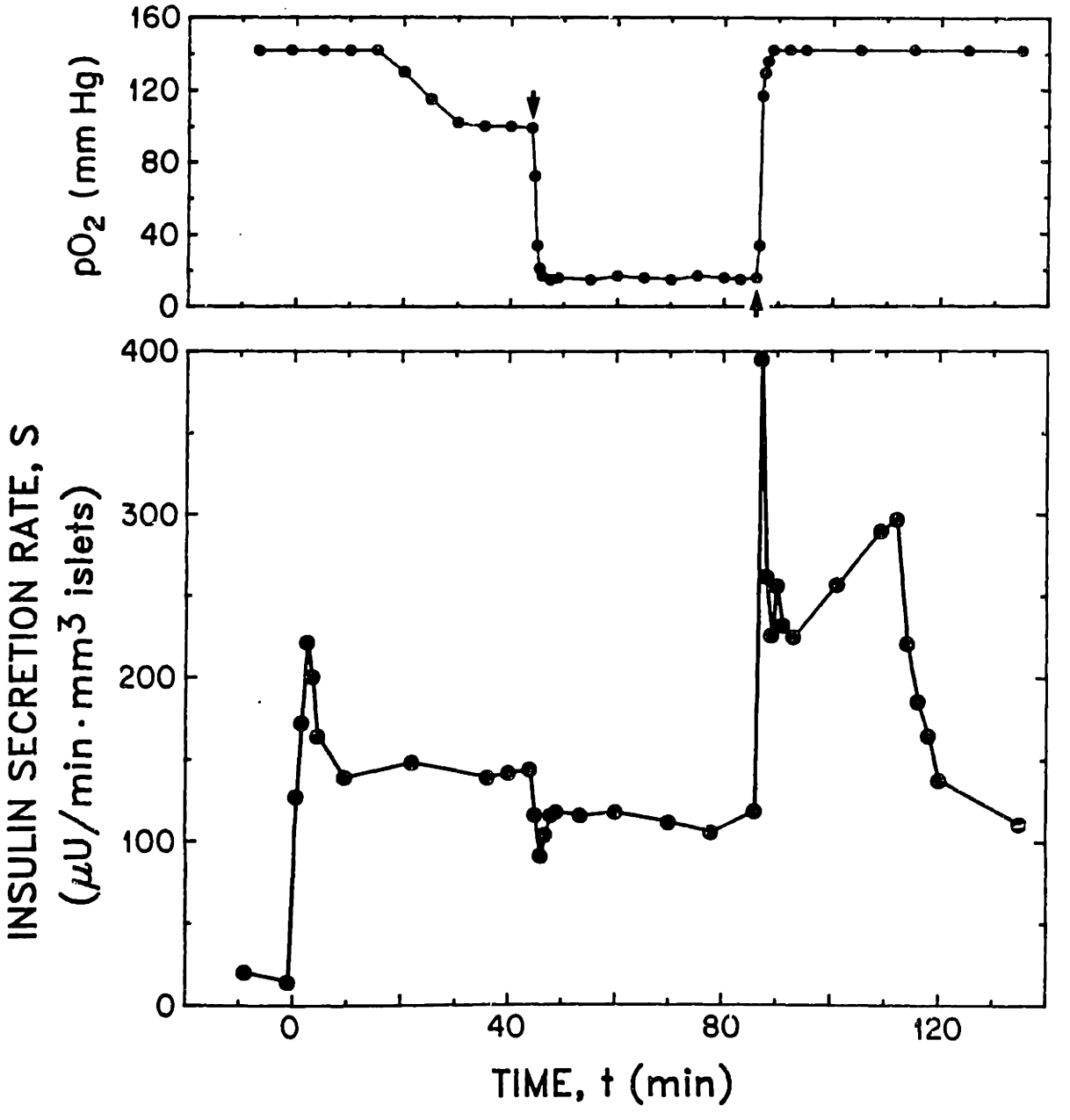

FIGURE 9. The effect of rapid changes in perfusate pO_2 on second phase insulin secretion rate of isolated rat islets. Changes in the perfusate pO_2 were made using the rapid oxygen switching system. Perfusate was collected over one min time intervals for 10 min following the step change in glucose from 100 to 300 mg/dl at t=0, the downward pO_2 step from 142 to 15 mm Hg at t=44 min, and the upward pO_2 step at t=86 min. At all other times, samples were collected over four min intervals. At t=112 min, the glucose concentration was switched back to 100 mg/dl.

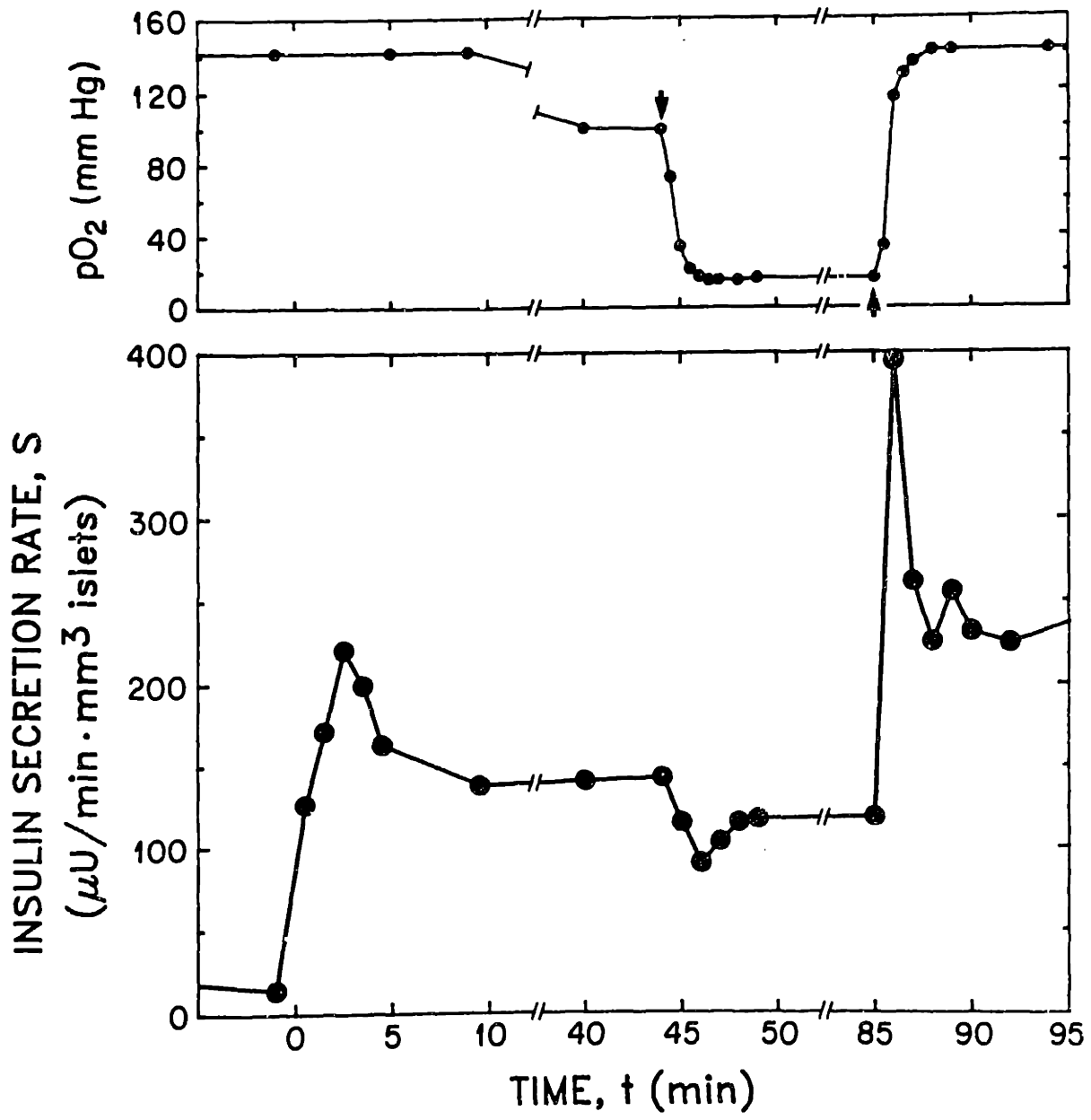

FIGURE 10. The data in Figure 9 is plotted with an expanded time scale for the periods following the glucose step up and the pO_2 steps down and up. Insulin secretion rate responds to changes in glucose and perfusate pO_2 within the first min following initiation of a change.

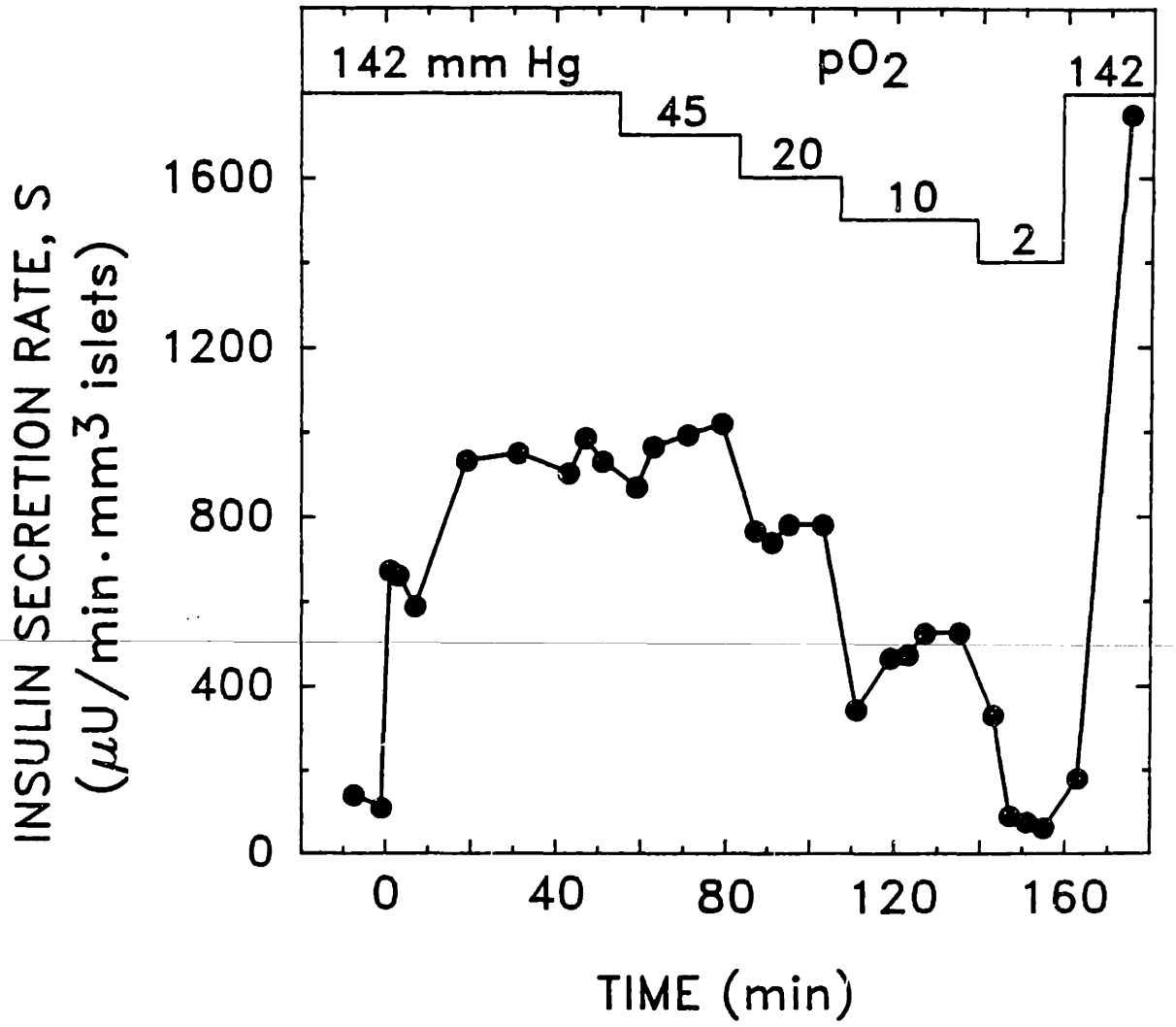

FIGURE 11. The effect of multiple hypoxic steps on insulin secretion from isolated rat islets of Langerhans. Islets were cultured for two weeks under normoxic static culture after isolation before being tested. Perfusate flowrate and time intervals for perfusate collection are the same as described in Figure 8.

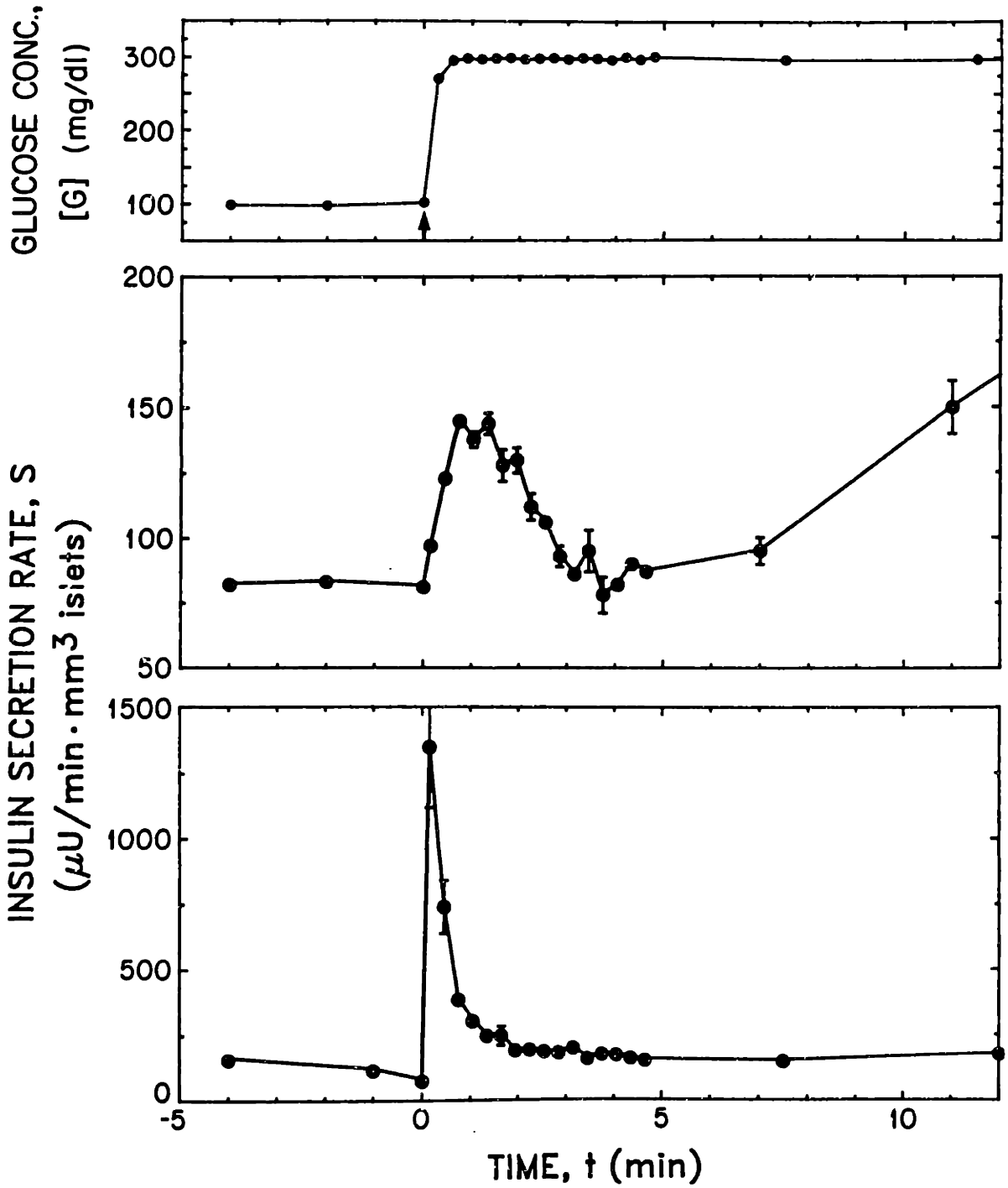

FIGURE 12. First phase insulin secretion rate from perifused islets in response to rapid step change in perfusate glucose from 100 to 300 mg/dl at t=0 min. Samples were collected over 18 sec time intervals from t=0 to 5 min. Secretion rate is plotted at the midpoint of the time interval for each sample. Results are shown for islets selected from the same isolation batch. Those corresponding to the upper panel were purified by hand-picking without ficoll purification whereas those in the bottom panel were first purified on a ficoll gradient and then handpicked for perifusion.

CHAPTER 3:

EFFECT OF HYPOXIA ON INSULIN SECRETION BY ISOLATED RAT AND CANINE ISLETS OF LANGERHANS

SUMMARY

The effect of oxygen partial pressures reduced below physiological levels on glucose-stimulated insulin secretion by isolated islets of Langerhans was investigated with a microperifusion apparatus which provided control of pO_2 and rapid dynamic response. Hypoxic levels of perfusate pO_2 between 5 and 60 mmHg had only modest effect on basal and first phase insulin secretion. Second phase insulin secretion was substantially reduced by hypoxia. The response to lowered pO_2 was rapid and reversible. Although the secretion rate under hypoxic conditions and the steady normoxic (pO_2 = 142 mmHg) second phase secretion rate varied widely from one islet preparation to another, the ratio between the two collapsed onto a single curve for all data and demonstrated a continuous reduction with decreasing pO_2. For rat islets perifused one day after isolation, the secretion rate was nearly 100% of the normoxic value at a pO_2 of 60 mmHg, 50% of 27 mmHg (P_{50}), and about 2% at two mmHg. Oxygen sensitivity of second phase secretion rate declined with increasing duration of <u>in vitro</u> culture: P_{50} was 13 mmHg after two to five weeks. Canine islets exhibited a P_{50} of 16 mm Hg after one week of culture. The reduction in insulin secretion is thought to be associated with the existence of pO_2 gradients outside and inside of isolated islets, resulting in exposure of islet cells to low pO_2 levels which decrease radially from the periphery to the core. We hypothesize the effect of low pO_2 on insulin secretion rate is manifested through depletion of the energy stores of the β-cells. The effect of hypoxia on insulin secretion rate may play a role in the effectiveness of transplanted islets prior to revascularization and of immuno-isolated islet implantation devices.

INTRODUCTION

Islets of Langerhans in vivo are highly vascularized by a glomerular-like network of capillaries that delivers arterial blood throughout the islet (Bonner-Weir and Orci, 1982; Bonner-Weir, 1984). This capillary network, combined with a very high islet blood flowrate (Lifson et al., 1980), ensures that β-cells throughout the islet receive oxygen and other nutrients at or near their arterial levels. However, when islets are isolated from the pancreas for in vitro studies or for use in transplantation (Scharp, 1984; Southerland et al., 1989; Andersson, Korsgren, and Jansson, 1989) or immunoisolated implantation devices (Scharp, Mason, and Sparks, 1984), their vascular access is destroyed, and the entire islet must be supplied with oxygen and other metabolic nutrients by diffusion through the islet periphery from the surrounding tissue or media. In the non-vascularized state, the consumption of oxygen by the cells leads to the establishment of oxygen concentration gradients both inside and outside of the islets. Consequently, the oxygen partial pressure (pO_2) in the β-cell rich islet core will be lower than that at the islet surface which, in turn, will be lower than the pO_2 in the surrounding medium or tissue.

It has been reported that short-term incubation of pieces of rabbit pancreas in static culture under an oxygen-free, 5% CO_2, 95% N_2 environment abolished their insulin secretion in response to glucose, leucine, and tolbutamide stimulation (Coore and Randle, 1964; Coore et al., 1967; Milner and Hales, 1969). Normal secretory responses were restored following 30 min of non-stimulated, normoxic culture. These results led us to hypothesize that exposure of islets to hypoxic pO_2 conditions above complete anoxia but below normal in vivo physiological levels might also affect insulin secretory response. The objective of our study is to investigate this phenomenon at intermediate pO_2 levels.

In an earlier paper, we described a micro-perifusion system with rapid dynamic response which could be used to regulate the pO_2 environment of perifused islets over a wide range (Dionne, Colton, and Yarmush, 1989-2). Preliminary experiments with this system showed that hypoxic perfusate pO_2 levels as high as 30 mmHg can cause reduction in the release of glucose-stimulated insulin secretion from intact isolated rat islets of Langerhans

(Dionne, Colton, and Yarmush, 1989A and 1989-2). In this paper, we report studies showing that intermediate levels of pO_2 (2 to 60 mmHg) reduce the insulin secretion of isolated, perifused islets of Langerhans in a graded fashion. In addition to quantifying the degree of reduction in secretory response and its dependence on perifusate pO_2, we also (1) compare the oxygen sensitivity of first and second phase insulin secretion, (2) investigate the dynamic response of islets to pO_2 changes, (3) examine the effect of in vitro culture time on the oxygen sensitivity of secretion, and (4) compare the oxygen sensitivity of canine and rat islets of Langerhans.

MATERIALS AND METHODS

Islet Isolation and Culture. Rat islets of Langerhans were isolated from male Sprague Dawley rats (200-350 g, Charles River Laboratories, Kingston NY) using a collagenase digestion / ficoll purification technique (Lacy and Kostianovsky, 1967; Dionne, Colton, and Yarmush 1989-2). Each isolation batch consisted of pancreata from two or three rats whose islets were mixed together in the isolation process. Briefly, rats were anaesthetized with sodium pentobarbital (0.1 ml/100 g body weight, 65 mg/ml, J.A. Webster, N. Billerica MA) injected in the peritoneal cavity. The pancreas was distended in situ by injecting 10-15 ml of ice cold Hanks solution without Ca^{++} and Mg^{++} (H2387 Sigma Chemical Co., St. Louis, MO) containing 1.7 mg/ml collagenase (108 8882 Boehringer Mannheim, Indianapolis, IN). The distended pancreas was dissected free and digested under mild agitation in a 37°C water bath for 15-18 min until islets were freed from acinar tissue as ascertained by microscopic examination. The slurry was then rinsed and purified on a discontinuous ficoll gradient (25%, 22%, 17.5%, 11% (w/w); F9378, Sigma Chemical Co) centrifuged at 1000 x g. The purified islet fraction was rinsed in Dulbecco's modified Eagles medium (DMEM, D5523, Sigma Chemical Co.) with 10% (v/v) newborn calf serum (NBCS, 200-6010AJ, GIBCO, Grand Island, NY), pelleted by centrifugation, hand-picked under a microscope through a series of four additional rinses with DMEM and 10% NBCS in order to thoroughly remove ficoll residues and ensure islet purity.

Purified rat islets to be perifused within 16-32 hr after isolation (referred to as one day of culture) were cultured in 50-mm diameter polystyrene bacteriological Petri dishes (Falcon 1007, Becton Dickinson Inc, Lincoln Park NJ) containing seven ml of DMEM with 5.6 mM (100 mg/dl) glucose, 50 U/ml penicillin, 50 μg/ml streptomycin (600-5140AG, GIBCO), and 10% NBCS. One hundred to two hundred islets were dispersed throughout each dish. Dishes were placed in a 37°C incubator with a gas environment of 95% air and 5% CO_2. Islets cultured for one day remained freely floating and did not attach. Islets cultured for longer than one day were placed in 50-mm diameter dishes pre-coated with a 0.5-mm thick layer of gelled rat tail collagen prepared by the method of Montesano et al. (1983). Each dish contained seven ml of DMEM prepared as described for short term culture except for the addition of 5% NBCS and 5% rat serum (200-6230AD, GIBCO). One to two hundred islets were placed in each dish. Cultured islets lightly attached to the collagen matrix which helped avoid islet aggregation and clumping. For long term cultures, medium was changed every other day.

Canine islets were isolated using a modification of standard collagenase digestion / ficoll purification techniques by Biohybrid Technologies, Shrewsbury MA, and generously donated by Dr. William Chick for these studies. Canine islets were received in and cultured in M-199 with Earle's salts (400-1100, GIBCO) containing 11.2 mM glucose and 10% (v/v) fetal bovine serum (GIBCO). Islets remained freely suspended under these conditions. Twelve hr before perifusion testing, canine islets were transferred to dishes containing DMEM with 5.6 mM glucose and 10% NBCS in order to equilibrate to the lower glucose concentration.

Perifusion System. The design, construction, and characterization of the oxygen regulating micro-perifusion system has been previously described (Dionne, Colton, and Yarmush, 1989-2). The system was capable of making rapid changes in perfusate glucose concentration and pO_2, had rapid dynamic response for measuring changes in insulin secretion rate as a result of these changes in perfusate composition, and was suitable for studying very small volumes of

tissue. In brief, the perifusion system consisted of two incubators, one nestled inside of the other. The outer incubator (continuous gas flow incubator, model 2210, Queue Systems Inc., Parkersburg WV) provided primary temperature control at about 37°C and isolated the system from the surrounding environment. The inner incubator, which contained the tissue perifusion chamber and gas exchange tubing, was formed by inverting a 600 ml pyrex bowl over a 0.5-cm thick neoprene rubber mat. The interface was sealed with silicon vacuum grease. All tubing and electrical or mechanical leads entered or exited the inner incubator through small holes cut in the rubber mat using a cork borer. The temperature in the inner incubator was continuously monitored and controlled at 37 ± 0.3 °C. The gas environment (pO_2, pCO_2) in the inner incubator was regulated by a steady flow (0.6 l/min) of humidified gas, the pO_2 and pCO_2 of which were set with the control system of the Queue incubator. Perfusion media pre-mixed with different concentrations of glucose were stored in separate reservoirs placed in the outer incubator. The perfusate was pumped through gas-permeable silicone rubber tubing coiled inside of the inner incubator where it equilibrated with the surrounding gas. The pO_2 and pH of the perfusate were monitored by in-line probes. After gas exchange, the perfusate entered a pinch clamp valve system which allowed switching between streams containing different concentrations of glucose. The selected medium flowed over the islets entrapped in a tissue chamber, which consisted of a cotton plug placed in the silicon rubber tubing, and then out of the inner and outer incubators directly into a fraction collector where it was collected for later analysis of glucose (Beckman Glucose Analyzer II, Beckman Instruments, Brea CA) and insulin by radioimmunoassay (Dionne, Colton, and Yarmush, 1989-2).

In a modification of the perifusion system used for more rapid pO_2 switching, a third perfusate line was equilibrated in a separate enclosed gas exchange flask. This line was directly connected to the perfusate switch via gas-impermeable stainless steel tubing. With this system in place, the perfusate pO_2 could be rapidly changed by switching between perfusates that had the same glucose concentration but were equilibrated at different pO_2 levels.

At a perfusate flowrate of 0.5 ml/min, a switch from a perfusate containing 100 mg/dl glucose to one containing 300 mg/dl resulted in a value equal to 50% of the approach to steady state at the outlet after 22 sec and 90% after 37 sec. In the normal oxygen switching system, a two-min burst of 5.3% CO_2 and 94.7% N_2 at 2.0 l/min was used to flush normoxic gas out of the humidification chambers, gas mixing flask, and inner incubator. After this flush, the gas pO_2 was set at the test level, and the flowrate was decreased back to 0.6 l/min. A switch in gas pO_2 settings from the normoxic (142 mmHg) to a hypoxic level required 2.2 min to reach 50% of the approach to steady state in the perfusate and 4.1 min to reach 90%. The rapid oxygen switching system achieved 50% of the approach to steady state in 9 sec and 90% in 71 sec (Dionne, Colton, and Yarmush, 1989-2). The normal oxygen switching system was used in all experiments unless indicated otherwise.

Islet Preparation and Perifusion Protocol. Two hr before a perifusion, a specified number of spheroidal islets (10-15 for rat, 35-40 for canine) of approximately uniform diameter (about 200 μm for rat islets, about 175 μm for canine islets) were hand-picked under a dissecting microscope by aspiration with a 20 μl micropipette (Pipetman, Rainin Instruments Inc.) and placed in a petri dish (Falcon 1007, Becton Dickinson) containing 10 ml of warmed (37°C) basal perfusion medium (DMEM with 10% NBCS, 50 μU/ml penicillin, 50 μg/ml streptomycin, and 5.6 mM glucose). The islet preparation was photographed under a microscope for later sizing using a calibrated reticule. The petri dish containing the islets was then placed in a 37°C incubator under a 5% CO_2, 95% air environment.

The micrograph of the islet sample was projected onto a screen, and the external dimensions of each islet were measured using the reticule grid. Slight deviations from a spherical shape were accounted for by measuring both the largest diameter and the diameter normal to it, assuming each islet could be represented by a prolate ellipsoid, and calculating its volume, v, from $v = \pi a^2 b/6$, where a and b are the smaller and larger axes, respectively. The equivalent spherical diameter, d, for each islet was calculated as that of a sphere of equal volume, $v = \pi d^3/6$; thus, $d = (a^2 b)^{1/3}$. For a typical perifusion preparation of twelve rat islets,

the number-average equivalent spherical diameter of the islets was 207 ± 17 μm, the ratio of a/b was 0.82 ± .09, and the total volume of perifused tissue was 0.060 mm^3.

Islets were transferred from the petri dish to the perifusion system in the tip of a 200 μl micropipette. The islets were loaded through a connection in the tubing located immediately upstream of the tissue chamber and were visually ascertained to be carried downstream by the perfusate until they became entrapped in the mesh of the cotton plug.

Once the inner incubator was resealed and the outer incubator closed, the temperature, pH, and pO_2 restabilized within about five min and the system was left for another 25 min to allow the islets to adjust to the basal perifusion conditions before collecting fractions for measurement of basal insulin secretion. Unless indicated otherwise, perfusate glucose concentration was switched from basal (5.6 mM or 100 mg/dl) to stimulated (16.7 mM or 300 mg/dl) conditions at time t=0.

The inner incubator was maintained at 37 ± 0.3°C. A perfusate flow rate of 0.5 ml/min was used, resulting in a superficial fluid velocity of 0.5 cm/sec relative to the islets. The perfusate pH was maintained at 7.45 . Normoxic perfusate pO_2 was 142 mm Hg (humidified 5.3% CO_2 and 94.7% air). Hypoxic pO_2 ranged from 2 to 60 mmHg. For twelve, 200 μm diameter rat islets cultured overnight after isolation, the basal insulin concentration in the outlet perfusate ranged between 2 - 10 μU/ml, and the glucose-stimulated insulin concentration rose to between 20 - 150 μU/ml. The insulin secretion rate, S, per unit volume of tissue, V_t, was calculated from the measured insulin concentration [I] in each sample according to

$$S = \frac{Q\,[I]}{V_t} \qquad (1)$$

where Q is the perfusate flowrate.

Islet viability was tested by vital staining. A solution of 0.06% (w/v) trypan blue (630-5250AG, GIBCO) was prepared in DMEM containing 2% NBCS. Islets were aspirated into petri dishes containing a warmed (37°C) and gas-equilibrated (5.3% CO_2 and 94.7% air) trypan blue solution and then placed in a 37°C incubator. After five min, the islets were

aspirated out of the staining solution with a micropipette, placed in DMEM with 10% NBCS, and examined under a dissecting microscope. Viable cells exclude trypan blue whereas dead cells which have lost their membrane integrity stain blue (Lillie, 1977).

Fresh isolated islets which were stained with trypan blue following collagenase digestion showed a diffuse pattern of blue staining. The intensity of staining decreased with time and disappeared after two days of culture. Although diffuse staining could be indicative of sublethal cell damage during isolation, a more likely explanation is that dye was trapped within the residual vascular elements of the islets, and that the disappearance of the stain corresponded to collapse of the vascular network (Andersson and Hellerstrom, 1977).

RESULTS

Effect of pO_2 on Insulin Secretion by Rat Islets (One Day of Culture). The insulin secretion profiles from seven normoxic rat islet perifusions are shown in Figure 1. The perifused islets responded to a glucose challenge with a burst of first phase insulin secretion which varied in magnitude from 100 to 600 μU insulin/min•mm^3 islet. First phase secretion lasted for 2-4 min, after which secretion rate usually decreased before second phase insulin secretion began. In most islet perifusions, second phase secretion rate reached a plateau about 30 - 40 min after the glucose concentration change and leveled off at a steady value which varied widely in magnitude from about 200 to 900 μU insulin/min•mm^3 islets. Despite the wide variation in magnitude, second phase secretion rate in each perifusion remained approximately constant throughout the period of glucose stimulation.

The effect of maintaining hypoxia during the entire perifusion experiment is shown in Figure 2 for two islet preparations from each of two different isolation batches. Thirty minutes prior to the glucose step, the perfusate pO_2 was set at either 10 mmHg (upper panel) or 25 mmHg (lower panel). Basal secretion rate was slightly reduced at a hypoxic pO_2 of 10 mmHg; no significant difference in basal release was observed between pO_2 of 20 and 142 mmHg. First phase insulin secretion rate was slightly lower in hypoxic perifusions, averaging 67 ± 19% of the paired normoxic controls. Whereas normoxic islets immediately began

secreting insulin at a steadily increasing rate, the second phase response was substantially reduced at 25 mmHg and was almost completely eliminated at 10 mmHg. The second phase secretion rate, averaged over t=10 to 60 min, was 47% of the normoxic value at 25 mmHg and 16% at 10 mmHg. With each isolation batch, the two different islet preparations gave results which were qualitatively similar but differed substantially quantitatively. This was usually observed whenever different islet preparations from the same isolation batch were studied.

Figure 3 shows the effect of changing from hypoxic to normoxic conditions. The perifusate pO_2 was lowered to 15 mmHg 30 min prior to a glucose challenge at t=0. Following a first phase burst of insulin, second phase secretion rate was negligible throughout the period of hypoxia. At 40 min, the pO_2 was raised to 142 mmHg. The islets responded to reoxygenation with a rapid burst of insulin, followed by a steadily increasing second phase secretion rate. The secretion rate dropped rapidly after the glucose concentration was switched back to its basal level. The increased insulin secretion rate observed upon reoxygenation indicates that the reduction in insulin secretion caused by short-term hypoxia was rapidly reversed.

The results presented to this point demonstrate the qualitative effect of hypoxia on basal, first, and second phase insulin secretion rate. However, the variability observed in normoxic, second phase secretion rate between preparations of small numbers of islets from different isolation batches, and even from the same batch, appeared to preclude quantitation of the effect of hypoxia. To circumvent this problem, a protocol was developed in which each islet preparation served as its own normoxic control, and the effect of hypoxia was normalized to the prior normoxic second phase level. After steady normoxic, glucose-stimulated second phase secretion rate was attained (30-40 min, Figure 1), perfusate pO_2 was decreased to the hypoxic test level for a period of 30-35 min and then increased back to normoxic conditions. The fraction of normoxic insulin secretion rate released during the hypoxic period was taken as a measure of the relative effect of hypoxia in reducing secretion rate. This fraction was defined as the steady hypoxic secretion rate, S_x, measured at pO_2 = x mmHg, divided by the normoxic secretion rate, S_{142}, measured at pO_2 = 142 mmHg.

Results from 16 representative perifusions of isolated rat islets in which the perfusate pO_2 during the hypoxic period ranged from 142 down to as low as 5 mmHg are shown in Figure 4. In virtually all experiments, a first phase insulin spike occurred after glucose stimulation at t=0, followed by a steadily increasing rate of second phase insulin secretion which usually reached a plateau after 30 - 40 min. When perfusate pO_2 was dropped to 60 mmHg, insulin secretion rate dipped in one case and then recovered; by the end of the hypoxic period there was no change between the hypoxic and normoxic secretion rates. In the other case, the secretion rate had not reached a steady level and continued to slowly rise. When perfusate pO_2 was further lowered to 45, 30, 15, or 5 mmHg, insulin secretion rate quickly dropped to a fraction of the normoxic rate and remained at the lower level throughout the period of hypoxia. The extent to which secretion rate was reduced was dependent on the degree of hypoxia in the perfusate; the lower the pO_2, the larger the drop in insulin secretion rate. With the exception of the normoxic control perifusions, the islets usually responded with a reoxygenation spike of insulin secretion upon the restoration of normoxia and then returned to a secretory rate similar to that seen before the onset of hypoxia. In the case of the hypoxic perifusions at 60 mmHg, the islets still displayed a small reoxygenation spike, even though secretion had recovered to the normoxic level before the end of the hypoxic period.

In order to calculate the fraction of normoxic insulin secretion rate, S_{142} and S_x were evaluated as the average of the three measurements over the 12 min period just before pO_2 was decreased and at the end of the hypoxic period, respectively. In about 10% of the perifusions, second phase secretion obviously did not reached a steady value prior to the hypoxic period, and S_{142} was evaluated using two or three data points from the post-hypoxic period.

At the termination of each perifusion, islets were removed from the cell chamber for examination under a dissecting microscopic and staining with the vital stain trypan blue. The islets retained their spheroidal integrity throughout the perifusion and did not fragment or agglomerate under perifusion conditions. Trypan blue staining beyond the diffuse staining

normally seen in freshly isolated islets was not observed in any of the islets examined following perifusion after one day of normoxic culture. The absence of increased trypan blue staining in all cases indicated that the hypoxia-induced reductions in insulin secretion were not a result of gross cell death. This is consistent with the elimination of reduced insulin secretion observed upon the restoration of normoxia in most of the perifusions.

In addition to perifusions of the type shown in Figure 4, several experiments were run in which the pO_2 was decreased stepwise to multiple hypoxic levels, followed by a corresponding return to normoxia. Representative examples of these perifusions are shown in Figure 5. As in Figure 4, normoxic second phase secretion was first allowed to reach a steady value. Insulin secretion rate was progressively reduced with each stepwise decrease in perfusate pO_2. Upon reoxygenation to sequentially higher pO_2, an insulin secretion spike was observed in all cases, even when the increase in pO_2 was small and the secretion rate was still limited by hypoxia. As a result of these successive reoxygenation spikes, it was not possible to measure a steady value of insulin secretion rate during the interval of each upward pO_2 step. S_x at each hypoxic pO_2 was therefore evaluated from the data during the downward pO_2 steps.

Perifusions of the types shown in Figures 4 and 5 each produced one or more paired values of the fraction of normoxic insulin secretion rate, S_x / S_{142}, and the bulk perfusate pO_2 = x mmHg. These values from all single- and multiple-step experiments with rat islets cultured for one day after isolation are plotted in Figure 6; they are represented by a single curve with modest scatter, despite the wide range in the individual values of both S_x and S_{142}. The fraction of normoxic insulin secretion rate decreased smoothly with reduction in perfusate pO_2 The fractional secretion rate began to decrease from 1.0 at pO_2 levels below about 60 mmHg, reached 0.5 at pO_2 = 27 mmHg (P_{50}), and was about 0.02 at 5 mmHg.

Figure 7 shows the temporal insulin secretion profile obtained using the rapid oxygen switching system. Ninety percent of the measured perfusate pO_2 drop to 22 mmHg was accomplished within 67 sec following the switch from normoxic to hypoxic perfusate. Insulin secretion rate began to drop during the first min following the downward pO_2 switch and

reached a steady level during the second min, which coincided with full establishment of the perfusate pO_2 drop. The response time of insulin secretion following the upward pO_2 switch was even more rapid. The reoxygenation insulin spike was well under way during the first min. The reoxygenation spike of insulin secretion peaked during the second min and leveled out after about seven min of reoxygenation.

Effect of Culture Time and Species on the Sensitivity of Insulin Secretion to Hypoxia.

Isolated islets were cultured under static normoxic conditions for 1, 2, 3 or 5 weeks following isolation. At the end of the specified period of time, the O_2 sensitivity of their insulin secretion was tested during hypoxic perifusion. During culture, certain changes occurred in islet morphology. First, islets developed a flattened surface on the side where they attached to the collagen coated petri dish. Second, after 4-5 days of culture, some islets began to display darkened core regions which were evident by light microscopy. The development of these darkened regions was size dependent: larger islets developed larger and more pronounced darkened cores. The darkened regions also grew in size with time of culture up to about two weeks, beginning as small discolored regions at the islet core and ending as large black regions covering 50% or more of the islet diameter in large ($\geq$250-μm diameter) islets. On exposure to trypan blue, the darkened regions appeared to take up dye although this was difficult to assess because of the darkness of the cores. These regions were assumed to represent necrotic cores.

Figure 8 illustrates the effect of hypoxia on second phase insulin secretion rate from three preparations of islets which were obtained from the same isolation batch and tested either on the day after isolation or following one week of static culture under 142 mmHg oxygen. The normoxic rate of insulin secretion was much higher for islets perifused following overnight culture than for islets cultured for one week. One-day old islets were more sensitive to 30 mmHg (S_{30}/S_{142} = 0.61) than were islets from the same isolation batch following one week of normoxic culture (S_{30}/S_{142} = 0.85). When the pO_2 was dropped to 15 mmHg, secretion by one-week old islets (S_{15}/S_{142} = 0.54) was comparable to that observed at

30 mmHg with one-day old islets. The reoxygenation spike of islets cultured for one week was less pronounced than for one-day old islets; however, the hypoxia-limited secretion was nevertheless reversible upon reoxygenation.

Figure 9 illustrates the insulin secretion profiles of rat islets perifused with multiple sequential hypoxic steps following one week (upper panels) or five weeks (lower panel) of static culture under normoxic conditions. As in the case with islets cultured for one day (Figure 5), insulin secretion rate decreased stepwise with progressive drops in perfusate pO_2. However, somewhat lower values of pO_2 were required to affect decreases in insulin secretion rate comparable to those observed with one-day old islets, as was the case for the data presented in Figure 8.

The effect of hypoxia in reducing second phase insulin secretion was not unique to rat islets, as is demonstrated by a representative secretion profile of one-week old, perifused canine islets in Figure 10. The patterns of insulin secretion rate with canine islets were qualitatively similar to those observed with rat islets. The extent of reduction of second phase insulin secretion rate as a consequence of exposure to specific hypoxic levels was quantitatively comparable for the two species.

The effect of perfusate pO_2 on the fraction of normoxic insulin secretion rate for islets cultured one or more weeks is summarized in Figure 11 and compared with the data for rat islets cultured for one day shown in Figure 6. In all cases, at any given value of pO_2, islets cultured one week or more yielded higher values of S_x/S_{142} than did islets cultured for one day. These results suggest that the sensitivity of islet insulin secretion rate to hypoxia decreases with time in culture. The estimates of P_{50} provide a measure of the shift in the data. The largest change for rat islets occurred during the first week of culture, during which time P_{50} dropped from 27 mm Hg to 13 mm Hg. After the second week of culture, no further changes in oxygen sensitivity were observed and the data from weeks 2-5 were combined and exhibited an overall P_{50} of 10 mm Hg. The data for rat and canine islets after one week of culture were almost identical and yielded P_{50} estimates of 13 and 16 mmHg, respectively.

The change in oxygen sensitivity with time of culture is further illustrated in Figure 13. At each of the hypoxic pO_2 test levels investigated, S_x/S_{142} increased substantially over the first week of culture. Subsequent changes were larger at lower pO_2, and oxygen sensitivity remained unchanged after two weeks of culture.

The average size and normoxic insulin secretion rate of fresh and cultured islets are summarized in Table 1. The average diameters of rat islets perifused after one day and one week of culture were almost identical at 214 and 210 μm respectively. Perifusions after longer culture times were carried out with slightly smaller islets, but the differences are not statistically significant. The average normoxic insulin secretion rate, S_{142}, decreased from one-day to one-week and then increased after two or more weeks of culture ($P \leq 0.01$). The average diameter of perifused canine islets was slightly smaller than that for rats, but S_{142} was the same as for the rat after the same culture time.

Effect of additional glucose stimulation on hypoxia-limited second phase insulin secretion

Perifusion experiments were carried out in order to examine if additional glucose stimulation would increase the insulin secretion rate during the hypoxic test period. Each of these perifusions began with glucose stimulation at t=0, followed by a single hypoxic test period. At t=84 min, perifusate glucose concentration was raised to 33.3 mM. Twenty five min later, perfusate pO_2 was raised to 142 mmHg.

Results from three perifusions are shown in Figure 13. The insulin secretion rate of one-day old islets in response to 16.7 mM glucose was substantially reduced at pO_2 = 25 mm Hg (panel A). When the perfusate glucose concentration was increased to 33 mM with pO_2 unchanged, the islets responded with an insulin secretion spike, followed by a rise of insulin secretion rate despite the constant hypoxic conditions. Secretion rate increased again following the increase in perfusate pO_2 to 142 mmHg. Exposure of one-day old islets to a pO_2 of 5 mmHg almost completely shut off second phase insulin secretion rate stimulated by 16.7 mM glucose (panel C). Little or no increase in insulin secretion rate occurred following increase of perfusate glucose concentration to 33.3 mM. The islet preparation used in this

experiment also failed to respond with an increase in insulin secretion rate after an increase in perfusate pO_2 to 142 mmHg which was observed in most, but not all, of the perifusions with a hypoxic test level of 5 mmHg.

The decrease in perfusate pO_2 to 25 mmHg did not significantly affect the second phase secretion of islets cultured for one week (panel B), and an increase in perfusate glucose concentration to 33.3 mM elicited a substantial increase in the rate at which insulin was released. An insulin secretion spike followed by elevated secretion rate nonetheless occurred when pO_2 was raised to 142 mmHg indicating an affect at pO_2 = 25 mmHg on insulin secretion rate in response to 33.3 mM glucose.

DISCUSSION

Effect of Intermediate Levels of pO_2 on Insulin Secretion

The effect of oxygen partial pressure on glucose-stimulated insulin secretion by isolated islets of Langerhans was investigated with perifusion experiments. A micro-perifusion system was employed which provided for regulation and monitoring of perfusate pO_2 and had a rapid dynamic response for measuring changes in insulin secretion rate as a result of changes in perfusate composition. Experiments were carried out in which (1) pO_2 was held constant during the entire period following an increase of glucose concentration from 5.6 to 16.7 mM, or (2) pO_2 was decreased from normoxic to hypoxic levels in one or more steps after steady second phase insulin secretion was established, followed by a return to normoxic conditions (perfusate pO_2 = 142 mm Hg).

Hypoxic levels of pO_2 over the range of 5 to 60 mmHg had little effect on basal insulin secretion and only modest effect on the first phase spike of insulin secretion following glucose stimulation. The largest effect of hypoxia was on the second phase insulin secretion rate. When pO_2 was decreased after normoxic second phase secretion was established, insulin secretion rate rapidly stabilized at a reduced level, sometimes after an initial dip in secretion rate, and remained at that level throughout the period of hypoxia. The extent of this reduction increased as pO_2 decreased. Following a subsequent increase in pO_2, islets rapidly

released a burst of insulin; this occurred whether the increase in pO_2 was small (10 mmHg) or represented complete return to normoxia (142 mmHg). The reoxygenation spike was absent or attenuated following severe (5 mmHg) hypoxia, but in most other cases it reached a magnitude greater than that of the normoxic second phase secretory rate. Using a rapid oxygen switching system, the reduction in second phase insulin secretion was shown to begin within about one minute following a decrease in the perfusate pO_2. Similarly, the reoxygenation spike of insulin secretion began within one min or less following an increase in perfusate pO_2. Following the reoxygenation spike, secretion usually returned to a rate similar to that of the normoxic state prior to the drop in pO_2. The reversibility of the hypoxia-induced reduction of insulin secretion rate upon reoxygenation and the absence of trypan blue staining in post-perifusion islets indicated that the phenomenon was not caused by loss of cell viability.

Although the normoxic insulin secretion rate, S_{142}, and the secretion rate, S_x, at a reduced pO_2 = x mm Hg, both varied substantially from one islet preparation to another, a plot of the ratio S_x/S_{142} versus perfusate pO_2 allowed all of the perifusion data to be represented by a single curve, suggesting that the fraction of normoxic secretion rate attained during the hypoxic test period was a unique and continuous function of perfusate pO_2 (Figure 6). The secretion rate under hypoxic conditions was nearly 100% of that under normoxic conditions at a pO_2 of 60 mmHg, 50% at 27 mmHg, and about 2% at five mmHg.

The pO_2 levels reported throughout this paper are those measured in the bulk perfusate. The actual pO_2 to which the β-cells within the perifused islets were exposed was lower. The islets consumed oxygen which was supplied by diffusion from the bulk perfusate. This produced a pO_2 diffusion gradient in the perfusate boundary layer immediately surrounding each islet as well as a pO_2 gradient within the islet itself. As a result of these gradients, the pO_2 at the islet surface was lower than that in the perfusate, and the pO_2 within the islet decreased radially from the periphery to the core. Therefore, peripheral β-cells, which were exposed to a higher pO_2 than those in the core, secreted a relatively higher fraction of their normoxic insulin secretion rate than did β-cells in the core. Consequently, the relationship

expressed by the data in Figure 6 does not represent an intrinsic property of individual β-cells. Instead, it reflects the complex interaction between islet oxygen consumption, boundary layer and intra-islet diffusion, and the effect of the local pO_2 on insulin secretion by β-cells. Dissecting apart these interactions from a quantitative standpoint requires additional information about islet oxygen consumption and diffusion properties and has provided motivation for further work in this area (Dionne, 1989).

Basal and first phase insulin secretion appeared to be less sensitive to hypoxia than was second phase release. The limited affect of pO_2 on basal secretion may be related, at least in part, to the lower oxygen consumption of islets in the basal as compared to the stimulated state (Hellerstrom, 1967; Hedeskov, Hertz, and Nissen, 1972; Andersson, Gunnarsson, and Hellerstrom, 1976; Lundgren et al., 1977; Hutton and Malaisse, 1980; Panten and Klein, 1982). Given the same perfusate pO_2, the lower oxygen uptake of basal respiration would result in higher pO_2 throughout the islet as compared to the pO_2 profile in an islet respiring under glucose stimulation, thereby leading to a higher fraction of normoxic basal insulin secretion. In the case of first phase secretion, the limited pO_2 effect suggests that insulin released during this period may be stored, at least partially, at a stage of the secretory process that is less, or not at all, affected by oxygen. Similarly, the burst of insulin secretion upon reoxygenation, which displayed a temporal pattern comparable to that of first phase release, may be due to the build-up of non-secreted insulin within the islet during the hypoxic period. Such a build-up could occur if some secretory steps prior to the actual exocytotic release of insulin are less influenced by hypoxia than is the final release.

The mechanism by which hypoxia limits insulin secretion is unknown. It seems reasonable to propose that it is related to the effect of low pO_2 on the energy stores of the β-cells. Previous reports in the literature have documented the ATP dependence of several of the steps in the exocytotic secretion of hormones (Randle and Hales, 1972; Gerich, Charles, and Grodsky, 1974; Baker and Whitaker, 1978; Knight and Baker, 1982; Brooks and Treml, 1983; Dunn and Holz, 1983; Moy et al., 1983), including the transport of secretion vesicles along microtubules (DeLisle and Williams, 1986; Sheetz et al., 1987), the operation of the

secretory vesicle osmotic pump (Hermans and Henquin, 1986; Knight and Baker, 1987), the glucose induced depolarization of the β-cell membrane (Cook and Hales, 1984; Cook et al., 1988), and the regulation of the transmembrane influx and efflux of ions such as Ca^{++} (Corkey et al., 1988;) and K^{+} (Cook and Hales, 1984; Misler et al., 1989). In addition, increased ATP turnover has been reported to occur in conjunction with stimulated secretion (Asplund and Freinkel, 1978; Trus et. al., 1980; Freinkel et al,. 1984). It is therefore possible that both complete anoxia (Coore and Randle, 1964; Coore et al., 1967; Milner and Hales, 1969) and the levels of hypoxia tested in this paper may affect insulin secretion by limiting the rate at which oxidative phosphorylation can replenish ATP energy supplies in the β-cells. The reversibility of hypoxia-limited secretion upon the restoration of normoxia could be mediated by a higher intra-cellular concentration of ATP fueled by an increase in oxidative phosphorylation. The ability of 33 mM glucose to increase insulin secretion rate in all but the most severely hypoxia-limited perifusions may therefore be caused by an increase in cellular ATP concentration produced by non-aerobic glycolysis.

Limited oxygen or ATP may potentially affect the entire insulin biosynthesis and secretion pathway at any number of steps. Because of the rapidity with which secretion is reduced or restored following a change in pO_2 (Figure 7), the location of the hypoxic rate limiting step is likely to be in one of the latter stages of exocytosis. Cessation of insulin biosynthesis, vesical packaging, or vesicle transport would not have an effect on insulin secretion over such a short time frame (Steiner et al., 1974). Whether or not earlier stages of insulin secretion or biosynthesis are also affected to some degree by hypoxia is unknown.

Effect of Culture Time on Oxygen Sensitivity of Insulin Secretion.

Perifusions containing hypoxic test periods were performed following normoxic static culture of different durations in order to determine if there was an effect of culture on the oxygen sensitivity of isolated islet insulin secretion. Islets which were perifused following one to two weeks of culture displayed a decreased sensitivity of insulin secretion to hypoxia. Oxygen sensitivity stabilized after two weeks of culture and remained the same after five

weeks of culture which was the longest period investigated. The measured P_{50} of rat islets was 27 mmHg, after one day of culture, 13 mmHg after one week, and 10 mmHg from 2 to 5 weeks of culture. Canine islets gave results very similar to those of rats after one week of culture. The change in oxygen sensitivity was not caused by differences in diameter of the perifused islets since the most profound changes in sensitivity occurred between one day and one week of culture and the average islet diameters for these periods were 214 μm and 210 μm, respectively.

There are several changes which may occur during culture of islets that could explain the apparent change in oxygen sensitivity of insulin secretion between freshly isolated and cultured islets. These include changes in the oxygen uptake rate of cultured versus freshly isolated islets, alteration of islet shape and cellular composition, and changes in the primary site of insulin secretion associated with the development of necrotic cores in cultured islets.

A change in the oxygen uptake rate of islet tissue with culture time would affect the oxygen gradients in the surrounding liquid boundary layer and throughout the islet, resulting in a change in the apparent sensitivity of insulin secretion to a given bulk perfusate pO_2. Islets freshly isolated by enzymatic digestion may pass through a period of abnormally high (or low) metabolic oxygen uptake due to reparation of enzymatic cell damage or to fundamental changes in the cell environment with the loss of neural, vascular and other in vivo connections. Whether these factors occur and tissue O_2 uptake changes with time of culture is unknown. The average rate of normoxic insulin secretion decreased from 547 to 318 $\mu U/min \cdot mm^3$ islet for islets culture for one week as compared to one day. This decrease may reflect a decrease in overall cell metabolism which would result in a lower oxygen uptake rate and correspondingly higher intra-islet pO_2 levels. However, the oxygen sensitivity of insulin secretion remained lower after two weeks of culture, even though the normoxic insulin secretion rate returned to a level comparable to that observed from islets after one day of culture.

Changes in the shape and cell composition of islets may occur over time as islets attach to culture surfaces and as the vascular network of intra-islet capillaries collapses. The

external geometry of attached islets changes as the islets spread out along the attachment surface (Goldman and Collie, 1976; Dionne, 1989). This spreading, which was limited to a flattening of the bottom side of cultured islets in the studies reported in this paper, exposes more islet surface area for substrate transport which would tend to make the islets less sensitive to external oxygen limitations. The collapse of capillaries and the exodus of vascular endothelial or fibroblastoid cells (Andersson and Hellerstrom, 1977; Dionne, 1989) in cultured islets could lead to larger intra-islet fractional voids which would enhance the diffusion of oxygen to the islet core. On the other hand, if the islet collapses into the void space, it may result in a smaller but more compact spheroid.

Even though islets were statically cultured at normoxic pO_2 (142 mmHg) and under a shallow layer of culture medium (the distance from the gas/liquid interface to the bottom of culture dishes was about 3.5 mm), islets still developed black, necrotic cores from 3 to 15 days into culture. The appearance of necrotic cores was size dependent with larger islets developing larger necrotic regions. The development of necrotic cores results in a lower overall apparent sensitivity of insulin secretion to hypoxic perfusate pO_2 in two ways. First, the lack of O_2 uptake in the atrophied core decreases the overall islet oxygen consumption rate, resulting in a higher pO_2 throughout the remainder of the viable islet. Second, central necrosis results in a correspondingly higher fraction of overall islet insulin secretion being supplied by peripheral islet β-cells. Such a shift to peripheral secretion may result in a decreased apparent sensitivity to hypoxia because peripheral pO_2 levels are higher than are core pO_2 levels in diffusion-limited, isolated islets.

Under certain circumstances, testing of insulin secretion from, isolated islets in static culture may also be affected by oxygen limitations. Although the liquid/gas interface of static culture systems is invariably above the 60 mmHg threshold at which effects of limited O_2 were observed with perifused islets, several factors may reduce the pO_2 at the islet surface to levels where O_2-limitation may occur in the islet core. These factors include the pO_2 drop through the unstirred static culture medium, the aggregation or close proximity of a large number of islets whose combined O_2 consumption may decrease the local pO_2, and the

presence of metabolic stimulating agents in the medium which increase the O_2 uptake rate of cultured islets. Sustained hypoxia may result in cell death and the development of necrotic cores as was observed in this study. Transient hypoxia, brought on as a result of any temporary stimulation of O_2 uptake by test substances may not be noticeable in terms of a loss of cell viability, but may nevertheless reduce the observed insulin secretion response to the test stimulation.

Relevance to Islet Transplantation and Immuno-Isolation Devices.

The pO_2 region over which islet insulin secretion is sensitive to pO_2 (below 60 mmHg for 200 μm diameter rat islets after one day of culture) is potentially important to implantation of islet immuno-isolation devices or transplantation of non-vascularized islets. Dispersed, non-encapsulated islet transplants begin to revascularize four days, and are usually fully vascularized 10-14 days, after transplantation (Griffith et al., 1977; Andersson, Korsgren, and Jansson, 1989; Menger et al., 1989). Islets transplanted in a single site underneath the kidney capsule require four weeks for revascularization throughout the tissue mass (Sandler and Jansson, 1987; Rooth et al., 1989). During the period of revascularization, islets depend on the diffusion of oxygen from the surrounding tissue to supply their metabolic requirements. This may lead to establishment of pO_2 gradients both outside and inside the islets in qualitatively the same manner as we have proposed to explain the results described in this paper. Intermediate pO_2 levels would compromise insulin secretion rate, and severe hypoxia might lead to loss of β-cell viability, especially in the islet core. The extent to which these phenomena might occur depends on the nature of the transplantation site and the pO_2 available from the surrounding tissue or blood. The extent of hypoxia might be further exacerbated if the islets aggregate into larger tissue masses.

Recent studies have shown that transplanted islets can suffer permanent damage, including the inability to establish normal vascularization when subjected to chronic hyperglycemia during this period (Korsgren, Jansson, and Andersson, 1989; Jansson and Sandler, 1989). One possible explanation for this sensitivity is that non-vascularized islets

subjected to chronic hyperglycemia may exist in a chronic state of hypoxia because of the higher metabolic oxygen requirements associated with glucose stimulation. Hypoxia-related damage to β-cells during the non-vascularized period may be one reason for the early loss of function seen in many islet grafts (Southerland et al., 1989). Once revascularization is complete, the increased oxygen demand during glucose stimulation can be supplied to the remaining viable cells by blood flow through the revascularized tissue.

An even larger potential exists for hypoxia to limit insulin secretion from encapsulated transplants which are prevented from revascularizing by an immuno-isolation membrane. The additional oxygen transport resistance of the membrane and any space between the membrane and the islet, as well as the larger effective size of the tissue if multiple islets are packed tightly together into a single device, might add additional external pO_2 gradients which would have the effect of shifting the curves shown in Figure 6 to the right. The development of an avascular layer of fibrotic overgrowth around an implant (Garvey et al., 1979; Scharp, Mason, and Sparks, 1984) would further exacerbate this situation by imposing an additional pO_2 gradient between the surface of the device and the nearest source of oxygen. On the other hand, use of smaller islets, dispersed pancreatic islet cells, or cell aggregates, may help to reduce internal pO_2 gradients. Whether encapsulated islets implanted in vivo for long periods of time will exhibit the high oxygen sensitivity observed with islets cultured for one day or the lower oxygen sensitivity exhibited by islets cultured for several weeks is unknown and may be a critical question in determining the effectiveness of immuno-isolated transplantations.

Oxygen limitations may be the cause of tissue atrophy or necrosis seen in some in vivo immuno-isolated transplantations (Garvey et al., 1979). Even if necrosis does not occur, the presence of viable graft tissue does not necessarily establish the functional secretory capacity of the encapsulated islets. Oxygen partial pressure may be sufficiently high throughout the islet to maintain cell viability and limited basal insulin biosynthesis and secretion, but there may be insufficient oxygen to support substantial second phase insulin secretion in response to post-prandial rises in blood glucose. The likelihood of such limitations occurring will be

affected by the size, choice of construction materials, and geometry of the immuno-isolated implant, the vascularization and pO_2 of the implantation site, and the magnitude of the stimulatory challenge and its resulting effect on islet cell oxygen uptake.

ACKNOWLEDGEMENTS

This work was supported in part by fellowships to Keith E. Dionne by the National Science Foundation and the John and Fannie Hertz Corporation and by grants from the Juvenile Diabetes Foundation and from Baxter Healthcare Corporation. Martin L. Yarmush is a Markey Scholar.

REFERENCES

Andersson, A, Gunnarsson, R, and Hellerstrom, C. (1976) Long-term Effects of a Low Extracellular Glucose Concentration on Glucose Metabolism and Insulin Biosynthesis and Release of Mouse Pancreatic Islets Maintained in Tissue Culture. Acta Endocrinol 82: 318-329.

Andersson, A, and Hellerstrom, C. (1977) Isolated Pancreatic Islets in Tissue Culture: An Investigative Tool for Studies of Islet Metabolism and Hormone Production. In *Pancreatic β-Cell Culture: Proceedings of the 5th Workshop. International Congress Series 408.* (October 5-9, Hoechst, Kitzbuhel; Excerpta Medica, NY.

Andersson, A, Korsgren, O, and Jansson, L. (1989) Intraportally transplanted pancreatic islets revascularized from hepatic arterial system. Diabetes 38 (Suppl. 1):192-195.

Asplund, K, and Freinkel, N. (1978) Phosphate Metabolism and Glucose-initiated Efflux of Phosphate Ions in Islets of Fetal Pancreas. Diabetes 27: 611-19.

Baker, P.F, and Whitaker, M.J. (1978) Influence of ATP and Calcium on the Cortical Reaction in Sea Urchin Eggs. Nature (London) 276: 513-515.

Bonner-Weir, S, and Orci, S. (1982). New Perspectives on the Microvasculature of the Islets of Langerhans in the Rat. Diabetes 31: 883-889.

Bonner-Weir, S. (1984) Morphological Evidence for β-cell Polarity Within the Islet of Langerhans in the Rat. Diabetes 33 (Suppl. 1): 81A.

Brooks, J.C, and Treml, S. (1983) Catecholamine Secretion by Chemically Skinned Cultured Chromaffin Cells. J Neurochem 40: 468-473.

Cook, D.L, and Hales, C.N. (1984) Intracellular ATP Directly Blocks K^+ Channels in Pancreatic β-Cells. Nature 311: 271-273.

Cook, D.L, Satin, L.S, Ashford, M.L.J, and Hales C.N. (1988) ATP-Sensitive K^+ Channels in Pancreatic β-Cells: Spare-Channel Hypothesis. Diabetes 37: 495-498.

Coore, H.G, and Randle, P.J. (1964) Regulation of Insulin Secretion Studied with Pieces of Rabbit Pancreas Incubated *in vitro*. Biochem J 93: 66-77.

Coore, H.G, Hellman, B., Idahl, L-A, and Taljedal, I-B. (1967). Diabetes Research at the Histological Department in Umea. Opuscula Medica 12:285-295.

Corkey, B.E, Deeney, J.T, Glennon, M.C, Matschinsky, F.M, and Prentki, M. (1988) Regulation of Steady-State Free Ca^{2+} Levels by the ATP/ADP Ratio and Orthophosphate in Permeabilized RINm5F Insulinoma Cells. J Biol Chem 263: 4247-4253.

De Lisle, R.C, and Williams, J.A. (1986) Regulation of Membrane Fusion in Secretory Exocytosis. Ann Rev Physiol 48: 225-238.

Dionne, K.E, Colton, C.K, and Yarmush, M.L. (1989A) Effect of Oxygen on Isolated Pancreatic Tissue. A.S.A.I.O Transactions (in press).

Dionne, K.E., Colton, C.K, and Yarmush, M.L. (1989-2) A Micro-Perifusion System with Environmental Control for Islet Insulin Secretion Studies. Biotech Progr (submitted).

Dionne, K.E. (1989). Effect of hypoxia on insulin secretion and viability of pancreatic islet tissue. Ph.D. Thesis, Department of Chemical Engineering, MIT, Cambridge, MA.

Dunn, L.A, and Holz, R.W. (1983) Catecholamine Secretion from Digitonin-treated Adrenal Medullary Chromaffin Cells. J Biol Chem 258: 4989-4993.

Freinkel, N, Lewis, N.J, Johnson, R, Swenne, I, Bone A, and Hellerstrom, C. (1984) Differential Effects of Age Versus Glycemic Stimulation on the Maturation of Insulin Stimulus-Secretion Coupling During Culture of Fetal Rat Islets. Diabetes 33: 1028-1038.

Garvey, J.F.W, Morris, P.J, Finch, D.R.A, Millard, P.R, and Poole, M. (1979) Experimental Pancreas Transplantation. The Lancet (May 5): 971-972.

Gerich, J.E, Charles, M.A, and Grodsky, G.M. (1976) Regulation of Pancreatic Insulin and Glucagon Secretion. Ann Rev Physiol 38: 353-388.

Goldman, H, and Colle, E. (1976) Human Pancreatic Islets in Culture: Effects of Supplementing the Medium with Homologous and Heterologous Serum. Science 182: 1014-1016.

Griffith, R.C., and Scharp, D.W., Hartman, B.K., Ballinger, W.F., Lacy, P.E. (1977) A morphologic study of intrahepatic portal-vein islet isografts. Diabetes 26: 201-14.

Hedeskov, C.J, Hertz, L, Nissen, C. (1972) The Effect of Mannoheptulose on Glucose- and Pyruvate-stimulated Oxygen Uptake in Normal Mouse Pancreatic Islets. Biochim Biophys Acta 261: 388.

Hellerstrom, C. (1967) Effects of Carbohydrates on the Oxygen Consumption of Isolated Pancreatic Islets of Mice. Endocrinology 81: 105-112.

Hellman, B, Idah, L.A, Sehlin, J, and Taljedal, I.B. (1975) Influence of Anoxia on Glucose Metabolism in Pancreatic Islets: Lack of correlation between fructose-1,6-diphosphate and apparent glycolytic flux. Diabetologia 11: 495-500.

Hermans, M.P, and Henquin, J.C. (1986) Is there a Role for Osmotic Events in the Exocytotic Release of Insulin? Endocrinology 119: 105-111.

Hutton, J.C, and Malaisse, W.J. (1980) Dynamics of Oxygen Consumption in Rat Pancreatic Islets. Diabetologia 18: 395.

Jansson, L, and Sandler, S. (1989) Influence of hyperglycemia on blood perfusion of autotransplanted pancreatic islets in diabetic rats. Diabetes 38 (Suppl. 1):196-98.

Knight, D.E, and Baker, P.F. (1982) Calcium-Dependence of Catecholamine Release from Bovine Adrenal Medullary Cells after Exposure to Intense Electric Fields. J Membrane Biol 68: 107-140.

Knight, D.E, and Baker, P.F. (1987) Exocytosis from the Vesicle Viewpoint: An overview. (Part VI. Exocytosis from the Perspective of the Secretory Vesicle; ed. Johnson, R.G.) Ann NY Acad Science 493: 504 - 522.

Korsgren, O, Jansson, L, and Andersson, A. (1989) Effects of hyperglycemia on function of isolated mouse pancreatic islets transplanted under kidney capsule. Diabetes 38:510-515.

Lacy, P.E. and Kostianovsky, M. (1967) Meithod for the Isolation of Intact Islets of Langerhans from the Rat Pancreas. Diabetes 16: 35-39.

Lifson, N, Kramlinger, K.G, Mayrand, F.F, and Lender, E.J. (1980) Blood flow to the Rabbit Pancreas with Special Reference to the Islets of Langerhans. Gastroenterology 79: 466-473.

Lillie, R.D. (ed) (1977). H.J. Conn's Biological Stains. Williams and Wilkins Co., Baltimore, MD.

Lundgren, G, Andersson, A, Borg, H, Buschard, K, Groth, C.G, Gunnarsson, R, Hellerstrom, C, Petersson, B, and Ostman, J. (1977) Structural and Functional Integrity of Isolated Human Islets of Langerhans Maintained in Tissue Culture for 1-3 Weeks. Trans Proc 9: 237-240.

Menger, M.D, Jaeger, S, Walter, P, Feifel, G, Hammersen, F, Messmer, K. (1989) Angiogenesis and hemodynamics of microvasculature of transplanted islets of Langerhans. Diabetes 38 (Suppl. 1):199-201.

Milner, R.D.G, and Hales, C.N. (1969) The Interaction of Various Inhibitors and Stimuli of Insulin Release Studied with Rabbit Pancreas *in vitro*. Biochem J 113: 473-479.

Misler, S, Gee, W. M, Gillis, K.D, Scharp, D.W, and Falke, L,C. (1989) Metabolite-Regulated ATP-Sensitive K^+ Channel in Human Pancreatic Islet Cells. Diabetes 38: 422-427.

Montesano, R, Mouron, P, Amherdt, M, and Orci, L. (1983). Collagen matrix promotes reorganization of pancreatic endocrine cell monolayers into islet-like organoids. J Cell Biol 97:935-939.

Moy, G.W, Kopf, G.S, Gache, C, and Vacquier, V.D. (1983) Calcium-Mediated Release of Glucanase Activity from Cortical Granules of Sea Urchin Eggs. Dev Biology 100: 267-274.

Panten, U, and Klein, H. (1982) Oxygen Consumption by Isolated Pancreatic Islets as Measured in a Microincubation System with a Clark-Type Electrode. Endocrinology 111: 1595-1600.

Randle, P.J, and Hales, C.N. (1972) Insulin Release Mechanisms in *Handbook of Physiology: Endocrinology I* (Chapter 13, pp. 219 - 35); Greep, R.O, and Astwood, E.B. (eds), American Physiological Society, Washington D.C.

Rooth, P, Dawidson, I, Lafferty, K, Diller, K, Armstrong, J, Pratt, P, Simonsen, R, Taljedal, I. (1989) Prevention of detrimental effect of cyclosporin A on vascular ingrowth of transplanted pancreatic islets with verapamil. Diabetes 38 (Suppl. 1):202-205.

Sandler, S, and Jansson, L. (1987) Blood flow measurements in autotransplanted pancreatic islets of the rat: Impairment of the blood perfusion of the graft during hyperglycemia. J Clin Invest 80:17-21.

Scharp, D.W, Downing, R, Merrel, R.C, and Greider, M. (1980) Isolating the Elusive Islet. Diabetes 29 (Suppl.1): 19-30.

Scharp, D.W. (1984) Isolation and Transplantation of Islet Tissue. World J Surgery 8: 143-151.

Scharp, D.W, Mason, N.S, and Sparks, R.E. (1984) Islet Immuno-isolation: The use of Hybrid Artificial Organs to Prevent Islet Tissue Rejection. World J Surg 8: 221-229.

Sheetz, M.P, Vale, R, Schnapp, B, Schroer, T, and Reese, T. (1987) Movements of Vesicles on Microtubules. Ann NY Acad Science 493: 409-416.

Southerland, D.E.R., Mondry, K.C., and Fry, D.S. (1989). Results of Pancreas-Transplant Registry. Diabetes 38(Suppl. 1):46-54.

Steiner, D.F, Kemmler, W, Tager, H.S, and Peterson, J.D. (1974). Proteolytic processing in the biosynthesis of insulin and other proteins. Fed Proc 33:2105-15.

Trus, M, Warner, H, and Matschinsky, F. (1980) Effects of Glucose on Insulin Release and on Intermediary Metabolism of Isolated Perifused Pancreatic Islets from Fed and Fasted Rats. Diabetes 29: 1-14.

Wilson, S.P, and Kirshner, N. (1983) Calcium-Evoked Secretion from Digitonin-Permeabilized Adrenal Medullary Chromaffin Cells. J Biol Chem 258: 4994-5000.

Table 1. Average Size and Insulin Secretion Rate of Perifused Islets Following Various Time Periods of Culture.

Species	Culture Time	Islet Diameter (μm)	S_{142}^{*} (μU/min•mm^3 islet)	Number of Samples
Rat	1 day	214 ± 14	550 ± 250	24
Rat	1 week	210 ± 13	320 ± 170	15
Rat	2 weeks	175 ± 34	770 ± 170	7
Rat	5 week	195 ± 35	600 ± 80	4
Canine	1 week	174 ± 10	290 ± 160	10

* Normoxic, second phase, glucose-stimulated insulin secretion rate evaluated as described in the text.

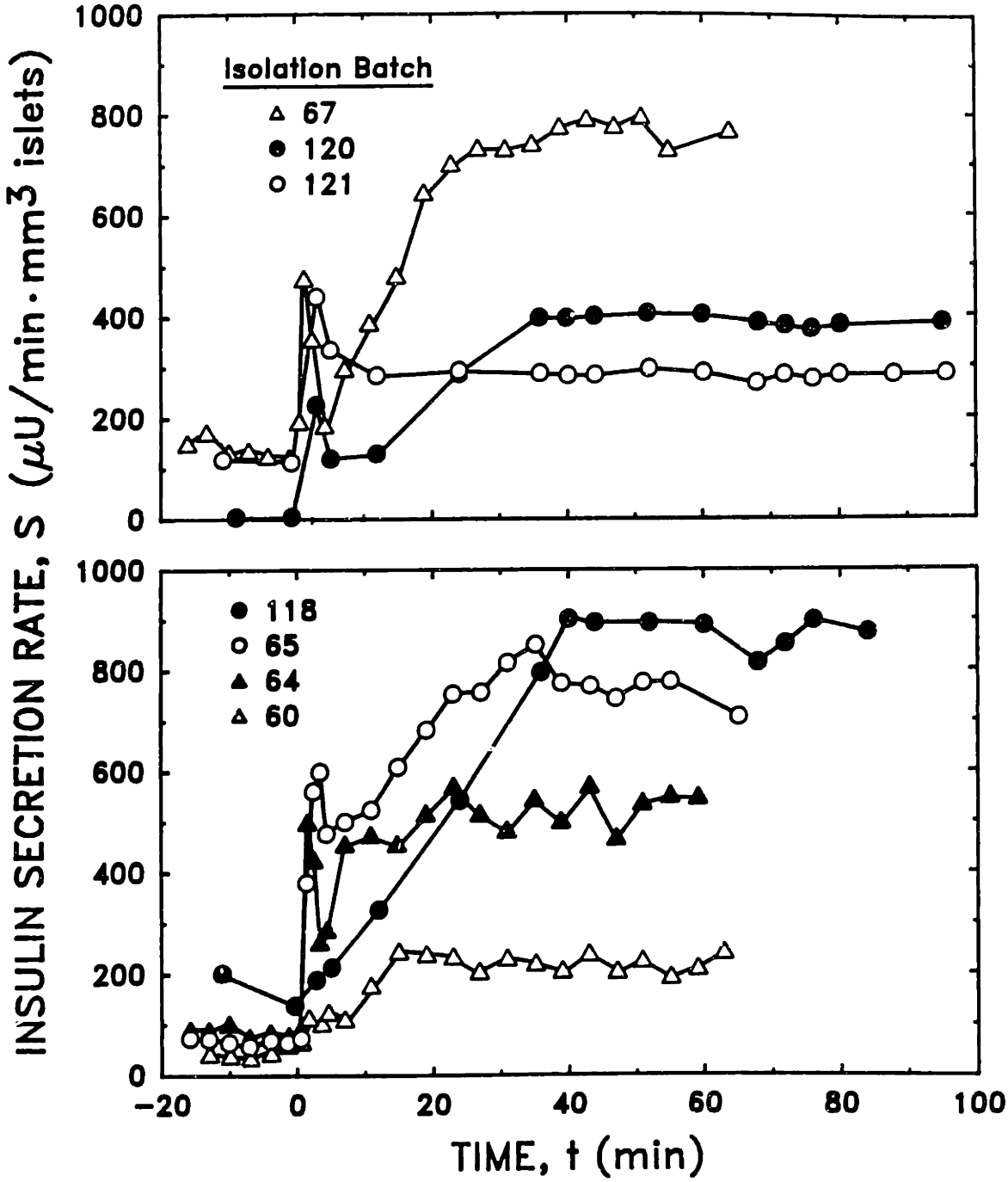

FIGURE 1. Insulin secretion from perifused rat islets under normoxic (142 mm Hg) conditions. The perifusion was carried out with 10-15 rat islets, each about 200 μm in diameter. Each set of data represents a different isolation batch. Islets were sized and perifused one day after isolation. At t=0, the glucose concentration was raised from 5.6 to 16.7 mM (100 to 300 mg/dl) glucose in DMEM with 10% NBCS. Insulin secretion rate is plotted at the midpoint of the time interval over which each sample was collected. Collection time was two min over the period from zero to six min and four min thereafter. Numbers on the figure refer to the isolation batch number.

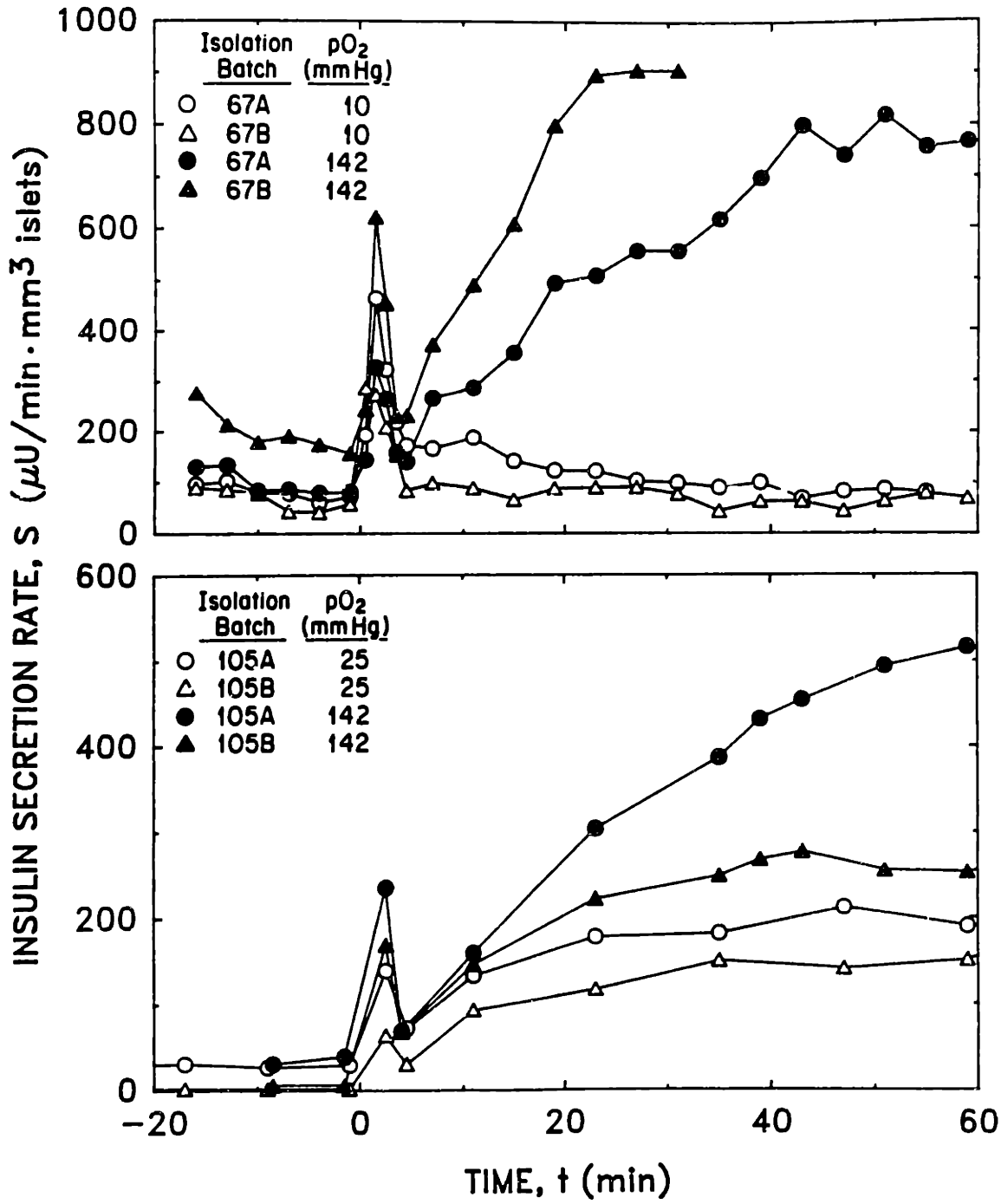

FIGURE 2. Effect of hypoxia on basal, first, and second phase insulin secretion from perifused rat islets. Normoxic islets were perifused as described in Figure 1. Thirty min prior to the glucose concentration change at t=0, the pO_2 of hypoxic perifusions was dropped to 10 mm Hg (upper panel) and 25 mm Hg (lower panel). Two separate islet samples (A,B and C,D) were used from each of two different isolation batches, shown separately in the upper and lower panels.

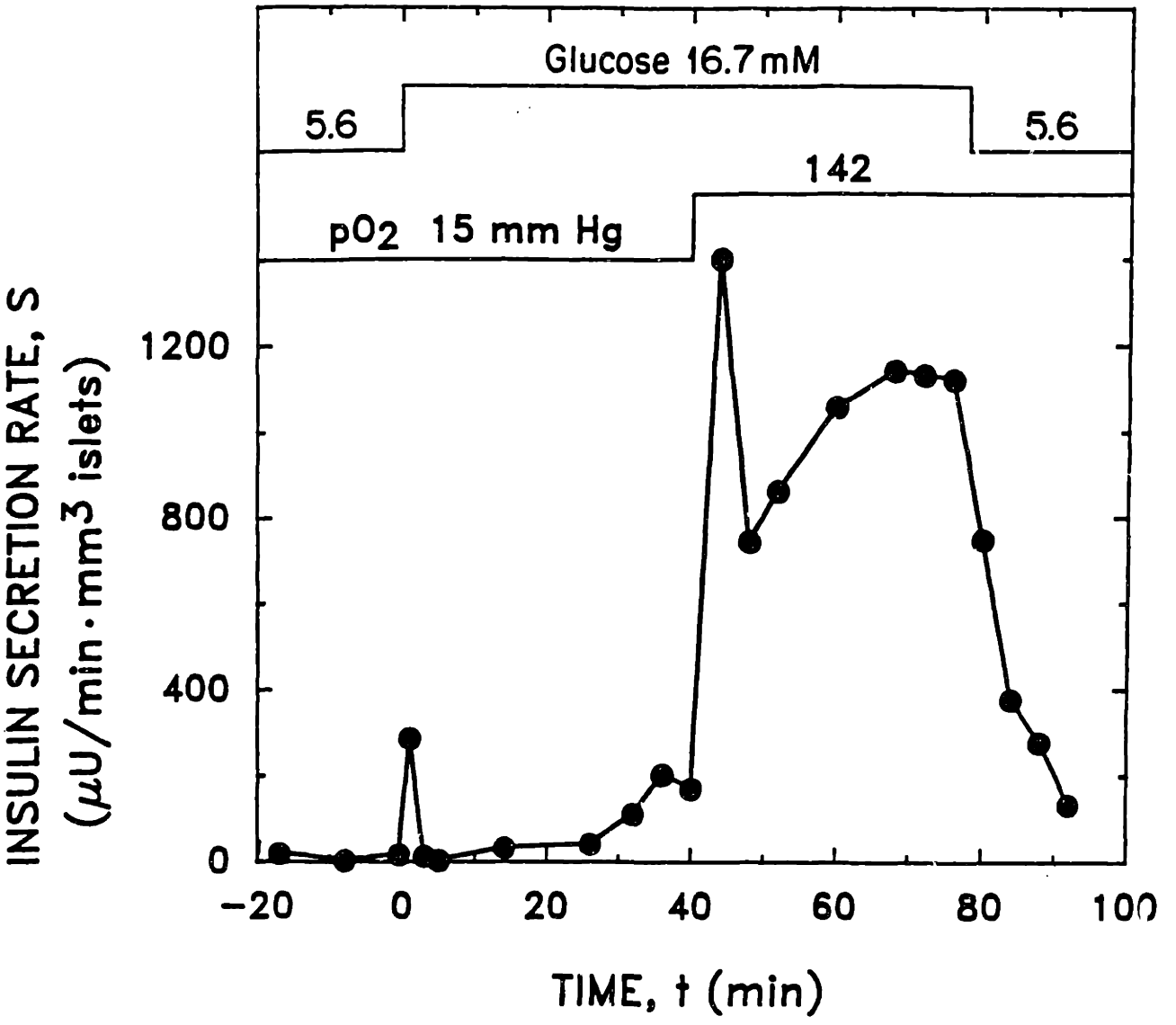

FIGURE 3. Reversibility of hypoxia-limited insulin secretion. At t=-30 min, perfusate pO_2 was decreased to 15 mm Hg. At t=0, perfusate glucose concentration was increased from 5.6 to 16.7 mM. At t=40 min, perfusate pO_2 was raised to 142 mm Hg. The profiles at the top of the figure indicate the times at which glucose and pO_2 were changed and do not represent data. The actual dynamic response of the system is described in the Materials and Methods section.

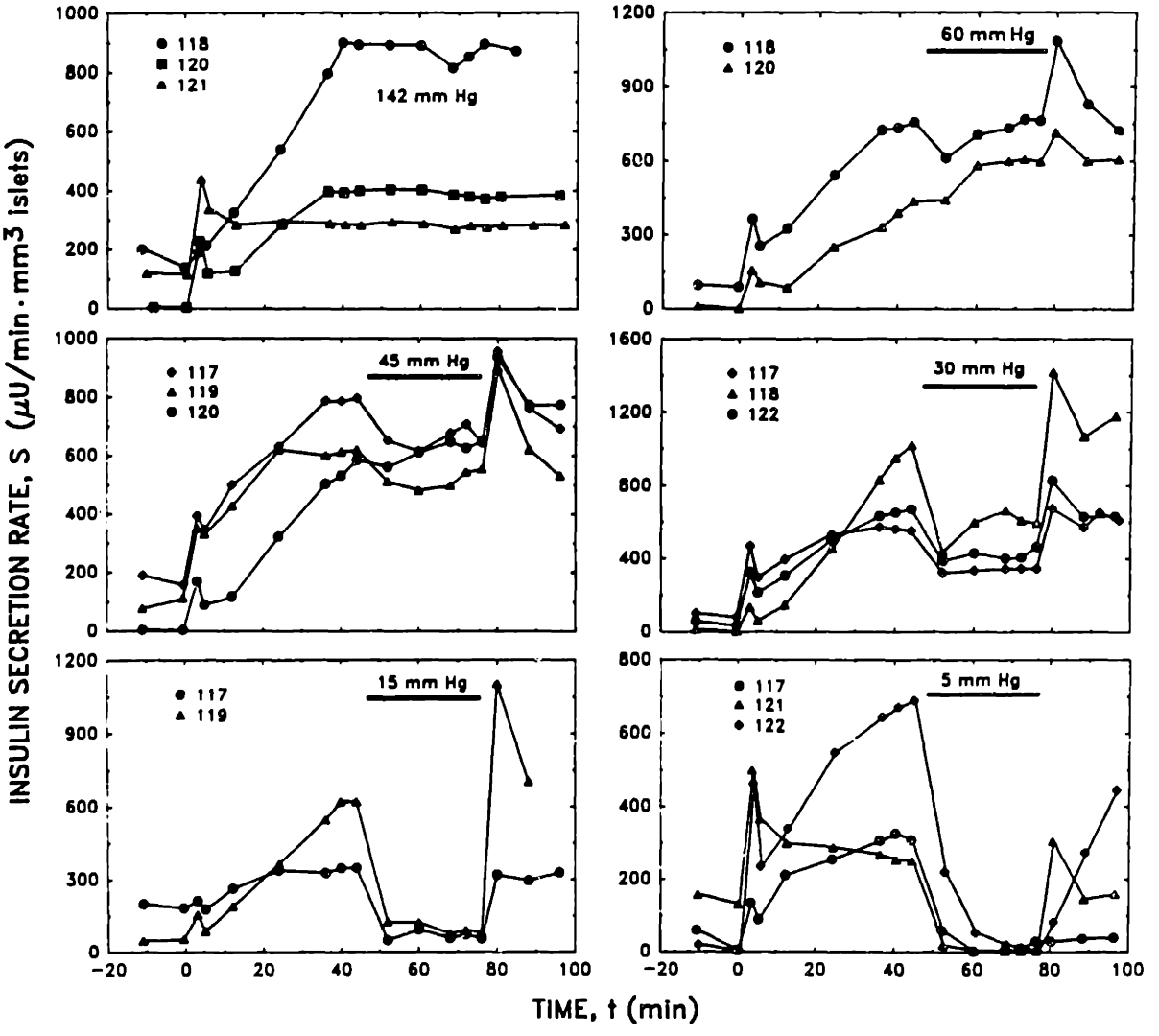

FIGURE 4. Effect of various levels of hypoxia on insulin secretion from perifused rat islets. Results are shown for perifusions of islets from multiple isolation batches cultured for one day after isolation. In all cases, pO_2 was initially 142 mm Hg and perfusate glucose concentration was increased from 5.6 to 16.7 mM at t=0. The perfusate pO_2 was dropped to the hypoxic test level at t=42-45 min and raised back to 142 mmHg at t=78 min. The bar in each panel indicates the time period during which the islets were exposed to the perfusate pO_2 indicated by the value over the bar.

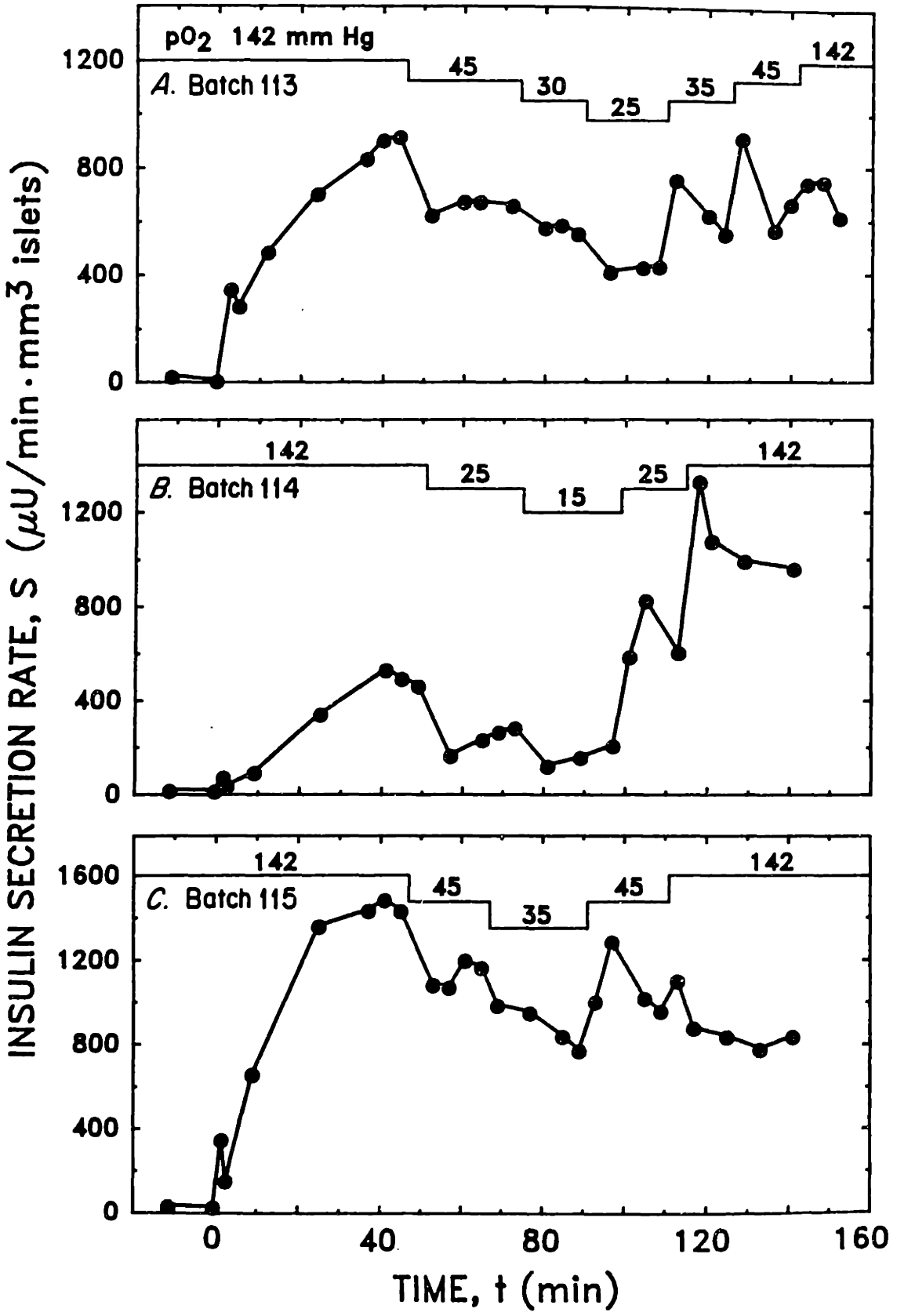

FIGURE 5. Effect of multiple sequential hypoxic steps on insulin secretion from perifused rat islets. Islets were perifused following culture for one day after isolation. Following 40-45 min of normoxic, glucose-stimulated secretion, perfusate pO_2 was progressively stepped down and then up in staircase fashion, as shown at the top of each panel, with each step lasting about 30 min.

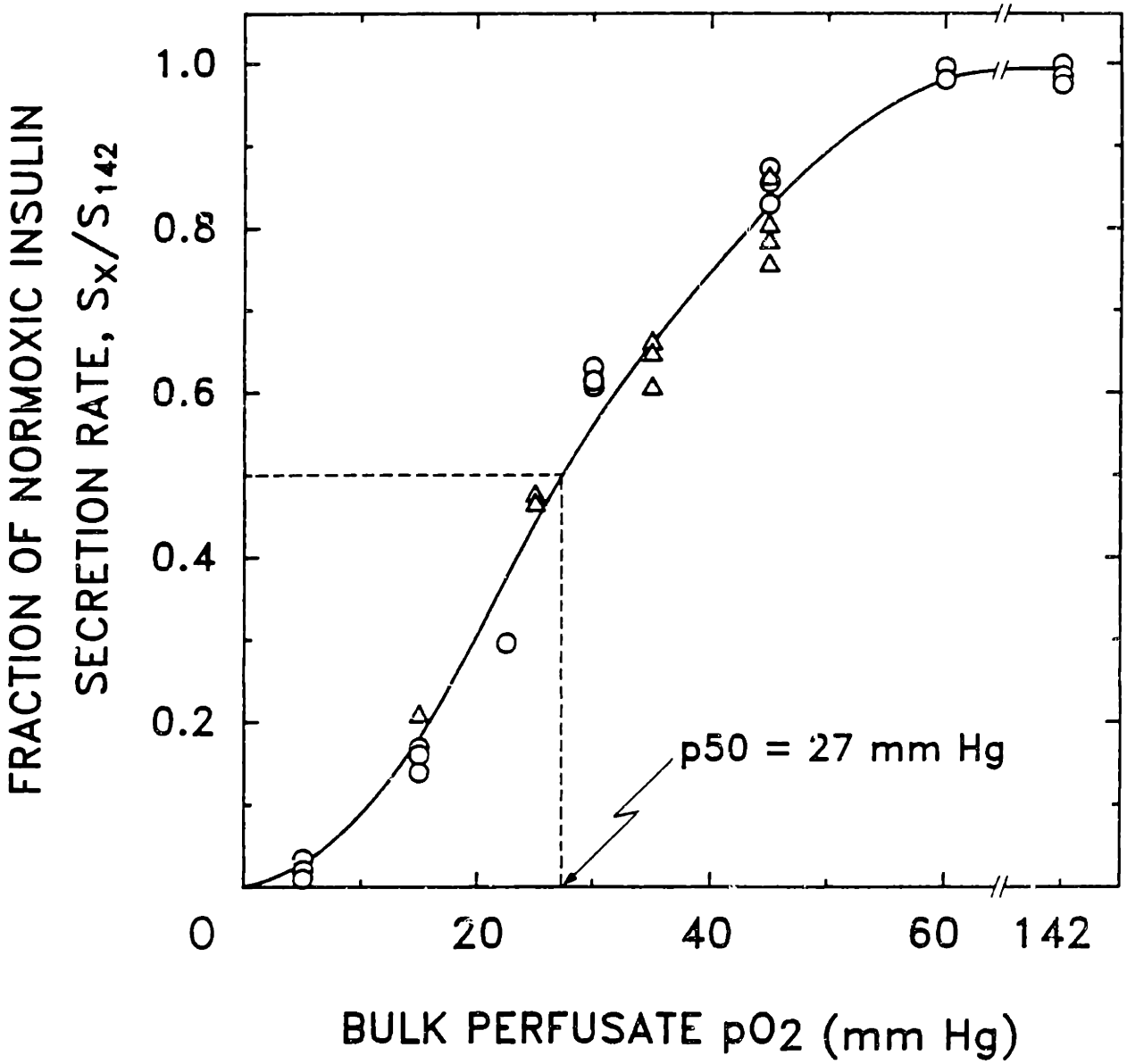

FIGURE 6. Fraction of normoxic second phase insulin secretion rate, S_x/S_{142}, as a function of bulk perfusate pO_2 for isolated rat islets cultured for one day after isolation. Diameter of islets averaged 214 ± 14 μm with an a/b ratio of 0.82 ± 0.9 (n=67). Data obtained with single hypoxic step is represented by circles, multiple steps by triangles. A single curve was drawn through all of the data by eye. P_{50}, the value of pO_2 at which $S_x/S_{142} = 0.5$, was evaluated from this curve.

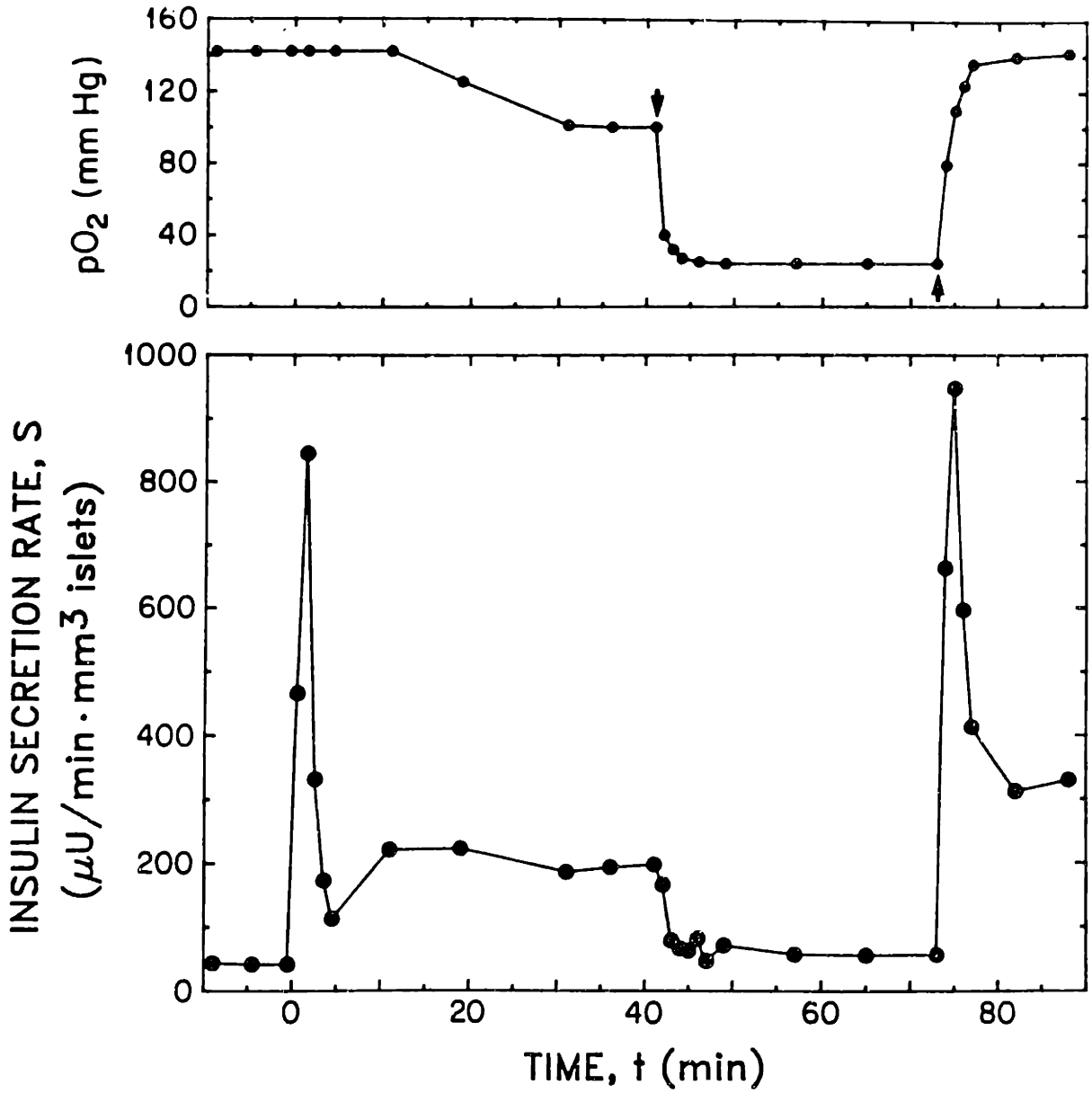

FIGURE 7. The effect of rapid changes in perfusate pO_2 on second phase insulin secretion rate of isolated rat islets. Changes in the perfusate pO_2 were made using the rapid oxygen switching system. Perfusate was collected over one min time intervals for five min following the step change in glucose from 5.6 to 16.7 mM at t=0, 10 min following the downward pO_2 step from 142 to 22 mm Hg at t=41 min, and four min following the upward pO_2 step at t=73 min. At all other times, samples were collected over four min intervals. Insulin secretion data is plotted at the midpoint of the time interval over which the sample was collected. Arrows indicate the time at which perfusate was switched from the normoxic to the hypoxic stream and vice versa.

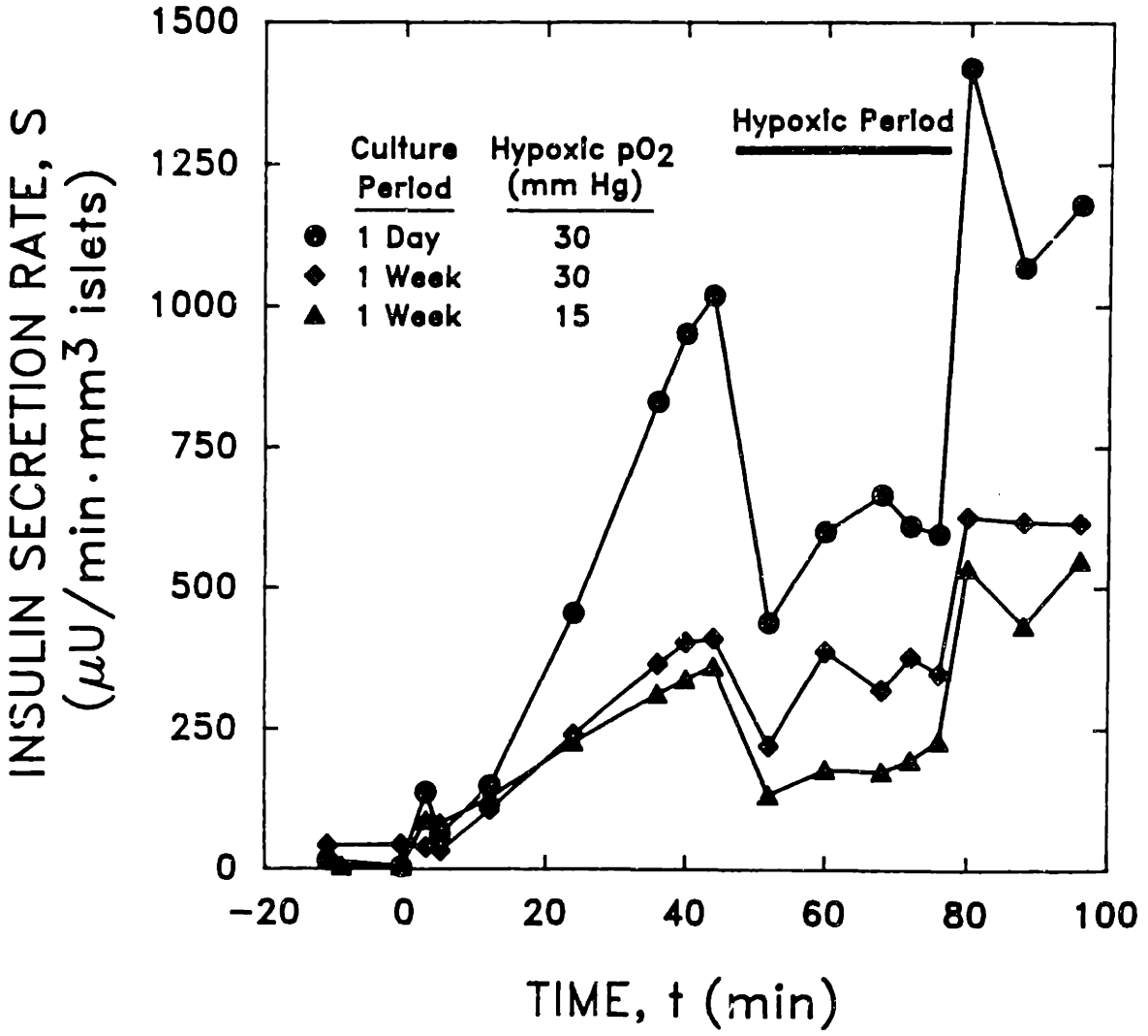

FIGURE 8. Comparison of the hypoxic sensitivity of insulin secretion from perifused islets following one day or one week of culture after isolation. Islets cultured for both one day (average diameter = 207 μm) and one week (average diameter = 203 μm) were selected from the same isolation batch (118). For one-week culture, islets were placed in collagen coated petri dishes in DMEM containing 5.6 mM glucose, 5% NBCS, and 5% rat serum at a pO_2 of 142 mm Hg.

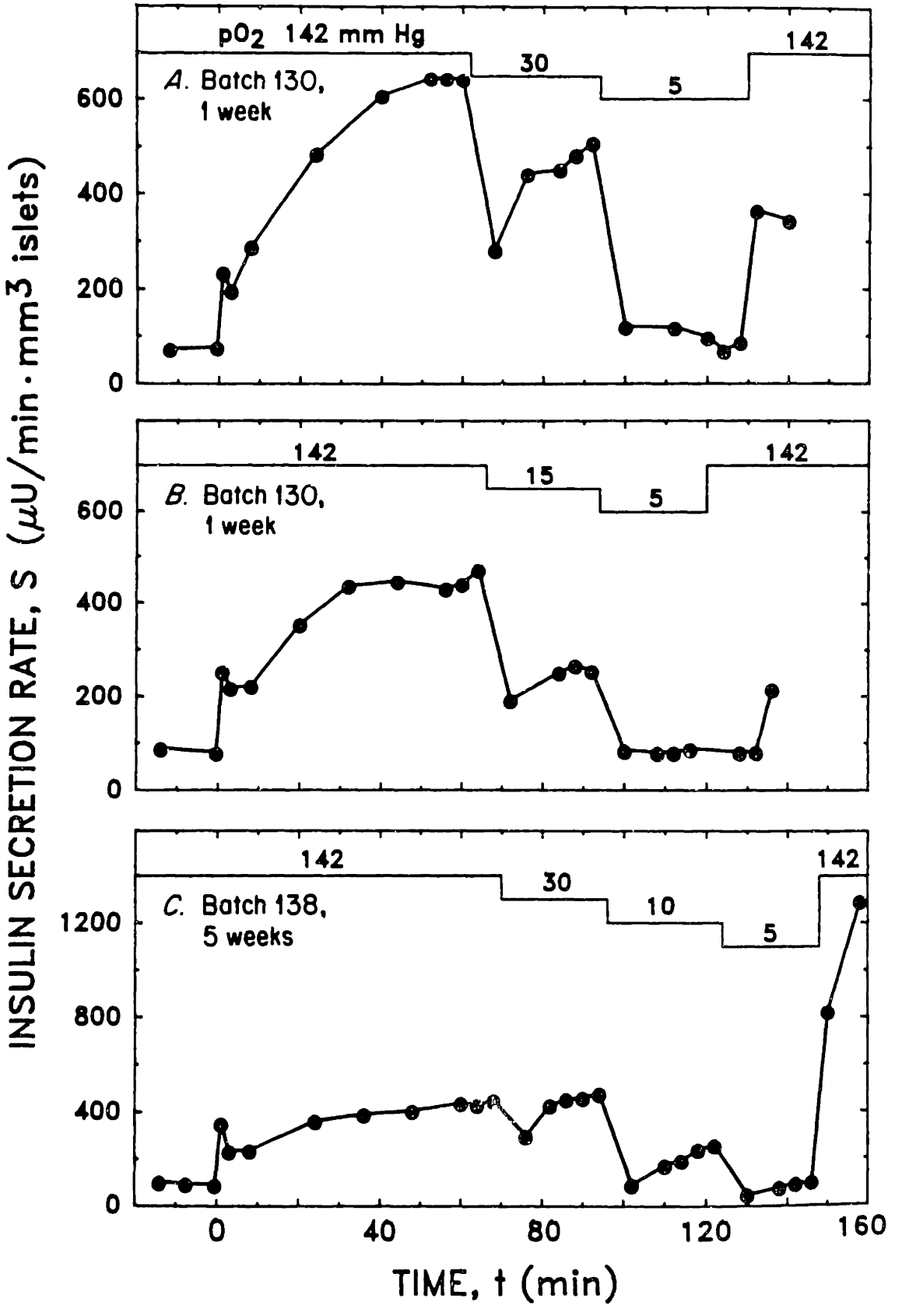

FIGURE 9. Effect of hypoxic pO_2 on insulin secretion from rat islets cultured for one or five weeks following isolation. The upper two panels were obtained with islet preparations from the same isolation batch (130). The lower panel is from a different isolation batch (138). Normoxic conditions were maintained until t=61-65 min to ensure attainment of steady-state glucose-stimulated second phase secretion. Perfusate pO_2 was progressively stepped down and then up in staircase fashion, as shown at he top of each panel, with each step lasting 18 - 30 min.

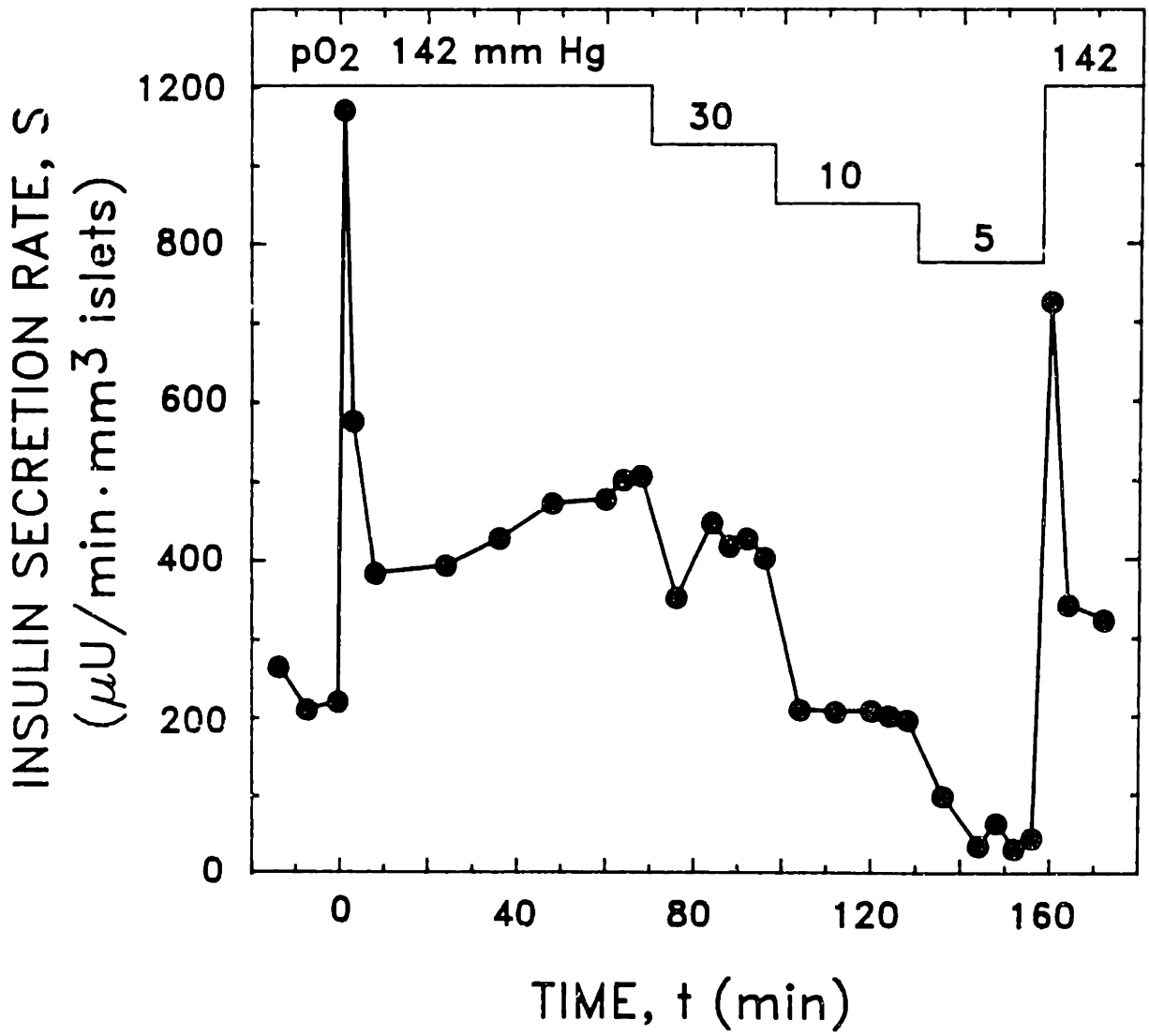

FIGURE 10. Effect of hypoxia on insulin secretion from perifused canine islets cultured for one week. Normoxic conditions were maintained until t=65 min, after which perfusate pO_2 was reduced stepwise for periods of 28-30 min and then increased back to 142 mm Hg.

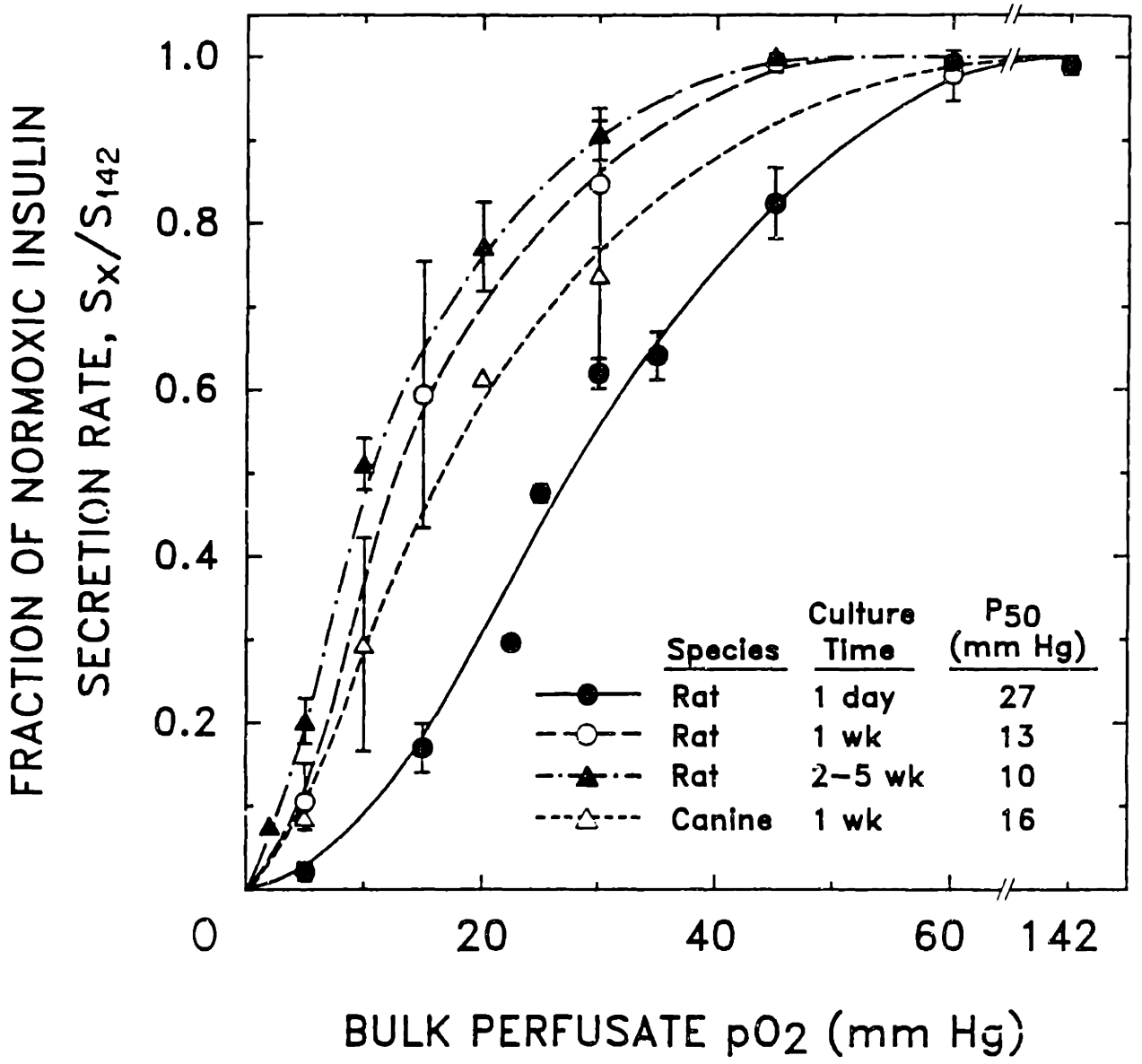

FIGURE 11. Fraction of normoxic second phase insulin secretion rate, S_x/S_{142}, as a function of bulk perfusate pO_2 for perifused rat islets cultured under normoxic conditions for one day, one week, and 2-5 weeks after isolation and for canine islets cultured one week after isolation. For one-day old rat islets, the symbols represent the mean ± SD of the data in Figure 6. All other symbols represent data from individual perifusion experiments. No distinction was made between data from single and multiple hypoxic step experiments. All curves were drawn by eye, and P_{50} for each data set was evaluated by linear interpolation between the data in the vicinity of $S_x/S_{142} = 0.5$.

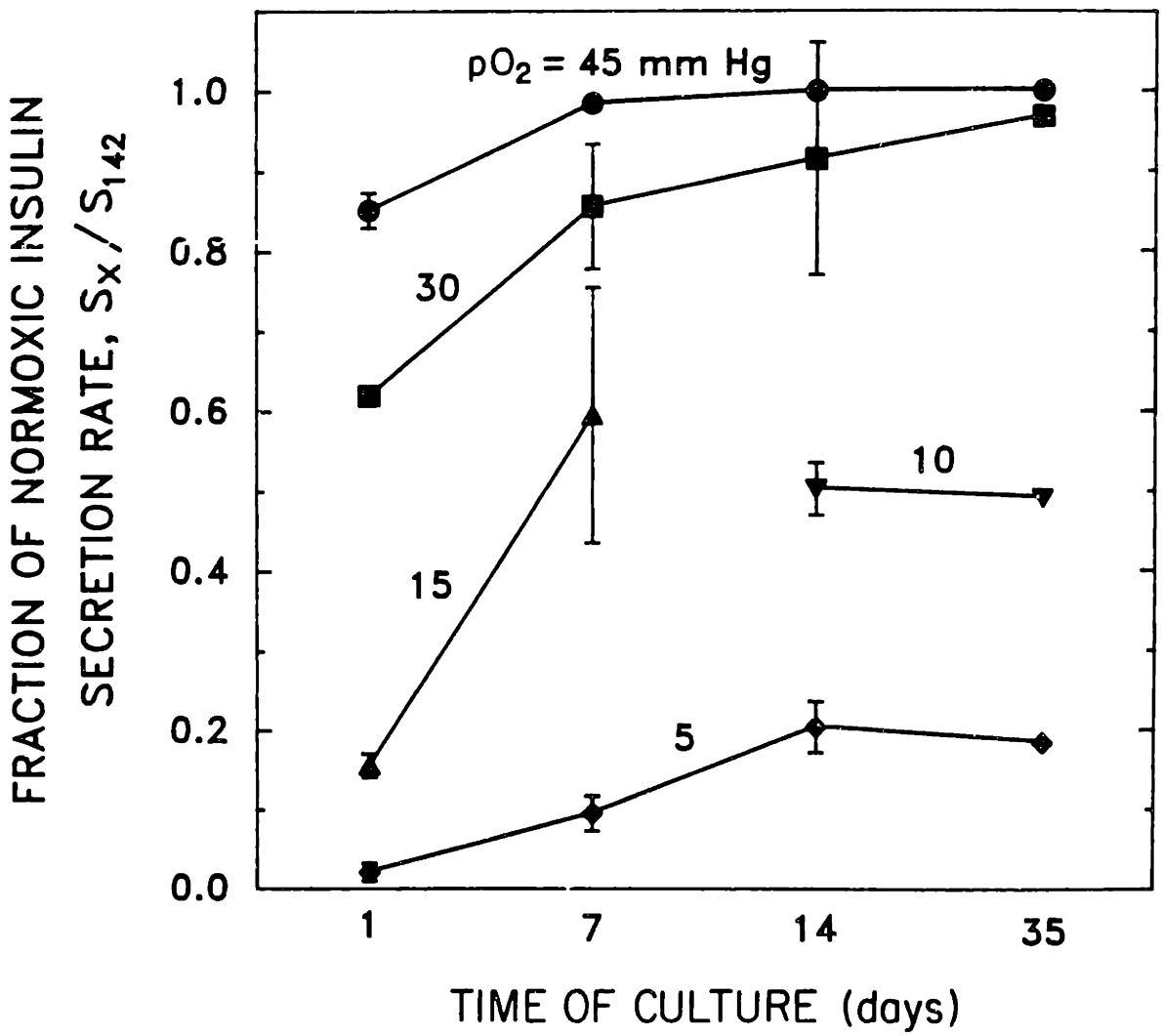

FIGURE 12. Effect of culture time on the oxygen sensitivity of insulin secretion from perifused rat islets. Average values of the fractional secretion rate, S_x / S_{142}, at specified values of pO_2 = x mm Hg, are plotted versus the time duration of normoxic static culture. Error bars represent standard deviation.

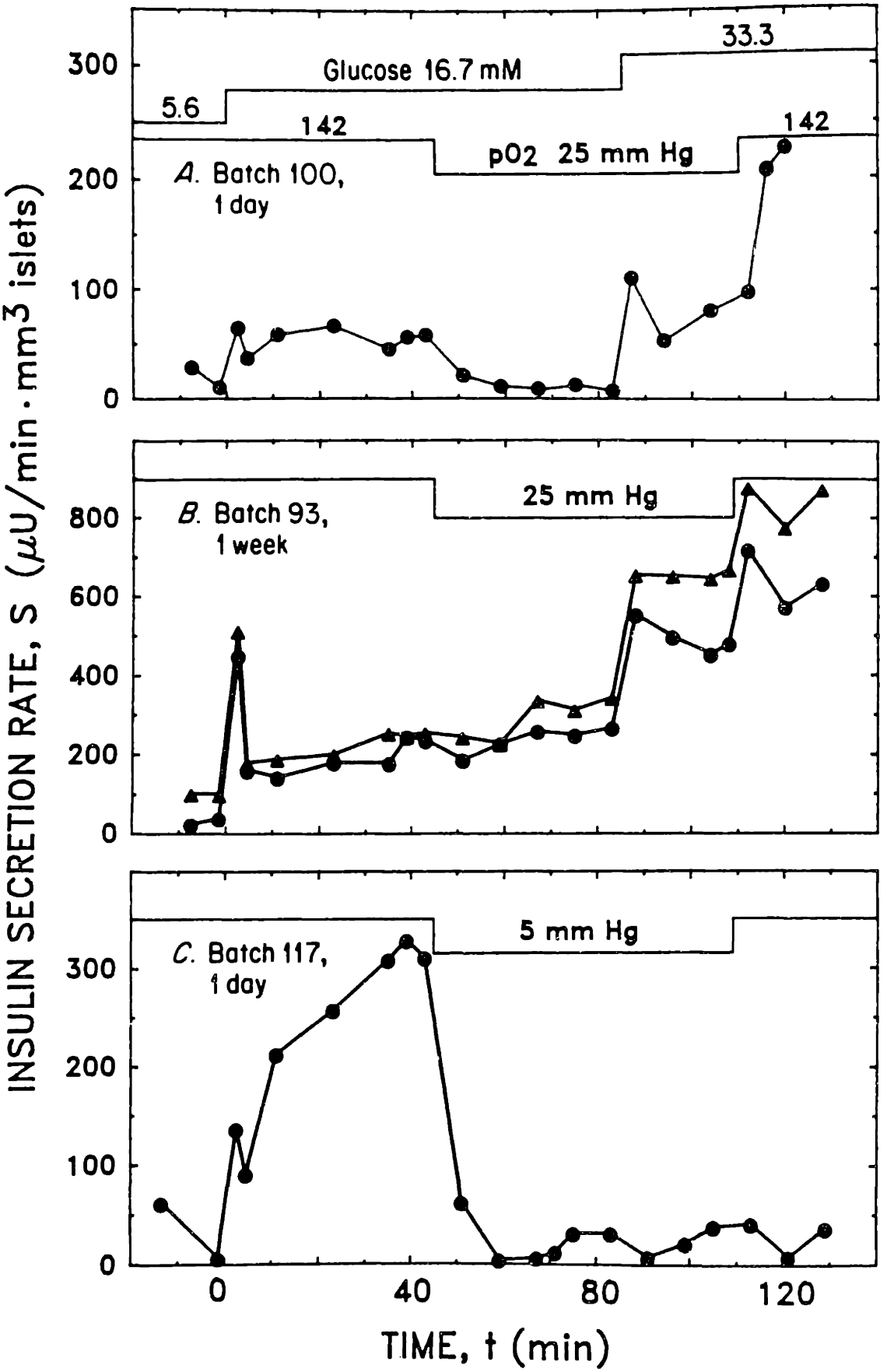

FIGURE 13. Effect of increasing the perifusate glucose concentration on hypoxia-limited second phase insulin secretion rate by perifused rat islets. At t = 0 min, glucose concentration was increased from 5.6 to 16.7 mM. At t = 45 min, perfusate pO_2 was decreased from 142 to either 25 mmHg (panel A, one-day old islets; panel B, one-week old islets) or 5 mmHg (panel C, one-day old islets). At t = 84 min, the perifusate glucose concentration was raised to 33.3 mM and pO_2 remained unchanged. At t = 109 min, perfusate pO_2 was raised to 142 mmHg while glucose concentration remained at 33.3 mM. Isolation batch number and culure time period are indicated on each panel.

CHAPTER 4:

EFFECT OF HYPOXIA ON INSULIN SECRETION FROM RAT AND CANINE ISLET CELL AGGREGATES

SUMMARY

The effect of reduced oxygen partial pressures (pO_2) on glucose-stimulated insulin secretion by aggregates of rat and canine islet cells was investigated with a microperifusion apparatus which provided control of perfusate pO_2. Aggregates were prepared from suspensions of single islet cells cultured for one (rat) or three (canine) days following trypsinization of whole islets. Second phase insulin secretion from small, 35 μm diameter, aggregated islet cell clusters was progressively decreased by reductions in the perfusate pO_2 below about 20 mm Hg. Secretion rate was reduced to 50% of its normoxic value at 5.0 mm Hg (P_{50}) and 20% at 2 mm Hg. These results provide an upper bound estimate of the intrinsic effect of pO_2 on second phase insulin secretion rate by individual β-cells. Insulin secretion from cell aggregates was more sensitive to hypoxia than was oxygen uptake (measured in a separate study), suggesting that environments may exist wherein the pO_2 is sufficiently high to maintain cell viability but is insufficient to support glucose stimulated insulin secretion. The perfusate pO_2 at which any specified reduction occurred in insulin secretion was much lower with small cell aggregates than with intact islets. This difference is consistent with the existence of substantial pO_2 gradients in isolated intact islets during the perifusion experiments.

INTRODUCTION

Internal vascularization (Bonner-Weir and Orci, 1982; Bonner-Weir 1984) and a high arterial blood flowrate to islets (Lifson et al, 1980) ensure that β-cells located in the vascularized in vivo pancreas are exposed to oxygen partial pressures (pO_2) close to arterial levels. In the absence of a functional vascular system, isolated islets or islet cells that are

cultured in vitro or encapsulated in immuno-isolation chambers must rely on the diffusion of oxygen from the surrounding environment to supply their metabolic requirements. We have previously reported that hypoxia reduces the insulin secretion rate by rat and canine islets of Langerhans. Second phase glucose-stimulated insulin secretion from intact rat islets which were perifused one day after isolation was affected at a bulk perfusate pO_2 level as high as 60 mm Hg and was reduced to one-half of normal at a perfusate pO_2 of 27 mm Hg (Dionne et al., 1989-3). To account for the relatively high pO_2 levels at which insulin secretion from intact islets was affected, we proposed that significant pO_2 gradients existed between the bulk perfusate and the islet surface as well as from the islet periphery to the islet core. As a consequence of these gradients, β-cells located at different radial positions throughout the islet would be exposed to a wide range of pO_2 making it difficult to determine the intrinsic effect of reduced pO_2 on insulin secretion by β-cells.

If pO_2 gradients were, in fact, responsible for a significant portion of the oxygen sensitivity measured in intact islets, then insulin secretion by single islet cells or small cell aggregates should be significantly less sensitive to hypoxic perfusate pO_2. Theoretically, perifusion of dispersed single islet cells would completely eliminate internal islet diffusion gradients and would also minimize gradients in the surrounding solution, thereby allowing measurement of intrinsic cellular kinetics. However, the glucose-stimulated insulin secretion rate of single islet cells is compromised to such a degree (Krause, Puchinger, and Wacker 1973; Halbon et al, 1982; Pipeleers et al, 1982; Pipeleers 1984; Weir et al, 1986) that it would be extremely difficult to measure its response to changes in the surrounding pO_2. Upon limited reaggregation, small clusters of islet cells regain their glucose responsiveness (Pipeleers et al, 1982; Chertow et al, 1983; Weir et al, 1984; Pipeleers et al, 1985) making them a useful tissue source for in vitro insulin secretion studies and possible in vivo transplantation. The small size of these cell aggregates should provide limited diffusional resistance to oxygen transport as compared to that of intact islets, and measurements made with aggregates should more closely approximate the intrinsic kinetics of dispersed β-cells.

In this paper, we report the effect of reductions in the bulk perfusate pO_2 on the glucose-stimulated insulin secretion rate from small perifused islet cell aggregates. The degree of reduction in secretory response and its dependence on perfusate pO_2 is quantified. As with intact islets, decreased levels of pO_2 reduce the insulin secretion rate from islet cell aggregates in graded fashion. However, sensitivity of insulin secretion rate to hypoxia is much lower with islet cell aggregates than that observed with intact islets. This phenomena is important in understanding and designing in vivo and in vitro systems that avoid oxygen limited secretion regimes and in understanding the effect of reduced oxygen levels on glucose induced insulin secretion at a cellular level.

MATERIALS AND METHODS

Isolation and Preparation of Islets, Single Cells, and Cell Aggregates. Islets of Langerhans were isolated from 200 - 350 g male Sprague-Dawley rats (Charles River Lab, Kingston, NJ) using a modified collagenase digestion / ficoll purification technique (Lacy and Kostianovsky, 1967; Scharp et al, 1980) which has previously been described (Dionne et al., 1989-2 and 1989-3). Briefly, the pancreas was distended in situ by injecting 10-15 ml of ice cold Hanks solution without Ca^{++}, Mg^{++} (H2387 Sigma Chemical Co., St Louis MO) containing 1.7 mg/ml collagenase (108 8882 Boehringer Mannheim, Indianapolis, IN). The distended pancreas was dissected free and digested under mild agitation at 37°C until the islets were free of acinar tissue as ascertained by microscopic examination. The slurry was then rinsed and purified by centrifugation on a discontinuous ficoll gradient. Separated islets were washed four times in Dulbecco's modified Eagles Medium (DMEM, D5523, Sigma Chemical Co.) with 10% (v/v) newborn calf serum (NBCS, 200-6010AJ, GIBCO), handpicked to remove remaining acinar contamination, and cultured in non-attaching petri dishes (8-757-12, Fisher Scientific Co, Pittsburgh PA) in DMEM with 10% NBS and 5.6 mM (100 mg/dl) glucose. Islets in petri dishes were cultured at 37°C under a 5% CO_2 / 95% air atmosphere.

Canine islets were isolated using a modification of standard collagenase digestion / ficoll purification techniques by Biohybrid Technologies, Shrewsbury MA and generously

donated by Dr. William Chick for these studies. Canine islets were received in and cultured in M-199 with Earle's salts (400-1100, GIBCO, Grand Island, NY) containing 11.2 mM glucose and 10% (v/v) fetal bovine serum (GIBCO) and were cultured at 37°C under 5% CO_2/95% air.

Slurries of single rat or canine islet cells were prepared from purified whole islets by digesting with trypsin (Pipeleers et al, 1982 and 1985; Halban et al, 1982; Dionne et al., 1989-6). Briefly, 500-1000 purified islets were rinsed three times by centrifugation at 100 x g in 50 ml Hanks solution containing 1mM ethylenedinitrilo-tetraacetic acid (EDTA, J.T. Baker Chemical Co, Phillipsburg, NJ). Following the final rinse, islets were resuspended in five ml / 1000 islets of the same solution in a polypropylene tube and gently agitated by aspiration and expulsion with a 200 μl pipette for eight min at room temperature, after which, 0.5 g/l trypsin (610 5305 GIBCO) and 25 μg/ml Dnase (10 159, Boehringer Mannheim, Indianapolis, IN), both in phosphate-buffered saline, were added to a final concentration of 25 μg/ml and 2 μg/ml, respectively. The tube was placed in a 30-32°C waterbath and islets were digested with digestion agitation by the pipette for approximately 10 min to produce a suspension of single cells. In experiments in which cells were to be allowed to reaggregate, digestion was continued until microscopic examination indicated that greater than 80% of the population represented single cells with the remaining fraction consisting of aggregates composed of two or three cells. At this point, the digestion was halted by adding ice cold DMEM. The slurry was centrifuged at 250xg for 6 min to form a cell pellet which was resuspended in DMEM with 10% NBCS and 5.6 mM glucose. The concentration and viability (by trypan blue exclusion) of single cells were determined by counting a sample of the cell slurry using a hemacytometer (Reichart Scientific Instruments, Buffalo NY). The cell slurry was then diluted with DMEM and aspirated into microbiological petri dishes (8-757-12, Fisher Scientific Co; 15 ml medium per 8.5 cm diameter dish) at a cell density of approximately 15 - 20,000 cells/cm^2, corresponding to 2-3% area coverage. Cells spontaneously reaggregated during normal static culture in Petri dishes to form small cell clusters. The number of cells in a cluster and the overall size of the cell aggregate was roughly controlled by adjusting the cell

density and the time of culture. With seeding densities in the range of 15- 20,000 cells / cm^2 surface area, the majority of cells formed small aggregates of 5 - 30 cells over a 1 - 3 day culture period.

Rat islet cells were allowed to reaggregate for 18 to 30 hr (one day) before they were perifused. Because a portion of the aggregates from trypsinized canine cell preparations was first used to measure aggregate oxygen uptake (Dionne et al., 1989-6), canine cells were cultured for a longer period (3 to 4 days) between the trypsinization and perifusion.

The size of the cell aggregates was determined by photographing an aggregate sample under a microscope. The photomicrographs were later projected onto a screen along with a calibrated reticule for sizing. The cell aggregates were individually sized in terms of the average number of cells per aggregate and the aggregate diffusion diameter (ADD), defined as the characteristic cross sectional diameter through which a solute would have to diffuse to reach all portions of the aggregate. For a spherical cell aggregate, the ADD was equal to the diameter. For a linear or branched chain, the ADD was equal to the diameter of the thickest section of the chain.

Single Cell and Aggregate Perifusions. The design, construction, and characterization of the oxygen regulated, micro-perifusion system has previously been described (Dionne, Colton, and Yarmush, 1989-pits). The system provided for temperature and gas control and was suitable for studying very small volumes of tissue. Cells or aggregates were loaded into a tissue chamber where they were perifused by the perfusate flowing over them. The pO_2 and pH of the perfusate were monitored by in-line probes. Exiting perfusate was collected in a fraction collector for later glucose (Beckman Glucose Analyzer II, Beckman Instruments, Brea CA) and insulin (radioimmunoassay; Dionne et al., 1989-2) analysis.

At a perfusate flowrate of 0.5 ml/min, 50% of a change in perfusate glucose concentration reached the outlet 22 sec after the switch was made and 100% was attained in under one min. A switch in gas pO_2 settings from a normoxic (142 mmHg) to a hypoxic (2-

25 mmHg) level required an average of 2.2 min to reach 50% of steady state in the perfusate and 4.1 min to reach 90% (Dionne et al., 1989-2).

Temperature was maintained at 37 ± 0.3 °C. The perifusate was DMEM with 10% NBCS, 50 μU/ml penicillin, and 50 μg/ml streptomycin (600 5140, GIBCO). Glucose concentration was 5.6 mM (100 mg/dl; basal) or 16.7 mM (300 mg/dl; stimulated). A perfusate flow of 0.5 ml/min resulted in a superficial fluid velocity of 0.5 cm/sec relative to the cell aggregates. Perfusate pH was maintained at 7.45 . Normoxic perfusate pO_2 was 142 mm Hg (humidified 5.3% CO_2 and 94.7% air). Hypoxic perfusate pO_2 ranged from 0 to 20 mm Hg. Normally 0.1 to 0.2 mm^3 of aggregates (1-2 x 10^5 cells, average cell diameter = 14.4 μm; Dionne et al., 1989-6) were used in each perifusion. For these loading conditions, the basal insulin concentration in the outlet media ranged between 5 - 15 μU/ml, whereas the glucose stimulated insulin concentration rose to between 30 - 60 μU/ml. The insulin secretion rate, S, per unit volume of tissue, V_t, was calculated from the measured insulin concentration [I] in each sample according to

$$S = \frac{Q\,[I]}{V_t} \qquad (1)$$

where Q is the perfusate flowrate.

The perfusion protocol was similar to that previously employed with intact islets (Dionne et al., 1989-3). After loading into the tissue perifusion chamber, aggregates were perfused with basal medium for 60 to 90 min in order to allow the cells to adjust to the perifusion conditions and to wash out insulin released as a result of handling procedures. Perfusate was collected for analysis of basal secretion, beginning 15 min before the perfusate glucose concentration was raised to 16.7 mM at time t=0. To investigate the effect of hypoxia, perfusate pO_2 was dropped to the test level after 40-60 min of glucose stimulated normoxic secretion. Aggregates were perifused at each hypoxic pO_2 for 30 - 40 min. Following one or more hypoxic steps, the perfusate pO_2 was raised to 142 mm Hg to test if the effect of hypoxia on insulin secretion was reversible. Perfusate fractions were collected over 2 min intervals from t=0-6 min and over 4 min intervals thereafter. All insulin secretion

data is plotted at the midpoint of the time period over which each fraction was collected. The relative effect of the hypoxic pO_2 on insulin secretion from the perifused tissue was quantified in terms of the ratio of the hypoxic insulin secretion rate, S_x, at pO_2 = x mm Hg (averaged over the final 12 min of the hypoxic period), divided by the normoxic insulin secretion rate, S_{142}, at pO_2 = 142 mm Hg (averaged over the 12 min period of normoxic secretion immediately preceding the hypoxic period).

RESULTS

Tissue Characterization. Figure 1 shows a series of photomicrographs which illustrate the aggregation state of canine islet cells following various periods of culture. Panel A shows a photograph taken 30 min after trypsinization. At the high cell density shown (about 10% area coverage, trypsinized cells had already begun to aggregate together, although they were easily separated by mild agitation. Following 18 hr of culture (panel B), the majority of cells had fused together to form aggregates composed of loose cell clusters and short branched chains. After four days of culture (panel C), branched cell chains had largely collapsed to form more tightly knit clusters, and after two weeks (panel D) these clusters had fused into small, compact spheroids.

Figure 2 contains photomicrographs of rat and canine aggregates taken at higher magnifications immediately prior to perifusion. Rat aggregates (panel A and B) were generally composed of more long branched cell chains than were canine aggregates (panel C and D) which consisted of more tightly packed cell clusters. The primary reason for this difference was the longer period of time that canine cells were cultured before perifusion as compared to rat cells (three verses one day), since both rat and canine cells passed through similar stages of reaggregation illustrated in Figure 1. Higher magnifications (panels B and D) show that the surfaces of cells within aggregates were in close apposition to one another after both one and four days of culture. The absence of staining on exposure to trypan blue dye (panels B and D) indicated that almost 100% of the cells in aggregates were viable.

Figure 3 illustrates the average size distribution of rat and canine islet cell aggregates in representative preparations immediately prior to perifusion. In both cases, approximately 30% of the total number of identifiable particles were non-aggregated single cells which accounted for less than five percent of the total cell volume. The majority of both rat (70%) and canine (74%) islet cells were located in aggregates containing from 6 to 30 cells. By comparison, a 200 μm diameter i..tact islet contains about 1800 cells. The volume fraction-weighted average number of cells was 17 and 20 for rat and canine aggregates, respectively. Aggregates were also sized according to their average aggregate diffusion diameter (ADD) for oxygen uptake experiments reported elsewhere (Dionne et al., 1989-6). The average volume fraction-weighted ADD of one-day old aggregate preparations was 39 μm for rat and 35 μm for canine aggregate preparations. For comparison, the volume-fraction weighted average diameter of an assorted, intact rat islet preparation was 214 μm.

Effect of Reduced pO_2 on Insulin Secretion. Non-aggregated single islet cells pose the least diffusion resistance to oxygen transport and theoretically should provide data that is most representative of intrinsic cellular secretion kinetics. Therefore, dispersed single islet cells were perifused immediately following trypsinization or after 24 hr culture under very dilute conditions in order to prevent cell aggregation. Results of several representative perifusions are shown in Figure 4. Freshly trypsinized cells (bottom panel) released insulin at very low rates (2 - 40 μU/min-mm^3 cells) and did not respond to glucose stimulation with a significant elevation of insulin secretion rate. Single cells cultured for 24 hr after isolation (top) had much higher basal insulin secretion rate (250 - 800 μU/min-mm^3 cells). These cells also displayed a measurable first phase insulin secretion spike upon stimulation with 16.7 mM glucose. However second phase secretion rate was neither stable nor significantly elevated above the basal rate. The absence of a second phase response to a glucose challenge and the elevated basal release rates indicate that dispersed single islet cells do not exhibit normal glucose-regulated insulin secretion.

Cell aggregates displayed secretion profiles qualitatively similar to those seen with intact islets (Dionne et al., 1989-3). The upper panel of Figure 5 shows insulin secretion from perifused rat islet cell aggregates under normoxic (142 mm Hg) conditions. Basal insulin secretion rate was about 200 $\mu U/min \cdot mm^3$ cells. Following glucose stimulation at t=0, a well-defined first phase insulin secretion spike occurred, followed by steadily increasing second phase secretion that reached a plateau 40-60 min after the onset of the glucose challenge. Second phase secretion rate remained elevated throughout the period of elevated glucose concentration and then fell when the perfusate glucose concentration was switched back to basal conditions, confirming that the elevated insulin secretion rate was glucose regulated.

Results in the lower panel of Figure 5 illustrate the effect of hypoxia on second phase insulin secretion rate from islet cell aggregates taken from the same cell preparation as were the aggregates used in the normoxic perifusion shown in the upper panel. After steady second phase secretion rate was established, the perfusate pO_2 was lowered to 4 mm Hg, and insulin secretion rate decreased until it reached a steady hypoxic rate that was substantially lower than the normoxic rate. When the perfusate pO_2 was raised to 142 mm Hg, the perifused aggregates responded with a burst of insulin followed by a return to the pre-hypoxic rate of secretion.

The effect of different levels of pO_2 on the second phase insulin secretion from cell aggregates is shown in Figure 7. Aggregates in both perifusions responded similarly to glucose stimulation at t=0 with a burst of first phase secretion and then rapidly attained a steady rate of second phase secretion. After perfusate pO_2 was lowered to either 6 or 12 mm Hg, insulin secretion rate rapidly fell; the decrease was much larger for the aggregates exposed to 6 mm Hg as compared to those exposed to 12 mm Hg. Upon reoxygenation at 78 min, the aggregates in both perifusions responded with a pronounced burst of insulin that peaked at a higher level than the steady normoxic rate. Secretion then returned to a rate similar to pre-hypoxic levels.

The effect of multiple sequential hypoxic steps on second phase insulin secretion rate is shown in Figure 7 for perifused canine cell aggregates. As in Figure 6, second phase secretion was first allowed to reach a steady value under normoxic conditions. The first hypoxic step in the perfusate pO_2 was made at t=55 (upper panel) or t=44 min (lower panel). Neither 12 nor 20 mm Hg had a significant effect on the rate of second phase insulin secretion rate of the aggregate preparations. However, subsequent steps to even lower pO_2 resulted in significant reductions in second phase insulin release that were proportionate to the degree of hypoxia.

The fraction of normoxic second phase insulin secretion, S_x/S_{142}, is plotted as a function of the hypoxic perfusate pO_2 in Figure 8 from data obtained with rat and canine islet cell aggregate perifusions involving both single and multiple hypoxic step experiments. Insulin secretion rate from cell aggregates began to be reduced when the perfusate pO_2 dropped below about 20 mm Hg, reached 50% of the normoxic rate when the pO_2 dropped to 5 mm Hg (P_{50}), and was reduced to about 20% of normal at about 2 mm Hg. No significant differences were seen between rat and canine cell aggregates.

A comparison of insulin secretion from aggregated rat islet cells and intact rat islets is shown in Figure 9. The average diameter was 37 μm for the cell aggregates (upper panel) and 215 μm for the perifused islets (lower panel). The basal insulin secretion rate of cell aggregates was elevated as compared to that of intact islets (200 versus 100 $\mu U/min \cdot mm^3$ tissue). Both intact islets and cell aggregates responded to a 16.7 mM glucose challenge at t=0 with a burst of first phase insulin release. As represented by these examples, second phase normoxic secretion rate from cell aggregates attained a steady value which was usually lower than that of intact islets. At about t=60 min, the perfusate pO_2 was dropped to 15 mm Hg in both perifusions. Whereas the insulin secretion rate of intact islets rapidly fell to about one-third of the normoxic rate, the insulin secretion rate of cell aggregates was unaffected at this pO_2. A subsequent drop in perfusate pO_2 at about t=90 min resulted in a decrease in the secretion rate from cell aggregates and a further decrease in that from intact islets. The ratio S_{15}/S_{142} was 1.0 for cell aggregates and 0.57 for intact islets cultured for one week. At the

lower pO_2, S_4/S_{142} = 0.49 for rat aggregates compared to S_5/S_{142} = 0.17 for intact cultured islets. In this particular experiment, cell aggregates did not immediately respond with a reoxygenation spike of insulin secretion when the perfusate pO_2 was raised back to 142 mm Hg at the end of the hypoxic period; a reoxygenation spike was observed in about two-thirds of all the cell aggregate perifusions.

A comparison of the oxygen sensitivity of cell aggregates and intact rat islets cultured for one day after isolation is shown in Figure 10. The curve for cell aggregates is shifted to the left of that for islets, and much lower perfusate pO_2 is required to achieve the same reduction in insulin secretion rate from islet cell aggregates than for intact islets. Whereas insulin secretion from intact islets began to be affected by hypoxia when the perfusate pO_2 dropped below about 60 mm Hg, secretion from cell aggregates was not affected until the pO_2 dropped below about 20 mm Hg. P_{50} was 27 mm Hg for intact islets (210 μm average diameter) whereas P_{50} of islet cell aggregates (37 μm average diameter) was 5.0 mm Hg. In contrast, the insulin secretion rate of intact islets at 5 mm Hg was reduced to about two percent of its normoxic level.

The average diameter, normoxic insulin secretion rate (S_{142}), and P_{50} for rat and canine cell aggregates and for intact rat and canine islets are shown in Table 1. The average diameters of canine and rat islet cell aggregates were very similar (about 37 μm) and smaller than the average diameter of intact islets by a factor of about five (canine) or six (rat). The normoxic rate of second phase insulin secretion of rat and canine cell aggregates (Average = 258, range = 107 - 500 $\mu U/min \cdot mm^3$ tissue) was lower (p=0.01) than that of one-day old intact islets by a factor of two but was not statistically different (p=.05) from that of rat and canine islets cultured for one week after isolation. The P_{50} of cell aggregates (5.0 mmHg) was significantly lower than the P_{50} of rat or canine islets after either one day (27 mmHg) or one week (13-16 mmHg) of culture following isolation.

DISCUSSION

We have previously reported that second phase insulin secretion from intact islets of Langerhans isolated from rat and canine pancreata is rapidly and reversibly reduced by hypoxic perfusate pO_2 levels below about 60 mm Hg (Dionne et al., 1989-3). Based on these results, we hypothesized the existence of significant pO_2 gradients within the islets and in the boundary layer of medium immediately surrounding the perifused islets. In order to test this hypothesis, we measured the effect of hypoxic pO_2 on second phase insulin secretion from perifused islet cell aggregates whose small size significantly diminished both internal and external oxygen gradients.

Single Islet Cells. We initially carried out perifusions of dispersed, single islet cells which would directly allow the measurement of the effect of pO_2 on β-cell insulin secretion. However, glucose-stimulated insulin secretion from non-aggregated, dispersed islet cells was drastically reduced from that of intact islets and of the islet cell aggregate preparations which we subsequently investigated. This finding is consistent with previous reports that glucose-stimulated insulin secretion is completely lacking (Krause, Puchinger, and Wacker 1973; Weir et al, 1986) or seriously deficient (Halban et al, 1982; Pipeleers et al, 1982; Pipeleers 1984) with single islet cells. In contrast, the use of aggregated islet cells has been reported to increase the β-cell insulin secretion in response to a glucose challenge compared to basal levels (Pipeleers et al, 1982; Halban et al, 1982; Chertow et al, 1983; Weir et al, 1984; Shizuru, Trager, and Merrell 1985; Pipeleers et al, 1985). In the only other study comparing insulin secretion from dispersed and aggregated islet cells, Pipeleers reported that slurries of β-cells (90% pure, >70% single cells) isolated from rat islets secreted about three percent as much second phase insulin as did the same number of β-cells situated in intact islets. When more than 65% of the β-cells were aggregated in 2-10 cell clusters, insulin secretion was four times greater than with single cells (Pipeleers et al, 1982). In the former experiments, a sizable fraction (~30%) of the β-cells were actually in small 2-4 cell aggregates, and it is possible that these aggregates were responsible for most of the reported glucose-stimulated insulin

secretion from single cells. In other studies which reported a decreased but measurable level of glucose induced secretion from dispersed single cells, the presence of some small aggregates may also be responsible for much of the observed secretion (Ono, Takaki, and Fukuma 1977; Chertow et al, 1983). Experiments in which insulin secretion from dispersed cells is measured using static culture techniques must be evaluated in light of the report by Weir et al, (1986) that cell handling artifacts caused 90+% of the insulin measured in their 90-min static tests to be released in the first 5 min, indicating that the vast majority of their reported insulin release was not glucose induced.

Islet Cell Aggregates. In the absence of glucose-stimulated second phase secretion from dispersed single islet cells, the closest approximation to intrinsic cellular kinetics was obtained by perifusing small, loosely aggregated cell clusters whose average diameter was about 2.5 times larger than that of an individual β-cell. These small aggregates displayed an insulin secretion profile that was qualitatively similar to that observed with perifused intact islets (Dionne et al., 1989-3) although it differed quantitatively in several respects. Basal release of insulin from cell aggregates was generally elevated as compared to release from intact islets. Both aggregates and islets responded to a step increase in perfusate glucose concentration from 5.6 to 16.7 mM with a first phase spike of insulin secretion. The peak first phase secretion rate was usually larger, relative to the subsequent second phase secretion rate, for cell aggregates than for intact islets. Second phase secretion rate from both types of tissue was elevated above basal levels but was higher, in terms of both absolute magnitude and in relation to basal levels, from intact islets cultured for one day after isolation. Hypoxia rapidly reduced second phase insulin secretion rate from both aggregates and intact islets. Following a return to normoxic pO_2, both types of tissue usually produced a burst of insulin secretion and then attained a post-hypoxic secretory rate similar in magnitude to their pre-hypoxic rate. Recovery of post-hypoxic secretion was slowed and sometimes not seen during the period over which samples were collected following perifusion at very low pO_2. The lack

of recovery of normoxic secretion rate upon reoxygenation was observed more frequently with cell aggregates than with intact islets.

Size Dependence of Oxygen Sensitivity. Although hypoxia reduced glucose-stimulated second phase insulin secretion from both cell aggregates and intact islets, much lower perfusate pO_2 levels were required to suppress cell aggregate secretion than were required to similarly limit secretion from intact islets. Secretion from intact, 210 μm diameter rat islets tested one day after isolation began to be compromised at a perfusate pO_2 below about 60 mm Hg, whereas secretion from 37 μm diameter cell aggregates tested one day after isolation and trypsinization was not affected until the perfusate pO_2 fell below about 20 mm Hg. Secretion from intact islets was reduced to 50% of the normoxic rate at a perfusate pO_2 of 27 mm Hg, whereas the P_{50} of cell aggregates was 5 mm Hg. The lowest perfusate pO_2 tested on one-day old intact islets was 5 mm Hg which reduced their secretion to less than 2% of their normoxic rate. The lowest pO_2 tested on cell aggregates was 2 mm Hg which reduced secretion to 20% of their normoxic rate.

The difference in the hypoxic sensitivity of cell aggregates and intact islets can be understood as a result of differences in their respective sizes. Whereas the average diameter of handpicked, intact, perifused rat and canine islets was between 175-215 μm, the average diameter of rat and canine islet cell aggregate preparations was approximately 36 μm. This size difference results in larger pO_2 diffusion gradients in the medium around the perifused tissue and throughout the tissue itself with intact islets as compared to cell aggregates. As a result of these larger diffusion gradients, the pO_2 actually seen by the insulin secreting β-cells at any given perfusate pO_2 will be lower for β-cells located in large intact islets than for β-cells located in cell aggregates.

Even in a perifusion system with a relatively high perfusate velocity, a thin boundary layer surrounds the perifused tissue. Oxygen required for cell metabolism must diffuse through this boundary layer from the bulk perfusate to reach the respiring tissue. In order to drive oxygen across this layer, an oxygen gradient must be established from the bulk

perifusate to the surface of the aggregate or islet tissue (Franko and Freedman, 1984). This gradient results in the pO_2 at the tissue surface being lower than the pO_2 measured in the bulk perfusate. The magnitude of the pO_2 drop across the external fluid layer is a function of the perfusate velocity, oxygen uptake rate, oxygen diffusivity in the medium, and the size or diameter of the perifused tissue. Thus, even if both islets and aggregates are perifused with identical perfusate flowrates, the pO_2 drop across the boundary layer is larger for large intact islets than for small cell aggregates. A mathematical model developed to describe this process indicates that for the perifusion flow conditions pertaining to the experiments described in this paper, the pO_2 drop across the boundary layer is approximately 5.6 mm Hg for 210 μm diameter islets and 0.2 mm Hg for 37 μm diameter cell aggregates when they are each fully respiring under glucose-stimulated conditions (Dionne et al., 1989-7 and 1989-8). The oxygen uptake of the perifused tissue is reduced as the perfusate pO_2 is lowered, and the magnitude of the pO_2 drop in the boundary layer decreases for both islets and cells in proportion to the decrease in the oxygen uptake of the tissue. For example, when the perfusate pO_2 is reduced to the point at which tissue oxygen consumption is one-half of normal, the boundary layer pO_2 drop would be 2.8 and 0.1 mm Hg for 210 μm diameter islets and 37 μm diameter cell aggregates, respectively. In summary, the pO_2 that the islet or aggregate surface is actually exposed to is lower than the pO_2 measured in the bulk perfusate because of the need for oxygen to diffuse to the tissue surface through a thin layer of fluid immediately surrounding the perifused tissue. This pO_2 drop can be decreased, but not eliminated, by increasing the perifusion velocity. However, the need to reduce perfusate volume to prevent dilution of secretion products and the danger of hydrodynamic cell shearing place practical limits on high perifusion velocities.

In addition to having a larger pO_2 drop across the perfusate boundary layer, the larger size of intact islets also causes a larger internal pO_2 gradient to form within the tissue. Oxygen must diffuse from the islet surface through the interior of the islet to supply the β-cells which are primarily located in the islet core (Orci, 1976). A large diffusion gradient results from the surface to the core, and the pO_2 at the islet core may be much lower than at

the islet surface. Because the diffusion distance is much shorter for small cell aggregates, the decrease in pO_2 from the surface to the core is much smaller for aggregates than for intact islets (Dionne, 1989-thesis). If the β-cells of the islet or aggregate individually respond to hypoxia according to the local pO_2 to which each cell is exposed, then the relatively more oxygenated β-cells in the periphery of both islets and aggregates will secrete at a higher fraction of their normoxic rate than will the relatively less oxygenated β-cells located at the tissue core. In the case of intact islets, the overall oxygen sensitivity observed reflects the radial pO_2 gradient and the wide range of actual secretion rates from β-cells located throughout the islet. Therefore, although the results for intact islets in Figure 11 are representative of the islet as a physiological unit, they do not represent the intrinsic oxygen sensitivity of any particular β-cells within the islet. The same argument is true for cell aggregates. However, because the average aggregate diameter was only 2.5 times that of a single islet cell (36 μm versus 14.4 μm), both the pO_2 drop from the aggregate surface to the core and the range of pO_2 seen by β-cells located throughout the aggregate will be much smaller. Therefore, the results from cell aggregates in Figure 11 provide an upper bound and a much closer estimate of the intrinsic oxygen sensitivity of β-cell insulin secretion to hypoxic pO_2 levels.

The existence of internal and external gradients and the possibility of non-secreting islet cores should be considered in the design of <u>in vitro</u> culture and non-vascularized immuno-isolation systems where diffusion-restricted conditions may threaten islet core viability or limit glucose-stimulated insulin secretion.

Mechanism of Oxygen Sensitivity. Recent data on the oxygen uptake rate of rat and canine islet cell aggregates can be fitted to a Michaelis-Menten kinetic expression for oxygen consumption with P_{50} (or apparent Km) averaging 1.12 mm Hg (Dionne, 1989-6). This value is about one-fifth of the estimate of P_{50} (5.0 mm Hg) for the dependence of second phase insulin secretion rate on pO_2 obtained with all aggregates in this study. It is unlikely that this significant difference can be accounted for on the basis of different magnitudes of pO_2

gradients present during the two measurements (Dionne, 1989). The larger value indicates that insulin secretion is much more sensitive to low pO_2 than is oxygen uptake. For example, at pO_2 = 5.0 mm Hg, where insulin secretion is reduced to 50% of its normoxic value, aggregate oxygen uptake would be 82% of its maximum value.

Although insulin secretion has a higher effective value of P_{50} than does oxygen uptake itself, the pO_2 range over which insulin secretion is affected by hypoxia nonetheless overlaps the range in which oxygen uptake begins to be reduced. Small decreases in oxygen consumption have been associated with changes in the cellular ratio of high energy to low energy metabolites such as the ATP/ADP ratio (Wilson et al, 1988). It has been suggested that small changes in these ratios can affect fuel induced insulin secretion (Randle and Hales 1972; Trus, Warner and Matschinsky 1980; Cook and Hales 1984; Corkey et al, 1988; Cook et al, 1988; Misler et al, 1989). Therefore, the effect of hypoxia on β-cell insulin secretion may be mediated by a hypoxia-induced lowering of the metabolic energy state of the β-cell.

In our previous study with islets (Dionne et al., 1989-2), we found that insulin secretion rate was affected within one min following a change in perfusate pO_2 to or from hypoxic levels. The rapidity with which insulin secretion is reduced or restored following changes in perfusate pO_2 suggests that the rate limiting step of hypoxia reduced insulin secretion occurs during the exocytotic release of insulin. Although hypoxia may also affect the rate of insulin biosynthesis, the processing of secretion vesicles in the golgi apparatus, or the initial stages of vesicle transport to the cell membrane, changes in the rate at which these steps occur, could not account for the rapidity with which hypoxia affects insulin secretion rate (Steiner et al, 1974). As in the case of intact islets (Dionne et al. 1989-3), the immediate spike of insulin often observed in the first sample collected following the reoxygenation of perifused aggregates suggests the possibility that some earlier stages of insulin biosynthesis and/or secretion may be less affected by hypoxia than is the actual exocytotic release of insulin, resulting in an accumulation of secretable insulin behind the rate limiting step.

Possible mechanisms by which hypoxia may limit the exocytosis of insulin include (1) reducing the cellular concentration of ATP which may inhibit membrane depolarization by

opening ATP gated K^+ channels (Cook and Hales 1984; Cook et al, 1988; Misler et al, 1989) or limiting the energy dependent transport of secretion vesicles along microtubules to the cell membrane where they are positioned for membrane fusing (De Lisle and Williams 1986; Sheetz et al, 1987); (2) shutdown of an as of yet unidentified oxygen- or ATP phosphorylation-dependent enzymatic reaction required for secretion (Knight and Barker 1987); or (3) lowering of the cellular ATP/ADP ratio which may affect a large number of cell functions through secondary messenger action (Randle and Hales 1972; Trus, Warner, and Matschinsky 1980; Wilson et al, 1988). Regardless of the mechanism, it appears possible to create hypoxic conditions under which β-cells maintain their viability but are unable to respond to a glucose challenge with normal insulin secretion. The higher hypoxic sensitivity of insulin secretion compared to oxygen uptake may be viewed as a built-in defense mechanism by which a metabolically threatened β-cell acts to reduce its energy expenditure in order to better survive the hypoxic threat (Hochachka 1986).

REFERENCES

Bonner-Weir, S, and Orci, S. (1982). New Perspectives on the Microvascular of the Islets of Langerhans in the Rat. Diabetes 31: 883-889.

Bonner-Weir, S. (1984) Morphological Evidence for β-cell Polarity Within the Islet of Langerhans in the Rat. Diabetes 33 (Suppl. 1): 81A.

Brian, P.L.T, and Hales, H.B. (1969) Effects of Transpiration and Changing Diameter on Heat and Mass Transfer to Spheres. A.I.Ch.E. J 15:419-425.

Brian, P.L.T, and Hales, H.B, and Sherwood, T.K. (1969) Transport of Heat and Mass Between Liquids and Spherical Particles in an Agitated Tank. A.I.Ch.E. J: 727-733.

Chertow, B.S, Baranetsky, N.G, Sivitz, W.I, Meda, P, Webb, M.D, and Shih, J.C. (1983) Cellular Mechanisms of Insulin Release: Effects of retinoids on rat islet cell-to-cell adhesion, reaggregation, and insulin release. Diabetes 32: 568-574.

Cook, D.L, and Hales, C.N. (1984) Intracellular ATP Directly Blocks K^+ Channels in Pancreatic β-Cells. Nature 311: 271-273.

Cook, D.L, Satin, L.S, Ashford, M.L.J, and Hales C.N. (1988) ATP-Sensitive K^+ Channels in Pancreatic β-Cells: Spare-Channel Hypothesis. Diabetes 37: 495-498.

Corkey, B.E, Deeney, J.T, Glennon, M.C, Matschinsky, F.M, and Prentki, M. (1988) Regulation of Steady-State Free Ca^{2+} Levels by the ATP/ADP Ratio and Orthophosphate in Permeabilized RINm5F Insulinoma Cells. J Biol Chem 263: 4247-4253.

De Lisle, R.C, and Williams, J.A. (1986) Regulation of Membrane Fusion in Secretory Exocytosis. Ann Rev Physiol 48: 225-238.

Dionne, K.D, Colton, C.K, and Yarmush, M.L. (1989) Effect of Oxygen on Isolated Pancreatic Tissue. A.S.A.I.O Transactions (submitted).

Dionne, K.E. (1989) Effect of oxygen on insulin secretion and viability of pancreatic islet tissue. (Ph.D. Thesis), Department of Chemical Engineering, Massachusetts Institute of Technology, Cambridge MA.

Dionne, K.E, Colton, C.K, and Yarmush, M.L. (1989-2) A Micro-Perifusion System with Environmental Control for Islet Insulin Secretion Studies. (Ph.D. Thesis, Chapter 2).

Dionne, K.E, Colton, C.K, and Yarmush, M.L. (1989-3) Effect of Hypoxia on Insulin Secretion by Isolated Rat and Canine Islets of Langerhans. (Ph.D. Thesis, Chapter 3).

Dionne, K.E, Colton, C.K, and Yarmush, M.L. (1989-7) Extraction of the intra-cellular and intra-islet oxyen diffusivity from experimental measurements of tissue oxygen uptake. (Ph.D. Thesis, Chapter 7).

Dionne, K.E, Colton, C.K, and Yarmush, M.L. (1989-8) Mathematical modeling of pO_2 profiles, O_2 consumption, and insulin secretion in isolated and immuno-isolated islets of Langerhans. (Ph.D. Thesis, Chapter 8).

Franko, A.J, and Freedman, H.I. (1984) Model of Diffusion of Oxygen to Spheroids Grown in Stationary Medium I. Complete Spherical Symmetry. Bull Mathematical Biology 46: 205-217.

Halban, P.A, Wollheim, C.B, Blondel, B, Meda, P, Niesor, E.N, and Mintz, D.H. (1982) The Possible Importance of Contact Between Pancreatic Islet Cells for the Control of Insulin Release. Endocrinology 111: 86-94.

Hochachka, P.W. (1986) Defense Strategies Against Hypoxia and Hypothermia. Science 231: 234-241.

Knight, D.E, and Baker, P.F. (1987) Exocytosis from the Vesicle Viewpoint: An overview. (Part VI. Exocytosis from the Perspective of the Secretory Vesicle; ed. Johnson, R.G.) Ann NY Acad Science 493: 504 - 522.

Krause, U, Puchinger, H, and Wacker, A. (1973) Inhibition of Glucose-induced Insulin Secretion in Trypsin-treated islets of Langerhans. Horm Metab Res 5:325.

Lacy, P.E. and Kostianovsky, M. (1967) Meithod for the Isolation of Intact Islets of Langerhans from the Rat Pancreas. Diabetes 16: 35-39.

Lifson, N, Kramlinger, K.G, Mayrand, F.F, and Lender, E.J. (1980) Blood flow to the Rabbit Pancreas with Special Reference to the Islets of Langerhans. Gastroenterology 79: 466-473.

Misler, S, Gee, W. M, Gillis, K.D, Scharp, D.W, and Falke, L,C. (1989) Metabolite-Regulated ATP-Sensitive K^+ Channel in Human Pancreatic Islet Cells. Diabetes 38: 422-427.

Ono, J, Takaki, R, and Fukuma, M. (1977) Preparation of Single Cells from Pancreatic Islets of Adult Rat by the Use of Dispase. Endocrinol Japon 24: 265-270.

Orci, L. (1976) The Microanatomy of the Islets of Langerhans. Metabolism 25: 1303.

Pipeleers, D, In't Veld, P, Maes, E, and Van De Winkel, M. (1982) Glucose-Induced Insulin Release Depends on Functional Cooperation Between Islet Cells. (Proc Natl Acad Sci 79: (USA) 7322-325.

Pipeleers, D. (1984) Islet Cell Interactions with Pancreatic β-Cells. Experientia 40: 1114-1126.

Pipeleers, D, In't Veld, P, Van De Winkel, M, Maes, E, Schuit, F.C, and Gepts, W. (1985) A New *in Vitro* Model for the Study of Pancreatic A and B Cells. Endocrinology 117: 806-816.

Pipeleers, D, Schuit, F.C, In't Veld, P, Maes, E, Hooghe-Peters, E.L, Van De Winkel, M, and Gepts, W. (1985a) Interplay of Nutrients and Hormones in the Regulation of Insulin Release. Endocrinology 117: 824-833.

Randle, P.J, and Hales, C.N. (1972) Insulin Release Mechanisms in *Handbook of Physiology: Endocrinology I* (Chapter 13, pp. 219 - 35); Greep, R.O, and Astwood, E.B. (eds), American Physiological Society, Washington D.C.

Scharp, D.W, Downing, R, Merrel, R.C, and Greider, M. (1980) Isolating the Elusive Islet. Diabetes 29 (Suppl.1): 19-30.

Sheetz, M.P, Vale, R, Schnapp, B, Schroer, T, and Reese, T. (1987) Movements of Vesicles on Microtubules. Ann NY Acad Science 493: 409-416.

Shizuru, J, Trager, D, and Merrell, R.C. (1985) Structure, Function, and Immune Properties of Reassociated Islets Cells. Diabetes 34: 898-903.

Steiner, D.F, Kemmler,W, Tager, H.S, and Peterson, J.D. (1974) Proteolytic Processing in the Biosynthesis of Insulin and Other Proteins. Federation Proc. 33: 2105-115.

Trus, M, Warner, H, and Matschinsky, F. (1980) Effects of Glucose on Insulin Release and on Intermediary Metabolism of Isolated Perifused Pancreatic Islets from Fed and Fasted Rats. Diabetes 29: 1-14.

Weir, G.C, Halban, P.A, Meda, P, Wollheim, C.B, Orci, L, and Renold, A.E. (1984) Dispersed Adult Rat Pancreatic Islet Cells in Culture: α, β, and δ Cell Function. Metabolism 33: 447-453.

Weir, G.C, Leahy, J.L, Barras, E, and Braunstein, L.P. (1986) Characteristics of Insulin and Glucagon Release from the Perfused Pancreas, Intact Isolated Islets, and Dispersed Islet Cells. Hormone Res 24: 62-72.

Wilson, D.F, Rumsey, W.L, Green, T.J, and Vanderkooi, J.M. (1988) The Oxygen Dependence of Mitochondrial Oxidative Phosphorylation Measured by a New Optical Method for Measuring Oxygen Concentration. J Biol Chem 263: 2712-718.

Table 1. Average Diameter, Normoxic Secretion Rate, and P_{50} for Insulin Secretion by Intact Islets and Islet Cell Aggregates.

Species	Type	Culture Time	Average Diameter (μm)	Secretion Rate, S_{142} (μU/min·mm^3 tissue)	(n)	P_{50} (mmHg)
Rat	Aggregate	1 Day	39 ± 8.5	240 ± 100	(9)	5.0
Canine	Aggregate	3 Days	35 ± 9.0	210 ± 150	(6)	
Rat	Islets*	1 Day	214 ± 14	550 ± 250	(24)	27
Rat	Islets*	1 Week	210 ± 13	320 ± 170	(15)	13
Canine	Islets*	1 Week	174 ± 10	290 ± 160	(10)	16

*Dionne et al., 1989-3.

A.
B.
C.
D.
100μm

FIGURE 1. Photomicrographs of reaggregated canine islet cells following different culture time periods. (A) Cells at a surface concentration of about 10% area coverage, 30 min after trypsinization. After cell counting, the preparation was diluted to approximately 3% (by area) and cultured in static petri dish culture. (B), (C), and (D) illustrate the degree of aggregation following 18 hr, four days, and two weeks of culture, respectively.

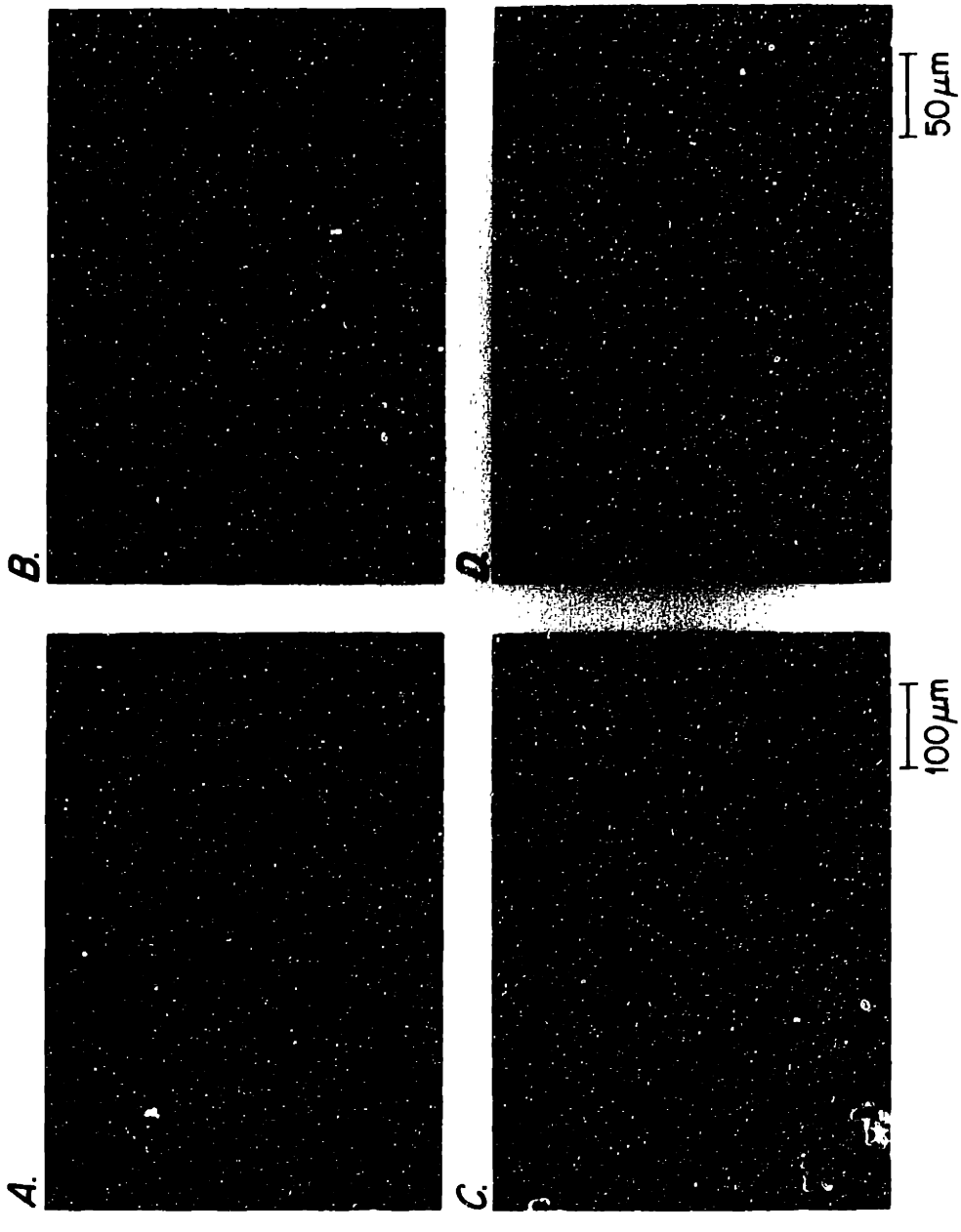
A.
B.
C.
D.
100μm
50μm

FIGURE 2. Photomicrographs of aggregated rat (A and B) and canine (C and D) islet cells immediately prior to perifusion following one day (rat) and four days (canine) of culture. Aggregates shown in panels B and D were stained with 1% trypan blue solution which indicated that greater than 70% of single non-aggregated cells and close to 100% of all reaggregated cells were viable.

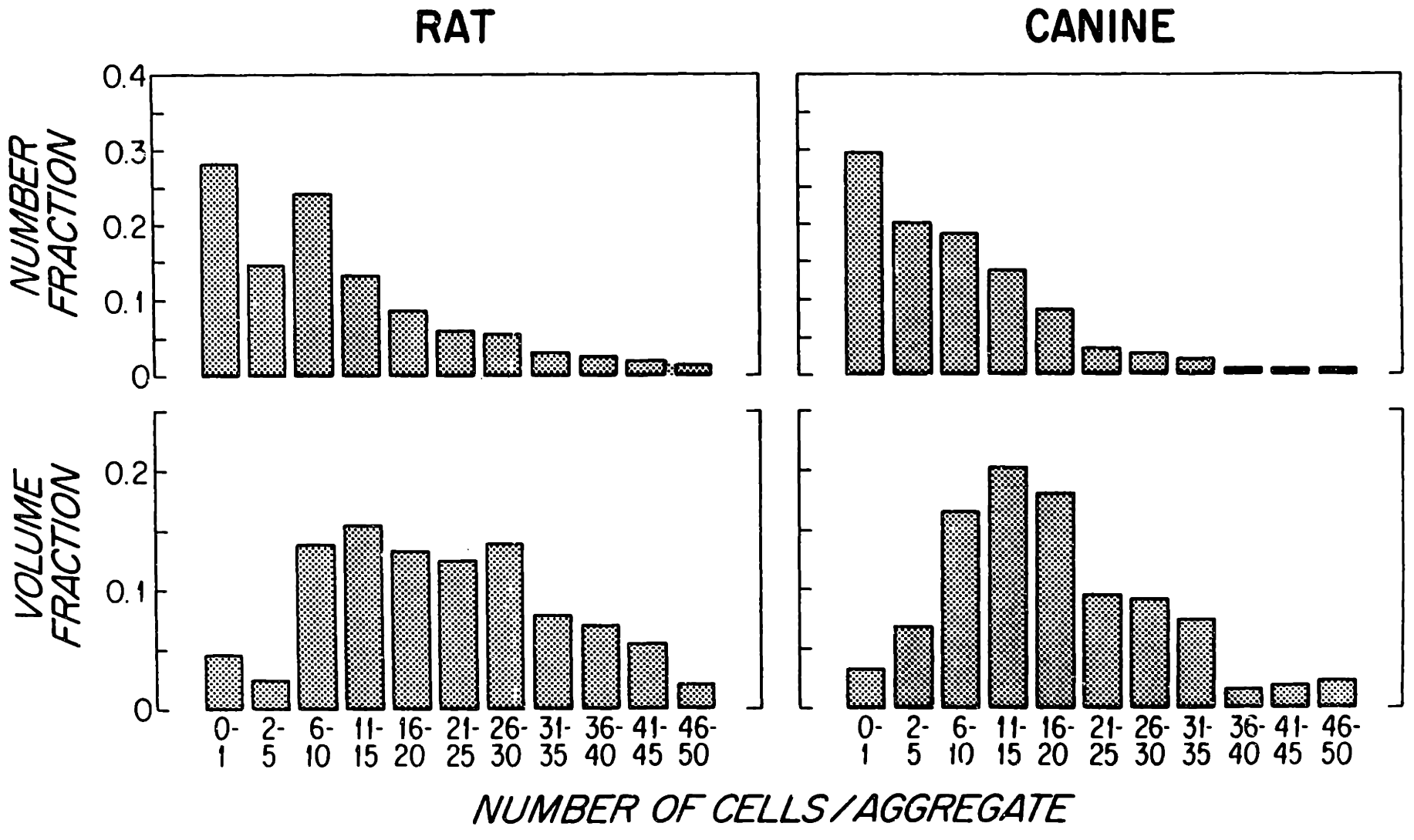

FIGURE 3. Number and volume fraction of representative rat and canine aggregate preparations. Aggregates are the same as those shown in Figure 2. Size was analyzed immediately prior to perifusion following one day (rat) or four days (canine) of culture. Number fraction was calculated as the number of aggregates in each indicated size range divided by the total number of aggregates counted (n = 221 for rat, 257 for canine). Volume fraction was calculated as the number of cells contained in aggregates in each indicated size range divided by the total number of cells in all of the aggregates counted.

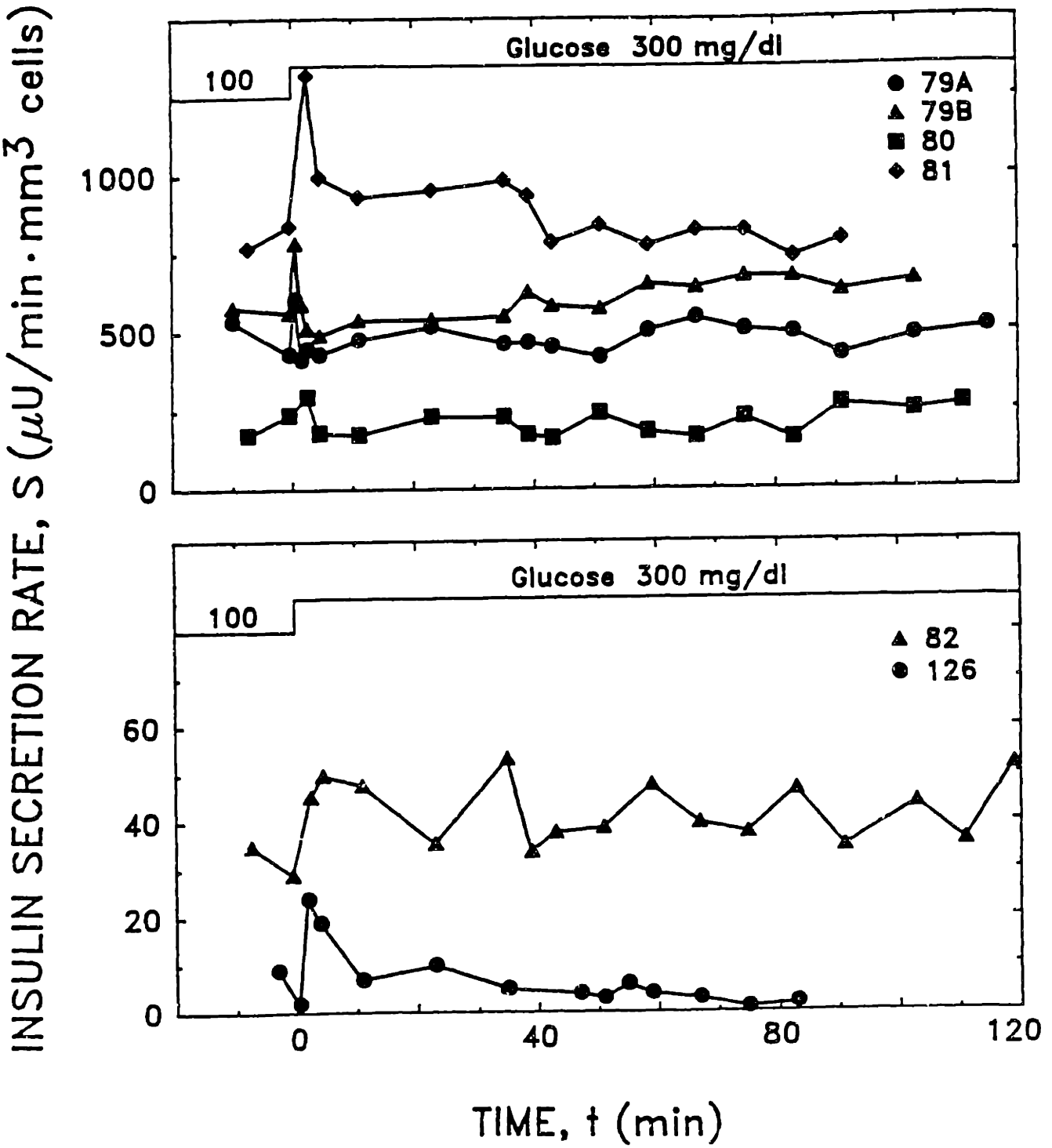

FIGURE 4. Insulin secretion from non-aggregated single rat islet cells. Cells were perifused either 2-4 hr after isolation (bottom) or after 24 hr culture under very dilute conditions (2,000 - 5,000 cells/cm^2) (top) in order to prevent spontaneous reaggregation. About 85% of the cells were viable by trypan blue staining. Cells were perifused with DMEM fortified with 10% NBCS and 5.6 mM glucose for one hr before the glucose concentration was raised to 16.7 mM at t=0 min.

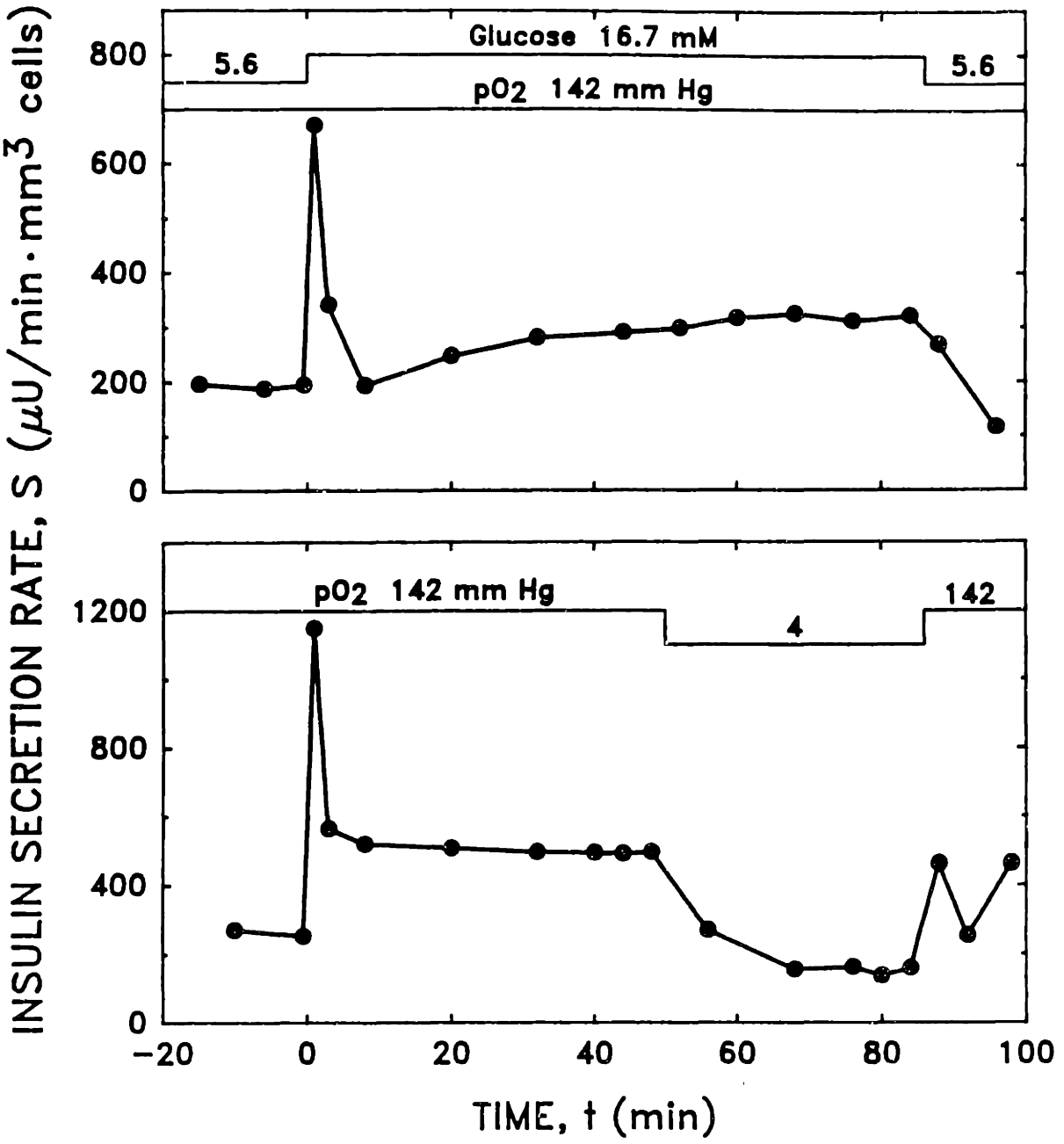

FIGURE 5. Insulin secretion under normoxic (upper panel) and hypoxic (lower panel) conditions from the same preparation of rat cell aggregates. Each perifusion was carried out with about 0.1 mm^3 tissue (containing about 7 x 10^4 cells) which had been allowed to aggregate for 18 hr after trypsinization. Aggregates were perifused with perfusate containing 5.6 mM glucose for one hr before the glucose concentration was raised to 16.7 mM at t=0. Perfusate glucose concentration was lowered back to 5.6 mM at t=88 min. The pO_2 of the normoxic perifusion was maintained at 142 mm Hg (humidified 5.3% CO_2 and 94.7% air) throughout the duration of the perifusion. Aggregates in the bottom panel were handled in an identical manner except that perfusate pO_2 was lowered to 4 mm Hg at t=50 min, and raised back to the normoxic level at t=85 min.

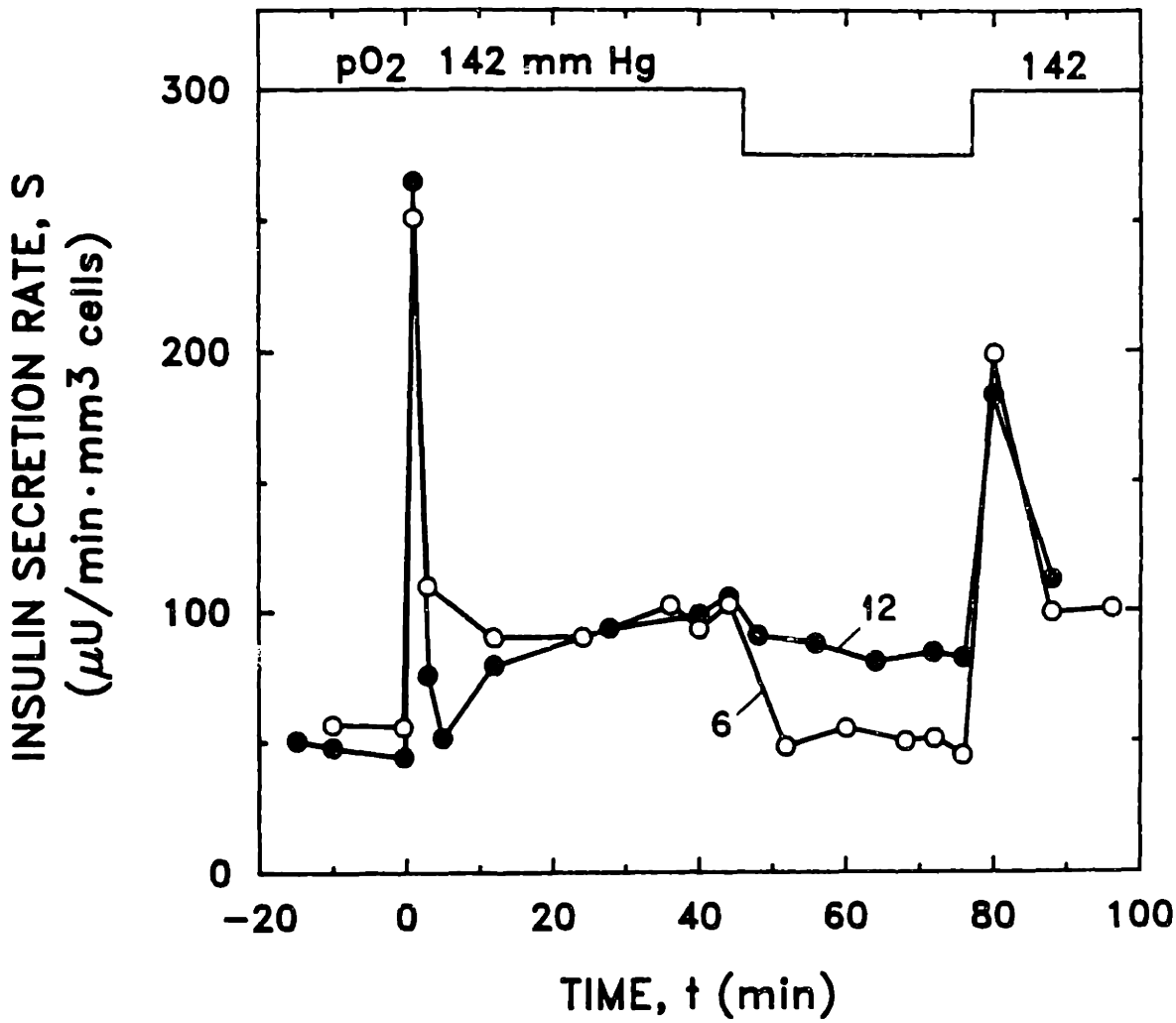

FIGURE 6. Effect of different levels of hypoxia on second phase glucose-stimulated insulin secretion from rat islet cell aggregates. Following one hr of basal equilibration, the glucose concentration of both perifusions was raised from 5.6 to 16.7 mM at t=0. At t=47 min, the perfusate pO_2 was dropped to either 6 or 12 mm Hg. Perfusate pO_2 was raised back to 142 mm Hg at t=78 min.

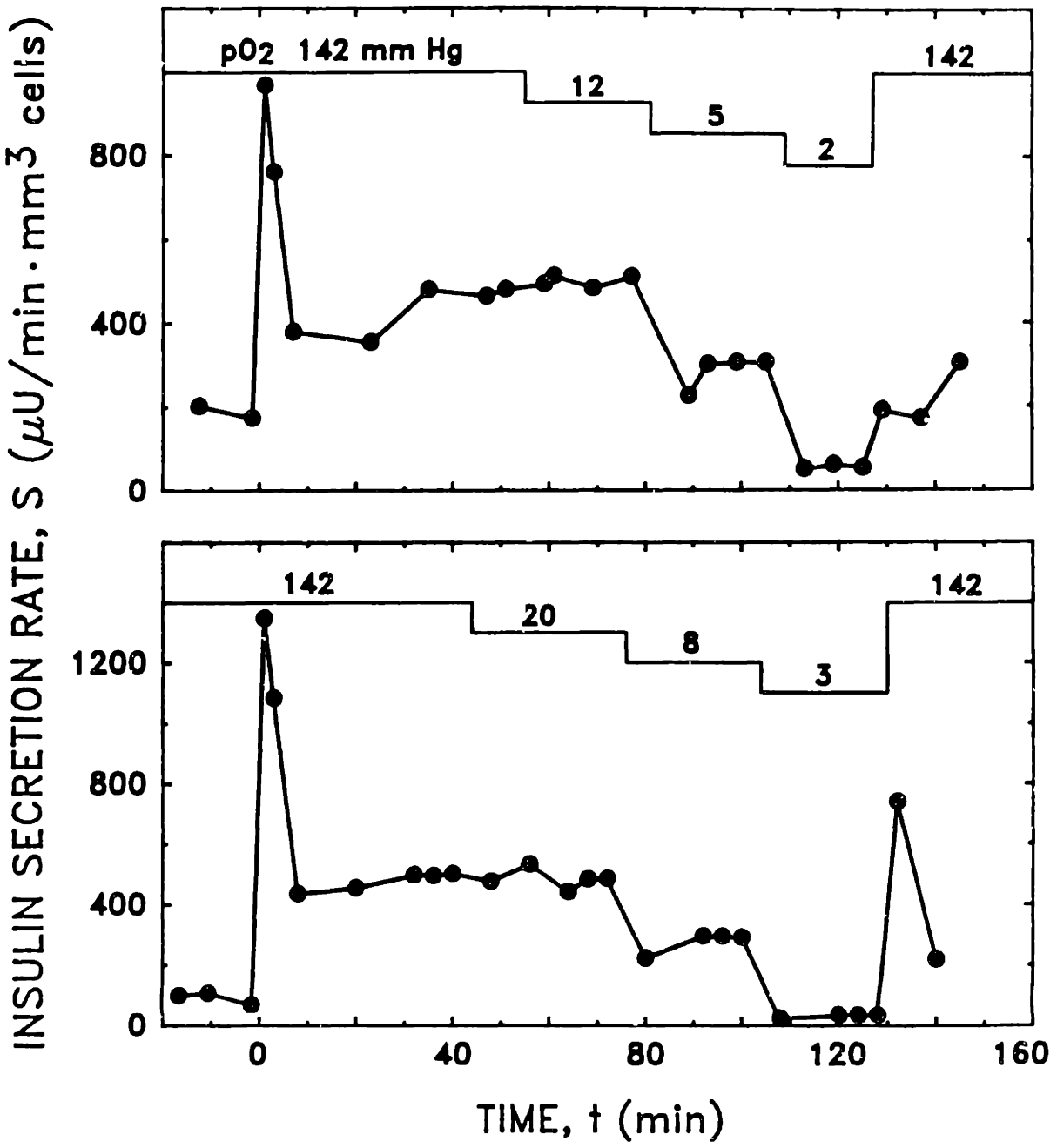

FIGURE 7. Effect of multiple sequential hypoxic steps on insulin secretion rate of two batches of aggregated canine islet cells taken from the same cell preparation. Aggregates were cultured for four days following trypsinization. Following 44 or 55 min of normoxic, glucose-stimulated secretion, perfusate pO_2 was progressively stepped down, as shown at the top of each panel, with each step lasting 18-30 min, and then back up to 142 mm Hg.

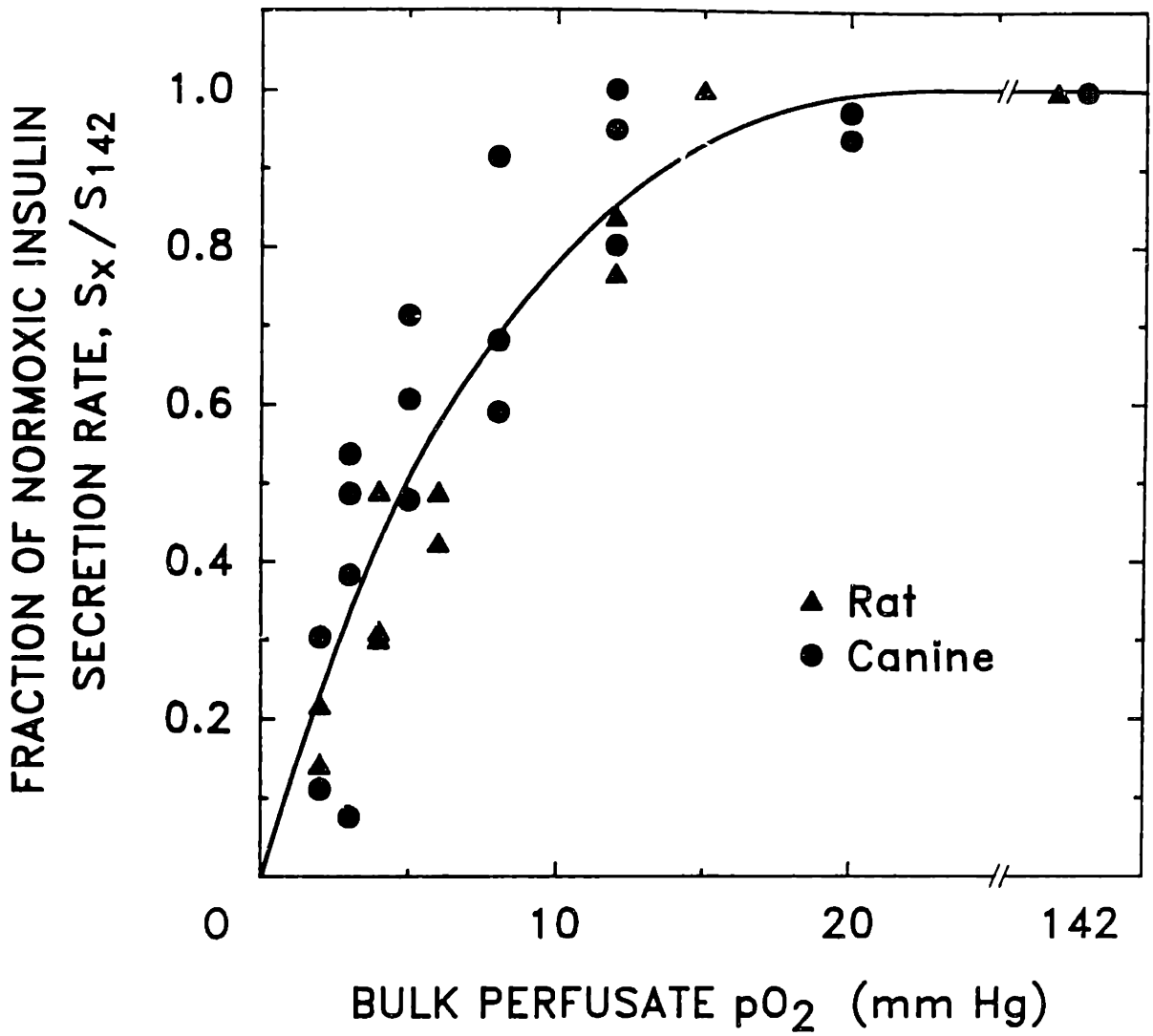

FIGURE 8. Fraction of normoxic second phase insulin secretion rate, S_x/S_{142}, as a function of bulk perfusate pO_2 = x mm Hg for perifused aggregates cultured one day (rat) or four days (canine) after preparation of islet cell suspensions. Data were obtained from 30 separate hypoxic periods collected during perifusions of rat and canine aggregates. The pO_2 at which S_x/S_{142} = 0.5 (P_{50}) was evaluated by linear interpolation amongst all the data obtained at perfusate pO_2 ranging from 3 to 8 mm Hg.

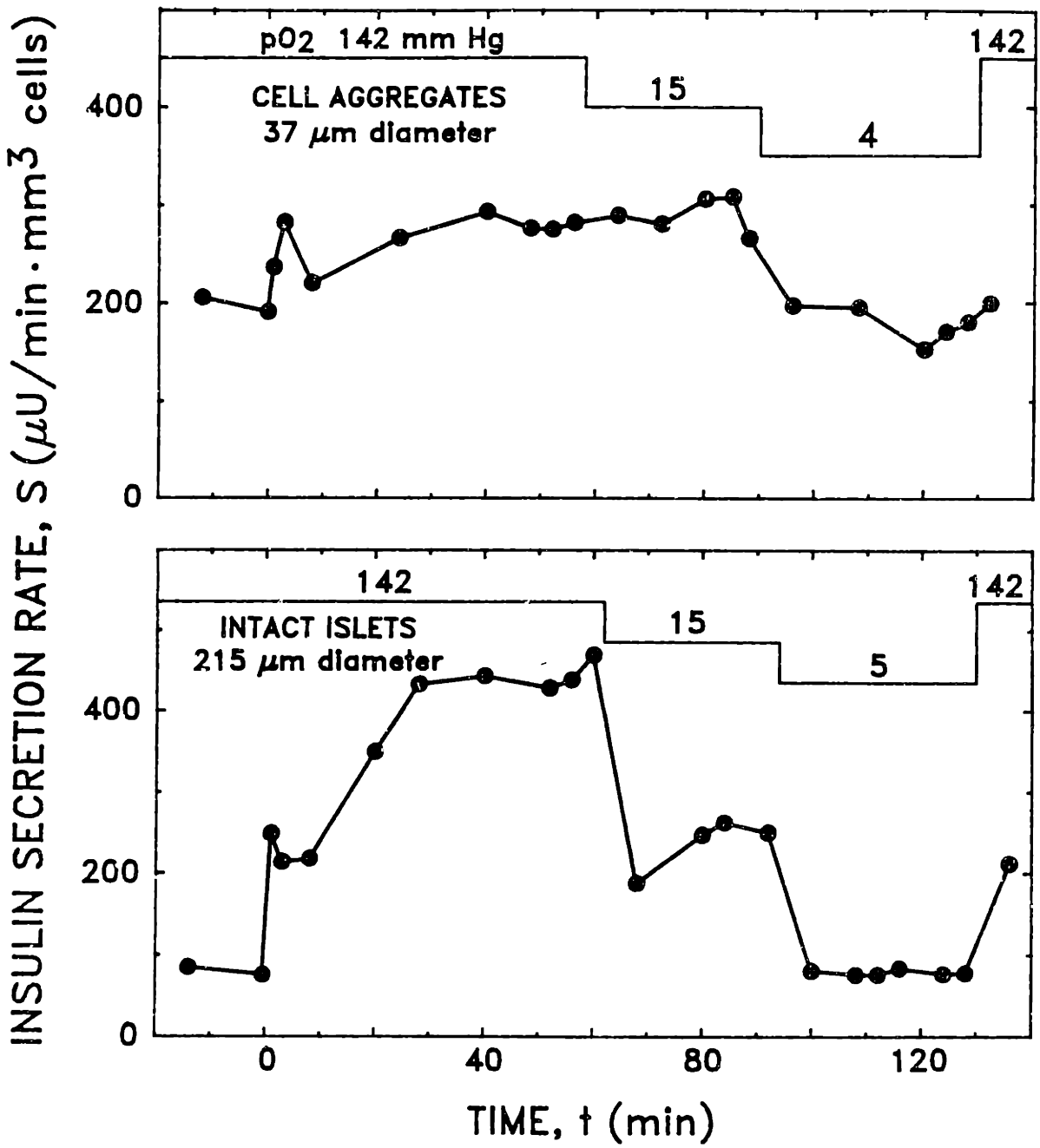

FIGURE 9. Comparison of the effect of hypoxia on glucose-stimulated insulin secretion rate from rat islet cell aggregates cultured for 18 hr after trypsinization and intact rat islets cultured in DMEM with 10% NBCS and 5.6 mM glucose under normoxic conditions for one week after isolation. Islets and aggregates, which were obtained from different isolation batches, were perifused on the same day. Twelve islets (0.06 mm^3 of tissue) and about 7 x 10^4 cells (0.10 mm^3) were used in the respective perifusions.

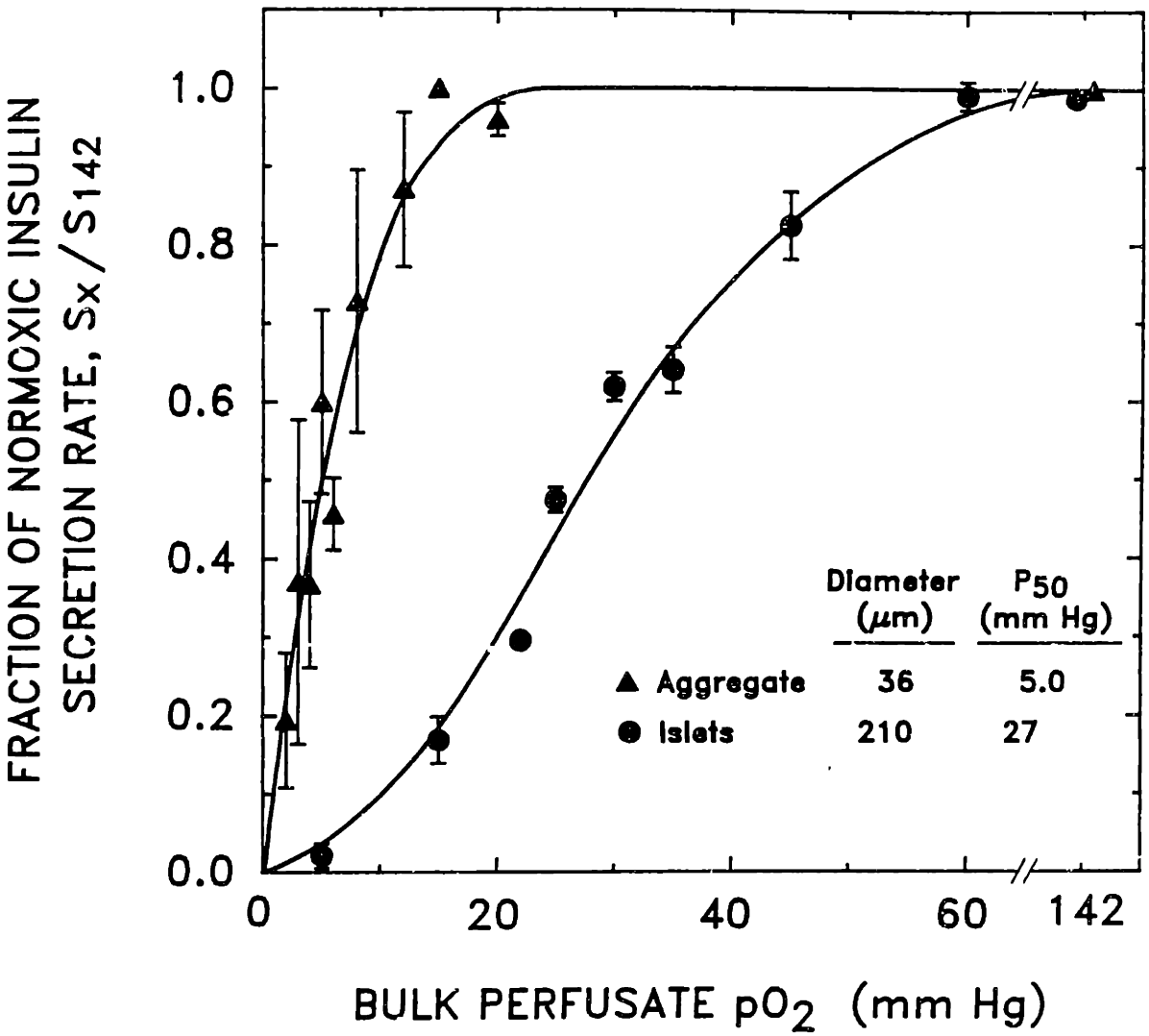

FIGURE 10. Comparison of the fraction of normoxic glucose-stimulated second phase insulin secretion rate as a function of perfusate pO_2 for cell aggregates and intact one-day old rat islets. Data at each perfusate pO_2 were combined and averaged. Data from perifusions from both rat and canine aggregates (Figure 8) are plotted. Error bars represent standard deviation. The S_x/S_{142} values for intact, 210 μm diameter rat islets cultured for one day after isolation have previously been reported (Dionne, Colton, and Yarmush 1989-3).

CHAPTER 5:

INSULIN SECRETION AND VIABILITY OF ISOLATED ISLETS OF LANGERHANS DURING LONG TERM OXYGEN-LIMITED STATIC CULTURE

SUMMARY

Using a static culture system with environmental control, the effect of various levels of oxygen partial pressure (pO_2) on the long-term (1 to 2 week) viability and insulin secretion of isolated rat islets of Langerhans was measured. Central necrotic cores were shown to develop in large (>200 μm diameter) isolated islets cultured for one or more weeks in normoxic (142 mm Hg) petri dish culture (medium depth = 6 mm). The size of the necrotic core increased with increasing islet diameter and with decreasing pO_2 in the gas above the culture medium. Glucose stimulated insulin secretion rate of islets cultured in static liquid overlay conditions was reduced with progressive reductions in gas pO_2 after both one day and one week of hypoxic culture. Islets did not acclimate to hypoxic pO_2 as the hypoxic fraction of normoxic secretion rate was further decreased after one week of hypoxic culture as compared to after one day of culture at the same pO_2. The effect of hypoxia in reducing insulin secretion was shown to be reversed following ten days of culture at 15 mm Hg by raising the pO_2 to either 30 or 142 mm Hg despite the presence of non-reversible black necrotic regions in the cores of the hypoxic cultured islets.

INTRODUCTION

We have previously reported that glucose-stimulated, second phase insulin secretion from both isolated islets and small pancreatic cell aggregates is reversibly reduced by intermediate levels of acute hypoxia (Dionne et al., 1989-3 and 1989-4). In perifusions of intact 200 μm diameter rat islets cultured for 24 hr after isolation, second phase insulin secretion began to decrease at a perfusate pO_2 of 60 mm Hg, reached one-half of normal at

27 mm Hg, and was less than 2% of normal at 5 mm Hg (Dionne et al., 1989-3). First phase secretion was less sensitive to hypoxia than was second phase secretion. Small clusters of reaggregated pancreatic islet cells (mean aggregate diameter = 36 μm) began to reduce their second phase secretion when the perfusate pO_2 was dropped below about 15 mm Hg oxygen, reached one-half of normal secretion at 5 mm Hg, and were at less than 20% of normal release at a perfusate pO_2 of 1-2 mm Hg (Dionne et al., 1989-4). Reduced insulin secretion has been shown to occurr over a similar range of pO_2 in which oxygen uptake is also reduced in both intact islets and cell aggregates (Dionne et al., 1989-6).

All of the reports of the effect of oxygen on insulin secretion involve acute periods of hypoxia lasting for 30-60 min (Coore and Randle, 1964; Coore et al., 1967; Milner and Hales, 1969; Dionne, Colton and Yarmush 1989-2,3,4) and indicate that the effects of acute hypoxia are reversible and are not caused by cell necrosis. In this paper, we report the effect of long-term (one to two weeks) hypoxia on insulin secretion and viability of isolated islets in static culture.

MATERIALS AND METHODS

Materials

Hanks Balanced Salt Solution (Hanks): Tissue digestions were performed using Hanks solution without Ca^{++}, Mg^{++} (H2387 Sigma Chemical Co., St Louis MO) fortified with 50 U/ml Penicillin and 50 μg/ml Streptomycin (600-5140AG, GIBCO, Grand Island, NY), and 0.35 g/l HEPES (H0763, Sigma Chemical Co.), pH buffered to 7.4 .

Dulbecco's Modified Eagles Media (DMEM): Islet tissue was cultured and tested in DMEM (D5523, Sigma Chemical Co) fortified with 50 U/ml Penicillin and 50 μg/ml Streptomycin, and containing either 1.0 or 3.0 mg/ml glucose, and either 10% Newborn Calf Serum (NBCS; 200-6010, GIBCO) or 5% NBCS and 5% rat serum (200-6230, GIBCO).

Construction of a Static Culture System with Oxygen Control

A static islet testing system was developed in order to culture islets for extended periods of time under various oxygen tensions. A schematic of this system is shown in Figure 1. A 37°C, continuous gas flow incubator (model 2210, Queue Systems Inc., Parkersburg WV) served as the outer shell around the entire culture system. The incubator protected the system from outside interference and maintained all of the components at a constant temperature of 37°C.

The gassing system of the Queue incubator provided a steady gas flow consisting of pulses of CO_2, air, and N_2, which could be set to any desired composition ranging from 0.0 to 99.9% using the incubator gas controls. The gas flowstream (0.4 l/min) was humidified by bubbling it through two water filled 250 ml erlenmeyer flasks connected in series with gas impermeable 3 mm i.d., 6.5 mm o.d. tubing (Tubing No 3814-1, Queue System Inc.; used for all gas lines). The gas then flowed directly into an inner oxygen regulated culture chamber formed by inverting a 600 ml pyrex bowl (Pyrex No. 3140) over a 0.5 cm thick neoprene rubber matt. The interface was sealed with silicon vacuum grease. Incoming gas flushed the culture chamber on average once every 1.5 min.

The gas pO_2 and pCO_2 were set by adjusting the percent air, N_2 or CO_2 gas flowing into the system using the Queue incubator controls. The percent air and N_2 were set to achieve to the desired pO_2 according the following formulas,

$$\% \text{ air} = \frac{100\ pO_2}{0.21\ (P_{atm} - pH_2O)} \qquad (1)$$

$$\% N_2 = 100 - (\%CO_2 + \% \text{ air}) \qquad (2)$$

The percent CO_2 was set at 5.3% in order to hold the pH of the culture medium at 7.45 . P_{atm} was taken to be a constant 760 mm Hg for use in Equation 1. At 37°C, the partial pressure of water, pH_2O, was 47 mm Hg (Weast, 1980). At 37°C, a fully humidified gas originally composed of 94.7% air and 5.3% CO_2 had a pO_2 of 141.8 mm Hg. To decrease the pO_2 to 25 mm Hg, air was replaced by N_2 gas such that the gas composition was 16.7% air, 5.3% CO_2, and 78.0% N_2. The pO_2 and pCO_2 of gas inside the culture chamber were

daily monitored using a fyrite gas analyzer (Fyrite model O_2 and CO_2; Bacharach Instruments, Pittsburgh PA). In some experiments, the chamber gas pO_2 was verified by continuously monitoring using a prototype fluorescent pO_2 probe (Bently OM-100, American Hospital Supply Co, Irvine CA; generously donated by Dr. Hal Heitzemann of Bentley Division, Baxter Healthcare Corp, Irvine CA) mounted inside of the culture chamber which directly measured the pO_2 of the gas in the chamber.

The temperature inside the culture chamber was maintained by the surrounding incubator and was monitored using a thermoresistor (YSI 511, VWR Scientific, Boston MA) connected to a digital readout (Digital thermometer 500, VWR Scientific, Boston MA). The external incubator temperature was monitored using the thermocouple of the Queue System incubator.

Islet isolation, batch preparation, culture and secretion testing

Islet Isolation: Islets of Langerhans were isolated from 200 - 350 g male Sprague-Dawley rats (Charles River Lab, Kingston, NJ) using collagenase digestion and ficoll purification (Lacy and Kostianovsky, 1967; Dionne, Colton, and Yarmush 1989-2). Briefly, the pancreas was distended in situ by injecting 10-15 ml of ice cold Hanks solution containing 1.7 mg/ml collagenase (108 8882 Boehringer Mannheim, Indianapolis, IN). The distended pancreas was dissected free, placed in a 50 ml T-flask, and digested under mild agitation in a 37°C water bath until islets were freed from acinar tissue as ascertained by microscopic examination (15 - 20 min). The slurry was then rinsed and purified by centrifugation on a discontinuous ficoll gradient. Ficoll purified islets were washed four times in DMEM with 10% NBCS, hand-picked to remove remaining acinar contamination, and placed in non-attaching petri dishes (Falcon 1007, Becton Dickinson Inc, Lincoln Park, NJ) containing 12 ml of DMEM with 10% NBCS and 100 mg/dl glucose.

Batch preparation: Following isolation, selected islets were sorted into batches by hand-picking five, approximately 200 μm diameter, spherical islets. Each batch of five islets was placed in a Petri dish containing DMEM culture medium and photographed under a

microscope for later sizing using a calibrated reticle grid. The micrograph of the islet sample was projected onto a screen, and the external dimensions of each islet were measured using the reticule grid. Slight deviations from a spherical shape were accounted for by measuring both the largest diameter and the diameter normal to it, assuming each islet could be represented by a prolate ellipsoid, and calculating its volume, v, from $v = \pi a^2 b/6$, where a and b are the smaller and larger axes, respectively. The equivalent spherical diameter, d, for each islet was calculated as that of a sphere of equal volume, $v = \pi d^3/6$; thus, $d = (a^2 b)^{1/3}$.

Following initial sizing, islet batches were prepared for culture in either free suspension or sandwiched between two layers of collagen. For free suspension culture studies, islets were transferred into 50 mm diameter, non-attaching polystyrene petri dishes (Falcon 1007, Becton Dickenson Inc) and cultured in either 12 (viability studies) or 6 (secretion studies) ml of DMEM with 100 mg/dl glucose and 10% NBCS. Culture medium was changed by transferring the islets into new petri dishes containing fresh, pre-warmed and gassed DMEM using a micropipette. Twenty μl of medium were transferred each time an islet batch was moved to a new dish.

Collagen/islet sandwiches were prepared by first attaching a thin patch or layer of collagen to the bottom of a 35 mm diameter petri dish (Falcon 3001). Collagen preparations were handled according to the methods described by Montesano et al. (1983). Solutions of rat tail collagen (1.2 mg collagen /ml buffered saline solution; pH = 4) and 10 times normal strength DMEM were placed on ice along with the petri dishes to be coated. One part 10X DMEM was added to nine parts collagen solution. The resulting rise in pH and ionic concentration caused the collagen to begin to slowly gel - a process that was slowed by the cold temperature. Before the solution had gelled, 60 μl of collagen/DMEM solution was spread into a thin patch approximately 1 1/2 cm in diameter in the center of each petri dish. The collagen coated petri dishes were then placed in a 37°C incubator for two hours to allow the collagen to firmly gel. At the end of two hr, the dishes were filled with 1.5 ml DMEM containing 10% NBCS and 100 mg/dl glucose and then allowed to incubate at 37°C, 94.7% air, 5.3% CO_2 for another two hours. At this time, one pre-sized batch of five islets was micro-

pipetted on top of each collagen patch. The dishes were then reincubated at 37°C, 94.7% air and 5.3% CO_2 for two days in order to allow islets to attach to the collagen layer beneath them. At the end of the second day, the culture medium was slowly aspirated out of the dish, leaving the islets attached to the collagen patch. At this time 40 μl of fresh collagen/DMEM were gently micropipetted on top of the islet/collagen patch to form the upper collagen layer. The second collagen layer rapidly gelled (< one min) and attached to the original collagen patch effectively sandwiching the islets between the two layers. At the end of one min, 1.5 ml of DMEM culture medium was slowly added to cover the collagen/islet patch. At later times, culture medium was changed by aspirating the supernate out of the petri dish and adding fresh, pre-gassed and pre-warmed medium to the petri dish containing each collagen/islet sandwich.

Some islets cultured for long periods of time were placed in 50-mm diameter dishes pre-coated with a 0.5-mm thick layer of gelled rat tail collagen. Each dish contained seven ml of DMEM prepared as described for short term culture except for the addition of 5% NBCS and 5% rat serum (200-6230AD, GIBCO). One to two hundred islets were placed in each dish. Cultured islets lightly attached to the collagen matrix which helped avoid islet aggregation and clumping. Once islets had attached (24 - 48 hr), medium was changed every other day.

Culture and secretion testing: Once islet batches were prepared in either free floating suspension or collagen patches, the effect of oxygen on their insulin secretion rate was tested by culturing one half of the dishes in a normal 37°C incubator under 142 mm Hg O_2 in the gas (94.7% air and 5.3% CO_2) and the other one half of the dishes in the static incubator system set at 37°C and at a preset hypoxic gas pO_2 ranging from 5 - 30 mm Hg (5.3% CO_2 and the appropriate air and N_2 fractions). Culture medium was changed every day using fresh DMEM containing 100 mg/dl glucose and 10% serum that had been pre-warmed and pre-gassed at the respective culture conditions. Basal insulin secretion was monitored by collecting the supernate following each media change and storing it at 4°C until it was assayed

for insulin by RIA (Dionne, Colton, and Yarmush, 1989-2). The glucose concentration of the medium was tested using a Beckman Glucose Analyzer II (Beckman Instruments, Brea CA).

The effect of glucose stimulation on insulin secretion rate was tested by measuring the insulin secretion rate during a 60-90 min glucose challenge with 300 mg/dl glucose in DMEM and 10% NBCS. Depending on whether islets were to be transferred to new petri dishes (free suspension culture) or whether the culture medium was to be replaced in the same petri dish (collagen/islet sandwiches), test medium was either placed in a large 75 mm petri dish or in individual 50 mm petri dishes and equilibrated overnight at the respective pO_2 levels of the islet culture. The glucose concentration of freely suspended islets was changed by micro-pipetting the five islets per petri dish into a fresh dish containing the pre-gassed and warmed test medium. The new dishes were immediately replaced in the respective incubators. The glucose concentration of collagen/islet sandwiches was changed by aspirating out the basal culture medium, adding the pre-gassed and warmed test medium to the petri dish containing the attached islets and immediately replacing the dish in its incubator. At the end of 60-90 min of glucose-stimulated secretion, the process was repeated except this time basal medium was added to each dish. Test medium was collected and analyzed for insulin content by radioimmuno-assay. The insulin secretion rate, S, per unit volume of tissue, V_t, was calculated for both basal and stimulated secretion periods from the insulin concentration [I] measured in the spent culture medium (volume Vm) according to

$$S = \frac{[I]\ Vm}{V_t\ t} \qquad (3)$$

where t is the time period during which islets secreted insulin into the culture medium.

Vital Staining: A fresh solution of 0.06% (by weight) trypan blue (630-5250 AG, GIBCO) in DMEM with 2% new born calf serum was made daily. Petri dishes (35 x 10 mm, Falcon 3001, Becton Dickinson Inc., Lincoln Park NJ) were filled with 1.5 mls of staining solution per dish and placed in a 37°C incubator for pre-warming and gassing. Using a micro-pipette, islets were transferred into the staining dishes which were then placed in a 37°C incubator for five min. After five min, the islets were micro-pipetted out of the staining dishes, placed in

fresh DMEM, and examined under a microscope for staining. The membrane of viable cells excludes trypan blue whereas the proteins in the cytosol of nonviable cells are stained (Lillie, 1977).

RESULTS

Effect of hypoxia on islet cell viability

Islets which were cultured at normoxic (142 mm Hg) pO_2 in either free suspension or attached to collagen coated petri dishes often developed black necrotic cores over time. Figure 2 shows a series of photomicrographs illustrating this phenomenon. Regardless of islet size, necrotic cores were never seen in islets during the first three days of culture (panel A). The first visible signs of necrotic cores appeared following 4-7 days of culture as small dark regions at the core of larger islets (panel B). By two weeks of culture, black regions assumed to be regions of necrosis were fully developed in the cores of larger islets (panel C). The size of the necrotic regions remained constant from two weeks until the culture was terminated at five weeks (panel D).

The size dependence of the development of necrotic cores is further illustrated in Figure 3. Small islets (< 150 μm in diameter, panel A) rarely developed necrotic regions. Mid-sized islets with diameters ranging between 150 and 180 μm occasionally developed visible necrotic regions (panel B), whereas large islets with diameters greater than 200 μm usually developed necrotic regions whose size was a function of the islet diameter (panels C and D).

The relationship between the size of the necrotic core region and the islet diameter following two weeks of normoxic culture was measured for a number of large islets and is shown in Figure 4. The largest islets that were measured (400 - 500 μm diameter) developed necrotic core regions which comprised about 90% of the total islet diameter. Assuming that islets are best described as spheroids, a necrotic core that occupied 90% of the islet diameter corresponded to about 72% of the islet volume because of the cubed dependence of volume on spheroid radius. The percent of the islet diameter that was necrotic decreased to 10 to 20% in

islets under 200 μm diameter. Necrotic cores were rarely observed in islets under 100 μm diameter (data not shown).

The effect of decreased culture pO_2 on the development of necrotic islet cores is shown in Figure 5. Large (220 - 250 μm diameter) islets cultured for ten days under normoxic conditions (panels A and B) developed black core regions whose diameters were about 50% of the diameter of the islet. Islets which were cultured for four days at normoxic and one day at hypoxic (9 mm Hg) gas pO_2 (panels C and D) developed much larger regions of central necrosis, the diameters of which represented about 80 - 90% of the overall islet diameter.

The necrotic core and overall diameters of a small number of islets cultured for one week at 142 mm Hg and one week at 30 mm Hg are shown in the right hand side of Figure 4. Although the necrotic fraction is higher in comparably sized large islets cultured at this mild hypoxic level, the differences are not large and appear to be non-existent in the few small islets that were measured.

It has been assumed that the black discoloration at the core of islets can be equated with necrosis of cell tissue. In order to test this assumption, cultured islets which had developed black cores were exposed to trypan blue in order to see if the regions of discoloration and trypan blue uptake overlapped. Enlarged photomicrographs of islets with black cores before (panel A) and after (panel B and C) exposure to trypan blue are shown in Figure 6. Although the degree of staining is difficult to assess in the black core region, qualitatively the region in which trypan blue stained and the region of black discoloration coincided. From this, it is assumed that intense black discolorization can be equated with the loss of cell viability, or at least with the loss of a cell's ability to exclude trypan blue.

Effect of hypoxia on insulin secretion

The effect of long-term hypoxia on the insulin secretion rate of statically cultured islets was tested in parallel cultures of normoxic and hypoxic islets. The culture pO_2 was set by adjusting the composition of the gas with which the culture medium was in equilibrium. Insulin secretion rate was determined by assaying spent culture medium for secreted insulin.

Islets were sized, transferred to petri dishes containing medium pre-equilibrated at the test pO_2, and then placed in 37°C incubators set at the respective pO_2 level for each run. Results of four pairs of normoxic and hypoxic secretion tests are shown in Figures 7 and 8. Each set of paired secretion studies was made with islets from different isolation batches. After the first day of culture, basal insulin secretion rate at all levels of hypoxia were generally reduced compared to the corresponding normoxic rate which averaged between 20 and 40 $\mu U/min \cdot mm^3$ islet. After the first day of culture, incidences in which hypoxic basal secretion was equal to or higher than the normoxic level generally occurred in the basal period immediately following glucose stimulation.

Quantitative comparisons between basal and stimulated secretion must be made with care because stimulated secretion was measured over 60 (Figure 7) or 90 min (Figure 8) period whereas basal secretion was collected over a 24 hr period; however in general, 300 mg/dl glucose stimulation increased the insulin secretion rate by a factor of 3 to 5 over that seen with basal glucose. The glucose-stimulated secretion rate was generally slightly lower following one week of culture as compared to the rate on day one or two. The stimulated secretion rate of the tests shown in both panels of Figure 8 are about a factor of three higher than the corresponding secretion rates of islets shown in Figure 7. This difference may reflect either intrinsic differences in secretion rate of islets from different isolation batches or the longer period of glucose stimulation (90 compared to 60 min) over which islets represented in Figure 8 were tested.

Hypoxia was observed to reduce glucose-stimulated insulin secretion rate at all of the pO_2 levels shown. Secretion was least affected at 27 mm Hg when measured in either absolute units or as a fraction of the paired normoxic secretion rate. In order to compare the effect of different levels of pO_2 on glucose stimulated insulin secretion, insulin secretion from each hypoxic glucose-stimulated secretion period was normalized by its paired normoxic secretion rate. The hypoxic fraction of normoxic insulin secretion rate, S_x/S_{142} where x is the reduced pO_2, for these and other runs are listed in Table 1. As can be seen from the data in this Table, glucose-stimulated insulin secretion rate decreased with falling pO_2 after both one

day and one week of hypoxic culture. The fraction of normoxic secretion rate was also decreased (or remained constant at $S_x/S_{142} = 0.1$) following one week compared to one day of culture at each hypoxic pO_2.

In order to test whether the effects of long-term hypoxia on insulin secretion and cell viability were reversible, insulin secretion from islets cultured under hypoxic conditions was first tested and then the islets were placed in a higher oxygen environment and allowed to recuperate before insulin secretion was again tested. For these experiments, batches of islets were sandwiched between two layers of collagen and cultured in paired normoxic and hypoxic (15 mm Hg) runs for ten days. On day ten, the hypoxic cultured islets were transferred to either a partially (30 mm Hg) or fully normoxic (142 mm Hg) environment. Photomicrographs of normoxic and hypoxic islets taken on day ten are shown in Figure 9. Both hypoxic and normoxic islets had spread out and attached to the collagen layers. Islets cultured under normoxia (panels A and B) exhibited no evidence of necrosis. (Note: the distance from the islet to the liquid/gas interface of islets in collagen patches was 1.6 mm compared to 3 mm for islets cultured in free suspension insulin secretion studies.) Islets cultured for ten days at 15 mm Hg displayed large central necrotic regions accounting for over 80% of the total islet diameter (about 50 to 65% of the islet volume depending on the actual geometry of sandwiched islets). Neither the area nor the intensity of the discolored regions were affected after two days of culture at a higher medium pO_2 level (data not shown).

The effect of raising the culture pO_2 on insulin secretion rate following prolonged hypoxia is shown in panels A and B of Figure 10. Glucose-stimulated insulin secretion was tested during the hypoxic period on days two and seven. The hypoxic insulin secretion rate was about 50% of the paired normoxic rate on day two and about 30% on day seven. On day ten, the hypoxic culture pO_2 was raised to either 30 (upper panel) or 142 mm Hg (lower panel). On day 12, following two days of culture at the higher pO_2, glucose stimulated secretion was approximately the same from all three sets of islets (normoxic, 15 to 30 mm Hg,

and 15 to 142 mm Hg) despite the large necrotic region of islets cultured at 15 mm Hg for ten days.

DISCUSSION

The effect of reduced oxygen partial pressure on cell viability and glucose-stimulated insulin secretion of isolated islets in static culture was investigated. Large islets (>200 μm diameter) were observed to develop central regions of necrosis over one to two weeks of culture at a gas pO_2 equal to 142 mm Hg and a culture medium depth of six mm. The region of necrosis appeared to be fully developed by two weeks of culture and did not measurably change in size or intensity from two to five weeks. The size of the necrotic cores was dependent on the diameter of the islet, with larger islets developing larger necrotic cores both in terms of the diameter of the necrotic region and in terms of the fraction of the overall islet that was necrotic. The size of the centrally necrotic regions increased both in terms of absolute diameter and as a fraction of the overall islet diameter when the culture pO_2 was lowered. All of these observations are consistent with the hypothesis that the necrotic regions are caused by insufficient oxygen delivery to the core region of isolated islets under these culture conditions.

The effect of reduced pO_2 on the glucose-stimulated insulin secretion rate of isolated islets cultured under static conditions was measured with both islets in free suspension and with islets sandwiched between two layers of collagen. The glucose-stimulated insulin secretion rate was substantially reduced at gas pO_2 levels of 15, 17, 20, 27 and 30 mm Hg - the range of partial pressures tested (See Table 1). The degree of reduction progressively increased with decreasing pO_2. For a given hypoxic pO_2 level, glucose-stimulated secretion was more reduced after one week of hypoxic culture than after one day of culture. The increased affect over time may be caused by the development of necrotic regions over time and is indicative that at least at these pO_2 levels, islets are unable to acclimatize to the hypoxic environment.

There are certain limitations in static culture systems that must be considered when directly comparing the set pO_2 and the pO_2 at which cell viability or insulin secretion are affected. First, the pO_2 set in the gas phase above the culture medium is not the pO_2 at the surface of cultured islets due to diffusion gradients in static medium. A mathematical analysis of transport to an oxygen consuming spheroid suspended in an infinite static reservoir (Dionne et al., 1989-7) indicates that the pO_2 drop through the static medium surrounding a 200 μm diameter islet without an anoxic core is about 30 mm Hg. The presence of other islets in the near vicinity and of the bottom of the petri dish will increase the pO_2 gradient from liquid/gas interface to the islet surface. The development of a non-consuming necrotic core will decrease the pO_2 drop to the islet as, to a certain degree, will decreasing the thickness of the medium between the gas/liquid surface and the tissue (Franko and Freedman, 1984). Evidence of the latter effect was seen by the absence of necrotic cores in islets cultured at 142 mm Hg in collagen patches where the medium depth was 1.6 mm, whereas islets of a similar size and at the same gas pO_2 cultured in free suspension (medium depth = 6 mm Hg) developed definite necrotic cores over time.

In addition to the pO_2 gradient in the surrounding static medium, a large pO_2 gradient will exist inside of an oxygen consuming islet resulting in a progressive reduction in pO_2 toward the islet core (Dionne et al., 1989-7 and 1989-8). It is as a result of these gradients that the core region of diffusion limited islets is the first to become necrotic under oxygen limiting circumstances. The larger the islet, the larger the pO_2 gradients in the surrounding medium and in the islet tissue, resulting in the development of larger regions of central necrosis in large islets.

Previous reports of the effect of acute (30-60 min) anoxia (Coore and Randle, 1964; Coore et al., 1967; Milner and Hales, 1969) or hypoxia (Dionne, Colton and Yarmush 1989-2,3,4) indicated that over short periods of time, the lack of oxygen reduced insulin secretion but did not affect islet cell viability. In these reports, hypoxia limited insulin secretion was reversed upon the return to higher pO_2 levels. In the present experiments, chronic (1 to 2 weeks) hypoxia was shown not only to reduce insulin secretion, but to also lead to cell

necrosis in the diffusion limited core of islets. Despite the development of necrotic regions over a ten day hypoxic period in which insulin secretion was also reduced to between 30 and 50% of the normoxic rate, the glucose-stimulated insulin secretion rate of hypoxic islets returned to the paired normoxic level following two days of culture at either 30 or 142 mm Hg (Figures 9 and 10). That the post-hypoxic rate returned to the full normoxic level was surprising since about 50% of the post-hypoxic islet volume was necrotic as ascertained by dark black staining which was shown to correspond to regions of trypan blue staining (Figure 6). There was no evidence of a change in the morphology of the necrotic core regions with the change to the higher pO_2 levels.

There are two possible explanations of this phenomenon. First, it is possible that necrotic core regions were still capable of secreting insulin in response to glucose stimulation. This is unlikely as trypan blue staining has been shown to be indicative of the absence of secretion in other experiments (Dionne et al., 1989-9). The other possibility is that the remaining viable tissue hypersecreted insulin in comparison to normal normoxic islet tissue. This could be caused by a variety of factors. During the hypoxic period, the insulin secretion rate of cells in the viable rim was reduced as ascertained by the higher level of secretion upon culture at higher oxygen tensions. It has previously been suggested that biosynthesis of insulin may continue to occur under conditions where there is inadequate oxygen to allow insulin secretion thus creating a build up of unsecreted insulin in hypoxia suppressed β-cells (Dionne et al., 1989-3). It is therefore possible that during the post-hypoxic glucose challenge, viable β-cells hypersecreted insulin that was previously built up during the hypoxic period. There is some evidence for this occurring in the insulin secretion studies shown in Figures 7 and 8. The basal secretion rate of hypoxic islets was generally elevated in the period immediately following glucose stimulation on day one or two. Such elevations could be caused by hypersecretion of built up insulin when islets were first transferred to new culture medium and temporarily exposed to higher pO_2 levels because of handling artifacts. If this hypothesis is true, then the glucose stimulated secretion of post-hypoxic islets would decrease to a lower fraction of the normoxic rate on successive glucose challenges.

The similarity of post-hypoxia glucose-stimulated secretion whether the pO_2 was raised to 30 or 142 mm Hg can be explained by the presence of the non-oxygen consuming necrotic cores. During the ten day culture at 15 mm Hg, each islet probably reached a pseudo-steady state wherein the outer layer of cells was viable, the next layer was viable but dormant, and the inner core was necrotic and dead. The relative proportions of each layer would be determined such that the oxygen consumption of the overall islet equaled the diffusion limited oxygen delivery to the islet at a gas pO_2 of 15 mm Hg. Therefore, whereas 30 mm Hg was shown to reduce the stimulated insulin secretion rate of non-necrotic islets to 80% of normal after one day of culture (Table 1), the decreased oxygen consumption of islets equilibrated at 15 mm Hg reduces the pO_2 gradient both in the medium surrounding the islet and through the islet mass itself such that the entire viable rim is sufficiently oxygenated at 30 mm Hg.

The results of these experiments have important implications for static islet cultures: (1) they indicate that under certain conditions both insulin secretion and viability of large, isolated islets can be adversely affected at standard culture pO_2 levels (5% CO_2, 95% air; 142 mm Hg); (2) they suggest that the ability of islets to secrete insulin following extraction from a potentially hypoxic environment (encapsulation device, non-vascularized hypoxic transplantation site, etc.) may not be indicative of secretion in the previous environment; and (3) they support the hypothesis that insulin secretion can be reduced, even over extended periods of time, at a pO_2 level that does not cause cell death. This latter phenomenon may be important in allowing cells to survive temporary or even extended periods of hypoxia and still retain their ability to secrete insulin in response to a glucose challenge upon the return to higher oxygen levels.

REFERENCES

Coore, H.G, and Randle, P.J. (1964) Regulation of Insulin Secretion Studied with Pieces of Rabbit Pancreas Incubated *in vitro*. Biochem J 93: 66-77.

Coore, H.G, Hellman, B., Idahl, L-A, and Taljedal, I-B. (1967). Diabetes Research at the Histological Department in Umea. Opuscula Medica 12:285-295.

Dionne, K.E, Colton, C.K, and Yarmush, M.L. (1989) Effect of Oxygen on Isolated Pancreatic Tissue. A.S.A.I.O Transactions (submitted).

Dionne, K.E, Colton, C.K, and Yarmush, M.L. (1989-2) A micro-perifusion system with environmental control for islet insulin secretion studies. (Ph.D. Thesis; Chapter 2).

Dionne, K.E, Colton, C.K, and Yarmush, M.L. (1989-3) Effect of hypoxia on insulin secretion by isolated rat and canine islets of Langerhans. (Ph.D.Thesis; Chapter 3).

Dionne, K.E, Colton, C.K, and Yarmush, M.L. (1989-4) Effect of hypoxia on insulin secretion from rat and canine islet cell aggregates. (Ph.D. Thesis; Chapter 4).

Dionne, K.E, Schlosser, C, Wilson, D.F, Yarmush, M.L, and Colton, C.K. (1989-6). Measurement of oxygen uptake of intact islets and reaggregated cells under oxygenated and oxygen limiting conditions. (Ph.D. Thesis; Chapter 6).

Dionne, K.E, Colton, C.K, and Yarmush, M.L. (1989-8). Mathematical modeling of O_2 profiles, O_2 consumption, and insulin secretion in isolated and immuno-isolated islets of Langerhans. (Ph.D. Thesis; Chapter 8).

Dionne, K.E, Colton, C.K, and Yarmush, M.L. (1989-9). A proposed metabolic pathway by which hypoxia reduces the exocytotic release of insulin from pancratic β-cells. (Ph.D. Thesis; Chapter 9).

Findlay, J.A, and Ashcroft, J.J.H. (1975) Cells of the islets of Langerhans. The Cell in Medical Science Volume III. Academic Press, NY.

Franko, A.J, and Freedman, H.I. (1984) Model of diffusion of oxygen to spheroids grown in stationary medium - I. complete spherical symmetry. Bull Math Biol 46:205-217.

Franko, A.J, Freedman, H.I, and Koch, C.J. (1984). Oxygen supply to spheroids in spinner and liquid-overlay culture. Rec Res Can Research 95:162-167.

Hellman, B, Idahl, L.A, and Danielson, A. (1969) Adenosine triphosphate levels of mammalian pancreatic β-cells after stimulation with glucose and hypoglycemic sulfonylureas. Diabetes 18:509-516.

Lacy, P.E. and Kostianovsky, M. (1967) Method for the isolation of intact islets of Langerhans from the rat pancreas. Diabetes 16: 35-39.

Lillie, R.D. (ed) (1977) *H.J. Conn's Biological Stains.* Williams and Wilkins Co., Baltimore, MD.

Malaisse, W.J. (1972) Hormonal and environmental modification of islet activity. in Greep, R.O, and Astwood, E.B. (eds), Handbook of PHysiology, Section 7: Endocrinology, Volume I. Endocrine Pancreas, p. 175-98, American Physiological Society, Washington, D.C.

Milner, R.D.G, and Hales, C.N. (1969) The Interaction of Various Inhibitors and Stimuli of Insulin Release Studied with Rabbit Pancreas *in vitro*. Biochem J 113: 473-479.

Misler, S, Gee, W. M, Gillis, K.D, Scharp, D.W, and Falke, L,C. (1989) Metabolite-regulated ATP-sensitive K^+ channel in human pancreatic islet cells. Diabetes 38: 422-427.

Montesano, R, Mouron, P, Amherdt, M, and Orci, L. (1983). Collagen matrix promotes reorganization of pancreatic endocrine cell monolayers into islet-like organoids. J Cell Biol 97:935-939.

Randle, P.J, and Hales, C.N. (1972) Insulin Release Mechanisms in *Handbook of Physiology: Endocrinology I* (Chapter 13, pp. 219 - 35); Greep, R.O, and Astwood, E.B. (eds), American Physiological Society, Washington D.C.

Sando, H, and Godsky, G.M. (1973) Dynamic synthesis and release of insulin and proinsulin from perifused islets. Diabetes 22:354-60.

Trus, M, Warner, H, and Matschinsky, F. (1980) Effects of glucose on insulin release and on intermediary metabolism of isolated perifused pancreatic islets from fed and fasted rats. Diabetes 29:1-14.

TABLE 1. SUMMARY OF INSULIN SECRETION FROM RAT ISLETS OF LANGERHANS CULTURED IN LIQUID OVERLAY AT VARIOUS HYPOXIC PO_2

Gas pO_2 (mm Hg)	Fraction of Normoxic Insulin Secretion Released during 60-90 min, 300 mg/dl Glucose Challenge[r]	
	Time of Hypoxic Culture	
	1 Day	1 Week
15	0.1	0.1
17	0.1	0.1
20	0.3	0.1
27	0.6	0.2
30	0.8	0.3
142	1.0	1.0

[r] Each measurement was calculated as the average secretion from islets in 5 separate petri dishes with each dish containing five, 200 - 220 μm diameter rat islets dispersed throughout the 5.4 cm diameter, Falcon 1007 petri dish. Culture medium was DMEM with 10% NBCS and 100 mg/dl glucose between 300 mg/dl glucose challenges. Medium depth (distance between islets and air/medium interface) was 2.6 - 3.0 mm.

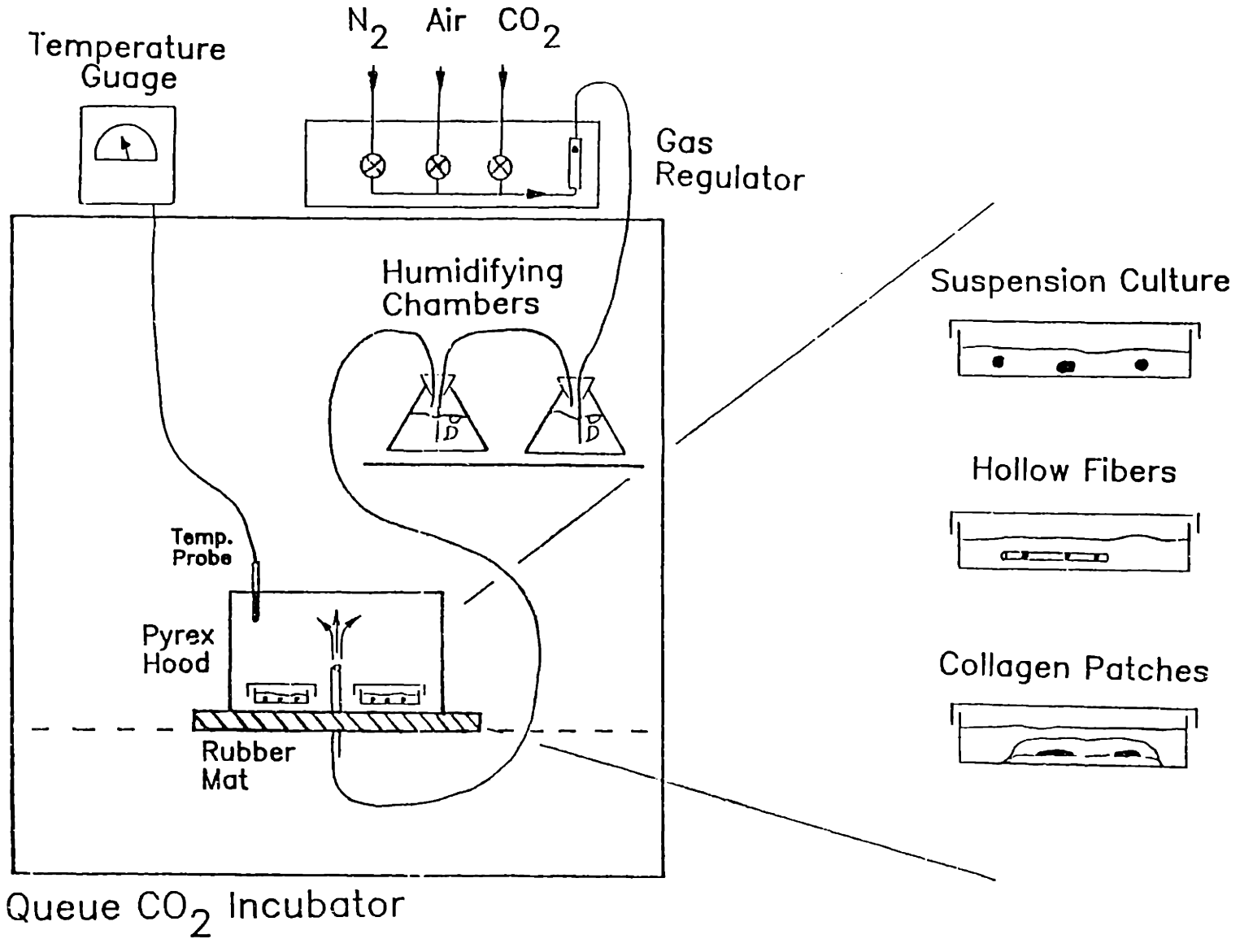

FIGURE 1. Schematic diagram of static islet culture system.

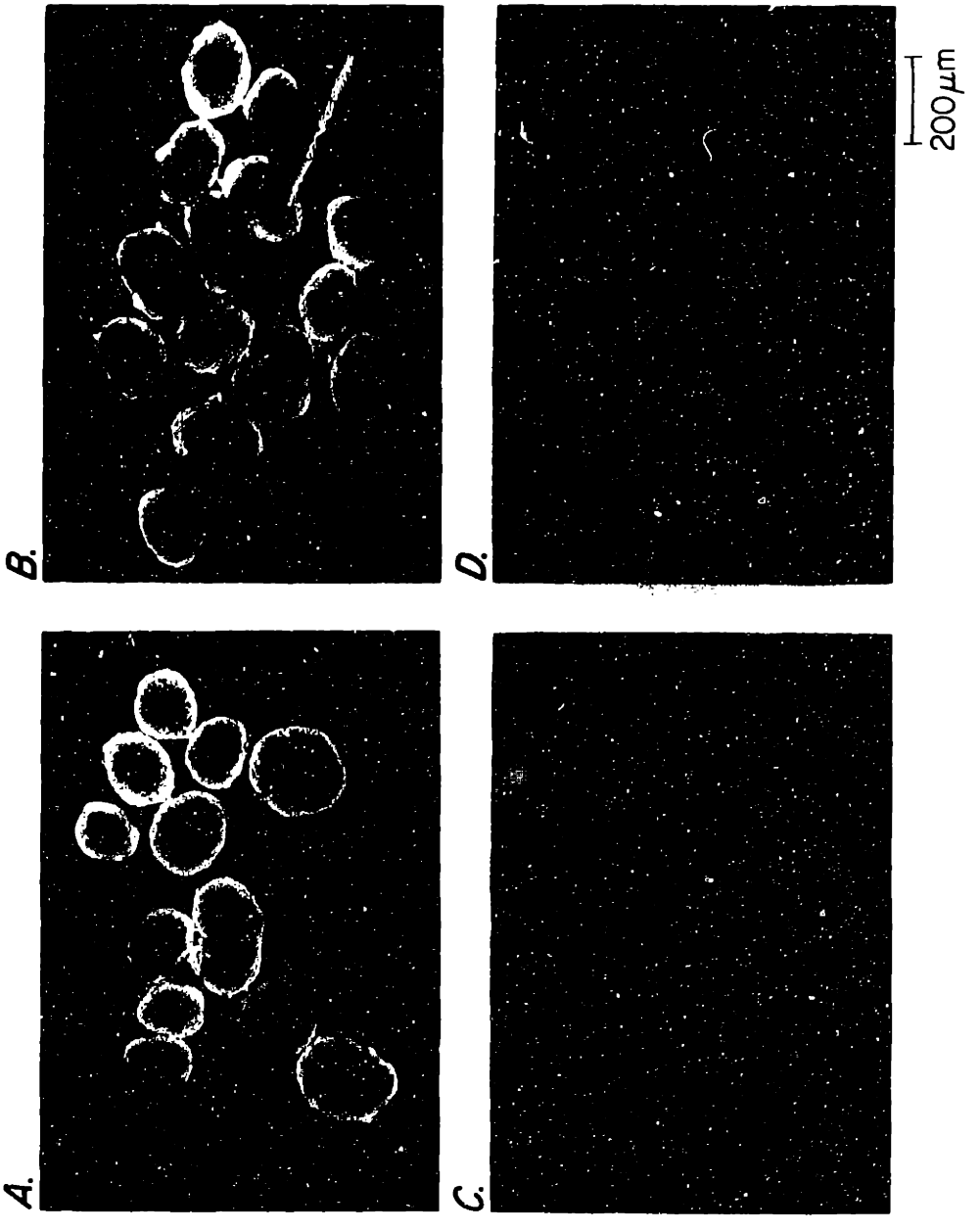
A.
B.
C.
D.
200μm

FIGURE 2. Photomicrograph illustrating the development of necrotic cores in cultured islets over time. Panels A-D represent 1 day, 1, 2, and 5 weeks of culture, respectively. Islets were cultured in DMEM with 10% serum petri dishes (Falcon 1007, 12 ml medium, medium depth = 6 mm) either freely suspended (panels A and B) or lightly attached to a collagen layer on the bottom of the dish (panels C and D).

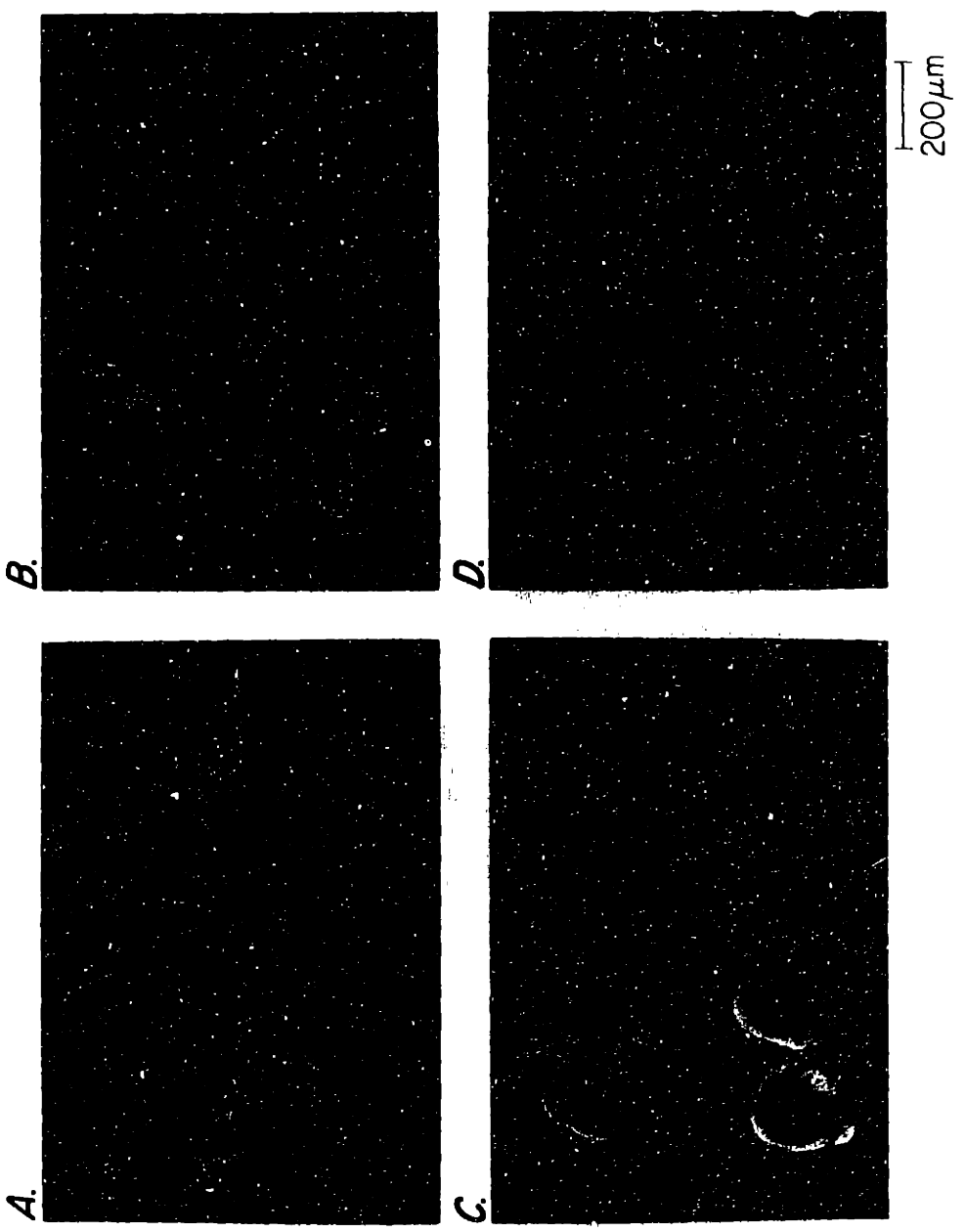
B.
D.
200μm
A.
C.

FIGURE 3. Islet size dependence of necrotic cores in islets cultured for two weeks. Islets in all photos are from the same preparation and were cultured together for two weeks in DMEM with 10% serum (6.0 mm depth). During culture, islets lightly attached to the collagen coated petri dish bottom. Islets in panels A-C were sorted according to their approximate diameters which averaged 134, 172, and 215 μm, respectively. Panel D shows islets before sorting for size.

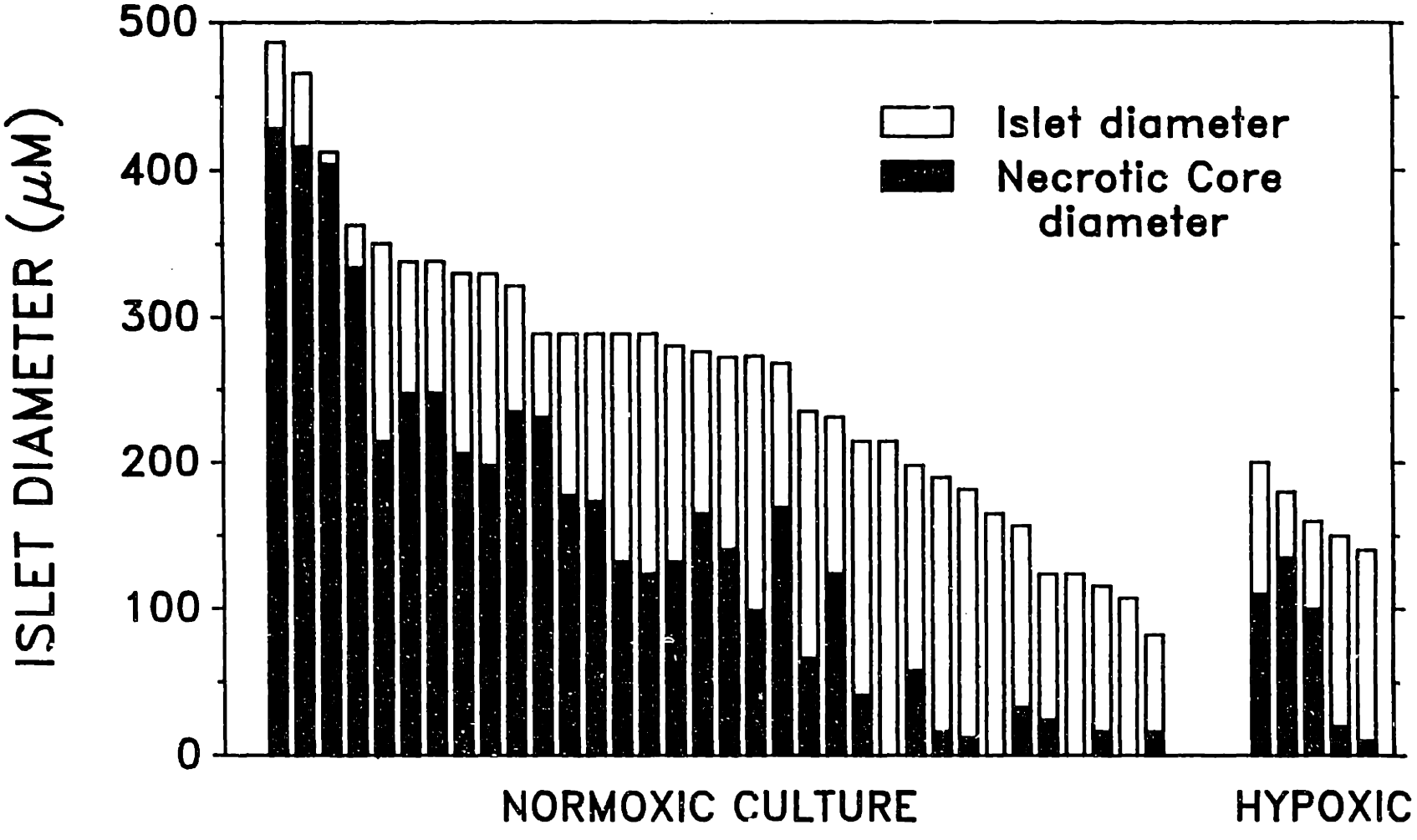

FIGURE 4. Bargraph illustrating the dependence of necrosis on islet diameter and medium pO_2. Normoxic islets were cultured for two weeks in static free suspension (medium depth = 6 mm) at a gas pO_2 = 142 mm Hg. Hypoxic islets were cultured for one week at a gas pO_2 = 142 mm Hg and then for one week at a reduced gas pO_2 = 30 mm Hg (depth = 6 mm). Medium was changed every third day. Necrotic diameters were measured as the region of black staining at the islet core. Islet size range covers the largest islets seen and is not representative of average sizes of islets.

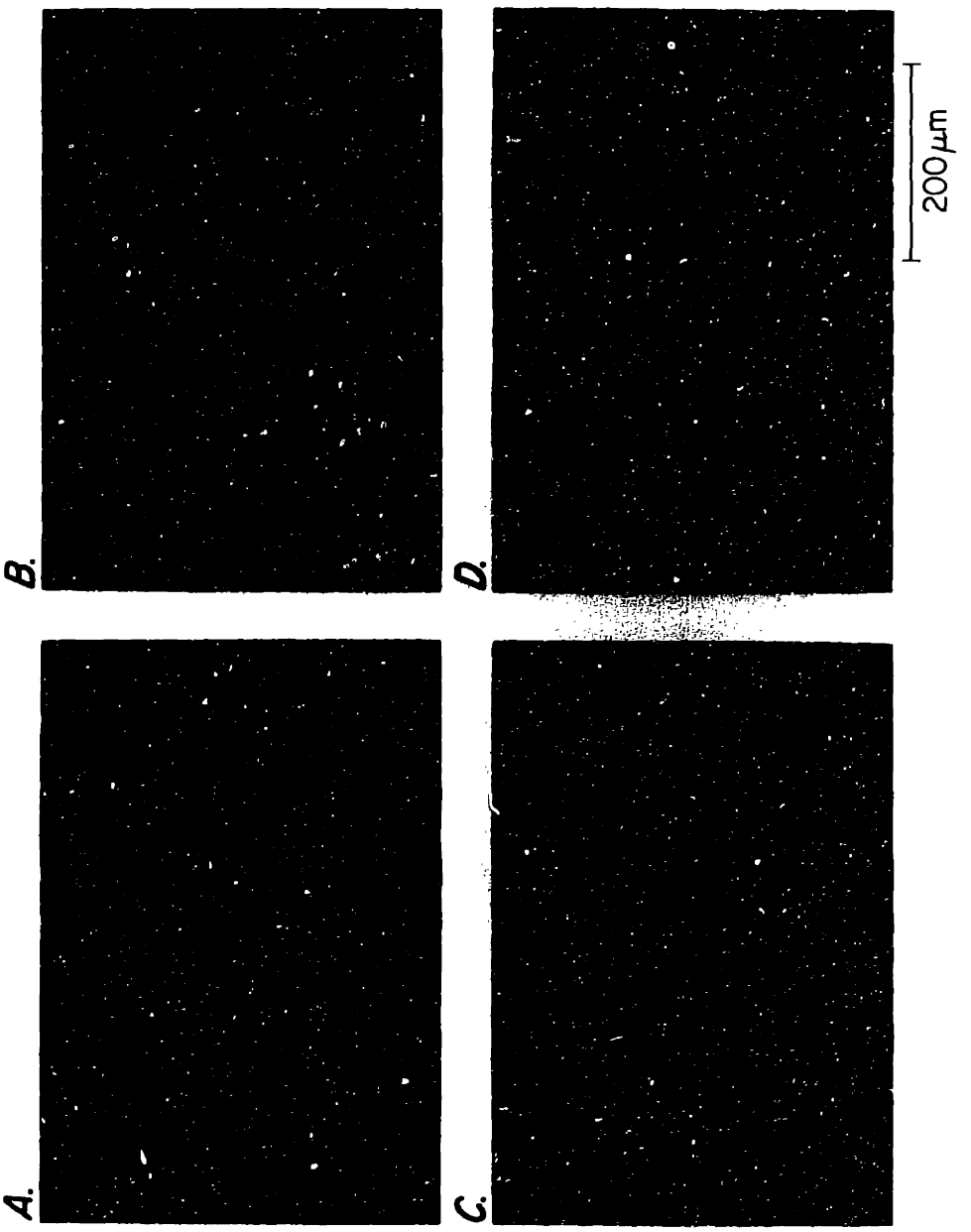
A.
B.
C.
D.
200μm

FIGURE 5. Effect of decreased culture pO_2 on the development of necrotic cores. Islets in panels A and B were cultured at normoxic gas pO_2 (142 mm Hg) for ten days. Islets in panels C and D were cultured for four days at normoxic pO_2, 24 hr at hypoxic pO_2 (9 mm Hg in the gas), followed by one day at normoxic pO_2. Culture medium depth equaled 6 mm in all cases.

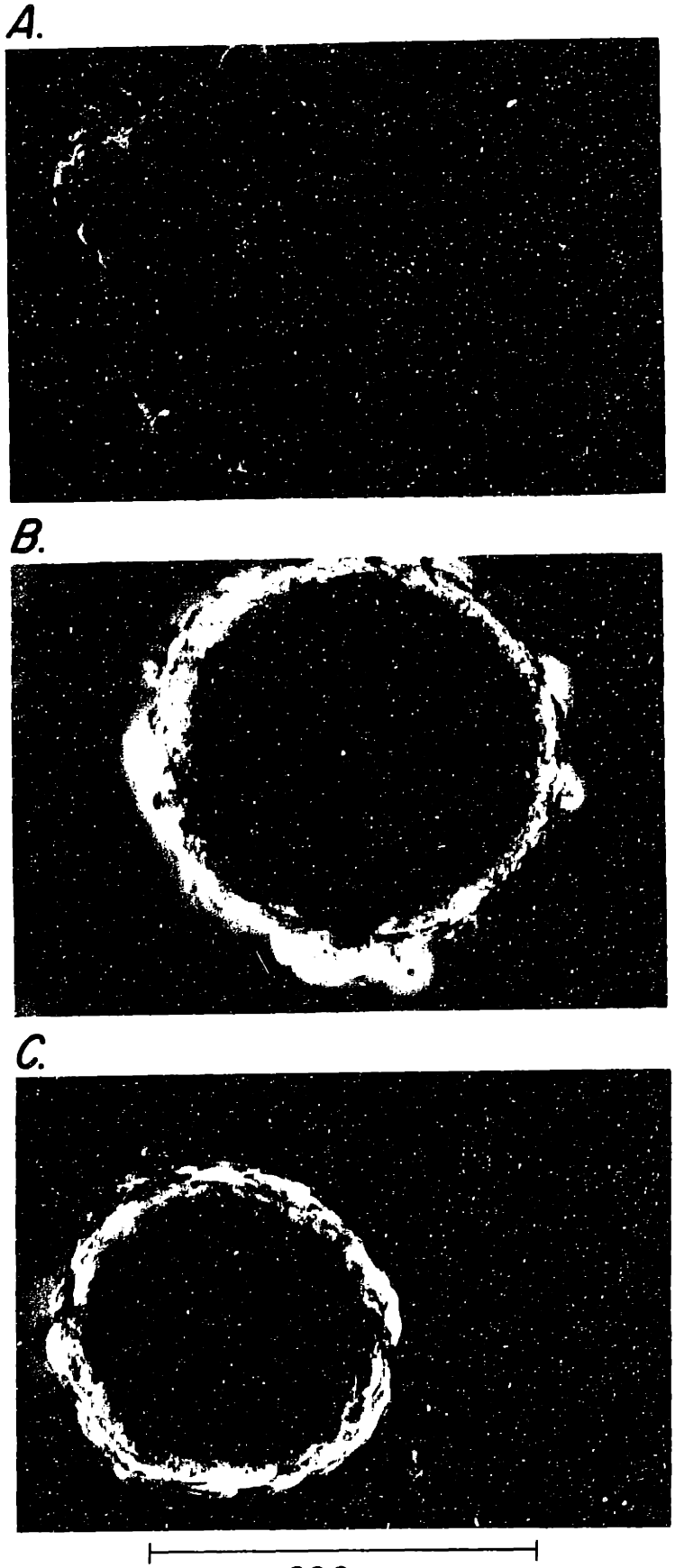
A.
B.
C.
200 μm

FIGURE 6. Comparison of black discolored regions to trypan blue stained cores. Islets were cultured as described in the caption of Figure 5 for panels C and D except that the hypoxic pO_2 was 11 mm Hg. Panel A shows an islet with a black discolored core which has not been stained with trypan blue. Islets in panels B and C were exposed to 0.06% (w/v) trypan blue for five min. Necrotic regions as ascertained by both trypan blue staining and black discoloration comprised about 80% of the islets' diameter.

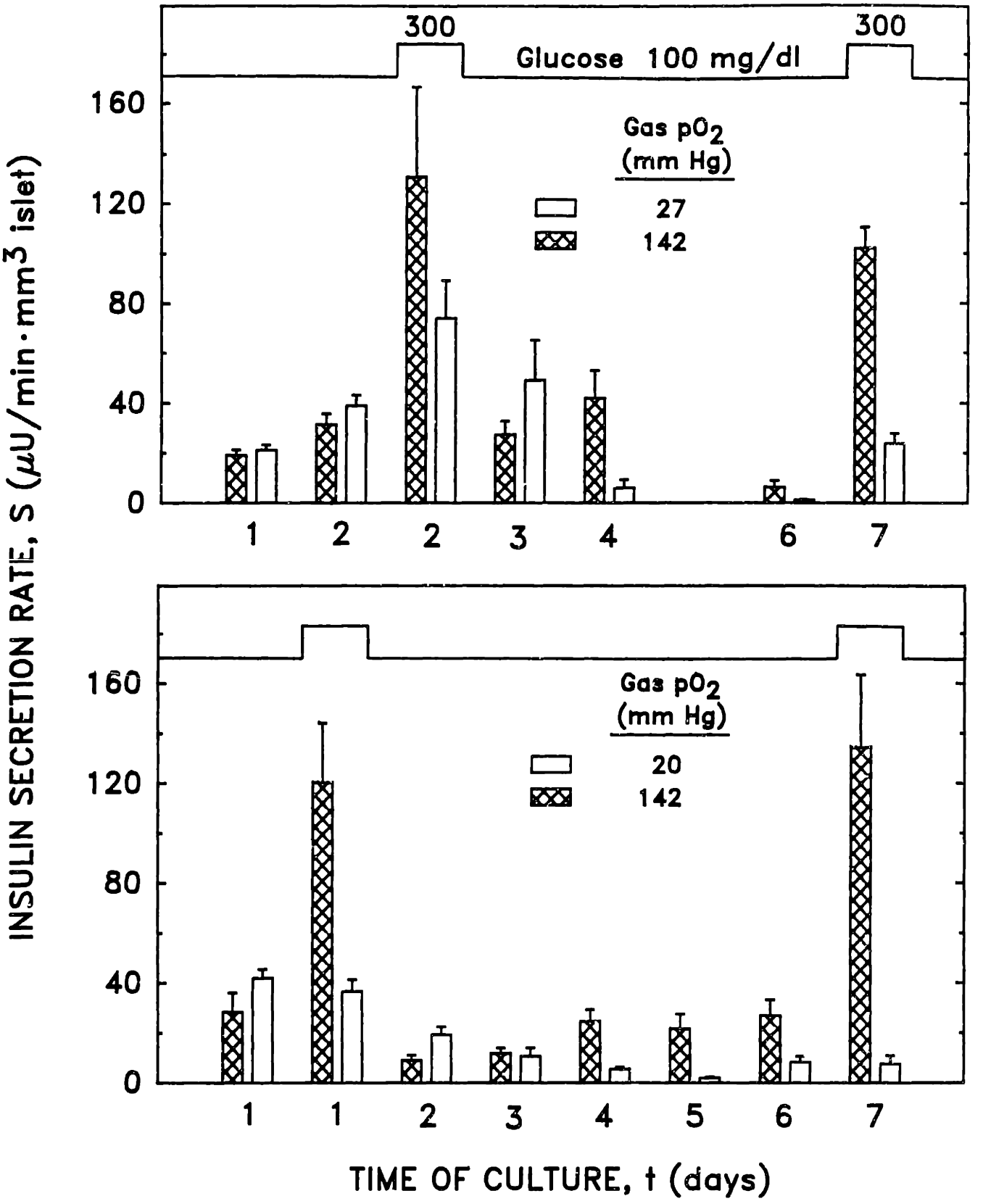

FIGURE 7. Effect of hypoxia on insulin secretion rate of islets cultured in static free suspension. For each batch, five approximately 200 μm diameter islets were placed in non-attaching petri dishes (Falcon 1007) containing six ml DMEM with 10% NBCS (culture medium depth = 3 mm). Five dishes were run per pO_2 level checked. The bars represent the average +/- sem. The pO_2 listed in each panel is the pO_2 in the gas phase. Islets were daily transferred by micropipette to new petri dishes containing fresh culture medium pre-equilibrated at 37°C and the respective culture pO_2. Old medium was daily assayed for basal secretion rate. The response of islets to 300 mg/dl glucose stimulation was measured in one-hr stimulation tests on days 2 and 7 in the upper panel and on days 1 and 7 in the lower panel.

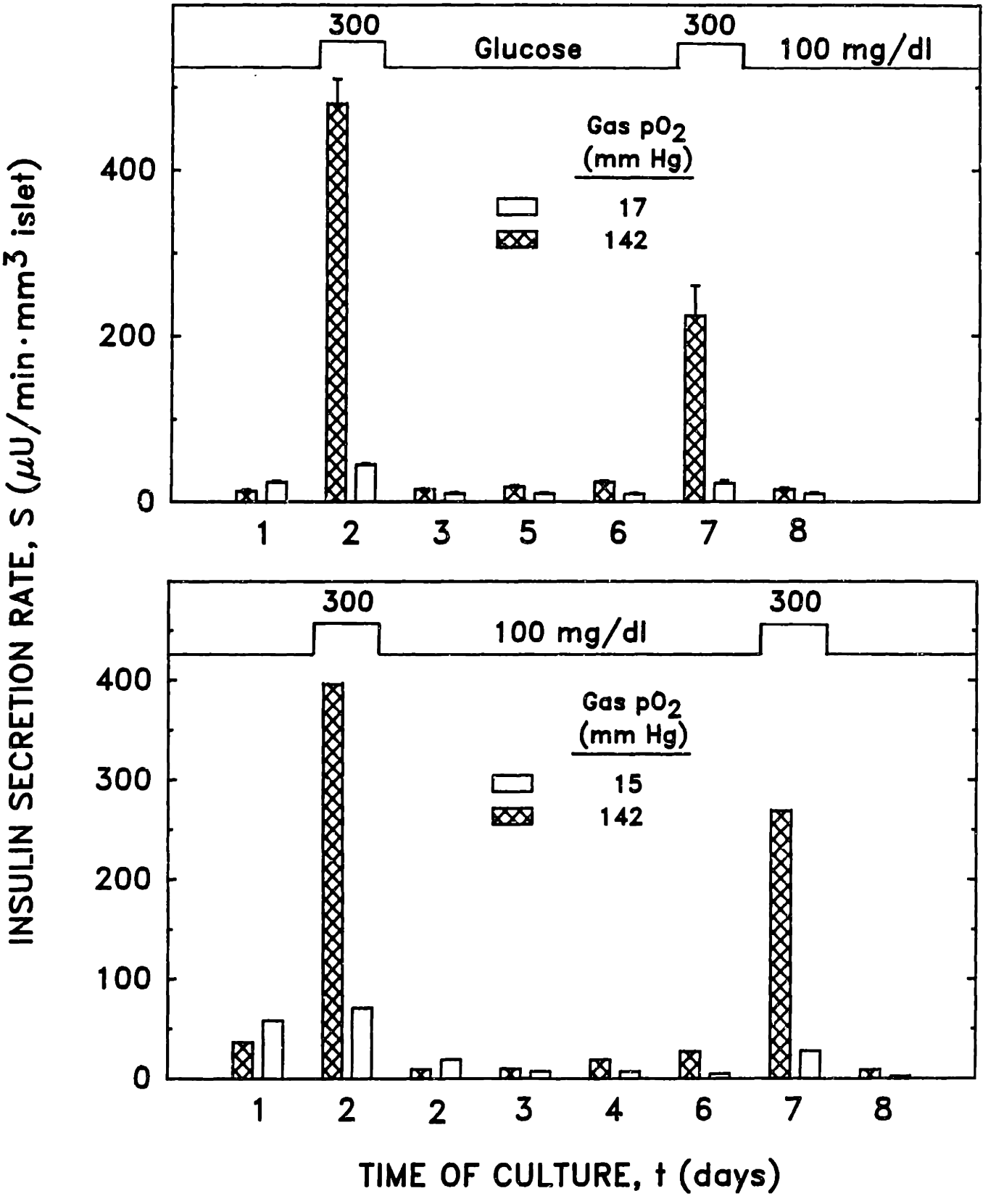

FIGURE 8. Effect of hypoxia on insulin secretion rate of islets cultured in static free suspension. Islet batch preparation is as described in caption of Figure 7. The response of islets to 300 mg/dl glucose stimulation was measured in 1 1/2 hr stimulation tests on days 2 and 7 in both panels.

A.
B.
C.
D.
200μm

FIGURE 9. Photomicrographs of islets cultured for ten days under 142 (panels A and B) or 15 mm Hg (panels C and D) oxygen. Islets were sandwiched between two layers of collagen on the bottom of petri dishes (Falcon 3001) to prevent loss of islet mass. Each dish contained 1.5 ml DMEM with 10% serum (medium depth = 1.6 mm). Culture medium was changed by aspirating out spent medium and gently pipetting fresh, temperature and gas equilibrated medium over the islet/collagen patch. Normoxic islets exhibited no evidence of central necrosis. Islets cultured for ten days at 15 mm Hg exhibited large central necrotic regions as evidenced by black discolored cores. Insulin secretion of these islets is shown in Figure 10.

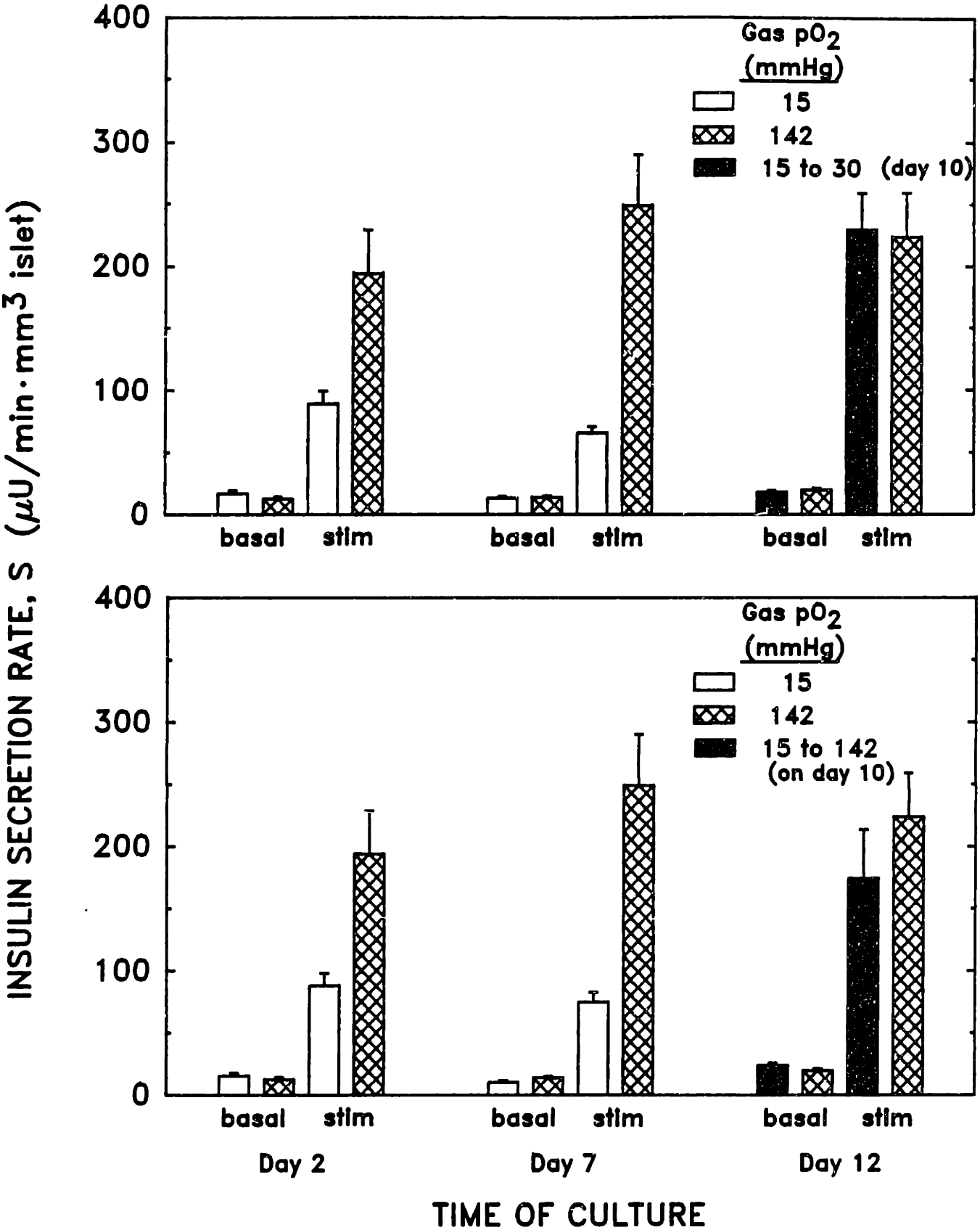

FIGURE 10. Reversibility of hypoxia reduced insulin secretion. Islets were cultured as described in the text and the caption of Figure 9. Normoxic islets were cultured at 142 mm Hg throughout the experiment. Hypoxic islets were cultured at a gas pO_2 of 15 mm Hg for 10 days at which time the pO_2 was raised to either 30 (upper panel) or 142 mm Hg (lower panel). Glucose (300 mg/dl) stimulated secretion was tested on days 2, 7 and 12. (n=5).

CHAPTER 6:

MEASUREMENT OF OXYGEN UPTAKE OF INTACT ISLETS AND REAGGREGATED CELLS UNDER OXYGENATED AND OXYGEN LIMITING CONDITIONS

SUMMARY

The maximum rate of oxygen uptake (Vmax) and the medium oxygen concentration at which oxygen uptake was reduced to one-half of maximum (P_{50}) was measured in stirred suspensions of intact rat islets of Langerhans and of small reaggregated canine and rat islet cell clusters. Glucose stimulated oxygen consumption by canine and rat cell aggregates was found to be well represented by Michaelis-Menten kinetics with Vmax of 3.98 and 4.38 x 10^{-8} mol $O_2/cm^3 \cdot sec$ and P_{50} of 1.16 and 1.05 mm Hg, respectively. Vmax of intact rat islets (3.14 x 10^{-8} mol $O_2/cm^3 \cdot sec$ was similar to that of cell aggregates, however the P_{50} of intact islets was 10-fold larger than that of small cell aggregates due to the large internal diffusion resistance of intact islets. Cells in an energy depleted state due to uncoupling with FCCP or to chronic hypoxia can temporarily double their oxygen uptake, Vmax = 8.9 x 10^{-8} mol $O_2/cm^3 \cdot sec$ and are best represented by a P_{50} that is diffusion limited. Comparison of the hypoxic pO_2 at which oxygen uptake and insulin secretion are affected indicates that oxygen uptake is reduced over the same range of pO_2 as is insulin secretion but to a lessor degree.

INTRODUCTION

Individual pancreatic islets of Langerhans in vivo are fed by at least one arteriole and are highly vascularized by a glomerular-like network of capillaries (Bonner-Weir and Orci, 1982). Consequently, cells throughout the islet are exposed to oxygen partial pressure (pO_2) levels that are probably never far below that of arterial blood. This arrangement not only supplies the oxygen requirements of the resting islet cell but can also accommodate the increased oxygen consumption that accompanies insulin secretion when cells are stimulated by a variety of insulin secretagogues, such as glucose (Hellerstrom, 1967; Andersson,

Gunnarsson, and Hellerstrom 1976; Panten and Klein, 1982; Malaisse and Sener, 1988); amino acids (Hellerstrom, 1967; Hellman, Sehlin, and Taljedal 1971; Lundgren et al, 1977; Welsh, Hellerstrom, and Andersson 1982) fatty acids, and other substances (Panten and Klein, 1982; Welsh, Hellerstrom, and Andersson 1982).

We have recently reported that the glucose-stimulated insulin secretion rate from isolated rat and canine islets measured in perifusion experiments (Dionne et al., 1989-3) is reduced upon exposure of the islets to perfusate pO_2 below 60 mm Hg. The extent of this reduction increases as pO_2 is decreased. The same phenomenon is observed with small aggregates (Dionne et al., 1989-4) prepared from suspensions of single islet cells, but the reduction in secretion rate is substantially less than observed with the larger intact islets at any given value of perfusate pO_2. This sensitivity of insulin secretion rate to hypoxic pO_2 levels is of particular importance in situations where intact islets are cut off from their normal blood supply and must receive nutrients and oxygen by diffusion from the external surroundings. These include any in vitro studies with whole islet preparations, islet transplants (Scharp, 1984; Southerland et al., 1989) prior to their revascularization in vivo (Griffith et al., 1977; Andersson et al., 1989; Menger et al., 1989), and islets encapsulated in immuno-isolation devices (Scharp et al., 1984) wherein the islet tissue is separated from the vascular supply by a semipermeable membrane.

The observed oxygen sensitivity of insulin secretion rate is determined by the intrinsic sensitivity of the β-cells and the local pO_2 to which these cells are exposed. The local pO_2 will be different from that of the external environment because of the presence of pO_2 gradients within and external to the tissue which are induced by cellular consumption of oxygen. The magnitude of these gradients is determined, in turn, by the oxygen consumption rate and its dependence on the local pO_2, the diffusion coefficient of oxygen within the tissue, and the oxygen transport properties of the surrounding environment. Quantitative information about each of these components is required in order to better understand the complex interplay between oxygen consumption, oxygen diffusion, and oxygen sensitivity of insulin secretion.

As a first step in this process, we have studied the oxygen consumption rate of islet tissue. The maximum oxygen uptake rate (Vmax) of isolated whole islets respiring at full oxygenation has previously been reported (Hellerstrom, 1967; Hedeskov, Hertz, and Nissen 1972; Andersson, Gunnarsson, and Hellerstrom 1976; Lundgren et al, 1977; Altman et al, 1979; Hutton and Malaisse, 1980; Panten and Klein, 1982). However, no data on the dependence on oxygen concentration has been described. In this paper, we report measurements of the oxygen consumption rate of isolated intact islets and of small islet cell aggregates as a function of bulk pO_2. Islet cell aggregates were studied, rather than single islet cells, because the aggregates display glucose-responsive insulin secretion properties similar to that of whole islets, whereas single cells do not (Dionne et al., 1989-4). Because of their small size, pO_2 gradients in and around aggregates should be much smaller than with islets, and the oxygen consumption properties of aggregates should provide a closer approximation to that of individual cells within islets than the properties displayed by intact islets themselves. Oxygen consumption rates were determined from measurements of the rate of oxygen depletion from a well-stirred suspension of islet tissue. Oxygen concentration was measured using a new optical method based upon the ability of oxygen to quench the phosphorescence of selected phosphors (Kautsky, 1939; Vanderkooi et al., 1986 and 1987). The technique has a very rapid response time and is sensitive to oxygen concentration over the entire range of interest. It has recently been used to characterize the oxygen dependence of respiration in mitochondria (Wilson et al., 1988) and various types of cells (Robiolio et al., 1988; Rumsey et al., 1989).

MATERIALS AND METHODS

Isolation and Preparation of Islets, Single Cells, and Cell Aggregates

Isolation and Culture of Islets of Langerhans. Islets of Langerhans were isolated from 200 - 350 g male Sprague-Dawley rats (Charles River Lab, Kingston, NJ) using a modified collagenase digestion / ficoll purification technique (Lacy and Kostianovsky, 1967; Scharp et al, 1980) which has previously been described (Dionne, Colton, and Yarmush 1989-2 and

1989-3). Briefly, the pancreas was distended in situ by injecting 10-15 ml of ice cold Hanks solution without Ca^{++}, Mg^{++} (H2387 Sigma Chemical Co., St Louis MO) containing 1.7 mg/ml collagenase (108 8882 Boehringer Mannheim, Indianapolis, IN). The distended pancreas was dissected free and digested under mild agitation at 37°C until the islets were free of acinar tissue as ascertained by microscopic examination. The slurry was then rinsed and purified by centrifugation on a discontinuous ficoll gradient. Separated islets were washed four times in Dulbecco's modified Eagles Medium (DMEM, D5523, Sigma Chemical Co.) with 10% (v/v) newborn calf serum (NBCS, 200-6010AJ, GIBCO), and hand-picked to remove remaining acinar contamination.

Purified rat islets were cultured in non-attaching polystyrene bacteriological Petri dishes (8-757-12, Fisher Scientific Co, Pittsburgh PA). The culture medium was Dulbecco's modified Eagles medium (DMEM, D5523, Sigma Chemical Co) containing 5.6 mM (100 mg/dl) glucose, 50 U/ml Penicillin, 50 μg/ml Streptomycin, and 10% (v/v) newborn calf serum (NBCS, 200-6010, GIBCO). Four to five hundred islets were dispersed throughout each dish. Dishes were placed in a 37°C incubator with a gas environment of 95% air and 5% CO_2. Islets remained freely floating and did not attach over the one-day period of culture before oxygen uptake testing.

Canine islets were isolated using a modification of standard collagenase digestion / ficoll purification techniques by Biohybrid Technologies, Shrewsbury MA and generously donated by Dr. William Chick for these studies. Canine islets were received in and cultured in M-199 with Earle's salts (400-1100, GIBCO, Grand Island, NY) containing 11.2 mM glucose and 10% (v/v) fetal bovine serum (GIBCO) and were cultured at 37°C under 5% CO_2/95% air. Islets remained freely suspended under these conditions. Twelve hr before oxygen uptake testing, canine islets were transferred to dishes containing normal culture medium with 5.6 mM glucose in order to equilibrate to the lower glucose concentration.

Preparation of Single Cell Suspensions. Slurries of single rat or canine islet cells were prepared from purified whole islets by digesting with trypsin (Pipeleers et al, 1982 & 1985;

Halban et al, 1982). Following one day of culture after isolation for rat islets, or two to three days for canine islets, approximately 3000 purified islets and the surrounding culture medium were transferred from petri dishes into a 50 ml centrifugation tube (Falcon 2098, Becton Dickinson Inc). Islets were rinsed three times by centrifugation at 100 x g and resuspension in digestion medium composed of Hanks balanced salt solution without Ca^{++}, Mg^{++} (H2387 Sigma Chemical Co., St Louis MO) to which was added 50 U/ml Penicillin, 50 μg/ml Streptomycin (600-5140AG, GIBCO, Grand Island, NY), and 0.35 g/l Hepes (H0763, Sigma Chemical Co.), pH 7.4, to which was added 1.0 mM ethylenedinitrilo-tetracetic acid (EDTA, J.T. Baker Chemical Co., Phillipsburg, NJ). Following the final rinse, islets were resuspended in five ml of digestion medium with EDTA per 1000 islets in a polypropylene tube and gently agitated by aspiration and expulsion with a 200 μl pipette for eight min at room temperature, after which, 0.5 g/l trypsin (610 5305 GIBCO) and 25 μg/ml Dnase (10 159, Boehringer Mannheim, Indianapolis, IN), both in phosphate-buffered saline, were added to a final concentration of 25 μg/ml and 2 μg/ml, respectively. The tube was placed in a 30-32°C waterbath and islets were digested with digestion agitation by the pipette for approximately 10 min to produce a suspension of single cells. In experiments in which cells were to be allowed to reaggregate, digestion was continued until microscopic examination indicated that greater than 80% of the population represented single cells with the remaining fraction consisting of aggregates composed of two or three cells. At this point, the digestion was halted by diluting with two ml of ice cold culture medium per ml of digestion medium. The slurry was centrifuged at 250 x g for 6 min to form a cell pellet. The supernatant was aspirated off and the pellet was resuspended in culture medium and transferred into non-attaching microbiological petri dishes (8-757-12, Fisher Scientific Co; 15 ml medium per 8.5 cm diameter dish). Cells spontaneously reaggregated during culture to form small, loosely-organized cell clusters. The number of cells in a cluster and the overall size of each aggregate were roughly controlled by adjusting the cell density and the time of culture. With densities in the range of 15 - 20,000 cells/cm^2 surface area, corresponding to 2-3% area coverage, the majority of cells formed small aggregates of 5-15 cells over a one-day culture period.

Sizing and Counting of Islets and Single Cells. Single cell concentration and viability were determined by counting a cell slurry sample of known volume diluted 1:1 with 0.06% (w/v) trypan blue (630-5250, GIBCO) in phosphate buffered saline using a hemacytometer (Reichart Scientific Instruments, Buffalo NY). Cells were counted immediately following trypsinization before they began to reaggregate and again after oxygen uptake testing when most of the cells were contained in aggregates. The number of cells counted in large aggregates was difficult to accurately determine, and the estimates for larger aggregates are approximate. The total tissue volume of cell aggregate preparations was calculated from the cell concentration measurements of each preparation made prior to aggregation and the average volume per cell. The number of intact islets in whole islet batches was determined before O_2 uptake testing by counting the number of islets in a sample of known volume of medium under a dissecting microscope.

Samples of cell aggregates and intact islets were photographed under a dissecting microscope on the day of O_2 uptake testing for later sizing using a calibrated reticule. The micrographs of the different tissues were projected onto a screen, and their exterior dimensions were measured using the calibrated grid. The size distribution of each aggregate preparation was evaluated two ways. First, the number of cells in each aggregate was counted. Secondly, a characteristic cross sectional diameter was estimated as twice the distance through which oxygen would have to diffuse in order to reach all portions of the aggregate. This distance, designated as the aggregate diffusion diameter (ADD), was taken as the diameter of a spherical aggregate and the cross-sectional diameter of a cylindrical chain-like aggregate. For the substantial fraction of aggregates with irregular shape, judgement was employed to estimate a reasonable dimension. The volume fraction of each diameter size range was calculated as the number of cells contained in aggregates having a diameter in that size range divided by the total number of cells in all of the aggregates examined.

The size distribution and total tissue volume of intact islets were based on individual measurements of the external dimensions of samples containing 5 to 10 percent of the islets in each preparation. Slight deviations from a spherical shape of each islet were accounted for by

measuring both the largest islet diameter and the diameter normal to it, assuming each islet could be represented by a prolate ellipsoid, and calculating its volume, v, from $v = \pi a^2 b/6$, where a and b are the smaller and larger axes, respectively. The equivalent spherical diameter, d, for each islet was calculated as that of a sphere of equal volume, $v = \pi d^3/6$; thus, $d = (a^2 b)^{1/3}$.

Cellular Volume Fraction of Islets

In order to estimate the volume fraction of intact islets, occupied by cells, spherical islets were handpicked, individually sized, and then trypsinized in a known volume of digestion medium, after which the cell concentration was immediately counted. Twelve to fifteen islets were individually sized using a calibrated reticule under a dissecting microscope. Three axes of an ellipsoid were evaluated, one major (a) and two minor (b and c). The minor semiaxis, or depth, c, was measured by individually turning each islet on edge using a 20 μl pipette. Only spherical or nearly spherical ellipsoidal islets were examined. The volume of each islet was calculated from $v = \pi abc/6$. Using a 20 μl pipette, sized islets were transferred by aspiration through three petri dishes filled with digestion medium containing 1 mM EDTA. Following the final rinse, islets were placed in a two ml glass test tube along with 100 μl of digestion medium with EDTA, 10 μl of 0.5 g/l trypsin, and 16 μl of 25 μg/ml Dnase. Islets were digested for approximately 10 min at 37°C with manual agitation using a 20 μl pipet. When microscopic examination revealed that essentially 100% of the population was represented by single cells, digestion was quenched by adding 20 μl ice cold culture medium and then immersing the outside of the test tube in 4°C water. A sample of the cell slurry was photographed under a microscope for later sizing in order to obtain the average diameter and volume per cell. The cell concentration was immediately determined by counting the number of cells in a known volume on a hemacytometer. The volume fraction of the islet that was composed of cells was calculated as the cell volume (total number of cells in the preparation times the volume per cell) divided by the volume of intact islets used to prepare the preparation.

Oxygen Uptake Measurements

Transport of Islet Tissue. Islet and cell aggregate preparations used for oxygen uptake studies were isolated and cultured for one day at Massachusetts Institute of Technology and transported by air to the University of Pennsylvania (UPa) on the day of oxygen uptake testing. The preparations were transferred to 50 ml centrifuge tubes (Falcon 2098, Becton Dickinson Inc) containing approximately 45 ml culture medium and five ml air, the latter to ensure adequate oxygenation during transport. Tubes were intermittently shaken to prevent settling and further aggregation. At UPa, the tubes containing the tissue samples were kept between 32-37°C in a water bath for 2 hr or more until aliquotes were withdrawn for actual testing. Trypan blue staining, microscopic examination, and glucose-stimulated insulin secretion with perifusion experiments verified that there was no change in islet tissue viability, morphology, or function as a result of this handling procedure.

Oxygen-Quenched Phosphorescence Measuring System. Tissue oxygen uptake was evaluated with an apparatus equipped for measuring the oxygen-dependent quenching of phosphorescence. The technique provides rapid, accurate measurements of oxygen concentration down to as low as 0.05 μM (Vanderkooi et al, 1987; Wilson et al, 1988; Robiolio et al, 1989). Briefly, the apparatus consisted of a glass cuvette (0.275 ml volume, square inside cross section, about 0.5 cm wide on each side) containing a small teflon-coated magnetic stirring bar (length about 0.4 cm, diameter about 0.1 cm) which functioned as the O_2 uptake chamber. The tissue sample was loaded in the chamber which was then completely filled with oxygen uptake medium supplemented with 0.01 μM palladium coproporphyrin (Porphyrin Products, Logan, UT), which served as the phosphorescence probe for oxygen, and 1-5 U/ml catalase (Sigma Chemical Co), which reacted with H_2O_2 injected into the cuvette to produce dissolved oxygen and water. The oxygen uptake medium was phosphate buffered saline (PBS: 8.67 g/l NaCl, 7.0 ml/l 1M K_2HPO_4 and 3 ml/l 1M KH_2PO_4), containing 0.35 g/l Hepes, 0.5 g/l bovine serum albumin (BSA, A2153, Sigma Chemical Co),

and either 50 or 300 g/dl glucose, pH7.4. The cuvette was capped with a ground glass stopper so as to completely eliminate the gas phase. The stopper contained a two-cm long one-mm diameter hole bored through its center which functioned as an unstirred oxygen diffusion barrier and allowed for injection of reagents into the uptake chamber without removing the cap. The sample cuvette was placed in an aluminum block seated on a magnetic stirrer. A xenon flash lamp was placed on one side of the cuvette and photomultiplier tube. on the other.

The rate of oxygen consumption by the tissue was measured by monitoring the oxygen concentration in the medium as a function of time. The phosphorescence of excited palladium coproporphyrin was quenched by dissolved oxygen; the higher the oxygen concentration, the shorter the lifetime of the phosphorescence. The xenon flash lamp was used to excite the luminophore to its triplet state with light of wavelengths between 380 and 440 nm. The lifetime of the emitted light (>635 nm) was used to calculate the oxygen concentration from the Stern-Volmer relationship (Wilson, Rumsey et al., 1988). The quenching constant was $1.4 \times 10^8 M\ sec^{-1}$ for the experimental conditions employed and was unaffected by the addition of reagents to the cuvette. At the normal operating frequency of the flash lamp, oxygen concentration data was collected at the rate of 50 phosphorescent lifetimes/sec. In these experiments, the measurements from 10-20 lifetimes were averaged per data point resulting in the generation of an oxygen concentration measurement every 0.1 to 0.2 sec, these data stored in computer for on-line display and subsequent data analysis.

The temperature of the uptake chamber was held at 36 ± 1°C by wrapping the aluminum block of the cuvette holder with heating tape connected to a variable voltage source. Temperature was monitored continuously by a rapidly-responding thermistor (Digital Thermometer 500, VWR, San Francisco CA) taped to the exterior surface of the cuvette and intermittently by placing a glass thermometer into the holder with the cuvette removed. These measurements indicated that the cuvette temperature reached 36°C within five min and remained constant between 35 and 37°C throughout the testing period. All data was collected after the initial five minute warm-up period.

Oxygen uptake of Cell Aggregates and Islets. Ten to fifteen min before loading islet tissue into the oxygen uptake chamber, the sample tissue was pelleted by centrifugation and resuspended in 25 ml of oxygen uptake medium. Immediately before testing, the islet tissue was again pelleted by centrifugation and transferred into the 0.275 ml glass cuvette in oxygen uptake medium supplemented with palladium coproporphyrin and catalase. The cuvette was capped and placed in its holder. Despite attempts to decrease the initial oxygen concentration of the oxygen uptake medium by bubbling with 5% CO_2, 95% N_2 prior to introduction into the cuvette, initial oxygen concentrations were usually close to that expected at room air equilibration and required five to ten min to drop to the test range in which measurements were recorded. This allowed adequate time for the sample cuvette temperature to stabilize at 36 ± 1°C. With aggregates, oxygen was recorded as it decreased from about 60 μM until it was totally depleted. At that time, the medium in the uptake chamber was immediately reoxygenated to a concentration of ≥ 60 μM by the injection of 0.5 - 2.0 μl of dilute (<0.2 mM) H_2O_2. With intact islets recording was begun at an oxygen concentration of about 100 μm. Normally one to four oxygenation / depletion cycles were measured with each tissue sample.

Under normal conditions in which the cells are exposed to a sufficiently high oxygen concentration, ATP generation by mitochondrial oxygen consumption. The cells are maintained at a high energy level with a high ratio of [ATP]/[ADP)(Pi)] (Rumsey et al., 1989), where each symbol represents intracellular concentrations. This condition, referred to as state 5 is applicable to all the cells in the islet tissues at least initially, in the experiments described above. Additional experiments were carried out to examine the effect of reducing the intracellular energy level on oxygen consumption. Following several of the oxygenation / depletion cycles under coupled conditions, oxygen uptake of tissue was uncoupled from ATP generation by the addition of 2 μl of 2 mM Carbonylcyanide-p-trifluoro-methoxyphenylhydrazone (FCCP, kindly donated by Dr. P. Heytler of E.I. duPont de Nemours Co., Wilmington, DE) to a final concentration of 15 μM. Uncoupling with FCCP

causes cell respiration to increase while the energy state decreases (Wilson et al., 1988). The concentration of FCCP was experimentally chosen to maximally stimulate oxygen consumption by the islet tissue.

Following several uncoupled oxygenation / deoxygenation cycles, mitochondrial respiration of was inhibited by the addition of Amytal (amobarbital sodium, Eli Lilly, Indianapolis, IN) which slows the rate at which oxygen is reduced through the electron transport chain of oxidative phosphorylation. Successive additions of Amytal were made in an attempt to bracket the uptake rate of normal, coupled tissue in order to compare the oxygen concentration dependence of uptake by coupled and metabolically uncoupled tissues under conditions of similar maximum oxygen uptake rates. Experiments to investigate inhibited oxygen uptake were carried out primarily with islet cell aggregates.

Each experiment yielded data for the chamber medium oxygen concentration $[O_2]$ versus the time at which each data point was collected. The rate of change of medium oxygen concentration, $d[O_2]/dt$ (mol/l/sec) was calculated as a function of time from the changes in each successive data point. For purposes of presentation, these data were also smoothed using a centered, seven-point running average. The data for oxygen uptake rate of the chamber as a whole, $Q = d[O_2]/dt$, was converted into an oxygen consumption rate per unit volume of tissue from

$$V = \frac{V_{ch}}{V_c} \frac{d[O_2]}{dt} \qquad (1)$$

where V_{ch} is the chamber volume (0.275 cm^3), V_c is the volume (cm^3) of tissue placed in the uptake chamber, and V is the oxygen consumption rate of the tissue (mol/sec•cm^3 tissue). Oxygen concentration was converted to oxygen partial pressure pO_2 (mm Hg) from

$$[O_2] = \alpha \, pO_2 \qquad (2)$$

where α is the bunsen solubility coefficient for oxygen which was taken as 1.27×10^{-9} mol/cm^3 mmHg for oxygen in buffered salt solutions at 37°C (Chen et al., 1985; Panten and Klein, 1982; McLimans et al., 1968; Altman and Dittmer, 1971).

In addition to the data for oxygen uptake rate as a function of $[O_2]$ (or pO_2), two parameters which characterize the data were of particular interest: V_{max}, the maximum uptake rate at high oxygen concentration, and $[O_2]_{50}$ (or P_{50}), the oxygen concentration or partial pressure at which $V = 1/2\ V_{max}$. These parameters were estimated three different ways: (1) Starting at the highest $[O_2]$ for which data was recorded, successive groups of 10 data points for decreasing $[O_2]$ were averaged. The average value of V_{max} (actually of Q_{max} which was then converted to V_{max} by Equation 1) was evaluated from all data groups down to the point where V showed a definite decrease from V_{max}. $[O_2]_{50}$ was calculated by linear interpolation amongst all data for which V/V_{max} lay between 0.48 and 0.52) (using usually about 20-25 data points for islets, five data points for aggregates). (2) The data was plotted on an expanded scale. The best curve through the data was drawn by eye, and V_{max} (actually Q_{max}) and $[O_2]_{50}$ were read off the graph. (3) The data was fit by nonlinear least squares regression to an expression in the form of Michaelis-Menten kinetics:

$$Q = \frac{d[O_2]}{dt} = \frac{Q_{max}\ [O_2]}{([O_2]_{50} + [O_2])} \qquad (3)$$

The chamber based values of Q and Q_{max} were directly converted to the cell volume based values of V and V_{max} using Equation 1.

RESULTS

Characterization of Islet Tissue

Photomicrographs of intact rat islets (panel A) and of rat (panel B) and canine (panel C) cell aggregates, taken on the day of oxygen uptake testing, are shown in Figure 1. Whereas intact islets were solid agglomerates of cells, islet cell following one day of reaggregation formed short linear or branched chains (panel B, rat) or small, loosely organized clusters (panel C, canine). Reaggregated cells were firmly attached together as ascertained by visual inspection and by attempts to disrupt them by expulsion through a micropipette. Whereas the compact nature of intact islets forces their interior to be supplied with oxygen by diffusion through the islet mass, the small size and more open structure of one-day old cell aggregates

allows better access of oxygen to individual cells. As a result, the oxygen uptake characteristics of small cell aggregates should approximate those of individual islet cells much more closely than would intact islets.

The size distributions of reaggregated rat and canine islet cells cultured for one day are shown in Figure 2. The aggregate diffusion diameter ranged between 13 and 60 μm. For both rat and canine preparations, about 15% of the aggregates were single cells which accounted for 80+% of the number of aggregates between 10 and 15 μm in diameter; about 65% of the volume was represented by aggregates between 25 and 45 μm in diameter. The number- and volume-average diffusion diameters were 31.1 ± 14.5 and 38.9 ± 8.5 μm, respectively, for rat aggregates and 28.1 ± 9.4 and 35.3 ± 9.0 μm, respectively for canine aggregates.

The equivalent spherical diameter of intact rat islets ranged from 70 to 310 μm (Figure 3). Although small islets far out numbered large islets (61% of the islets were 190 μm or less in diameter), the majority of the volume mass was represented by relatively large islets (islets larger than 190 μm diameter comprised about 67% of the total volume. The number and volume-average diameter of sampled islets was 173 ± 47 and 214 ± 55 μm, respectively, or nearly six times larger than the diffusion diameter of the islet cell aggregates.

The fraction of the total volume of rat islets that was occupied by cells was calculated by carefully measuring the volume of a small number of intact islets, dispersing the cells by trypsinization, and then measuring the total volume of the cells in the resulting slurry. Islet volume was calculated from the three measured axes of an ellipsoid, a, b, and c. For the islets sample examined, the ratio of axes was a/b = 0.85 ± 0.09 and b/c = 0.87 ± 0.11 (n=35). The volume of cells was calculated by counting the number of cells and multiplying by the volume per cell. Islet cells were spherical with diameters ranging from to μm. The number average diameter was 14.4 ± 2.1 μm (n=50). The cell volume fraction of intact islets cultured for one day after isolation averaged 0.67 ± 0.14 (n=3). The remaining one third of the islet volume not occupied by cells presumably consisted of extra-cellular and vascular space. Based on these data, each islet was calculated to contain an average of 1.8×10^3 cells.

For oxygen uptake experiments, the volume of each islet was calculated by assuming that the two minor axes were identical, i.e., b = c. The calculated volume was corrected by multiplying it by c/b using the ratio of b/c reported above. This corrected volume was used to calculate the oxygen uptake rate per unit volume.

Oxygen Uptake of Coupled Tissue

Cell Aggregates. In order to measure the oxygen uptake rate of islet cell aggregates, approximately two million aggregated cells comprising about 2.5 - 3.0 mm^3 tissue volume were loaded into the 0.275 ml oxygen uptake chamber for each run. The oxygen uptake medium contained either 50 or 300 mg/dl glucose to simulate basal or glucose-stimulated conditions, respectively. A sufficiently large volume of cells was required in order to rapidly deplete the dissolved oxygen once the oxygen uptake rate became oxygen-concentration dependent in order to limit the degree to which the phosphorylation state ratio ([ATP]/([ADP][Pi])) of cells changed throughout the measurement period.

Aggregates formed a uniformly stirred cell suspension within the oxygen uptake cuvette, the respiration of which followed by monitoring the depletion of $[O_2]$ in the oxygen uptake medium within the cuvette (Figure 4). Following the complete depletion of oxygen, the cuvette medium was reoxygenated by injecting 1-3 μl dilute H_2O_2 into the cuvette which was immediately converted to dissolved oxygen and water by catalase included in the uptake medium. Cell aggregates were passed through several sequential oxygenation/deoxygenation cycles without permanently affecting their respiratory rate as long as the hypoxic period was relatively short (about one min or less) and they were reoxygenated to a minimum of 65 μM in order to give the cells adequate time to recover from the hypoxic period of the previous cycle.

The data from the first oxygen uptake curve shown in Figure 4 is replotted in the upper panel of Figure 5. The oxygen uptake rate in the medium, Q, was calculated by computing the derivative of the oxygen verses time curve, $(d[O_2]/dt)$, and is plotted verses the medium $[O_2]$ in the lower panel of Figure 5 (point-by-point derivative). Respiration of the

cell aggregates resulted in a linear decrease in medium $[O_2]$ until oxygen became rate limiting at low $[O_2]$ (< 15 μM). At $[O_2]$ below about 15 μM, oxygen consumption of cell aggregates was progressively reduced with falling $[O_2]$ resulting in the curvature of the $[O_2]$ verses time curve.

The oxygen uptake rate as a function of medium $[O_2]$ was fit by least squares non-linear regression to Michaelis-Menten kinetics in order to determine values for Qmax and $[O_2]_{50}$ for the aggregate preparation. The best fit of the Michaelis-Menten kinetic expression is shown as the solid, smooth line through the data in Figure 5C. The best parameter fits for this preparation were: Qmax = 0.35 μM/sec; $[O_2]_{50}$ = 0.91 μM. Estimates of Vmax and P_{50} obtained directly from the data by numerical or graphical analysis agreed very closely with estimates obtained by fitting a Michaelis-Menten kinetic expression to the data (Q_{max} agreed to within ± 0.01 μM/sec and $[O_2]_{50}$ to within ± 0.03 μM). Similar close agreement was observed in all oxygen uptake experiments with coupled cell aggregates on the first oxygen depletion cycle. The oxygen uptake rate predicted by the fitted Michaelis-Menten kinetics is compared to the experimental data at low oxygen concentrations in Figure 6.

Qmax was converted to a tissue volume basis by multiplying by the volume of medium in the cuvette and dividing by the volume of tissue used in the experiment (Equation 1). For this oxygen uptake run, Batch 3K4A1, $Vmax_{cell}$ = 3.56 x 10^{-8} mol O_2/sec•cm^3 tissue. P_{50}, converted from μM oxygen concentration to mm Hg oxygen partial pressure by dividing by the oxygen solubility coefficient at 37°C (Equation 2), was 0.72 mm Hg.

Oxygen concentration and rate of oxygen uptake curves for two different preparations of rat islet cell aggregates in medium with 300 mg/dl glucose are shown in Figure 7. Data were analyzed as described for canine aggregates and similar trends were found. The relative deficit in oxygen uptake rate observed in both sets of rat aggregate data from about 10 to 20 μM oxygen concentration, and to a lesser extent with canine aggregates (Figure 5) over the range 5 to 10 μM, may be indicative of the presence of a second oxygen consuming reaction with a higher P_{50} than the main oxygen consuming reaction. This pattern was observed in roughly 75% of all of the uptake runs with aggregates.

Values for the coupled Vmax and P_{50} of cell aggregates were obtained from repeated oxygenation cycles of the same aggregate preparation, different preparations from the same cell isolation batch, and different isolation batches. A summary of these values is contained in Table 1. Vmax is reported for each experimental run in terms of mol O_2 / cm^3 cells • sec, P_{50} is reported in mm Hg. The mean ± s.d. is reported for each tissue batch in the latter two columns.

Values of Vmax and P_{50} from multiple oxygenation/deoxygenation cycles of the same sample were in close agreement providing that there was adequate reoxygenation between cycles. Close inspection of the 2nd through 4th oxygen depletion curves of Figure 4 reveals that after the first cycle, immediately after reoxygenation the slope ($d[O_2]/dt$) of succeeding oxygen consumption curve was initially significantly higher than either the slope of the first cycle or the slope of the same curve after about one min. This phenomenon, which is seen more clearly in the plot of Q verses time shown in Figure 8, is caused by cells hyper-respiring following a period of oxygen depletion in order to restore the normal [ATP]/([ADP][Pi]). Because of this phenomenon, failure to reoxygenate to a sufficiently high level (or for a sufficiently long time) could result in the hyper-respiration being interpreted as the normal V_{max} and the decrease in consumption seen at about one min in Figure 8 as being caused by oxygen limited consumption. Several oxygen uptake runs were eliminated because of this possibility (for example 3K5A1 and 2 listed in Table 1).

Table 2 summarizes the average values of Vmax and P_{50} for different species and glucose concentrations. The maximum oxygen uptake rate of canine islet cell aggregates exposed to basal (50 mg/dl) glucose was 3.51 ± .40 x 10^{-8} mol O_2 /sec•cm^3 tissue. Vmax was increased ($p \leq .025$) when the glucose concentration was raised to 300 mg/dl glucose ($Vmax_{stim}$ = 3.98 ± .44 x 10^{-8} mol O_2 /sec•cm^3 tissue). The value of P_{50} was also elevated in aggregates exposed to 300 compared to 50 mg/dl glucose ($p \leq .01$). Glucose-stimulated Vmax of rat aggregates (4.38 ± .22 x 10^{-8} mol O_2 /sec•cm^3 tissue) was slightly higher ($p \leq .05$) than the corresponding glucose-stimulated Vmax of canine aggregates; however, the respective values of P_{50} were not statistically different ($p \leq .01$).

Intact Islets. Intact rat islets loaded into the oxygen uptake chamber retained their integrity and formed a well-stirred heterogenous mixture of respiring spheroids. Islets recovered following several coupled oxygen uptake cycles were observed to be viable, intact spheroids by microscopic analysis and vital staining. The depletion of $[O_2]$ in the oxygen uptake medium for two representative O_2 uptake runs are plotted versus time in the upper panels of Figures 9A and 9B. Whereas oxygen depletion caused by cell aggregate respiration was linear with time until the $[O_2]$ dropped below about 15 μM, oxygen consumption by intact islets became dependent on the medium $[O_2]$ at levels as high as 50-60 μM. The rate of oxygen uptake as a function of medium $[O_2]$ for intact islet preparations is plotted in the lower panels of Figures 9A and 9B. The values of Qmax were measured graphically and numerically over the flat section of the uptake curve above 60 μM oxygen. The values of $[O_2]_{50}$ were manually extracted (see Methods) from the data at the $[O_2]$ where Q equaled 1/2 of Qmax. The values of P_{50} measured in intact islets is about an order of magnitude larger than the corresponding values for cell aggregates.

The solid and dashed curves in the lower panels of Figures 9A and 9B illustrate the lack of fit of islet oxygen uptake data to that predicted by a Michaelis-Menten type expression. In the data of Figure 9B, Michaelis-Menten parameters extracted from least squares non-linear regression significantly overpredicted the values of Qmax (1.33 μM/sec) and $[O_2]_{50}$ (35.9 μM) in order to fit the data below 60 μM oxygen. Michaelis-Menten predictions based on the graphically and numerically measured values of Qmax (0.80 μM/sec) and $[O_2]_{50}$ (13.1 μM) significantly underpredicted the data over most of the $[O_2]$ range measured. As a result, oxygen uptake of intact islets cannot be adequately described by a Michaelis-Menten kinetic expression using an overall Vmax and P_{50} based on whole islet consumption.

Individual Vmax and P_{50} values for seven islet oxygen uptake runs are shown in Table 1. The mean ± standard deviation of the data is included in Table 2. The P_{50} of intact rat islets (10.7 ± 3.1 mm Hg) was significantly higher ($p \leq .001$) than the P_{50} of either rat or canine aggregates. The glucose-stimulated Vmax of intact rat islets ($3.14 \pm .55 \times 10^{-8}$ mol O_2 /sec•cm^3 tissue) was lower ($p \leq .01$) than that of either rat or canine aggregates.

Oxygen uptake of FCCP Uncoupled and Amytal Inhibited Tissue

Following several oxygenation/depletion cycles under coupled conditions, cellular mitochondrial respiration was uncoupled from ATP synthesis by the addition of FCCP, lowering the energy state of the cells. Under these conditions, normal metabolic control over cell respiration was lost resulting in maximal, zero-order oxygen uptake with an intrinsic mitochondrial Km for oxygen uptake equal to zero. Under these conditions, the measured P_{50} is simply an indication of the $[O_2]$ at which cell aggregate oxygen uptake is reduced to 50% of normal due to oxygen diffusion limitations to the tissue. After one to three uncoupled oxygenation/deoxygenation cycles, uncoupled mitochondrial respiration was inhibited by the addition of Amytal. Incremental doses of amytal were added in an attempt to match the value of Vmax for uncoupled, amytal-inhibited tissue to the value normal coupled tissue.

Figure 10 illustrates the Michaelis-Menten fit of coupled and uncoupled oxygen consumption from the same preparation (Batch 4K4) of canine aggregates. Uncoupling increased Qmax (and hence Vmax) to more than double the normal coupled rate. This increased consumption rate in turn resulted in an increase in the $[O_2]_{50}$ from 0.95 to 2.01 μM as diffusion became more limiting at the higher oxygen uptake rate. When the oxygen uptake of FCCP uncoupled aggregates was inhibited back to the normal coupled level using Amytal (Qmax = 0.34 μM/s), the $[O_2]_{50}$ decreased to 0.77 μM as compared to 0.95 μM for coupled aggregates at a similar Qmax (data not shown). The relative magnitudes of the coupled and uncoupled/inhibited $[O_2]_{50}$ values at the same Qmax are indicative that some portion of the coupled $[O_2]_{50}$ is the result of the intrinsic kinetics of coupled cell intra-cellular mitochondrial oxygen uptake but that a major portion of the magnitude of the $[O_2]_{50}$ is caused by diffusion limitations in and around the aggregates.

Figure 11 illustrates the oxygen uptake curve (upper panel) and oxygen consumption curve (lower panel) of FCCP uncoupled and Amytal inhibited intact rat islets. In contrast to small cell aggregates, when intact islets are uncoupled and inhibited back to the normal coupled level of Vmax, the $[O_2]_{50}$ did not change. At a Qmax of 0.62 and 0.54 μM/s for

coupled (Figure 9A) and uncoupled islets, respectively, the respective values of $[O_2]_{50}$ were 10.5 and 11.1 μM for the same preparation of islets. The lack of sensitivity of $[O_2]_{50}$ to the coupled state of the tissue is indicative that oxygen diffusion limitations are the major cause of the high $[O_2]_{50}$ measured in intact islet preparations. Table 3 shows the mean ± standard deviation or range of Vmax and P_{50} for uncoupled and inhibited tissues, respectively.

DISCUSSION

Characterization of Islet Tissue

Small reaggregates of canine and rat pancreatic islet cells rather than single cells were used to approximate intrinsic cellular oxygen uptake because reaggregated cells more accurately reflect the secretion properties of β-cells located within the normal islet matrix. Insulin secretion from pure single cells has been found to be very low or non-responsive to a glucose challenge (Pipeleers et al, 1985; Weir et al, 1984; Dionne et al., 1989-4), whereas reaggregated cells respond to glucose with both first and second phase insulin secretion that is similar in magnitude to that of cells in intact isolated islets (Pipeleers et al, 1982; Dionne et al., 1989-4). The time of, and cell concentration during, reaggregation were important parameters in forming loose reaggregated strings and small clusters of cells with minimal internal diffusion resistance. Cells reaggregated for one day at a density of 15 - 20,000 cells/cm^2 formed branched strings and/or loose clusters with an average diffusion diameter equal to 35 and 39 μm for canine and rat aggregates, respectively. The ADD of aggregates was approximately 2 1/2 times larger than the diameter of single β-cells (14.4 ± 2.1 μm) and about 1/6 the diameter (1/36 to 1/216 the volume) of intact islets.

Though generally spheroidal in shape, the actual dimensions of random intact islets was found to be more ellipsoidal with a ratio of major to minor axes averaging 0.81 ± 0.13 . Some ellipsoids were slightly flattened and the average ratio of the minor axes of selected islets was 0.87 ± 0.11 . The equivalent spherical diameter of unsorted islets ranged between 70 and 310 μm with a volume weighted average of 214 μm. Approximately two thirds (0.67 ± 0.13) of

the volume of islets cultured for one day after isolation were accounted for by cells. The remaining one third of the islet volume was presumably vascular and extracellular space.

O_2 Consumption of Cell Aggregates and Intact Islets (Coupled)

The oxygen uptake of intact rat islets of Langerhans and small reaggregated clusters of rat and canine islet cells was measured as a function of oxygen concentration. Oxygen consumption of small reaggregated cell clusters was found to be fit by Michaelis-Menten kinetics with values of Vmax between 3.51 - 4.38 x 10^{-8} mol/sec•cm^3 and of P_{50} between 0.93 - 1.16 mm Hg. The specific values of Vmax and P_{50} varied with metabolic stimulus and tissue species (See Tables 1 and 2). Increasing the glucose concentration in oxygen uptake medium from 50 to 300 mg/dl resulted in an increase in both the Vmax ($p=.05$) and P_{50} ($p=.01$) of canine aggregates. The glucose stimulated Vmax of rat aggregates was slightly higher than that of canine aggregates although the P_{50} was not statistically different ($p=.05$).

The oxygen uptake of intact islets is of particular interest because islets are the naturally occurring state of insulin secreting β-cells. Whereas normal, in vivo islets are highly vascularized by a network of capillaries (Bonner-Weir and Orci, 1982) which deliver oxygen and other metabolites throughout the islet, isolated islets lose their vascular connections and must rely on diffusion of oxygen and other metabolites from the surrounding environment to supply their metabolic requirements. Because of the relatively large size of islets, it is possible that islet cell oxygen consumption and the resulting internal diffusion gradients could result in the development of hypoxic or anoxic islet cores, especially during elevated oxygen uptake during stimulated secretion.

Values of Vmax (3.14 ± 0.55 x 10^{-8} mol/cm^3•sec) and P_{50} (10.7 ± 3.1 mm Hg) were numerically and graphically measured for glucose-stimulated oxygen uptake of intact rat islets; however, overall Michaelis-Menten type kinetic expressions did not adequately fit the actual oxygen consumption data (see Figure 9B). The non-oxygen limited value of Vmax compared closely with Vmax data in the literature for glucose stimulated, oxygenated, intact islets obtained using cartesian divers (Hellerstrom, 1967; Andersson, Gunnarsson, and

Hellerstrom 1976; Lundgrun et al, 1977) and clark style pO_2 electrodes (Panten and Klein, 1982). The literature values ranged from 2.94 - 4.90 x 10^{-8} moles $O_2/cm^3 \cdot sec$, and averaged 3.90 ± .93 x 10^{-8} moles $O_2/cm^3 \cdot sec$ (data converted to similar units for comparison purposes).

Oxygen uptake parameters of islet cell aggregates have not previously been reported. However, the Vmax values of aggregates and islets were measured at high medium $[O_2]$ where the $[O_2]$ was not rate limiting. Under these conditions the diffusion resistance of intact islets is not important and Vmax of cell aggregates can be compared to that of intact islets. Vmax of canine islet cell aggregates under basal (50 mg/dl) glucose stimulation (3.51 ± .40 x 10^{-8} mol $O_2/cm^3 \cdot sec$) fit within the range of the values of basal whole islet respiration reported in the literature (0.9 - 4.8 (ave = 2.4 ± 1.2) x 10^{-8} moles $O_2/cm^3 \cdot sec$; Hellerstrom, 1967; Hedeskov, Hertz, and Nissen, 1972; Andersson, Gunnarsson, and Hellerstrom 1976; Lundgrun et al, 1977; Hutton and Malaisse, 1980; Panten and Klein, 1982). The glucose stimulated Vmax of rat (4.38 ± .22 x 10^{-8} mol $O_2/cm^3 \cdot sec$) and canine (3.98 ± .44 x 10^{-8} mol $O_2/cm^3 \cdot sec$) aggregates also fits within the range of Vmax reported for intact islets (2.94 - 4.90 x 10^{-8} moles $O_2/cm^3 \cdot sec$).

The slightly higher values of Vmax measured in aggregates as compared to islets may be reflective of a different metabolic state of reaggregated cells or may be due to differences in the volume basis of the two measurements. One reason that basal oxygen uptake by aggregates is higher than the average basal islet oxygen uptake may be that although insulin secretion is quiescent at basal glucose levels for both aggregates and islets, aggregates have the additional energy expenditure associated with cell reaggregation and reattachment. This would explain the relatively small difference between glucose stimulated and basal aggregate Vmax. It is therefore possible that the oxygen uptake of cell aggregates cultured to a stable aggregate size or immobilized in a gel may decrease to a rate similar to that reported for intact islets.

Conversely, the similarity between measured Vmax of cell aggregates and intact islets is enhanced if the Vmax of either islets or aggregates is corrected by the cellular volume fraction of the islet (V_f = 0.67 ± 0.13). Multiplying aggregate oxygen consumption rates by

0.67 to account for the void fraction in islets results in a glucose stimulated rat islet cell aggregate consumption of 2.94 x 10^{-8} mol O_2/cm^3islet•sec which is very close to the value of 3.14 x 10^{-8} mol/cm^3islet•sec measured for intact rat islets.

Oxygen consumption under oxygen limiting conditions has not previously been reported for either islet cell aggregates or intact islets. However, comparison of the P_{50} measured with reaggregated islet cells (0.93 - 1.16 mm Hg) to the P_{50} measured with other cells in the same oxygen uptake system indicates that aggregate P_{50} values are within the range of cell P_{50} values: neuroblastoma cells (0.8 mm Hg; Robiolio et al., 1989), M21 cells (1.14 mm Hg; unpublished results), SK-MEL-2 cells (1.41 mm Hg; unpublished results) and cardiac myocytes (1.39 mm Hg; Rumsey et al., 1989). The P_{50} of islet cell aggregates is higher than the Km measured for isolated mitochondria at high ATP/ADP (Km = 0.44 mm Hg; 25°C, Wilson et al, 1988).

The extent to which oxygen consumption of metabolically coupled islet cell aggregates is decreased by low medium [O_2] is a combination of intrinsic kinetic and of diffusive transport limitations. The relative contribution of each of these factors is quantitatively analyzed in detail elsewhere in order to extract an intra-tissue value of the oxygen diffusivity (Dionne et al., 1989-7). Qualitatively, even in small oxygen consuming particles such as cell aggregates, an oxygen diffusion gradient exists within the tissue such that the pO_2 at the aggregate surface is higher than the pO_2 at the aggregate core. In addition, because of hydrodynamic and transport limitations, even in a well stirred system the pO_2 at the aggregate surface is lower than the pO_2 in the stirred bulk medium where the pO_2 is monitored. As a result an oxygen gradient exists from the bulk medium to the aggregate surface and from the aggregate surface to the core of the aggregate. The overall oxygen consumption of the aggregate is furthermore a summation of the oxygen uptake of mitochondria dispersed throughout the aggregate, whose oxygen consumption is probably based on the local pO_2 which varies with radial position. As a result of these considerations, the pO_2 in the medium which reduces a tissue's oxygen consumption to any particular level must be taken as an upper bound to the actual pO_2 in the tissue which results in an intrinsic reduction in the local

oxygen uptake. The reported values of P_{50} therefore represent upper bounds to the actual tissue pO_2 at which local tissue oxygen consumption is reduced to one half of maximum. It has been suggested, and preliminarily supported with a quantitative model of oxygen uptake by myocytes, that the intrinsic P_{50} of cells may be equal to the Km of the mitochondrial oxygen uptake and that the difference between the mitochondrial Km and the cellular P_{50} is due to diffusion gradients in and around oxygen consuming cells (Rumsey et al., 1989-Appendix).

Whereas the Vmax values of cell aggregates and intact islets indicated similar oxygen uptake rates of identical cells in different organizational structures, the 10 fold larger P_{50} of intact islets as compared to cell aggregates is indicative of much greater diffusion limitations in large islets. It is probable that the intrinsic kinetics of oxygen uptake of cells incorporated in aggregates or in islets are quite similar and that the difference in measured P_{50} values are entirely caused by the larger diffusion gradients in and around intact islets.

While the large value of whole islet P_{50} is not indicative of intrinsic reaction properties, it does suggest that oxygen limitations within the islet as a whole can be a serious factor in many experiments with isolated islets even at relatively high surrounding pO_2 levels. Furthermore, slight reductions in the rate of oxygen consumption may result in large changes in the secretion of insulin or other hormones from islet cells. The potential effect of oxygen limitations on insulin secretion if of particular concern since the insulin secreting β-cells are concentrated in the islet core (Orci, 1981) where oxygen consumption is most reduced due to the gradient in pO_2 throughout the islet. We have previously reported that insulin secretion from intact, 200 μm diameter rat islets cultured for one day after isolation was reduced to one-half of maximum by a reduction in perfusate pO_2 to 27 mm Hg (Dionne et al., 1989-3). In contrast, oxygen consumption of one day old rat islets averaging 214 μm in diameter reported in this paper was only reduced to about 80% of maximum at 27 mm Hg and was not reduced to one-half of maximum until the medium pO_2 reached 10.7 mm Hg. This difference could be caused by either a higher sensitivity of secretion verses uptake to hypoxia or to the generally lower pO_2 of the insulin secreting β-cell core.

The potential for oxygen limitations in intact islets is further increased in non-stirred systems, if several islets are clumped or packed together, or if the oxygen consumption of the islets is significantly raised by exposure to insulin secretagogues. The potential for oxygen limitations is decreased in stirred systems using small, non-clumped islets respiring under basal stimulation.

Uncoupled/inhibited and chronically hypoxic cell aggregates and islets

FCCP uncouples oxidative phosphorylation from ATP synthesis. Thus when cells are uncoupled, their energy state - represented by the [ATP]/[ADP][Pi] ratio - decreases. In response, the intrinsic Km of mitochondrial oxygen uptake drops to about zero and the Vmax increases to some cellular limit as cells utilize as much oxygen as possible in an attempt to regain their normal energy state (Wilson et al, 1988). In a similar fashion, tissue exposed to hypoxia will become energy depleted as ATP is reduced to ADP (Hellman, Idahl, and Danielson, 1969; Wettermark et al, 1970; Randle and Hales, 1972). As the energy state of the cell changes, the intrinsic Km of cellular mitochondria will approach zero, the theoretical value of Vmax will increase, and the local tissue oxygen consumption will best be described by zero order kinetics.

In tissue with a low [ATP]/[ADP][Pi] ratio as a result either of FCCP uncoupling or of depleted energy due to chronic hypoxia, oxygen consumption will be limited only by the maximum rate at which oxygen can be reduced in the cell and by diffusion limitations of oxygen to the tissue. This effect was observed both immediately following reoxygenation of previously hypoxic tissue and when oxygen uptake of islet cell aggregates was uncoupled with FCCP. The oxygen uptake of aggregates following a period of hypoxia was elevated above the normal Vmax for about one min immediately following reoxygenation (Figure 8). Following FCCP uncoupling, the oxygen consumption rate increased to about double the normal Vmax which also resulted in a higher P_{50} as the higher oxygen consumption created larger diffusion gradients in and around the aggregates. When uncoupled aggregate oxygen uptake was inhibited with amytal such that the uncoupled, inhibited Vmax was the same as

the normal coupled Vmax, the uncoupled P_{50} was always lower than the normal coupled P_{50}. This was true because the uncoupled P_{50} was only diffusion limited rather than a combination of diffusion and reaction limited. If the coupled P_{50} were simply a result of diffusion limitations, then the coupled P_{50} would be the same as the uncoupled value for similar Vmax.

The reduction in intrinsic Km with decreasing cellular [ATP]/[ADP][Pi] may affect the pO_2 gradient within tissue which is prone to developing hypoxic regions such as may be the case with isolated or encapsulated islets, spheroids, etc. As the pO_2 approaches hypoxic levels away from the oxygenation source (toward the spheroid core), the mitochondrial Km of cells located within the core will drop toward zero. Thus, in a chronically hypoxic islet, it is possible that the intrinsic Km may range from normal state 5 conditions (0.44 mm Hg) in cells that are in a high energy state near the relatively oxygenated periphery to close to 0 mmHg in cells that are in the relatively anoxic core. As a result, the oxygen drop off may be steeper than that predicted by models incorporating Michaelis-Menten kinetics using a Km value measured under oxygenated conditions.

REFERENCES

Altman, G.J., Panol, G., Hayner, N. and Galletti, P.M. (1979) Oxygen Requirements of Freshly Isolated Cells. Artif Organs 3: 290 (abstract).

Altman, P.L. and Dittmer, D.S. (eds) (1971) Respiration and Circulation. Fed Am Soc Exp Biol Bethesda Md; p. 16.

Andersson, A., Gunnarsson, R. and Hellerstrom, C. (1976) Long-Term Effects of a Low Extracellular Glucose Concentration on Glucose Metabolism and Insulin biosynthesis and Release of Mouse Pancreatic Islets Maintained in Tissue Culture. Acta Endocrinologica 82: 318-329.

Andersson, A., Christensen, N., Groth, C.G., Hellerstrom, C., Petersson, B., and Sandler, S. (1984) Survival of Human Fetal Pancreatic Explants in Organ Culture as Reflected in Insulin Secretion and Oxygen Consumption. Transplantation 37: 499-503.

Andersson, A, Korsgren, O, and Jansson, L. (1989) Intraportally transplanted pancreatic islets revascularized from hepatic arterial system. Diabetes 38 (Suppl. 1):192-195.

Bonner-Weir, S, and Orci, S. (1982). New Perspectives on the Microvascular of the Islets of Langerhans in the Rat. Diabetes 31: 883-889.

Bonner-Weir, S. (1984) Morphological Evidence for β-cell Polarity within the Islet of Langerhans in the Rat. Diabetes 33: (Suppl. 1): 81A.

Chen, J, Tannahill, A.L, and Shuler, M.L. (1985) Design of a System of the Control of Low Dissolved Oxygen Concentrations. Biotech & Bioengr 27: 151-155.

Dionne, K.E, Colton, C.K, and Yarmush, M.L. (1989-3) Effect of hypoxia on insulin secretion by isolated rat and canine islets of Langerhans. (Ph.D.Thesis; Chapter 3).

Dionne, K.E, Colton, C.K, and Yarmush, M.L. (1989-4) Effect of hypoxia on insulin secretion from rat and canine islet cell aggregates. (Ph.D. Thesis; Chapter 4).

Dionne, K.E, Colton, C.K, and Yarmush, M.L. (1989-8). Mathematical modeling of O_2 profiles, O_2 consumption, and insulin secretion in isolated and immuno-isolated islets of Langerhans. (Ph.D. Thesis; Chapter 8).

Dionne, K.E, Colton, C.K, and Yarmush, M.L. (1989-9). A proposed metabolic pathway by which hypoxia reduces the exocytotic release of insulin from pancratic β-cells. (Ph.D. Thesis; Chapter 9).

Griffith, R.C., and Scharp, D.W., Hartman, B.K., Ballinger, W.F., Lacy, P.E. (1977) A morphologic study of intrahepatic portal-vein islet isografts. Diabetes 26: 201-14.

Halban, P.A., Wollheim, C.B., Blondel, B., Meda, P., Niesor, E.N. and Mintz D.H. (1982) The Possible Importance of Contact between Pancreatic Islet Cells for the Control of Insulin Release Endocrinology 111: 86-94.

Hedeskov, C.J, Hertz, L, and Nissen, C. (1972) The Effect of Mannoheptulose on Glucose- and Pyruvate- stimulated Oxygen Uptake in Normal Mouse Pancreatic Islets. Biochim Biophys Acta 261: 388.

Hellerstrom, C. (1967) Effects of Carbohydrates on the Oxygen Consumption of Isolated Pancreatic Islets of Mice. Endocrinology 81: 105-112.

Hellman, B., Idahl, L.A. and Danielson, A. (1969) Adenosine Triphosphate Levels of Mammalian Pancreatic β-cells after Stimulation with Glucose and Hypoglycemic Sulfonylureas. Diabetes 18: 509-516.

Hellman, B., Sehlin, J. and Taljedal, I.B. (1971) Effects of Glucose and other Modifiers of Insulin Release on the Oxidative Metabolism of Amino Acids in Micro-Dissected Pancreatic Islets. Biochem J 123: 513-521.

Hermans, M.P. and Henquin, J.C. (1986) Is there a Role for Osmotic Events in the Exocytotic Release of Insulin? Endocrinology 119: 105-111.

Hutton, J.C, and Malaisse, W.J. (1980) Dynamics of Oxygen Consumption in Rat Pancreatic Islets. Diabetologia 18: 395.

Jones, D.P, and Kennedy, F.G. (1982) Intracellular Oxygen Supply during Hypoxia. Am J Physiol 243: C247-C253.

Kautsky, H. (1939). Quenching of Luminescence by Oxygen. Trans Faraday Soc 35:216-219.

Lacy,P.E. and Kostianovsky, M. (1967) Method for the Isolation of Intact Islets of Langerhans from the Rat Pancreas. Diabetes 16: 35-39.

Lundgren, G., Andersson, A., Borg, H., Buschard, K., Groth, C.G., Gunnarsson, R., Hellerstrom, C., Petersson, B. and Ostman, J. (1977) Structural and Functional Integrity of Isolated Human Islets of Langerhans Maintained in Tissue Culture for 1-3 Weeks. Trans Proc 9:237-240.

Malaisse, W.J. and Sener, A. (1988) Hexose Metabolism in Pancreatic Islets. Feedback Control of D-Glucose Oxidation by Functional Events. Biochim Biophys Acta (Netherlands) 971: 246-254.

McLimans, W, Blumenson, L, and Tunnah, K. (1968) Kinetics of Gas Diffusion in Mammalian Cell Culture Systems II. Theory. Biotech & Bioengr X: 741-763.

Menger, M.D, Jaeger, S, Walter, P, Feifel, G, Hammersen, F, Messmer, K. (1989) Angiogenesis and hemodynamics of microvasculature of transplanted islets of Langerhans. Diabetes 38 (Suppl. 1):199-201.

Orci, L. (1976) Microanatomy of the Islets of Langerhans. Metabolism 25: 1303.

Pace, C.S. and Goldsmith, K.T. (1986) Phospholipase C and Melittin Enhancement of Glucose-Induced Electrical Activity. Endocrinology 118: 102-107.

Panten, U. and Klein, H. (1982) Oxygen Consumption by Isolated Pancreatic Islets, as Measured in a Microincubation System with a Clark-Type Electrode. Endocrinology 111: 1595-1600.

Pipeleers, D.G., In't Veld, P.A., Maes, E., and Van De Winkel, M. (1982) Glucose-Induced Insulin Release Depends on Functional Cooperation between Islet Cells. Proc Natl Acad Sci 79: 7322-7325.

Pipeleers, D.G., In't Veld, P.A., Van De Winkel, M., Maes, E., Schuit, F.C. and Gepts, W. (1985) A New *In Vitro* Model for the Study of Pancreatic A and β Cells. Endocrinology 117:806-816.

Pipeleers, D.G., Schuit,F.C., In't Veld, P.A., Maes, E., Hooghe-Peters, E.L., Van De Winkel, M. and Gepts, W. (1985) Interplay of Nutrients and Hormones in the Regulation of Insulin Release. Endocrinology 117: 824-833.

Randle, P.J. and Hales, C.N. (1972) Insulin Release Mechanisms. in *Handbook of Physiology: Endocrinology I* (Chapter 13, pp.219-35); Greep, R.O. and Astwood, E.B. (eds), American Physiological Society, Washington D.C.

Robiolio, M., Rumsey, W.L. and Wilson, D.F. (1989) Oxygen Diffusion and Mitochondrial Respiration in Neuroblastoma Cells. Science (in press).

Rumsey, W.L, Schlosser, C, Nuutinen, E.M, Robiolio, M, and Wilson, D.F. (1989) Cellular energetics and the oxygen dependence of respiration in cardiac myocytes isolated from adult rat. (Appendix: Dionne, K.E. (1989) Oxygen transport to respiring myocytes. (Submitted).

Scharp,D.W., Downing, R., Merrell, R.C., and Greider, M. (1980) Isolating the Elusive Islet. Diabetes 29 (Suppl. 1): 19-30.

Scharp, D.W. (1984) Isolation and Transplantation of Islet Tissue. World J Surgery 8: 143-151.

Scharp, D.W, Mason, N.S, and Sparks, R.E. (1984) Islet Immuno-isolation: The use of Hybrid Artificial Organs to Prevent Islet Tissue Rejection. World J Surg 8: 221-229.

Shizuru, J., Trager, D. and Merrell, R.C. (1985) Structure, Function, and Immune Properties of Reassociated Islet Cells. Diabetes 34: 898-903.

Trus, M., Warner, H. and Matschinsky, F. (1980) Effects of Glucose on Insulin Release and on Intermediary Metabolism of Isolated Perifused Pancreatic Islets from Fed and Fasted Rats. Diabetes 29: 1-14.

Vanderkooi, J.M., Maniara, G., Green, T.J. and Wilson, D.F. (1987) An Optical Method for Measurement of Dioxygen Concentration Based upon Quenching of Phosphorescence. J Biological Chemistry 262: 5476-5482.

Weir, G.C., Halban, P.A., Meda, P., Wollheim, C.B., Orci, L. and Renold, A.E. (1984) Dispersed Adult Rat Pancreatic Islet Cells in Culture: A, B, and D Cell Function. Metabolism 33: 447-453.

Welsh, M., Hellerstrom, C. and Andersson, A. (1982) Respiration and Insulin Release in Mouse Pancreatic Islets: Effects of L-leucine and 2-ketoisocaproate in combination with D-glucose and L-glutamine. Biochimica et Biophysica Acta 721: 178-184.

Wettermark, G., Tegner, G., Brolin, S.E. and Borglund, E. (1970) Photokinetic Measurements of the ATP and ADP Levels in Isolated Islets of Langerhans. In: *The Structure and Metabolism of the Pancreatic Islets*, Falkmer, S., Hellman, B. and Taljedal, I.B. (eds), Osford: Pergamon Press, pp. 275-282.

Wilson, D.F., Rumsey, W.L., Green, T.J. and Vanderkooi, J.M. (1988) The Oxygen Dependence of Mitochondrial Oxidative Phosphorylation Measured by a New Optical Method for Measuring Oxygen Concentration. J Biological Chemistry 263: 2712-2718.

Zawalich, W.S. (1979) Intermediary metabolism and inulin secretion from isolated rat islets of Langerhans. Diabetes 28:252-262.

TABLE 1. COUPLED Vmax AND P50 OF RAT AND CANINE CELL AGGREGATES AND OF INTACT RAT ISLETS

Cell Type	Batch #[d]		Vmax x 10^8 (mole/cm^3·sec)	P_{50} (mmHg)	Batch Averages[a] Vmax (ave)	P_{50} (ave)
Canine, Cell Agg 50 mg/dl glucose						
	2K3A	1	2.99	0.82		
		2	3.06	1.00	3.03 ±.91	0.91 ±.13
	3K4A	1	3.56	0.72		
		2	3.88	1.00		
		3	3.86	1.04		
		4	3.75	0.97	3.76 ±.14	0.93 ±.14
Canine, Cell Agg 300 mg/dl glucose						
	2K1A	1	3.19	1.29	3.19	1.29
	2K2A	1	3.54	0.95		
		2	3.90	1.14	3.72 ±.25	1.05 ±.13
	3K3A	1	4.56	1.23		
		2	4.71	1.30		
		3	5.78[b]	1.66[b]	4.63 ±.11	1.27 ±.05
	3K5A	1	4.06	1.18		
		2	6.12[b]	2.48[b]		
		3	6.41[b]	2.07[b]		
		4	4.30	1.39		
		5	3.93	1.24		
	3K5B	1	4.10	1.15	4.10 ±.15	1.24 ±.11
	4K4A	1	3.62	0.95		
		2	3.83	1.01	3.73 ±.15	0.98 ±.04
Rat, Cell Agg 300 mg/dl glucose						
	1K1A	1	3.56[c]	1.23[c]		
	3K2B	1	4.56	1.28	4.56	1.28
	4K3A	1	4.34	1.00		
		2	4.53	0.96		
	4K3B	1	4.46	1.16		
		2	4.02	0.84	4.34 ±.23	0.99 ±.13
Rat, Whole Islet 300 mg/dl glucose						
	2K4A	1	3.71	8.7	3.71	8.7
	3K1A	1	3.17	11.2		
		2	4.02	17.4	3.60 ±.60	14.3 ± 4.4
	4K2A	1	2.42	8.3		
	4K2B	1	2.83	8.9		
		2	2.94	10.3		
		3	2.87	9.8	2.76 ±.23	9.3 ± 0.9

[a] Average of multiple runs for each batch ± st. dev.
[b] Insufficient reoxygenation (<30 mmHg), not included in data averaging.
[c] Uptake was measured at 28°C instead of 35-37°C.
[d] Batch # designation: 2K3A 1: 2 refers to the trip to UPa during which the data was collected; K3 refers to different tissue samples (therefore 2K3 and 2K4 would be uptake from different tissue samples); A is used only to refer to the correct computer data bank in which the data was stored; 1 refers to the oxygenation cycle and begins new with each data bank.

TABLE 2. SUMMARY OF COUPLED Vmax AND P_{50} OF RAT AND CANINE CELL AGGREGATES AND OF INTACT RAT ISLETS*

		Vmax (moles O_2/cm^3-sec x 10^6)	P_{50} (mmHg O_2)
Dog:	Cell aggregates 50 mg/dl glucose	3.51 ± .40 *(n=6)*	0.93 ± .13 *(n=6)*
Dog:	Cell aggregates 300 mg/dl glucose	3.98 ± .44 *(n=11)*	1.16 ± .15 *(n=11)*
Rat:	Cell aggregates 300 mg/dl glucose	4.38 ± .22 *(n=5)*	1.05 ± .17 *(n=5)*
Rat:	Intact islets 300 mg/dl glucose	3.14 ± .55 *(n=7)*	10.7 ± 3.1 *(n=7)*

* mean ± standard deviation

TABLE 3. Vmax AND P_{50} OF FCCP UNCOUPLED AND AMYTAL INHIBITED CANINE CELL AGGREGATES AND INTACT RAT ISLETS

		Vmax* (moles $O_2/cm^3 \cdot sec \times 10^8$)	P_{50}* (mmHg O_2)
Dog:	Coupled Cells 300 mg/ml glucose	3.98 ± .44 *(n=11)*	1.16 ± .15 *(n=11)*
Dog:	FCCP Uncoupled Cells 300 mg/ml glucose	8.86 ± .80 *(n=7)*	2.43 ± .72 *(n=7)*
Dog:	Amytal Inhibited Cells	1.07 - 4.72 *(n=8)*	.224 - 1.02 *(n=8)*
Rat:	Intact Islets FCCP Uncoupled Amytal Inhibited	0.96 - 2.54 *(n=2)*	2.3 - 8.7 *(n=2)*

* mean ± standard deviation

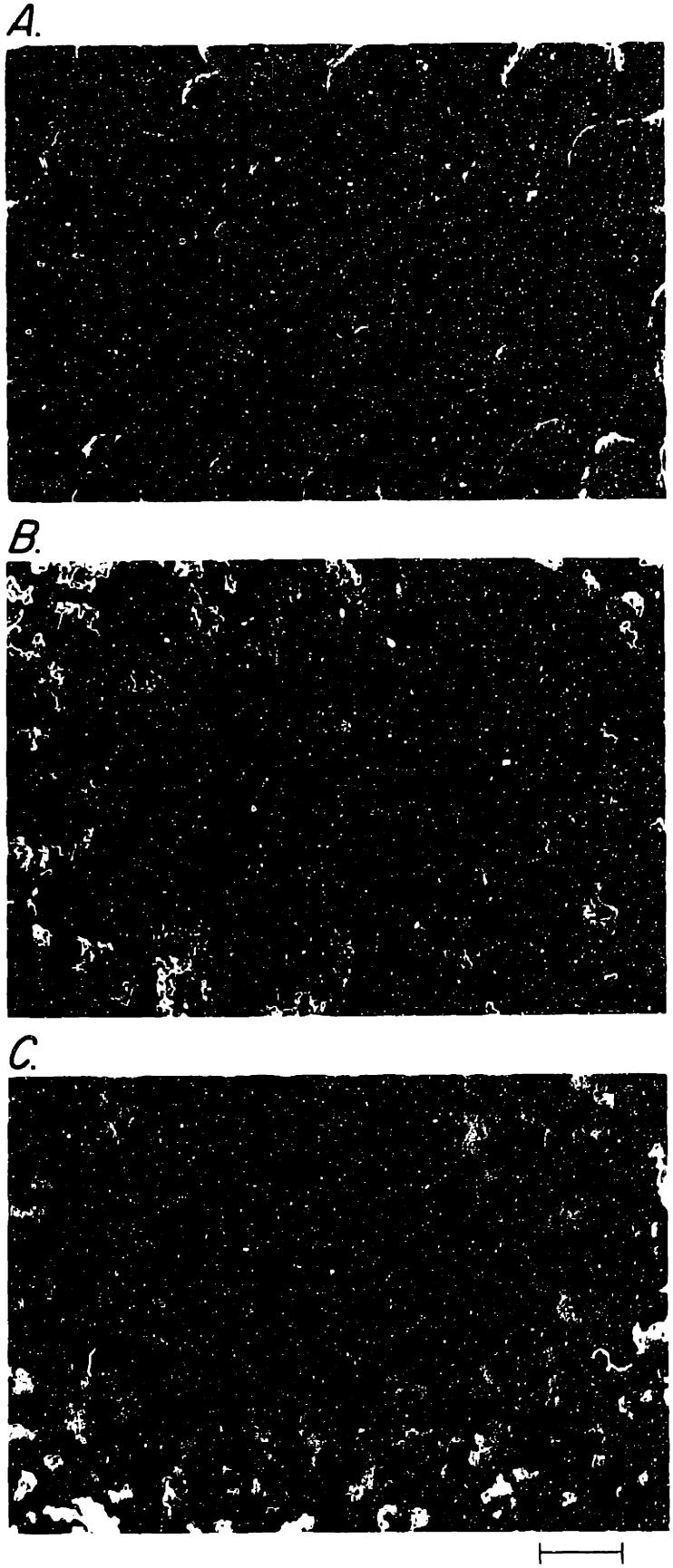
A.
B.
C.
200 μm

FIGURE 1. Photomicrographs of intact rat islets (A), re-aggregated rat (B) and canine (C) islet cell clusters. Islets were cultured for one day after isolation. Cell aggregates were cultured for one day following trypsinization to single cells. Cells were approximately 90% viable by trypan blue exclusion.

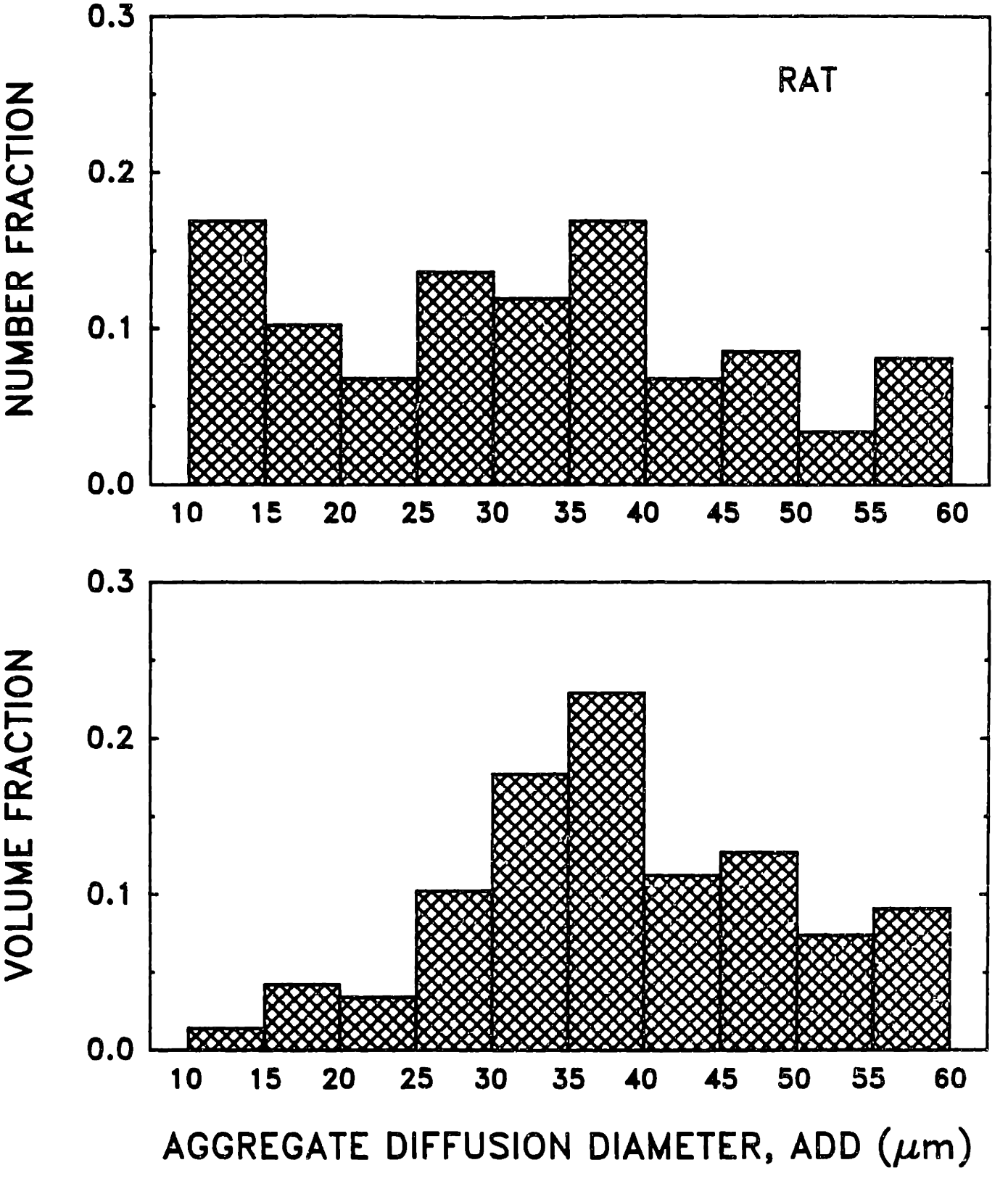

FIGURES 2A & 2B. Size distribution of rat and canine islet cell aggregates following one day of culture after trypsinization. Photomicrographs for size analysis were taken on the day of oxygen uptake testing. Data shown represents pooled results from two isolation batches for each species. Number fraction was calculated as the number of aggregates in each indicated size range divided by the total number of aggregates counted (n = 59 for rat, 84 for canine). Volume fraction was calculated as the number of cells contained in aggregates in each indicated size range divided by the total number of cells in all of the aggregates counted. The volume average diameter was calculated as the volume fraction times the diameter, summed over all particles.

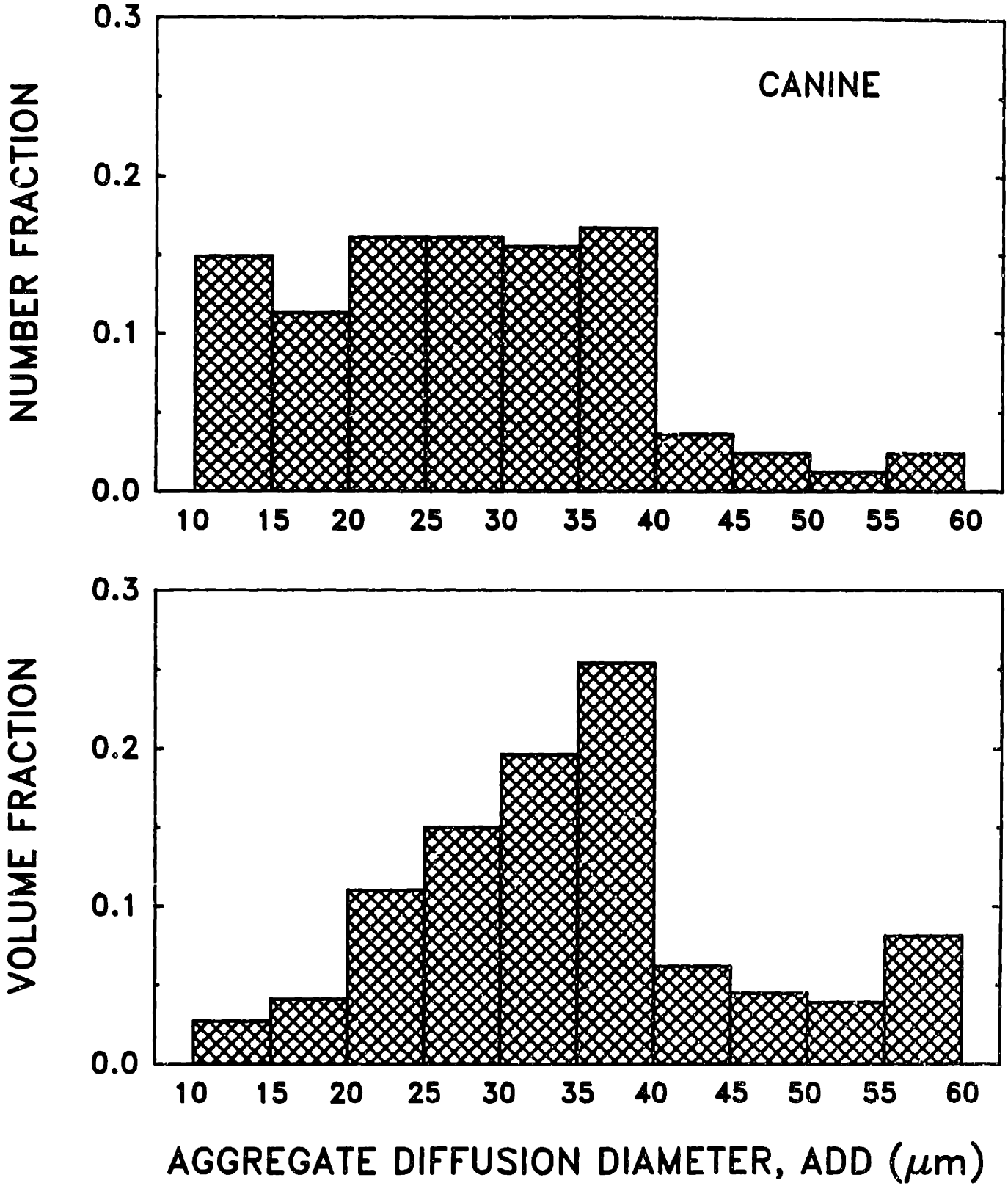

FIGURE 2B. Size distribution of canine aggregates. (See caption of Figure 2A).

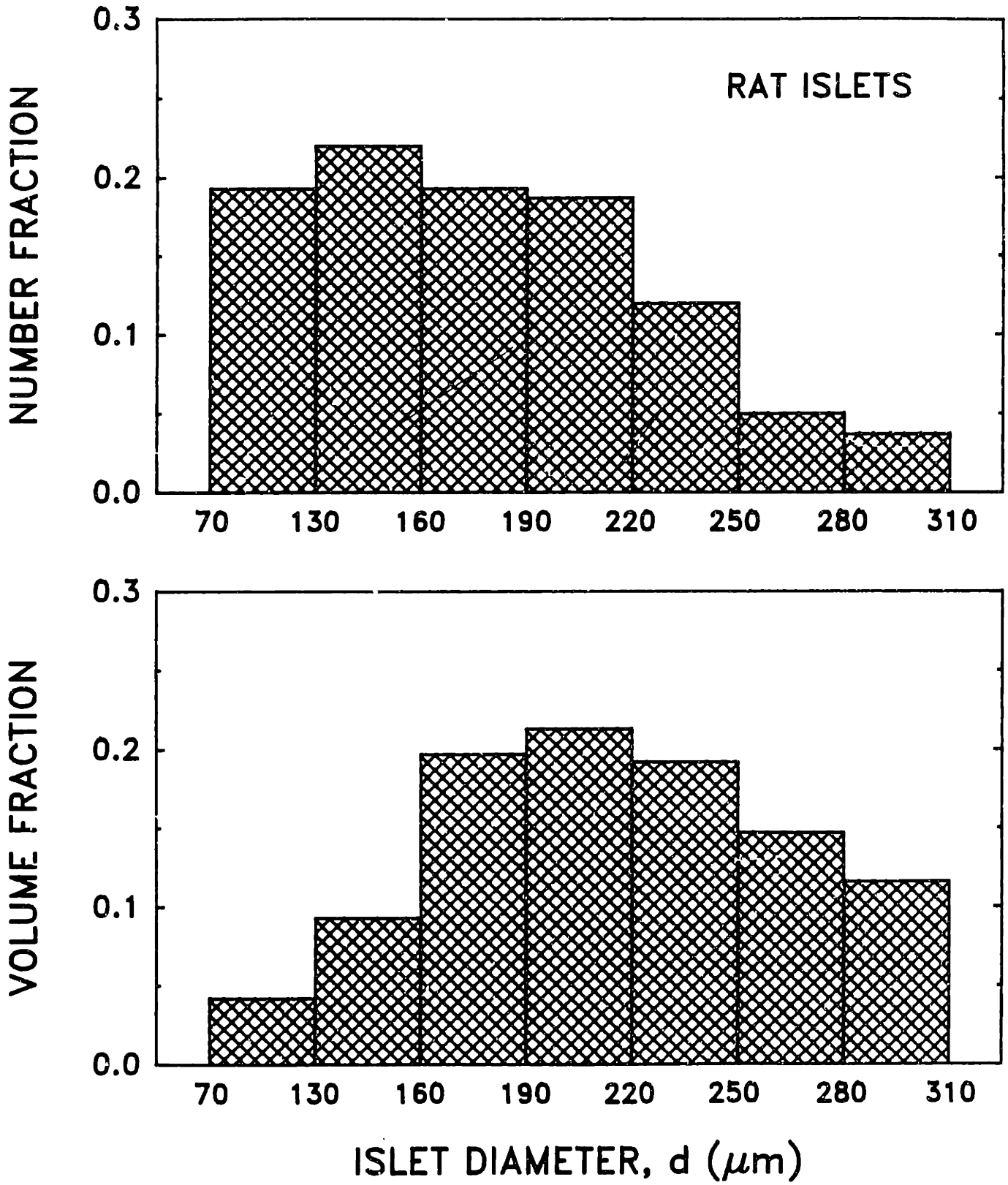

FIGURE 3. Size distribution of intact rat islets following one day of culture after isolation. Data shown represents pooled results from the three isolation batches studied (n=154). Number fraction of islets was calculated as described for cell aggregates (Figure 2). Volume fraction was based on the calculated volume of each islet.

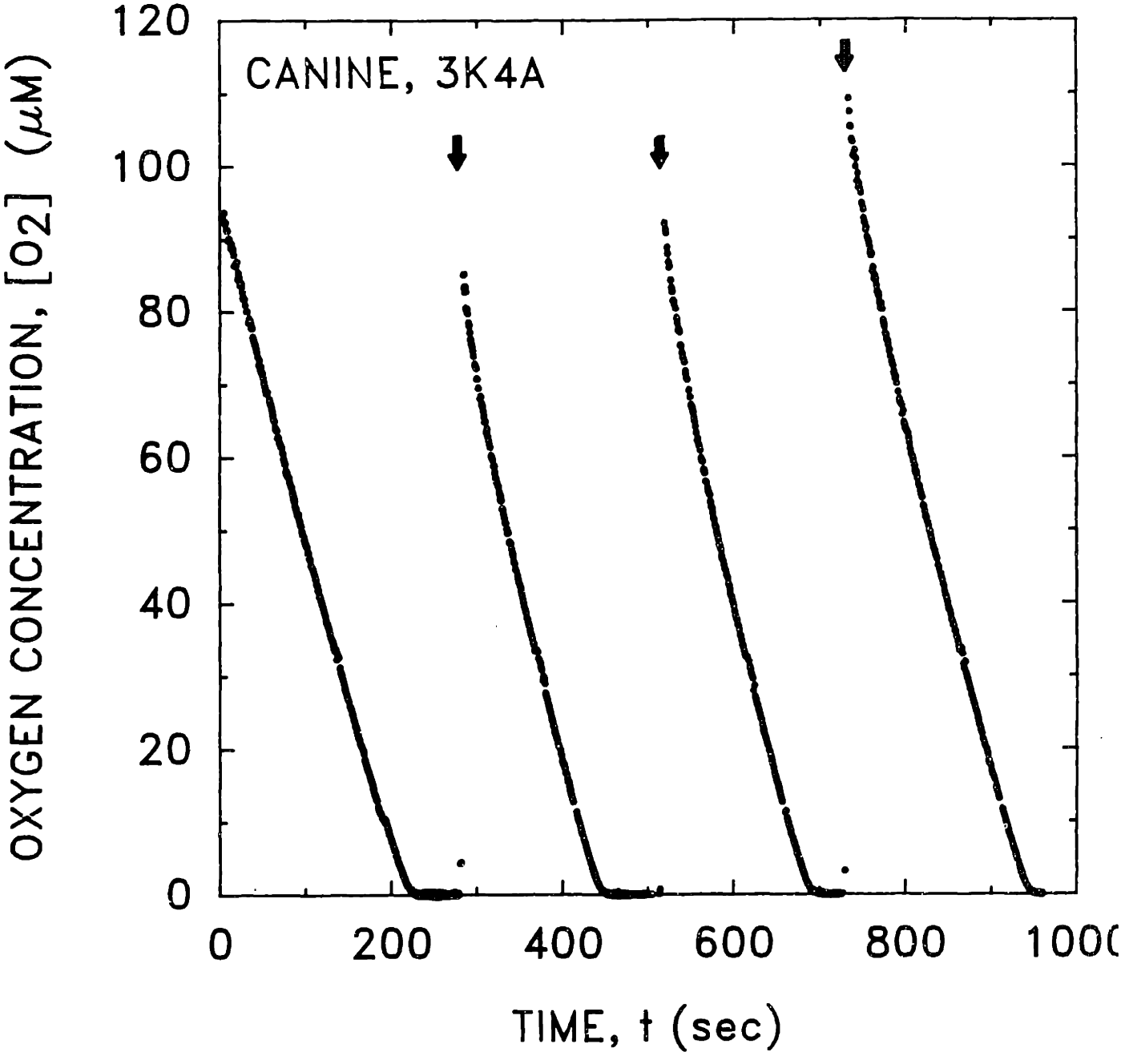

FIGURE 4. Oxygen uptake of canine aggregates (1.9 million cells comprising cm^3 tissue) in medium containing 50 mg/dl glucose. Oxygen concentration in the uptake chamber is plotted versus time. Each data point represents $[O_2]$ from the average of 15 phosphorescence lifetime measurements. Data was collected at the rate of about one point per sec. Following oxygen depletion, medium was reoxygenated by injecting 1-2 μl of dilute (<0.2 mM) H_2O_2 into the cuvette medium through the central hole bored through the cuvette cap. Sequential oxygen uptake runs were performed using the same aggregate preparation with almost identical results. Tissue oxygen uptake runs are identified by a batch number, 3K4A, which indicates isolation batch (3), O_2 uptake tissue preparation (4K), run and peak number (A-1,2,3, 4).

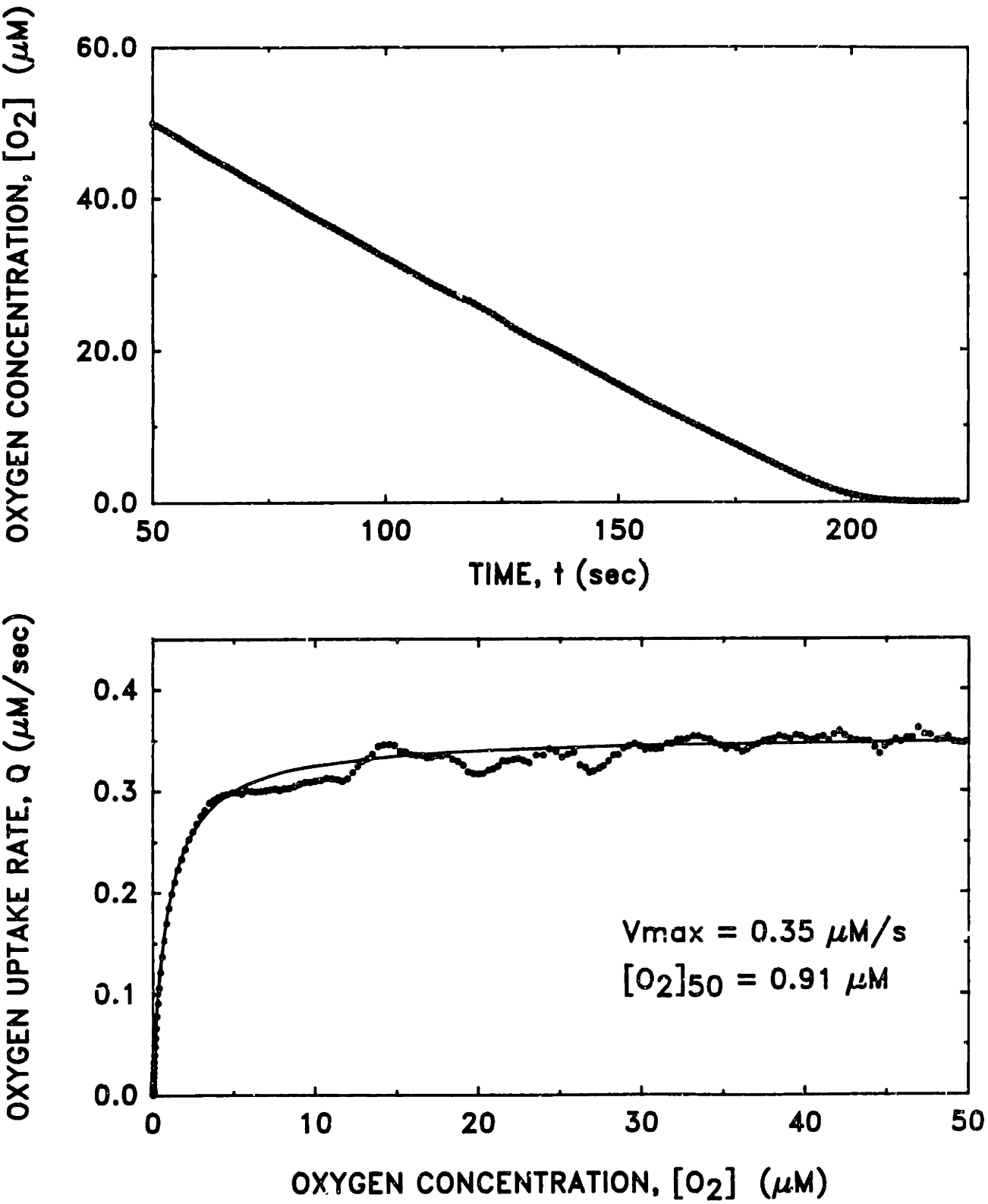

FIGURE 5. Oxygen uptake of canine islet cell aggregates from first run in Figure 4. (Upper panel) Depletion of medium $[O_2]$ as a result of cell respiration as a function of time. Overlapping of data points (about one per sec) creates the appearance of a connected line. (Lower panel) Rate of oxygen uptake calculated as the point to point derivative of the $[O_2]$ verses time data shown in the upper panel. The derivative was smoothed with a seven point moving average. Smoothing did not affect the values of Qmax or $[O_2]_{50}$ calculated by any of the three methods.

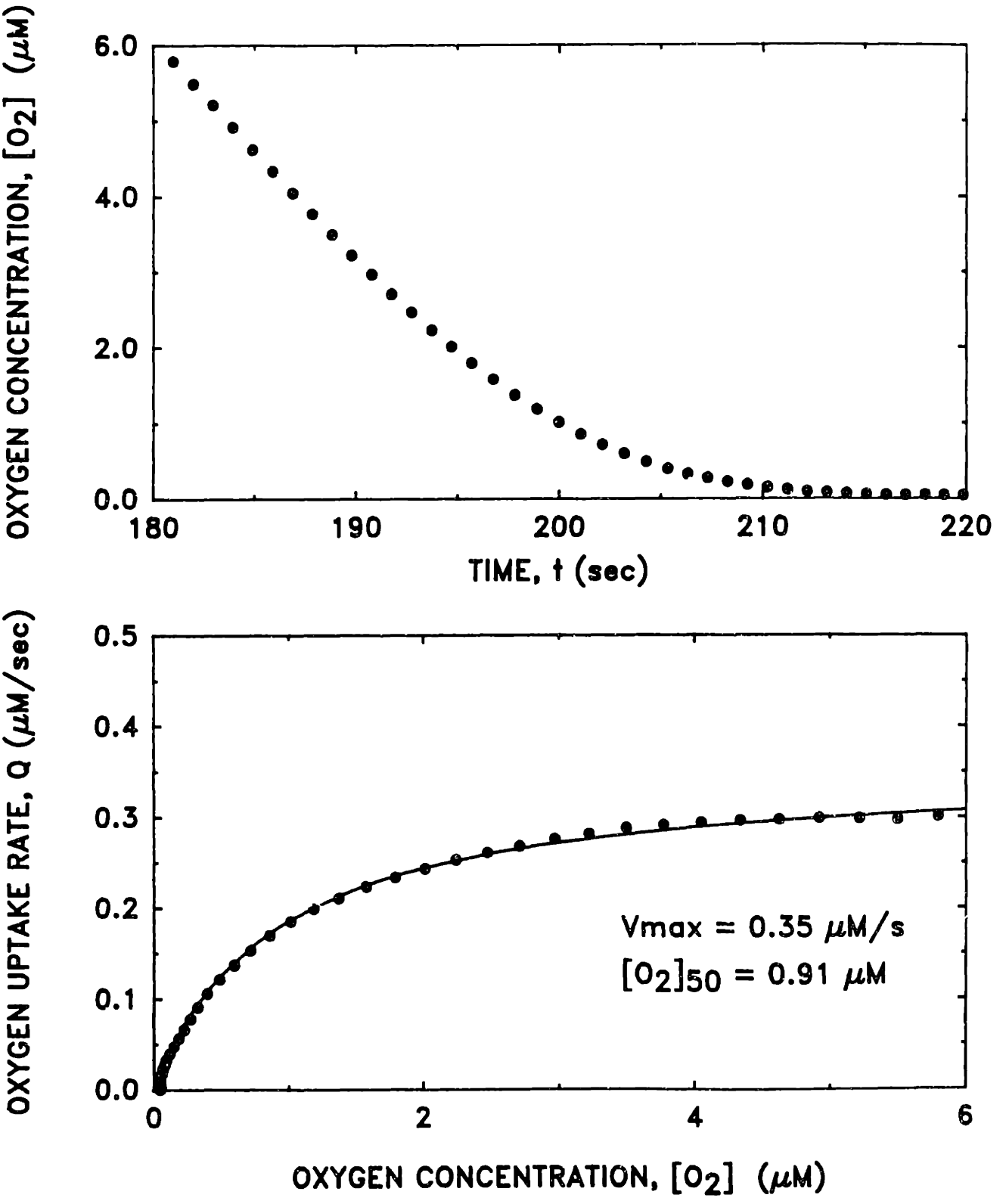

FIGURE 6. Oxygen-limited region of the oxygen uptake run shown in Figure 5 plotted on an expanded scale, showing the curvature of the oxygen depletion curve (upper panel) and the corresponding decrease in oxygen uptake under oxygen limited conditions (lower panel). The lower panel also illustrates the agreement between the values of Q predicted by the fitted Michaelis-Menten kinetics and the experimental data.

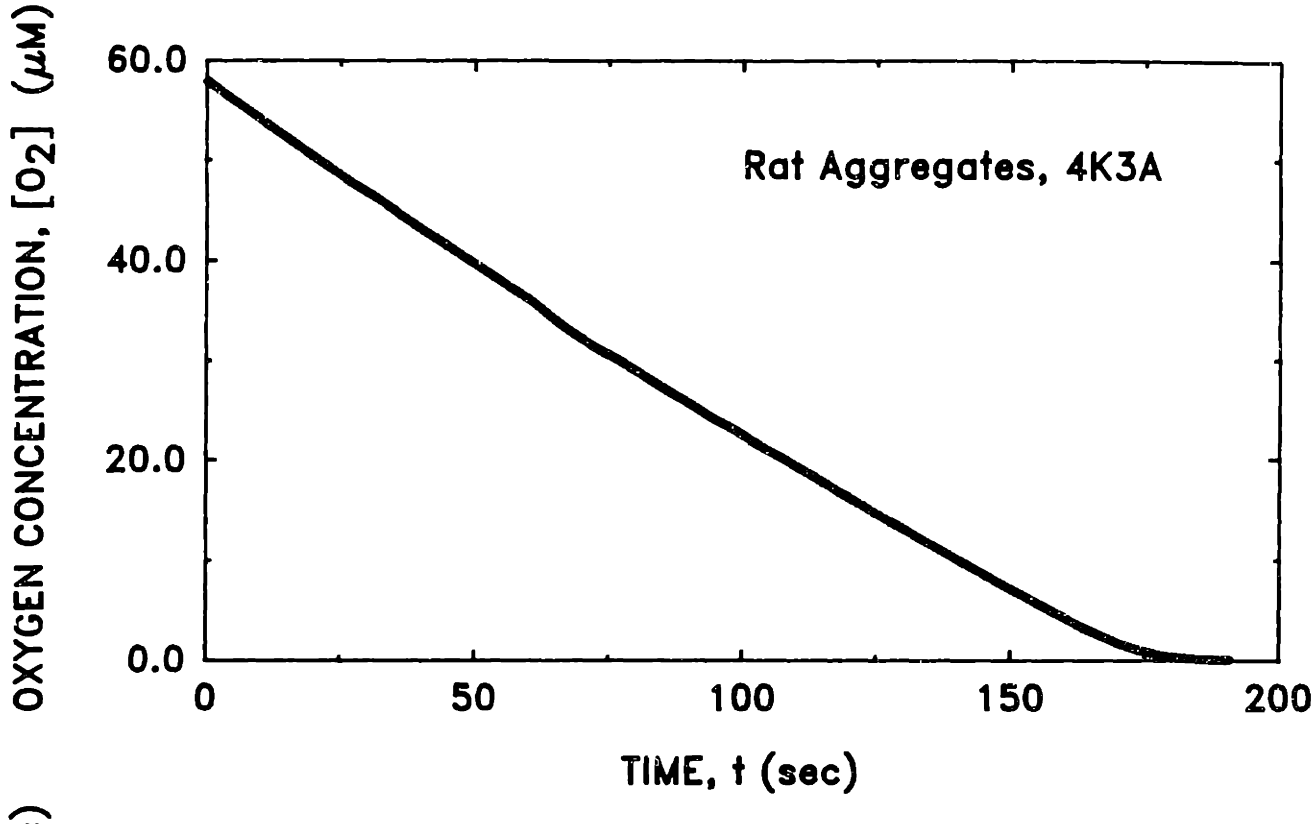

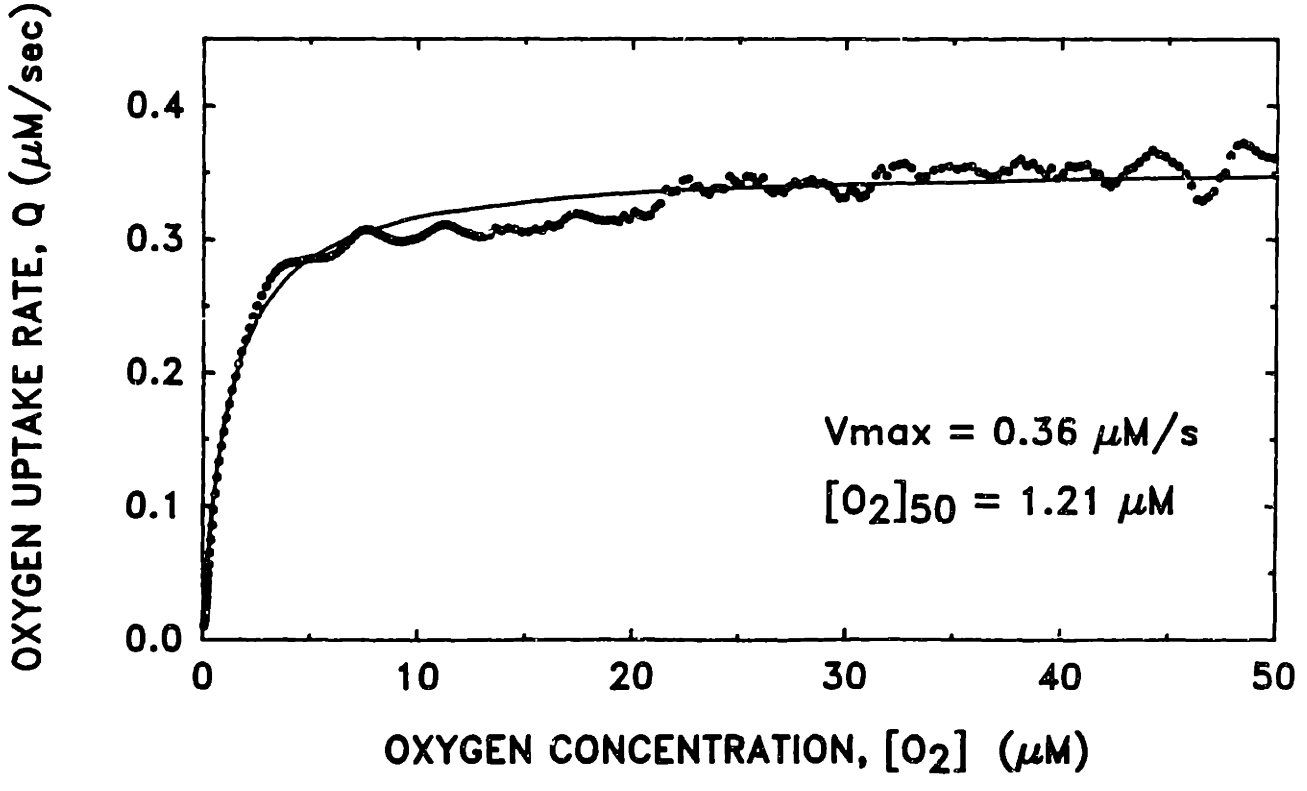

FIGURES 7A & 7B. Oxygen uptake of two preparations of rat islet cell aggregates from the same isolation batch (each with about 1.5 million cells) in the presence of 300 mg/dl glucose in the medium. Data was analyzed as described in the caption of Figure 6.

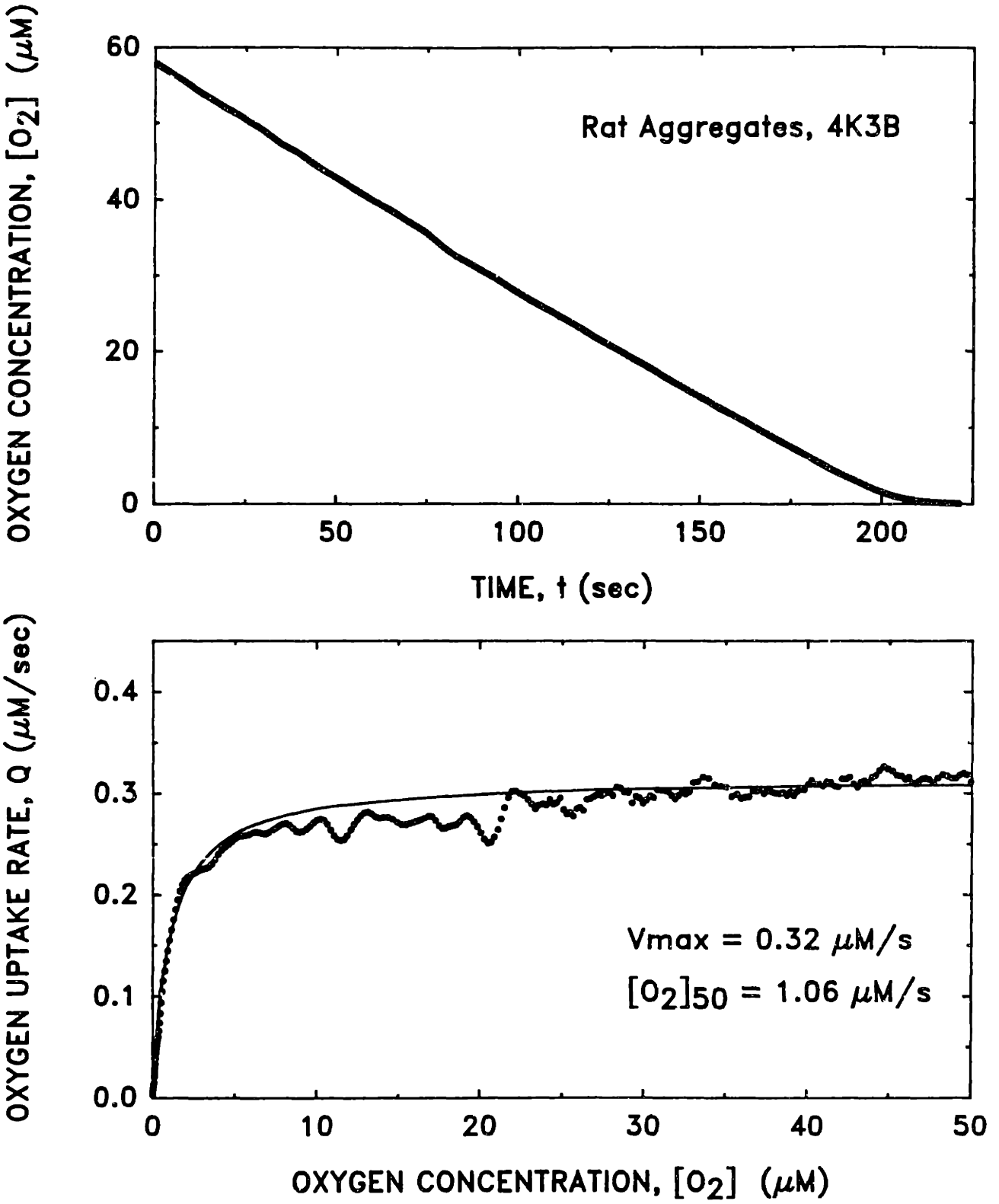

FIGURE 7B. Oxygen uptake of rat islet cell aggregates. (See caption of Figure 7A).

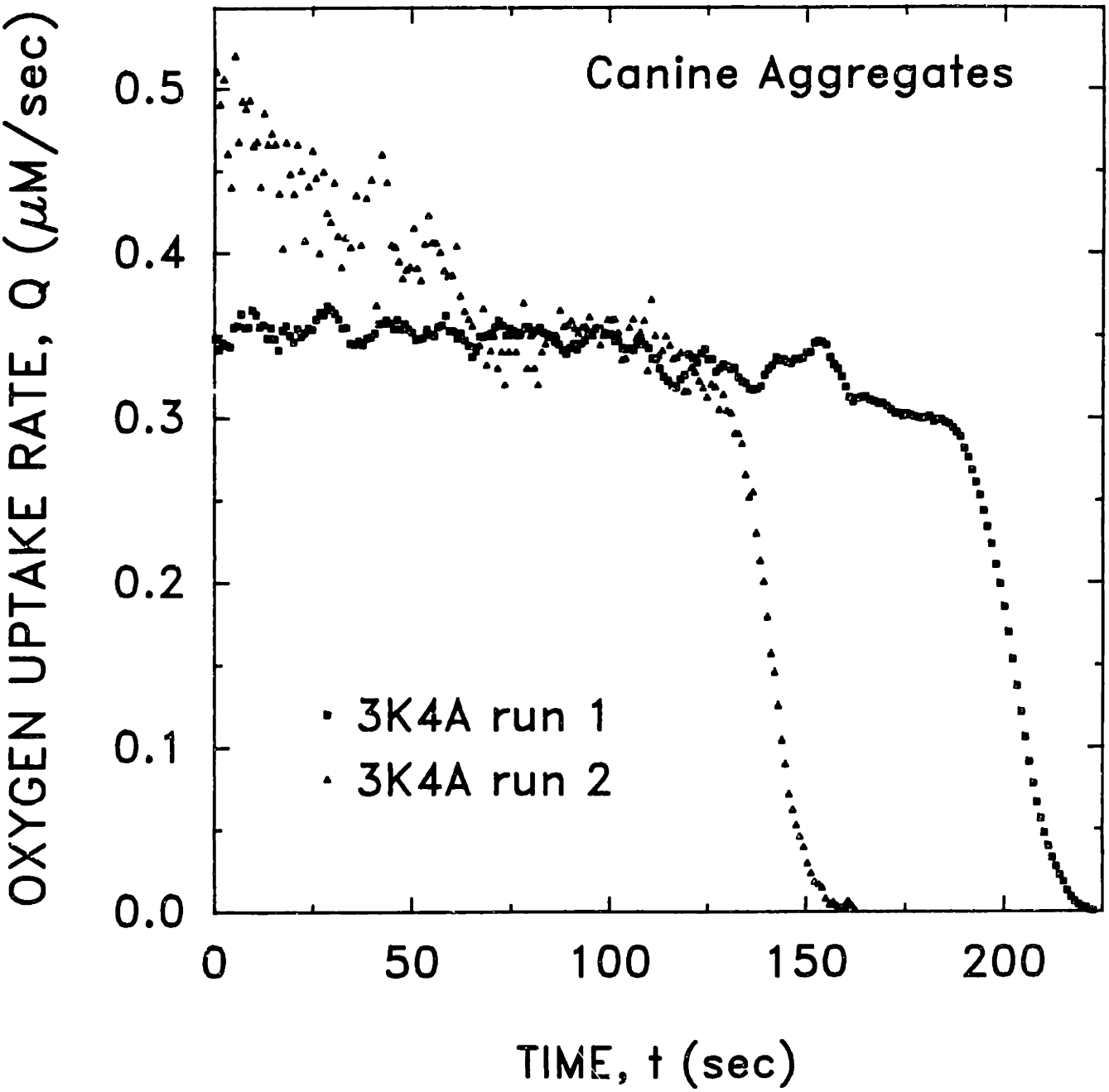

FIGURE 8. Oxygen uptake rate, Q, as a function of time after reoxygenation. The curves represent the oxygen consumption rate calculated as the point by point derivative of the first and second oxygen depletion curves shown in Figure 4. Data was smoothed by a running seven point average.

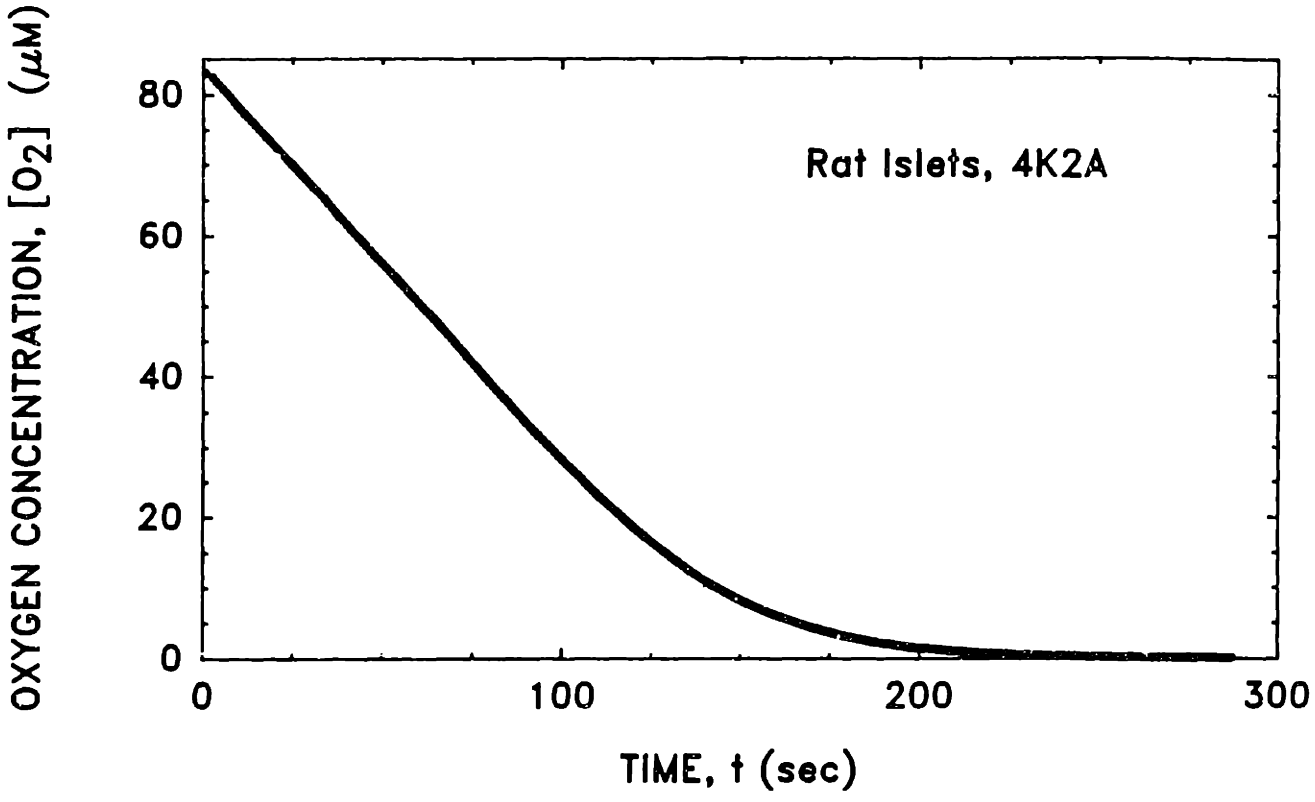

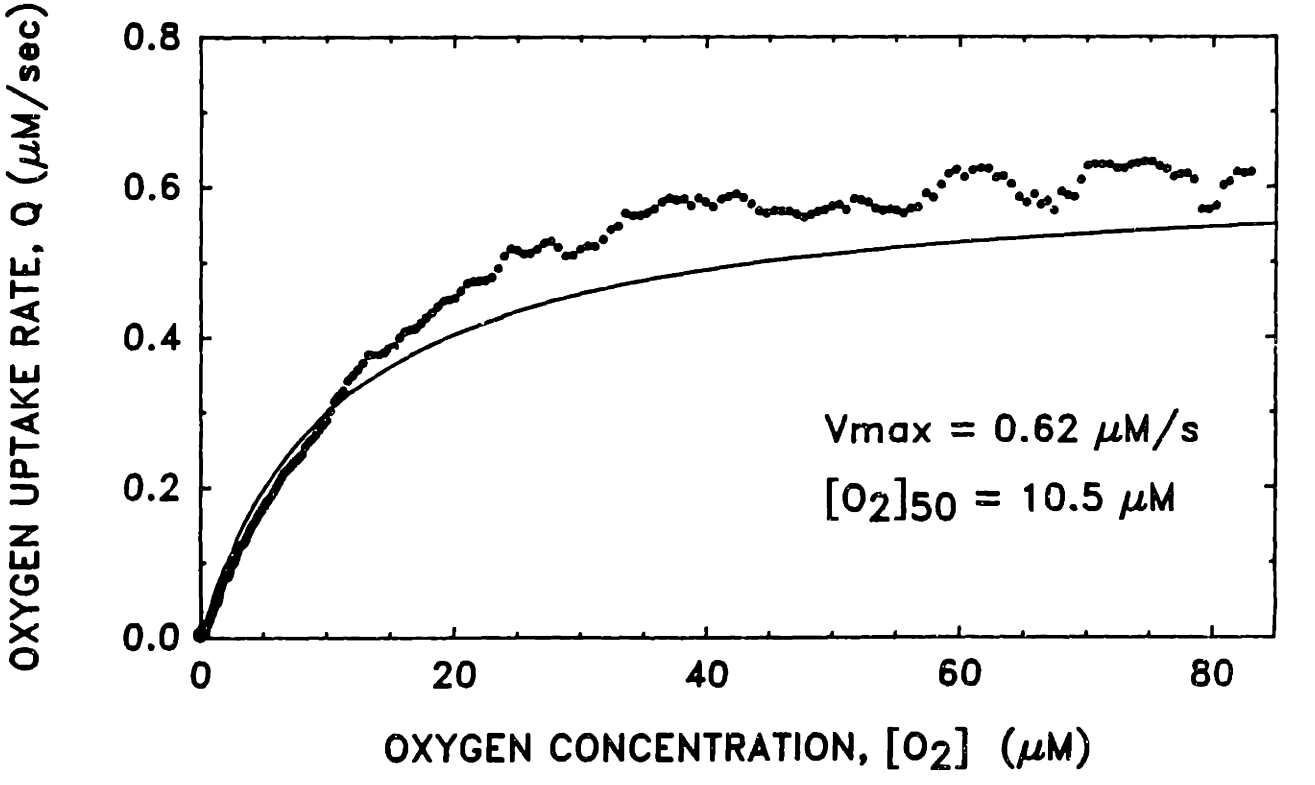

FIGURES 9A & 9B. Oxygen uptake by two preparations of intact rat islets each containing about 1500 islets or 7.4 mm^3 tissue. Islet oxygen uptake was measured in the same manner previously described for aggregate oxygen uptake. However, in contrast to cell aggregates, oxygen consumption of intact islets (volume-average diameter = 214 μm) became oxygen limited at much higher $[O_2]$ (>50 μM). The values of Vmax and P_{50} were measured directly from the data.

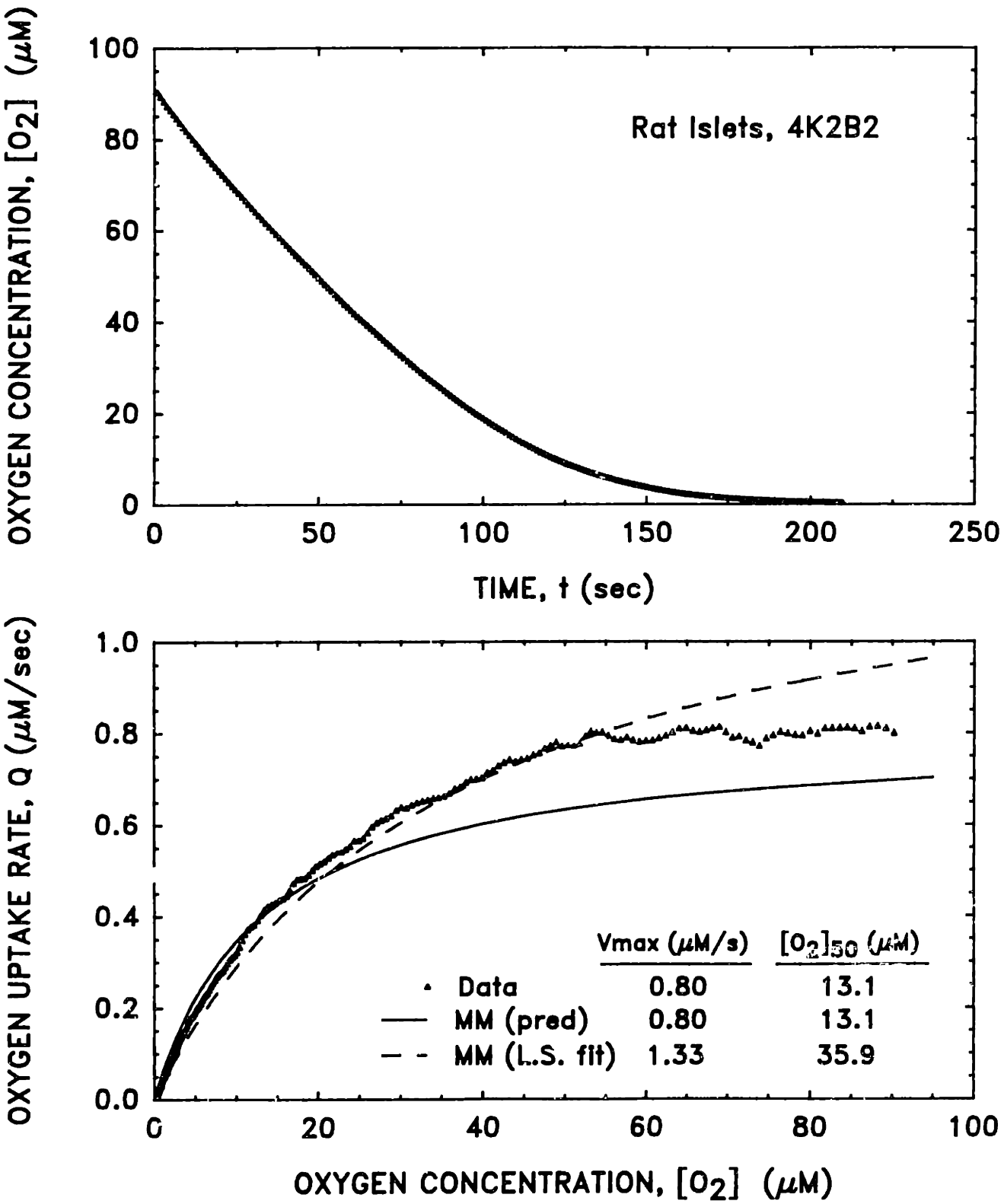

FIGURE 9B. Oxygen uptake of intact rat islets. (See caption of Figure 9A.) The oxygen uptake rate predicted by Michaelis-Menten kinetics using parameters measured directly from the data significantly under-predicts Q above P_{50} and overpredicts Q below P_{50} (lower panel). The values of Vmax and P_{50} fit by linear regression to a Michaelis-Menten type expression are significantly larger than the true values.

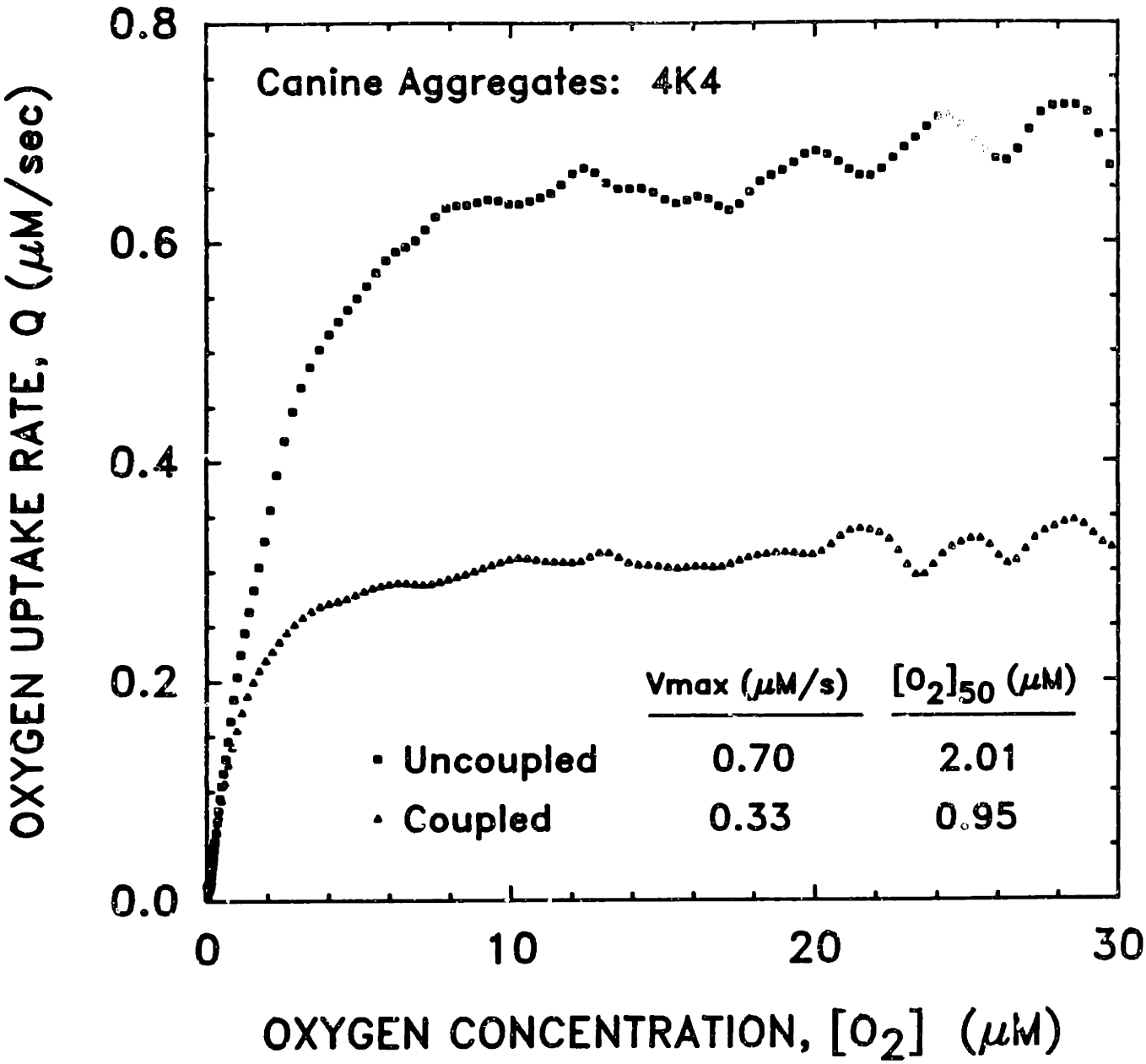

FIGURE 10. Oxygen uptake curves for normal coupled and FCCP uncoupled respiration from a preparation of canine aggregates (4K4). Cells were uncoupled and inhibited as described in Methods. Qmax and $[O_2]_{50}$ were measured directly from the data.

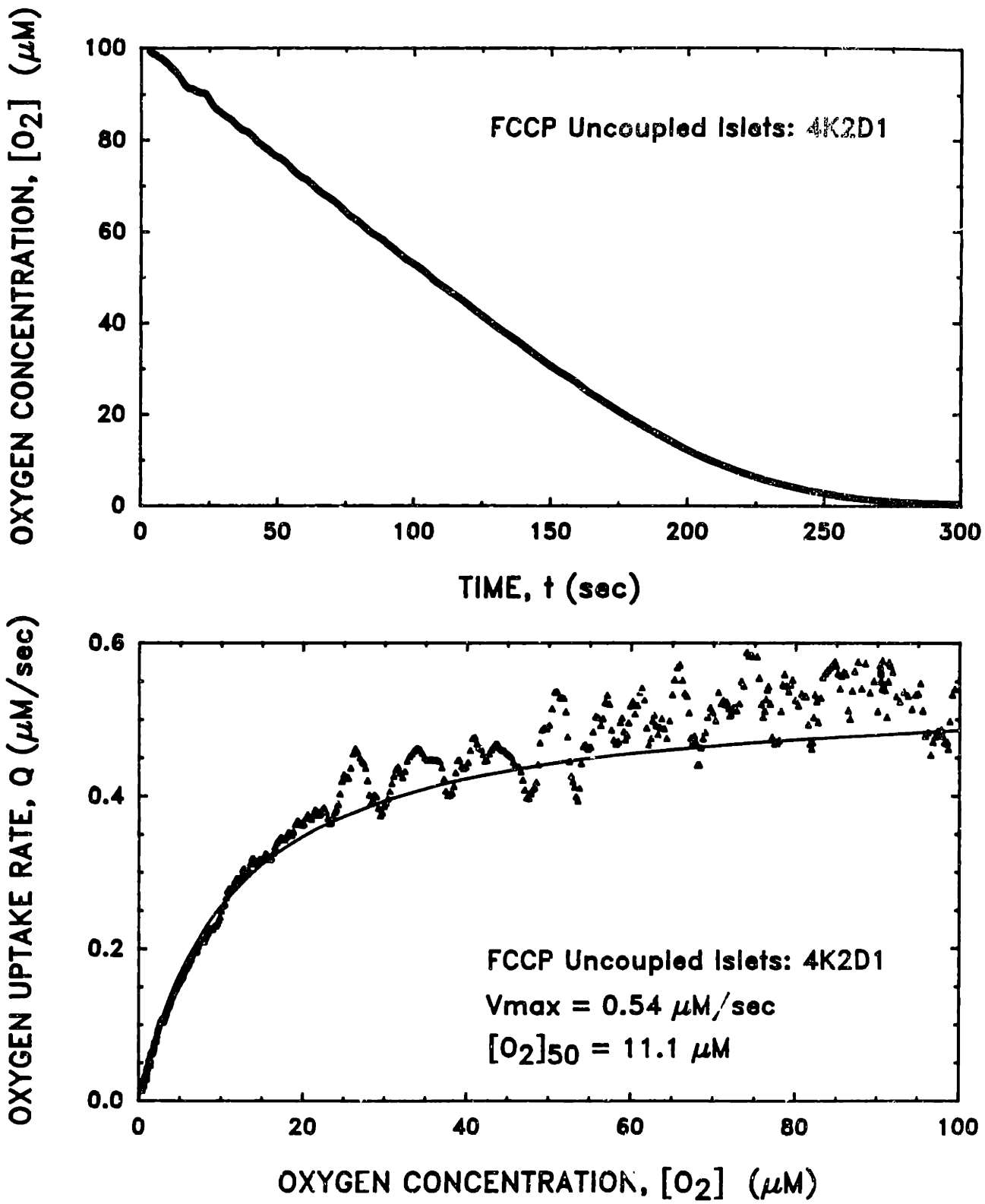

FIGURE 11. Oxygen uptake of FCCP uncoupled and Amytal inhibited intact rat islets. Islet preparation is the same as that shown in Figure 9A in the coupled state. The depletion of oxygen in medium is shown in upper panel and the corresponding rate of oxygen uptake in the lower panel. Qmax and $[O_2]_{50}$ were measured directly from the data. The solid curve in lower panel is the oxygen uptake rate predicted by an overall Michaelis-Menten type expression using the measured parameter values.

CHAPTER 7:

EXTRACTION OF THE INTRA-CELLULAR AND INTRA-ISLET OXYGEN DIFFUSIVITY FROM EXPERIMENTAL MEASUREMENTS OF TISSUE OXYGEN UPTAKE

SUMMARY

Values of intra-cellular and intra-islet oxygen diffusivities were estimated from experimental oxygen uptake measurements of small islet cell aggregates and intact isolated islets of Langerhans using mathematical reaction/diffusion models to calculate intra-tissue pO_2 profiles and oxygen consumption. The best estimate of the intra-cellular oxygen diffusivity, D_{O2c}, using uncoupled, 0-order cell aggregates was 2.3 - 4.6 x 10^{-6} cm^2/sec. The best estimate of the intra-islet oxygen diffusivity, D_{O2I}, was 1.53 x 10^{-5} cm^2/sec. The larger value of the intra-islet diffusivity in comparison to the intra-cellular diffusivity is in agreement with other measurements of the oxygen diffusivity in cells and heterogeneous tissues. The tissue oxygen diffusivity is an important parameter in helping to understand the role of limited oxygen penetration in the viability of isolated islet and cell samples and is the final tissue parameter required in order to model pO_2 gradients in isolated and immuno-isolated islet.

INTRODUCTION

In this paper, analytical and numerical models are developed in order to extract an estimate of the intra-cellular ($D_{O2\ c}$) and intra-islet ($D_{O2\ I}$) value of oxygen diffusivity from experimental measurements of the tissue oxygen uptake rate. The oxygen uptake rate, V, of pancreatic islet cell aggregates and of intact islets of Langerhans was measured as a function of the partial pressure of oxygen (pO_2) in the surrounding medium and was reported in a previous paper (Dionne et al, 1989-6).

Islets of Langerhans or their cellular derivatives that are removed from the pancreas and isolated from their internal vascularization must depend on the diffusion of substrates

from the surrounding medium through their periphery to supply their cellular metabolic requirements. To characterize the penetration of oxygen into an islet or aggregate requires both metabolic uptake and transport parameters. In the companion paper, we measured the oxygen uptake rate of small cell aggregates (mean diameter = 37 μm diameter) and of intact islets (mean diameter = 214 μm) in a stirred oxygen uptake chamber. Tissue oxygen uptake as a function of the surrounding medium pO_2 was measured by following the rate at which oxygen was depleted in the medium of the closed chamber using an oxygen quenched phosphorescent probe (Vanderkooi et al., 1986 and 1987). Based on these measurements, we reported V (including Vmax defined as the maximum tissue oxygen uptake rate in the absence of oxygen limitations) as a function of the bulk medium pO_2 (including P_{50} defined as the bulk medium pO_2 at which V=1/2 Vmax). The dependence of V on medium pO_2 of coupled cell aggregates was shown to be closely fit by a global (or tissue averaged) Michaelis-Menten type expression for oxygen consumption based on the measured values of Vmax and P_{50}. We also showed that metabolically uncoupled cell aggregates follow zero-order uptake kinetics which could be qualitatively described using a global Michaelis-Menten type expression based on an elevated Vmax and a diffusion limited P_{50}. Vmax and P_{50} data of cell aggregates from these experiments are tabulated in Tables 1 an 2 of this paper. The overall oxygen uptake of intact islets was measured and was found to have a Vmax similar to that of cell aggregates however the P_{50} of intact islet preparations was 10-fold higher than that measured in small cell aggregates. This difference was attributed to the larger diffusion resistance of intact islets. The oxygen uptake curve of intact islets plotted as V verses medium pO_2 was shown not to be fit by a global Michaelis-Menten type expression based on the measured values of Vmax and P_{50}. Therefore the oxygen uptake curves of intact islets are repeated in their entirety in Appendix 7A of this paper.

Oxygen diffusion limitations in both cell aggregates and intact islets result in the development of pO_2 gradients in and around consuming tissue. These gradients in conjunction with intrinsic oxygen consumption kinetics of respiring mitochondria within the tissue determine the degree to which the overall oxygen uptake of the tissue is affected by

changing medium pO_2. Thus in the oxygen limited regime, oxygen uptake is a function of the local or intrinsic rate of tissue oxygen consumption, the intra-tissue oxygen diffusivity, the intra-tissue diffusion distance, and of the fluid properties in the surrounding medium. In this paper, we use measured values of oxygen limited consumption in the diffusion limited regime, intra-tissue diffusion distances, and fluid properties in conjunction with a mathematical reaction/diffusion model to extract the value of the intra-tissue oxygen diffusivity.

RATIONALE

Extraction of D_{O2} from Uncoupled 0-Order Consumption Data

Exposure to Carbonylcyanide-p-trifluoro-methoxyphenylhydrazone (FCCP) uncouples mitochondrial oxygen uptake from oxidative phosphorylation effectively reducing the Michaelis-Menten coefficient (Km) of mitochondrial oxygen uptake to zero (Wilson et al., 1988). As a result, the intrinsic oxygen uptake of FCCP uncoupled cells can best be described by zero-order oxygen uptake kinetics (Robiolio et al., 1989; Rumsey et al., 1989; Dionne et al., 1989-6). Under these conditions, the experimentally measured value of P_x, the bulk medium pO_2 at which overall tissue consumption is reduced to V_x defined as the fraction of maximum oxygen uptake V/Vmax = x, is actually a measure of the medium pO_2 at which x fraction of the tissue volume is consuming oxygen at Vmax and 1-x fraction of the tissue is anoxic and is therefore not contributing to oxygen consumption. For the case of a spheroidal aggregate at P_{50}, the outer one-half of the aggregate's volume (r/R = 0.794 to 1.0; where r is the radial position and R is the aggregate radius) would be is consuming O_2 at Vmax whereas the O_2 consumption of the inner one-half of the aggregate volume would be zero due to anoxia. Therefore, the measured $P_{50uncoupled}$ is actually a measure of O_2 diffusion limitations to the interior volume of the tissue. Assuming homogeneous O_2 uptake within an aggregate or islet (homogeneously dispersed mitochondria), the O_2 profile within uncoupled tissue can be analytically solved using 0-order, O_2 uptake kinetics. This model requires information on the tissue size, the intra-tissue effective oxygen diffusivity (D_{O2}), paired P_x

and V_x data, and characteristics of the liquid medium surrounding the aggregates -- all of which have been measured (Dionne et al, 1989-6) or are generally available from the literature (see Table 1) with the exception of D_{O2}. The pO_2 drop in the stagnant layer of medium immediately surrounding stirred aggregates or islets may be neglected for small particles (Case I) or taken into account using a mass transport analogy (Brian and Hales, 1969) to determine the O_2 mass transfer coefficient, kc, across the liquid boundary layer (Case II).

Extraction of D_{O2} from Coupled Michaelis-Menten O_2 Uptake

Oxygen consumption of coupled mitochondria (Wilson et al., 1988) and of cells (Robiolio et al., 1989; Rumsey et al., 1989) including pancreatic islet cells (Dionne et al., 1989-6) can be described by Michaelis-Menten oxygen uptake kinetics. Under these conditions, the measured value of P_{50} in stirred tissue suspensions is a result of a combination of intrinsic kinetics (Km mitochondria), and to O_2 diffusion limitations throughout the tissue and in the stagnant boundary layer immediately surrounding the oxygen consuming tissue. The medium pO_2, P_x, at which overall tissue oxygen uptake is reduced to V/Vmax = x is a function of all of these parameters. An estimate of the intra-tissue oxygen diffusivity can be calculated by solving the reaction/diffusion equation with Michaelis-Menten reaction kinetics at a medium $pO_2 = P_x$ and iterating over D_{O2} in order to force the integrated tissue oxygen consumption to equal V_x. Because of the non-linear nature of Michaelis-Menten kinetics, the oxygen profile of coupled aggregates/islets must be modeled numerically. The model requires information on tissue size, paired V_x and P_x data, mitochondrial Km, and characteristics of the surrounding liquid medium, and an initial guess for the tissue D_{O2}.

MATHEMATICAL MODEL DEVELOPMENT

Estimation of the intra-tissue D_{O2} from uncoupled, 0-Order oxygen uptake data

Case I. Well-stirred tissue (Ps = Pm): The case of an oxygen consuming spheroid with an anoxic core well stirred medium such that the pO_2 at tissue surface, Ps, is equal to the pO_2 in the bulk medium, Pm, is depicted in Figure 1. The anoxic core (Region I) extends from r=0

to r=a; the oxygen consumption in the anoxic core is equal to zero. The viable rim (region II) extends from the outer radius of the anoxic core r=a to the outer radius of the spheroid r=R; the oxygen uptake rate in the viable rim is equal to Vmax. The reaction/diffusion equation simplified for the assumptions of steady state, 0-order oxygen uptake, radial diffusion in a spheroid of constant density, ρ, and diffusivity, D_{O2}, is written for each region along with the appropriate boundary conditions. The boundary conditions are derived for symmetry at the cell core, r=0; for both zero pO_2 and zero flux at the anoxic interface, r=a; and for no drop in pO_2 from the medium (Pm) to the cell surface (Ps) in a well stirred system. This last boundary condition will be relaxed to include a ΔpO_2 across the stagnant liquid boundary layer surrounding the suspended tissue in Case II.

The characteristic reaction/diffusion equations listed in Figure 1 can be integrated to produce the general solutions:

$$\text{Region I:} \qquad P(r) = \frac{A}{r} + B \tag{1}$$

$$\text{Region II:} \qquad P(r) = \frac{Vmax\ R^2}{6\ \alpha\ D_{O2}} + \frac{E}{r} - F \tag{2}$$

The solution of Equation 1 for region I is trivial: by the first boundary condition, "A" must be zero; by the second BC, "B" must also be zero. Therefore, as defined, the pO_2 everywhere within the anoxic core is zero.

To solve for the profile in region II, the 4th BC is first applied to Equation 2.

$$\text{BC \#4:} \qquad P(R) = Pm = \frac{Vmax\ R^2}{6\ \alpha\ D_{O2}} + \frac{E}{R} - F \tag{3}$$

Solving for "F" yields,

$$F = Pm + \frac{E}{R} - \frac{Vmax\ R^2}{6\ \alpha\ D_{O2}} \tag{4}$$

Applying the 3rd BC to Equation 2 yields,

$$\text{BC \#3:} \qquad \frac{dP(a)}{dr} = 0 = \frac{Vmax\ a}{3\ \alpha\ D_{O2}} + \frac{E}{a^2} \tag{5}$$

Therefore,

$$E = -\frac{Vmax\ a^3}{3\ \alpha\ D_{O2}} \tag{6}$$

Inserting the solutions for "E" and "F" contained in Equations 4 and 6 into the general solution of Equation 2 yields an equation that describes the pO_2 profile within the 0-order respiring rim of an O_2 consuming spheroid.

$$P(r) = Pm - \frac{Vmax}{6\ \alpha\ D_{O2}}(R^2 - r^2) + \frac{Vmax\ a^3}{3\ \alpha\ D_{O2}}(1/r - 1/R) \tag{7}$$

valid between: $a \leq r \leq R$.

Equation 7 contains the defined but unknown parameter "a" - the radius of the anoxic core. A correlation for "a" can be obtained by noting that Equation 8 must also meet the additional constraint imposed by the 2nd BC: that is at r=a, P(a) = 0.

$$P(a) = 0 = Pm - \frac{Vmax}{6\ \alpha\ D_{O2}}(R^2 - a^2) + \frac{Vmax\ a^3}{3\ \alpha\ D_{O2}}(1/a - 1/R) \tag{8}$$

Equation 8 can be implicitly solved for "a" - the radial position at which O_2 is depleted leaving an anoxic tissue core, or alternatively, it can be directly solved for the oxygen diffusivity, D_{O2}, within the spheroid. The latter approach yields:

$$D_{O2} = \frac{Vmax}{6\ \alpha\ Pm}(R^2 - a^2) - \frac{Vmax\ a^3}{3\ \alpha\ Pm}(1/a - 1/R) \tag{9}$$

Equation 9 can be solved for D_{O2} if another correlation can be found for the anoxic radius, "a". By definition, at Pm = P_x the overall tissue oxygen consumption, V, equals V_x. If a cell's mitochondria are homogeneously dispersed and uncoupled so that their intrinsic Km is equal to zero, then under the resulting O-order kinetics at P_x, x fraction of the tissue volume is oxygenated and 1-x is anoxic. Therefore, at Pm = P_x,

$$\frac{\text{anoxic core vol}}{\text{total cell vol}} = 1\text{-}x = \frac{4/3\ \pi\ a^3}{4/3\ \pi\ R^3} = \frac{a^3}{R^3} \tag{10}$$

or

$$a = (1\text{-}x)^{1/3}\ R \tag{11}$$

For the specific case where x = .5, $P_x = P_{50}$, and Equation 11 reduces to,

$$a = 0.5^{1/3} R \tag{12}$$

Either Equation 11 or 12 can be inserted into Equation 9 to yield an expression for the intra-tissue oxygen diffusivity in terms of Vmax, α, R, and P_x. For the explicit case of $P_x = P_{50}$,

$$D_{O2} = \frac{Vmax\ R^2}{6\ \alpha\ P_{50}} (1 - .5^{2/3}) + \frac{Vmax\ .5\ R^2}{3\ \alpha\ P_{50}} (1/.5^{1/3} - 1) \tag{13}$$

or,

$$D_{O2} = .0183\ \frac{Vmax\ R^2}{P_{50}\ \alpha} \tag{14}$$

Equation 14 can be used directly to solve for the intra-tissue D_{O2} in spheroids of known radius provided that uncoupled, experimental data relating the medium P_{50} to the cell Vmax is available. Alternatively, an equivalent expression can be derived for analyzing data relating P_x to Vmax where $x \neq 0.5$, by inserting Equation 11 into Equation 9 and solving for the appropriate dimensionless constant. An expression analogous to Equation 14 can be derived for other tissue geometries. The solution for infinitely long, rod shaped tissue of radius R is equivalent to Equation 14 except that the dimensionless constant 0.0183 is replaced by 0.0384 valid at $P_x = P_{50}$.

Case II: Stagnant liquid boundary layer surrounding tissue: ($Ps = Pm - \Delta P$): In the previous case, it was assumed that in a stirred system, the pO_2 at the tissue surface was equal to the pO_2 in the surrounding medium. This assumption is at best valid for small aggregates at low respiration rates in well stirred systems. In order to estimate the pO_2 drop across the stagnant liquid boundary layer surrounding oxygen consuming tissue particles, a mass transfer analogy based on the Sherwood number (Sh) for mass transfer to spheroids in stirred tank reactors was employed (Phipps, 1967; Brian and Hales, 1969; Brian, Hales and Sherwood, 1969; Wadia, 1974). The power input by the stir bar, Po, was calculated as a function of the stirring speed, ω (20 rev/sec), of the 0.4 cm diameter (d_s) impeller, the fluid density, ρ (1.0 g/cm^3), and the

dimensionless power number, Np which was taken as 0.5 based on the geometry of the stirred tank and on the impeller Reynolds number (580) (Phipps, 1967).

$$Po = Np\ \omega^3\ d_s^5\ \rho \tag{15}$$

The power input was in turn converted into a dimensionless power group, ϵ^* where

$$\epsilon^* = \left[\frac{Po\ (2R)^4}{m\ \nu^3} \right]^{1/3} \tag{16}$$

where m is the mass of fluid in stirred tank (0.275 g), ν is the kinematic viscosity of the medium at 37°C (0.0069 g/cm•sec), and R is the average radius of the oxygen consuming particles (cm). Correlations of ϵ^* to particle Sherwood number have been published for different experimental conditions (Brian, Hales and Sherwood, 1969; Wadia, 1974). Using a numerical fit to a correlation reported by Wadia (1974; Figure 1.23), a numerical relationship for the Sherwood number as a function of ϵ^* was formulated,

$$Sh = 2.0 + 6.3\ \exp[-0.393 + 0.382\ \ln\epsilon^* + 0.038\ (\ln\epsilon^*)^2] \tag{17}$$

where 6.3 is a constant derived from $(\nu/D_{O2m})^{1/3}$. Equation 17 provides an approximation of Sh under the experimental conditions at which oxygen uptake data was measured in our system and should not be interpreted as a general equation.

The mass transfer coefficient, kc, across the stagnant liquid boundary layer is equal to:

$$kc = \frac{Sh\ D_{O2m}}{2\ R} \tag{18}$$

The mass transfer coefficient, kc, in the above equation is used to determine the flux, N, of oxygen across a stagnant layer of medium according to the following equation,

$$\text{Flux of oxygen:} \quad N = kc\ \alpha_m\ (Pm - Ps) \tag{19}$$

where α_m is the solubility of oxygen in the medium and (Pm - Ps) represents the driving force or the ΔpO_2 between the bulk medium and the spheroid surface. Equation 18 can be inserted into Equation 19 which can then be solved for the partial pressure at the spheroid surface, Ps. Before doing this, one more relationship is required in order to eliminate the flux, N, from the resulting equation. This relationship can be obtained by realizing that at steady state, the

flux of oxygen into the aggregate must be equal to the consumption of oxygen within the spheroid. In other words, the flux per unit surface area must equal the O_2 consumption per unit volume, V, multiplied by the volume. For a spheroid this reduces to:

$$N = V \frac{4/3\ \pi\ R^3}{4\ \pi\ R^2} = V \frac{R}{3} \tag{20}$$

For a given value of P_x, V in Equation 20 can be replaced by $Vx = x \cdot Vmax$; therefore,

$$\text{at } Pm = P_x\ ;\quad N = \frac{x\ Vmax\ R}{3} \tag{21}$$

In particular, at $Pm = P_{50}$, the oxygen consumption within the aggregate is equal to one half of maximum. Therefore at P_{50}: $N = Vmax\ R/6$.

Equations 17, 18 and 21 can be combined to solve for the pO_2 at the aggregate surface, Ps, at any given P_x in terms of V_x and other known or measurable quantities.

$$Ps_x = P_x - \frac{2\ R^2\ V_x}{3\ Sh\ \alpha_m\ D_{O2m}} \tag{22}$$

Using Equation 22, the value of pO_2 at the spheroid surface at which overall tissue oxygen consumption is reduced to $V_x = x \cdot Vmax$ can be calculated from the value of P_x that is measured in the bulk medium.

The final step in developing a closed, analytical solution for the intra-tissue oxygen diffusivity of 0-order spheroids is to substitute Ps_x from Equation 22 for Pm in Equation 9 and solving it for a given value of x. This effectively relaxes the previous assumption that the pO_2 at the tissue surface being equal to the pO_2 in the stirred medium and allows for consideration of the pO_2 drop across the stagnant liquid boundary layer as calculated by equation 22. The analytical solution for D_{O2} at any given value of x is:

$$D_{O2} = \frac{Vmax}{6\ \alpha\ Ps_x} [1.5 - x - 1.5\ (1-x)^{2/3}] \tag{23}$$

Equation 23 is generally valid for any 0-order relationship between P_x and Vmax in spheroids provided that the Sherwood number mass transfer analogy used is applicable to the

conditions under which the relationship between P_x and V_x are measured. The appropriate units for the parameters are those used in Table 1.

For the particular case of $P_x = P_{50}$, Equation 23 reduces to:

$$D_{O2} = .0183 \frac{Vmax\ R^2}{Ps_{50}\ \alpha} \tag{24}$$

where the value of Ps_{50} is obtained by evaluating Equation 22 at $x = 0.5$. If it is assumed that the mass transfer analogy used to derive the pO_2 drop across the stagnant boundary layer can be extended to cylindrical rods, then Equation 24 can be used to calculate the intra-tissue diffusivity from data collected from rod-shaped tissue by replacing the constant 0.0183 with 0.0384.

Extraction of tissue D_{O2} from coupled, Michaelis-Menten consumption data

Mathematical formulation. The extraction of a tissue oxygen diffusivity from coupled, Michaelis-Menten consuming tissue must be done numerically because of the non-linear nature of the Michaelis-Menten kinetics resulting in an iterative solution. The general steps are, however, similar to those used in the analytical solution of 0-order kinetics: (1) the tissue O_2 profile must be solved using initial parameter values at some value of medium pO_2 equal to P_x; (2) tissue O_2 consumption is integrated and compared to the experimental value of V_x; (3) the guess of the tissue oxygen diffusivity is updated and the process is repeated until the solution converges. The additional complications of non-uniform spheroid sizes are dealt with by solving the pO_2 profile and by integrating O_2 consumption over multiple size ranges of islets. The consumption of the entire preparation is calculated as the volume fraction weighted sum of the consumption calculated in each size range.

The basic equations that must be solved are those for an oxygen consuming spheroid immersed in a well stirred liquid. The spheroid is assumed to be at steady state. Oxygen transport within the tissue is by radial diffusion only with no convection. The tissue oxygen diffusivity, D_{O2}, and the mass density, ρ, are assumed to be constant throughout the spheroid. Finally, oxygen consumption is assumed to be homogeneous throughout the aggregate or islet

and is described by local Michaelis-Menten uptake kinetics. A schematic of these conditions along with the appropriate characteristic reaction/diffusion equation for these assumptions is shown in Figure 2. Nomenclature is defined at the bottom of Figure 2. At the spheroid core, symmetry requires that the flux be zero, hence the boundary condition at r=0 is dP(0)/dr = 0. Even in a well stirred system, it cannot be assumed that the pO_2 at the spheroid surface, Ps, for large islets is equal to the pO_2 in the bulk medium, Pm. Instead, the spheroid surface pO_2 is set equal to the bulk medium pO_2 minus the pO_2 drop across the stagnant liquid boundary layer calculated by the Sherwood number mass transfer analogy previously described. The mass transfer coefficient, kc, is again defined such that,

$$\text{Flux of oxygen:} \quad N = kc\ \alpha_m\ (Pm - Ps) \tag{25}$$

At steady state, the flux into the spheroid multiplied by the area around the spheroid must equal the consumption within the spheroid.

$$N = q_{act}\ \frac{Vol}{Area} = q_{act}\ \frac{4/3\ \pi\ R^3}{4\ \pi\ R^2} = q_{act}\ \frac{R}{3} \tag{26}$$

Substituting "N" from Equation 26 into Equation 25, solving for Ps, and substituting Equation 18 for kc yields the boundary condition at r=R, the interface between the spheroid and the medium.

$$P(R) = Ps = Pm - \frac{q_{act}\ 2\ R^2}{3\ Sh\ \alpha_m\ D_{O2m}} \tag{27}$$

The pO_2 drop in the liquid boundary layer increases with increasing tissue oxygen consumption and spheroid radius and decreases with increasing medium oxygen diffusivity and power input.

Solution algorithm. The set of equations shown in Figure 2 are solved by iteration to extract the tissue D_{O2} using a finite difference algorithm to compute the non-linear oxygen profile. The solution algorithm is shown in flowchart form in Figure 3 and is discussed here as it pertains to a multi-sized ensemble of intact spheroidal islets.

The program input includes constant parameters such as oxygen solubility: α_m and α_I, number of radial steps (n), stirring speed, the experimental values of Pm_{50}, Vmax, Km intrinsic, and the size distribution and volume fraction of the islet preparation. An initial guess of the intra-islet diffusivity, (D_{O2} (l=1)) is also entered.

After initialization, the diameter, Dia(k), and volume fraction, Volf(k), of the kth size range of islets are read. The pO_2 at the islet surface for this kth size range is calculated using the boundary condition at the islet surface which requires an initial (j=1) guess for the fractional rate of oxygen uptake for that size islet, [q_{act} / q_{max} (k)]. The oxygen profile within the islet is calculated using Euler's form of a centered finite difference algorithm with LU decomposition and back substitution to solve a non-dimensionalized form of the characteristic equation shown in Figure 2. The "j+1"th estimate of the fractional oxygen consumption of the kth size range of spheroids, [q_{act} / q_{max} (k)]$_{(j+1)}$, is computed by numerically integrating the oxygen consumption over the "i=1→n" radial segments of the spheroid based on each averaged local pO_2 in the volume segment, P(i), and the intrinsic Michaelis-Menten coefficient, Km, for mitochondrial O_2 uptake.

$$\left[\frac{q_{act}}{q_{max}}(k)\right]_{j+1} = \sum_{i=1}^{n} \frac{q(i)\ Vol(i)}{Vmax\ Vol_{tot}} - \sum_{i=1}^{n} \frac{P(i)}{Km + P(i)} \frac{r^3_{(i+1)} - r^3_{(i)}}{R^3} \qquad (28)$$

The "j+1" value of [q_{act} / q_{max} (k)] calculated in Equation 27 is compared to the previous "j"th value which was used to determine the Δ pO_2 drop across the stagnant fluid layer. If these two values converge, then [q_{act} / q_{max} (k)] is stored for the kth size range, and the program drops down to the "k+1"th size range and volume fraction. If the fractional oxygen consumption fails to converge then Ps_{50} for the kth size range is recalculated using the new "j+1"th value of [q_{act} / q_{max} (k)]. The islet pO_2 profile and islet oxygen consumption are recalculated based on the new Ps_{50} and [q_{act} / q_{max} (k)] is again checked for convergence. This loop continues until the "j+1"th integrated consumption equals the consumption used to determine the islet surface pO_2 (jth iteration).

Once the value of $[q_{act} / q_{max}(k)]$ has been calculated for all ranges of the islet size distribution, the overall fractional oxygen uptake of the system is calculated by summing the fractional uptake of each size range weighted by the volume fraction of that size range.

$$\frac{Q_{act\ sys}}{Q_{max\ sys}} = \sum_{k} \frac{q_{act}}{q_{max}}(k)\ \frac{Vol(k)}{Vol_{tot}} \stackrel{?}{=} x \qquad (29)$$

The computed $[Q_{act} / Q_{max}]_{sys}$ ($P_{x\ sys}$) is compared to "x", the experimental fraction of maximum oxygen uptake corresponding to the medium pO_2, P_x, for which this simulation is being run. If the calculated $P_{x\ sys} \neq x \pm .002$ then D_{O2} is updated and the entire set of computations is repeated (as depicted in Figure 3) until convergence occurs. Once convergence is achieved, the final fit of D_{O2} is printed out along with the $P_{x\ sys}$, the final $[q_{act} / q_{max}(k)]$, and $Ps_x(k)$ for each size range of the islet ensemble. The algorithm was written in advanced Basic and run on an IBM PC AT. Convergence over an ensemble of 7 islet sizes requires an average of 3-4 hours of computation time. The computer code is listed in Appendix 8B.

RESULTS

Intra-Cellular or Intra-aggregate Oxygen Diffusivity

Four different mathematical approaches were used to extract the value of the intra-cellular O_2 diffusivity, D_{O2}, from two different sets of data relating the maximum aggregate oxygen consumption to the medium pO_2 at which the rate of consumption was reduced to 1/2 of maximum. First, an analytical solution (Equation 14) was developed based on the 0-order, O_2 uptake kinetics of FCCP - uncoupled cells. Equation 14 assumes that there was no pO_2 drop in the medium surrounding the stirred aggregates: $Ps_{50} = Pm_{50}$. This equation was applied to 23 sets of experimentally derived Vmax and P_{50} data (Dionne et al, 1989-6) to produce an estimate of the intra-cellular oxygen diffusivity, D_{O2c}, for each data set. Individual values of Vmax, P_{50}, and the resulting predicted values of D_{O2c} are listed in Table

2. The average intra-cellular O_2 diffusivity extracted from these well stirred, uncoupled measurements assuming spheroidal geometry was 1.71 x 10^{-6} cm^2/sec ± 0.65 x 10^{-6} (st. dev.; n=23).

The second method used to extract an intra-cellular oxygen diffusivity used the same 0-order uncoupled Vmax and P_{50} data as the previous solution but allowed for an portion of the P_{50} to be accounted for by a pO_2 drop in the layer of medium immediately surrounding the stirred aggregates: $Ps_{50} = Pm_{50} - \Delta pO_2$. Equation 24 represents the resulting expression for the intra-cellular oxygen diffusivity. In addition to Vmax and P_{50} data, Equation 24 also requires information on the mixing characteristics of the stirred medium. The calculated values of D_{O2c} based on Equation 24 are shown in column 4 of Table 2 for each set of 0-order Vmax and P_{50} data. The average value of D_{O2c} calculated including the ΔpO_2 drop was 2.32 ± 1.30 x 10^{-6} cm^2/sec (n=23). The addition of the ΔpO_2 drop across the boundary layer resulted in an increase in the predicted D_{O2c} because with the lower pO_2 at the cell surface, a higher permeability was required for O_2 to penetrate to the same depth of the aggregate.

The third method used to extract the intra-cellular oxygen diffusivity from uncoupled, 0-order data was based on Equation 24 but assumed that aggregates were more closely represented by infinitely long cylindrical rods of radius, R, than by spheroids. The actual shape of aggregates is somewhere between these two assumptions. The average value of D_{O2c} based on the assumption of stirred cylinders was 4.57 ± 2.77 x 10^{-6} cm^2/sec (n=23).

The fourth method used to predict intracellular D_{O2} was based on the Vmax and P_{50} of coupled cell aggregates whose O_2 consumption was represented by Michaelis-Menten kinetics. The method required the numerical solution of the intra-aggregate O_2 profile due to the non-linear Michaelis-Menten kinetics. The pO_2 drop in the liquid boundary layer surrounding he stirred aggregates was taken into account using a mass transfer coefficient as in Method 2. The numerical algorithm is summarized in Figure 3. The values of the coupled Vmax and P_{50} as well as the predicted intra-cellular O_2 diffusivity are listed in Table 3. The average value of D_{O2c} was 9.1 ± 3.6 x 10^{-6} cm^2/sec (n=26).

The different estimates of D_{O2c} from the two sets of experimental data and the four mathematical algorithms are listed together in Table 5.

Intra-Islet Oxygen Diffusivity

The diffusivity of O_2 within an intact, isolated islet of Langerhans was predicted using the same numerical algorithm used to extract the intra-cellular D_{O2} from coupled cell aggregates. The additional complexity of a large variety of islet sizes in the test population was accounted for by dividing each islet sample into seven size ranges, solving the O_2 profile in each size range, numerically integrating the fraction of maximum O_2 consumption for each size range, and summing the O_2 consumption of each size range weighted by its respective volume fraction to obtain the fractional O_2 consumption of the overall islet ensemble. The intra-islet diffusivity was extracted from eight different measurements of P_x and x between x = 0.2 to 0.9 . Experimental values of P_x at which oxygen consumption was reduced to x = Q/Qmax were measured from the full oxygen uptake curves for each islet preparation run (See Appendix 7A). The individual values of D_{O2} calculated at each value of P_x are listed in Table 5 for five separate, coupled intact rat islet oxygen uptake runs. The calculated value of D_{O2I} was strongly influenced by the value of x at which the data was run. Possible explanations for this phenomenon are addressed in the discussion; however for a variety of reasons, the values of D_{O2I} extracted at high values of x were deemed most reliable. The best estimate of the true intra-islet diffusivity was estimated as the value of D_{O2I} linearly extrapolated to x=1 for each uptake run. In addition to coupled estimates, D_{O2} for intact islets was extracted from two FCCP uncoupled oxygen consumption runs using the same solution algorithm described for coupled islets but with an intrinsic Km value = 0.05 mm Hg. The value of D_{O2I} calculated from these runs (see Table 4) was much less sensitive to x. The mean ± standard deviation of the best estimates (x=1) from each islet run was $1.55 \pm .41 \times 10^{-5}$ cm^2/sec (n=7).

DISCUSSION

Best Value of D_{O2c} based on Different Experimental and Mathematical Techniques.

The three methods of extracting the intra-cellular oxygen diffusivity from uncoupled aggregates all yielded values of D_{O2c} within a similar range: ~ 1 - 5 x 10^{-6} cm^2/sec; however, these diffusivities were consistently lower than the diffusivities extracted from numerical analysis of coupled cell aggregates at their P_{50}: D_{O2c} = 9.1 ± 3.6 x 10^{-6} cm^2/sec. It is unlikely that this difference is due to a real change in the oxygen permeability of coupled vs uncoupled cells. Rather it is more probable that the difference is due to the techniques used to extract the value of D_{O2c} from the different tissues. Among the choices of uncoupled diffusivities, the estimation of D_{O2c} based on the incorporation of the liquid boundary layer (Equation 24) is an obvious improvement over the estimate (Equation 14) which neglects its influence.

Values of D_{O2c} extracted from coupled, Michaelis-Menten respiring aggregates are questionable because of consistent trends in the predicted value of D_{O2c} depending on at what experimental value of Q/Qmax the diffusivity was extracted similar to the trends seen in intact islets. The reason for these trends in coupled aggregates is believed to be the changing value of Km of mitochondrial respiration as the aggregates become energy depleted in the oxygen limited uptake range. Because the medium pO_2 at which oxygen uptake is affected is the same order of magnitude as is the mitochondrial Km, small changes in the value of Km can have large affects on the calculated oxygen uptake and hence on estimated value of oxygen diffusivity. In sample calculations it was observed that a change in Km of 25%, from 0.44 to 0.33 mm Hg, could completely reverse the calculated trend of lower predicted $D_{O2}c$ values at low Q/Qmax ratios. Because the exact relationship of Km to the energy state of the cell or to the oxygen uptake rate is unknown, it is not possible to correct for the changing value of Km in these experiments. Since the Km of uncoupled aggregates is zero, this affect is not seen in uncoupled aggregates. Because of this, the values of D_{O2c} extracted from uncoupled aggregates are better estimates of the real intra-cellular oxygen diffusivity. Since the true geometry of aggregates is somewhere between a spheroid and an infinite cylindrical

rod, the best estimate of the intra-cellular diffusivity is bounded by the estimates using these two extremes: 2.3×10^{-6} cm^2/sec $\leq D_{O2c} \leq 4.85 \times 10^{-6}$ cm^2/sec.

Comparison of Islet Tissue D_{O2} to D_{O2} Values Measured in Other Tissue Systems

There have been many reports and several reviews published on the diffusivity of oxygen in cell tissue and biofilms. In a review of measured D_{O2} values in packed cells and biofilms, Karel and coworkers listed reports of the ratio of $D_{O2\ tissue}/D_{O2\ water}$ ranging from 0.1 to 1.1 (Karel, Libicki, and Robertson, 1985); Ngian and Lin cited five reports of $D_{O2\ tissue}/D_{O2\ water}$ ranging from 0.016 - 0.92 (Ngian and Lin, 1976); Evans quoted a narrower range of ratios between 0.54 - 0.89 for eight mammalian tissues (Evans, Naylor, and Quinton, 1981); Clark summarized reported ratios of four additional mammalian tissues between 0.54 - 0.78 (Clark et al, 1987). The ratios of $D_{O2\ tissue}/D_{O2\ water}$ reported in the present paper are 0.08 - 0.17 for cellular aggregates and 0.55 for intact islets which is within range of values reported in the literature for a variety of cellular tissues and/or aggregations.

Intra-Cellular Oxygen Diffusivity

The vast majority of the reported values of tissue D_{O2} have been measured in intact tissue slices which represent a heterogeneous mixture of cellular and extra-cellular spaces. It is not clear that these measurements represent the intrinsic intra-cellular diffusivity of oxygen, which may be much lower than that measured in heterogenous tissue beds.

Mueller and coworkers measured the intra-floc O_2 diffusivity in pure cultured flocs of Zoogloea ramigera I-16M using a technique similar to the 0-order kinetic model described in the present paper (Mueller, Boyle, and Lightfoot, 1968). They developed an anoxic core, 0-order kinetics model of diffusion/reaction within floc particles and applied it to O_2 consumption as a function of O_2 concentration data measured in a stirred suspension of consuming floc particles. Although their model neglected the ΔpO_2 drop in the liquid boundary layer and required the estimation of a specific spherical diameter form very non-spherical particles, it nevertheless predicted an intra-floc O_2 diffusivity of $2.1 \pm .95 \times 10^{-6}$

cm^2/sec (30°C) which is very close to the values of intra-cellular oxygen diffusivity calculated in the present paper using 0-order kinetic data.

Presently, the only experimental/theoretical predictions of the intra-cellular oxygen diffusivity in mammalian cells are those of Jones and coworkers (Jones and Kennedy, 1982; Jones 1984; Jones and Kennedy, 1986). They used differences in the oxygen P_{50} of electron transport chain cytochromes measured in intact cells (P_{50cell} = 6.0 μM (or ~4.3 mmHg); in isolated hepatocytes) vs the P_{50} measured in isolated, suspended mitochondria ($P_{50mitochondria}$ = 0.69 μM (or ~ 0.49 mmHg) to extract values of intra-cellular D_{O2}. Their primary assumption was that at a medium $pO_2 = P_{50cell}$, the pO_2 at the surface of the intra-cellular mitochondria must on average be equal to the P_{50} measured for isolated mitochondria. The ΔpO_2 (P_{50cell} - $P_{50mitochondria}$) was attributed to the resistance of the cytosol to oxygen diffusion. This assumption was analyzed using a model developed by Boag for diffusion to a consuming spheroid (mitochondria) surrounded by an infinite layer of stagnant media (cell cytosol). This equation (Equation 30, Boag, 1969; Equation 1, Jones and Kennedy, 1982) is repeated here for clarity.

$$C(r) = C_\infty - \frac{Q_{mit}\, b^3}{3\, D\, r} \qquad (30)$$

where C(r) is the $[O_2]$ at radial distance "r" from the center of the consuming spheroid, C_∞ is the $[O_2]$ at r=∞, Q_{mit} is the 0-order, O_2 uptake rate (Vmax) of the spheroid which in this case is the mitochondria (Q_{mit} = 6.2 x 10^{-4} moles/liter-sec), b is the radius of the consuming spheroid (set equal to 0.6 μm for a single mitochondria), and D is the oxygen diffusivity in the surrounding medium which in this case is the intra-cellular cytosol. All values are those reported by Jones et al.

Equation 30 was evaluated at r=b. C(b) was set equal to the $P_{50mitochondria}$ when C_∞ was set equal to the P_{50cell}. Solution of Equation 30 (or of its cylindrical equivalent) for "D" using the parameters reported by Jones, including a very high estimate of the effective

mitochondrial cluster radius: b=2μm; yielded an estimate of intra-cellular D_{O2} between 1.7 - 4 x 10^{-6} cm^2/sec (Jones and Kennedy, 1982; Jones 1984; Jones and Kennedy, 1986).

Despite the excellent agreement with the values of intra-cellular oxygen diffusivity predicted in the present paper, there are several limitations in the approach as described above, which require an unrealistically high assumption of the mitochondrial radius in order to raise the predicted D_{O2} to this level: (1) The model used to extract the D_{O2} was developed for diffusion to a consuming spheroid through an infinitely stagnant medium. However, in the present case, the model was applied to the case of diffusion through a finite distance from the cell membrane to the mitochondrial surface. The addition of the correction factor to account for the finite distance is small if the mitochondria is far from the cell membrane but approaches a factor of "2" as the distance from the mitochondria surface to the cell membrane approaches the magnitude of the mitochondria radius. (2) The model assumes an average ΔpO_2 from the cell surface to the mitochondria surface rather than incorporating the spatial effect of a distribution of mitochondria throughout a macroscopic intra-cellular pO_2 gradient extending from the membrane to the cell core. This assumption eliminates the cell radius from the equation and instead inserts the mitochondrial radius as the most sensitive parameter, which is a more difficult parameter to measure. (3) The analysis either neglects the pO_2 drop in the liquid boundary layer (Jones and Kennedy, 1982) or assumes a ΔpO_2 drop based on an arbitrary thickness of the stagnant layer of medium around the stirred cells (Jones 1984; Jones and Kennedy 1986). Although these three limitations of the mathematical analysis used to extract the value of D_{O2} are troublesome, they do not appear to cause a major discrepancy in the outcome. Substitution of the average P_{50cell} (1.10 mm Hg) reported for O_2 uptake in rat and canine islet cell aggregates in the accompanying experimental paper (Dionne et al, 1989) into Equation 30 along with the accepted value (b=0.6 μm) for the radius of an individual mitochondria reported by Jones and others, and neglecting the ΔpO_2 in the liquid boundary layer, yields a predicted intra-cellular D_{O2} of 1.3 x 10^{-6} cm^2/sec which is only slightly lower than the value obtained using the more complete mathematical extraction described in the present paper.

The larger problem which forces Jones and coworkers to assume a very high value for the effective radius of clustered mitochondria: "b" = 2 μm (or an effective diameter of clustered mitochondria = 4 μm or ~ 37 mitochondria per cluster); is an abnormally high value of cellular P_{50}. Jones' values of P_{50cell} were reported as 6.0 μM (~ 4.3 mmHg for media at 30°C) for hepatocytes (Jones and Kennedy, 1982) and 8.5 μM (~ 6.0 mmHg) for myocytes (Jones and Kennedy, 1986). These values are much higher than those measured by other investigators which all range below 2.5 μM for similar cells (Longmuir, 1957; Robiolio et al, 1989; Dionne et al, 1989; Rumsey et al, 1989). One possible explanation for the abnormally high values of P_{50cell} is the double pulse technique used by Jones to measure O_2 consumption rates. Especially at low O_2 levels, this technique is prone to error as the magnitude of the "pulse" of O_2 added to the oxygen consumption chamber becomes large with respect to the nominal value of the pO_2 at which oxygen consumption is being measured. Our experience has indicated that the Vmax of cells increases when their energy state becomes depleted following periods of hypoxia as short as 30 sec or less (Dionne et al., 1989) and remain elevated until cells have been exposed to high oxygen levels for a long enough time (about one min) to replenish their metabolic energy supplies. The combination of this "pseudo-uncoupled" Vmax and a relatively large $\Delta pO_{2\ pulse}$ in comparison to the nominal medium pO_2 may explain why the values reported by Jones are abnormally large. In order to compensate for the high value of P_{50cell}, Jones assigned mitochondria to clusters with an average radius of 2 μm. Since in his model the mitochondria radius is the most sensitive parameter, the effect is to increase the predicted $D_{O2\ c}$ by a factor of $(b_{cluster}/b_{mitochondria})^2 = (2/.6)^2 = 11$.

In summary, the intra-cellular diffusivity predicted by Jones and coworkers agrees with the value calculated in the present paper but required very large estimates of the effective mitochondria radius because of very high experimental values of P_{50cell}. However, using more generally accepted values of P_{50cell} in the same analysis used by Jones, yields an estimate of D_{O2c} which fits in the range reported by Jones and coworkers and which is only slightly lower than the values calculated in the present paper without the need to assume an arbitrarily high level of mitochondria clustering.

It appears that the intra-cellular diffusivity of oxygen may be significantly lower than the diffusivity of oxygen measured in heterogeneous tissues which consist of both cellular and extra-cellular compartments. This statement is supported by several observations. (1) In the present paper, the intra-cellular D_{O2} values measured by all three techniques (1.7 - 4.6 x 10^{-6} cm^2/sec) were lower than the D_{O2} measured in intact islets (15.3 x 10^{-6} cm^2/sec), the latter being more representative of heterogenous tissue. (2) The analysis of Jones using either his data assumptions or using generally accepted P_{50cell} values, yielded similarly low estimates of intra-cellular D_{O2} ranging from 1.0 - 4.0 x 10^{-6} cm^2/sec; whereas Evans' summary of eight D_{O2} values measured in intact tissue slices yielded values 5-10 times higher (1.45 - 2.3 x 10^{-6} cm^2/sec) (Evans, Naylor, and Quinton, 1981) than the intra-cellular values. (3) Ho correlated a linear decrease of composite D_{O2} with increasing volume fraction of cells in a suspended heterogenous cell slurry (Ho, 1987). Finally, (4) Tai and Chang used a heterogeneous model of oxygen diffusion to predict the ratio of extra-cellular to intra-cellular oxygen permeability, Ke/Kc, and found that the best fit to experimental data was obtained with a cellular permeability approximately 1/10 that of the extra-cellular or medium permeability.

Comparison of the D_{O2} in Intact Islets to D_{O2} in Multi-cellular Spheroids

The similarity in shape and composition of isolated islets of Langerhans to multi-cell spheroids suggests the comparison of intra-islet to intra-spheroid oxygen diffusivities. Mueller-Klieser and coworkers have developed a technique using microprobes to measure the pO_2 gradient in and around an O_2 consuming spheroid. From the gradient in the stagnant media, they extract an overall spheroid oxygen uptake rate, Q, and from the gradient within the spheroid, they extract a value for the Krogh's diffusion constant, Ks = $(\alpha D)_s$, in the spheroid (Mueller-Klieser 1984; Mueller-Klieser and Sutherland, 1984). The values of the intra-spheroid diffusivity obtained using this technique were 1.82 x 10^{-5} cm^2/sec for EMT6 spheroids and 1.69 x 10^{-5} cm^2/sec for V79 spheroids with a standard deviation of 10-25%. These values are quite close to the mean intra-islet D_{O2} measured in this paper (1.53 x 10^{-5} cm^2/sec).

The agreement may be even better than reported due to two factors. First, Mueller-Klieser used an average value of α_I, the O_2 solubility in tissue, of 0.88 x 10^{-9} mole/cm^3-mmHg, which is ~ 15% lower than the tissue averaged value used in the present paper of 1.02 x 10^{-9} mole/cm^3-mmHg (See Table 1 for references), which is between the value used by Mueller-Klieser and that cited by Evans as the average of eight mammalian tissues reported in the literature: α_I = 1.29 ± .17 x 10^{-9} mole/cm^3-mmHg (Evans, Naylor, and Quinton, 1981). Since the Krogh diffusivity is the product of α_I x D_{O2}, a decrease in the value of α_I results in an inversely proportional increase in the predicted value of D_{O2}. Use of the α_I used by Mueller-Klieser would result in a predicted intra-islet D_{O2} of 1.93 x 10^{-5} cm^2/sec, whereas use of α_I = 1.02 x 10^{-9} mole/cm^3-mmHg in Mueller-Klieser's analysis would result in an intra-spheroid D_{O2} of 1.46 - 1.58 x 10^{-6} cm^2/sec, therefore the values of the Krogh diffusivity actually overlap.

Second, the agreement of islet to spheroid diffusivities may be even closer due to the possibility of heterogeneous oxygen consumption in the spheroids as reported by Mueller-Klieser et al. Their analysis assumes that Oxygen consumption is uniform throughout the spheroid or at least throughout the viable rim of non-necrotic respiring cells. The intra-spheroid diffusivity is extracted from measurements of the pO_2 gradient at a radial position, r, in the spheroid using the first integral of the diffusion / reaction equation for 0-order O_2 consumption in a spheroid. The resulting equation, solved for K_s, (Equation 5a of Mueller-Klieser, 1984) is repeated here for the case of a spheroid with no necrotic core.

$$K_s = (\alpha D)_s = \frac{Q\ r}{3\ \frac{dP_s(r)}{dr}} \qquad (31)$$

where "Q" is the O_2 uptake rate of the viable tissue <u>interior</u> to the radial position "r" at which the pO_2 gradient, dP(r)/dr, is measured. However, the "Q" that is actually substituted into Equation 30 is an overall "$Q_{spheroid}$" based on the average oxygen consumption of the entire viable region of the spheroid. In Table 2 of Mueller-Klieser 1984, and in Figure 1 of Mueller-Klieser and Southerland, 1984, the authors point out that their data showed either a

linear or exponential decrease in the predicted overall "$Q_{spheroid}$" with increasing spheroid diameter. (This decrease was not due to inclusion of non-consuming necrotic core regions as all consumption data was based on the volume of viable tissue as ascertained by histologic examination.) Only in the very smallest spheroids (diameter < 400 μm) did the overall uptake rate of spheroids equal the uptake rate of single cells. The majority of data from which D_{O2} values were calculated, was collected from spheroids whose diameter ranged from 500 - 2000 μm: the overall oxygen consumption of which dropped to less than 1/3 of that measured in small spheroids or in single cells. If, as suggested by this data, the oxygen consumption of non-necrotic, cells located toward the core of large spheroids was lower than the oxygen consumption of peripheral cells because of limited core oxygenation under test conditions, variations in growth conditions, or intrinsic differences in the cell state, then this would directly lead to an over prediction of the tissue diffusivity since the correct "Q" of the tissue interior to the position "r" where the gradient was measured in Equation 31 would be less than the average overall "$Q_{spheroid}$" which was actually used in the equation and on which the values of intra-spheroid D_{O2} were based.

REFERENCES

Boag, J.W. (1969) Oxygen Diffusion and Oxygen Depletion Problems in Radiobiology. Curr Topics Radiat Res 5: 141-195.

Brian, P.L.T, and Hales H.B. (1969) Effects of Transpiration and Changing Diameter on Heat and Mass Transfer to Spheres. AIChE J 15: 419-425.

Brian, P.L.T, Hales, H.B, and Sherwood, T.K. (1969) Transport of Heat and Mass Between Liquids and Spherical Particles in an Agitated Tank. AIChE J 15: 727-733.

Clark, A, Clark, P.A.A, Connett, R.J, Gayeski, T.E.J, and Honig, C.R. (1987) How Large is the drop in pO_2 between Cytosol and Mitochondrion? Am J Physiol 252 (Cell Physiol. 21): C583-C587.

Evans, N.T.S, Naylor, P.F.D, and Quinton, T.H. (1981) The Diffusion Coefficient of Oxygen in Respiring Kidney and Tumour Tissue. Respiration Physiology 43: 179-188.

Ho, C.S. (1987) Oxygen Transfer and Diffusion in Mycelial Biofilms. Doctoral Thesis submitted to Department of Chemical Engineering, Massachusetts Institute of Technology, Cambridge MA; July 27, 1987.

Jones, D.P, and Kennedy, F.G. (1982) Intracellular Oxygen Supply during Hypoxia. Am J Physiol 243: C247-C253.

Jones, D.P. (1984) Effect of Mitochondrial Clustering on O_2 supply in Hepatocytes. Am. J. Physiol. 247 (Cell Physiol 16): C83-C89.

Jones, D.P, and Kennedy, F.G. (1986) Analysis of Intracellular Oxygenation of Isolated Adult Cardiac Myocytes. Am J Physiol 250 (Cell Physiol 19): C384-C390.

Karel, S.F, Libicki, S.B, and Robertson, C.R. (1985) The Immobilization of Whole Cells: Engineering Principles. Chem Engr Sci 40: 1321-54.

Levich, V.G. (1962) Physiocochemical Hydrodynamics. Prentice-Hall, Englewood Cliffs, NJ.

Longmuir, I.S. (1957) Respiration Rate of Rat-Liver Cells at Low Oxygen Concentrations Biochem J 65: 378-382.

Mueller, J.A, Boyle, W.C, and Lightfoot, E.N. (1968) Oxygen Diffusion Through Zooglocal Flocs. Biotech & Bioeng 10: 331-358.

Mueller-Klieser, W.F. (1984) Method for the Determination of Oxgyen Consumption Rates and Diffusion Coefficients in Multicelluar Spheroids. Biophys J 46: 343-348.

Mueller-Klieser, W.F, and Sutherland, R.M. (1984) Oxygen Consumption and Oxygen Diffusion properties of Multicellular Spheroids from Two Different Cell Lines. Adv in Exp Medicine and Biology 180; Oxygen Transport to Tissue VI; Proceedings of the International Society of Oxgyen Transport to Tissue held Aug 16-20, 1983, in Ruston, Louisiana; pp311-321.

Phipps, D.L. (1967). Mass transfer in a mechanically agitated batch dialyzer. M.S. Thesis; Department of Chemical Engineering; Massachusetts Institute of Technology, Cambridge, MA.

Tai, R.C, and Chang, H-K. (1974) Oxygen Transport in Heterogeneous Tissue. J Theor Biol 43: 265-276.

Wadia, P.H. (1974). Mass transfer from spheres and discs in turbulent agitated vessels. (Ph.D. Thesis; Department of Chemical Engineering; Massachusetts Institute of Technology, Cambridge, MA.

Wilson, D.F., Rumsey, W.L., Green, T.J. and Vanderkooi, J.M. (1988) The Oxygen Dependence of Mitochondrial Oxidative Phosphorylation Measured by a New Optical Method for Measuring Oxygen Concentration. J Biological Chemistry 263: 2712-2718.

TABLE 1. Experimental Parameters For Single Cell Aggregate And Whole Islet Oxygen Uptake

---

Average Tissue Size

Volume average size of cell aggregates*[1]

Rat aggregate diameter	38.9 ± 8.5 μm
Canine aggregate diameter	35.3 ± 9.0 μm

Average size distribution of intact islets*[1]

Diameter (μm)	Volume %
≤ 120	4.2
121 - 150	9.3
151 - 180	19.7
181 - 210	21.3
211 - 240	19.2
241 - 280	14.7
281 - 310	11.6

System Parameters at 37 °C

Diffusivity of Oxygen in media[τ1]	2.96×10^{-5} cm^2 / sec
Solubility of Oxygen in media[τ2]	1.27×10^{-9} mole / cm^3 - torr
Solubility of Oxygen in tissue[τ3]	1.02×10^{-9} mole / cm^3 - torr
Kinematic viscosity of media[τ4]	6.92×10^{-3} cm^2 / sec
Km for state 5 Mitochondria[τ5]	0.44 mmHg

[τ1] Literature values: 2.86×10^{-5}, H_2O corrected to 37°C (Goldstick and Fatt, 1970); 2.98×10^{-5}, H_2O corrected to 37°C (Stroeve et al, 1971); 3.53×10^{-5}, H_2O corrected to 37°C (Grossman, 1984; data of Grote, 1987); 2.72×10^{-5}, H_2O corrected to 37°C (Treybal, 1980); 2.51 - 3.28×10^{-5}, Reported range in literature for H_2O corrected to 37°C (Goldstic and Fatt, 1970; reported in Stroeve et al, 1976); 2.78×10^{-5}, isotonic saline corrected to 37°C (Goldstick and Fatt, 1970); 2.96×10^{-5}, isotonic saline corrected to 37°C (Stroeve et al, 1976)

[τ2] Averaged from: 1.33×10^{-9}, Balanced Salt Sol. (Chen et al, 1985); 1.22×10^{-9}, BSS (Panten and Klein, 1982); 1.32×10^{-9}, Burks media (Chen et al, 1985); 1.29×10^{-9}, Ringer's Sol (McLimans et al, 1968); 1.24×10^{-9}, plasma (Colton and Drake, 1971); 1.24×10^{-9}, isotonic saline (Altman and Dittmer, 1971).

[τ3] Averaged from: 1.11×10^{-9}, frog sartorius muscle (Mahler, 1978); 1.20×10^{-9}, D.S. Carcinosarcoma cells (Grossman, 1984; data of Grote et al, 1977); 0.915×10^{-9}, EMT6 spheroids, 87.2 % H_2O, (Mueller-Klieser 1984 & 1985); 0.866×10^{-9}, EMT6 spheroids, 85.5 % H_2O, (Mueller-Klieser 1984 & 1985).

[τ4] From National Bureau of Standards, H_2O at 37°C, reported in CRC Handbook of Chemistry and Physics, 60th ed.

[τ5] Km of isolated, suspended mitochondria measured in same O_2 uptake system as was the islet tissue and reported by Wilson et al, 1988.

TABLE 2. Intra-Cellular Oxygen Diffusivity: Uncoupled Cells

Vmax ($\times 10^8$ mol/cm^3-sec)	P_{50} media (mm Hg)	DO_2 No BL: Eq.14 ($\times 10^6$ cm^2/sec)	DO_2 BL: Eq. 24 ($\times 10^6$ cm^2/sec)	DO_2 BL: Cylinder ($\times 10^6$ cm^2/sec)
9.25	2.22	1.84	2.41	5.03
9.25	1.66	2.46	3.59	5.51
8.71	2.96	1.30	1.56	3.26
8.28	3.02	1.21	1.43	2.99
8.23	2.01	1.81	2.35	4.92
8.00	3.46	1.02	1.17	2.45
4.72	0.64	3.25	5.59	11.67
4.13	1.07	1.70	2.18	4.55
4.11	1.11	1.63	2.07	4.32
4.06	0.52	3.45	6.17	12.90
3.99	1.04	1.69	2.16	4.52
3.71	1.02	1.61	2.02	4.22
3.70	1.02	1.60	2.01	4.21
3.59	1.10	1.44	1.77	3.69
3.06	1.00	1.35	1.63	3.41
2.99	0.82	1.61	2.03	4.24
2.77	0.98	1.25	1.48	3.10
2.51	1.02	1.09	1.26	2.64
2.41	0.79	1.35	1.63	3.40
2.35	0.44	2.36	3.38	7.06
1.91	0.78	1.08	1.25	2.62
1.91	0.78	1.08	1.25	2.62
1.07	0.22	2.15	2.96	6.19
	Average =	1.71×10^{-6} cm^2/s	2.32×10^{-6}	4.85×10^{-6}
	St. dev =	± 0.65	± 1.30	± 2.71
		(n=23)	(n=23)	(n=23)

Parameters used in Equations 14 and 24 are listed in Table 1 along with their sources. $D_{O2m} = 2.78 \times 10^{-5}$ cm^2/sec; $\alpha_m = 1.27 \times 10^{-9}$ mole/cm^3-mmHg; $\alpha = 1.02 \times 10^{-9}$ mole/cm^3-mmHg.

TABLE 3. Intra-Cellular Oxygen Diffusivity: Coupled Cells[a]

Batch	Vmax ($\times 10^8$ mol/cm^3-sec)	P_{50} media (mmHg)	DO_2 Stirred ($\times 10^6$ cm^2/sec)
Canine aggregates			
2K3A1	2.99	0.82	14.0
2K3A2	3.06	1.00	8.0
3K4A1	3.56	0.72	27.5[b]
3K4A2	3.88	1.00	11.0
3K4A3	3.86	1.04	9.5
3K4A4	3.75	0.97	12.5
2K1A1	3.19	1.29	4.5
2K2A1	3.54	0.95	12.5
2K2A2	3.90	1.14	8.0
3K3A1	4.56	1.23	8.0
3K3A2	4.71	1.30	8.0
3K3A3	5.78	1.66	5.5
3K5A1	4.06	1.18	8.0
3K5A2	6.12	2.48	2.5
3K5A3	6.41	2.07	4.5
3K5A4	4.30	1.39	5.5
3K5A5	3.93	1.24	6.5
3K5B1	4.10	1.15	8.0
4K4A1	3.62	0.95	12.5
4K4A2	3.83	1.01	11.0
Rat aggregates			
1K1A1	3.56	1.23	8.0
2K2B1	4.56	1.28	9.5
4K3A2	4.34	1.00	18.5
4K3B1	4.46	1.16	24.5[b]
4K3B2	4.02	0.84	12.5
		Average =	9.06×10^{-6} cm^2/s
		St. dev =	$\pm 3.65 \times 10^{-6}$ (n=25)

[a] Parameters used to solve for coupled O_2 diffusivity are listed in Table 1 along with their sources.

[b] Data point excluded from mean

TABLE 4. Intra-Islet Oxgyen Diffusivity Calculated at Q/Qmax (Q_x) of 0.2 to 0.9

Islet Batch #	D_{O2I} (x 10^5 cm^2/sec) Q_x: 0.2	0.3	0.4	0.5	0.6	0.7	0.8	0.9	1.0[a]
2K4A1	-	-	1.87	1.95	2.11	2.22	2.22	2.54	2.22
4K2A1	0.67	0.83	1.01	1.12	1.20	1.35	1.50	1.55	1.69
4K2B1	0.65	0.85	0.98	1.12	1.22	1.30	1.45	1.43	1.58
4K2B2	0.67	0.77	0.92	1.00	1.10	1.20	1.30	1.50	1.56
4K2B3	0.62	0.75	0.87	0.92	0.97	1.02	1.05	1.15	1.18
4K2D	0.44	0.58	0.71	0.82	0.89	0.91	0.84	0.87	0.93
2K4F	1.45	1.60	1.60	1.45	1.64	1.60	1.75	1.55	1.66
					Mean at Q/Qmax = 1.0 :				1.55×10^{-5} cm^2/sec $\pm 0.41 \times 10^{-5}$
					Mean[b] at Q/Qmax = 1.0 :				1.53×10^{-5} cm^2/sec $\pm 0.21 \times 10^{-5}$

[a] Data extrapolated to Q/Qmax = 1.0 by linear interpolation of the data from 0.4 to 0.9 .

[b] Excluding stray highest and lowest values: 2K4A1 and 4K2D.

TABLE 5. Summary of Calculated Tissue Oxygen Diffusivity Values.

Intra-Cellular Oxygen Diffusivity		
Extracted from Uncoupled Data		
No stagnant fluid layer	$1.71 \pm .65 \times 10^{-6}$ cm^2/sec	(n=23)
With a liquid boundary layer	$2.32 \pm 1.30 \times 10^{-6}$ cm^2/sec	(n=23)
Cylindrical rod with B.L.	$4.85 \pm 2.71 \times 10^{-6}$ cm^2/sec	(n=23)
Extracted from Coupled Data		
With a liquid boundary layer	$9.1 \pm 3.6 \times 10^{-6}$ cm^2/sec	(n=24)
Intra-Islet Oxygen Diffusivity		
Extracted from Coupled Islet Data		
With a liquid boundary layer	$15.3 \pm 2.1 \times 10^{-6}$ cm^2/sec	(n=5)

FIGURE 1. SPHEROID MODEL FOR EXTRACTING INTRA-TISSUE OXGYEN DIFFUSIVITY FROM 0-ORDER O_2 UPTAKE DATA.

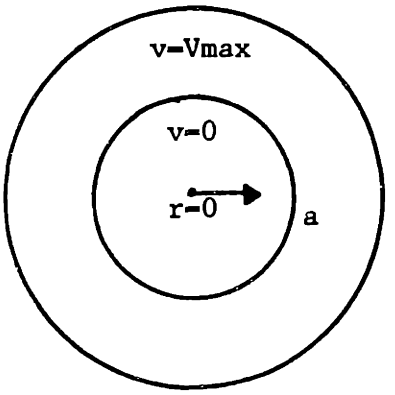

Characteristic Equations

Assumptions: Steady state spheroid, no convection, radial diffusion, Constant intra-cellular diffusivity (D_{O2}) and density (ρ), homogeneous 0-order Oxygen consumption for $pO_2 > 0$ (Region II; $a \leq r \leq R$), zero Oxygen consumption for $pO_2 = 0$ (Region I; $0 \leq r < a$).

Region I

$$D_{O2} \alpha \left[\frac{d^2 P(r)}{d r^2} + \frac{2}{r} \frac{dP(r)}{dr} \right] = 0$$

Regicn II

$$D_{O2} \alpha \left[\frac{d^2 P(r)}{d r^2} + \frac{2}{r} \frac{dP(r)}{dr} \right] = Vmax$$

Boundary Conditions

#1: $r = 0, \quad \frac{dP_I(0)}{dr} = 0$

#2: $r = a, \quad P_I(a) = P_{II}(a) = 0$

#3: $r = a, \quad D_{O2} \alpha \left[\frac{dP(a)}{dr}\right]_I = D_{O2} \alpha \left[\frac{dP(a)}{dr}\right]_{II} = 0$

#4: $r = R, \quad P_{II}(R) = Ps = Pm$

List of Symbols

α	Tissue oxygen solubility (mole/cm^3-mmHg)
a	Anoxic core radius (μm)
D_{O2}	Tissue oxygen diffusivity (cm^2/sec)
P(r)	Partial Pressure of Oxygen at radial position r, (mm Hg)
Pm	Partial Pressure of Oxygen in bulk media (mm Hg)
Ps	Partial Pressure of Oxygen at aggregate surface (mm Hg)
r	Radial position within tissue (μm)
R	Outer radius of spheroidal tissue partical (μm)
v	local O_2 uptake of tissue (moles/cm^3-sec)
Vmax	Maximum cell O_2 uptake (moles/cm^3-sec)

FIGURE 2. SPHEROID MODEL FOR EXTRACTING INTRA-TISSUE OXGYEN DIFFUSIVITY FROM COUPLED O_2 UPTAKE DATA.

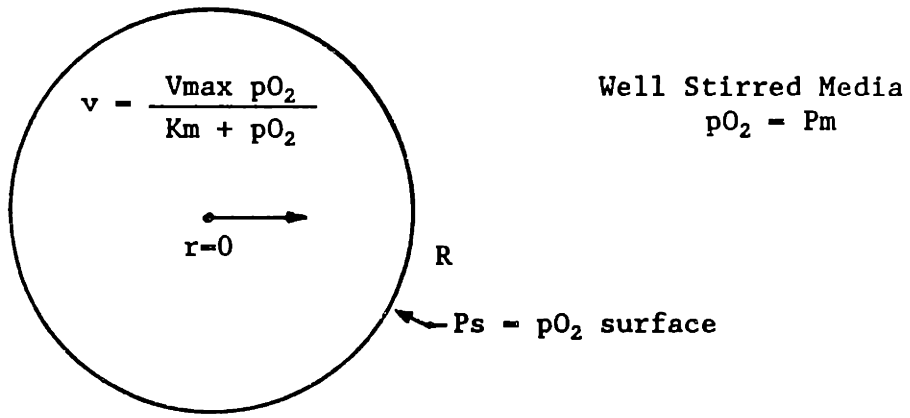

Characteristic Equation

Assumptions: Steady state spheroid, no convection, radial diffusion, Constant tissue diffusivity (D_{02}) and density (ρ), homogeneous O_2 consumption described by Michaelis-Menten kinetics.

$$D_{02}\,\alpha\left[\frac{d^2\,P(r)}{d\,r^2}+\frac{2}{r}\,\frac{dP(r)}{dr}\right]=\frac{Vmax\;\;P(r)}{Km\;+\;P(r)}$$

$$\text{BC \#1:}\quad r=0,\qquad \frac{dP(0)}{dr}=0$$

$$\text{BC \#2:}\quad r=R,\quad P(R)=Ps=Pm-\frac{q_{act}\;R}{3\;kc\;\alpha_m}$$

List of Symbols

D_{02}	Tissue oxygen diffusivity (cm^2/sec)
kc	O_2 Mass transfer coefficient in liquid boundary layer (cm/sec)
Km	M-M coefficient for mitochondrial O_2 uptake (mm Hg)
P(r)	Partial Pressure of Oxygen at radial position r, (mm Hg)
Pm	Partial Pressure of Oxygen in bulk media (mm Hg)
Ps	Partial Pressure of Oxygen at islet surface (mm Hg)
q_{act}	Actual overall O_2 uptake of tissue particle (moles/cm^3-sec)
r	Radial position within tissue (μm)
R	Outer radius of tissue spheroid (μm)
v	local O_2 uptake of tissue (moles/cm^3-sec)
Vmax	Maximum intrinsic O_2 uptake rate (moles/cm^3-sec)
α	Tissue oxgyen solubility (mole/cm^3-mm Hg)
α_m	Liquid medium oxygen solubility (mole/cm^3-mm Hg)

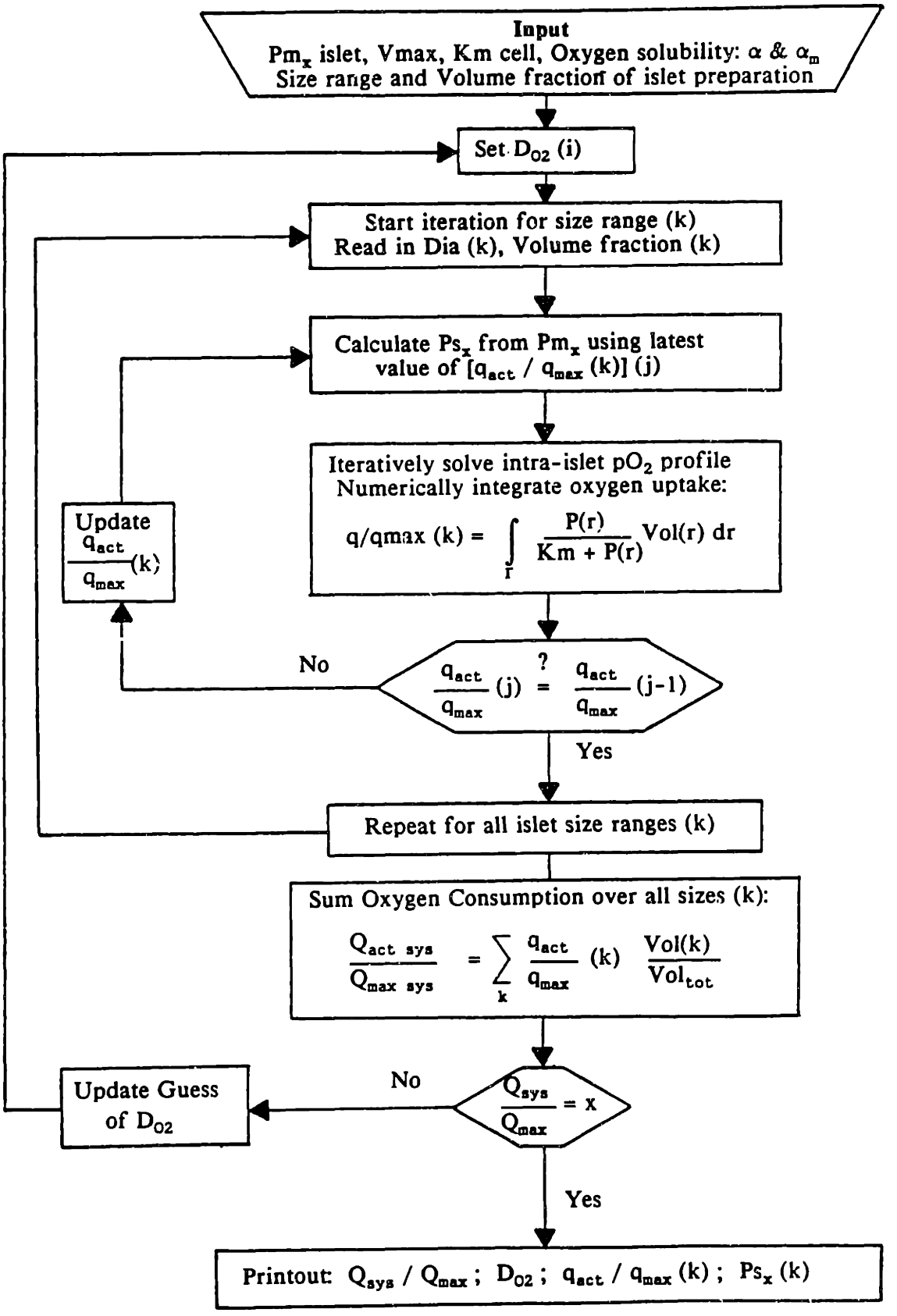

FIGURE 3. FLOWCHART OF NUMERICAL MODEL TO EXTRACT D_{O2} FROM COUPLED SPHEROIDS

CHAPTER 8:

MATHEMATICAL MODELING OF O_2 PROFILES, O_2 CONSUMPTION, AND INSULIN SECRETION IN ISOLATED ISLETS OF LANGERHANS

INTRODUCTION

In previous chapters, it has been demonstrated that both tissue oxygen consumption and insulin secretion are functions of the oxygen concentration or partial pressure in the surrounding medium. Insulin secretion from intact, one-day old rat islets of Langerhans averaging 210 μm in diameter begins to be affected at about 60 mm Hg and reaches one-half of maximum at 27 mm Hg oxygen in the perfusate (Dionne et al., 1989-3). Oxygen consumption from a slurry of intact islets ranging from 70 to 300 μm in diameter and averaging 214 μm was first noticeably affected below about 50 mm Hg oxygen and was reduced to one-half of maximum at about 11 mm Hg (Dionne et al., 1989-6). That much of the reason that intact islets display such a high sensitivity to reduced medium pO_2 levels is due to diffusion gradients both in and around the islets was established by measuring the insulin secretion and oxygen uptake of small reaggregated clusters of islets cells. These aggregates which should provide an upper bound to the intrinsic properties of single β-cells had a P_{50} of 5.0 mm Hg and about 1.1 mm Hg for insulin secretion and oxygen uptake, respectively (Dionne et al., 1989-4 and 1989-6).

With the measurement of tissue oxygen uptake parameters (Dionne et al., 1989-6) and the calculation a value of the intra-tissue oxygen diffusivity (Dionne et al., 1989-7) it is now possible to model oxygen levels in the interior of isolated islets. We have therefore developed a mathematical model to predict intra-islet pO_2 levels and their effect on local intra-islet oxygen consumption and insulin secretion. This model not only provides further information on the oxygen requirements of insulin secretion but also allows the prediction of insulin secretion as a function of the local oxygen tension.

Initially, a model of oxygen diffusion and reaction in a spherical islet is developed which can predict intra-islet pO_2 profiles and oxygen consumption as a function of islet size, metabolic stimulus, and exterior medium pO_2. This model is then extend to include islet insulin secretion as a function of local pO_2 throughout the islet and is used to extract the local oxygen dependence of β-cells in intact islets based on experimental data on the effect of reduced perfusate pO_2 on insulin secretion from intact islets (Dionne et al., 1989-3). The predicted secretion kinetics are compared to experimental secretion data. The resulting model is capable of predicting both oxygen-limited oxygen uptake and insulin secretion from isolated, whole islets of Langerhans.

PO_2 PROFILES AND O_2 CONSUMPTION IN ISOLATED ISLET SPHEROIDS

Mathematical Model Development

The oxygen consumption of a perifused, isolated, spherical islet is described by the equation of continuity written in spherical coordinates for the diffusion and reaction of oxygen in an oxygen consuming spheroid (Bird, Stewart, and Lightfoot, 1960). The islet is assumed to be at steady state, suspended in a flowing stream of perfusate which is assumed to be described by laminar flow. Oxygen transport within the tissue is by radial diffusion only with no convection. The tissue oxygen diffusivity, D_{O2I}, and the tissue density, ρ, are assumed to be constant throughout the spheroid. Finally, oxygen consumption is assumed to be homogeneous throughout the islet and is described by Michaelis-Menten uptake kinetics. A schematic of these conditions is shown in Figure 1. Included in this Figure is the characteristic diffusion/reaction equation derived from the equation of continuity under the assumptions listed above and the appropriate boundary conditions. Symbols are defined at the bottom of the Figure.

The first boundary condition, $dP(0)/dr = 0$, at $r=0$, is derived from the symmetry requirement of zero flux at the islet core. The second boundary condition is derived for oxygen diffusion through a liquid boundary layer surrounding the respiring islet. The magnitude of the ΔpO_2 drop through the boundary layer is calculated using a Sherwood

number mass transfer analogy to estimate the mass transfer coefficient, kc, of oxygen across the stagnant layer of medium composing the boundary layer. Levich (Levich, 1962) derived the following relationship for the mass transfer coefficient across a stagnant layer surrounding a spheroid under the experimental conditions of low Reynolds (Re) number and moderate to high Peclet (Pe) number. (For the conditions under which oxygen uptake and insulin secretion were experimentally measured: $2 \leq Re \leq 10$; $600 \leq Pe \leq 3000$) (Dionne et al., 1989-3 and 1989-6):

$$Sh\ \# = \frac{2Rkc}{D_{O2m}} = .997\ Pe^{1/3} \approx \left[\frac{2\ R\ v_l}{D_{O2m}}\right]^{1/3} \qquad (1)$$

Which can be rewritten as:

$$kc \approx \frac{D_{O2m}}{2\ R}\left[\frac{2\ R\ v_l}{D_{O2m}}\right]^{1/3} \qquad (2)$$

Where "kc" is the mass transfer coefficient across the boundary layer, D_{O2m} is the oxygen diffusivity in the media, v_l is the averaged perfusate or medium velocity relative to the islet surface and, all other symbols are as defined in Figure 1. The flux of oxygen to the islet is defined such that:

$$\text{Flux of oxygen:} \quad N = kc\ \alpha_m\ (Pm - Ps) \qquad (3)$$

At steady state, the flux into the spheroid multiplied by the area around the spheroid must equal the consumption within the spheroid:

$$N = Q_{islet}\frac{Vol}{Area} = Q_{islet}\frac{4/3\ \pi\ R^3}{4\ \pi\ R^2} = Q_{islet}\frac{R}{3} \qquad (4)$$

Substituting "N" from Equation 4 into Equation 3, solving for Ps, and replacing the mass transfer coefficient, kc, with the appropriate expression from Equation 2 yields the boundary condition at the spheroid / medium interface, r=R:

$$P(R) = Ps = Pm - \frac{Q_{islet}\ (2\ R)^{5/3}}{12\ \alpha_m\ D_{O2m}^{2/3}\ v_l^{1/3}} \qquad (5)$$

The pO_2 drop across the boundary layer increases with increasing consumption and islet radius and decreases with increasing medium oxygen diffusivity and relative velocity.

The characteristic reaction/diffusion equation in a spheroid (shown in Figure 1) must be solved numerically because of the non-linear Michaelis-Menten oxygen uptake kinetics. The equations were discretized using centered finite differences to approximate the first and second order derivatives. The Equations were solved using Euler's finite difference technique and L/U decomposition to solve the tridiagonal Jacobian matrix (See Finlayson, 1980). The program was written in advanced Basic and run on an IBM PC AT.

Extraction of a Value of Km_I for Insulin Secretion

It was hypothesized that the effect of oxygen on intrinsic insulin secretion of β-cells located within intact islets of Langerhans could be represented by a Michaelis-Menten type secretion expression,

$$S(r) = \frac{Smax\ P(r)}{Km_I + P(r)} \qquad (6)$$

where S(r) and P(r) are, respectively, the local insulin secretion rate and local pO_2 at radial position, r. Smax is the maximum oxygenated insulin secretion rate and Km_I is a pseudo-Michaelis-Menten constant for insulin secretion.

The internal oxygen profile, P(r), of perifused islets was calculated as described above for bulk perfusate pO_2 levels for which experimental S_x/S_{142} was available (Dionne et al., 1989-3). P(r) was calculated at the same conditions for which the islets were experimentally perifused using the experimentally measured oxygen uptake and transport parameters. Using the resulting intra-tissue pO_2 profile and an initial guess of Km_I in the kinetic expression of Equation 2, the insulin secretion was integrated throughout the islet β-cell core. The β-cell core was assumed to extend from r = 0 to r = β, where $\beta = 0.75^{1/3}$ based on the report that 75% of the islet volume is composed of β-cells which are primarily located in islet core (Colella et al., 1985). The predicted insulin secretion rate in terms of S_x/Smax was compared to the experimental S_x/S_{142} data at x equal to the nine bulk perfusate pO_2 levels experimentally tested. Km_I was iterated to find the closest fit to the nine experimentally measured values of S_x/S_{142} fractions by the method of least squares.

Experimental Parameters

The mathematical diffusion/reaction model requires input of tissue oxygen uptake and transport parameters including: Vmax, the maximum O_2 consumption rate; Km, the pO_2 at which mitochondrial oxygen consumption is reduced to one-half of normal; D_{O2I}, the intra-islet oxygen diffusivity; α_I, the solubility of oxygen in the islet tissue; and R, the islet radius. Required input of liquid medium parameters include: D_{O2m}, the oxygen diffusivity in medium; α_m, the medium oxygen solubility; and v_1, the average medium velocity relative to the islet surface. The value of each of these parameters along with its source is listed in Table 1.

Oxygen uptake, including Vmax, of intact islets and small cell aggregates were measured in an oxygen uptake chamber under glucose stimulated (300 mg/dl glucose) and basal (50 mg/dl glucose) conditions (Dionne et al., 1989-6). The Km (P_{50}) of isolated, state 5 mitochondria was measured in the same system (Wilson et al., 1988). The intra-tissue oxygen diffusivity was extracted from the oxygen uptake curves of intact islets and small cell aggregates (Dionne et al., 1989-7). The intra-islet oxygen solubility was taken as the average of the oxygen solubility in several tissues (Evans et al, 1981; see Dionne et al., 1989-7). The islet diameter and the relative fluid velocity with respect to the islet surface were chosen so as to coincide with values measured in experimental perifusion studies of the effect of various perfusate pO_2 levels on islet insulin secretion (Dionne et al., 1989-3). The values of the medium oxygen solubility and oxygen diffusivity at 37°C are well established in the literature and their selection is discussed elsewhere (Dionne et al., 1989-7).

RESULTS

Results of the modeled pO_2 profiles in spherical islets are shown in Figures 2-4. In Figure 2, the tissue pO_2 is plotted verses the islet radius for a range of bulk medium pO_2 levels from 5 to 142 mmHg. For a glucose stimulated, 210 μm diameter, non-oxygen limited islet, the pO_2 drop from the bulk perfusate to the islet surface was calculated to be 8.0 mm

Hg at a superficial perfusate velocity of 0.75 cm/sec. As can be seen from Equation 5, the ΔpO_2 from the bulk medium to the islet surface is directly proportional to the O_2 uptake rate of the islet. Thus the ΔpO_2 drop in the liquid phase can be calculated for each curve of Figure 2 by multiplying 8.0 mm Hg by the fraction of normoxic oxygen uptake, Qx, shown in the Figure for each pO_2 profile. As can be seen from Figure 2, the pO_2 steadily decreases from a high at the islet surface, $P(r) = Ps = Pm - \Delta pO_2$, to a low at the islet core, $P(r) = 0$. The model predicts that under the conditions represented by the simulations, the pO_2 at the islet core will become hypoxic when the bulk medium pO_2 level drops below about 40 mm Hg. As the pO_2 in the bulk medium is further decreased, the hypoxic region at the islet core expands outward radially and the overall fraction of islet oxygen uptake progressively decreases. Under the conditions represented by this set of simulations, the overall islet oxygen respiration is reduced to one-half of normal, P_{50} at a bulk medium pO_2 of about 10.5 mm Hg. This corresponds closely with a mean value of P_{50} equal to 10.7 ± 3.1 mm Hg measured in a stirred tank system with an ensemble of islets averaging 214 μm in diameter with fluid dynamics which resulted in a similar ΔpO_2 drop across the boundary layer (Dionne et al., 1989-6 and 1989-7).

Figure 3 illustrates the effect of the islet size on the oxygen penetration into the islet and on the overall islet oxygen uptake. The tissue pO_2 profile is plotted verses the islet radius for 50 - 300 μm diameter islets. Under glucose stimulated respiration, at a medium pO_2 of 45 mm Hg and a medium superficial velocity of 0.75 cm/sec, islets smaller than about 200 μm in diameter are oxygenated ($pO_2 \geq$ 2 mm Hg) throughout their volume whereas islets larger than 200 μm diameter become progressively more hypoxic in the core region and suffer form reduced overall oxygen uptake. The ΔpO_2 drop across the boundary layer also increases with increasing islet diameter going from less than one mm Hg for fully consuming 50 μm diameter islets to 11.5 mm Hg for 300 μm diameter islets consuming oxygen at 77% of their maximum rate which corresponds to a 15 mm Hg drop under non-oxygen limited consumption.

Figure 4 illustrates the effect of the islet respiration rate on the tissue pO_2 profile. Two hundred and ten micron diameter islets respiring under basal (50 mg/dl glucose) stimulation in bulk media at 30 mm Hg O_2, are oxygenated throughout their volume with a Q/Qm ratio of 0.95 . Glucose stimulation (300 mg/dl) increases islet respiration rate over the basal uptake rate and results in a steeper oxygen profile, a hypoxic core, and a decrease in overall oxygen uptake to Q/Qm = 0.89 .

Figure 5 is a plot of the normalized local oxygen uptake rate, V(r)/Vmax, throughout a 210 μm diameter, glucose-stimulated islet exposed to a range of bulk medium pO_2 levels from 5 to 142 mm Hg. Assuming that local, intrinsic oxygen uptake can be represented by Michaelis-Menten uptake kinetics, with a Mitochondrial Km equal to 0.44 mm Hg, the local Q(r) remains elevated as long as the local pO_2, P(r), remains high relative to Km = 0.44 mm Hg. However, V(r)/Vmax drops rapidly as the tissue pO_2 passes through the region of Km, and then flattens out at a very low level to form the sigmoidal curves shown in Figure 5. The result of these kinetics is that V(r) forms a front with increasing penetration as the bulk medium pO_2 is raised. Plotted as a dashed line in Figure 5 is the fraction of the islet volume that lies interior to the radial position, r. Because of the cubed dependence of volume on radius, the interior volume fraction drops very rapidly with penetration into the islet. The relationship between Vol(r)/Vol and P(r) illustrates why the Q/Qm ratios shown in Figures 2 and 3 seem to be relatively insensitive to apparently large (as determined by the fraction of the overall diameter) regions of hypoxia in the core. For example, at a bulk medium pO_2 = 25 mm Hg, the inner 45 μm of a 105 μm radius islet (about 43% of the diameter) are predicted to be hypoxic. However, this region only accounts for 7.9% of the islet volume therefore, despite the hypoxic core, the overall oxygen uptake of the islet is predicted to be 83% of its maximum level.

Figure 6 illustrates the remarkably close fit of oxygen uptake predicted by the theoretical model to oxygen uptake data measured in a stirred tank under fluid dynamic conditions where the liquid boundary layers were similar. The modeled predictions are for the steady state consumption of 210 μm diameter, glucose-stimulated islets based on the

parameters described in Table 1. The experimental data was measured as the dynamic oxygen uptake of an ensemble of islets averaging 214 μm in diameter in a closed, stirred oxygen uptake chamber. The experimental uptake curve is one of several curves used in extracting the intra-islet oxygen diffusivity (Dionne et al., 1989-7).

Hypoxia-limited insulin secretion was theoretically modelled using the pO_2 profiles run at experimentally tested perfusate pO_2 levels and the intrinsic kinetic expression of Equation 6. The value of Km_I which best fit the data as ascertained by the method of least squares was 4.2 mm Hg. This value agrees well with the upper limit of the intrinsic Km_I measured with small cell aggregates (5.0 mm Hg; Dionne et al., 1989-4). A comparison of the predicted insulin secretion to the experimentally measured reductions in secretion with hypoxic pO_2 (Figure 7) indicates that the model not only correctly predicts the value of S_x/Smax to within ± 10% of the experimental values but also reproduces the sigmoidal nature of the experimental S_x/S_{142} curve.

DISCUSSION

The tissue parameters used in the diffusion / reaction model were all specifically measured for rat islets with the exception of the tissue oxygen solubility, α_I, which was taken as the average in mammalian tissues and the Km for mitochondrial oxygen uptake which was measured with mitochondria isolated from hepatocytes. The Km is bounded on the upper side by the P_{50} of 1.05 mm Hg measured in rat cell aggregates and on the lower side by zero mm Hg - or zero order uptake kinetics. A Km of zero would replace the sigmoidal V(r) curves of Figure 5 with a vertical penetration front and would slightly increase the slope of the oxygen profile curves of Figures 2-4, however the overall Q/Qm ratios would be only moderately affected. An increase in the Km to 1.05 mm Hg would increase the sigmoidal V(r) curves of Figure 5 and would tend to flatten out the oxygen profiles of Figures 2-4.

One good indication of the applicability of the oxygen reaction/diffusion model is its ability to predict the effect of reduced bulk medium pO_2 on islet oxygen consumption as seen in Figure 6 throughout the range of Q/Qm from 0 to 0.99 . The experimental P_{50} of intact

islets averaging 214 μm in diameter was reported to be 10.7 ± 3.1 mm Hg for a series of seven oxygen uptake runs (Dionne et al., 1989-6). The P_{50} of 210 μm diameter islets predicted by the diffusion / reaction model with the parameters as reported is about 10.5 mm Hg. Although the fluid dynamics of the two systems are different (stirred tank verses perifused flow), the predicted fluid resistance to oxygen transport was similar in both cases (Dionne et al., 1989-7). Other differences which may have been expected to influence the comparison include the fact that the model assumes a steady state profile whereas the experimental data was collected from a dynamic system, and that the experimental data was collected from an ensemble of islets averaging 214 μm diameter whereas the model was for a single sized islet of 210 μm diameter. Either these differences are not important or else the model is insensitive to them.

Using the oxygen dependent insulin secretion model with a value of Km_I equal to 4.2 mm Hg, we can model oxygen-limited insulin from perifused rat islets to within plus or minus ten percent. The estimate of Km_I is bounded on the upper side by measurements of small islet cell aggregates which produced a value of $S_x/S_{142} = 0.5$ at $x = 5.0$ mm Hg (Dionne et al., 1989-4). The close fit of the modelled insulin secretion to experimental data both in terms of islet cell aggregates and to fitting both qualitatively and quantitatively the secretion from intact islets suggests that the simple Michaelis-Menten secretion expression for the dependence of insulin secretion on local pO_2 may be adequate to use for predicting insulin secretion as a function of tissue pO_2. Preliminary models incorporating the pO_2 drop through membrane encapsulated islets await experimental verification to see if the model can be extended to immuno-isolation devices. If so, then this approach provides a powerful tool for designing and developing immuno-isolation systems that avoid hypoxia-limited insulin secretion regimes.

REFERENCES

Altman, P.L. and Dittmer, D.S. (eds) (1971) Respiration and Circulation. Fed Am Soc Exp Biol Bethesda Md; p. 16.

Brian, P.L.T, and Hales H.B. (1969) Effects of Transpiration and Changing Diameter on Heat and Mass Transfer to Spheres. AIChE J 15: 419-425.

Brian, P.L.T, Hales, H.B, and Sherwood, T.K. (1969) Transport of Heat and Mass Between Liquids and Spherical Particles in an Agitated Tank. AIChE J 15: 727-733.

Chen, J, Tannahill, A.L, and Shuler, M.L. (1985) Design of a System of the Control of Low Dissolved Oxygen Concentrations. Biotech & Bioengr 27: 151-155.

Clark, A, Clark, P.A.A, Connett, R.J, Gayeski, T.E.J, and Honig, C.R. (1987) How Large is the drop in pO_2 between Cytosol and Mitochondrion? Am J Physiol 252 (Cell Physiol. 21): C583-C587.

Colella, R.M, Bonner-Weir, S, Braunstein, L.P, Schwalke, M, and Weir, G.C. (1985) Pancreatic islets of variable size-insulin secretion and glucose utilization. Life Sci 37:1059-1065.

Dionne, K.E, Colton, C.K, and Yarmush, M.L. (1989-3) Effect of hypoxia on insulin secretion by isolated rat and canine islets of Langerhans. (Ph.D.Thesis; Chapter 3).

Dionne, K.E, Colton, C.K, and Yarmush, M.L. (1989-4) Effect of hypoxia on insulin secretion from rat and canine islet cell aggregates. (Ph.D. Thesis; Chapter 4).

Dionne, K.E, Colton, C.K, and Yarmush, M.L. (1989-8). Mathematical modeling of O_2 profiles, O_2 consumption, and insulin secretion in isolated and immuno-isolated islets of Langerhans. (Ph.D. Thesis; Chapter 8).

Evans, N.T.S, Naylor, P.F.D, and Quinton, T.H. (1981) The Diffusion Coefficient of Oxygen in Respiring Kidney and Tumour Tissue. Respiration Physiology 43: 179-188.

Karel, S.F, Libicki, S.B, and Robertson, C.R. (1985) The Immobilization of Whole Cells: Engineering Principles. Chem Engr Sci 40: 1321-54.

Levich, V.G. (1962) Physiocochemical Hydrodynamics. Prentice-Hall, Englewood Cliffs, NJ.

McLimans, W, Blumenson, L, and Tunnah, K. (1968) Kinetics of Gas Diffusion in Mammalian Cell Culture Systems II. Theory. Biotech & Bioengr X: 741-763.

Mueller, J.A, Boyle, W.C, and Lightfoot, E.N. (1968) Oxygen Diffusion Through Zooglocal Flocs. Biotech & Bioeng 10: 331-358.

Mueller-Klieser, W.F. (1984) Method for the Determination of Oxgyen Consumption Rates and Diffusion Coefficients in Multicelluar Spheroids. Biophys J 46: 343-348.

Mueller-Klieser, W.F, and Sutherland, R.M. (1984) Oxygen Consumption and Oxygen Diffusion properties of Multicellular Spheroids from Two Different Cell Lines. Adv in Exp Medicine and Biology 180; Oxygen Transport to Tissue VI; Proceedings of the International Society of Oxgyen Transport to Tissue held Aug 16-20, 1983, in Ruston, Louisiana; pp311-321.

Panten, U. and Klein, H. (1982) Oxygen Consumption by Isolated Pancreatic Islets, as Measured in a Microincubation System with a Clark-Type Electrode. Endocrinology 111: 1595-1600.

Tai, R.C, and Chang, H-K. (1974) Oxygen Transport in Heterogeneous Tissue. J Theor Biol 43: 265-276.

Wilson, D.F., Rumsey, W.L., Green, T.J. and Vanderkooi, J.M. (1988) The Oxygen Dependence of Mitochondrial Oxidative Phosphorylation Measured by a New Optical Method for Measuring Oxygen Concentration. J Biological Chemistry 263: 2712-2718.

TABLE 1. Experimental Parameters For Modeling the Oxygen Profile in Intact, Spherical Islets of Langerhans

Tissue Parameters (37°C)	
Vmax of Intact Islets[τ1]	
Stimulated (300 mg/dl glucose)	3.14×10^{-8} mol/cm^3-sec
Basal (est) (50 mg/dl glucose)	$2.3\text{-}2.7 \times 10^{-8}$ mol/cm^3-sec
P_{50} of Islets, cell aggregates, and isolated mitochondria	
Intact Islets (214 ± 55 μm dia)[τ1]	10.7 ± 3.1 mm Hg
Cell aggregates (38.9 ± 8.5 μm dia; rat)[τ1]	1.05 ± .17 mm Hg
Isolated Mitochondria (state 5; rat)[τ2]	0.44 mm Hg
Diffusivity of Oxygen in Islets[τ3]	1.53×10^{-5} cm^2 / sec
Solubility of Oxygen in tissue[τ4]	1.02×10^{-9} mole / cm^3 - torr
Islet Radius[τ5]	
Average of Experimental Perifusions	105 μm
Range of Isolated Islet radii	25 - 250 μm
Medium Parameters (37°C)	
Fluid velocity relative to perifused islets[m1]	0.75 cm / sec
Diffusivity of Oxygen in medium[m2]	2.78×10^{-5} cm^2 / sec
Solubility of Oxygen in medium[m3]	1.27×10^{-9} mole / cm^3 - torr

[τ1] Experimentally measured in Oxygen uptake chamber (Dionne et al., 1989-6)

[τ2] Mitochondria isolated from rat hepatocytes; state 5 conditions (Wilson et al., 1988)

[τ3] Calculated from Vmax and P_{50} data for rat islets and cells (Dionne et al., 1989-7)

[τ4] Averaged from: 1.11×10^{-9}, frog sartorius muscle (Mahler, 1978); 1.20×10^{-9}, D.S. Carcinosarcoma cells (Grossman, 1984; data of Grote et al, 1977); 0.915×10^{-9}, EMT6 spheroids, 87.2 % H_2O, (Mueller-Klieser 1984 & 1985); 0.866×10^{-9}, EMT6 spheroids, 85.5 % H_2O, (Mueller-Klieser 1984 & 1985).

[τ5] Microscopically measured radius of 24hr post isolation rat islets handpicked for perifusion studies (Dionne et al., 1989-3)

[m1] Superficial velocity of perifusion media with respect to islet surface (Dionne et al., 1989-3)

[m2] Literature values: 2.86×10^{-5}, H_2O corrected to 37°C (Goldstick and Fatt, 1970); 2.98×10^{-5}, H_2O corrected to 37°C (Stroeve et al, 1971); 3.53×10^{-5}, H_2O corrected to 37°C (Grossman, 1984; data of Grote, 1967); 2.72×10^{-5}, H_2O corrected to 37°C (Treybal, 1980); 2.51 - 3.28×10^{-5}, Reported range in literature for H_2O corrected to 37°C (Goldstic and Fatt, 1970; reported in Stroeve et al, 1976); 2.78×10^{-5}, isotonic saline corrected to 37°C (Goldstick and Fatt, 1970); 2.96×10^{-5}, isotonic saline corrected to 37°C (Stroeve et al, 1976)

[m3] Averaged from: 1.33×10^{-9}, Balanced Salt Sol. (Chen et al, 1985); 1.22×10^{-9}, BSS (Panten and Klein, 1982); 1.32×10^{-9}, Burks media (Chen et al, 1985); 1.29×10^{-9}, Ringer's Sol (McLimans et al, 1968); 1.24×10^{-9}, plasma (Colton and Drake, 1971); 1.24×10^{-9}, isotonic saline (Altman and Dittmer, 1971).

FIGURE 1. MATHEMATICAL DIFFUSION/REACTION MODEL FOR CALCULATING OXYGEN PROFILES IN SPHERICAL ISLETS

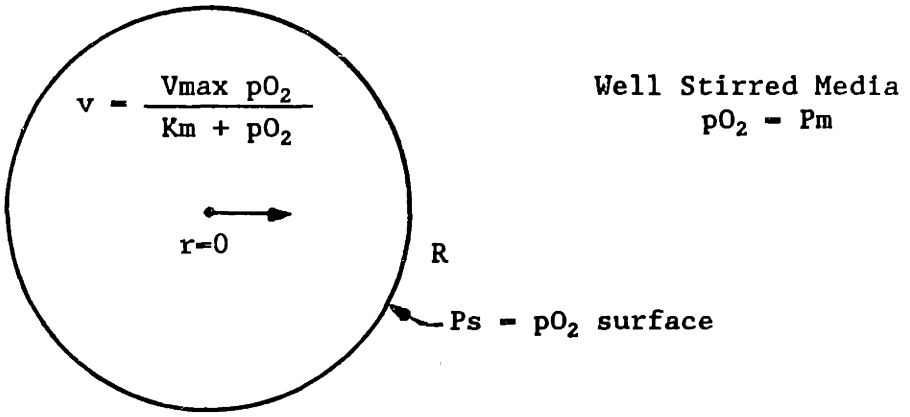

Characteristic Equation

Assumptions: Steady state spheroid, no convection, radial diffusion, Constant tissue diffusivity (D_{O2}) and density (ρ), homogeneous O_2 consumption described by Michaelis-Menten kinetics.

$$D_{O2}\,\alpha\left[\frac{d^2P(r)}{d\,r^2}+\frac{2}{r}\,\frac{dP(r)}{dr}\right]=\frac{Vmax\;\;P(r)}{Km\;+\;P(r)}$$

$$\text{BC \#1:}\quad r=0,\qquad \frac{dP(0)}{dr}=0$$

$$\text{BC \#2:}\quad r=R,\quad P(R)=Ps=Pm-\frac{q_{act}\;R}{3\;kc\;\alpha_m}$$

List of Symbols

D_{O2}	Tissue oxygen diffusivity (cm^2/sec)
kc	O_2 Mass transfer coefficient in liquid boundary layer (cm/sec)
Km	M-M coefficient for mitochondrial O_2 uptake (mm Hg)
P(r)	Partial Pressure of Oxygen at radial position r, (mm Hg)
Pm	Partial Pressure of Oxygen in bulk media (mm Hg)
Ps	Partial Pressure of Oxygen at islet surface (mm Hg)
q_{act}	Actual overall O_2 uptake of tissue particle (moles/cm^3-sec)
r	Radial position within tissue (μm)
R	Outer radius of tissue spheroid (μm)
v	local O_2 uptake of tissue (moles/cm^3-sec)
Vmax	Maximum intrinsic O_2 uptake rate (moles/cm^3-sec)
α	Tissue oxgyen solubility (mole/cm^3-mm Hg)
α_m	Liquid medium oxygen solubility (mole/cm^3-mm Hg)

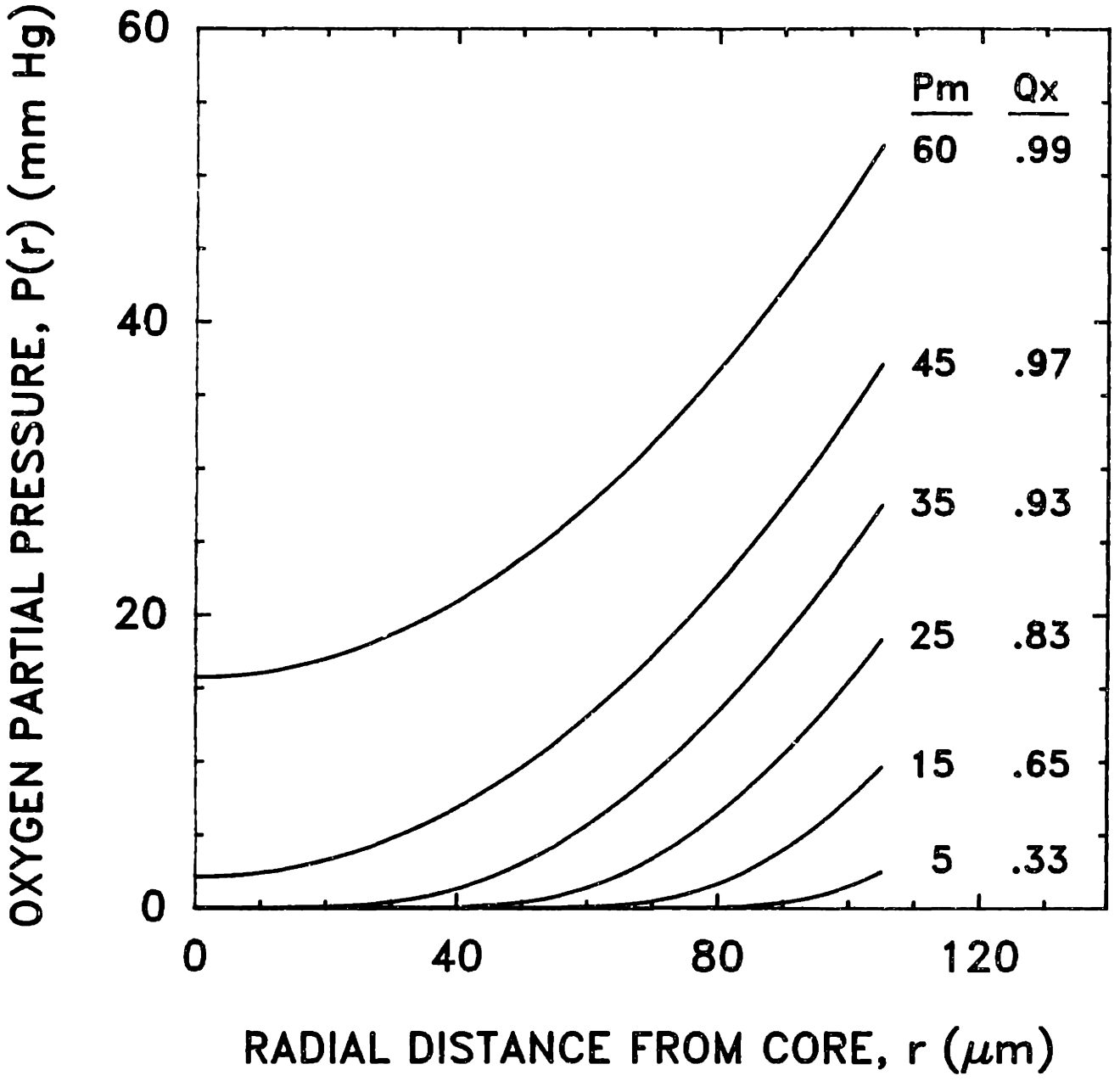

FIGURE 2. Modeled intra-islet pO_2 profiles as a function of bulk medium pO_2, Pm. Profiles were modeled as described in the text. Pm is the bulk medium pO_2 at which each simulation was run. Qx is the fraction of maximum oxygen uptake of the islet calculated by integrating the oxygen consumption throughout the islet. Islet diameter was 210 μm. Other parameters are as described in Table 1 for glucose stimulated conditions.

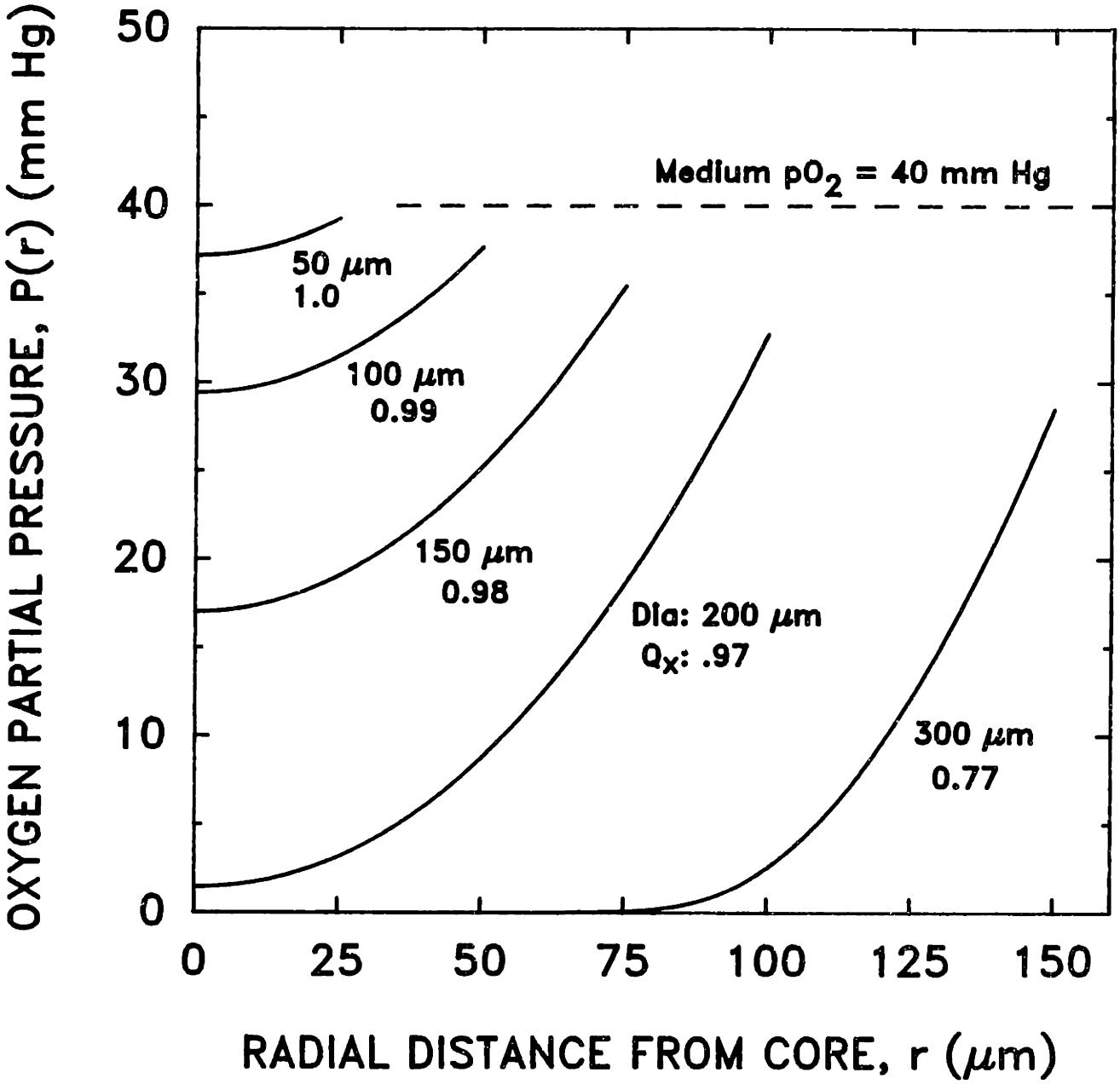

FIGURE 3. Modeled intra-islet pO_2 profiles as a function of islet diameter. Simulation is run at a bulk medium pO_2 of 40 mm Hg for 50, 100, 150, 200, and 300 μm diameter, glucose-stimulated islets. Qx is the calculated fraction of maximum oxygen consumption.

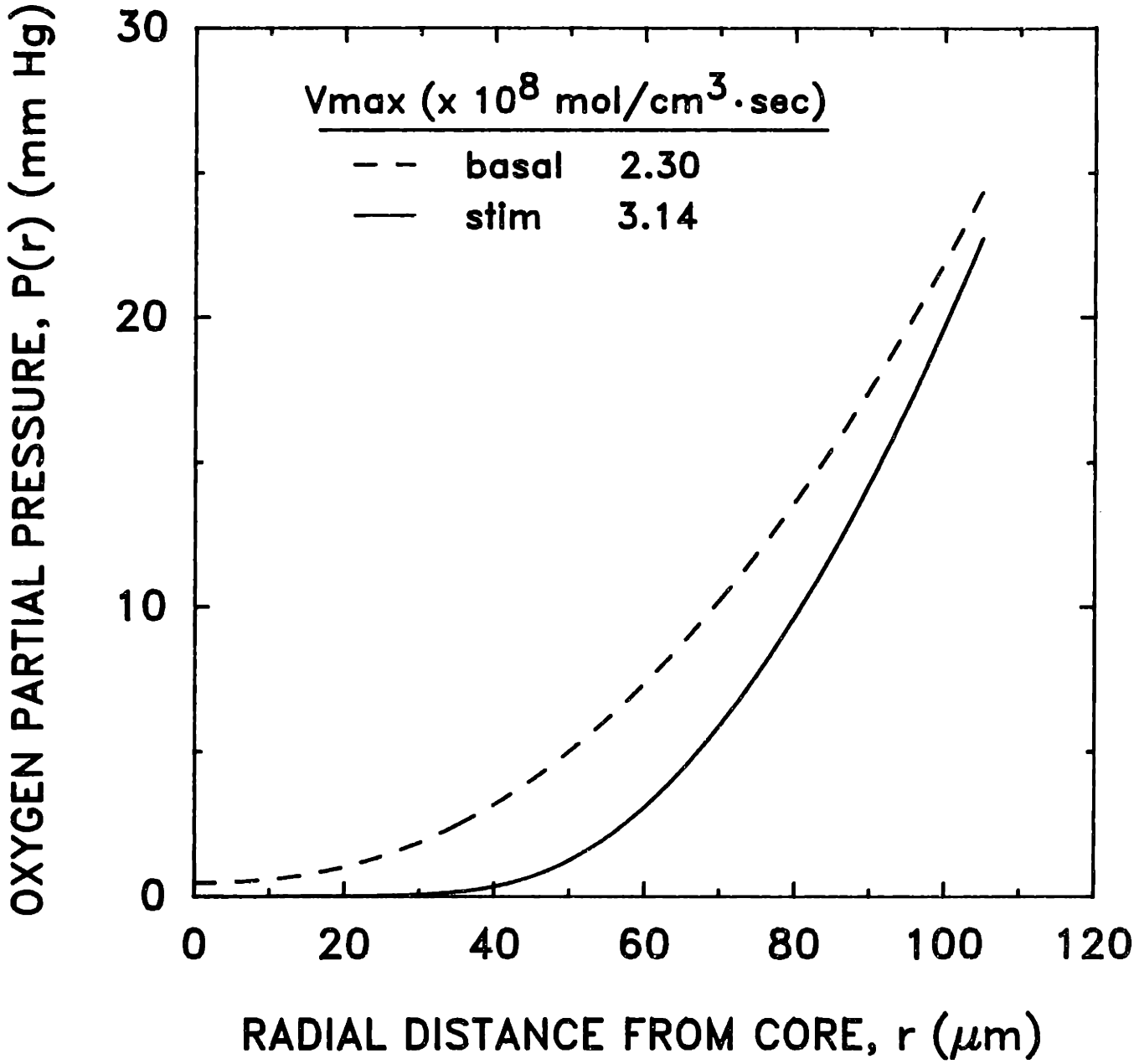

FIGURE 4. Modeled intra-islet pO_2 profiles as a function of glucose-stimulated oxygen uptake rate, Vmax. Stimulated oxygen uptake was measured at 300 mg/dl; basal uptake was estimated at 50 mg/dl (See Table 1).

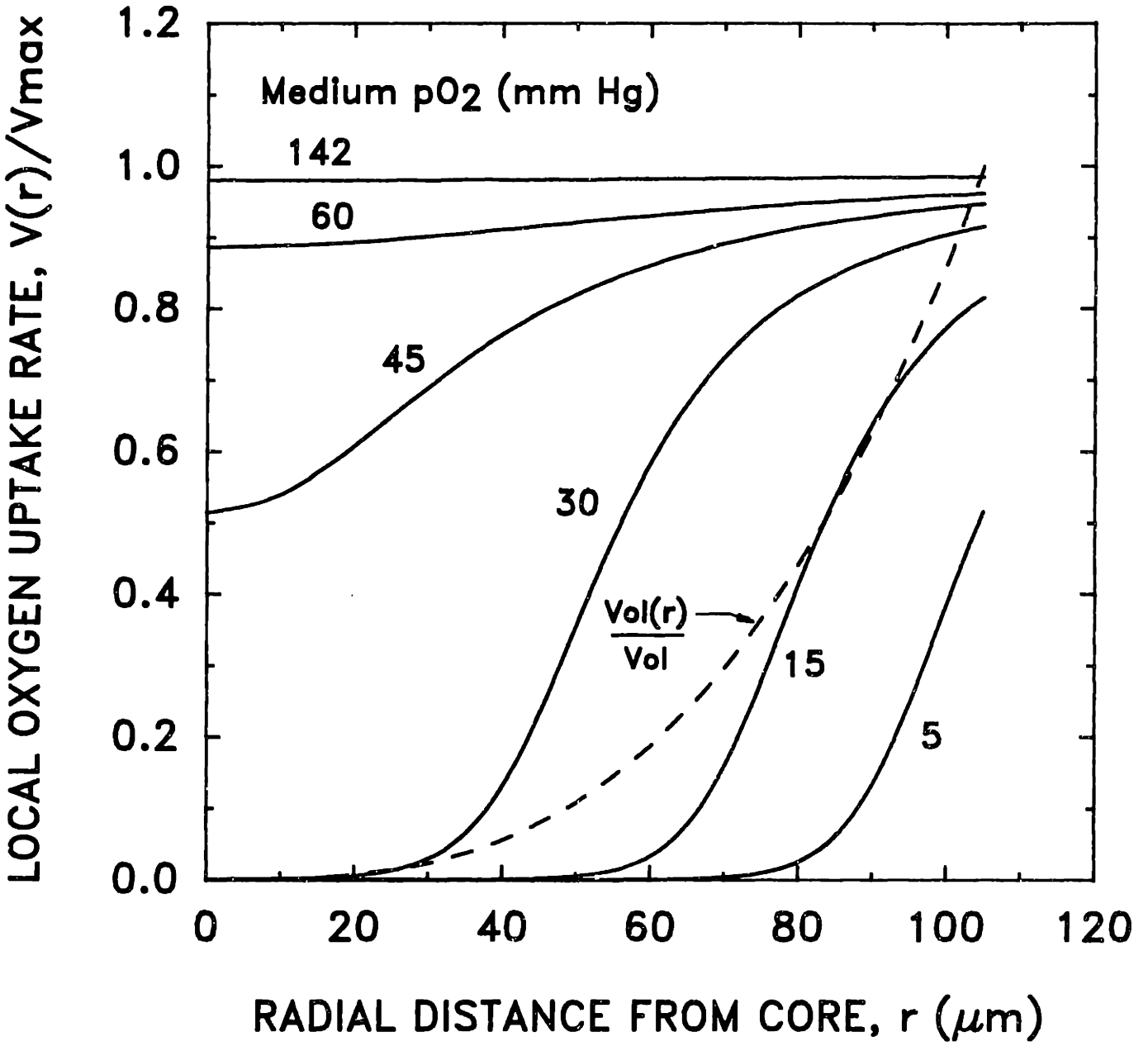

FIGURE 5. Local tissue oxygen uptake rate, V(r), as a function of radial position and bulk medium pO_2. V(r) is the calculated oxygen uptake rate based on the local tissue pO_2, P(r), and the Km for mitochondrial oxygen consumption (0.44 mm Hg). Medium pO_2 is the bulk medium pO_2 of each simulation. Islet diameter is 210 μm. All other parameters are as given in Table 1 for glucose stimulated uptake. The dashed line represents the fraction of the total volume interior to the radial position, r, and can be read directly off of the y axis.

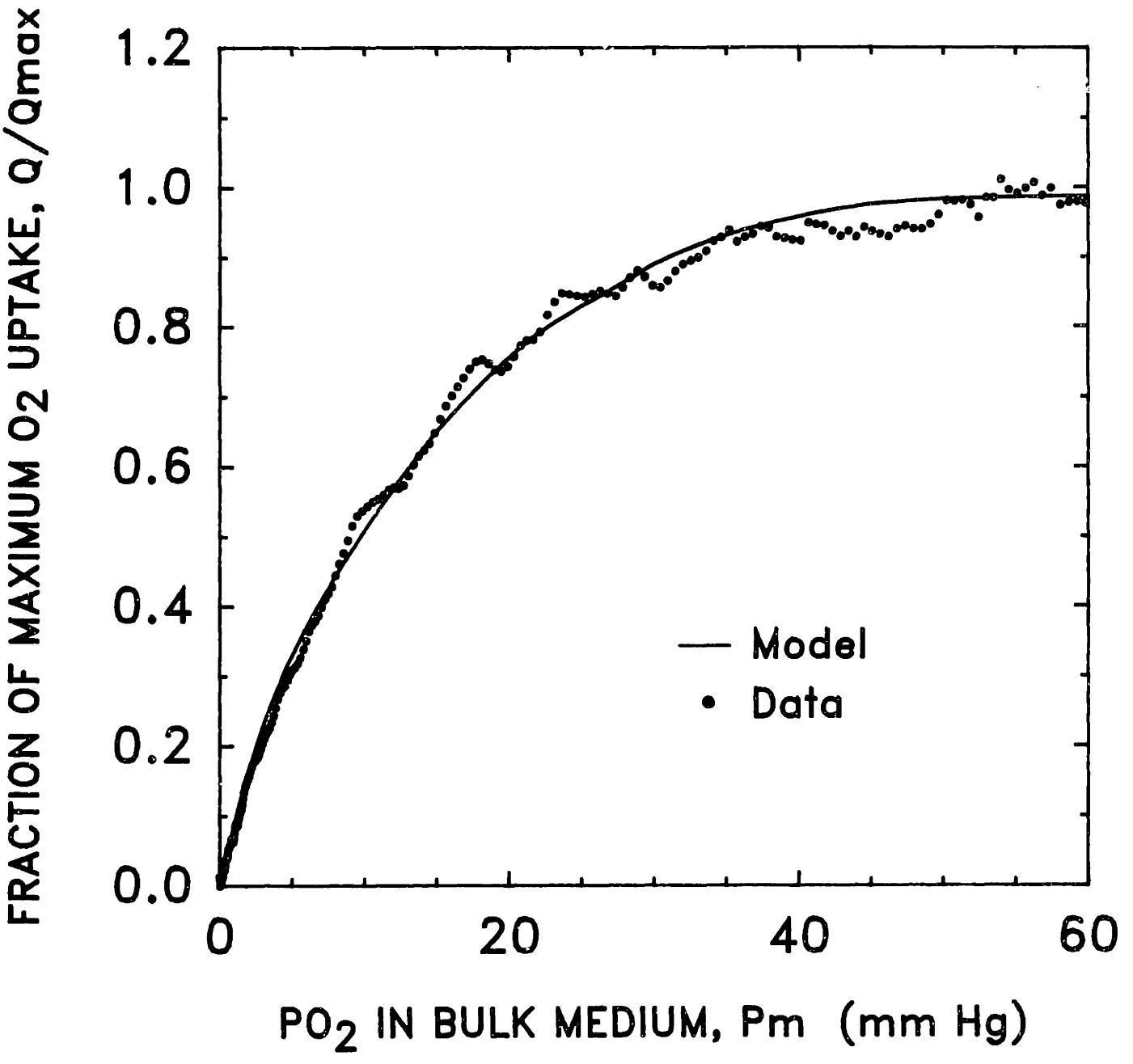

FIGURE 6. Comparison of oxygen uptake predicted by the theoretical model to experimental uptake data. Model predictions are for 210 μm diameter islets under 300 mg/dl glucose stimulated, perifused conditions. Experimental data was measured in a stirred tank oxygen uptake system for an ensemble of 300 mg/dl glucose-stimulated rat islets averaging 214 μm in diameter (Dionne et al., 1989-6).

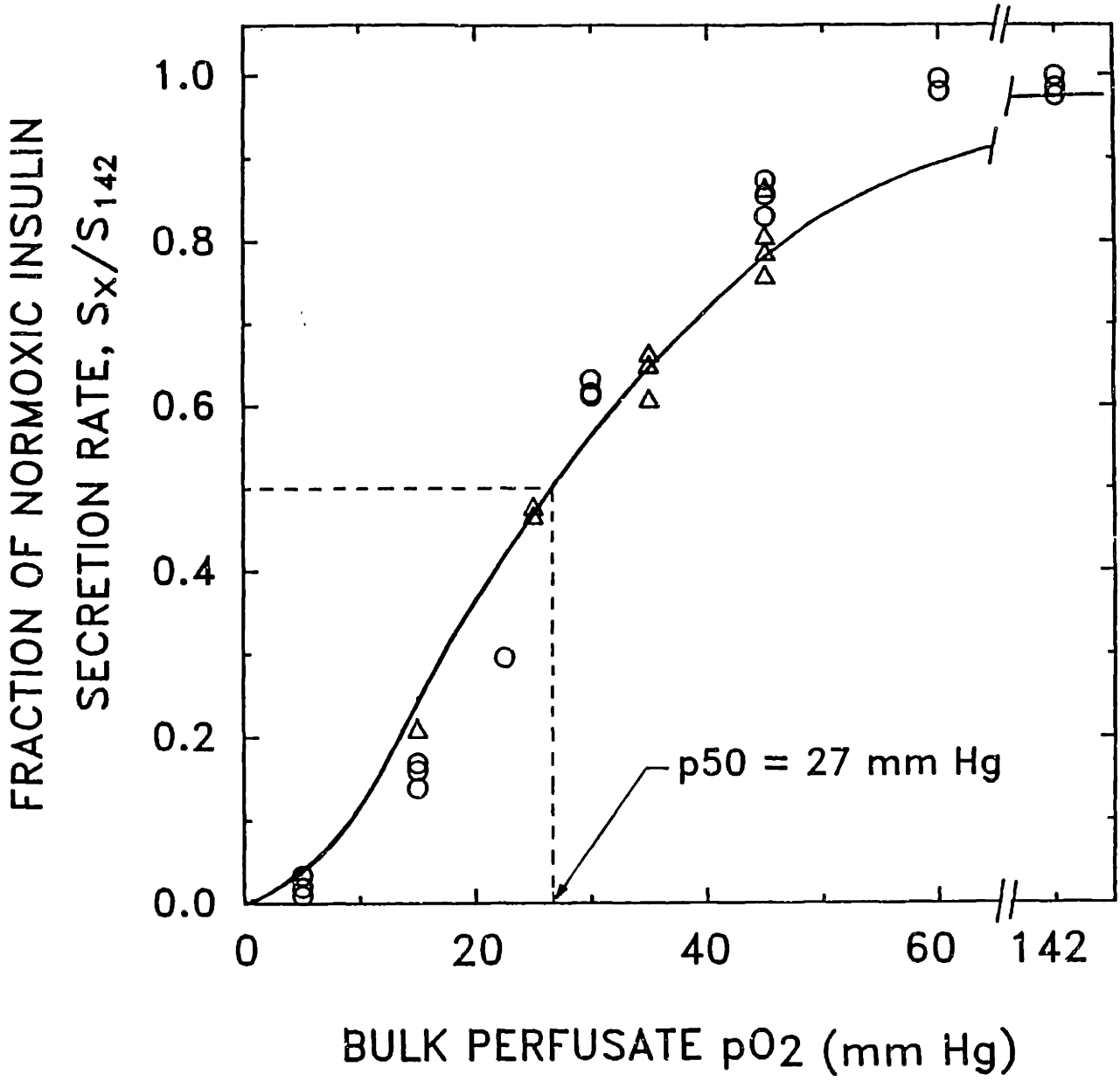

FIGURE 7. Comparison of modeled fraction of normoxic insulin secretion, S_x/S_{142}, from intact islets to experimental S_x/S_{142} values measured in rat islet perifusions. Modelled prediction was based in the integrated insulin secretion assuming a Michaelis-Menten type expression to represent local insulin secretion with a best fit value of Km_I = 4.2 mm Hg, and the local pO_2, P(r), predicted as previously described for 210 μm diameter islets. Experimental data was obtained from perifusions of one-day old rat islets averaging 210 ± 14 μm in diameter (Dionne et al., 1989-3).

CHAPTER 9:

A PROPOSED METABOLIC PATHWAY BY WHICH HYPOXIA REDUCES THE EXOCYTOTIC RELEASE OF INSULIN FROM PANCREATIC BETA-CELLS

INTRODUCTION

It has previously been demonstrated that glucose-stimulated, second phase insulin secretion from both isolated islets and small pancreatic cell aggregates is reversibly reduced by intermediate levels of both acute and chronic hypoxia (Dionne et al., 1989-3 and 1989-4). In perifusions of intact 200 μm diameter rat islets cultured for 24 hr after isolation, second phase insulin secretion began to decrease at a media pO_2 of 60 mmHg, reached one-half of normal at 27 mmHg, and was less than 2% of normal at 5 mmHg (Dionne, Colton, and Yarmush, 1989-3). First phase secretion in these perifusions was much more refractory to hypoxia than was second phase secretion. Small clusters of reaggregated pancreatic cells (mean diameter 37 μm) began to reduce their second phase secretion in response to about 15 mm Hg oxygen, reached one-half of normal secretion at 5.0 mm Hg, and were at less than 20% of normal release at a perfusate pO_2 of 1-2 mmHg (Dionne, Colton, and Yarmush, 1989-4). A mathematical model describing the oxygen profile and insulin secretion within isolated islets indicated that experimental secretion data could be fit by a model using a Michaelis-Menten type expression for insulin secretion with an intrinsic secretory Km for insulin secretion of 4.2 mm Hg oxygen (Dionne, Colton, and Yarmush, 1989-8). Reduced insulin secretion has been shown to correlate closely with reduced oxygen uptake in both intact islets and cell aggregates (Dionne et al., 1989-6 and 1989-8). Reductions in secretion caused by both acute (30-60 min) and chronic (10 day) exposure to hypoxia have been shown to be reversible upon the restoration of normoxic conditions (Coore and Randle, 1964; Coore et al, 1967; Milner and Hales, 1969; Dionne et al., 1989-3, 4, and 5). Perifusion experiments

indicate that insulin secretion is reduced within 30-60 sec of the onset of hypoxia and is increased within a similar time frame upon the restoration of normoxia (Dionne et al., 1989-2).

The purpose of this paper is to describe a mechanism by which hypoxia may affect glucose stimulated insulin secretion and to describe preliminary experimental evidence which supports this mechanism. A brief review of insulin biosynthesis and secretion is included in order to provide a background for the proposed mechanism of hypoxia limited secretion.

Mechanism of Insulin Biosynthesis and Exocytosis

1. Insulin Biosynthesis

The insulin biosynthetic mechanism of the pancreatic β-cell (Steiner et al, 1974) is summarized in Figure 1. The initial biosynthetic step is the transcription of the insulin gene in the nucleus to produce insulin messenger RNA (mRNA). The insulin mRNA is transported to the cytoplasm where it is translated into pre-proinsulin by ribosomes associated with the rough endoplasmic reticulum (RER). Pre-proinsulin is rapidly cleaved to form proinsulin in the microsomes of the RER. Proinsulin, the biosynthetic precursor to insulin, is a single chain polypeptide (MW 9600) consisting of the disulfide linked A and B chains of insulin (MW 5800) and a connecting peptide (C-peptide; MW 3800). The newly formed proinsulin rapidly undergoes sulfhydryl oxidation and peptide chain folding to assume its normal configuration either before or during its energy dependent transport to the Golgi complex via the cisternae of the RER (Steiner, 1972).

In the Golgi apparatus, proinsulin is incorporated into newly formed secretion sacs derived from the Golgi tubules. Once enclosed within the premature secretion sacs, the C-peptide is cleaved from the proinsulin by the proteolytic enzymes trypsin and carboxypeptidase B (Kemmler et al., 1971; Steiner et al., 1974) to form insulin. As insulin is liberated from proinsulin, it complexes with zinc to form a dense rhombic dodecahedral crystalline matrix which accumulates at the center of the 0.2 -0.3 μm diameter granule (Steiner et al., 1974; Howell, 1982). The separated C-peptide forms a semi-fluid region

within the sac surrounding the granular insulin core. A well granulated β-cell may have some thirteen thousand mature granules (Howell, 1984).

The secretion vesicles continue to mature as they are transported toward the cell membrane by an energy dependent process along the microtubular-microfilament network in the cell cytoplasm (Lacy, Walker, and Fink, 1972; Strutfield and Howell, 1984; Sheetz et al., 1987). Experiments in which the microtubular system has been destroyed (via administration of vinblastine or colchicine) or paralyzed (deuterium oxide) have shown that both first and second phase insulin secretion is transported through this system (Lacy, Walker, and Fink, 1972). Upon arrival at the cell membrane, the vesicles marginate along the interior membrane surface waiting to be released by exocytosis. Exocytosis is the process by which the membranous sac encasing the granule fuses with the plasma membrane thus releasing the vesicle's contents into the extracellular space. Upon release, the crystalline insulin granules undergo rapid dissolution due to the high concentration of sodium in the extracellular fluid (Howell et al., 1969; Lacy and Greider, 1972).

The time frame for the various stages in the biosynthetic sequence is shown in the time scale on the right hand side of Figure 1. The values represent experimental results obtained by introducing radioactive amino acids into beta cells and monitoring their movement through the synthesis sequence (Steiner et al, 1974). Labeled amino acids begin to be incorporated into proinsulin within 10-20 min of incubation. Another 10-15 min are required before labeled proinsulin is detected in granules. The conversion of proinsulin to insulin behaves like a first order reaction with a half-life of approximately one hour (Steiner, 1967). This maturation occurs concurrent with the transport of secretion vesicles along the microtubule system to the plasma membrane and accounts for the majority of the overall time delay of about one hour before the first labeled insulin begins to appear as a secretory product (Steiner, 1967; Sando and Grodsky, 1973). Mature granules can be secreted immediately or can wait for hours or days before they are released by exocytosis.

2. Modified Fuel Theory of Exocytosis

The basic fuel theory of exocytosis states that glucose and other insulin secretagogues

trigger β-cell insulin secretion by increasing the metabolic energy state of the cell through the increased production of high energy compounds such as ATP. Besides providing the necessary fuel to drive energy dependent stages of insulin biosynthesis and transport, an increase in the energy supplies of the β-cell may also directly trigger the process of exocytosis. One proposed mechanism for this triggering effect is shown in Figure 2. An increase in the influx of glucose or other metabolites into the cell fuels an increase in the rate of glycolysis and oxidative phosphorylation which in turn result in an increase in the intra-cellular concentrations of H^+ and ATP as well as of other high energy compounds. The increased intra-cellular concentrations of ATP and H^+ block a larger percentage of ATP (Cook and Hales, 1984; Misler et al., 1989) and H^+ (Cook, Ikeuchi, and Fujimoto, 1984) gated K^+ channels which decreases the efflux of K^+ ions from the cell. The decreased efflux of K^+ ions contributes to the depolarization of the β-cell plasma membrane - an event which is integrally associated with exocytosis (Ashcroft, Harrison, and Ashcroft, 1984; Wollheim and Biden, 1987). Among other possible interactions, membrane depolarization may open voltage gated Ca^{++} channels (Dean and Mathews, 1970; Ronner, 1987) to allow an influx of Ca^{++} ions which are essential for the exocytotic release of insulin regardless of the secretagogue (Rubin, 1970; Findlay and Ashcroft, 1975; Hellman, 1975; Cerasi, 1975; Hellman, 1977; Nabor, McDaniel, and Lacy, 1977).

The links between membrane depolarization and/or calcium influx and the exocytotic fusing of the secretion vesicle to the plasma membrane are largely unknown. However, some potential pathways may include: bursting of the secretion vesicle due to increased osmotic pressure caused by an intra-vesicle influx of Ca^{++} and other ions (Brown et al., 1978; Howell, 1984); an electrostatic attraction of the depolarized cell plasma membrane for the polarized membrane of the secretion vesicle (Howell and Tyhurst, 1977; Howell, 1984); or a combination of these events to decrease the resistance of the energy dependent movement of the secretion vesicles along the final nanometers of the microtubule system until they abut against the plasma membrane (Howell, 1984).

The role of rising intra-cellular ATP concentration in directly triggering exocytosis via membrane depolarization was originally questioned since ATP sensitive K^+ channels were found to be one-half maximally inhibited by 15 μM ATP (Cook and Hales, 1984; Rorsman and Trube, 1985) whereas intra-cellular β-cell ATP concentrations are in the mM range (Ashcroft, Weerasinghe, and Randle, 1973; Trus, Warner, and Matschinsky, 1980; Ronner, 1987). However, Cook et al., (1988) have recently developed a "spare channel" hypothesis which mathematically demonstrates the desirability that greater than 99% of the K^+ be closed in order to control the membrane potential in the physiologic range. Their model suggests that the increase in intra-cellular ATP concentration associated with exposure to increased glucose concentrations can block enough additional K^+ channels to cause membrane depolarization.

Proposed Mechanism by which Intermediate Levels of Hypoxia Reduce Insulin Secretion

Potential pathways by which hypoxia may affect insulin secretion include: inhibition of a hypothetical oxygen sensitive enzymatic pathway through which glucose triggers β-cell insulin secretion; cell necrosis or death brought about by hypoxia; reduction of the metabolic energy state of the cell brought about by altered ATP production and utilization. Following preliminary experiments, we believe that the most probable route by which hypoxia affects insulin secretion is via a metabolic pathway.

Hypothesis: Hypoxia reduces second phase insulin secretion from isolated islet tissue via reductions in the intra-cellular metabolic energy state of β-cells - most likely by limiting the production of ATP through oxidative phosphorylation. ATP induced membrane depolarization or the energy dependent transport of secretion vesicles along microtubules to the plasma membrane may be the steps that are the most sensitive to hypoxia though earlier stages of insulin biosynthesis may also be affected.

Studies on insulin secretion, hypoxic viability, and hypoxic amino acid uptake in isolated rat islets were performed in order to gather support for this hypothesis.

MATERIALS AND METHODS

1. Medias and Reagents.

Hanks Balanced Salt Solution (Hanks). Tissue digestions were performed using Hanks solution without Ca^{++}, Mg^{++} (H2387 Sigma Chemical Co., St Louis MO) fortified with 50 U/ml Penicillin and 50 μg/ml Streptomycin (600-5140AG, GIBCO, Grand Island, NY), and 0.35 g/l HEPES (H0763, Sigma Chemical Co.), pH buffered to 7.4 .

Dulbecco's Modified Eagles Media (DMEM). Islet tissue was cultured and tested in DMEM (D5523, Sigma Chemical Co) containing either 1.0 or 3.0 mg/ml glucose, fortified with 50 U/ml Penicillin and 50 μg/ml Streptomycin, and 10% Newborn Calf Serum (NBCS) (200-6010AJ, GIBCO) unless otherwise specified.

Potassium Cyanide (KCN). (6881, Mallinckrodt Inc, Paris, KY) Solutions of 2-4 mM KCN in DMEM were prepared in order to induce a cellular state of chemical anoxia. CN^- inhibits the respiratory electron transport chain by competitively displacing O_2 from its binding site on the final cytochrome c oxidase of the respiratory chain, thereby preventing the transfer of electrons to O_2 (Rawn, 1983).

Antimycin A. (A-2006, Sigma Chemical Co, St. Louis MO) Solutions of 0.56 and 5.6 μM Antimycin A were prepared in DMEM as a second "chemically anoxic" media. Antimycin A blocks the respiratory electron transport chain earlier in tis sequence than does CN^- by specifically inhibiting the action of cytochrome c reductase (Rawn, 1983).

Carbonylcyanide-p-trifluoromethoxyphenylhydrazone (FCCP). (Donated by Dr. P. Heytler of E.I. duPont de Nemours company of Wilmington, DE.) A solution of 12 μM FCCP was

prepared in DMEM. FCCP uncouples the respiratory electron transport chain from ATP synthesis, allowing the reduction of oxygen to continue but without the concurrent production of ATP from oxidative phosphorylation.

2. Islet Isolation and Culture.

Rat Islet Isolation. Islets of Langerhans were isolated from 200 - 350 g male Sprague-Dawley rats (Charles River Lab, Kingston, NJ) using a collagenase digestion / ficoll purification technique (Lacy and Kostianovsky, 1967; Scharp et al, 1980; Dionne et al., 1989-2). Briefly, the pancreas was distended in situ by injecting 10-15 ml of ice cold Hanks solution with 1.7 mg/ml collagenase (108 8882 Boehringer Mannheim, Indianapolis, IN). The distended pancreas was dissected free, placed in a 50 ml T-flask, and digested under mild agitation in a 37°C water bath until islets were freed from acinar tissue as ascertained by microscopic examination (15 - 20 min). The slurry was then rinsed and purified on a discontinuous ficoll gradient (25%, 22%, 17.5%, 11%; F9378, Sigma Chemical Co) and centrifuged at 1000 g for 10 minutes. Separated islets were washed four times in DMEM, handpicked to remove remaining acinar contamination, and cultured in non-attaching petri dishes (8-757-12, Fisher Scientific Co, Pittsburgh PA) in DMEM with 1 mg/ml glucose. Islets in petri dishes were cultured at 37°C under a 5% CO_2 / 95% air atmosphere with media changes every second day.

3. Islet Secretion, Viability and Uptake Testing.

Perifusion Secretion Testing.

The design, construction, and characterization of an oxygen regulating, micro-perifusion system has previously been described (Dionne et al., 1989-2). In brief, the perifusion system is enclosed inside a 37°C incubator for temperature and gas control. Media from separate reservoirs is pumped through gas permeable silastic tubing where it equilibrates with the surrounding gas pO_2 and pCO_2 to provide dissolved oxygen and pH control.

Following gas equilibration, the media flows into a valve which permits rapid switching between media streams containing different concentrations of test substrates. After passing through the valve, media flows into the islet cell chamber. Islets loaded upstream of the cell chamber are entrapped in a cotton mesh membrane and are perifused by the media flowing over them. Before leaving the system, the media pO_2 and pH are monitored by micro in-line probes. Exiting media is collected in a fraction collector for later glucose (Beckman Glucose Analyzer II, Beckman Instruments, Brea CA) and insulin radioimmunoassay analysis (Dionne et al., 1989-2).

The lag between the time at which perfusate streams containing different substrate concentrations were switched at the perfusate switching valve and when one hundred percent of the change was seen in the perfusate exiting into the sample collection tubes was less than one minute. By pre-equilibrating a second media stream at the test pO_2, 90% of a desired oxygen step was achieved in media passing through the in-line pO_2 probe 67 sec after the switch was made and full equilibration was reached 63 sec later.

Batches of 10 - 20 islets were handpicked under a microscope, photographed for later volumetric sizing using a calibrated reticule, and loaded into the perifusion system via an in-line loading port. Islets were perifused at 37°C with DMEM containing basal (100 mg/dl) glucose for 1 hr in order to allow them to equilibrate at basal conditions. Following basal equilibration, insulin secretion was stimulated by switching the media to DMEM containing 300 mg/dl glucose. Islets were perifused with 300 mg/dl glucose for 40-60 min during which time their insulin secretion usually reached a steady release rate. After 40-60 min of stimulated secretion, the media was switched to DMEM with 300 mg/dl glucose either at a reduced pO_2 or which contained a test substance. The test conditions were maintained for 20-40 min after which the perfusate was switched back to normal glucose stimulated conditions. At the conclusion of the perifusion, islets were collected for vital staining and microscopic examination.

Static Secretion Testing. Sized batches of 5 islets each were handpicked and placed into pre-incubated polystyrene petri dishes (35 x 10 mm, 3001 Falcon) containing 1.5 ml DMEM with 100 or 300 mg/dl glucose and the appropriate test substance. The dishes were placed in a 37°C incubator gassed with 5% CO_2 and 95% air for 90 min. At the end of 90 min, the islets were removed from the petri dish by handpicking with a micro-pipette and the supernate was collected for glucose and insulin measurement.

Vital Staining. Trypan Blue. A fresh solution of 0.06% (by weight) trypan blue (630-5250 AG, GIBCO) in DMEM with 2% new born calf serum was made daily. Multiple petri dishes (35 x 10 mm, Falcon 3001, Becton Dickinson Inc., Lincoln Park NJ) were filled with 1.5 ml of staining solution per dish and placed in a 37°C incubator for prewarming and gassing. Using a micro-pipette, test islets were placed in the staining dishes which were then placed in the incubator for 5 min. After 5 min, the islets were micro-pipetted out of the staining dishes, placed in fresh DMEM, and examined under a microscope for staining.
Neutral Red. The procedure for staining with neutral red was similar to that of trypan blue with the exceptions that 0.005% (by weight) neutral red (86,125-1, Aldrich Chemical. Co., Milwaukee WI) was used and the incubation time was increased to 20 min. Viable cells exclude trypan blue and concentrate neutral red whereas nonviable cells do not exclude trypan blue and do not concentrate neutral red stain (Lillie, 1977).

^{14}C-Leucine Uptake. The effect of hypoxia on the rate of ^{14}C-L-leucine uptake by isolated rat islets was measured because changes in the incorporation of amino acids into islet cells during hypoxia may provide a clue as to the effect of hypoxia on early stages of insulin biosynthesis. Batches of 5 islets were handpicked into petri dishes and photographed under a microscope for later volume sizing using a calibrated reticule. The islets were pre-incubated at 37°C in a petri dish containing DMEM with 300 mg/dl glucose under 142 mmHg oxygen for 30 minutes. During pre-incubation, a pyrex test tube (10 x 75 mm) containing 200 μl of DMEM with 2.9 mM L-leucine labeled with ^{14}C-L-leucine (1.25 mCi/mmol L-leucine; NEC-

169; New England Nuclear, Boston MA) was set up in a 37°C waterbath on a wrist shaker (Model 75, Burrell Co, Pittsburgh PA; setting #1). The media in the test tube was gassed with pre-warmed and humidified gas at either 142 mmHg (5.4% CO_2, 94.6% air) or 5 mmHg (91.4% N_2, 5.4% CO_2, and 3.2% air) oxygen. After pre-incubation, the islets were transferred with a micro-pipette to the media in the pyrex tube containing the ^{14}C-L-leucine. The pyrex test tube was then resealed except for the gas inlet and outlet. The islets were incubated for 30 min with mild shaking to reduce any substrate gradients in the media. After incubation, the islets were quickly pipetted out of the radio-labeled media, placed in a pre-warmed petri dish containing 5 ml of DMEM with 100 mg/dl glucose, and rinsed. A series of three, 2-min rinses were performed, each time transferring the islets to a new petri dish with 5 ml of fresh DMEM using a new pipette tip between rinses and transferring less than 5 μl of media with each transfer. After the final rinse, the islets and 200 μl of the last rinse solution were pipetted into a glass scintillation vial. Five hundred and twenty microliters of Protosol (NEF-935, New England Nuclear) were added to the vial which was then capped and allowed to digest for 30 minutes. Following digestion, 9.28 ml Biofluor scintillation fluid (NEF-961, New England Nuclear) were added to each vial after which the vials were counted in a liquid scintillation counter. Background DMEM, control rinse solutions, and total ^{14}C-leucine incubation media vials were prepared and counted at the same time.

RESULTS

Figure 3 shows the results of decreasing the media pO_2 on insulin secretion from perifused islets. The islets were perifused in DMEM with 100 mg/dl for 1 hr in order to allow them to equilibrate to the perifusion conditions. Perfusate fractions were collected over 1 minute intervals following changes in glucose and oxygen concentrations in order to determine the time lag between changes in media substrates and the insulin secretion response by perifused islets. At time zero, the glucose concentration was raised to 300 mg/dl and the islets responded with a rapid burst of 1st phase insulin secretion which peaked during the second minute following the glucose switch. Second phase secretion stabilized at a steady rate

over the next 30 min and remained at that level throughout the normoxic period. At 42 min, the oxygen concentration was rapidly lowered from 142 mmHg to 22 mmHg. Insulin secretion collected during the 1st minute following the switch to low oxygen showed a slight drop, whereas during the second minute of collection (during which time the oxygen drop reached its full hypoxic level) secretion was fully reduced to a hypoxia-limited rate. Secretion remained at about 29-30% of the normoxic rate throughout the period of hypoxia. At 73 min, the media oxygen concentration was raised to 142 mmHg. During the 1st minute following the initiation of the reoxygenation step (before oxygen had reached its full value), the islets responded with a burst of insulin secretion. The reoxygenation spike of insulin secretion peaked during the 2nd min of collection after which secretion returned to a rate similar to the pre-hypoxic level.

Figure 4 illustrates the insulin secretion profile of perifused rat islets subjected to a 40 min exposure to 2 mM KCN. CN^- inhibits the respiratory electron transport chain by competing with O_2 for its binding site on the final cytochrome c oxidase thus producing a pseudo-hypoxic state in the cell. As in the hypoxic perifusion, islets were first equilibrated for 1 hr at 100 mg/dl glucose in DMEM. At time zero, the glucose concentration was raised to 300 mg/dl and the islets responded with a 1st phase spike of insulin secretion which was followed by second phase release which rapidly reached a steady level. At 42 min, the media was switched to DMEM containing 300 mg/dl glucose and 2 mM KCN. Insulin secretion was rapidly diminished to 12 - 14 % of its normoxic rate by the presence of CN^-, and remained at that level throughout the exposure to KCN. At 83 min, the perifusate was switched back to DMEM without KCN and within 2 min, insulin secretion began to rise, demonstrating that insulin suppression by KCN is reversible.

To further test the ability of "chemical anoxia" agents to suppress insulin secretion, islets were perifused with media containing two different concentrations of Antimycin A. Antimycin A specifically inhibits the respiratory cytochrome c reductase, thus blocking the electron transport chain higher up than does KCN. The upper portion of Figure 5 illustrates the insulin secretion profile of perifused islets subjected to a low (0.56 μM) concentration of

Antimycin A. Following an initial dip in secretion, there was only a minor reduction in insulin release throughout the exposure to this concentration of Antimycin A. However, upon the removal of Antimycin A from the perfusate, insulin secretion rapidly began to increase indicating a suppressive effect of the low dosage respiratory poison. When islets were perifused with a 10 fold higher concentration of Antimycin A (5.6 μM), secretion was rapidly shut down (See lower portion of Figure 5). At this high concentration of Antimycin A, the reduction in secretion was not reversible.

Perifused islets were treated with FCCP in order to measure insulin secretion under conditions of reduced intra-cellular ATP but with a normal oxygen concentration and functional electron transport chain. Rather than blocking the respiratory chain, FCCP uncouples electron transport from ATP synthesis. Figure 6 illustrates that 12 μM FCCP rapidly reduced second phase secretion. The reduction was reversible upon the removal of FCCP from the perfusate.

The ability of high extra-cellular K^+ levels to elicit insulin secretion from hypoxia suppressed islets was tested by flushing islets perifused with hypoxic media with similar media containing 50 mM K^+. The insulin secretion profile of hypoxic islets perifused with a bolus of K^+ is shown in Figure 7. Normal second phase secretion was established in perifused rat islets and then suppressed by decreasing the media pO_2 to 10 mmHg. Twenty minutes later, the perifusate was switched to a media containing 50 mM K^+ which elicited an immediate burst of insulin secretion lasting less than 3 min following which secretion remained slightly elevated above its previous hypoxic level throughout the period of high K^+ perifusion. Upon the removal of K^+ from the media, secretion dropped to its previous hypoxic rate. When normoxia was restored, there was no reoxygenation spike and insulin secretion was slow to rise. Whether the reoxygenation spike was absent because the insulin normally released upon reoxygenation was previously secreted in response to the K^+ flush or whether the spike was simply absent from this perifusion is unknown and requires further experimentation.

The effect of hypoxic pO_2 levels on the ability of islets to incorporate amino-acids was determined by measuring the uptake of ^{14}C-L-leucine by islets cultured in either hypoxic (5 mmHg oxygen) or normoxic (142 mmHg) environments. The results of these experiments are shown in Figure 8. The cpm of ^{14}C-L-leucine incorporated per volume of islet tissue are plotted for six experimental runs in which islets were incubated for 30 min at 37°C in KREB/DMEM media containing 2.9 mM L-leucine (1.25 mCi/mmol L-leucine). Islets incubated under 5 mmHg oxygen incorporated approximately 1/5th (20.8%) as much ^{14}C-L-leucine as did normoxic islets during 30 min of glucose stimulated incubation.

Islets were stained with the vital stains trypan blue and neutral red in order to assess their viability following various chemical and hypoxic procedures. Trypan blue staining was never seen in islets following perifusions wherein they were exposed to short term (30 - 60 min) periods of hypoxia ranging from 5 to 60 mmHg. Exposure to longer periods (16 - 32 hr) of severe hypoxia (10 mmHg) in static petri dish culture resulted in trypan blue staining of islet cores whereas the islet periphery was unstained and presumably viable.

Islets exposed to 3mM KCN for 0-2 hours stained in neutral red and did not stain in trypan blue - both indicating viable tissue. Exposure to 3 hr of 3 mM KCN produced speckled staining throughout the islets by both trypan blue and neutral red. After 4 hr, islets were qualitatively judged to be >80% non-viable by both trypan blue and neutral red staining patterns. By the end of 6 hr, islets were completely stained by trypan blue and were judged to be entirely dead. Similar results were obtained when islets were cultured in 5.6 μM Antimycin A.

The correlation between vital staining and insulin secretion was established by measuring the insulin secretion from islets judged to be viable or non-viable by trypan blue and neutral red staining. Secretion results are shown in Figure 9 for normal non-stained islets and for islets following 4 hr of 3 mM KCN culture. Trypan blue stained (hence non-neutral red stained) islets exhibited a basal secretion rate that was 76% lower than normal islets and a stimulated rate that was 97% lower than non-trypan blue stained islets. Stained islets showed

no insulin response to a glucose challenge whereas normal islets showed a 3-fold increase in insulin secretion when the glucose concentration was raised from 100 to 300 mg/dl.

DISCUSSION

1. Pathway by Which Hypoxia Affects Insulin Secretion.

Several experimental observations support the hypothesis that low oxygen tensions reduce insulin secretion through a metabolic pathway rather than by limiting a critical oxygen requiring enzyme that triggers insulin secretion or by causing cell necrosis or death. Cell death is eliminated as a pathway because: a) hypoxia reduced insulin secretion was reversed upon the restoration of normal oxygen tensions after both the 40 min period of hypoxia shown in Figure 3 (and in other similar perifusions; Dionne et al., 1989-3) and over a ten day period of secretion limiting hypoxia (Dionne et al., 1989-5); and b) vital staining by trypan blue and neutral red indicated that both short term hypoxic and chemically anoxic islets were viable both during, and for several hours after, the period of limited insulin secretion. It appears that severe hypoxia over long periods of time may result in cell death and hence decreased insulin secretion since longer periods of hypoxia (16-32 hr of static culture at 10 mmHg O_2) resulted in the development of necrotic cells in the core region of islets. However this long term cell necrosis is not the mechanism that appears to be the cause of short term, rapid depression of insulin secretion by hypoxia.

Although the existence of an oxygen sensitive enzyme that is essential for glucose to trigger insulin secretion cannot be absolutely eliminated, the experimental evidence does not support the existence of this pathway. Such a pathway should be specific to oxygen, however, islet perifusions with KCN and Antimycin A which block the metabolic reduction of oxygen but do not affect its concentration, simulated the effect of hypoxia in reversibly reducing insulin secretion. FCCP, which leaves the respiratory chain intact and functioning but decouples ATP synthesis, also resulted in a reversible reduction of insulin secretion similar to that seen with hypoxia. These experiments do not prove that an oxygen sensitive enzyme does not exist but they do suggest that even should such an enzymatic pathway exist,

its functional importance would be questionable because of the concurrent requirement of oxygen to provide metabolic energy for insulin secretion.

There are several lines of evidence that suggest that hypoxia reduces insulin secretion through a metabolic pathway. First, intra-cellular ATP has been shown to be essential for insulin secretion regardless of the stimulus (Malaisse, 1972; Findlay and Ashcroft, 1975; Cerasi, 1975) and to increase in concentration during glucose stimulated insulin secretion (Randle and Hales, 1972; Ashcroft et al., 1974; Malaisse and Sener, 1987). Complete anoxia has been shown to decrease the ATP concentration in β-cells (Matschinsky and Ellerman, 1968; Hellman, Idahl and Danielson, 1969; Wettermark et al., 1970; Randle and Hales, 1972). Although no experimental correlation has been directly measured between the degree of hypoxia and the degree to which the intra-cellular concentration of ATP is reduced in β-cells, such a correlation has been measured in isolated hepatocytes (Jones and Mason, 1978) and it is probable that such a relationship also exists in β-cells. A progressive decline in intra-cellular ATP concentration would explain the progressive reduction of insulin secretion as the media pO_2 is incrementally lowered.

Second, perifusions with KCN, Antimycin A, FCCP, and hypoxia all of which inhibit oxidative phosphorylation, all had a similar affect on insulin secretion despite the fact that KCN, Antimycin A, and FCCP have no effect on intracellular oxygen concentration and only affect the metabolic use of oxygen.

Third, the respective values of the Km (state 5) of mitochondrial oxidative phosphorylation (0.44 mm Hg; Wilson et al., 1988) and the calculated intrinsic cellular dependence of insulin secretion on oxygen (intrinsic Km_I = 4.2 mm Hg pO_2; Dionne et al., 1989-8) indicate that hypoxia-limited insulin secretion is modulated over a range of pO_2 where oxgygen uptake is just beginning to be affected. Although at a given pO_2 the hypoxic depression of insulin secretion is more severe than is the reduction in oxygen uptake, the effect on insulin secretion neverthelss coincides with a range where reductions in oxgyen uptake and hence metabolic ATP production by oxidative phosphorylation are predicted to occurr although to a lessor degree.

Fourth, one postulated role of hypoxia in limiting insulin secretion is that hypoxia reduces the intra-cellular ATP concentration thereby opening ATP gated K^+ channels and preventing membrane depolarization. If such were true, then another method of blocking or slowing the K^+ efflux out of the cell would lead to membrane depolarization and insulin secretion. This is in complete agreement with the hypoxic K^+ flush experiment in which insulin secretion was elicited from hypoxia suppressed islets by flushing the extra-cellular space with a high concentration of K^+ ions in order to halt the β-cell K^+ efflux.

Finally, perifusions using a rapid media oxygen switching technique and a low perifusate residence time, indicated that islets responded to changes in media pO_2 within 30 - 60 sec or less from the time of the media pO_2 change. Such a rapid response is in agreement with potential changes in intra-cellular ATP concentrations. Randle and Hales (1972) estimated that glucose stimulated β-cell ATP turnover was on the order to 37 - 42 μmole ATP / min-gram dry wt. The normal intra-cellular concentration of ATP in β-cells is between 10 - 17 μmole / gram-dry wt (Randle and Hales, 1972; Trus, Warner, and Matschinsky, 1980). These numbers indicate that in the absence of ATP generation, β-cell ATP supplies are depleted within 15 to 25 seconds of normal energy expenditures, therefore even a slight decrease in ATP synthesis could rapidly affect the cellular ATP concentration and hence insulin secretion.

2. Hypoxia Appears to Limit Insulin Secretion During the Exocytotic Stage of Release.

Hypoxia probably also limits earlier states of biosynthesis and vesicle transport but the rapidity with which hypoxia reduces insulin secretion in perifused islets indicates that the reduction must also occur during the exocytotic stage of secretion. Perifused insulin secretion responded within 30 - 60 seconds or less to changes in the media pO_2. The time scale of biosynthetic events shown on the right hand side of Figure 1 indicates that any changes occurring upstream of vesicle exocytosis, though perhaps occurring, would not affect insulin secretion over this short of a period of time.

There are several lines of evidence that suggest that exocytosis may be more sensitive to hypoxia than are earlier stages of biosynthesis or of the secretion process and that some earlier states of synthesis and secretion may continue to operate at a higher rate than that defined by the actual rate at which insulin is released. First, when normoxia is restored after 20 - 40 min of hypoxia reduced insulin secretion, a burst of insulin is released that is much higher than either the previous normoxic rate or the subsequent post-hypoxic rate of release. This reoxygenation spike is suggestive of a build-up of insulin that "dams up" against the slower acting exocytotic release mechanism. Upon reoxygenation, the exocytotic limitations are released and the built-up insulin is rapidly secreted.

Second, experiments in which the uptake of ^{14}C-L-leucine was measured in hypoxic islets indicated that amino acid incorporation was only reduced to approximately 21% of its normal rate whereas insulin secretion under similar conditions was reduced to less than 2% of its normal rate (Dionne et al., 1989-3). The reduced, yet still significant uptake of l-leucine suggests that some earlier stages of biosynthesis may continue to occur during intermediate levels of hypoxia at a higher rate than is the final exocytotic release of insulin.

When hypoxic islets were flushed for 20 min with a high concentration of K^+, they released a single spike of insulin and then decreased their secretion to a level significantly less than their normoxic rate but slightly elevated with respect to the hypoxic secretion rate in the absence of K^+. This indicates the presence of a body of insulin that can be secreted if the K^+ efflux can be prevented by a means other than ATP closing off of ATP gated K^+ channels. This suggests that ATP closure of ATP gated K^+ channels may be the secretory step that is the most sensitive to hypoxia reduced ATP levels. That K^+ did not induce a larger sustained release of insulin could be due either to the spike-like nature of perfused K^+ induced insulin secretion (Dawson et al, 1986) or to other hypoxia suppressed secretory steps which limited the availability of secretable granules.

Finally, the ability of islets to survive periods of gaseous and chemical (KCN, Antimycin A) hypoxia over extended periods of time (1 to 10 days depending on the degree of gaseous hypoxia; Dionne et al., 1989-5; 2 - 4 hr of KCN or Antimycin A) indicates that

some cell activity, including possibly the biosynthesis of essential proteins, still occurs in hypoxic cells. The apparent gap between loss of insulin secretion and the onset of β-cell death could teleologically be understood as a defense mechanism which allows the cell to survive during anoxic stress by shutting down a major drain on the cell's energy supplies (Hochachka, 1986).

SUMMARY - HYPOTHESIS

It is hypothesized that hypoxia most directly reduces second phase insulin secretion from isolated islet tissue by limiting the oxidative phosphorylative production of ATP. Besides limiting the energy available for insulin biosynthesis and intra-cellular vesicle transport, hypoxia reduced ATP concentrations may also prevent membrane depolarization by increasing the K^+ conductance out of the cell by opening ATP gated K^+ channels.

REFERENCES

Ashcroft, S.J.H, Chatra, C, Weersinghe, C, and Randle, P.J. (1973) Interrelationships of islet metabolism, adenosine triphosphate content and insulin release. Biochem J 132:223-31.

Ashcroft, F.M, Harrison, D.E, and Ashcroft, J.H. (1984) Nature 312:446-448.

Ashcroft, S.J.H, Weerasinghe, L.C.C, and Randle, P.J. (1973) Biochem J 132:223-231.

Brown, E.M, Pazoles, C.J, Kreutz, C.E, Aurbach, G.D, and Pollard, H.B. (1978) Role of aniions inparathyroid hormone release from dispersed bovine parathyroid cells. Proc Natl Acad Sci (USA) 75:876-880.

Cerasi, E. (1975) Mechanism of glucose stimulated insulin secretion in health and in diabetes: some re-evaluations and proposals. Diabetologia 11:1-13.

Cook, D.L, and Hales, C.N. (1984) Intracellular ATP directly blocks K^+ channels in pancreatic β-cells. Nature 311: 271-273.

Cook, D.L, Ikeuchi, M, and Fujimoto, W.Y. (1984) Lowering of pH_i inhibits Ca^{2+}-activated K^+ channels in pancreatic β-cells. Nature 311:269-271.

Cook, D.L., Satin, L.S, Ashford, M.L.J, and Hales, C.N. (1988) ATP-Sensitive K^+ Channels in Pancreatic β-Cells: Spare-channel hypothesis. Diabetes 37:495-98.

Dawson, C.M, Lebrun, P, Herchuelz, A, Malaisse, W.J, Goncalves, A.A, and Atwater, I. (1985) Effect of temperature upon potassuim-stimulated insulin release and calcium entry in mouse and rat islets. Horm Metabol Res 18:221-224.

Dean, P.M, and Mathews, E.K. (1970) Electrical activity in pancreatic islet cells: effect of ions J Physiol (Lond)210:265-275.

Dionne, K.E, Colton, C.K, and Yarmush, M.L. (1989) Effect of Oxygen on Isolated Pancreatic Tissue. A.S.A.I.O Transactions (submitted).

Dionne, K.E, Colton, C.K, and Yarmush, M.L. (1989-2) A micro-perifusion system with environmental control for islet insulin secretion studies. (Ph.D. Thesis; Chapter 2).

Dionne, K.E, Colton, C.K, and Yarmush, M.L. (1989-3) Effect of hypoxia on insulin secretion by isolated rat and canine islets of Langerhans. (Ph.D.Thesis; Chapter 3).

Dionne, K.E, Colton, C.K, and Yarmush, M.L. (1989-4) Effect of hypoxia on insulin secretion from rat and canine islet cell aggregates. (Ph.D. Thesis; Chapter 4).

Dionne, K.E, Schlosser, C, Wilson, D.F, Yarmush, M.L, and Colton, C.K. (1989-6). Measurement of oxygen uptake of intact islets and reaggregated cells under oxygenated and oxygen limiting conditions. (Ph.D. Thesis; Chapter 6).

Dionne, K.E, Colton, C.K, and Yarmush, M.L. (1989-8). Mathematical modeling of O_2 profiles, O_2 consumption, and insulin secretion in isolated and immuno-isolated islets of Langerhans. (Ph.D. Thesis; Chapter 8).

Findlay, J.A, and Ashcroft, J.J.H. (1975) Cells of the islets of Langerhans. The Cell in Medical Science Volume III. Academic Press, NY.

Hellman, B, Idahl, L.A, and Danielson, A. (1969) Adenosine triphosphate levels of mammalian pancreatic β-cells after stimulation with glucose and hypoglycemic sulfonylureas. Diabetes 18:509-516.

Hochachka, P.W. (1986) Defense strategies against hypoxia and hypothermia. Science 231:234-241.

Howell, S.L, and Taylor, K.W. (1967) The secretion of newly synthesized insulin *in vitro*. Biochem J 102:922.

Howell, S.L, Young, D.A, and Lacy, P.E. (1969) Isolation and properties of secretory granules from rat islets of Langerhans. III. Studies of the stability of the isolated beta granules. J Cell Biol 41:167-76.

Howell, S.L. (1982) The insulin storage granule. in Poisner, A.M, and Trifaro, J.M. (eds) The Secretory Granule Elsevier Medical. Amsterdam. p. 155-172.

Howell, S.L. (1984) The mechanism of insulin secretion. Diabetologia 26:319-327.

Grodsky, G.M, and Bennett, L.L. (1966) Cation requirements for insulin secretion in the isolated perfused pancreas. Diabetes 15:910-13.

Jones, D,P, and Mason, H.S. (1978) Gradients of O_2 concentration in hepatocytes. J Biol Chem 253:4874-80.

Kemmler, W, Peterson, J.D, Gorg, J, Nehrlich, S, and STeiner, D.F. (1971) On the transformation of proinsulin to insulin *in vitro* and *in vivo*. Diabetes 20(suppl 1):332.

Knight, D.E, and Baker, P.F. (1987) Exocytosis from the vesicle viewpoint: An overview. (Part VI. Exocytosis from the Perspective of the Secretory Vesicle; ed. Johnson, R.G.) Ann NY Acad Science 493: 504 - 522.

Lacy P.E, Walder, M.M, and Fink, C.J. (1972) Perifusion of isolated rat islets in vitro: Participation of the microtubular system in the biphasic release of insulin. Diabetes 21:987-98.

Lacy, P.E, and Greider, M.H. (1972) Ultrastructural organization of mammalian pancreatic islets. in Greep, R.O, and Astwood, E.B. (eds), Handbook of PHysiology, Section 7: Endocrinology, Volume I. Endocrine Pancreas, p. 77-89, American Physiological Society, Washington, D.C.

Lillie, R.D. (ed) (1977) *H.J. Conn's Biological Stains*. Williams and Wilkins Co., Baltimore, MD.

Malaisse, W.J. (1972) Hormonal and environmental modification of islet activity. in Greep, R.O, and Astwood, E.B. (eds), Handbook of PHysiology, Section 7: Endocrinology, Volume I. Endocrine Pancreas, p. 175-98, American Physiological Society, Washington, D.C.

Malaisse, W.J, and Sener, A. (1987) Glucose-induced changes in cytosolic ATP content in pancratic islets. Biochim Biophys Acta 927:190-95.

Matschinsky, F.M, and Ellerman, J.E. (1968) Metabolism of glucose in the islets of Langerhans. J Biol Chem 243:2730-36.

Misler, S, Gee, W. M, Gillis, K.D, Scharp, D.W, and Falke, L,C. (1989) Metabolite-regulated ATP-sensitive K^+ channel in human pancreatic islet cells. Diabetes 38: 422-427.

Randle, P.J, and Hales, C.N. (1972) Insulin Release Mechanisms in *Handbook of Physiology: Endocrinology I* (Chapter 13, pp. 219 - 35); Greep, R.O, and Astwood, E.B. (eds), American Physiological Society, Washington D.C.

Ronner, P. (1984) Transmembrane ion distribution and insulin secretion. Ann NY Acad Science 493:341-355.

Sando, H, and Godsky, G.M. (1973) Dynamic synthesis and release of insulin and proinsulin from perifused islets. Diabetes 22:354-60.

Sheetz, M.P, Vale, R, Schnapp, B, Schroer, T, and Reese, T. (1987) Movements of vesicles on microtubules. Ann NY Acad Science 493: 409-416.

Steiner, D.F. (1967) Evidence for a precursor in the biosynthesis of insulin. Trans NY Acad SCi Ser II 30:60-68.

Steiner, D.F, Kemmler, W, Clark, J.L, Oyer, P.E, and Rubenstein, A.H. (1972) The biosynthesis of insulin. in Greep, R.O, and Astwood, E.B. (eds), Handbook of PHysiology, Section 7: Endocrinology, Volume I, Endocrine Pancreas, p. 175-198, American Physiological Society, Washington, D.C.

Steiner, D.F, Kemmler, W, Tager, H.S, and Peterson, J.D. (1974). Proteolytic processing in the biosynthesis of insulin and other proteins. Fed Proc 33:2105-15.

Stutchfield, J, and Howell, S.L. (1984) The effect of phallodin on insulin secretion from islets of Langerhans isolated from rat pancreas. FEBS LET 175:393-396.

Trus, M, Warner, H, and Matschinsky, F. (1980) Effects of glucose on insulin release and on intermediary metabolism of isolated perifused pancreatic islets from fed and fasted rats. Diabetes 29:1-14.

Wettermark, G, Tegner, L, Brolin, S.E, and Borglund, E. (1970) Photokinetic measurements of the ATP and ADP levels in isolated islets of Langerhans. in *The Structure and Metabolism of the Pancreatic Islets*, edited by S. Falkmer, B. Hellman, and I.B. Taljedal. Oxford: Pergamon Press. p. 275-282.

Wilson, D.F, Rumsey, W.L, Green, T.J, and Vanderkooi, J.M. (1988) The oxygen dependence of mitochondrial oxidative phosphorylation measured by a new optical method for measuring oxygen concentration. J Biol Chem 263:2712-18.

Wollheim, C.B, and Biden, T.J. (1987) Signal transduction in insulin secretion: Comparison between fuel stimuli and receptor agonists. Ann NY Acad Science 493:317-333.

FIGURE CAPTIONS

Figure 1. Schematic representation of insulin biosynthesis in the β-cell. (Steiner et al., 1974)

Figure 2. Schematic representation of the pathway by which increased intra-cellular ATP concentration may lead to membrane depolarization and insulin exocytosis. Increased metabolic fuels lead to increased production of ATP, which blocks ATP gated K^+ channels halting the efflux of K^+ from the cell and initiating membrane depolarization. Depolarization opens voltage gated Ca^{++} channels initiating an influx of Ca^{++}. The actual process by which vesicle and plasma membrane fuse is unknown but may involve a combination of osmotic and electrostatic forces.

Figure 3. Effect of hypoxia on second phase insulin secretion from perifused rat islets.

Figure 4. Effect of KCN on second phase insulin secretion from perifused rat islets. CN^- causes a form of chemical anoxia by competitively displacing O_2 from its binding site on the final cytochrome c oxidase of the respiratory chain.

Figure 5. Effect of the respiratory chain poison Antimycin A on second phase insulin secretion from perifused rat islets.

Figure 6. Effect of metabolic uncoupler FCCP on second phase insulin secretion from perifused rat islets. FCCP uncouples oxidative phosphorylation from ATP synthesis.

Figure 7. The effect of high concentration of extra-cellular K^+ on hypoxia suppressed insulin secretion. Extra-cellular K^+ may cause membrane depolarization and exocytosis by reducing the efflux of K^+ ions through ATP gated K^+ channels left open because of a hypoxia reduced intra-cellular ATP concentration.

Figure 8. The effect of hypoxia on the uptake of l-^{14}C-leucine by glucose stimulated islets. Islets were pre-incubated at 300 mg/dl glucose for 30 min and then incubated in DMEM containing 2.9 mM l-leucine (1.25 mCi/mmole l-leucine) and 300 mg/dl glucose at either 5 or 142 mmHg oxygen.

Figure 9. Correlation between trypan blue and neutral red vital staining patterns and insulin secretion. Islets cultured in 3 mM KCN for 4 hr stained with trypan blue and did not incorporate neutral red - both indicating non-viable cells. When insulin secretion was tested 2 hr later, islets deemed "non-viable" by vital staining showed decreased basal and the absence of glucose stimulated insulin secretion in 1.5 hr static secretion tests.

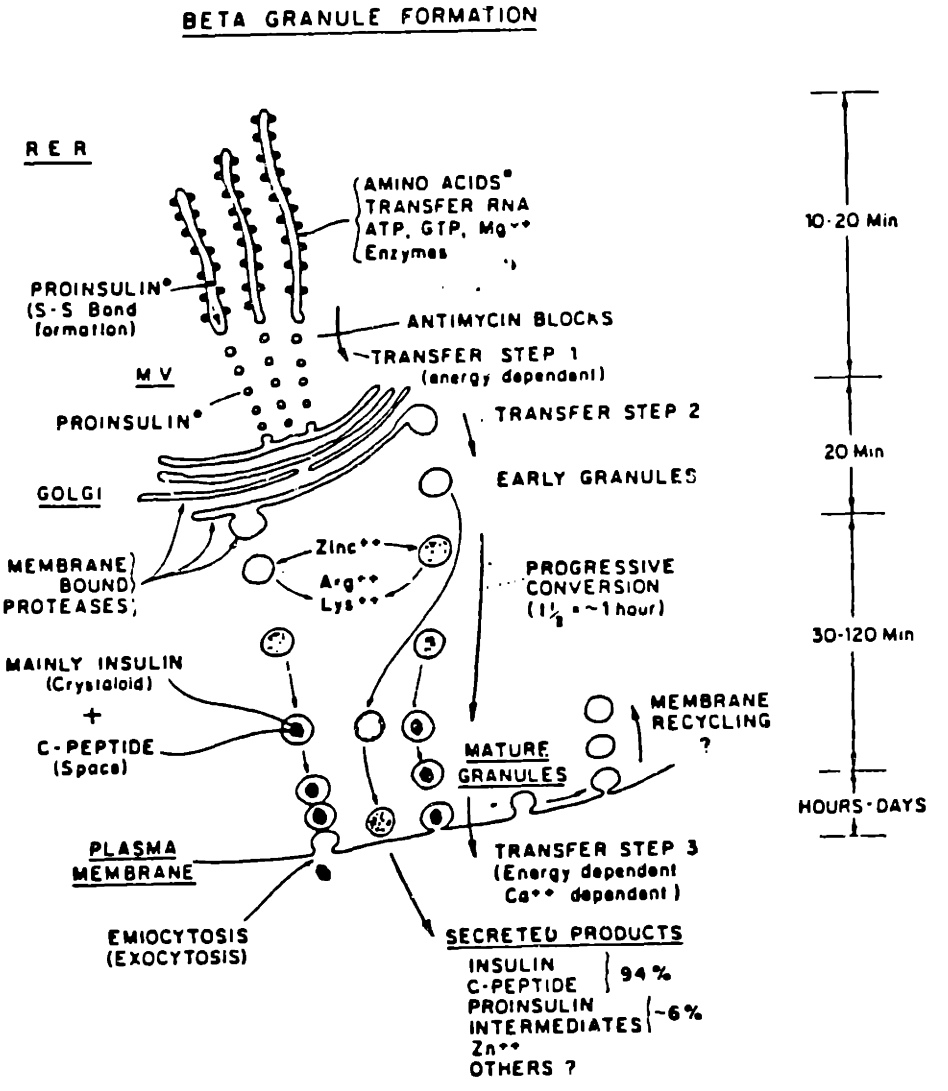

FIGURE 1. Schematic representation of insulin biosynthesis in the β-cell. (Steiner et al., 1974)

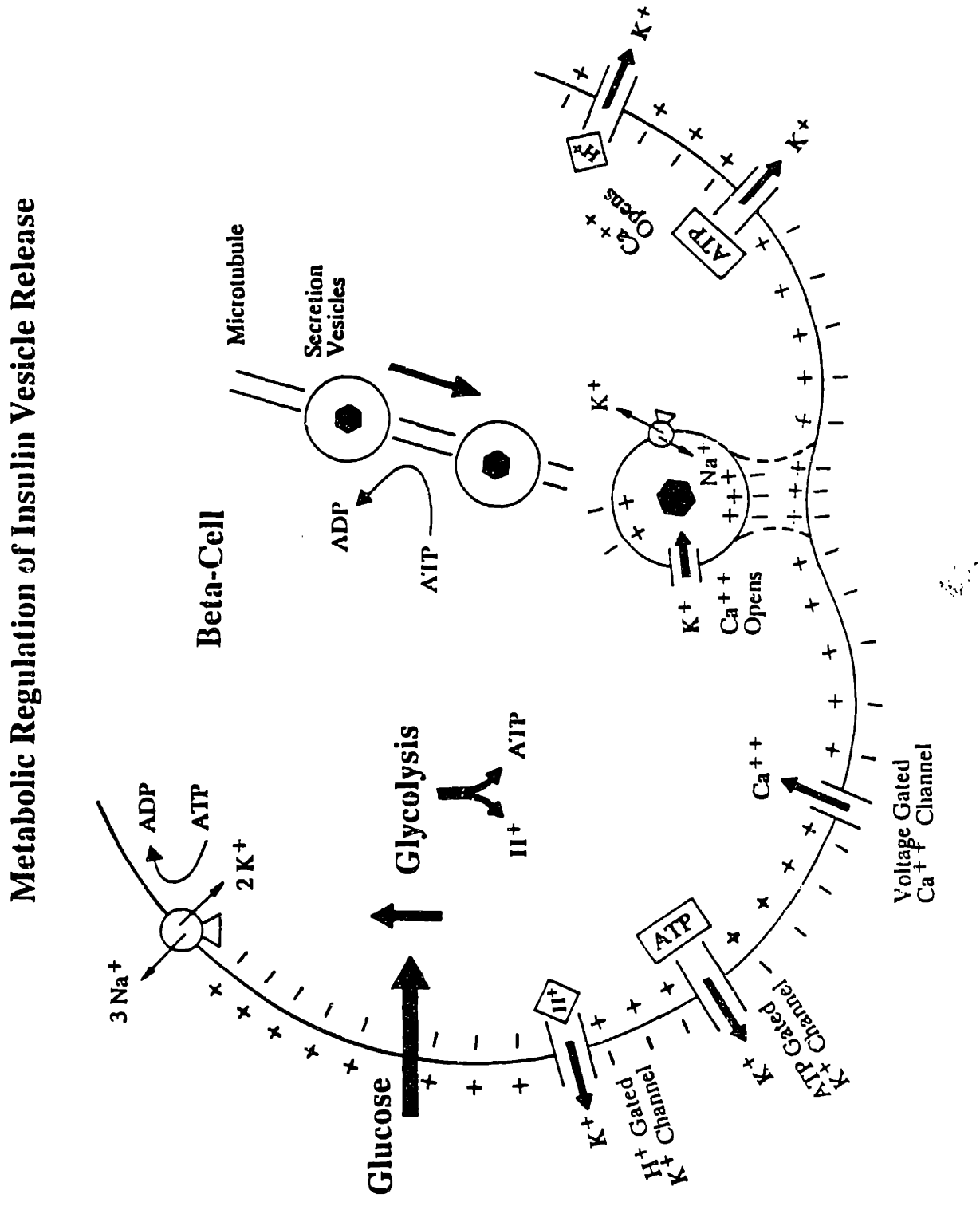

FIGURE 2. Schematic representation of the pathway by which increased intra-cellular ATP concentration may lead to membrane depolarization and insulin exocytosis. Increased metabolic fuels lead to increased production of ATP, which blocks ATP gated K^+ channels halting the efflux of K^+ from the cell and initiating membrane depolarization. Depolarization opens voltage gated Ca^{++} channels initiating an influx of Ca^{++}. The actual process by which vesicle and plasma membrane fuse is unknown but may involve a combination of osmotic and electrostatic forces.

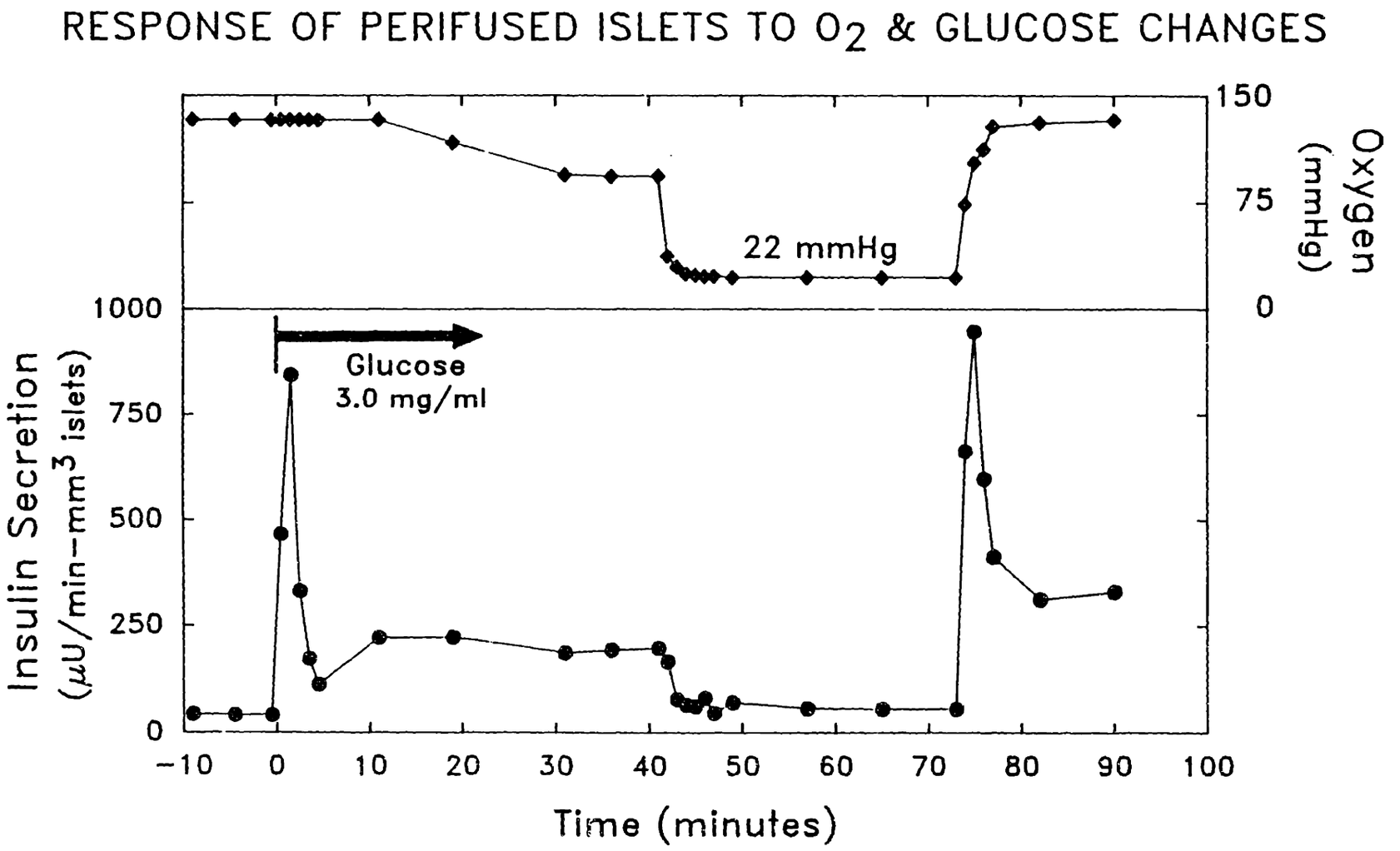

FIGURE 3. Effect of hypoxia on second phase insulin secretion from perifused rat islets.

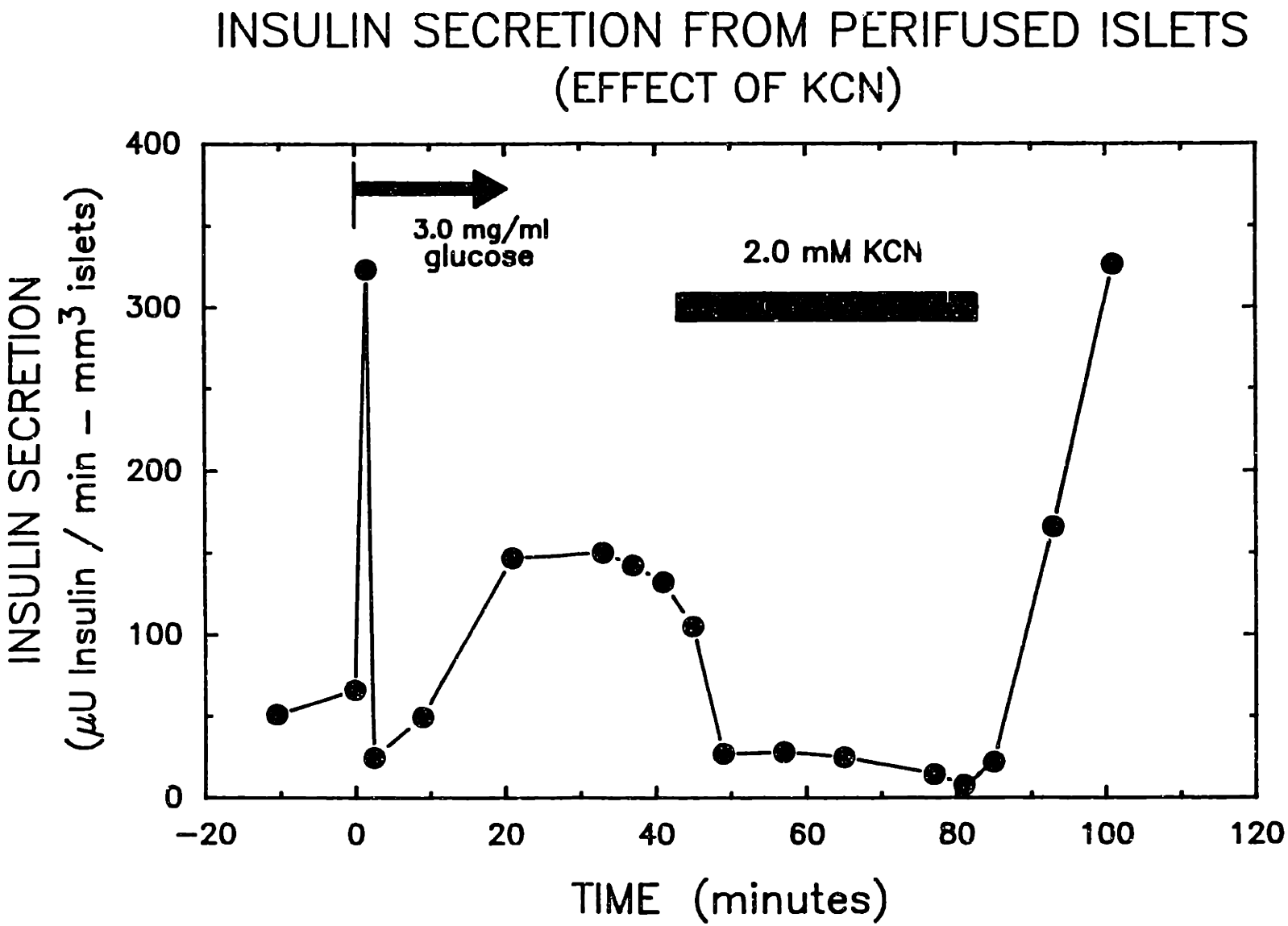

FIGURE 4. Effect of KCN on second phase insulin secretion from perifused rat islets. CN^- causes a form of chemical anoxia by competitively displacing O_2 from its binding site on the final cytochrome c oxidase of the respiratory chain.

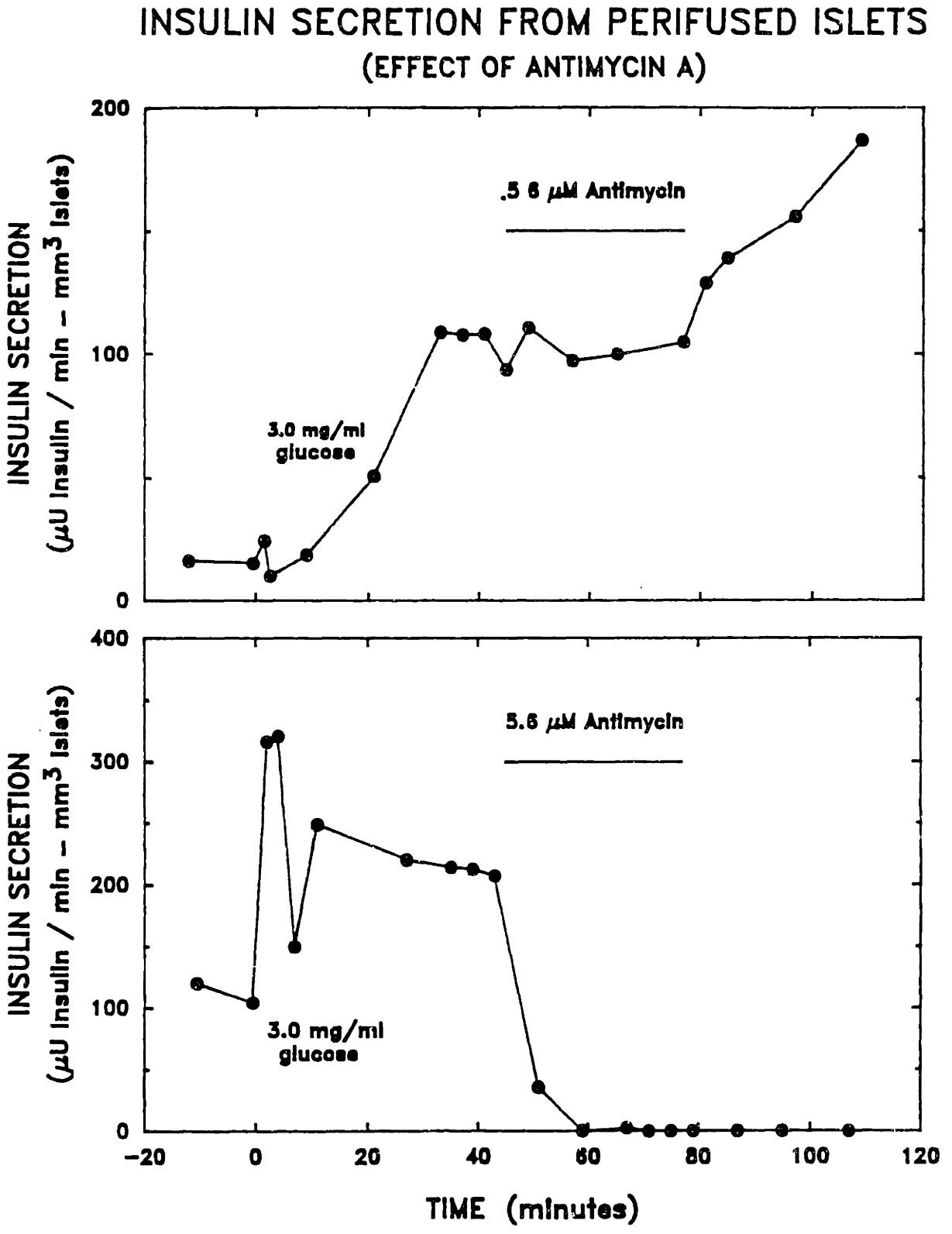

FIGURE 5. Effect of the respiratory chain poison Antimycin A on second phase insulin secretion from perifused rat islets.

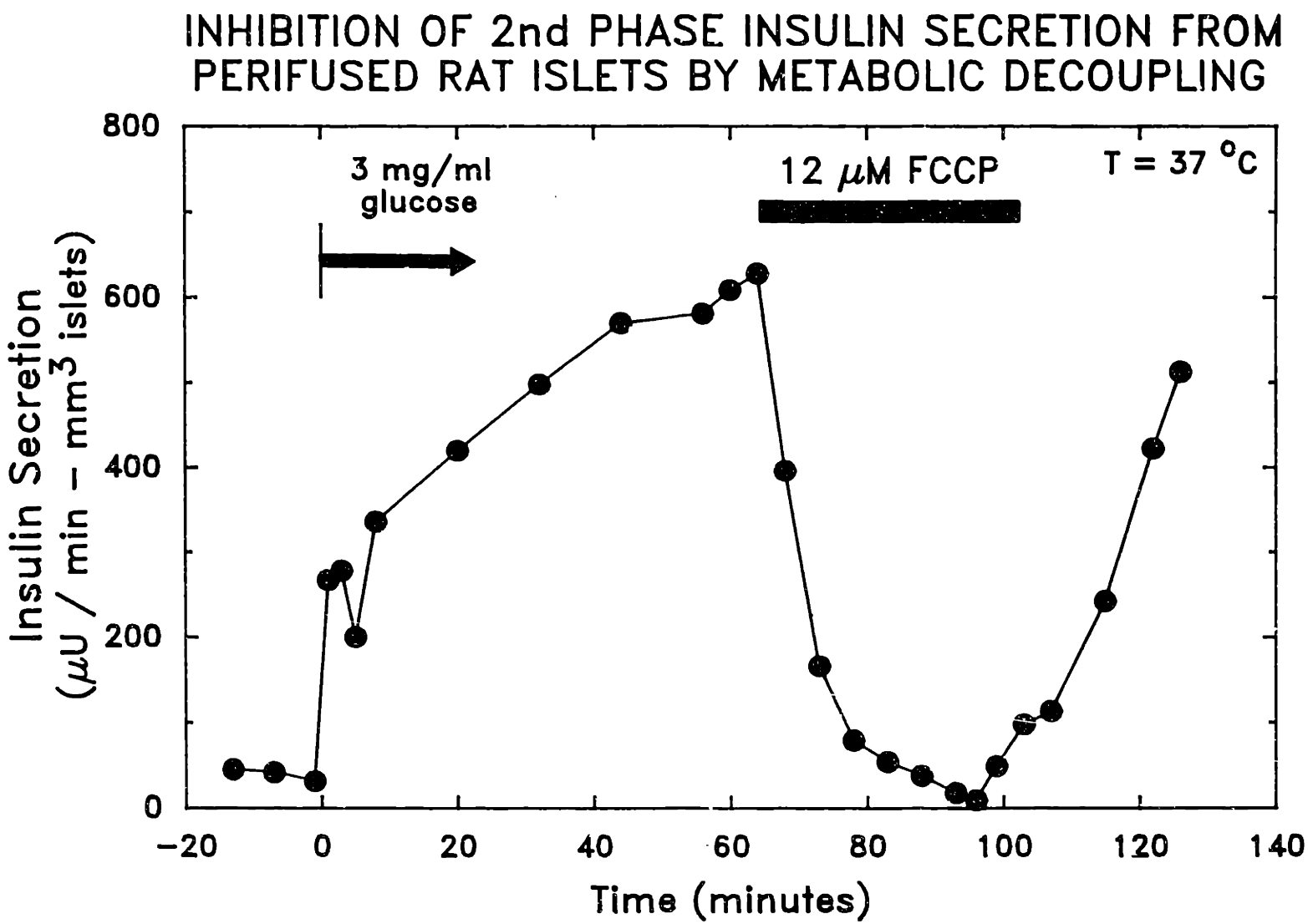

FIGURE 6. Effect of metabolic uncoupler FCCP on second phase insulin secretion from perifused rat islets. FCCP uncouples oxidative phosphorylation from ATP synthesis.

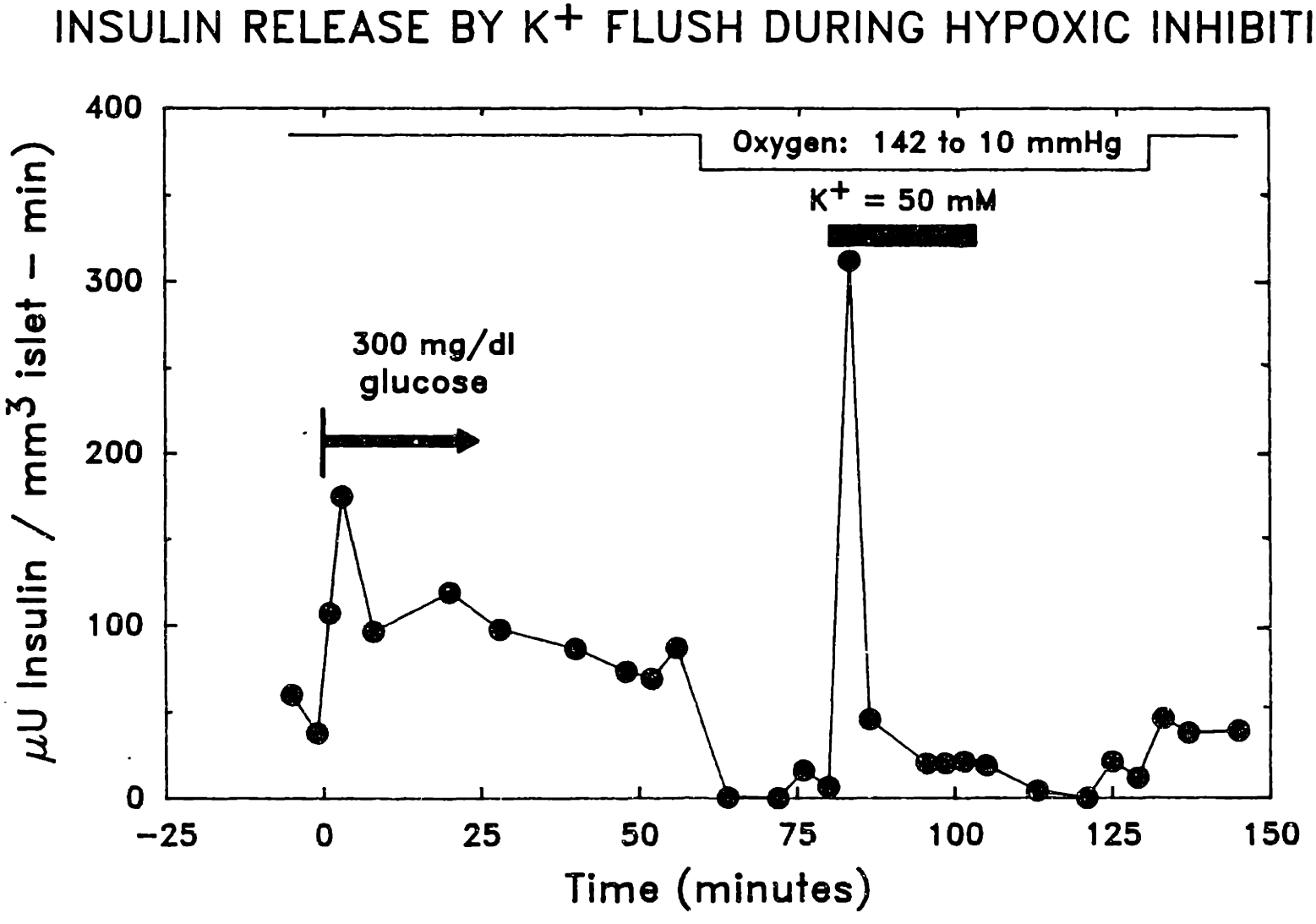

FIGURE 7. The effect of high concentration of extra-cellular K^+ on hypoxia suppressed insulin secretion. Extra-cellular K^+ may cause membrane depolarization and exocytosis by reducing the efflux of K^+ ions through ATP gated K^+ channels left open because of a hypoxia reduced intra-cellular ATP concentration.

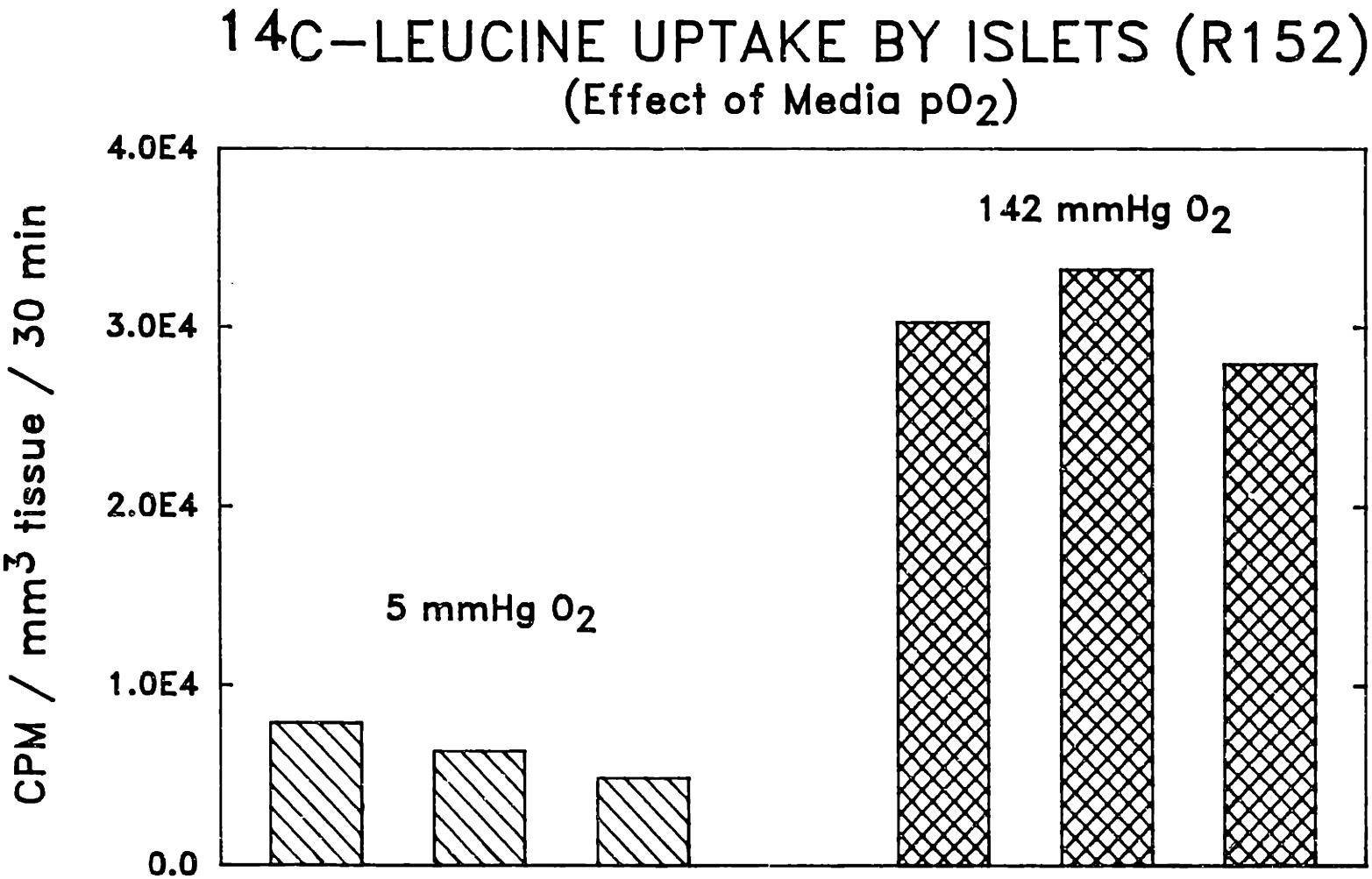

FIGURE 8. The effect of hypoxia on the uptake of l-^{14}C-leucine by glucose stimulated islets. Islets were pre-incubated at 300 mg/dl glucose for 30 min and then incubated in DMEM containing 2.9 mM l-leucine (1.25 mCi/mmole l-leucine) and 300 mg/dl glucose at either 5 or 142 mmHg oxygen.

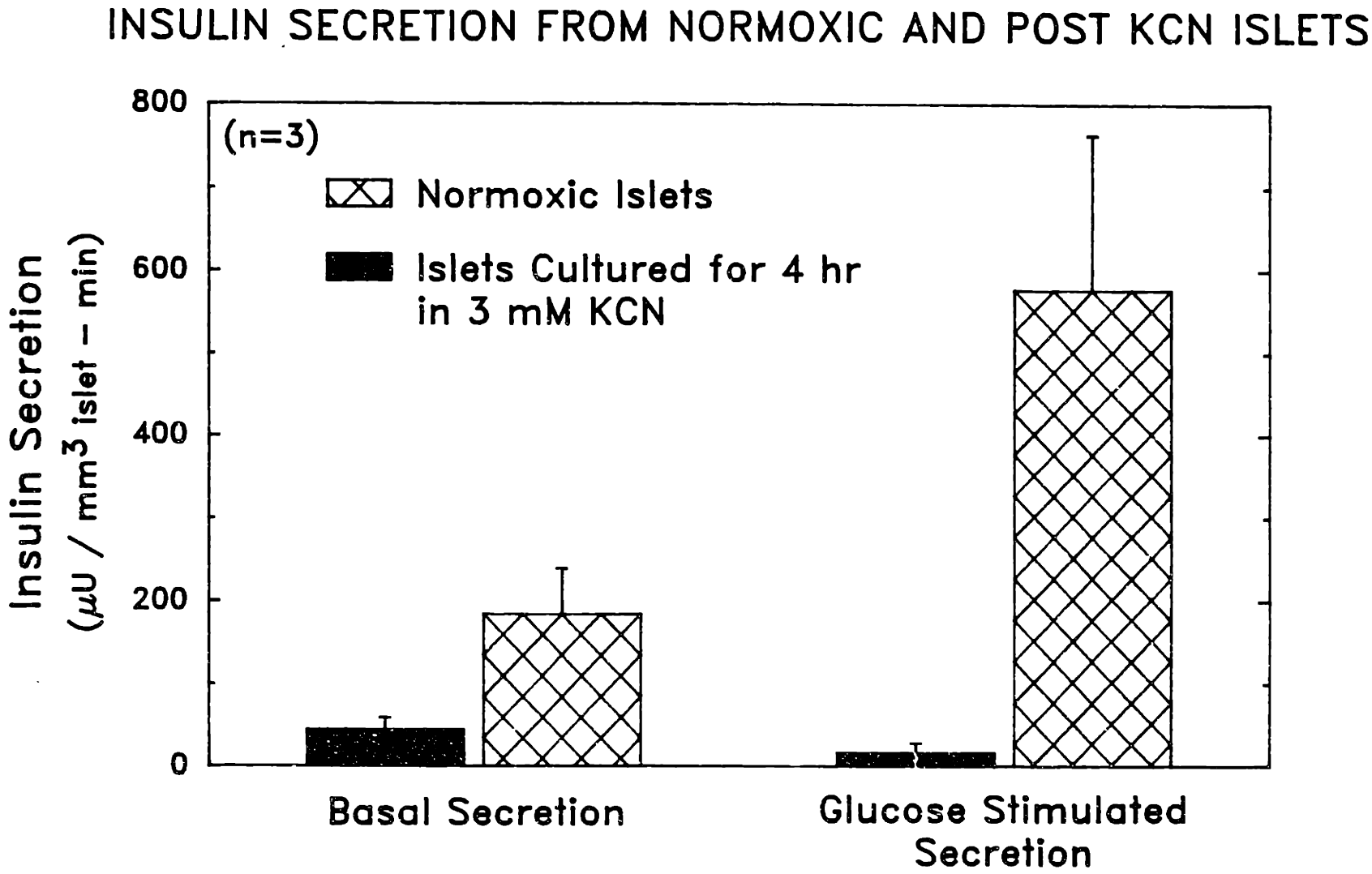

FIGURE 9. Correlation between trypan blue and neutral red vital staining patterns and insulin secretion. Islets cultured in 3 mM KCN for 4 hr stained with trypan blue and did not incorporate neutral red - both indicating non-viable cells. When insulin secretion was tested 2 hr later, islets deemed "non-viable" by vital staining showed decreased basal and the absence of glucose stimulated insulin secretion in 1.5 hr static secretion tests.

APPENDICES

APPENDIX 2A:

ISOLATION AND PURIFICATION OF ISLETS OF LANGERHANS

I. Pancreatomy, Collagenase Digestion, and Ficoll Purification

Materials

Rats: Sprague-Dawley, Male, 200-350 g, obtained from Charles River Laboratories through the MIT Division of Comparative Medicine, Cambridge, MA.

Collagenase: 1088 882, Collagenase D, Boehringer Mannheim Biochemicals, Indianapolis IN Stored at 4°C in an air tight bottle.

Ficoll: Type 400-DL, Dialyzed and Lyophilized; F9378, Sigma Chemical Co., St. Louis MO.

Hanks Media: w/o Ca^{++}, Mg^{++}; H2387, Sigma Chemical Co., St. Louis MO. Fortified with 50 U/ml Penicillin & 50 μg/ml Streptomycin (600-5140 AG, GIBCO, Grand Island, NY), 0.35 g/l HEPES (1088 882, Boehringer Mannheim), and 0.35 g/l Sodium bicarbonate; pH = 7.4.

DMEM: Dulbecco's Modified Eagles Media with 1.0 g/l glucose (D5523, Sigma Chemical Co.). Fortified with 50 U/ml Penicillin & 50 μg/ml Streptomycin, 10% Newborn Calf Serum (NBCS) (200-6010 AJ, GIBCO), and 3.7 g/l sodium bicarbonate; pH = 7.4.

Advance Preparation

Media. All powdered medias are mixed according to instructions, pH balanced, sterilized by filtration (.45 μm pore, Nalgene Filters; 450-0045, Nalge Co., Rochester NY), and stored at 4°C.

Ficoll Gradient Fractions: Preparation of Stock Solution. A 25% ficoll solution is prepared by adding 100 g of dialyzed and lyophilized ficoll to 300 g of Hanks solution in an autoclavable media bottle (Sigma Chemical Co.) using a teflon coated stirring bar to mix the components together. Once the ficoll powder is completely dissolved, the bottle is loosely capped, weighed, covered with autoclavable paper or aluminum foil, and autoclaved for 30 min. After cooling, the bottle is reweighed and an additional volume of sterile filtered water

is added to make up for evaporation losses during autoclaving. The stock 25% ficoll solution is stored sealed at 4°C.

Preparation of 25%, 22%, 17.5%, & 11% fractions. Ficoll fractions are made up in sterile 50 ml conical tubes (Falcon 2098, Becton Dickinson, Lincoln Park NJ), 25 g (approximately 25 ml) at a time. To prepare 22%, 17.5%, & 11% ficoll solutions, 22 g, 17.5 g, & 11 g of 25% ficoll stock are pipetted into labeled 50 ml conical tubes using a balance placed in a sterile laminar flow hood to weigh the appropriate quantities. Sufficient Hanks solution is added to each tube to bring its contents up to a total of 25 g. (Example: 17.5% ficoll requires 17.5 g of 25% ficoll stock and 7.5 g of Hanks solution). Tubes are capped, inverted to mix the solutions, and stored at 4°C for up to 1 month.

Surgical Procedure

The procedure is a variation of techniques used by Dr. David Scharp at Childrens Hospital, St. Louis MO, and Dr. Philip Halbon, Joslin Diabetes Center, Boston MA.

1. Anaesthesia. Rats are temporarily rendered quasi-unconscious by a 10 sec exposure to CO_2 gas. During the 30 sec period in which they are incapacitated, they are injected intra-peritoneally with 0.1 ml of sodium pentobarbital per 100 g body weight.
2. Collagenase. Weigh out 1.7 mg collagenase / ml Hanks solution; Make up 20 mls of solution per rat and place in a sterile 50 ml conical tube. (Note: The collagenase concentration will change between different lots of collagenase and must be tested for each lot.)
3. Surgery. Surgery is performed in a sterile laminar flow hood (Labguard, Nuaire Inc., Plymouth MN). Surgical implements are clean but not sterile. Media and flasks are sterile. The surgical procedure is clean but non-sterile. Sterile technique is followed once the pancreas is dissected free from the rat. Sterilized implements, gloves, and surgical procedures may be used if desired but have not proven necessary for sterile islet preparations.

a) The anaesthetized rat is laid on a teflon base pad placed in the sterile hood with its head towards the surgeon.

b) Wash the rat's belly with 70% ethyl alcohol. (Optionally the rat's belly may be shaved and then washed with alcohol).

c) Holding loose belly skin with toothed forceps, using scissors make a midline incision form the xyphoid to the bladder. Make certain that only skin is cut.

d) With a toothed forceps and straight scissors, lift up muscle by xyphoid. Make a straight midline incision form xyphoid to groin. Cut only muscle.

e) Lift up xyphoid with forceps and clip off with scissors. Do not nick liver or diaphragm.

f) Wet sterile gauze or Kimwipes with Hanks solution, place over rib area. Push down and out on ribs from both sides to force the liver up and out of the peritoneal cavity. Pull the liver out over the gauze and fold the gauze over the liver to pull the liver over the sternum and out of the way.

g) With toothed forceps, carefully pull up the duodenum and trace the bile duct through the pancreas to its junction with the duodenum. Using blunt dissection, isolate the bile duct at this juncture and ligate it with silk suture.

h) Trace the bile duct to the opposite end where it passes from the liver into the pancreas. This is where the duct will be cannulated. Using blunt dissection, tease fascia from the duct in the area of cannulation primarily with small curved forceps.

i) After choosing the site for cannulation, tie a loose suture around the duct inferior (towards the pancreas) to the site.

j) If doing multiple rats, bring all rats up to this point. Cover the surgical site with gauze or kimwipes wet with Hanks solution.

k) Add Hanks (20 ml/rat) to collagenase in 50 ml conical tube. Mix. Draw into syringe. Fit 22 gauge needle onto syringe. Fit 5" long section of catheter tubing (#7410, Intramedic Polyethylene Tubing; .023" i.d., .038" o.d.; Clay Adams, division of Becton Dickinson Co., Parsippany, NJ). Cut bevel into free end of catheter. Place loaded syringe next to rat.

l) Hold the bile duct from underneath with small curved forceps. Stabilizing small curved scissors on the gauze make a tiny nick on the top of the duct. DO NOT cut all of the way through the duct.

m) Supporting the bile duct from below with forceps, guide the cannula into the nick and up the duct toward the pancreas. Make certain that the cannula goes into the duct toward the pancreas and not towards the liver. Keep the area wet with Hanks solution at all times. The cannula should go in about 1/2 cm.

n) Pull knot forward and tighten at edge of cut. This holds cannula in duct. Alternatively, the cannula can be held in place by gently gripping the bile duct where the cannula is inserted into it and holding them together with small curved forceps.

o) Slowly inject 10 - 15 ml of distention fluid over about 1/2 to 1 min into the pancreas. The pancreas should visibly distend with minimal leakage. Too much pressure can break the duct, rupture the membrane, or pop the catheter out of the duct. If the pancreas is not distending, check the duodenum. If the duodenum is blowing up, carefully religate the bile duct. Also check for leaks in the cannula, the cannulation site and in the wall of the pancreas. If found take appropriate action (retie suture, move site of cannulation, cover with finger, etc.).

p) Rapidly dissect the pancreas free following distention. Trim along duodenum, then along the stomach. Clip the bile duct and other attachments near the liver. Pull up on the pancreas with blunt forceps and clip restricting attachments underneath the pancreas. Pull up spleen and trim free. Tease/trim pancreas away from remaining attachments to stomach, duodenum, and gut while pulling pancreas away with blunt forceps. Place removed pancreas on clean portion of teflon base pad. Trim away lymph nodes, fat, blood clots, and any non distended sections of pancreas. Place the pancreas in a 50 ml tissue culture flask (Falcon 3013, Becton Dickinson Inc.).

q) Euthanize the rat via cardiac puncture while the rat is still under anaesthesia.

Collagenase Digestion

1. Add remaining collagenase solution (~10 ml/rat) not used for distention to the pancreas in tissue flask.
2. Immerse bottom 1/2 of tissue flask in a 37°C water bath and clamp flask to a wrist shaker (Model 75, Burrell Co, Pittsburgh PA, setting 1 - mild agitation).
3. Shake for 10 min.
4. Remove, shake vigorously by hand for 5 - 10 sec, and return to digestion flask for 3 more minutes of digestion.
5. Shake vigorously by hand (5 - 10 sec), examine to see if slurry is homogeneous. Withdraw a 2-3 drop sample of the slurry. Dilute it in DMEM and examine under a microscope to see if islets are free of acinar tissue. If not, replace the flask on the shaker for 2 - 3 min and repeat.
6. Digestion is complete when islets are free of acinar and vascular attachments.

Post-Digestion Islet Rinses

1. When digestion is complete, immediately add ice cold DMEM with 10% NBCS to halt digestion.
2. Shake capped flask to ensure complete mixing. Filter slurry through 500 μm mesh filter (145765, Spectra/mesh macroporous filter; Spectrum Medical Ind., Los Angeles CA) into sterile 50 ml conical tube.
3. Centrifuge at 100 g for 1 min.
4. Aspirate off supernate.
5. Resuspend the precipitate in DMEM with serum. Mix to a homogeneous suspension using a 10 ml pipet.
6. Centrifuge at 100 g for 1 min.
7. Aspirate off supernate. The remaining tissue pellet should consist of 1 - 1 1/2 ml of tissue per rat.

Ficoll Purification (Ficoll should be at room temperature)

1. Resuspend tissue in 7 ml of 25% ficoll solution.
2. Carefully vortex and/or aspirate through a 10 ml pipet to resuspend into a homogeneous slurry.
3. Carefully layer 5 ml each of 22%, 17.5%, and 11% ficoll in successive layers.
4. Centrifuge for 12 min at 1000 g. Acinar tissue will settle to the bottom. Islets will settle at the 22/17.5 interface. Dead cells, fat and some islets will rise to the 17.5/11 interface.
5. Using a 1 ml pipet, aspirate islets off of the interface between the 17.5% and 22% layers and place them in a 50 ml sterile conical tube pre-filled with 30 ml DMEM with 10% NBCS. Try to transfer as little ficoll solution as possible during this step (2-3 ml).

Post-Ficoll Purification Rinses

1. Fill the 50 ml tube the rest of the way with DMEM with 10% NBCS. Invert to mix. Centrifuge at 100 g for 1 min.
2. Using a 10 ml pipet pre-loaded with 5ml of DMEM with NBCS, aspirate islet pellet off the bottom of the conical tube taking as little surrounding solution as possible. Transfer into a petri dish (Falcon 1007, Becton Dickinson Inc) pre-filled with 10 ml DMEM with 10% NBCS.

Final Rinses and Purification by Hand-picking

1. Place microscope in sterile laminar flow hood.
2. Hand pick islets using a 100 μl micro pipet (Pipetman, Rainin Instrument Co, Woburn MA). Gently swirl petri dish. This "gold panning" motion causes the islets to move to the center of dish. Pipet islets and resuspend in a second petri dish pre-filled with 10 ml DMEM. Repeat swirling / pipetting until most islets are transferred.
3. Repeat step "b" a minimum of 3 times or until desired purity is reached.

Islet Culture

1. Non-attached. Culture purified islets in Falcon 1007 petri dishes, 7 ml DMEM with 10% NBCS and 1.0 g/l glucose, in a 37°C incubator under 95% air, 5% CO_2. Disperse the islets across the dish to discourage clumping. Change the media every 2nd day by "gold panning" the islets to the center and pipetting them to a new petri dish.
2. Collagen-attached. Pre-coat Falcon 1007 petri dishes with 1 ml of 1.25 mg/ml rat tail collagen. This forms a layer of collagen 0.5 mm thick. Collagen is gelled by adding 1 part 10X (ten times concentrated) DMEM to 9 parts collagen solution (1.25 mg collagen per ml of Hanks solution, pH = 2-4) with both solutions on ice. Collagen gels at neutral pH and higher salt concentration of final solution. Cold temperature slows the gelling process. Islets lightly attached to collagen layer which prevented islet aggregation. Media was changed every other day by gently aspirating supernate off of attached islets and very gently pipetting new media on top of collagen layer so as not to dislocate islets.

Worksheet Protocol -- RAT PANCREATOMY

ISOLATION NUMBER: R 6 7 . DATE : 6/30/87

PURPOSE OF ISOLATION: Perifusion : Normal + Hypotic 1st Phase
Static : Long Term pH, pO_2 Study

OF RATS: 2

APPROXIMATE WEIGHTS: 350g, 350g, ____ grams

SODIUM PENTABARBITOL DOSAGE: .4 ml . .4 ml , ____ mls

COLLAGENASE LOT # : ____

COLLAGENASE CONCENTRATION: 1.7 mg/ml. VOLUME/RAT 20 mls/rat

TIME - SURGERY STARTS: 8:50 am

TIME - DISTENTION: 9:10 am.

QUALITY OF DISTENTION: Rat one: Excellent

Rat two: Good

Rat three: ____

DIGESTION :

	TIME (min)			
SHAKER BATH	15 min	5	2	
SETTING	1	.7	.7	
HANDSHAKES	10 sec. Vig	Quick	Quick	
		– close		

TIME - FINAL RINSE: 10:40

ELAPSED TIME (DISTENTION TO FINAL RINSE): 90 min

OF ISLETS : < 100 µm : ~ 400
100 - 250 µm : ~ 400
> 250 µm : ~ 100

QUALTIY OF ISLETS: Excellent. Free of Acinar

NOTES:

Massachusetts Institute of Technology

COMMITTEE ON ANIMAL CARE

PROTOCOL REVIEW FORM

Protocol Number 86-124
Date Submitted 5/21/86
Date DCM Approved / /
Date CAC Approved / /
USDA Pain Category
(For office use only)

PLEASE TYPE OR PRINT CLEARLY

I. GENERAL INFORMATION

DATE SUBMITTED: 5/21/86

A. PRINCIPAL INVESTIGATOR NAME: CLARK COLTON DEPT: Chemical Engineering
B. OFFICE EXT: 4585 LAB EXT: 5483 HOME PHONE NO. IN CASE OF EMERGENCY: 965-0271
C. OTHER PERSONNEL INVOLVED: MARTIN YARMUSH, KEITH DIONNE
D. TITLE OF PROPOSAL: Development of an Artificial Pancreas
E. AGENCY FUNDING THIS PROJECT: none
F. PERIOD OF TIME TO BE COVERED BY GRANT: FROM: -/-/-- TO: / /

II. WRITE A BRIEF DESCRIPTION OF THE PURPOSE OF THE STUDY

The objective of the study is to characterize insulin and glucagon secretion from isolated islets of Langerhans under the physiologic conditions encountered in a biologic artificial pancreas. In particular, the impact of isolation procedures, acute and chronic hypoxia, the synergistic relationship of secretagogues, and variations in device design will be examined as to their effect on insulin release

PLEASE NOTE: A SUBSTANTIAL CHANGE IN PROTOCOL, AN INCREASE IN THE NUMBER OF ANIMALS USED OR A CHANGE IN THE ANIMAL SPECIES USED, WILL NECESSITATE THAT THIS FORM BE RESUBMITTED.

III. SPECIES INFORMATION

A. ANIMAL SPECIES TO BE USED a: Rats b: c: d:
B. ESTIMATED NUMBER OF ANIMALS OF EACH SPECIES
TO BE USED IN THIS STUDY a: 100 b: c: d:
TO BE HOUSED PER DAY a: 5 b: c: d:
C. CHECK FOR EACH SPECIES WHEN APPLICABLE:

a	b	c	d	
				1. RATIONALE FOR USE OF ANIMALS:
—	—	—	—	Studies involve analysis of a process/mechanism that cannot be reconstructed in vitro.
—	—	—	—	Studies cannot or should not be undertaken in humans.
X	—	—	—	Other, explain Studies require animal (pancreatic) tissue
				2. APPROPRIATENESS OF THE SPECIES:
—	—	—	—	Demonstrated similarity of the process under study to that in humans.
X	—	—	—	Large amount of relevant data already has been derived from species.
—	—	—	—	Manipulations required for the experiment (e.g., surgery) require an animal greater than _____ in size.
—	—	—	—	Other, explain
				3. NUMBERS USED:
X	—	—	—	To establish statistical significance of experimental results.
X	—	—	—	To obtain sufficient biological materials to permit the studies proposed.
—	—	—	—	Other, explain

IV. **WRITE A BRIEF DESCRIPTION OF THE PROTOCOL** (Include any particular husbandry requirements, such as special diet or housing.)

The study will utilize normal, healthy laboratory rats (primarily male C-D rats) weighing between 150 and 400 grams as a source of islets of Langerhans to be used for in vitro testing. From arrival until the day of operation, the rats will be fed ad libitum and allowed full freedom of their cages (eg. no special pre-operative procedures are required.).

On the day of surgery, the rats will be anesthetized and their pancreas will be distended and removed (according to the procedure described in section VIII) following which the rats will be sacrificed. The distended pancreas will be digested with collagenase and/or trypsin. The resulting slurry of exocrine and endocrine cells will be purified on a dicontinuous Ficoll gradient. The islets of Langerhans will be handpicked, counted and loaded into a perfusion chamber. The insulin release of the perfused islets will be measured in response to glucose and arginine as a function of oxygen concentration, islet size, and culture time.

On the basis of the secretion data obtained in the above experiments, an artificial device will be modeled, designed, built, and tested in vitro. These are important initial steps toward the ultimate goal of the project which is to develop a rapid acting bio-compatible pancreas suitable for human implantation.

V. SPECIAL QUESTIONS

A. What relevant training have the personnel of this project had in conducting animal experimentation?

Principal investigator: C. Colton: Previous experience with rabbits

Associate investigator(s): M. Yarmush: Medical Training (MD)

Technician(s): _____

Student(s): K.Dionne: Specific training in isolation techniques by D. Scharp (MD) & P. Halbon (MD)

B. Are any animal restraint devices used in this project? YES___ NO X

If "yes", what method and duration? _____

C. Is surgery to be performed? YES X NO___

Is any other manipulation to be performed which would lead to pain or other discomfort which alters well being? YES___ NO X

(If the answer to either of these is "yes", complete Surgical Report/Invasive Procedures section, pages 4 and 5)

Is more than one survival surgical procedure proposed for any animal in this study? YES___ NO X

If "yes", provide justification for multiple survival surgery _____

D. How will the animal be euthanatized? Cardiac puncture while anesthetized

E. Are radionuclides to be used? YES___ NO X

If "yes", indicate Radiation Protection Office approval # _____

F. Are biohazards involved in this study? YES___ NO X

If "yes", date of Committee on Assessment of Biohazards approval _____ / /

G. Will any aspect of the animal experimentation in this study be conducted at another institution? YES___ NO X

Describe the facility and the nature and duration of this activity _____

H. Signature of Principal investigator: _____ / /

date

SURGICAL REPORT/INVASIVE PROCEDURES

(this form must be completed if answer to V-C is "yes")

VI. GENERAL INFORMATION

A. INDIVIDUAL(S) RESPONSIBLE FOR SURGERY & POSTOPERATIVE CARE: Keith Dionne

B. LAB EXT: 3-6483 HOME PHONE NO. IN CASE OF EMERGENCY: 492-7428

C. CHECK LETTER CORRESPONDING TO SPECIES USED: XX a ____ b ____ c ____ d

VII. EXPERIMENTAL DESIGN

A. PREANESTHETICS: 10 sec exposure to Carbon Dioxide

B. ANESTHETIC AGENT(S): Diabutol

C. DOSAGE: 0.08 ml per 100 grams body weight

D. FREQUENCY OF DOSAGE (e.g., daily, weekly): Once 15 minutes before surgery

E. ROUTE OF ADMINISTRATION: Intra-peritoneal

VIII. SURGICAL PROCEDURE: (Please provide detailed information and attach additional pages if necessary.)

On the day of surgery, the rats will be brought to a cell culture room in traveling cages and anesthetized with 0.08 ml diabutol per]00 gram body wieght injected intra-peritoneally. All further procedures are performed while the rat is under anesthesia. Should the rat begin to wake before the operation is completed, additional anethesia will be administered by dripping .05 ml diabutol into the peritoneal cavity.

The surgical protocol consists of the following steps:

1. Holding loose belly skin with toothed forceps, make midline incision from xyphoid to bladder. Make certain only skin is cut.
2. With a toothed forceps and straight scissors, pick up muscle by xyphoid. Make a straight midline incision from xyphoid to groin. Cut only muscle.
3. Lift up xyphoid with forceps, clip off. Be extremely careful not to nick liver or diaphragm.
4. Unfold gauze sponge, place over rib area. Push down and out exposing liver lobes. Pull out liver over sponge and fold sponge over to pull liver out of the way.
5. With curved point of hemostat up, carefully pull up duodenum, trace bile duct to its junction with gut. Carefully clamp gut across at this point. This prevents the gut from distending. Lay hemostat with handles toward the tail, curve up. This exposes bile duct.
6. Quickly and carefully, tease fascia from duct in area of cannulation with small curved forceps.
7. After choosing site for cannulation, tie a loose suture around the duct inferior to the site.
8. Pick up syringe loaded with Hanks solution, push all air out, lay beside rat. Poke bevel of 20 gauge catheter connected to syring through gauze.
9. Stabilizing small curved scissors on the gauze and holding the duct with curved forceps, make a tiny nick on the top of the duct.
10. Supporting duct from below with forceps, guide the cannula into the nick and up the duct toward the pancreas. Make certain cannula goes into the duct toward the pancreas and not the liver. Keep the area wet with Hanks solution at all times. The cannula should go in about 5 mm.
11. Pull knot forward and tighten at edge of cut. This holds cannula in duct.

(continued on page 5)

VIII. SURGICAL PROCEDURE (continued):

12. Slowly inject the distention fluid checking to make certain that the pancreas is blowing up. Too much pressure can break the duct or rupture the membrane. If the pancreas is not distending, check the gut. If the gut is blowing up, carefully reclamp the duct, and start again. Also check for leaks in the cannula or in the wall of the pancreas. Take appropriate action (retie suture, move site of cannulation, cover leak with finger, etc.)

13. Rapidly remove the pancreas following distention. Pull up spleen by fat, remove spleen and pull fat off. Tease pancreas from stomach, duodenum, and gut. Pick up pancreas, tease away all remaining attachments. Pick off lymph nodes, fat, blood clots. Place the pancreas in a chopping bowl with Hanks solution.

14. Euthanize the rat via cardiac puncture while the rat is still under anesthesia.

'end'

IX. POSTOPERATIVE CARE:

none

X. DESCRIBE THE DAILY CARE AND MAINTENANCE PROCEDURES OF SURGICALLY IMPLANTED DEVICES:

none

XI. DESCRIBE ANY NONSURGICAL PROCEDURES THAT ARE PAINFUL OR STRESSFUL TO THE ANIMALS:

none

IX. ADDITIONAL COMMENTS

Procedures for isolating islets of Langerhans have been developed by serveral research teams attempting to develop biologic replacements to the natural pancreas. These procedures and their variations have been summarized in: Diabetes 29, No. 2, Suppl.1, (1980) pp. 19-30. ; and in, World Journal of Surgery 8, (1984) pp. 143-151. The procedure described under our protocol is well researched and is fairly standard among research groups for rat isolations.

For office use only: ☐ ☐ ☐ ☐ ☐ ☐ ☐

Massachusetts Institute of Technology
DIVISION OF COMPARATIVE MEDICINE
45-102 • 37 Vassar Street • Cambridge, MA 02139
(617) 253-1733 or -1718

No. 86- 0644

REQUEST FOR LABORATORY ANIMAL PURCHASE AND CARE

PROJECT

Title (specify) Development of an Art. Pancreas			CAC Protocol Approval # 86-124
Investigator Clark Colton		Authorized Personnel Keith E Dionne	
Telephone # 253-6483	Room # 66-453	Department Chem. Engr.	

TO BE COMPLETED BY REQUISITIONER

A

1. Will radioisotopes be used? ☒ No ☐ Yes*
   If yes, Radiation Protection Office Authorization # _____
2. Will any biohazardous agent be used? (Chemicals, carcinogens, toxic substances, infectious agents, etc.) ☒ No ☐ Yes*
3. Will a surgical procedure be performed? ☐ No ☒ Yes*
4a. Number of animals used where no pain, distress, or use of pain relieving drugs are involved: 0
4b. Number of animals involving pain or distress where appropriate anesthetic, analgesic, or tranquilizer will be used: 20
4c. Number of animals involving pain or distress without use of appropriate anesthetic, analgesic, or tranquilizer ** 0

5. Hazardous Precautions Required:
   ☒ None
   ☐ Biological
   ☐ Chemical
   ☐ Carcinogenic
   ☐ Radioactive
   ☐ Other**

6. Required Protective Clothing:
   ☒ None
   ☐ Mask
   ☐ Gloves
   ☐ Lab Coat
   ☐ Footwear
   ☐ Head Gear
   ☐ Other**

B

1. Species	2. Strain	3. Sex	4. Age	5. Weight	6. Quantity	7. Est. Stay
Sprague/Dawley	+ Rat	M		150-175 g	20	1 month

8. Other specifications: none

9. Special requirements for animal care: none

10. Est. #/cage

11. Date needed:

12. Vendor: Charles River

* If yes, complete DCM form(s), if not previously submitted for this project or if modification of procedure requires new form.
** Attach brief explanation..

REQUEST AND FINANCIAL APPROVAL

Authorized Agent (signature) Keith E Dionne		Date 10/20/86
Administrative Officer (signature)		Date
Purchase Account # 97612	Care Account # 97612	Expiration Date:

TO BE COMPLETED BY DCM

A *Arrangements*

1. Vendor:	3. Other
2. Location	4. Approval (Facility Mgr) Date

B *Purchase*

1. Date confirmed _____ with	5. Charge	6. Purchasing Agent
	Vendor $ _____	7. Debit Acct # .589
2. Lot #	Shipping $ _____	8. Credit Acct # 11449.146
3. Delivery date	Processing $ _____	9. Billing Agent
4. Tattoo	Total $ _____	10. Comments

WHITE: DCM COPY / CANARY: ANIMAL FACILITIES MANAGER / PINK: ACCOUNTING COPY / GOLD: DEPARTMENT COPY

APPENDIX 2B:

INSULIN RADIOIMMUNOASSAY

PURPOSE

This Appendix describes a radio-immuno-assay designed to measure nanogram per ml quantities of insulin utilizing insulin labeled with ^{125}I as a tracer. The protocol was submitted to Massachusetts Institute of Technology's Radiation Protection Office and approved in June, 1986.

DESCRIPTION

Insulin concentration is assayed by a competitive double antibody radio-immuno-assay. In brief, a measured aliquot of media containing the unknown concentration of insulin is mixed with a known volume and concentration of ^{125}I-insulin. An anti-insulin antibody is added to this mixture and competitively binds to the labeled and unlabeled insulin in proportion to their respective concentrations. Thus the higher the concentration of unknown insulin, the less ^{125}I-insulin is bound. Total antibody bound insulin is precipitated out of solution by adding a second antibody which binds to the anti-insulin antibody. The precipitate containing bound labeled and unlabeled insulin is separated from the supernate containing free labeled and unlabeled insulin by centrifugation after which the supernate is decanted off. The bound ^{125}I-insulin is counted in a gamma counter and the bound/free ration of ^{125}I-insulin is computed and compared to a standard curve prepared in an identical manner except with known concentrations of unlabeled insulin.

MATERIALS PREPARATION

Basic Phosphate Buffer (Make up 2-5 liters at a time) (per liter)

1.0	liter deionized/distilled water
7.3	grams EDTA salt (0.025 M)
6.9	grams Monobasic Sodium Phosphate (0.05 M)
0.1	grams Thimersol (0.1g/l) (#T-5125, Sigma Chemical Co, St. Louis MO)

Mix with stirring bar. pH to 7.5 using 1 N HCl or 1 N NaOH.
Storage: 4°C, Indefinite but Thimersol is light sensitive.
Poison: Thimersol. Prevent absorption through skin.

Phosphate Buffer with PEG

1.0 liter basic phosphate buffer
30.0 grams Polyethylene glycol 8000 (PEG) (P-2139, Sigma Chemical Co)

Mix with stirring bar.
Storage: 4°C, Indefinite but Thimersol is light sensitive.
Poison: Thimersol. Prevent adsorption through skin.
Volume use: ~ 100 ml per 100 tube assay.

Phosphate Buffer with 1% BSA

1.0 liter basic phosphate buffer
10.0 grams Bovine Serum Albumin (BSA) RIA grade (A-7888, Sigma Chemical Co)

Mix with stirring bar.
Storage: 4°C, Indefinite but Thimersol is light sensitive.
Poison: Thimersol. Prevent adsorption through skin.
Volume use: ~ 60 ml per 100 tube assay.

Guinea Pig Serum

Initial Mixing

5.0 ml Guinea pig serum (S-3634, Sigma Chemical Co). Reconstitute lyophilized powder with 5 ml of any phosphate buffer.
350 ml phosphate buffer with PEG.

Forms a 1/70 dilution. Mix with stirring bar.
Freeze in 50 ml aliquotes (-70 or -20°C).

Day of Assay (Required on 2nd day)

Thaw 10 ml of sera per 100 tubes of assay.
i) if hand pipeting: Pipet 100 µl of 1/70 GPS into each sample tube.
ii) if using Gilson diluter 401: Mix 50 ml of 1/70 GPS with 400 ml phosphate buffer with PEG and 100 ml of phosphate buffer with 1% BSA. Use this mixture as the reservoir fluid in the diluter and add 1100 µl per sample.
Refrigerate remaining mixed or unmixed GPS.

^{125}I-Insulin Tracer

^{125}I-Porcine Insulin. (~140 µCi/µg; #130, Cambridge Medical Diagnostics, Billirica MA. (617) 935-4050.) Order 5 - 10 µCi per shipment, 60 day half-life, can use up to 45 - 60 days after arrival.

On Arrival of Shipment

Record shipment information	(example)
Lot #	130-8720
Total Activity	10 µCi
Specific Activity	140 µCi/µg
Date of Assay	6/9/86

Calculate total μU of insulin

$$\frac{\text{Total activity}}{\text{Specific activity}} = \frac{10\ \mu Ci}{140 \mu Ci/\mu g}\ (25{,}000\ \mu U/\mu g) = 1785\ \mu U$$

Reconstitute and store ^{125}I-Insulin

Reconstitute lyophilized ^{125}I-insulin with Phosphate buffer with 1% BSA to approximately 10 μU/ml.
Either
i) Aliquot insulin into 10 - 50 ml tubes, label and freeze at -70°C, or
ii) Refrigerate bulk solution at 4°C in a tightly covered flask.

Day of Assay

Thaw/remove 10 ml of ^{125}I-insulin for every 100 samples in the assay.
i) if hand pipeting: aliquot 100 μl of 10 μU/ml ^{125}I-insulin to each sample tube using a micro-pipet; or,
ii) if using Gilson diluter 401: Dilute 10μU/ml ^{125}I-insulin to ~3.0 μU/ml ^{125}I-insulin using phosphate buffer with 1% BSA. Use this mixture as the reservoir fluid in the auto-diluter and add 300 μl to each sample or standard tube.
Refrigerate remaining ^{125}I-insulin in sealed flask.

Antibody #1: Guinea Pig Anti-Rat Insulin Serum

(Ron Gingerich; Linco Research, Inc.; P.O. Box 641;
Eureka MO 63025; phone (314) 527-2188)

On Arrival of Shipment

Record shipment information	(example)
Lot #	ARI-02
Date of Shipment	6/9/86

Reconstitute and titrate antibody concentration

Reconstitute antibody serum with 10 ml of phosphate buffer with 1% BSA.
To determine correct level of dilution, dilute an aliquot of antibody serum to find the concentration which binds between 35 - 45% of the ^{125}I-insulin in an assay containing 0 μU/ml unlabeled insulin.
Dilute remainder of antibody serum with phosphate buffer with 1% BSA according to the above titration. (This will usually be a total addition of 100 ml buffer for a 1000 assay-tube antibody shipment.)
Aliquot diluted antibody into 10 - 50 ml polypropylene test tubes and freeze at -70°C.

On Day of Assay

Thaw / remove 10 ml of anti-insulin antibody per 100 sample tubes of assay.
Aliquot 100 μl per sample tube using either a hand micro-pipet or the Gilson dilutor.
Refrigerate the remaining antibody for up to 4 weeks.

Antibody #2: Goat Anti-Guinea Pig IgG (Pretitered, Linco Research Inc.)

On Arrival of Shipment

Record shipment information	(example)
Lot #	2012
Date of Shipment	6/9/86

Reconstitute and Aliquot for storage

Reconstitute lyophilized powder with 10 ml of phosphate buffer with 1% BSA.
Dilute to 100 ml for a 1000 assay-tube shipment using phosphate buffer with PEG.
Aliquot diluted antibody into 10 - 50 ml polypropylene test tubes and freeze at -70°C.

On Day of Assay (Required on 2nd day)

Thaw / remove 10 ml of Goat Anti-Guinea Pig IgG per 100 sample tubes of assay.
Aliquot 100 µl per sample tube using either a hand micro-pipet or the Gilson dilutor.
Refrigerate the remaining antibody for up to 4 weeks.

Insulin Standards

Desired Standard Range

0.0	ng/ml	-	0.0	µU/ml	
0.12	ng/ml	-	3.125	µU/ml	
0.25	ng/ml	-	6.25	µU/ml	
0.5	ng/ml	-	12.5	µU/ml	
1.0	ng/ml	-	25.0	µU/ml	
2.0	ng/ml	-	50.0	µU/ml	
4.0	ng/ml	-	100.0	µU/ml	
8.0	ng/ml	-	200.0	µU/ml	
16.0	ng/ml	-	400.0	µU/ml	(optional)

Preparation of Stock Solution

Rat insulin standard was generously donated by Eli Lilly & Co (Indianapolis, IN)
Resuspend the 10,000 ng of lyophilized insulin standard from Eli Lilly in 10.00 ml of 0.1 N HCl, or of 0.6% Acetic Acid or of phosphate buffer with 1% BSA.
This is the stock solution. Keep refrigerated at 4°C. Do Not Freeze.
Keep tightly sealed. Do not leave open. Do not contaminate.

Standard Preparation

Prepare new standards every 6 months or if there is any question of contamination.

a) Pre-wet all glassware, test tubes, and pipets with phosphate buffer with 1% BSA to pre-adsorb all surfaces in order to prevent adsorption of insulin. Use a minimum # of implements, and a minimum of exposed surface area. Never use an implement exposed to higher concentrations of Insulin to mix a lower concentration. (Note: Increased accuracy can often be achieved by weighing the fractions rather than volumetrically measuring them).

b) 400 μU/ml: Make up 50 ml of 400 μU/ml insulin in a 50 ml centrifugation tube.

c) 200 μU/ml: Pipet 5.0 ml of phosphate buffer with 1% BSA into a 10 ml polypropylene test tube. With the same pipet add 5.0 mol of 400 μU/ml insulin. Mix.

d) 100 μU/ml: Using the same pipet, add 5.0 ml of 200 μU/ml to new pre-adsorbed 10 ml test tube. Dispose of pipet. With new pipet add 5.0 ml of phosphate buffer with 1% BSA. Mix.

e) Prepare the remainder of the standards according to this protocol.

f) Cap and refrigerate all standards. Do not mix caps. Rinse all pipet tips before withdrawing a standard sample.

INSULIN RADIO-IMMUNO-ASSAY WORKSHEET

Action	Sample	Standard	Q.Control	Total Insulin
Day One				
1. Fill Assay tubes				
Unknown media sample	100 µl	---	---	---
^{125}I-insulin (3 µU/ml)	300 µl	300 µl	300 µl	300 µl
Anti-insulin antibody	100 µl	100 µl	100 µl	---
Insulin standard	---	100 µl	---	---
Quality control sample	---	---	100 µl	---
2. Incubate overnight at 4°C (or at least 4 hrs)	yes	yes	yes	yes
Day Two				
3. Add 100 µl of anti-guinea pig IgG	yes	yes	yes	no
4. Add 100 µl of guinea pig sera diluted 1/70.	yes	yes	yes	no
5. Add 1000 µl of phosphate buffer with PEG & 0.2% BSA	yes	yes	yes	no
6. Incubate for 2 hrs at 4°C.	yes	yes	yes	---
Two hours later				
7. Centrifuge for 15 min at 1000 g.	yes	yes	yes	no
8. Immediately invert tubes & blot to remove supernate.	yes	yes	yes	no
Whenever				
9. Count tubes on gamma counter.	yes	yes	yes	yes
10. Calculate Bound/Free ratios.	yes	yes	yes	---
11. Compute µU/ml using standard curve.	yes	yes	yes	---

STANDARD CURVE PREPARATION AND DATA REDUCTION

The gamma counter averages the bound counts per minute (cpm) of the sample duplicates and of the triplicate standards. The standard curve is prepared using the RS/1 software package (BBN Software Products Co, Cambridge MA). The nominal value of the standards in μU/ml is loaded in column 1 of the spreadsheet. The averaged bound cpm of the standards is loaded in column 2. The bound/free (B/F) ratio of ^{125}I-insulin is calculated in column 3 by dividing the bound cpm in column 2 by the total cpm minus the bound cpm.

$$B/F = \frac{\text{Bound cpm}}{\text{Total cpm - Bound cpm}} \qquad 1$$

The standard curve is formed by plotting the nominal standard values (col 1) vs the B/F ratios (col 3) with the latter as the X-axis. The RS/1 graph is edited to include only B/F ratios > 0 on the X-axis so as not to divide by zero when the data is curve fit. Using the curve fitting option, the data is fit to a polynomial equation of the form:

$$Y = A + B(X) + C(X)^2 + D/X + E/X^2 \qquad 2$$

where "Y" is the value of the nominal standard in μU/ml and "X" is the B/F ratios. The comparison of the curve fit to the data can be checked in the residual table of the curve fitting routine. If necessary, the lower μU/ml values can be weighted so as to insure a good fit over the lower range of the standard curve.

A typical RS/1 standard curve is shown in Figure 1. The discrepancy between the data points and the curve for 100 and 200 μU/ml points as well as the jerkiness of the curve are results of the RS/1 plotting routine and are not real. The residual table comparing the actual fit of the standard curve to the nominal standard values shown in Table 1. As indicated in this table, the polynomial curve follows the actual data very closely. The nominal values of the standards, the mean experimental values, and the standard deviations (in both μU/ml and in % variation) of replicate standard samples are shown in Table 2 for a set of standards (n=4) and for a set of quality control replicates (n=8). In absolute terms, the standard deviation of the standards is between ± 1-2 μU/ml over the entire range of the curve except at the very

highest (in terms of μU/ml) end. In terms of % variation, the lower end of the curve shows correspondingly higher % deviations as the 1-2 μU/ml absolute variation forms a larger percentage of the value being measured. Similar results are seen in the quality control replicates. The standard curves and the quality control points are plotted with standard deviations using Sigmaplot (Jandel Scientific, Sausalito, CA) in Figure 2. In most cases the error bars are contained within the data points.

The advantage of curve fitting the standard curve is that B/F ratios of sample data can be input as the "X" values of the curve fit in order to quickly convert B/F ratios into μU/ml of insulin. On RS/1, this is done by substituting the column containing the B/F ratios for "X" in the curve fit of equation 2 using the values of the constants "A - E" determined with the standards. Once the sample data has been converted to its final form on RS/1, it can either be plotted as an RS/1 plot or printed out as a table of "μU insulin / min - mm^3 islets" vs time (min) and subsequently plotted on Sigmaplot for presentation purposes.

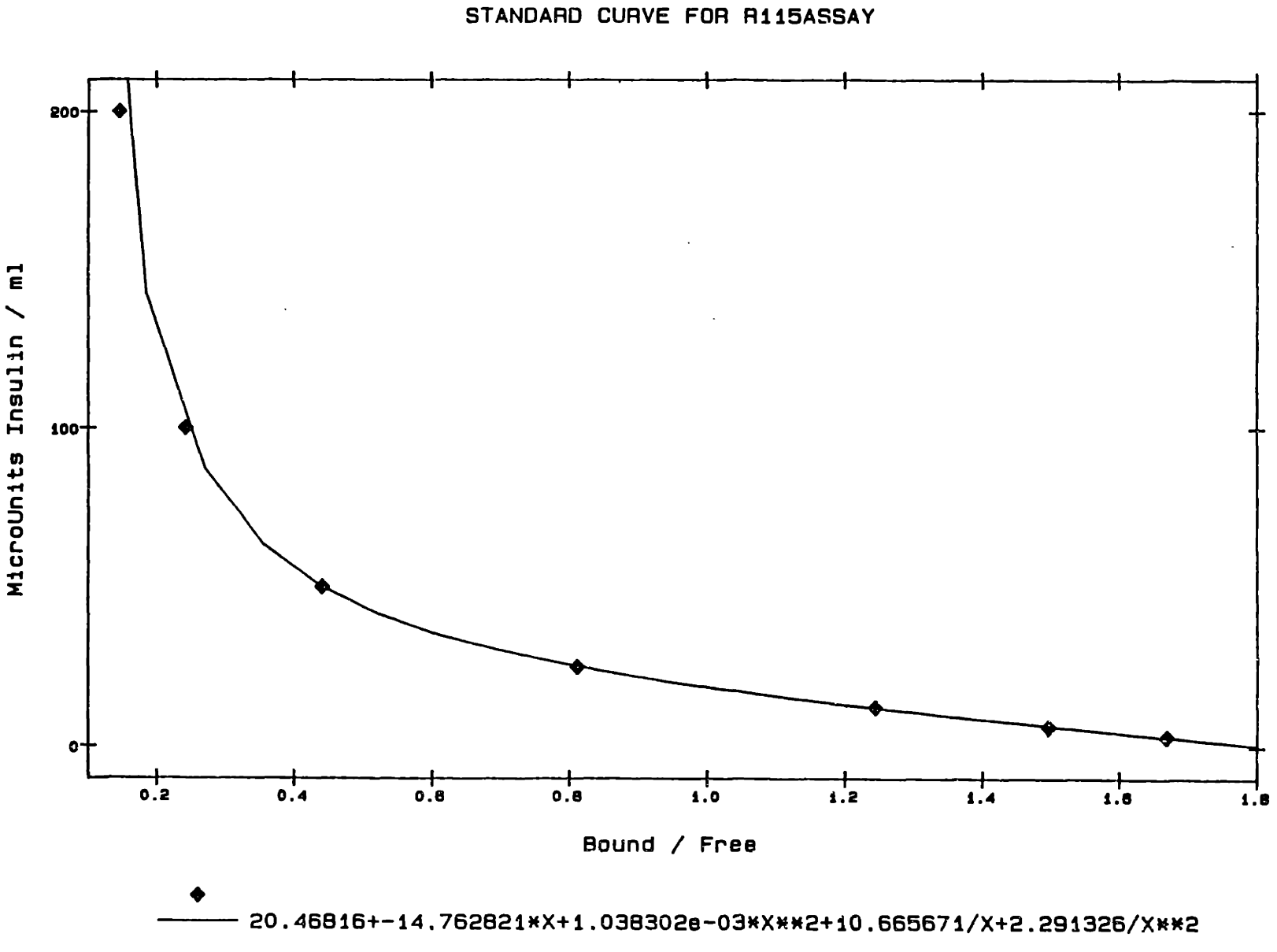
STANDARD CURVE FOR R115ASSAY
MicroUnits Insulin / ml
200
100
0
0.2
0.4
0.6
0.8
1.0
1.2
1.4
1.6
1.8
Bound / Free
20.46816+-14.762821*X+1.038302e-03*X**2+10.665671/X+2.291326/X**2

TABLE 1. RESIDUAL TABLE OF STANDARD CURVE (R115)

B / F	Nominal μU/ml	Fit μU/ml	Residual
1.668698	3.125	3.050835	0.074165
1.496813	6.250	6.521596	-0.271596
1.244572	12.500	12.145398	0.354602
0.810949	25.000	25.133212	-0.133212
0.441045	50.000	49.919305	0.080695
0.242156	100.000	100.012612	-0.012612
0.145429	200.000	199.998908	0.001092

TABLE 2. STATISTICAL ANALYSIS OF STANDARD CURVE AND QUALITY CONTROL POINTS

Standard Curve R115 (n=4)

B/F	Nominal μU/ml	Ave Fit	St. Dev. (n=4)	% Variation
1.668	3.125	3.05	1.36	44.7
1.496	6.25	6.50	1.25	19.2
1.244	12.5	12.13	2.21	18.1
0.811	25.0	25.16	2.25	8.9
0.441	50.0	49.93	1.15	2.3
0.242	100.0	100.00	1.54	1.5
0.145	200.0	200.47	9.47	4.7

Quality Control Samples (n=8)

---	---	9.01	1.20	13.3
---	---	129.40	8.00	6.2
---	---	229.30	11.57	5.0

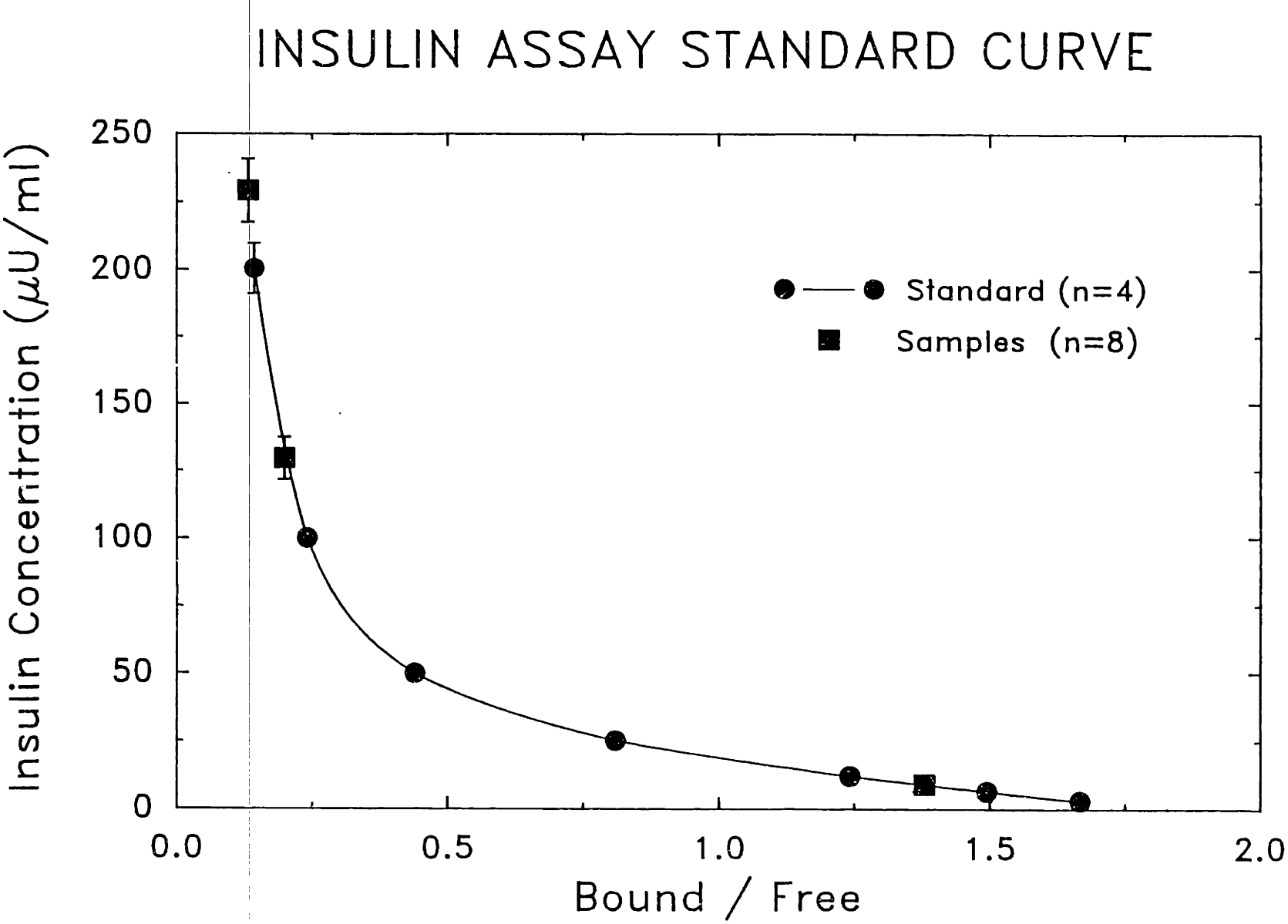
INSULIN ASSAY STANDARD CURVE
Insulin Concentration (μU/ml)
250
200
150
100
50
0
0.0
0.5
1.0
1.5
2.0
Bound / Free
Standard (n=4)
Samples (n=8)

APPENDIX 3A:

REDUCED OXYGEN ISLET PERIFUSIONS

I. Summary

II. 1-Day, Rat, data tables

III. 1-Week, Rat, data tables

IV. 1-Week, Canine, data tables

V. 2-5-Week, Rat, data tables

ISLET PERIFUSION SUMMARY: RAT ISLETS, 1-DAY CULTURE

Perifusion #-pO_2)	S/Smax	Max Secretion ($\mu U/mm^3$-min)	Diameter (μm)
R122D2-5	1.6	668	220 ± 20
R117(600)-5	3.4	314	207 ± 35
R121D2-5	1.4	272	212 ± 20
R117D2-15	16.4	348	214 ± 17
R119D2-15	13.9	598	190 ± 24
R128D2-15	16.5	160	---
R114D2(M)-15	21.0		
R126D2-22	29.6	197	
R113D2(M)-25	47.6		
R114D2(M)-25	47.4		
R117D2-30	63.1	653	218 ± 25
R118D2-30	61.1	985	207
R122D2-30	61.5	564	227 ± 28
R113D2(M)-35	64.9		
R113D2(Mp)-35	66.3		
R115D2(M)-35	60.8		
R117D2-45	85.5	792	210 ± 15
R119D2-45	87.3	612	214 ± 27
R120D2-45	82.9	774	235 ± 23
R113D2(M)-45	75.8		
R113D2(Mp)-45	80.6		
R115D2(M)-45	78.6		
R115D2(Mp)-45	86.3		
R118D2-60	99.5	738	197 ± 17
R120D2-60	98.9	603	240 ± 19
R118D2-142	97.8	894	205 ± 18
R120D2-142	99.9	380	236 ± 23
R121D2-142	98.2	286	198 ± 20
	Average ± stdev:	546.6 ± 246	214 ± 14.5

(M) Indicates data is from a multiple hypoxic step perifusion
(Mp) Indicates data is estimated from post-minimun hypoxia steps.

ISLET PERIFUSION SUMMARY: RAT ISLETS, 1 WEEK

Perifusion #-pO_2)	S/Smax	Max Secretion ($\mu U/mm^3$-min)	Diameter (μm)
R130WK(15)-2	1.0	445	226
R119WK-5	11.2	281	212
R1282K-5	9.0	316	188
R130WK(30)-5	12.6	641	209
R121WK-5	10.8	180	204
R120WK-5	3.2	230	---
R120WK-15	60.0	220	216
R118WK-15	54.3	337	208
R128WK-15	85.3	253	188
R130WK-15	56.9	445	226
R124WK-15	40.3	194	227
R124WK-30	91.9	132	211
R130WK-30	76.8	641	209
R118WK-30	85.3	392	197
R125WK-45	98.4	158	210
R121EK-60	100.0	110	203
R125WK-60	95.6	170	220
R125WK-142	99.4	145	230
	Average ± stdev:	318 ± 166	210.7 ± 13.1

ISLET PERIFUSION SUMMARY: CANINE ISLETS, 1 WEEK

Perifusion #-pO_2)	S/Smax	Max Secretion ($\mu U/mm^3$-min)	Diameter (μm)
C3D7(30,10)-5	8.6	183	173
D3WK(30,10)-5	8.8	500	185
C3D7(30)-10	15.1	183	173
C3D6(45,20)-10	33.0	177	165
D3WK(30)-10	40.0	500	185
C3D6(45)-20	61.4	177	165
C3D7-30	65.7	183	173
D3WK-30	81.8	500	185
C3D7-45	100	177	165
	Average:	287	174

APPENDIX 3A:

REDUCED OXYGEN ISLET PERIFUSIONS

II. 1-Day, Rat, data tables

0 r121d2 142mmhg	1 bound	2 b/f	3 micU/ml	4 flow ml/min	5 micU/ min-mm3	6 time min
1	3806	0.761505	15.867602	0.5	119.305275	-10.5
2	3834	0.771429	15.351120	0.5	115.421957	-4.5
3	2161	0.325305	58.512749	0.5	439.945480	2.0
4	2509	0.398570	44.759240	0.5	336.535637	4.0
5	2749	0.454005	37.752189	0.5	283.851042	11.0
6	2693	0.440681	39.261772	0.5	295.201291	27.0
7	2727	0.448741	38.337361	0.5	288.250835	35.0
8	2745	0.453045	37.857850	0.5	284.645492	39.0
9	2750	0.454245	37.725823	0.5	283.652807	43.0
10	2690	0.439974	39.344551	0.5	295.823695	51.0
11	2726	0.448503	38.364197	0.5	288.452608	59.0
12	2821	0.471503	35.902746	0.5	269.945460	67.0
13	2760	0.456651	37.463264	0.5	281.678674	71.0
14	2791	0.464161	36.661622	0.5	275.651292	75.0
15	2751	0.454485	37.699478	0.5	283.454722	79.0
16				0.5	284.000000	87.0
17				0.5	285.000000	95.0
18				0.5		

0 r121d2 142mmhg	7 %max
1	41.785260
2	40.425174
3	154.085696
4	117.867623
5	99.415467
6	103.390758
7	100.956443
8	99.693714
9	99.346038
10	103.608747
11	101.027111
12	94.545202
13	98.654621
14	96.543602
15	99.276661
16	
17	
18	

$$\frac{Q_{142}}{Q_N} = \frac{280.5 \pm 4}{285.7 \pm 2} = 98.2$$

$$Dia = 198 \pm 20$$

R120D2142 18R x 7C 07-SEP-89 18:31 Page 1

0 r120d2 142mmhg	1 bound	2 b/f	3 micU/ml	4 flow ml/min	5 micU/ min-mm3	6 time min	
1	4629	1.119197	0.000000	0.5	0.000000	-10.5	
2	4665	1.137805	0.000000	0.5	0.000000	-4.5	
3	2499	0.398819	44.722898	0.5	227.019785	2.0	
4	3380	0.627669	23.542184	0.5	119.503471	4.0	
5	3299	0.603549	25.124294	0.5	127.534488	11.0	
6	2198	0.334704	56.316867	0.5	285.872420	27.0	
7	1829	0.263697	78.442430	0.5	398.184922	35.0	Q_N
8	1836	0.264973	77.895652	0.5	395.409403	39.0	
9	1733	0.246445	79.874400	0.5	400.765000	43.0	
10	1722	0.244498	80.008760	0.5	405.889700	51.0	
11	1806	0.259520	79.976000	0.5	403.875500	59.0	
12	1859	0.269186	76.142999	0.5	386.512683	67.0	
13	1875	0.272134	74.962066	0.5	380.518099	71.0	
14	1896	0.276023	73.457622	0.5	372.881328	75.0	
15	1875	0.272134	74.962066	0.5	380.518099	79.0	Q_{142}
16	1863	0.269922	75.844880	0.5	384.999393	95.0	
17				0.5			
18				0.5			

0 r120d2 142mmhg	7 %max
1	0.000000
2	0.000000
3	55.219835
4	29.067783
5	31.021232
6	69.535031
7	96.853698
8	96.178586
9	106.971998
10	108.243560
11	99.128431
12	94.014566
13	92.556455
14	90.698903
15	92.556455
16	93.646476
17	
18	

$$\frac{Q_{142}}{Q_N} = \frac{379.3}{380.0} = 99.9$$

$Dia = 236 \pm 23$

	0 r118 d2 142 mmhg	1 b	2 b/f	3 mic/ml	4 flow ml/min	5 micu/ mm3-min	6 time min	
1		1566	0.401538	52.551195	0.5	415.753129	-13.5	
2		2417	0.792719	17.590779	0.5	139.167554	-4.5	
3		2229	0.688601	23.968108	0.5	189.621104	3.0	
4		2148	0.647378	26.878270	0.5	212.644544	5.0	
5		1792	0.487752	41.260554	0.5	326.428432	12.0	
6		1324	0.319652	68.278797	0.5	540.180358	24.0	
7		1013	0.227487	100.649643	0.5	796.278821	36.0	
8		929	0.204761	114.101067	0.5	902.698319	40.0	
9		934	0.206090	113.212015	0.5	895.664673	44.0	Q_N
10		935	0.206356	113.035696	0.5	894.269749	52.0	
11		937	0.206889	112.684535	0.5	891.491573	60.0	
12		996	0.222819	103.138033	0.5	815.965455	68.0	
13		965	0.214397	107.966058	0.5	854.161853	72.0	
14		933	0.205824	113.388828	0.5	897.063509	76.0	Q_{142}
15		950	0.210363	110.448862	0.5	873.804292	80.0	
16					0.5		88.0	
17					0.5		96.0	
18					0.5			
19					0.5			
20					0.5			

	0 r118 d2 142 mmhg	7
1		48.063946
2		16.088735
3		21.921515
4		24.583184
5		37.737391
6		62.448596
7		92.055355
8		104.358187
9		103.545049
10		103.383786
11		103.062610
12		94.331266
13		98.747035
14		103.706764
15		101.017837
16		
17		
18		
19		
20		

$$Q_{142} = \frac{875.0}{894.5} = 97.8$$

$$Q_N =$$

$$Q_{iu} = 205 \pm 12$$

R11860 20R x 7C 28-OCT-88 16:11 Page 1

	0 r118 d2 60mmHg	1 b	2 b/f	3 mic/ml	4 flow ml/min	5 micu/ min-mm3	6 time min	
1		2684	0.930975	10.798475	0.5	96.243092	-13.5	
2		2710	0.948547	10.049095	0.5	89.564129	-4.5	
3		1831	0.490096	40.999683	0.5	365.416070	3.0	
4		2143	0.625876	28.500871	0.5	254.018461	5.0	
5		1935	0.532764	36.566668	0.5	325.906135	12.0	
6		1453	0.353184	60.982679	0.5	543.517639	24.0	
7		1197	0.273913	81.270931	0.5	724.339852	36.0	
8		1187	0.271005	82.260987	0.5	733.163875	40.0	Q_N
9		1161	0.263504	84.928779	0.5	756.940992	44.0	
10		1343	0.317945	68.692219	0.5	612.230112	52.0	
11		1220	0.280653	79.064850	0.5	704.677808	60.0	
12		1188	0.271295	82.161108	0.5	732.273692	68.0	Q_{60}
13		1149	0.260072	86.208268	0.5	768.344636	72.0	
14		1155	0.261786	85.564577	0.5	762.607636	76.0	
15		905	0.194123	121.776653	0.5	1085.353417	80.0	
16		1089	0.243189	93.118393	0.5	829.932198	88.0	
17		1200	0.274788	80.977647	0.5	721.725911	96.0	
18					0.5			
19					0.5			
20					0.5			

	0 r118 d2 60mmHg 7
1	13.041069
2	12.136061
3	49.514373
4	34.419846
5	44.160723
6	73.647377
7	98.149031
8	99.344698
9	102.566530
10	82.958010
11	95.484798
12	99.224077
13	104.111739
14	103.334368
15	147.066859
16	112.456937
17	97.794839
18	
19	
20	

$$Q_{60} = \frac{734}{738.1 \pm 16.9} = 995$$

Q_N

$Dia = 197 \pm 17$

R120D260 19R x 7C 28-OCT-88 16:35 Page 1

0 r120d2 60mmhg	1 bound	2 b/f	3 micU/ml	4 flow ml/min	5 micU/ min-mm3	6 time min	
1	4512	1.044928	2.500764	0.5	12.270678	-10.5	
2	4834	1.209710	0.000000	0.5	0.000000	-4.5	
3	2992	0.512504	32.049571	0.5	157.259918	2.0	
4	3506	0.658527	21.626268	0.5	106.115153	4.0	
5	3724	0.729338	17.581749	0.5	86.269622	11.0	
6	2334	0.359298	51.261059	0.5	251.526295	27.0	
7	2006	0.293962	67.222466	0.5	329.845272	35.0	
8	1832	0.261789	79.273531	0.5	388.977090	39.0	
9	1720	0.241913	89.071813	0.5	437.055022	43.0	drop @ 60
10	1710	0.240169	90.044231	0.5	441.826451	51.0	
11	1479	0.201197	118.558103	0.5	581.737501	59.0	
12	1457	0.197613	122.038494	0.5	598.814983	67.0	Q_{60}
13	1446	0.195829	123.841625	0.5	607.662539	71.0	
14	1461	0.198263	121.393392	0.5	595.649615	75.0	Raise @ N
15	1330	0.177333	145.822792	0.5	715.519099	79.0	
16	1457	0.197613	122.038494	0.5	598.814983	87.0	
17	1446	0.195829	123.841625	0.5	607.662539	95.0	Q_N
18				0.5			
19							

0 r120d2 60mmhg	7 %max
1	3.184707
2	0.000000
3	40.814928
4	27.540917
5	22.390247
6	65.280637
7	85.607389
8	100.954345
9	113.432396
10	114.670763
11	150.983000
12	155.415257
13	157.711534
14	154.593723
15	185.704412
16	155.415257
17	157.711534
18	
19	

$$Q_{60} = \frac{596}{603 \pm 6} = 98.9\ \%$$

$Q_{N_{post}}$ = peak

$$Dia = 240 \pm 19$$

R1200245 18R x 7C 28-OCT-88 16:36 Page 1

0 r120d2 45mmhg	1 bound	2 b/f	3 micU/ml	4 flow ml/min	5 micU/ min-mm3	6 time min	
1	4738	1.139216	0.000000	0.5	0.000000	-10.5	
2	4928	1.241623	0.000000	0.5	0.000000	-4.5	
3	2992	0.506689	32.560852	0.5	168.884087	2.0	
4	3758	0.731271	17.476892	0.5	90.647781	4.0	
5	3461	0.636681	22.971015	0.5	119.144268	11.0	
6	2106	0.310116	62.437951	0.5	323.848293	27.0	
7	1654	0.228358	97.203080	0.5	504.165352	35.0	
8	1606	0.220272	102.761150	0.5	532.993519	39.0	Q_{Npre}
9	1527	0.207191	113.130368	0.5	586.775769	43.0	Drop 45
10	1560	0.212621	108.598283	0.5	563.269105	51.0	
11	1492	0.201485	118.286022	0.5	613.516710	59.0	
12	1449	0.194549	125.165531	0.5	649.198810	67.0	Q_{45}
13	1475	0.198733	120.930387	0.5	627.232296	71.0	
14	1447	0.194228	125.501288	0.5	650.940289	75.0	77 - Reset N.
15	1203	0.156356	180.744136	0.5	937.469584	79.0	
16	1325	0.174987	149.116842	0.5	773.427603	87.0	Q_{Npost}
17	1323	0.174677	149.562318	0.5	775.738163	95.0	
18				0.5			

0 r120d2 45mmhg	7 %max
1	0.000000
2	0.000000
3	31.217022
4	16.755597
5	22.022970
6	59.861052
7	93.191377
8	98.520059
9	108.461325
10	104.116286
11	113.404198
12	119.999780
13	115.939426
14	120.321680
15	173.284581
16	142.962588
17	143.389679
18	

$Q_{Npre} = 586$

$Q_{N\,post} = 774$

$Q_{45} = 642 \pm 13$

$$\frac{Q_{45}}{Q_{Npost}} = \frac{642}{774} = 82.9\ \%$$

$Dia = 235 \pm 23.5$

R11945 20R x 7C 28-OCT-88 16:13 Page 1

0 r119 d2 45mmHg	1 b	2 b/f	3 nic/ml	4 flow ml/min	5 micu/ min-mm3	6 time min	
1	2648	0.912789	11.599249	0.5	78.056858	-13.5	
2	2476	0.805727	16.877648	0.5	113.577711	-4.5	
3	1598	0.404455	52.102371	0.5	350.621606	3.0	
4	1649	0.422821	49.402059	0.5	332.449923	5.0	
5	1406	0.339368	63.813534	0.5	429.431587	12.0	
6	1091	0.244729	92.441737	0.5	622.084366	24.0	
7	1118	0.252313	89.249846	0.5	600.604615	36.0	
8	1101	0.247527	91.237296	0.5	613.979114	40.0	Q_N
9	1092	0.245008	92.320077	0.5	621.265658	44.0	— Drop to 45
10	1246	0.289565	76.322481	0.5	513.610235	52.0	
11	1299	0.305647	71.813274	0.5	483.265637	60.0	
12	1269	0.296495	74.314604	0.5	500.098274	68.0	
13	1194	0.274168	81.185397	0.5	546.335111	72.0	Q_{45}
14	1179	0.269794	82.680162	0.5	556.394095	76.0	— Raise
15	846	0.179885	133.903295	0.5	901.098890	80.0	
16	1090	0.244449	92.563671	0.5	622.904917	88.0	
17	1215	0.280341	79.164304	0.5	532.734209	96.0	
18				0.5			
19				0.5			
20				0.5			

0 r119 d2 45mmHg	7
1	12.754389
2	18.558450
3	57.291112
4	54.321883
5	70.168560
6	101.647772
7	98.138009
8	100.323385
9	101.513996
10	83.923241
11	78.964973
12	81.715404
13	89.270443
14	90.914068
15	147.238381
16	101.781849
17	87.048073
18	
19	
20	

$$Q_{45} = \frac{534}{Q_N = 612 \pm 10} = 87.3$$

$$Dia = 214 \pm 27$$

R11745 20R x 7C 28-OCT-88 16:12 Page 1

0 r117 d2 45	1 b	2 b/f	3 mic/ml	4 flow ml/min	5 micu/ min-mm3	6 time min	
1	2203	0.661959	25.820124	0.5	190.695156	-13.5	
2	2331	0.728437	21.377255	0.5	157.882236	-4.5	
3	1571	0.396717	53.306236	0.5	393.694506	3.0	
4	1693	0.441115	46.907123	0.5	346.433702	5.0	
5	1345	0.321309	67.881955	0.5	501.343834	12.0	
6	1146	0.261345	85.729133	0.5	633.154601	24.0	
7	983	0.216139	106.929193	0.5	789.728162	36.0	
8	985	0.216674	106.614898	0.5	787.406926	40.0	Q_N
9	976	0.214270	108.042321	0.5	797.949197	44.0	
10	1122	0.254479	88.379012	0.5	652.725345	52.0	— Drop to 45
11	1168	0.267706	83.413422	0.5	616.051859	60.0	
12	1092	0.246001	91.889924	0.5	678.655272	68.0	
13	1059	0.236807	96.035156	0.5	709.269988	72.0	Q_{45}
14	1133	0.257617	87.147803	0.5	643.632223	76.0	
15	862	0.184622	129.600112	0.5	957.164783	80.0	— Raise to 142
16	1008	0.222861	103.115000	0.5	761.558348	88.0	
17	1076	0.241526	93.860554	0.5	693.209408	96.0	
18				0.5			
19				0.5			
20				0.5			

0 r117 d2 45	7
1	24.077671
2	19.934626
3	49.708902
4	43.741629
5	63.300989
6	79.943763
7	99.713152
8	99.420066
9	100.751161
10	32.414816
11	77.784326
12	85.688797
13	89.554291
14	81.266695
15	120.854139
16	96.156357
17	87.526440
18	
19	
20	

$$Q_{45} = \frac{677 \pm 32}{791.7 \pm 7.6} = 85.5$$

$Q_N =$

$$Dia = 210 \pm 15$$

R11730 20R x 7C 28-OCT-88 16:16 Page 1

0 r117 d2 30mmHg	1 b	2 b/f	3 mic/ml	4 flow ml/min	5 micu/ mm3-min	6 time min	
1	2692	0.967301	9.275099	0.5	59.152417	-13.5	
2	2814	1.057497	5.904783	0.5	37.658055	-4.5	
3	1596	0.411446	51.049383	0.5	325.570047	3.0	
4	1971	0.562500	33.781580	0.5	215.443748	5.0	
5	1644	0.429131	48.520952	0.5	309.444849	12.0	
6	1202	0.281301	78.859011	0.5	502.927364	24.0	
7	1025	0.230337	99.190607	0.5	632.593156	36.0	
8	1002	0.224011	102.490639	0.5	653.639278	40.0	Q_w
9	983	0.218833	105.365612	0.5	671.974567	44.0	— Drop to 30
10	1432	0.354192	60.784622	0.5	387.657028	52.0	
11	1336	0.322783	67.532398	0.5	430.691311	60.0	
12	1399	0.343229	62.999736	0.5	401.784033	68.0	Q_{30}
13	1388	0.339613	63.761176	0.5	406.640151	72.0	
14	1269	0.301712	72.868909	0.5	464.725187	?76.0	— Raise to 142
15	851	0.184040	130.113547	0.5	829.805785	80.0	
16	1028	0.231167	98.773875	0.5	629.935424	88.0	
17	1024	0.230061	99.330200	0.5	633.483422	96.0	
18				0.5			
19				0.5			
20				0.5			

$$Q_{30} = \frac{412}{653} = 63.1$$

$Q_w =$

0 r117 d2 30mmHg	7
1	9.058563
2	5.766930
3	49.857588
4	32.992917
5	47.388185
6	77.017973
7	96.874909
8	100.097899
9	102.905753
10	59.365548
11	65.955790
12	61.528948
13	62.272611
14	71.167716
15	127.075924
16	96.467906
17	97.011244
18	
19	
20	

$D_{TL} = 210 \pm 25$

R1180230 20R x 7C 28-OCT-88 16:17 Page 1

0 r118 d2 30mmhg	1 b	2 b/f	3 mic/ml	4 flow ml/min	5 micu/ mm3-min	6 time min	
1	2977	1.187475	1.992530	0.5	15.049321	-13.5	
2	3065	1.267053	0.105174	0.5	0.794364	-4.5	
3	2409	0.783415	18.111310	0.5	136.792372	3.0	
4	2735	0.994907	8.182804	0.5	61.803658	5.0	
5	2361	0.756004	19.697660	0.5	148.773865	12.0	
6	1443	0.357090	60.221489	0.5	454.845080	24.0	
7	956	0.211131	109.967288	0.5	830.568644	36.0	
8	871	0.188814	126.023107	0.5	951.836156	40.0	Q_{140}
9	831	0.178594	135.127519	0.5	1020.600594	44.0	— Drop to 30
10	1478	0.368947	58.005965	0.5	438.111514	52.0	
11	1198	0.279515	79.429183	0.5	599.918303	60.0	
12	1114	0.254920	88.204061	0.5	666.193814	68.0	
13	1184	0.275349	80.790857	0.5	610.202847	72.0	Q_{30}
14	1204	0.281308	78.856723	0.5	595.594588	76.0	— Raise to 140
15	670	0.139177	187.913111	0.5	1419.283314	80.0	
16	806	0.172296	141.448352	0.5	1068.341030	88.0	
17	755	0.159653	156.161335	0.5	1179.466274	96.0	
18				0.5			
19				0.5			
20				0.5			

$$Q_{30} = \frac{602}{985} = 61.1\ \%$$

Q_N

0 r118 d2 30mmhg	7
1	1.609553
2	0.084959
3	14.630200
4	6.610017
5	15.911643
6	48.646533
7	88.830871
8	101.800658
9	109.155144
10	46.856846
11	64.162385
12	71.250675
13	65.262337
14	63.699956
15	151.795007
16	114.261073
17	126.146126
18	
19	
20	

$Dia = 207$

0 r122d2 30mmhg	1 bound	2 b/f	3 micU/ml	4 flow ml/min	5 micU/ min-mm3	6 time min	
1	3729	0.714368	18.402821	0.5	103.619489	-10.5	
2	3925	0.781250	14.845176	0.5	83.587702	-4.5	
3	1802	0.252134	83.757563	0.5	471.607897	2.0	
4	2320	0.349977	53.070805	0.5	298.822101	4.0	
5	1978	0.283747	70.638912	0.5	397.741620	11.0	
6	1684	0.231796	95.009686	0.5	534.964448	27.0	
7	1623	0.221540	101.850238	0.5	573.481067	35.0	
8	1744	0.242054	99.450000	0.5	563.091825	39.0	Q_N
9	1653	0.226562	98.387578	0.5	553.984111	43.0	
10	2217	0.329323	57.553987	0.5	324.065241	51.0	— Drop to 30
11	2173	0.320691	59.653039	0.5	335.884227	59.0	
12	2138	0.313904	61.411571	0.5	345.785872	67.0	
13	2133	0.312940	61.669595	0.5	347.238711	71.0	Q_{30}
14	2136	0.313518	61.514571	0.5	346.365829	75.0	
15	1487	0.199276	120.400212	0.5	677.929123	79.0	— Raise to 1
16	1623	0.221540	101.850238	0.5	573.481067	87.0	
17	1513	0.203470	116.444745	0.5	655.657348	95.0	
18	1568	0.212437	108.746006	0.5	612.308592		
19	1539	0.207692	112.697537				
20	1526	0.205577	114.546040				
21							

0 r122d2 30mmhg	7 %max
1	19.088052
2	15.397937
3	86.876282
4	55.046901
5	73.269157
6	98.547379
7	105.642639
8	104.307602
9	102.051047
10	59.697014
11	61.874224
12	63.698236
13	63.965867
14	63.805071
15	124.883324
16	105.642639
17	120.780574
18	112.795172

$$\frac{Q_{30}}{Q_N} = \frac{346.5 \pm .7}{563.7} = 61.5\%$$

$Dia = 227 \pm 28$

R126D222 30R x 9C 03-OCT-88 12:51 Page 1

0 r126d222 rapid	1 bound	2 b/f	3 micU/ml	4 micU/ min-mm3	5 time	6 o2:mmHg	
1	3972	0.863854	7.027631	43.922691	-9.0	142	
2	3988	0.870362	6.716399	41.977495	-4.5	142	
3	3988	0.870362	6.716399	41.977495	0.0	142	
4	1746	0.255862	74.553699	465.991868	0.5	142	
5	1246	0.170126	135.161589	844.759934	1.5	142	
6	2160	0.336973	53.025963	331.412269	2.5	142	
7	3026	0.545815	27.634521	172.715759	3.5	142	
8	3442	0.671217	18.103045	113.144032	4.5	142	
9	2717	0.464206	35.390717	221.191984	11.0	142	
10	2707	0.461709	35.656705	222.854404	19.0	125	
11	2939	0.521932	29.741502	185.884388	31.0	101	Q_{24}
12	2890	0.508803	30.951533	193.447083	36.0	100	
13	2865	0.502191	31.576111	197.350693	41.0	100	— Drop to 22
14	3072	0.558749	26.539535	165.872094	42.0	40	
15	3699	0.759392	12.570026	78.562660	43.0	32	
16	3795	0.794764	10.575909	66.099433	44.0	27	
17	3825	0.806112	9.962060	62.262875	45.0	26	
18	3677	0.751482	13.033006	81.456289	46.0	25	
19	3948	0.854176	7.497688	46.860553	47.0	25	
20	3757	0.780594	11.359984	70.999900	49.0	24	
21	3863	0.820693	9.191396	57.446228	57.0	24	Q_{22}
22	3877	0.826124	8.909488	55.684300	65.0	24	
23	3867	0.822241	9.110738	56.942111	73.0	24	— Raise to 142
24	1421	0.198769	105.996892	662.480573	74.0	79	
25	1174	0.158734	151.608761	947.554754	75.0	110	
26	1508	0.213537	95.431917	596.449484	76.0	120	
27	1882	0.281400	66.053646	412.835289	77.0	137	
28	2242	0.354298	49.918814	311.992587	82.0	140	
29	2165	0.338017	52.829010	330.181313	90.0	142	
30							

D 2

R11715 20R x 7C 28-OCT-88 16:18 Page 1

0 r117 d2 15mmHg	1 b	2 b/f	3 mic/ml	4 flow ml/min	5 micu/ min-mm3	6 time min	
1	1998	0.566969	33.381638	0.5	231.816931	-13.5	
2	2183	0.653789	26.409007	0.5	183.395885	-4.5	
3	2072	0.600580	30.513165	0.5	211.896980	3.0	
4	2209	0.666767	25.478290	0.5	176.932571	5.0	
5	1886	0.518702	37.965935	0.5	263.652327	12.0	
6	1654	0.427611	48.731088	0.5	338.410332	24.0	
7	1688	0.440271	47.018324	0.5	326.516142	36.0	
8	1630	0.418808	49.974287	0.5	347.043663	40.0	Q_N
9	1626	0.417351	50.184386	0.5	348.502677	44.0	Drop to 15
10	2788	1.019751	7.246261	0.5	50.321255	52.0	
11	2568	0.869330	13.621282	0.5	94.592239	60.0	
12	2742	0.986331	8.516249	0.5	59.140617	68.0	
13	2672	0.937544	10.515564	0.5	73.024753	72.0	Q_{15}
14	2766	1.003628	7.849099	0.5	54.507631	76.0	
15	1707	0.447444	46.084381	0.5	320.030422	80.0	Raise to 142
16	1779	0.475287	42.681517	0.5	296.399423	88.0	
17	1681	0.437646	47.366506	0.5	328.934068	96.0	
18				0.5			
19				0.5			
20				0.5			

0 r117 d2 15mmHg	7 normalized values
1	67.981505
2	53.781785
3	62.139877
4	51.886384
5	77.317398
6	99.240567
7	95.752534
8	101.772335
9	102.200199
10	14.756966
11	27.739660
12	17.343289
13	21.414884
14	15.984642
15	93.850564
16	86.920652
17	96.461604
18	
19	
20	

$Q_{15} = 62.2$

$Q_N = 347.8$

$\frac{62.2}{347.8} = 16.4$

Dia = 214 ± 17.7

D2

R11915 20R x 7C 28-OCT-88 16:19 Page 1

0 r119 d2 15 mmHg	1 b	2 b/f	3 mic/ml	4 flow ml/min	5 micu/ min-mm3	6 time min	
1	2912	1.085757	4.962754	0.5	48.182079	-13.5	
2	2889	1.068022	5.547797	0.5	53.862105	-4.5	
3	2522	0.820964	16.063444	0.5	155.955769	3.0	
4	2761	0.974585	8.981520	0.5	87.199226	5.0	
5	2411	0.757462	19.611252	0.5	190.400506	12.0	
6	1923	0.523835	37.448553	0.5	363.578185	24.0	
7	1536	0.378512	56.314952	0.5	546.747108	36.0	Q_N
8	1411	0.337318	64.253160	0.5	623.817083	40.0	
9	1414	0.338278	64.046654	0.5	621.812173	44.0	— Drop to 15
10	2622	0.882234	13.004477	0.5	126.257057	52.0	
11	2632	0.888589	12.705900	0.5	123.358253	60.0	
12	2799	1.001431	7.932669	0.5	77.016203	68.0	
13	2742	0.961431	9.514577	0.5	92.374529	72.0	Q_{15}
14	2786	0.992165	8.288840	0.5	80.474176	76.0	
15	952	0.205084	113.383580	0.5	1105.665823	80.0	— Raise to 142
16	1300	0.302748	72.588108	0.5	704.738913	88.0	
17				0.5		96.0	
18				0.5			
19				0.5			
20				0.5			

$$\frac{Q_{15}}{Q_N} = \frac{83.3}{597.7} = 13.9\ \%$$

0 r119 d2 15 mmHg	7
1	8.057204
2	9.007041
3	26.079560
4	14.581810
5	31.839549
6	60.799028
7	91.429282
8	104.317238
9	103.981969
10	21.113220
11	20.628470
12	12.878964
13	15.447246
14	13.457220
15	184.893950
16	117.849317
17	
18	
19	
20	

Dia = 190 ± 24

R128D215 25R x 6C 03-OCT-88 12:04 Page 1

0 r128d215 1st phase	1 bound	2 b/f	3 micU/ml	4 micU/mm3-min	5 Time min	6 % norm	
1	977	0.843696	0.774572		-30.0	0.817059	15 mm Hg
2	969	0.831046	1.599471		-20.0	1.687205	
3	982	0.851691	0.256528		-10.0	0.270599	
4	971	0.834192	1.393694		-0.5	1.470141	
5	743	0.533764	24.006205		1.0	25.323001	
6	974	0.838932	1.084473		3.0	1.143959	
7	991	0.866259	0.000000		5.0	0.000000	
8	958	0.813934	2.726115		14.0	2.875649	
9	951	0.803209	3.438753		26.0	3.627377	
10	892	0.717619	9.336477		32.0	9.848604	
11	814	0.616200	16.973855	} 15.6	36.0	17.904910	Q15
12	842	0.651199	14.238159		40.0	15.019155	— 42 - N air.
13	305	0.166667	121.635616		44.0	128.307612	
14	462	0.276151	62.318864		48.0	65.737199	
15	421	0.245624	72.221030		52.0	76.182521	
16	370	0.209632	88.678488		60.0	93.542709	
17	353	0.198092	95.652163	} 94.8	68.0	100.898906	
18	355	0.199438	94.782887		72.0	99.981948	QN
19	357	0.200787	93.927296		76.0	99.079427	— 100 Glucose.
20	460	0.274627	62.751675		80.0	66.193750	
21	671	0.458333	31.553784		84.0	33.284582	
22	751	0.542630	23.200570		88.0	24.473175	
23	873	0.691759	11.205237		92.0	11.819871	
24							
25							

$$\frac{Q_{15}}{Q_N} = \frac{15.6}{94.8} = 16.5\%$$

p2

R1175600 21R x 7C 28-OCT-88 16:20 Page 1

0 r117 d3 5mmHg 600G	1 b	2 b/f	3 mic/ml	4 flow ml/min	5 micu/ min-mm3	6 time min	
1	2774	0.990007	8.372674	0.5	60.062224	-13.5	
2	3133	1.282440	0.000000	0.5	0.000000	-4.5	
3	2428	0.771283	18.803475	0.5	134.888627	3.0	
4	2631	0.893379	12.483065	0.5	89.548530	5.0	
5	2120	0.613426	29.476624	0.5	211.453546	12.0	
6	1960	0.542035	35.674109	0.5	255.911833	24.0	
7	1795	0.474742	42.745010	0.5	306.635655	36.0	Q_N
8	1734	0.451327	45.589155	0.5	327.038413	40.0	Q_N
9	1787	0.471628	43.10997(	0.5	309.253776	44.0	Q_N — Drop to 5
10	2774	0.990007	8.372674	0.5	60.062224	52.0	
11	3105	1.256576	0.332503	0.5	2.385243	60.0	
12	3090	1.242961	0.637440	0.5	4.572741	68.0	Q_5
13	3051	1.208317	1.462157	0.5	10.488931	72.0	Q_5
14	2937	1.112922	4.106085	0.5	29.455414	76.0	Q_5
15	2937	1.112922	4.106085	0.5	29.455414	80.0	
16	3079	1.233080	0.865483	0.5	6.208633	88.0	Raise to 14
17	2894	1.079045	5.181737	0.5	37.171714	96.0	
18	2879	1.067482	5.565927	0.5	39.927742		
19	3075	1.229508	0.949315	0.5	6.810005		
20	2903	1.086046	4.953399	0.5	35.533706		
21							

$$\frac{Q_5 = 11.8}{Q_N = 314} = 3.74\ \%$$

0 r117 d3 5mmHg 600G	7
1	19.128097
2	0.000000
3	42.958161
4	28.518640
5	67.341894
6	81.500584
7	97.654667
8	104.152361
9	98.488464
10	19.128097
11	0.759632
12	1.456287
13	3.340424
14	9.380705
15	9.380705
16	1.977272
17	11.838125
18	12.715849
19	2.168791
20	11.316467
21	

Dia = 207 ± 35

R121D25 18R x 7C 07-SEP-89 17:31 Page 1

0 r121d2 5mmhg	1 bound	2 b/f	3 micU/ml	4 flow ml/min	5 micU/ min-mm3	6 time min	
1	3428	0.645939	22.394523	0.5	158.377108	-10.5	
2	3622	0.708390	18.735250	0.5	132.498234	-4.5	
3	1931	0.283804	70.619009	0.5	499.427224	2.0	
4	2301	0.357631	51.575977	0.5	364.752309	4.0	
5	2570	0.416869	42.217934	0.5	298.570964	11.0	
6	2620	0.428455	40.734824	0.5	288.082207	27.0	
7	2720	0.452203	37.950941	0.5	268.394210	35.0	Q_N
8	2795	0.470539	36.001036	0.5	254.604213	39.0	Q_N
9	2813	0.475008	35.548556	0.5	251.404212	43.0	Q_N — Drop to 5
10	4452	1.039458	2.741199	0.5	19.386129	51.0	
11	4791	1.214757	0.512430	0.5	3.532450	59.0	
12	4752	1.193071	0.493420	0.5	3.334250	67.0	Q_5
13	4687	1.157856	0.523240	0.5	3.732450	71.0	Q_5
14	4686	1.157323	0.513240	0.5	3.534250	75.0	Q_5
15	2542	0.410463	43.078219	0.5	304.655011	79.0	— Raise to 11
16	3520	0.674976	20.647368	0.5	146.020989	87.0	
17	3414	0.641609	22.662934	0.5	160.275345	95.0	
18				0.5			

0 r121d2 5mmhg	7 %max
1	61.355560
2	51.330041
3	193.478954
4	141.305664
5	115.666898
6	111.603536
7	103.976372
8	98.634104
9	97.394418
10	7.510219
11	0.000000
12	0.000000
13	0.000000
14	0.000000
15	118.023868
16	56.568779
17	62.090940
18	

$$\frac{Q_5}{Q_N} = \frac{3.5}{258.1} = 1.4\ \%$$

Dia = 212 ± 20.4

R122D25 18R x 7C 28-OCT-88 16:41 Page 1

0 r122d2 5mmhg	1 bound	2 b/f	3 micU/ml	4 flow ml/min	5 micU/ min-mm3	6 time min
1	4477	1.031567	3.088836	0.5	19.574373	-10.5
2	4623	1.102289	0.002827	0.5	0.017916	-4.5
3	1912	0.276901	73.126117	0.5	463.410119	2.0
4	2781	0.460736	37.023984	0.5	234.626010	4.0
5	2271	0.346929	53.689402	0.5	340.237020	11.0
6	1744	0.246571	86.571118	0.5	548.612914	27.0
7	1600	0.221699	101.737070	0.5	644.721607	35.0
8	1566	0.215970	105.968258	0.5	671.535220	39.0
9	1543	0.212125	108.997837	0.5	690.734076	43.0
10	2863	0.480853	34.969286	0.5	221.605109	51.0
11	4207	0.912581	8.464062	0.5	53.637909	59.0
12	4470	1.028295	3.233219	0.5	20.489348	67.0
13	4538	1.060528	1.817317	0.5	11.516585	71.0
14	4629	1.105301	-0.127259	0.5	-0.806459	75.0
15	3963	0.816440	13.070821	0.5	82.831565	79.0
16	2568	0.410946	43.012390	0.5	272.575349	87.0
17	1953	0.284528	70.365699	0.5	445.916980	95.0
18				0.5		

Q_N

Q_5

0 r122d2 5mmhg	7 %max
1	2.925915
2	0.002678
3	69.269076
4	35.071152
5	50.857552
6	82.004920
7	96.370943
8	100.378957
9	103.248741
10	33.124829
11	8.017625
12	3.062683
13	1.721463
14	-0.120547
15	12.381400
16	40.743699
17	66.654257
18	

$Q_5 = \frac{10.6 \pm 10.3}{668 \pm 23} = 1.6\ \%$

$Dia = 220 \pm 20$

0 R100 600G Cham B PERI	1 Bound	2 b/f	3 mic/ml	4 flow ml/min	5 micu/ min-mm3	6 time min
1	8878	1.562732	4.457780	0.66	28.453913	-7.5
2	9010	1.730198	1.562696	0.66	9.974658	-1.5
3	8607	1.276104	10.046990	0.66	64.129727	2.5
4	8818	1.493219	5.722609	0.66	36.527290	4.5
5	8654	1.321128	9.091943	0.66	58.033677	11.0
6	8594	1.263957	10.311102	0.66	65.815542	23.0
7	8753	1.422047	7.069263	0.66	45.122953	35.0
8	8665	1.331924	8.868186	0.66	56.605445	39.0
9	8651	1.318201	9.152944	0.66	58.423046	43.0
10	8932	1.628694	3.295225	0.66	21.033348	51.0
11	9002	1.719428	1.743781	0.66	11.130515	59.0
12	9018	1.741054	1.380754	0.66	8.813322	67.0
13	8990	1.703431	2.013850	0.66	12.854365	75.0
14	9029	1.756122	1.129136	0.66	7.207254	83.0
15	8253	0.985956	17.421295	0.66	111.199756	88.0
16	8686	1.352816	8.440536	0.66	53.875761	96.0
17	8475	1.158513	12.739163	0.66	81.313806	104.0
18	8350	1.057836	15.340118	0.66	97.915648	112.0
19	7666	0.639417	32.439482	0.66	207.060525	115.0
20	7573	0.595314	35.425939	0.66	226.123018	123.0

0 R113 day2	1 b	2 b/f	3 mic/ml	4 flo ml/min	5 micu/ min-mm3	6 time	
1	1749	0.971667	3.355539	0.5	18.641882	-14	
2	1798	1.026842	0.341247	0.5	1.895814	-6	
3	771	0.277538	61.828384	0.5	343.491022	3	
4	888	0.333709	50.631104	0.5	281.283911	5	
5	600	0.203459	86.791711	0.5	482.176170	12	
6	454	0.146688	125.820434	0.5	699.002409	24	
7	400	0.127024	149.077595	0.5	828.208862	36	
8	377	0.118852	161.461320	0.5	897.007332	40	S_n
9	373	0.117443	163.805184	0.5	910.028802	44	Drop to
10	496	0.162463	111.824410	0.5	621.246720	52	
11	468	0.151899	120.824296	0.5	671.246091	60	
12	468	0.151899	120.824296	0.5	671.246091	64	S_{45}
13	476	0.154897	118.125143	0.5	656.250797	72	Drop to 35
14	526	0.173999	103.419109	0.5	574.550606	80	
15	519	0.171287	105.278848	0.5	584.882489	84	S_{35}
16	543	0.180639	99.134153	0.5	550.745295	88	prop to 2
17	681	0.237448	73.236096	0.5	406.867199	96	
18	662	0.229304	76.082442	0.5	422.680231	104	S_{25}
19	658	0.227603	76.705053	0.5	426.139185	108	Raise to 3
20	431	0.138230	134.874315	0.5	749.301749	112	
21	498	0.163225	111.227018	0.5	617.927876	120	S_{35p}
22	546	0.181818	98.410091	0.5	546.722730	124	Raise to 4
23	375	0.118147	162.625653	0.5	903.475851	128	
24	535	0.177505	101.111156	0.5	561.728642	136	S_{45p}
25	474	0.154146	118.789831	0.5	659.943508	140	Raise to 5
26	436	0.140058	132.808911	0.5	737.827284	144	
27	433	0.138960	134.041307	0.5	744.673929	148	
28	501	0.164370	110.341427	0.5	613.007926	152	
29							

S_n = 878.3

S_{45} = 666

S_{35} = 570

S_{25} = 418

$S_{35\,post}$ = 582

$S_{45\,post}$ = 611

32 708

$\frac{S_{45}}{S_n} = \frac{666.0}{878.3} = .758$

$\frac{S_{35}}{S_n} = \frac{570}{878.3} = .649$

$\frac{S_{25}}{S_n} = \frac{418.3}{878.3} = .478$

$\frac{S_{35\,post}}{S_n} = \frac{582}{878.3} = .663$

$\frac{S_{45\,post}}{S_n} = \frac{611}{878.3} = .696$

$= .806$

Dia = 236 ± 20 μ

0 r114d2	1 b	2 b/f	3 mic/ml	4 flo ml/min	5 micu/ min-mm3	6 time min	
1	4713	1.715690	2.137756	0.5	13.035095	-12.0	
2	4796	1.800300	0.525362	0.5	3.203427	-6.0	
3	4193	1.283440	11.223914	0.5	68.438499	1.5	
4	4546	1.560055	5.218075	0.5	31.817530	2.5	
5	3995	1.152958	14.423019	0.5	87.945236	9.0	
6	2136	0.401202	55.364836	0.5	337.590462	25.0	
7	1596	0.272169	86.569979	0.5	527.865725	41.0	
8	1675	0.289542	80.361686	0.5	490.010283	S_n 45.0	
9	1748	0.306022	75.270068	0.5	458.963830	49.0	
10	3269	0.780005	26.393679	0.5	160.937066	57.0	— Drop to 25
11	2710	0.570526	37.779760	0.5	230.364390	65.0	
12	2504	0.505246	43.095375	0.5	262.776678	S_{25} 69.0	
13	2411	0.477520	45.802930	0.5	279.286157	73.0	
14	3694	0.980882	19.243653	0.5	117.339350	81.0	— Drop to 15
15	3347	0.813761	25.022204	0.5	152.574414	S_{15} 89.0	
16	2898	0.635248	33.558383	0.5	204.624287	97.0	
17	1497	0.251048	95.602346	0.5	582.941135	101.0	— Raise to 25
18	1203	0.192265	135.088921	0.5	823.712934	S_{25_p} 105.0	
19	1467	0.244786	98.665745	0.5	601.620394	113.0	
20	881	0.133911	225.916411	0.5	1377.539091	117.0	— Raise to 492
21	1021	0.158565	176.523320	0.5	1076.361706	121.0	
22	1073	0.167997	162.661180	0.5	991.836462	S_{n_p} 129.0	
23	1096	0.172219	157.111629	0.5	957.997740	137.0	
24							

$S_n = 492$

$S_{25} = 233$

$\frac{S_{25}}{S_n} = \frac{233}{492} = .474$

$S_{15} = 158$

$\frac{S_{15}}{S_n} = \frac{158}{492} = .320$

$S_{25\,post} = 669$

$\frac{S_{25\,post}}{S_{n\,post}} = \frac{669}{1010} = .663$

$S_{n\,post} = 1010$

$\frac{S_{15\,post}}{S_{n\,post}} = \frac{158}{1010} = .156$

Arranged

$S_{n15} = \frac{158}{\frac{1}{2}(1010 + 492)} = 2.21$

Dia = 212 ± 18

0 r115d3	1 b	2 b/f	3 mic/ml	4 flo ml/min	5 micu/ min-mm3	6 time min	
1	4600	1.605585	4.299570	0.5	33.485745	-12.0	
2	4683	1.683321	2.765253	0.5	21.536239	-6.0	
3	4677	1.677547	2.877872	0.5	22.413334	1.5	
4	4771	1.770973	1.079932	0.5	8.410686	2.5	
5	4639	1.641543	3.584821	0.5	27.919165	9.0	
6	4523	1.537390	5.681364	0.5	44.247381	21.0	
7	4265	1.332812	10.086190	0.5	78.552879	33.0	
8	4370	1.411955	8.328959	0.5	64.867285	37.0	
9	4254	1.324821	10.268026	0.5	79.969051	41.0	Pour #10
10	4517	1.532225	5.787515	0.5	45.074106	49.0	
11	4254	1.324821	10.268026	0.5	79.969051	57.0	
12	4393	1.430013	7.938187	0.5	61.823890	S_{10} 61.0	
13	4305	1.362342	9.421571	0.5	73.376722	65.0	Raise #20
14	3865	1.073611	16.542110	0.5	128.832634	69.0	
15	3533	0.898525	21.912529	0.5	170.658327	S_{20} 77.0	
16	2980	0.664437	31.901989	0.5	248.457855	85.0	Raise to 1x2
17	3075	0.700456	30.024827	0.5	233.838213	89.0	
18	2760	0.586610	36.649054	0.5	285.428769	93.0	
19	2736	0.578558	37.207601	0.5	289.778826	S_n 101.0	
20	2610	0.537590	40.300274	0.5	313.865062	109.0	
21							

$S_n = 296$

$S_{10} = 71.7$ $\quad \frac{S_{10}}{S_{n\,post}} = \frac{71.7}{296} = .242$

$S_{20} = 182$ $\quad \frac{S_{20}}{S_{n\,post}} = \frac{182}{296} = .615$

$D_{ia} = 194 \pm 26$

R115D1 26R x 6C 07-SEP-89 20:52 Page 1

0 r115 d1	1 b	2 b/f	3 mic/ml	4 flo ml/min	5 micu/ min-mm3	6 time min	
1	4561	1.562521	5.167908	0.5	28.903291	-12.0	
2	4606	1.602644	4.358418	0.5	24.375938	-6.0	
3	1996	0.363968	61.695581	0.5	345.053582	1.5	
4	3261	0.772932	26.692446	0.5	149.286609	2.5	
5	1319	0.214089	117.118516	0.5	655.025259	9.0	
6	847	0.127695	242.628331	0.5	1356.981716	25.0	
7	831	0.124981	250.650288	0.5	1401.847249	37.0	S_n
8	784	0.117085	276.975229	0.5	1549.078464	41.0	S_n
9	829	0.124643	251.684224	0.5	1407.629889	45.0	S_n — Drop to 45
10	969	0.148825	193.387936	0.5	1081.588009	53.0	
11	976	0.150062	191.081440	0.5	1068.688143	57.0	S_{45}
12	913	0.139028	213.675398	0.5	1195.052564	61.0	S_{45}
13	928	0.141636	207.899640	0.5	1162.749665	65.0	S_{45} — Drop to 35
14	1027	0.159151	175.597465	0.5	982.088732	69.0	S_{35}
15	1049	0.163116	169.564902	0.5	948.349562	77.0	S_{35}
16	1133	0.178510	149.487179	0.5	836.058049	85.0	S_{35}
17	1194	0.189946	137.322943	0.5	768.025408	89.0	S_{35} — Raise to 45
18	1016	0.157178	178.752464	0.5	999.734137	93.0	
19	876	0.132647	229.140963	0.5	1281.549012	97.0	
20	1006	0.155391	181.705373	0.5	1016.249288	105.0	S_{45p}
21	1044	0.162213	170.904585	0.5	955.842198	109.0	S_{45p}
22	960	0.147239	196.423588	0.5	1098.565926	113.0	S_{45p} — Raise to 45
23	1102	0.172781	156.399248	0.5	874.716155	117.0	S_{45post}
24	1134	0.178695	149.272966	0.5	834.859986	125.0	S_{45post}
25	1187	0.188622	138.630959	0.5	775.340934	133.0	S_{45post}
26							

$S_n = 1453$

$S_{45} = 1142$ $\quad \frac{S_{45}}{S_n} = \frac{1142}{1453} = .786$

$S_{35} = 883.0$ $\quad \frac{S_{35}}{S_n} = \frac{883.0}{1453} = .608$

$S_{45post} = 985$ $\quad \frac{S_{45post}}{S_{n\,ave}} = \frac{985}{(1453+838)/2} = .863$

Dia = 226 ± 33.7.

APPENDIX 3A:

REDUCED OXYGEN ISLET PERIFUSIONS

III. 1-Week, Rat, data tables

R125WK142 25R x 9C 03-OCT-88 12:49 Page 1

0 r125wk142	1 bound	2 b/f	3 micU/ml	4 micU/ min-mm3	5 time	6	7	8	9
1	3900	0.807453	9.890296	55.191385	-3				
2	3901	0.807828	9.870307	55.079840	0				
3	3776	0.762212	12.406501	69.232703	2				
4	3819	0.777642	11.525808	64.318123	4				
5	3630	0.711765	15.454844	86.243548	11				
6	3459	0.656232	19.129545	106.749691	23				
7	3230	0.587273	24.226456	135.192276 } Q_N	35				
8	3244	0.591323	23.908555	133.418274 }	47				
9	3118	0.555595	26.803722	149.574341	59				
10	3140	0.561717	26.292432	146.721159	71				
11	3200	0.578662	24.910727	139.010754	83				
12	3256	0.594812	23.636771	131.901626 } Q_{142}	95				
13	3235	0.588717	24.112817	134.558132 }	107				
14									
15									
16									
17									
18									
19									
20									
21									
22									
23									
24									
25									

$$\frac{Q_{142}}{Q_N} = \frac{133.5}{134.3} = 99.4$$

Dia = 230

R125WK60 28R x 9C 03-OCT-88 12:50 Page 1

0 r125wk60	1 bound	2 b/f	3 micU/ml	4 micU/ min-mm3	5 time	6	7	8	9
1	3934	0.846750	7.864252	49.151576	-6				
2	4178	0.949114	3.257566	20.359786	0				
3	3375	0.648415	19.675832	122.973952	2				
4	3688	0.753884	12.891747	80.573418	4				
5	3720	0.765432	12.220772	76.379823	11				
6	3475	0.680705	17.466725	109.167033	23				
7	3395	0.654773	19.230922	120.193263	35				
8	3317	0.630249	20.974982	131.093638	47				
9	3304	0.626232	21.268023	132.925142	59				
10	3337	0.636468	20.525486	128.284288	63				
11	3327	0.633352	20.750033	129.687705	67				
12	3493	0.686652	17.073169	106.707304	75				
13	3247	0.608851	22.561181	141.007380	87				
14	3237	0.606000	22.600000	142.000000	99				
15	3320	0.636400	20.800000	130.000000	103				
16	3134	0.575468	25.167510	157.296935	107				
17	2572	0.428096	39.459816	240.000000	111				
18	3099	0.565408	25.987391	162.421193	123				
19	3023	0.543999	27.790816	173.692600	135				
20	3007	0.539566	28.174829	176.092679	147				
21	3138	0.576626	25.074210	156.713809	159				
22	3305	0.626540	21.245457	132.784104	171				
23	3342	0.638030	20.413363	127.583517	175				
24	3681	0.751378	13.039128	81.494549	179				
25	3798	0.794228	10.605215	66.282591	183				
26	3838	0.809363	9.788449	61.177807	191				
27	3812	0.799497	10.318403	64.490019	199				
28									

S_N } S_N

S_{60} } S_{60}

S_{NP} } S_{NP}

Prop to 60

Raise to 142

Drop to 100 Glucose

$S_N = 130.3$

$S_{NP} = 168.7$

$S_{60} = 143.0$

$$\frac{S_{60}}{\frac{1}{2}(S_N + S_{NP})} = \frac{143.0}{(130.3 + 168.7).5} = 95.6$$

0 r121 1wk 60 mmHg O2	1 bound	2 b/f	3 micU/ml	4 flow ml/min	5 micU/ min-mm3	6 time min	
1	4269	0.944051	7.015043	0.5	38.249960	-10.5	
2	4263	0.941475	7.132841	0.5	38.892262	-4.5	
3	3440	0.642870	22.582895	0.5	123.134649	2.0	
4	4026	0.844911	11.674178	0.5	63.654189	4.0	
5	3872	0.787152	14.543458	0.5	79.299115	11.0	
6	3784	0.755742	16.169736	0.5	88.166501	27.0	
7	3812	0.765616	15.652758	0.5	85.347645	35.0	
8	3697	0.725756	17.776183	0.5	96.925755	39.0	S_n
9	3849	0.778834	14.969020	0.5	81.619523	43.0	↓60
10	4201	0.915251	8.340844	0.5	45.478975	51.0	
11	3760	0.747366	16.612741	0.5	90.582012	59.0	
12	3717	0.732558	17.406649	0.5	94.910845	67.0	S_{60}
13	3681	0.720352	18.072018	0.5	98.538809	71.0	
14	3565	0.682166	20.226611	0.5	110.286863	75.0	↑ MAX
15	2819	0.472036	35.842779	0.5	195.435000	79.0	
16	3787	0.756795	16.114356	0.5	87.864539	87.0	
17				0.5		95.0	
18				0.5			

0 r121 1wk 60 mmHg O2	7 %max
1	43.814387
2	44.550128
3	141.047708
4	72.914306
5	90.835183
6	100.992556
7	97.763626
8	111.026065
9	93.493153
10	52.095045
11	103.759464
12	108.718036
13	112.873779
14	126.330885
15	223.865979
16	100.646665
17	
18	

$$\frac{S_{60}}{S_n} = \frac{94.0}{88.2} = 106.6$$

$$\Rightarrow 100.0\%.$$

R125WK45 25R x 9C 03-OCT-88 12:50 Page 1

0 r125wk45	1 bound	2 b/f	3 micU/ml	4 micU/ min-mm3	5 time	6	7	8	9
1	3634	0.733253	14.124161	87.510290	-3				
2	3680	0.749491	13.150522	81.477832	0				
3	2827	0.490543	32.703049	202.621121	2				
4	3339	0.635879	20.567829	127.433885	4				
5	3039	0.547469	27.492802	170.339539	15				
6	3078	0.558418	26.567152	164.604410	27				
7	3245	0.607109	22.693030	140.601175	39				
8	3403	0.656063	19.141274	118.595254	51				
9	3412	0.658942	18.941944	117.360249	59				
10	3409	0.657981	19.008353	117.771702	63				
11	3387	0.650971	19.496412	120.795612	67				
12	3450	0.671206	18.103763	112.167059	75				
13	3359	0.642133	20.120303	124.661107	83				
14	3409	0.657981	19.008353	117.771702	91				
15	3299	0.623512	21.467697	~~133.009276~~	95				
16	3423	0.662473	18.698743	115.853424	99				
17	2667	0.450279	36.901521	228.633962	103				
18	3136	0.574991	25.206037	156.171234	111				
19									
20									
21									
22									
23									
24									
25									

S_n = 118.7

S_{45} = 116.8

$\frac{S_{45}}{S_n}$ = 98.4

R124WK30 25R x 9C 03-OCT-88 12:48 Page 1

0 r124wk30	1 bound	2 b/f	3 micU/ml	4 micU/ min-mm3	5 time	6	7	8	9
1	3880	0.822034	9.121518	65.716991	-3				
2	4050	0.890110	5.795948	41.757552	0				
3	3276	0.615327	22.074495	159.038151	2				
4	3636	0.732474	14.171542	102.100447	4				
5	3658	0.740186	13.705111	98.739991	11				
6	3498	0.685613	17.141621	123.498710	23				
7	3569	0.709402	15.604179	112.422038	39				
8	3641	0.734221	14.065358	101.335435	55				
9	3591	0.716910	15.131779	109.018580	71				
10	3443	0.667636	18.345902	132.175085	83				
11	3462	0.673803	17.928571	129.168381	91				
12	3440	0.666667	18.411922	132.650736	95				
13	3422	0.660873	18.808768	135.509858	99				
14	3568	0.709062	15.625697	112.577067	107				
15	3460	0.673152	17.972436	129.484408	115				
16	3498	0.685613	17.141621	123.498710	123				
17	3036	0.545651	27.648664	199.197864	127				
18									
19									
20									
21									
22									
23									
24									
25									

15.6
17.9
17.1
} 16.8 = S_n

= 91.9 %

18.8
18.4
17.9
18.3
} 18.35 S_n

0 r118 1wk 30 mmHg	1 b	2 b/f	3 mic/ml	4 flow ml/min	5 micu/ min-mm3	6 time min
1	2908	1.104863	4.355286	0.5	41.637534	-13.5
2	2900	1.098485	4.555472	0.5	43.551354	-4.5
3	2920	1.114504	4.057638	0.5	38.791954	3.0
4	2945	1.134875	3.447998	0.5	32.963650	5.0
5	2660	0.923611	11.119579	0.5	106.305727	12.0
6	2231	0.674222	24.955034	0.5	238.575851	24.0
7	1888	0.516977	38.141522	0.5	364.641705	36.0
8	1797	0.480096	42.126341	0.5	402.737484	40.0
9	1780	0.473404	42.901352	0.5	410.146771	44.0
10	2287	0.703043	23.005209	0.5	219.935076	52.0
11	1833	0.494470	40.518261	0.5	387.363872	60.0
12	2006	0.567629	33.323020	0.5	318.575716	68.0
13	1858	0.504617	39.426475	0.5	376.926151	72.0
14	1930	0.534626	36.385582	0.5	347.854511	76.0
15	1380	0.331731	65.479116	0.5	625.995368	80.0
16	1393	0.335905	64.559167	0.5	617.200445	88.0
17	1396	0.336873	64.349332	0.5	615.194381	96.0
18				0.5		
19				0.5		
20				0.5		

↓ 30

↑ 142

0 r118 1wk 7 30 mmHg
1 8.377773
2 8.762848
3 7.805222
4 6.632525
5 21.389482
6 48.003189
7 73.368552
8 81.033699
9 82.524501
10 44.252530
11 77.940417
12 64.099742
13 75.840272
14 69.990847
15 125.954802
16 124.185200
17 123.781566
18
19

$$\frac{S_{10}}{S_n} = \frac{347.0}{406.5} = 85.3$$

0 r130 wk 30 to 5mmHg	1 b	2 b/f	3 mic/ml	4 flow ml/min	5 micu/ min-mm3	6 time min	
1	3941	1.017295	13.880473	0.4	70.728524	-6.0	
2	3914	1.003332	14.420057	0.4	73.477999	-0.5	
3	2453	0.457479	45.327917	0.4	230.970280	1.0	
4	2757	0.545077	38.059096	0.4	193.931699	3.0	
5	2476	0.463757	44.733958	0.5	284.929666	8.0	
6	1693	0.276544	75.472081	0.5	480.713892	24.0	
7	1458	0.229353	94.757326	0.5	603.549845	40.0	
8	1403	0.218808	100.821508	0.5	642.175210	52.0	
9	1403	0.218808	100.821508	0.5	642.175210	56.0	S_n
10	1407	0.219569	100.354477	0.5	639.200492	60.0	620
11	2511	0.473416	43.846814	0.5	279.279072	68.0	
12	1803	0.299900	68.974085	0.5	439.325385	76.0	
13	1775	0.293874	70.515750	0.5	449.144902	84.0	
14	1697	0.277378	75.213536	0.5	479.067109	88.0	S_{30}
15	1637	0.264972	79.296300	0.5	505.071975	92.0	494
16	3712	0.904704	18.461411	0.5	117.588602	100.0	
17	3729	0.912628	18.121247	0.5	115.421956	112.0	
18	3897	0.994640	14.759937	0.5	94.012340	120.0	
19	4120	1.115020	10.317022	0.5	65.713518	124.0	S_5
20	3973	1.034097	13.241425	0.5	84.340284	128.0	130
21	2081	0.362923	56.684663	0.5	361.048807	132.0	
22	2177	0.386130	53.355876	0.5	339.846345	140.0	
23							

$S_n = 641$

$S_{30} = 492$

$S_5 = 81$

$\frac{S_{30}}{S_n} = .768$

$S_5/S_n = .126$

Basal ~ 71

0 r118 1wk 15 mmHg	1 b	2 b/f	3 mic/ml	4 flow ml/min	5 micu/ min-mm3	6 time min	
1	3195	1.326827	0.000000	0.5	0.000000	-13.5	
2	3222	1.353213	0.000000	0.5	0.000000	-4.5	
3	2643	0.892905	12.504995	0.5	87.447520	3.0	
4	2663	0.905782	11.914759	0.5	83.319996	5.0	
5	2460	0.782692	18.152127	0.5	126.937952	12.0	
6	2056	0.579645	32.271814	0.5	225.677022	24.0	
7	1762	0.458735	44.663779	0.5	312.334118	36.0	
8	1686	0.430431	48.342102	0.5	338.056660	40.0	S_n
9	1622	0.407435	51.649529	0.5	361.185519	44.0	
10	2432	0.766950	19.054469	0.5	133.248038	52.0	
11	2240	0.666072	25.527511	0.5	178.514066	60.0	
12	2254	0.673037	25.037680	0.5	175.088672	68.0	S_{15}
13	2172	0.633052	27.950821	0.5	195.460284	72.0	
14	2044	0.574319	32.733841	0.5	228.907978	76.0	
15	1256	0.288935	76.510386	0.5	535.037662	80.0	
16	1449	0.348820	61.852862	0.5	432.537499	88.0	
17	1234	0.282444	78.498320	0.5	548.939302	96.0	
18				0.5			
19				0.5			
20				0.5			
21							
22							
23							
24							

$\frac{S_{15}}{S_n} = \frac{1828}{337} = .543$

R120WK15 18R x 7C 08-SEP-89 12:26 Page 1

0 r120 wk 15mmHg O2	1 bound	2 b/f	3 micU/ml	4 flow ml/min	5 micU/ min-mm3	6 time min	
1	2488	0.388993	46.190063	0.5	310.834881	-10.5	
2	2755	0.449502	38.245207	0.5	257.370168	-4.5	
3	2921	0.489854	34.098150	0.5	229.462652	2.0	
4	3145	0.548005	29.129578	0.5	196.026772	4.0	
5	3087	0.532517	30.361246	0.5	204.315250	11.0	
6	2989	0.507040	32.525197	0.5	218.877504	27.0	
7	2956	0.498650	33.280572	0.5	223.960778	35.0	
8	2969	0.501944	32.981263	0.5	221.946587	39.0	S_n
9	2949	0.496883	33.442699	0.5	225.051808	43.0	
10	3661	0.700938	19.152714	0.5	128.887709	51.0	Drop*
11	3466	0.639719	22.779061	0.5	153.291122	59.0	
12	3558	0.668044	21.055390	0.5	141.691725	67.0	
13	3628	0.690259	19.759946	0.5	132.974067	71.0	S_{15}
14	3606	0.683213	20.165893	0.5	135.705875	75.0	
15	2952	0.497640	33.373132	0.5	224.583663	79.0	Raise
16	3117	0.540489	29.720028	0.5	200.000188	87.0	
17	3183	0.558323	28.339800	0.5	190.711978	95.0	
18				0.5			

0 r120 wk 15mmHg O2	7 %max
1	138.982732
2	115.077204
3	102.598995
4	87.648903
5	91.354907
6	97.866087
7	100.138957
8	99.238358
9	100.626786
10	57.629201
11	68.540632
12	63.354225
13	59.456323
14	60.677789
15	100.417466
16	89.425525
17	85.272514
18	

$$\frac{S_{15}}{S_n} = \frac{134.4}{223.7} = 60.0$$

R124WK15 25R x 9C 03-OCT-88 12:47 Page 1

0 r124wk15	1 bound	2 b/f	3 micU/ml	4 micU/ min-mm3	5 time	6	7	8	9
1	3700	0.738523	13.805179	79.891081	-3				
2	3647	0.720324	14.918939	86.336455	0				
3	2752	0.461900	35.636294	206.228556	2				
4	2996	0.524326	29.524992	170.862224	4				
5	3087	0.548995	27.362451	158.347517	11				
6	2829	0.481041	33.649274	194.729596	23				
7	2868	0.490928	32.665269	189.035123	35				
8	2799	0.473524	34.416106	199.167277	47				
9	2842	0.484322	33.319705	192.822365	59				
10	2954	0.513204	30.541573	176.745214	63				
11	3825	0.783009	11.224971	64.959323	75				
12	3767	0.762088	12.413707	71.838581	83				
13	3795	0.772126	11.837932	68.506554	91				
14	3798	0.773208	11.776451	68.150756	95				
15	3623	0.712208	15.426922	89.276168	99				
16	2155	0.328757	54.625275	316.118487	103				
17	2543	0.412356	41.407577	239.627180	107				
18									
19									
20									
21									
22									
23									
24									
25									

S_n

Drop to 15

S_{15}

Raise to 142

$$\frac{S_{15}}{S_n} = \frac{75.3}{189} = .40$$

R128WK15 17R x 6C

24-OCT-88 13:15 Page 1

0 r128 wk 15mmHg	1 b	2 b/f	3 mic/ml	4 flow ml/min	5 micu/ min-mm3	6 time min	
1	3660	0.890511	19.077724	0.4	169.203760	-8.0	
2	3998	1.059915	12.281039	0.4	108.922743	-0.5	
3	3228	0.710700	27.789416	0.5	308.086657	1.0	
4	3253	0.720168	27.281840	0.5	302.459421	3.0	
5	3718	0.917572	17.910482	0.5	198.564103	10.0	
6	3415	0.784156	24.008547	0.5	266.170150	26.0	
7	3481	0.811611	22.679480	0.5	251.435478	42.0	
8	3530	0.832547	21.693395	0.5	240.503271	58.0	
9	3664	0.892353	18.997231	0.5	210.612320	74.0	
10	3671	0.895584	18.856366	0.5	209.050625	78.0	
11	3632	0.877719	19.641145	0.5	217.751051	82.0	
12	3638	0.880445	19.520416	0.5	216.412592	94.0	
13	3575	0.852205	20.787993	0.5	230.465551	106.0	
14	3622	0.873192	19.842355	0.5	219.981767	110.0	
15	3730	0.923267	17.668962	0.5	195.886496	114.0	
16	2673	0.524426	39.605533	0.5	439.085734	122.0	
17	3353	0.759113	25.258810	0.5	280.031157	130.0	

Normal: 210.6, 209.0, 217.9 → 212.4 ± 4.6 ; 266.2, 251.4, 240.6 → 252.7 ± 12.8

Low: 230.5, 219.9, 195.9 → 215.4 ± 17.7

basal: 108

$$\frac{(252-108)-(215-108)}{(252-108)} = 74.3\%$$ of Normal Secretion basal subtracted.

$$= 85.3\%$$ of Normal Secretion w/o basal subtracted

0 r130 wk 15to2 mmHg	1 b	2 b/f	3 mic/ml	4 flow ml/min	5 micu/ min-mm3	6 time min	
1	3810	0.940741	16.936855	0.4	85.539671	-9.0	
2	3901	0.985350	15.126585	0.4	76.396894	-0.5	
3	2715	0.527697	39.354950	0.5	248.452968	1.0	
4	2968	0.606705	33.866835	0.5	213.805774	3.0	
5	2936	0.596263	34.539238	0.5	218.050742	8.0	
6	2127	0.371010	55.471114	0.5	350.196429	20.0	
7	1820	0.301325	68.621816	0.5	433.218535	32.0	
8	1792	0.295320	70.138152	0.5	442.791363	44.0	
9	1835	0.304564	67.836918	0.5	428.263371	56.0	
10	1807	0.298530	69.317335	0.5	437.609441	60.0	S_n
11	1720	0.280130	74.376238	0.5	469.546957	64.0	66; ↓ 15
12	3168	0.675192	29.753985	0.5	187.840816	72.0	
13	2728	0.531567	39.061304	0.5	246.599141	84.0	
14	2617	0.499142	41.623523	0.5	262.774769	88.0	S_{15}
15	2706	0.525029	39.559168	0.5	249.742223	92.0	
16	4020	1.046875	12.762857	0.5	80.573593	100.0	94 ↓ 2
17	4052	1.064076	12.128701	0.5	76.570084	108.0	
18	4053	1.064618	12.108898	0.5	76.445065	112.0	S_2
19	3991	1.031533	13.338228	0.5	84.205983	116.0	
20	4045	1.060288	12.267348	0.5	77.445379	128.0	120 ↑ 14
21	4036	1.055439	12.445672	0.5	78.571162	132.0	
22	2981	0.610986	33.595039	0.5	212.089893	140.0	

S_n = 445.1

S_{15} = 253.0 ± .85

S_2 = 76.5

S_{basal} = 76

w/ basal

S_{15}/S_n = .569

S_2/S_n = .172

w/o Basal S_2/S_n = ~.01

R128WK5 18R x 6C

24-OCT-88 12:37 Page 1

0 r128 wk 5mmHg O2	1 b	2 b/f	3 mic/ml	4 flow ml/min	5 micu/ min-mm3	6 time min	
1	4190	1.175316	8.298869	0.4	73.604160	-6.0	
2	4258	1.217615	6.963129	0.4	61.757239	-0.5	
3	3553	0.845550	21.092354	0.5	233.839850	1.0	
4	3866	0.994086	14.781712	0.5	163.877078	3.0	
5	4164	1.159566	8.813018	0.5	97.705297	8.0	
6	3442	0.798052	23.330599	0.5	258.654090	24.0	
7	3036	0.643357	31.606863	0.5	350.408680	40.0	
8	3215	0.708150	27.927258	0.5	309.614831	52.0	
9	3252	0.722185	27.174544	0.5	301.269886	60.0	
10	3074	0.656697	30.818983	0.5	341.673871	64.0	
11	3230	0.713812	27.621867	0.5	306.229122	68.0	70 - 5 mm Hg
12	4279	1.231013	6.553683	0.5	72.657244	76.0	
13	4421	1.326035	3.836006	0.5	42.527780	84.0	
14	4482	1.369386	2.703884	0.5	29.976538	92.0	
15	4497	1.380295	2.429578	0.5	26.935450	96.0	40 - 0 mm
16	3767	0.944584	16.777605	0.5	186.004491	104.0	
17	3839	0.980337	15.325881	0.5	169.909989	108.0	
18							

Normal

301
341
306
} 316 ± 21.8

5 mm Hg

29.9
26.9
} 28.4 ± 2.12

Basal

61.75.

w/o - basal

$\frac{Q_5}{Q_N} = \frac{28.4}{316} = 9\%$

Subtract basal

$\frac{0}{} = 0\%$

0 r119 1wk 5mmHg	1 b	2 b/f	3 mic/ml	4 flow ml/min	5 micu/ min-mm3	6 time min	
1	2873	1.070019	5.480908	0.5	38.597942	-13.5	
2	2998	1.171094	2.427703	0.5	17.096500	-4.5	
3	2718	0.957042	9.695251	0.5	68.276414	3.0	
4	2726	0.962571	9.467874	0.5	66.675166	5.0	
5	2532	0.836748	15.243125	0.5	107.345950	12.0	
6	2006	0.564752	33.579460	0.5	236.475073	24.0	
7	1843	0.496097	40.340868	0.5	284.090618	36.0	
8	1871	0.507459	39.126811	0.5	275.540920	40.0	S_n
9	1847	0.497710	40.165936	0.5	282.858701	44.0	— Drop 4 5
10	2437	0.780839	18.256951	0.5	128.570077	52.0	
11	2625	0.894988	12.408614	0.5	87.384604	60.0	
12	2908	1.097358	4.591093	0.5	32.331643	68.0	
13	2887	1.080869	5.121962	0.5	36.070155	72.0	
14	2937	1.120565	3.873529	0.5	27.278372	76.0	
15	2824	1.032919	6.767289	0.5	47.656962	80.0	
16	2615	0.888549	12.707755	0.5	89.491229	88.0	
17	2490	0.811604	16.560971	0.5	116.626554	96.0	
18				0.5			
19				0.5			
20				0.5			

0 r119 1wk 5mmHg	7
1	13.735923
2	6.084164
3	24.297656
4	23.727817
5	38.201406
6	84.154830
7	101.099864
8	98.057267
9	100.661459
10	45.754476
11	31.097724
12	11.505923
13	12.836354
14	9.707606
15	16.959773
16	31.847412
17	41.504112
18	
19	

$$\frac{S_5}{S_n} = \frac{31.6}{280.8} = 11.2$$

0 r121 wk 5mmhg bubble	1 bound	2 b/f	3 micU/ml	4 flow ml/min	5 micU/ min-mm3	6 time min
1	3660	0.704117	18.963772	0.5	125.921460	-10.5
2	3915	0.792029	14.285500	0.5	94.857237	-4.5
3	3217	0.570289	27.441909	0.5	182.217192	35.0
4	3384	0.618195	24.141974	0.5	160.305271	S_n 39.0
5	3378	0.616423	24.257698	0.5	161.073689	43.0
6	4488	1.027002	3.281409	0.5	21.788905	67.0
7	4516	1.040074	2.705237	0.5	17.963064	S_s 71.0
8	4532	1.047619	2.373767	0.5	15.762068	75.0
9	3190	0.562809	27.993561	0.5	185.380220	87.0
10				0.5		
11				0.5		
12				0.5		
13				0.5		
14				0.5		
15				0.5		
16				0.5		
17				0.5		
18				0.5		

0 r121 wk 5mmhg bubble	7 %max
1	75.011295
2	56.506366
3	108.546608
4	95.493698
5	95.951444
6	12.979630
7	10.700580
8	9.389449
9	110.728671
10	
11	
12	
13	
14	
15	
16	
17	
18	

$$\frac{S_s}{S_n} = \frac{18.2}{167.8} \simeq 10.8$$

0 r120 wk 5mmHg O2	1 bound	2 b/f	3 micU/ml	4 flow ml/min	5 micU/ min-mm3	6 time min
1	4942	1.221453	0.000000	0.5	0.000000	-10.5
2	4887	1.191661	0.000000	0.5	0.000000	-4.5
3	4715	1.103440	0.000000	0.5	0.000000	2.0
4	4731	1.111346	0.000000	0.5	0.000000	4.0
5	4619	1.057221	1.963069	0.5	14.894304	11.0
6	3890	0.763044	15.786856	0.5	119.778877	27.0
7	3481	0.632105	23.258045	0.5	176.464678	35.0
8	3136	0.535885	30.088389	0.5	228.288236 } S_n	39.0
9	3081	0.521585	31.267307	0.5	237.232980 }	43.0
10	4385	0.952640	6.623365	0.5	50.253151	51.0
11	4670	1.081519	0.903864	0.5	6.857842 $-S_5$	59.0
12	4845	1.169442	0.000000	0.5	0.000000	67.0
13	4866	1.180495	0.000000	0.5	0.000000	71.0
14	4890	1.193265	0.000000	0.5	0.000000	75.0
15	3753	0.716905	18.261816	0.5	138.557024	79.0
16	3629	0.677179	20.517154	0.5	155.668846	87.0
17	3041	0.511350	32.145812	0.5	243.898424	95.0
18				0.5		
19						

0 r120 wk 5mmHg O2	7 %max
1	0.000000
2	0.000000
3	0.000000
4	0.000000
5	6.960280
6	55.974053
7	82.463984
8	106.681731
9	110.861713
10	23.483878
11	3.204749 $\leftarrow S_5$
12	0.000000
13	0.000000
14	0.000000
15	64.749299
16	72.745851
17	113.976552
18	
19	

$\frac{S_5}{S_n} \sim .032$

APPENDIX 3A:

REDUCED OXYGEN ISLET PERIFUSIONS

IV. 1-Week, Canine, data tables

C3D730 24R x 6C 01-FEB-89 16:32 Page 1

0 C3D730	1 b	2 b/f	3 mic/ml	4 flow	5 micu/ min-mm3	6 time	
1	4895	1.281414	7.315533	0.5	31.424110	-7.5	
2	4882	1.273676	7.528296	0.5	32.338040	1.5	
3	3590	0.700488	29.293658	0.5	125.831866	1.0	
4	3094	0.550436	41.088678	0.5	176.497758	3.0	
5	3756	0.757411	26.050474	0.5	111.900663	7.0	
6	3530	0.680810	30.535443	0.5	131.165993	23.0	
7	3324	0.616583	35.144604	0.5	150.964795	35.0	
8	3310	0.612396	35.479949	0.5	152.405278	39.0	
9	3217	0.585122	37.789801	0.5	162.327324	43.0	↓ 30 mm Hg
10	4060	0.872180	20.671251	0.5	88.794033	51.0	
11	3875	0.800620	23.871757	0.5	102.541913	63.0	
12	4012	0.853073	21.483121	0.5	92.281447	67.0	
13	3782	0.766673	25.565065	0.5	109.815571	71.0	↓ 10 mm Hg
14	4970	1.327103	6.074039	0.5	26.091234	79.0	
15	4989	1.338969	5.755335	0.5	24.722230	91.0	
16	5195	1.475852	2.159889	0.5	~~9.277873~~	95.0	
17	5019	1.357955	5.248275	0.5	22.544135	99.0	↓ 5 mm Hg
18	5391	1.621841	0.000000	0.5	~~.000000~~	107.0	
19	5170	1.458392	2.612069	0.5	11.220229	119.0	
20	5231	1.501435	1.499698	0.5	6.442002	123.0	
21	5020	1.358593	5.231288	0.5	22.471169	127.0	↑ 142 mm Hg
22	3966	0.835123	22.272607	0.5	95.672712	131.0	
23	4890	1.278431	7.397443	0.5	31.775958	135.0	
24				0.5			

S_n = 155.2

S_{30} = 101.6

S_{10} = 23.6

S_5 = 13.4

S_{10}/S_n = .657

S_{10}/S_n = .152

S_5/S_n = .086

C3D745 25R x 6C 01-FEB-89 16:32 Page 1

0 c3d745	1 b	2 b/f	3 mic/ml	4 flow	5 mic/ min-mm3	6 time min	
1	5154	1.400163	4.131977	0.5	20.435097	-7.5	
2	5349	1.534423	0.651785	0.5	3.223466	-1.5	
3	3442	0.638235	33.484217	0.5	165.599489	1.0	
4	3471	0.647092	32.838243	0.5	162.404761	3.0	
5	4651	1.111616	12.218197	0.5	60.426296	7.0	
6	4152	0.886611	20.076185	0.5	99.288751	23.0	
7	3853	0.773384	25.219924	0.5	124.727618	35.0	
8	3623	0.695127	29.625153	0.5	146.514110	39.0	
9	3751	0.737805	27.114536	0.5	134.097608	43.0	↓ 145 mm Hg
10	4015	0.832988	22.368378	0.5	110.625015	51.0	
11	3418	0.630977	34.027571	0.5	168.286702	59.0	
12	3579	0.680936	30.527264	0.5	150.975589	63.0	
13	3707	0.722894	27.959625	0.5	138.277077	67.0	↓ 20
14	4249	0.926515	18.503373	0.5	91.510252	75.0	
15	3865	0.777666	25.002484	0.5	123.652243	87.0	
16	3804	0.756112	26.119391	0.5	129.176020	91.0	
17	4102	0.866681	20.902047	0.5	103.373130	95.0	↓ 10
18	5038	1.326837	6.081195	0.5	30.075148	103.0	
19	4614	1.093106	12.791005	0.5	63.259172	115.0	
20	4630	1.101070	12.543369	0.5	62.034465	123.0	
21	4842	1.212622	9.237513	0.5	45.685031	127.0	
22	4625	1.098575	12.620763	0.5	62.417227	131.0	↑ 142 mm Hg
23	2587	0.414052	60.416311	0.5	298.794810	135.0	
24	3942	0.805641	23.631877	0.5	116.873772	143.0	
25				0.5			

$S_{max} = 168.3 = S_{145}$ $\quad S_{145}/S_{max} = 100\%$

$S_{20} = 103.4$ $\quad S_{20}/S_{max} = 103.4/168.3 = 61.4\%$

$S_{10} = 56.7$ $\quad S_{10} = 56.7/168.3 = 33.0\%$

$Dia = 165.3$

0 dog 30	wk 6 time min	2 b/f	3 mic/ml	%max		
1	-13.5	0.818312	28.646558	53.147603		
2	-7.5	0.971127	22.513133	41.768335		
3	-1.5	0.929346	24.052338	44.624003		
4	1.0	0.292646	105.539353	195.805849		
5	3.0	0.439654	62.412423	115.792993		
6	8.0	0.608668	41.519814	77.031195		
7	24.0	0.597910	42.446387	78.750253		
8	36.0	0.556279	46.423159	86.128311		
9	48.0	0.513460	51.305946	95.187285		
10	60.0	0.508980	51.872809	96.238978		
11	64.0	0.488997	54.550662	101.207166	142	$S_{142}/S_m \equiv 100$
12	68.0	0.483220	55.373626	102.734001		
13	76.0	0.651404	38.178364	70.831845		
14	84.0	0.537193	48.487181	89.957665		
15	88.0	0.567124	45.322077	84.085486		
16	92.0	0.556913	46.357440	86.006383	30	$S_{30}/S_m = 83.7\ \%$
17	96.0	0.584992	43.610688	80.910366		
18	104.0	0.965048	22.732426	42.175188		
19	112.0	0.975711	22.348714	41.463292		
20	120.0	0.970111	22.549675	41.836132		
21	124.0	0.989591	21.855516	40.548268	10	$S_{10}/S_m = 40.6\ \%$
22	128.0	1.007351	21.233911	39.395012		
23	136.0	1.330387	10.591410	19.650112		
24	144.0	1.530950	3.537755	6.563552		
25	148.0	1.442031	6.762745	12.546837		
26	152.0	1.541888	3.128354	5.803996	5	$S_5/S_m = 7.2\ \%$
27	156.0	1.501963	4.608730	8.550519		
28	160.0	0.365601	79.057068	146.673596		
29	164.0	0.665432	37.185194	68.989228		
30	172.0	0.697225	35.094482	65.110356		
31						

$$\frac{54.5\,\mu V}{\text{ml}} \left| \frac{.5\,\text{ml}}{\text{min}} \right| \frac{}{.0545\,m^2} = 500\ \frac{\mu V}{m^2 \cdot \text{min}}$$

142
55
54 } 54.5

30
45
46
43 } 44.6

10
21
21.8
22.5 } 21.8

5
4.6
3.1
6.7 } 4.8

$$\frac{S_{30}}{S_{142}} = \frac{44.6}{54.5} = 81.8\ \%$$

$$\frac{S_{10}}{S_{142}} = \frac{21.8}{54.5} = 40.0\ \%$$

$$\frac{S_5}{S_{142}} = \frac{4.8}{54.5} = 8.8\ \%$$

APPENDIX 3A:

REDUCED OXYGEN ISLET PERIFUSIONS

V. 2-5-Week, Rat, data tables

R1382WKL60 27R x 6C 01-FEB-89 16:29 Page 1

0 r138 2wk L60	1 b	2 b/f	3 mic/ml	4 flow	5 micu/ min-mm3	6 time
1	4224	0.966369	17.025578	0.5	155.059909	-7.5
2	4377	1.037696	14.568290	0.5	132.680236	-1.5
3	3344	0.636831	33.588294	0.5	305.904321	1.0
4	3523	0.694598	29.658123	0.5	270.110407	3.0
5	3652	0.738823	27.058022	0.5	246.430069	7.0
6	3184	0.588431	37.497266	0.5	341.505157	19.0
7	3055	0.551444	40.986310	0.5	373.281510	31.0
8	3255	0.609551	35.710610	0.5	325.233242	43.0
9	3153	0.579383	38.305776	0.5	348.868632	55.0
10	3227	0.601155	36.404749	0.5	331.555093	59.0
11	3156	0.580254	38.226743	0.5	348.148845	67.0
12	2851	0.496344	47.276723	0.5	430.571245	79.0
13	2918	0.514004	45.092900	0.5	410.682149	83.0
14	2867	0.500524	46.743785	0.5	425.717530	87.0
15	3068	0.555093	40.619244	0.5	369.938468	95.0
16	2705	0.459253	52.507000	0.5	478.205826	103.0
17	2604	0.434652	56.566092	0.5	515.173878	111.0
18	2531	0.417381	59.762830	0.5	544.288071	115.0
19	2590	0.431307	57.161059	0.5	520.592526	127.0
20	3668	0.744469	26.747056	0.5	243.597959	135.0
21	3455	0.672179	31.102767	0.5	283.267459	143.0
22	3357	0.640893	33.288372	0.5	303.172791	147.0
23	3284	0.618339	35.005391	0.5	318.810484	151.0
24	3214	0.597287	36.731594	0.5	334.531818	155.0
25	2243	0.353117	75.132587	0.5	684.267637	163.0
26	2207	0.345492	77.437801	0.5	705.262306	
27				0.5		

$S_{mic\ pre} = 36.8$

$S_{60} = 46.4$

$S_{30} = 57.9$

$S_{10} = 35.0$

$S_{mic\ post} = 76.3$

S_{60} - no offset - $\Rightarrow 100\%$

$S_{30}/S_{mic\ post} = 57.9/76.3 = 75.8\%$

$S_{10}/S_{mic\ post} = 35.0/76.3 = 45.8\%$

$Dia = 215\ \mu m$

0 r138 2wk L45	1 b	2 b/f	3 mic/ml	4 flow	5 micu/ min-mm3	6 time min
1	4121	0.889297	19.978322	0.5	171.340673	-1.5
2	3277	0.598211	36.669802	0.5	314.492299	1.0
3	3471	0.656889	32.159733	0.5	275.812464	3.0
4	3569	0.688199	30.075508	0.5	257.937465	7.0
5	3297	0.604067	36.178175	0.5	310.275943	19.0
6	3132	0.556998	40.447710	0.5	346.892880	35.0
7	3276	0.597919	36.694559	0.5	314.704622	47.0
8	3243	0.588353	37.521143	0.5	321.793676	51.0
9	3255	0.591818	37.218387	0.5	319.197147	55.0
10	3060	0.537313	42.478986	0.5	364.313771	63.0
11	2962	0.511307	45.434768	0.5	389.663536	75.0
12	2940	0.505589	46.131345	0.5	395.637607	79.0
13	2927	0.502231	46.549009	0.5	399.219632	83.0
14	3463	0.654384	32.335138	0.5	277.316795	91.0
15	3089	0.545182	41.647355	0.5	357.181430	103.0
16	3014	0.524996	43.837474	0.5	375.964611	107.0
17	2972	0.513920	45.122310	0.5	386.983790	111.0
18	4375	0.998858	15.889423	0.5	136.272923	119.0
19	4559	1.086511	13.006655	0.5	111.549358	131.0
20	4428	1.023342	15.055736	0.5	129.122952	135.0
21	4611	1.112693	12.194134	0.5	104.580905	139.0
22	3239	0.587201	37.622624	0.5	322.664012	143.0
23	2566	0.414607	60.330773	0.5	517.416582	151.0
24				0.5		

$S_{142\ post}$ = 37.1

S_{45} = 46.0

S_{20} = 43.5

S_5 = 13.4

$S_{142\ post}$ = 60.3

$S_{20}/S_{142\ post}$ = 43.5/60.3 = 72.1

$S_5/S_{142\ post}$ = 13.4/60.3 = 22.2

Dia = 219 μm

R1382WKM45 26R x 6C 01-FEB-89 16:31 Page 1

0 r138 2wk M45	1 b	2 b/f	3 mic/ml		4 flow	5 micu/ min-mm3	6 time
1	3056	0.532497	42.982940		0.5	467.205869	-7.5
2	2308	0.355789	74.354355		0.5	808.199509	-1.5
3	2184	0.330358	82.414847		0.5	895.813558	1.0
4	2570	0.412851	60.655255		0.5	659.296247	3.0
5	2336	0.361666	72.392770		0.5	790.138799	7.0
6	2365	0.367807	71.027337		0.5	772.036274	19.0
7	2285	0.350998	75.760412		0.5	823.482742	31.0
8	2292	0.352453	75.328451		0.5	818.787512	43.0
9	2134	0.320372	86.029527	42	0.5	935.103557	47.0
10	2387	0.372503	69.799958		0.5	758.695200	51.0
11	2036	0.301228	93.829205		0.5	1019.882664	59.0
12	1978	0.290157	98.952450	45	0.5	1075.570109	71.0
13	2101	0.313863	88.544798		0.5	962.443459	75.0
14	2716	0.446784	54.497535		0.5	592.364509	79.0
15	2492	0.395367	64.335933		0.5	699.303625	87.0
16	2360	0.366744	71.310567	20	0.5	775.114862	99.0
17	2306	0.355371	74.475121		0.5	809.512186	103.0
18	4109	0.876867	20.476340		0.5	222.568911	107.0
19	4461	1.029303	14.846636		0.5	161.376483	115.0
20	4405	1.003417	15.722366	5	0.5	170.895287	127.0
21	4334	0.971531	16.840187		0.5	183.045508	135.0
22	3157	0.559950	40.138900		0.5	436.292389	139.0
23	2403	0.375939	68.926149		0.5	749.197269	143.0
24	1943	0.283567	102.250005		0.5	1111.413096	147.0
25					0.5		158.0
26					0.5		

$S_{mn} = S_{45} = 93.8 + 99.9 + 88.5 = 93.7 \rightarrow 100\%$

$S_{20} = 64.3 + 71.3 + 74.5 = 70.0 \rightarrow 74.7\%$

$S_5 = 14.8 + 15.7 + 16.8 = 15.7 \rightarrow 16.7\%$

$D_{ia} = 185.2$

R1382WKM30 23R x 6C 01-FEB-89 16:31 Page 1

0 r138 2wk m30	1 b	2 b/f	3 mic/ml	4 flow	5 micu/ min-mm3	6 time min
1	3940	0.828601	22.566340	0.5	299.288326	-5
2	4084	0.885708	20.112990	0.5	266.750526	-1
3	2698	0.449892	53.989122	0.5	716.036100	1
4	2965	0.517452	44.686441	0.5	592.658371	3
5	3007	0.528657	43.407292	0.5	575.693526	9
6	2935	0.509549	45.627419	0.5	605.138185	21
7	2669	0.442914	55.142623	0.5	731.334521	37
8	2682	0.446034	54.621575	0.5	724.424077	49
9	2667	0.442435	55.223364	0.5	732.405359	53
10	2598	0.426111	58.107755	0.5	770.659882	57
11	2621	0.431511	57.124432	0.5	757.618462	65
12	2511	0.406048	62.041400	0.5	822.830241	73
13	2628	0.433163	56.829584	0.5	753.708008	81
14	2528	0.409924	61.244836	0.5	812.265735	85
15	2291	0.357745	73.793584	0.5	978.694743	89
16	3630	0.716683	28.321408	0.5	375.615497	97
17	3327	0.619784	34.891495	0.5	462.751917	105
18	3398	0.641495	33.244282	0.5	440.905598	113
19	3351	0.627058	34.326331	0.5	455.256373	117
20	3269	0.602470	36.294696	0.5	481.362016	121
21	2033	0.305164	92.122802	0.5	1221.787820	125
22	1679	0.239310	130.790413	0.5	1734.620858	137
23				0.5		

$S_{max} = S_{30} = 63.9$ $\Rightarrow$ 100%

$S_{10} = 34.6$ $S_{10}/S_{max} = 34.6/63.9 = 54.1\%$

$S_{max,post} = 111.0$

$D_{1a} = 172.6$

n r138 2wk m20	1 b	2 b/f	3 mic/ml	4 flow	5 micu/ min-mm3	6 time min
1	4337	0.977242	16.636565	0.5	262.406387	-5
2	4111	0.881432	20.288028	0.5	320.000449	-1
3	2707	0.446111	54.608800	0.5	861.337534	1
4	3265	0.592559	37.137289	0.5	585.761651	3
5	3549	0.679104	30.646412	0.5	483.381899	9
6	2948	0.505921	46.070671	0.5	726.666742	21
7	2904	0.494635	47.497685	0.5	749.174836	32
8	2954	0.507473	45.880130	0.5	723.661351	44
9	2817	0.472810	50.483450 } S_{142}	0.5	796.268930	48
10	2776	0.462744	51.972522 }	0.5	819.755870	52
11	3371	0.623797	34.577988	0.5	545.394128	60
12	3050	0.532751	42.955100	0.5	677.525240	68
13	3130	0.554473	40.681250 }	0.5	641.660095	76
14	3018	0.524231	43.905074 } S_{20}	0.5	692.509048	80
15	2973	0.512410	45.282958 }	0.5	714.242247	84
16	4122	0.885880	20.105976	0.5	317.128957	92
17	3914	0.805184	23.653585 }	0.5	373.084943	100
18	3732	0.740036	26.990844 {	0.5	425.723087	108
19	3772	0.753948	26.234735 {	0.5	413.797080	112
20	3418	0.638044	33.498356 }	0.5	528.365234	116
21	2149	0.324328	84.563593	0.5	1333.810610	120
22	1798	0.257704	117.362870 } S_{mL}	0.5	1851.149370	132
23	1679	0.236612	132.994451 } $S_{mL\,pit}$	0.5	2097.704278	144
24				0.5		

$S_m = S_{142} = 51.25$

$S_{20} = 43.3$

$S_{11} = 27.5$

$S_{mL\,pit} = 125$

$S_{20}/S_m = 433/51.25 = 84.5$

$S_{11}/S_m = /51.25 = 53.7$

R1382WKS45 31R x 6C 02-FEB-89 11:14 Page 1

0 r138 2wk s45	1 b	2 b/f	3 mic/ml	4 flow	5 micu/ min-mm3	6 time
1	4468	1.077405	13.284627	0.5	140.429459	-7.5
2	4646	1.170572	10.451733	0.5	110.483435	-1.5
3	2454	0.398312	63.688221	0.5	673.237014	1.0
4	2477	0.403552	62.564341	0.5	661.356668	3.0
5	2631	0.439672	55.693455	0.5	588.725738	7.0
6	2061	0.314464	88.306852	0.5	933.476241	19.0
7	2041	0.310465	89.911606	0.5	950.439808	31.0
8	2098	0.321927	85.447851	0.5	903.254240	43.0
9	2000	0.302343	93.339880	0.5	986.679495	47.0
10	2064	0.315066	88.069808	0.5	930.970488	51.0
11	2141	0.330707	82.293550	0.5	869.910672	59.0
12	2024	0.307085	91.309950	0.5	965.221463	63.0
13	1992	0.300770	94.031504	0.5	993.990526	71.0
14	1964	0.295294	96.513517	0.5	1020.227449	79.0
15	2291	0.362271	72.525610	0.5	766.655498	87.0
16	2336	0.372034	69.920898	0.5	739.121542	91.0
17	2267	0.357120	73.971813	0.5	781.943051	95.0
18	2268	0.357334	73.910731	0.5	781.297370	103.0
19	3395	0.650383	32.602794	0.5	344.638409	111.0
20	2956	0.522354	44.119167	0.5	466.375967	119.0
21	2932	0.515925	44.865712	0.5	474.267567	123.0
22	2790	0.478970	49.608408	0.5	524.401775	127.0
23	2785	0.477702	49.786415	0.5	526.283456	135.0
24	3445	0.666344	31.494607	0.5	332.923965	143.0
25	4766	1.238244	8.513226	0.5	89.991821	147.0
26	4852	1.289397	7.096826	0.5	75.019307	151.0
27	4930	1.337856	5.785174	0.5	61.154055	155.0
28	4229	0.964204	17.103724	0.5	180.800461	163.0
29	1431	0.199193	172.124202	0.5	1819.494735	175.0
30	1250	0.169722	220.342846	0.5	2329.205565	
31				0.5		

$S_{MAX\,pos} = 89.9$

$S_m = S_{45} = 93.9 = 100\%$

$S_{20} = 72.6$ $\quad S_{20}/S_m = 72.6/93.9 = 77.3$

$S_{10} = 47.7$ $\quad S_{10}/S_m = 47.7/93.9 = 50.8$

$S_2 = 7.13$ $\quad S_2/S_m = 7.13/93.9 = 7.6$

$S_{MAX\,neg} = 106$

$Dia = 1361.3$

R1382WKS45 31R x 6C 02-FEB-89 11:14 Page 1

0 r138 2wk s45	1 b	2 b/f	3 mic/ml	4 flow	5 micu/ min-mm3	6 time
1	4468	1.077405	13.284627	0.5	140.429459	-7.5
2	4646	1.170572	10.451733	0.5	110.483435	-1.5
3	2454	0.398312	63.688221	0.5	673.237014	1.0
4	2477	0.403552	62.564341	0.5	661.356668	3.0
5	2631	0.439672	55.693455	0.5	588.725738	7.0
6	2061	0.314464	88.306852	0.5	933.476241	19.0
7	2041	0.310465	89.911606	0.5	950.439808	31.0
8	2098	0.321927	85.447851	0.5	903.254240	43.0
9	2000	0.302343	93.339880	0.5	986.679495	47.0
10	2064	0.315066	88.069808	0.5	930.970488	51.0
11	2141	0.330707	82.293550	0.5	869.910672	59.0
12	2024	0.307085	91.309950	0.5	965.221463	63.0
13	1992	0.300770	94.031504	0.5	993.990526	71.0
14	1964	0.295294	96.513517	0.5	1020.227449	79.0
15	2291	0.362271	72.525610	0.5	766.655498	87.0
16	2336	0.372034	69.920898	0.5	739.121542	91.0
17	2267	0.357120	73.971813	0.5	781.943051	95.0
18	2268	0.357334	73.910731	0.5	781.297370	103.0
19	3395	0.650383	32.602794	0.5	344.638409	111.0
20	2956	0.522354	44.119167	0.5	466.375967	119.0
21	2932	0.515925	44.865712	0.5	474.267567	123.0
22	2790	0.478970	49.608408	0.5	524.401775	127.0
23	2785	0.477702	49.786415	0.5	526.283456	135.0
24	3445	0.666344	31.494607	0.5	332.923965	143.0
25	4766	1.238244	8.513226	0.5	89.991821	147.0
26	4852	1.289397	7.096826	0.5	75.019307	151.0
27	4930	1.337856	5.785174	0.5	61.154055	155.0
28	4229	0.964204	17.103724	0.5	180.800461	163.0
29	1431	0.199193	172.124202	0.5	1819.494735	175.0
30	1250	0.169722	220.342846	0.5	2329.205565	
31				0.5		

$S_{m2\,pk} = 88.9$

$S_m = S_{45} = 93.9 = 100\%$

$S_{20} = 72.6$ $\quad S_{20}/S_m = 72.6/93.9 = 77.3$

$S_{10} = 47.7$ $\quad S_{10}/S_m = 47.7/93.9 = 50.8$

$S_2 = 7.13$ $\quad S_2/S_m = 7.13/93.9 = 7.6$

$S_{M2\,pos} = 106$

$Dia = 154.3$

R1382WKS30 26R x 6C 02-FEB-89 11:15 Page 1

0 r138 2wk s30	1 b	2 b/f	3 mic/ml	4 flow	5 micu/ min-mm3	6 time
1	5113	1.435430	3.209064	0.5	50.298810	-7.5
2	5252	1.534327	0.654268	0.5	10.254987	-1.5
3	3847	0.796810	24.055496	0.5	377.045393	1.0
4	3983	0.848892	21.664603	0.5	339.570587	3.0
5	4031	0.868002	20.846405	0.5	326.746152	7.0
6	3244	0.597312	36.729468	0.5	575.696998	19.0
7	3067	0.546897	41.451312	0.5	649.707092	31.0
8	2984	0.524337	43.893118	0.5	687.979911	43.0
9	2920	0.507385	45.890903	0.5	719.293157	47.0
10	2977	0.522464	44.106547	0.5	691.325187	51.0
11	3191	0.581875	38.080383	0.5	596.871206	59.0
12	2788	0.473586	50.371720	0.5	789.525398	71.0
13	2751	0.464382	51.724950	0.5	810.735895	75.0
14	2671	0.444870	54.814889	0.5	859.167532	79.0
15	3817	0.785714	24.599448	0.5	385.571293	87.0
16	3762	0.765724	25.614353	0.5	401.478892	99.0
17	3709	0.746879	26.615685	0.5	417.173749	103.0
18	3537	0.688400	30.048201	0.5	470.974943	107.0
19	4942	1.323868	6.161161	0.5	96.569924	115.0
20	4934	1.318899	6.295227	0.5	98.671270	123.0
21	4793	1.234673	8.613527	0.5	135.008253	135.0
22	4554	1.105072	12.419625	0.5	194.664968	139.0
23	4440	1.048406	14.216777	0.5	222.833492	143.0
24	2205	0.340804	78.919818	0.5	1236.987747	147.0
25	2147	0.328891	82.928567	-0.5	1299.820804	155.0
26				0.5		

$S_{14:\mu\dots} = 44.6$

$S_m = S_{20} = 52.3 \Rightarrow 100\%$

$S_{10} = 27.4$

$S_5 = 11.7$

$S_{\dots\mu\dots} = 81.0$

$S_{10}/S_m = 27.4/52.3 = 49.9$

$S_5/S_m = 27.4/52.3 = 22.4$

$Dia = 136.2\ \mu m$

R1383WK30 25R x 6C 01-FEB-89 16:28 Page 1

0 r138 3wk 30	1 b	2 b/f	3 mic/ml	4 flow	5 micu/ min-mm3	6 time min
1	4286	0.946346	17.757415	0.5	103.240783	-7.5
2	4926	1.266650	7.722194	0.5	44.896477	-1.5
3	2834	0.473834	50.336122	0.5	292.651869	1.0
4	3302	0.598948	36.590678	0.5	212.736501	3.0
5	3264	0.588002	37.534973	0.5	218.226589	7.0
6	2696	0.440595	55.535722	0.5	322.882107	19.0
7	2198	0.332175	81.787064	0.5	475.506183	31.0
8	1837	0.263256	113.789368	0.5	661.566093	43.0
9	1997	0.292901	97.635800	0.5	567.649998	47.0
10	1870	0.269258	110.141786	0.5	640.359218	51.0
11	1929	0.280134	104.048119	0.5	604.930922	59.0
12	1560	0.215024	153.341559	0.5	891.520690	71.0
13	1575	0.217541	150.689178	0.5	876.099871	75.0
14	1485	0.202592	167.756672	0.5	975.329487	79.0
15	4338	0.968952	16.932639	0.5	98.445574	83.0
16	3684	0.717989	28.244864	0.5	164.214324	95.0
17	3558	0.676812	30.796453	0.5	179.049146	99.0
18	3526	0.666667	31.472778	0.5	182.981266	103.0
19	5356	1.548424	0.292836	0.5	1.702536	111.0
20	5267	1.484498	1.936477	0.5	11.258587	123.0
21	5322	1.523619	0.929140	0.5	5.401977	127.0
22	5423	1.598762	0.000000	0.5	0.000000	131.0
23	3194	0.568226	39.341349	0.5	228.728771	135.0
24	1485	0.202592	167.756672	0.5	975.329487	147.0
25				0.5		

$S_{max\ pk} = 167.7$

$S_m \quad S_{20} = 157$

$S_{10} = 30.2$

$S_5 = .95$

$S_{max} = 167.7$

$S_{10}/S_m = \frac{30.2}{157} = 19.2$

$S_5/S_m = .95/157 = 0.6$

$Dia = 191.5$

0 r138 5wk 30	1 b	2 b/f	3 mic/ml		4 flow ml/min	5 micu/ mm3-min	6 time min
1	4075	1.141137	16.772070		0.4		-13.5
2	4142	1.182078	15.444670		0.4		-7.5
3	4177	1.204093	14.731768		0.4		-1.5
4	2361	0.446736	61.157374		0.5		1.0
5	2943	0.625771	40.121030		0.5		3.0
6	2915	0.616149	40.897179		0.5		8.0
7	2318	0.435060	63.252272		0.5		24.0
8	2221	0.409401	68.356405		0.5		36.0
9	2176	0.397806	70.919641		0.5		48.0
10	2079	0.373451	76.920900	S_{142}	0.5		60.0
11	2103	0.379397	75.371669		0.5		64.0
12	2051	0.366577	78.785514		0.5		68.0
13	2585	0.510769	51.645065		0.5		76.0
14	2106	0.380144	75.181103	S_{30}	0.5		82.0
15	2037	0.363166	79.741752		0.5		86.0
16	2018	0.358564	81.065887		0.5		90.0
17	1976	0.348501	84.105327		0.5		94.0
18	4172	1.200921	14.834522		0.5		102.0
19	3377	0.791052	29.933009		0.5		110.0
20	3207	0.722460	33.573624	S_{10}	0.5		114.0
21	2879	0.603944	41.922086		0.5		118.0
22	2773	0.569054	45.131267		0.5		122.0
23	4498	1.428844	7.226590		0.5		130.0
24	4282	1.272889	12.492823		0.5		138.0
25	4136	1.178348	15.565445	S_5	0.5		142.0
26	4064	1.134562	16.985915		0.5		146.0
27	1420	0.228076	146.286211		0.5		150.0
28	1067	0.162183	229.532355	$S_{142\,post}$	0.5		158.0
29	979	0.146843	262.019080		0.5		162.0
30							

$Vol = .0671\ mm^3$

Ave d.a = 195.4 μm

$S_{142} = 77.0$

$S_{30} = 74.3$

$S_{10} = 40.2$

$S_5 = 15.0$

$S_{142\,post} = 245.5$

$S_{30}/S_{142} = \frac{74.3}{77.0} = 96.4$

$S_{10}/S_{142} = \frac{40.2}{77.0} = 52.2$

$S_5/S_{142} = \frac{15.0}{77.0} = 19.5$

APPENDIX 4A:

REDUCED OXYGEN ISLET CELL AGGREGATE PERIFUSIONS

RAT SINGLE CELL AGGREGATE SUMMARY: DAY-2

Perifusion #-pO_2)	S/Smax	Ave ± st.dev.	Max Secretion ($\mu U/mm^3$-min)
R129D2SC142-142	100	100	316
R131D2SC152-15	100	100	150
R128D2SC12-12	83.8	80.2 ± 5.1	245
R135D2SC7-12	76.6		271
R127D2SC7-6	48.9	45.6 ± 4.6	190
R135D2SC7-6	42.4		271
R113D12SC-4	30.1		115
R129D2SC4-4	31.1	36.7 ± 10.6	494
R131D2SC152-4	49.0		150
R130D2SC71-(1.5-2.5)	21.8	18.0 ± 5.4	210
R130D2SC72-(1.5-2.5)	14.2		200

CANINE SINGLE CELL AGGREGATE SUMMARY

Perifusion #-pO_2)	S/Smax	Ave ± st.dev.	Max Secretion ($\mu U/mm^3$-min)
C2SC20-20	93.6		230
D3SC20-20	97.3	96.0 ± 2.1	500
C1SC16-20	97.1		107
C1SC12-12	94.8		115
C2SC12-12	80.2	91.6 ± 10.2	177
D3SC12-12	100		500
C2SC20-8	68.1		230
C1SC16-8	91.4	72.8 ± 16.7	107
D3SC20-8	59.1		500
C1SC12-5	71.3		15
C2SC12-5	47.9	60.0 ± 11.7	177
D3SC12-5	60.7		500
C1SC12-3	53.7		115
C2SC12-3	38.3	37.1 ± 20.6	177
D3SC20-3	7.6		500
C1SC16-3	48.7		107
C2SC20-(1.5-2.5)	30.4	20.7 ± 13.6	230
D3SC12-(1.5-2.5)	11.1		500

CANINE AND RAT SINGLE CELL AGGREGATE SUMMARY

Perifusion #-pO_2)	S/Smax	Ave ± st.dev.	Max Secretion ($\mu U/mm^3$-min)
R129D2SC142-142	100	100	316
C2SC20-20	93.6		230
D3SC20-20	97.3	96.0 ± 2.1	500
C1SC16-20	97.1		107
R131D2SC152-15	100	100	150
C1SC12-12	94.8		115
C2SC12-12	80.2		177
D3SC12-12	100	87.1 ± 9.9	500
R128D2SC12-12	83.8		245
R135D2SC7-12	76.6		271
C2SC20-8	68.1		230
C1SC16-8	91.4	72.8 ± 16.7	107
D3SC20-8	59.1		500
R127D2SC7-6	48.9	45.7 ± 4.6	190
R135D2SC7-6	42.4		271
C1SC12-5	71.3		150
C2SC12-5	47.9	60.0 ± 11/7	177
D3SC12-5	60.7		500
R113D12SC-4	30.1		115
R129D2SC4-4	31.1	36.7 ± 10.6	494
R131D2SC152-4	49.0		150
C1SC12-3	53.7		115
C2SC12-3	38.3	37.1 ± 20.7	177
D3SC20-3	7.6		500
C1SC16-3	48.7		107
C2SC20-(1.5-2.5)	30.4		230
D3SC12-(1.5-2.5)	11.1	19.4 ± 8.6	500
R130D2SC71-(1.5-2.5)	21.8		210
R130D2SC72-(1.5-2.5)	14.2		200

0 clsc16, 8,3 (1.5)	1 b	2 b/f	3 mic/ml	4 flow ml/min	5 micu/ min-mm3	6 time min
1	1618	0.641046	29.278289	0.5	77.867790	-10.5
2	1627	0.646918	28.924605	0.5	76.927141	-1.0
3	766	0.226896	108.310396	0.5	288.059563	1.0
4	926	0.287935	79.912113	0.5	212.532216	3.0
5	1357	0.487253	41.349069	0.5	109.970928	8.0
6	1365	0.491538	40.905794	0.5	108.792005	-20.0
7	1402	0.511679	38.931559	0.5	103.541380	28.0
8	1440	0.532939	37.022833	0.5	98.464982	36.0
9	1480	0.555973	35.127939	0.5	93.425370	40.0
10	1454	0.540923	36.347089	0.5	96.667790	44.0
11	1413	0.517772	38.367295	0.5	102.040678	52.0
12	1393	0.506730	39.400724	0.5	104.789159	60.0
13	1384	0.501813	39.876849	0.5	106.055451	68.0
14	1413	0.517772	38.367295	0.5	102.040678	72.0
15	1434	0.529542	37.316800	0.5	99.246809	76.0
16	1494	0.564199	34.489518	0.5	91.727441	84.0
17	1435	0.530107	37.267620	0.5	99.116010	92.0
18	1397	0.508925	39.191359	0.5	104.232337	100.0
19	1366	0.492075	40.850811	0.5	108.645773	104.0
20	1410	0.516105	38.520204	0.5	102.447352	108.0
21	1831	0.792298	21.286047	0.5	56.611827	120.0
22	1791	0.761803	22.766171	0.5	60.548326	128.0
23	1858	0.813485	20.276915	0.5	53.927964	132.0
24	1931	0.873360	17.469107	0.5	46.460391	136.0
25	1567	0.608544	31.337219	0.5	83.343667	140.0
26	1471	0.550730	35.544881	0.5	94.534257	144.0
27	1089	0.356698	60.920024	0.5	162.021340	156.0
28						

→

76

142
109.9
108.5
103.5 } 107.4

16
104.7
103
105 } 104.2

8
91.7
99
104 } 98.2

3
46.5
54
56.6 } 52.3

$\frac{S_{16}}{S_{107.4}} = \frac{104.2}{107.4} = 97.1$

$\frac{S_8}{S_{107.4}} = \frac{98.2}{107.4} = 91.4$

$\frac{S_3}{S_{107.4}} = \frac{52.3}{107.4} = 48.7$

0 c2sc20, 8,1.5	1 b	2 b/f	3 mic/ml	4 flow ml/min	5 micu/ min-mm3	6 time min
1	1815	0.788445	21.471034	0.5	106.292248	-10.5
2	1941	0.892004	16.598612	0.5	82.171347	-1.0
3	654	0.188854	136.843906	0.5	677.445081	1.0
4	658	0.190228	135.587753	0.5	671.226499	3.0
5	1157	0.390878	54.318308	0.5	268.902517	8.0
6	1204	0.413320	50.670152	0.5	250.842337	20.0
7	1257	0.439510	46.955369	0.5	232.452324	28.0
8	1226	0.424075	49.080275	0.5	242.971658	36.0
9	1304	0.463562	43.966916	0.5	217.658000	S_{142} 40.0
10	1265	0.443548	46.427623	0.5	229.839718	44.0
11	1402	0.516390	38.493981	0.5	190.564261	52.0 20
12	1255	0.438505	47.088590	0.5	233.111830	60.0
13	1327	0.475627	42.596987	0.5	210.876172	S_1, 68.0
14	1359	0.492748	40.782083	0.5	201.891502	72.0
15	1420	0.526511	37.582544	0.5	186.052199	76.0 — 8
16	1642	0.663434	27.955937	0.5	138.395726	84.0
17	1531	0.592034	32.458774	0.5	160.687000	96.0
18	1583	0.624704	30.290792	0.5	149.954414	104.0
19	1538	0.596355	32.159725	0.5	159.206560	S_P 108.0
20	1529	0.590804	32.544664	0.5	161.112200	112.0
21	1862	0.825721	19.699229	0.5	97.520937	116.0 1
22	1961	0.909555	15.777291	0.5	78.105401	124.0
23	2036	0.978376	12.510386	0.5	61.932605	$S_{1.5}$ 128.0
24	1965	0.913104	15.610830	0.5	77.281338	132.0
25	1740	0.732015	24.256990	0.5	120.084109	136.0 IV
26	1351	0.488431	41.226349	0.5	204.090838	140.0
27				0.5		

→

Point = P2

142

230
212 } 230
213

$$\frac{S_{20}}{S_{142}} = \frac{215.3}{230} = 93.6$$

20

233
211 } 215.3
202

$$\frac{S_P}{S_{142}} = \frac{156.7}{230} = 68.$$

8

161
159 } 156.7
150

$$\frac{S_{1.5}}{S_{142}} = \frac{70}{230} = 30.4$$

1.5

62
78 } 70.0

0 c2sc12, 5,3	1 b	2 b/f	3 mic/ml	4 flow ml/min	5 micu/ min-mm3	6 time	
1	1975	0.913506	15.591971	0.5	77.187976	-10.5	
2	2051	0.983221	12.276224	0.5	60.773387	-1.0	
3	792	0.236771	102.576329	0.5	507.803609	1.0	
4	916	0.284384	81.185853	0.5	401.910165	3.0	
5	1464	0.547699	35.789630	0.5	177.176384	8.0	
6	1321	0.469105	43.327621	0.5	214.493173	20.0	
7	1533	0.588710	32.691626	0.5	161.839732	32.0	
8	1459	0.544810	36.025585	0.5	178.344482	44.0	
9	1489	0.562311	34.634398	0.5	171.457414	48.0	S_{102}
10	1445	0.536776	36.695448	0.5	181.660632	52.0	
11	1671	0.677616	27.152005	0.5	134.415865	60.0	12
12	1636	0.654138	28.496592	0.5	141.072238	68.0	
13	1593	0.626179	30.197589	0.5	149.493016	76.0	
14	1639	0.656125	28.380091	0.5	140.495500	80.0	S_{12}
15	1662	0.671515	27.494894	0.5	136.113335	84.0	
16	2021	0.955104	13.626221	0.5	67.456542	92.0	5
17	1920	0.866035	17.811036	0.5	88.173447	100.0	
18	2005	0.941342	14.280065	0.5	70.693390	108.0	
19	1892	0.842762	18.899012	0.5	93.559464	112.0	S_5
20	1909	0.856822	18.241294	0.5	90.303437	116.0	
21	2055	0.987032	12.091622	0.5	59.859513	124.0	3
22	1975	0.913506	15.591971	0.5	77.187976	136.0	
23	1985	0.922398	15.174214	0.5	75.119869	144.0	
24	2028	0.961593	13.316447	0.5	65.923003	148.0	
25	2043	0.975645	12.642070	0.5	62.584506	152.0	
26	935	0.292005	78.496417	0.5	388.596123	156.0	N
27	1878	0.831341	19.434812	0.5	96.211938	160.0	
28	1611	0.637767	29.478016	0.5	145.930771	168.0	
29				0.5			

→

$\frac{S_{12}}{S_{102}} = \frac{102}{177} = 80.2$

$\frac{S_5}{S_{102}} \quad \frac{84.9}{177} = 47.9$

$\frac{S_3}{S_{102}} = \frac{67.9}{177} \quad 38.3$

142
182
172
178 } 177.3

12
136
140.5
149.5 } 142.3

5
90.3
93.5
71.5 } 84.9

3
62.6
66
75.1 } 67.9

0 clscl2, 5,3	1 b	2 b/f	3 mic/ml	4 flow	5 micu/ min-mm3	6 time min	
1	1491	0.568867	34.135497	0.5	74.207603	-10.5	
2	1688	0.696370	26.123293	0.5	56.789766	-1.0	
3	842	0.257492	92.155035	0.5	200.337034	1.0	
4	845	0.258647	91.630065	0.5	199.195794	3.0	
5	1338	0.482336	41.868644	0.5	91.018791	8.0	
6	1450	0.544703	36.034317	0.5	78.335472	20.0	
7	1498	0.573068	33.821705	0.5	73.525446	28.0	
8	1460	0.550528	35.561120	0.5	77.306782	36.0	
9	1446	0.542386	36.225519	0.5	78.751129	40.0	
10	1495	0.571265	33.955838	0.5	73.817039	44.0	
11	1468	0.555219	35.187376	0.5	76.494295	52.0	12
12	1317	0.471199	43.090612	0.5	93.675243	60.0	
13	1195	0.409667	51.232171	0.5	111.374284	68.0	
14	1224	0.423823	49.116456	0.5	106.774904	72.0	
15	1216	0.419890	49.687708	0.5	108.016756	76.0	
16	1505	0.577292	33.510730	0.5	72.849414	84.0	5
17	1484	0.564688	34.452187	0.5	74.896060	92.0	
18	1427	0.531471	37.149353	0.5	80.759463	100.0	
19	1417	0.525788	37.646362	0.5	81.839917	104.0	
20	1403	0.517903	38.355302	0.5	83.381091	108.0	
21	1607	0.641517	29.249732	0.5	63.586374	120.0	3
22	1646	0.667478	27.724245	0.5	60.270098	128.0	
23	1621	0.650743	28.696984	0.5	62.384748	132.0	
24	1644	0.666126	27.801449	0.5	60.437933	136.0	
25	891	0.276622	84.101023	0.5	182.828311	140.0	10
26	1137	0.382185	55.866806	0.5	121.449578	144.0	
27				0.5			

→

Pre-Shock

Post-Shock

56.

$S_1 = \frac{\quad}{\quad} = 100$

$S_1 = \frac{\quad}{\quad} = 94.1$

102

$S_5 = \frac{\quad}{\quad} = 75.2$

$S_5 = \frac{\quad}{\quad} = 67.8$

78
74
73 } 75

$S_3 = \frac{61.7}{109} = 56.6$

$S_3 = \frac{\quad}{\quad} = 51.0$

102 post: 121

Average Post-Shock

12

$S_1 = \frac{109}{(\text{average})} = 94.8$

108
107
111 } 109

$S_5 = \frac{\quad}{\quad} = 71.3$

$S_3 = \frac{61.7}{(\text{average})} = 53.7$

5

83
82
81 } 82

3

60
62
59 } 61.7

0 d3sc20	1 b	2 b/f	3 mic/ml	4 flow	5 micu/ min-mm3	6 time min	
1	3097	0.559227	40.209832	0.5		-16.5	
2	2975	0.525618	43.748037	0.5		-10.5	
3	3639	0.728383	27.644764	0.5		-1.5	
4	820	0.104926	481.400692	0.5		1.0	
5	978	0.127726	347.306822	0.5		3.0	
6	1606	0.228482	140.057785	0.5		8.0	
7	1568	0.221876	146.309249	0.5		20.0	
8	1494	0.209214	159.791897	0.5		32.0	
9	1499	0.210062	158.821341	0.5		36.0	142
10	1488	0.208199	160.968760	0.5		40.0	20
11	1531	0.215512	152.820607	0.5		48.0	
12	1440	0.200139	170.888270	0.5		56.0	
13	1594	0.226388	141.986652	0.5		64.0	
14	1521	0.213804	154.657563	0.5		68.0	
15	1516	0.212951	155.588899	0.5		72.0	
16	2314	0.366081	71.488310	0.5		80.0	8
17	1985	0.298496	95.047828	0.5		92.0	
18	1988	0.299082	94.783972	0.5		96.0	
19	2000	0.301432	93.739427	0.5		100.0	
20	4815	1.260471	7.893249	0.5		108.0	3
21	4612	1.146408	11.165832	0.5		120.0	
22	4610	1.145342	11.197653	0.5		124.0	
23	4597	1.138435	11.404366	0.5		128.0	
24	1204	0.162024	236.998061	0.5		132.0	
25	2335	0.370635	70.283603	0.5		140.0	142
26				0.5			

S_{142} S_{20} S_8 S_3

142 ppm
160
159
161
} 160

20 ppm
142
156
} 156

$\frac{S_{20}}{S_{142}} = \frac{156}{160} = .973$

8
95.0
94.8
93.7
} 94.5

$\frac{S_8}{S_{142}} = \frac{94.5}{160} = .591$

3
11.2
11.3
11.4
} 11.3

$\frac{S_3}{S_{142}} = \frac{11.3}{160} = .076$

142 ppm
937

0 d3sc12	1 b	2 b/f	3 mic/ml	4 flow	5 micu/ min-mm3	6 time	
1	3709	0.749899	26.452121	0.5		-7.5	
2	3914	0.825564	22.704440	0.5		-1.5	
3	1644	0.234489	134.776661	0.5		1.0	
4	1948	0.290443	98.813791	0.5		3.0	
5	2803	0.478982	49.606787	0.5		7.0	
6	2901	0.504171	46.287075	0.5		23.0	
7	2493	0.404576	62.348698	0.5		35.0	
8	2538	0.414909	60.246895	0.5		47.0	
9	2493	0.404576	62.348698	0.5		51.0	142
10	2578	0.424222	58.458834	0.5		59.0	12
11	2409	0.385687	66.551529	0.5		61.0	
12	2488	0.403438	62.588411 } 12	0.5		69.0	
13	2415	0.387019	66.238446	0.5		77.0	
14	3561	0.699058	29.381600	0.5		89.0	5
15	3143	0.570210	39.153923	0.5		93.0	
16	3123	0.564534	39.694023 } 5	0.5		97.0	
17	3127	0.565666	39.585363	0.5		105.0	
18	4897	1.303087	6.723600	0.5		117.0	1.5
19	4820	1.256845	7.993900 } 1.5	0.5		121.0	
20	4883	1.294539	6.956378	0.5		125.0	
21	3800	0.782698	24.749628	0.5		129.0	
22	3945	0.837580	22.162945	0.5		137.0	142
23	3125	0.565099	39.639653	0.5		145.0	
24				0.5			

142 pre
62.3
60.2 } 61.6
62.3

12
66.6
62.6 } 65.1
66.2

$\frac{S_{12}}{S_{142\,pre}} = \frac{65.1}{65.1} = 100$

5
39.2
39.7 } 39.5
39.6

$\frac{S_{5}}{S_{142\,pre}} = \frac{39.5}{65.1} = .60.7$

1.5
6.72
7.99 } 7.22
6.96

$\frac{S_{1.5}}{S_{142\,pre}} = \frac{7.22}{65.1} = 11.1$

142 post
39.6

R135D2SC7 26R x 6C

0 r135d2 sc 7 7	1 b	2 b/f	3 mic/ml	4 flow ml/min	5 mic/min	6 time min
1	1064	0.315353	70.233901	0.5	35.116951	-27.5
2	973	0.280808	82.775887	0.5	41.387943	-12.5
3	913	0.259007	92.915705	0.5	46.457852	-2.5
4	864	0.241746	102.583659	0.5	51.291829	1.0
5	219	0.051908	916.374823	0.5	458.187411	2.0
6	255	0.060961	726.643788	0.5	363.321894	3.0
7	405	0.100422	358.077231	0.5	179.038616	9.0
8	349	0.085351	450.358273	0.5	225.179137	21.0
9	294	0.070946	585.148926	0.5	292.574463	29.0
10	317	0.076923	521.690947	0.5	260.845473	37.0
11	300	0.072499	567.419541	0.5	283.709770	41.0
12	312	0.075618	534.496576	0.5	267.248288	45.0
13	334	0.081384	481.685415	0.5	240.842708	53.0
14	380	0.093642	395.144550	0.5	197.572275	61.0
15	347	0.084820	454.341958	0.5	227.170979	69.0
16	373	0.091759	406.626757	0.5	203.313378	73.0
17	375	0.092296	403.292235	0.5	201.646118	77.0
18	578	0.149741	203.633021	0.5	101.816510	85.0
19	564	0.145586	211.931863	0.5	105.965931	93.0
20	566	0.146178	210.715610	0.5	105.357805	101.0
21	526	0.134458	237.206153	0.5	118.603077	109.0
22	555	0.142931	217.537644	0.5	108.768822	113.0
23	530	0.135619	234.336864	0.5	117.168432	117.0
24	233	0.055410	833.686627	0.5	416.843313	125.0
25	348	0.085086	452.343034	0.5	226.171517	133.0
26						

$1/\alpha = .245$

S_n = 260.8, 283.7, 267.2 } 270.6

S_{12} = 197.6, 227.2, 203.3, 201.6 } 207.4

$S_{6.5}$ = 105.4, 118.6, 108.8, 117.2 } 114.8

$\frac{S_{12}}{S_n} = \frac{207.4}{270.6} = 76.6$

$\frac{S_{6.5}}{S_n} = \frac{114.8}{270.6} = 42.4$

R127D2SC7 25R x 6C 03-OCT-88 12:06 Page 1

0 r127d2 sc7	1 bound	2 b/f	3 micU/ml	4 micU/min-mm3	5 time min	6 % max
1	438	0.255841	68.594709	311.794132	-105.0	159.522579
2	542	0.337065	48.514139	220.518814	-65.0	112.823579
3	628	0.412615	36.984728	168.112399	-45.0	86.010995
4	670	0.452703	32.181185	146.278115	-25.0	74.839966
5	740	0.524823	24.834550	112.884317	-10.0	57.754767
6	745	0.530249	24.330740	110.594273	-0.5	56.583116
7	330	0.181319	107.990597	490.866350	1.0	251.140923
8	549	0.342911	47.456810	215.712774	3.0	110.364675
9	613	0.398829	38.805060	176.386638	12.0	90.244326
10	612	0.397919	38.928729	176.948766	24.0	90.531927
11	573	0.363348	44.016653	200.075697	36.0	102.364310
12	600	0.387097	40.437191	183.805414	40.0	94.039979
13	569	0.359899	44.571614	202.598248	44.0	103.654917 — 46. Drop to 6. — Ns. (Queue = 5 prob.)
14	781	0.570489	20.754844	94.340199	52.0	48.267078
15	749	0.534618	23.929142	108.768826	60.0	55.649167
16	772	0.560232	21.641593	98.370878	68.0	50.329286
17	769	0.556843	21.938112	99.718691	72.0	51.018865
18	794	0.585546	19.480375	88.547157	76.0	45.303197 — 77P. Raise to Normal.
19	380	0.214689	85.938121	390.627822	80.0	199.856095
20	582	0.371173	42.792460	194.511182	88.0	99.517349
21	576	0.365947	43.604899	198.204088	96.0	101.406743
22						
23						
24						
25						

$$\frac{Q6}{Qn} = \left.\begin{matrix}45.3\\51.01\\50.3\end{matrix}\right\} - 48.9\ \%$$

R128D2SC12 25R x 6C 03-OCT-88 12:05 Page 1

0 r128d2 sc12	1 bound	2 b/f	3 micU/ml	4 micU/mm3-min	5 time min	6 %max
1	505	0.309816	53.972605	122.665011	-20.0	51.402481
2	521	0.322800	51.253641	116.485549	-10.0	48.812992
3	543	0.341080	47.783934	108.599851	-0.5	45.508509
4	191	0.098251	279.068047	634.245560	1.0	265.779092
5	392	0.224900	80.877317	183.812085	3.0	77.026016
6	498	0.304215	55.221204	125.502737	5.0	52.591623
7	380	0.216524	84.982681	193.142456	12.0	80.935886
8	345	0.192737	99.280860	225.638318	28.0	94.553200
9	333	0.184795	105.183117	239.052538	40.0	100.174397
10	320	0.176309	112.307412	255.244118	44.0	106.959440
11	352	0.197420	96.099726	218.408469	48.0	91.523549
12	359	0.202140	93.092411	211.573661	56.0	88.659439
13	379	0.215831	85.340874	193.956532	64.0	81.277023
14	368	0.208263	89.459371	203.316753	72.0	85.199401
15	372	0.211004	87.922760	199.824455	76.0	83.735962
16	324	0.178907	110.027148	250.061700	80.0	104.787760
17	233	0.122503	193.989784	440.885872	84.0	184.752175
18	309	0.169222	119.026175	270.514033	92.0	113.358262
19						
20						
21						
22						
23						
24						
25						

50 - Acute 12

P2 - Normal

w/o basal

$\frac{Q_{12}}{Q_N} = \frac{P1.3,\ P3.7,\ P5.2}{3} \rightarrow P3.P$

Q over Prob

$\frac{199.}{237}$

R130D2SC71 20R x 6C

24-OCT-88 12:44 Page 1

0 r130d2sc 7mmHg #1	1 b	2 b/f	3 mic/ml	4 flow	5 mic/min	6 time
1	2068	0.361728	56.869275	0.4	22.747710	-20.0
2	2226	0.400432	51.515285	0.4	20.606114	-10.0
3	2331	0.427393	48.392099	0.4	19.356840	-0.5
4	857	0.123701	248.816788	0.4 4.5	99.526715	1.0
5	1632	0.265236	79.203742	0.4 .5	31.681497	3.0
6	1780	0.296420	69.854174	0.4 ↓	27.941670	8.0
7	1785	0.297500	69.578020	0.4	27.831208	20.0
8	1722	0.284018	73.231832	0.4	29.292733	32.0
9	1775	0.295341	70.132603 }	0.4	28.053041	40.0
10	1781	0.296636	69.798763 } S_{n4L}	0.4	27.919505	44.0
11	1766	0.293404	70.639600 }	0.4	28.255840	48.0 5'
12	3193	0.695340	28.627039	0.4	11.450816	56.0
13	3753	0.930804	17.351582	0.4	6.940633	68.0
14	3735	0.922222	17.713171	0.4	7.085268	80.0
15	3774	0.940912	16.929724 }	0.4	6.771890	92.0
16	3821	0.963925	15.985625 } S_{b}	0.4	6.394250	100.0
17	3962	1.036359	13.156240 }	0.4	5.262496	104.0 100 - ~ 0_L
18	3609	0.854224	20.243832	0.4	8.097533	108.0
19	3606	0.862886	20.304075	0.4	8.121630	116.0
20				0.4		

S_b ~ 1? question ... 70.2 ...

Normal

70.6
64.7 } 70.1
70.1

w/o basal

$\frac{S_{1.5-2.5}}{S_{N4L}} = \frac{15.3}{70.1} = 21.8\ \%$

1.5-2.5

13.1
15.4 } 15.3
16.9

basal (conc)

36

R130D2SC72 19R x 6C

24-OCT-88 12:45 Page 1

0 r130 d2sc 7mmHg #2	1 b	2 b/f	3 mic/ml	4 flow	5 mic/min	6 time min
1	2611	0.500287	41.528759	0.4	16.611504	-10.0
2	2665	0.515973	40.263792	0.4	16.105517	-0.5
3	1023	0.150286	177.562706	0.5	88.781353	1.0
4	1679	0.272964	76.606341	0.5	38.303170	3.0
5	1946	0.330727	62.225370	0.5	31.112685	10.0
6	1935	0.328244	62.708792	0.5	31.354396	22.0
7	1978	0.338004	60.859855	0.5	30.429927	34.0
8	2006	0.344437	59.712004	0.5	29.856002	42.0
9	2104	0.367447	55.998239	0.5	27.999120	46.0
10	2050	0.354671	57.989555	0.5	28.994777	50.0
11	4096	1.096947	10.948450	0.5	5.474225	58.0
12	4183	1.146970	9.230792	0.5	4.615396	70.0
13	4368	1.261698	5.640439	0.5	2.820219	78.0
14	4295	1.214993	7.044030	0.5	3.522015	86.0
15	4198	1.155837	8.936077	0.5	4.468038	90.0
16	4214	1.165376	8.622271	0.5	4.311135	94.0
17	3936	1.010786	14.131046	0.5	7.065523	102.0
18	3892	0.988319	15.009025	0.5	7.504512	110.0
19						

S_{1+2}

S_x

Normal

58.0
56.0
59.7
} 57.9

Wt'g Basal

$\frac{S_{1.5-2.5}}{S_{1+2}} = \frac{8.2}{57.9} = 14.2$

1.5-2.5

7.0
8.9
8.6
} 8.2

Basal (cum)

30

R131D2SC152 23R x 6C

24-OCT-88 12:47 Page 1

0 r131d2sc 15mmHg #2	1 b	2 b/f	3 mic/ml	4 flow	5 mic/min	6 time	
1	3314	0.726595	26.940950	0.4	10.776380	-10.0	
2	3498	0.799178	23.276184	0.4	9.310474	-0.5	
3	3509	0.803710	23.057661	0.5	11.528831	1.0	
4	3287	0.716434	27.481246	0.5	13.740623	3.0	
5	3588	0.836949	21.488967	0.5	10.744484	8.0	
6	3363	0.745346	25.962527	0.5	12.981263	24.0	
7	3234	0.696833	28.544839	0.5	14.272419	40.0	
8	3315	0.726974	26.920957	0.5	13.460478	48.0	
9	3320	0.728869	26.821006	0.5	13.410503	52.0	N
10	3287	0.716434	27.481246	0.5	13.740623	56.0	50 mmHg
11	3251	0.703071	28.203206	0.5	14.101603	64.0	
12	3294	0.719057	27.341080	0.5	13.670540	72.0	
13	3165	0.671975	29.937077	0.5	14.968539	80.0	S_{15}
14	3150	0.666667	30.241111	0.5	15.120556	84.0	
15	3365	0.746120	25.922641	0.5	12.961321	88.0	40 -
16	3701	0.886679	19.245682	0.5	9.622841	96.0	
17	3709	0.890302	19.086846	0.5	9.543423	108.0	
18	3921	0.991654	14.877403	0.5	7.438701	120.0	
19	3836	0.949740	16.564924	0.5	8.282462	124.0	
20	3787	0.926370	17.538002	0.5	8.769001	128.0	10 - Rand
21	3691	0.882170	19.444221	0.5	9.722111	132.0	
22	4078	1.074006	11.767798	0.5	5.883899	140.0	
23							

w/o Basal s

$S_{15} = \frac{14.1}{13.5} = 100$

Normal

13.7
13.4
13.5 } 13.53

$S_4 = \frac{7.4}{15.0} = 49$

15 mm Hg

13.6
Peak { 14.9
15.1
12.9 } 14.1

S_4

7.4 } 7.4

Basal

9.3

R129D2SC4 18R x 6C

24-OCT-88 12:43 Page 1

0 r129d2sc 4mmHg	1 b	2 b/f	3 mic/ml	4 flow	5 micu/ min-mm3	6 time min
1	2378	0.434973	47.582825	0.4	271.901858	-10.0
2	2506	0.469376	44.214088	0.4	252.651933	-0.5
3	1062	0.156568	165.971904	0.5	1185.513597	1.0
4	1645	0.265323	79.173606	0.5	565.525761	3.0
5	1741	0.285223	72.885869	0.5	520.613349	8.0
6	1769	0.291145	71.242484	0.5	508.874886	20.0
7	1798	0.297338	69.619378	0.5	497.281274	32.0
8	1803	0.298411	69.347221	0.5	495.337296	40.0
9	1813	0.300564	68.809435	0.5	491.495966	44.0
10	1798	0.297338	69.619378	0.5	497.281274	48.0
11	2769	0.545508	38.027675	0.5	271.626250	56.0
12	3554	0.828245	21.894150	0.5	156.386786	68.0
13	3507	0.808437	22.831006	0.5	163.078611	80.0
14	3683	0.884911	19.323428	0.5	138.024488	84.0
15	3525	0.815972	22.472167	0.5	160.515475	88.0
16	1890	0.317380	64.938050	0.5	463.843213	92.0
17	2871	0.577201	35.803883	0.5	255.742021	96.0
18	1887	0.316717	65.080572	0.5	464.861232	104.0

Normal

495
491
497
} 494.3

w/o basal

$\frac{Q_4}{Q_N} = \frac{154}{494.3} = 31.1\ \%$

54 mm Hg

163
138
160
} 154

basal

252

R129D2SC142 18R x 6C

24-OCT-88 12:41 Page 1

0 r129d2sc 142mmHg	1 b	2 b/f	3 mic/ml	4 flow ml/min	5 micu/ min-mm3	6 time min
1	2913	0.596071	34.551731	0.4	197.438461	-15.0
2	2988	0.620948	32.970926	0.4	188.405293	-6.0
3	2931	0.601972	34.169937	0.4	195.256785	-0.5
4	1441	0.226608	96.255003	0.5	687.535737	1.0
5	2357	0.433033	47.787376	0.5	341.338400	3.0
6	3268	0.721094	27.232534	0.5	194.518097	8.0
7	2904	0.593137	34.743247	0.5	248.166050	20.0
8	2690	0.526419	39.452600	0.5	281.804283	32.0
9	2775	0.552239	37.541492	0.5	268.153516	44.0
10	2598	0.499423	41.600201	0.5	297.144294	52.0
11	2494	0.470034	44.153939	0.5	315.385279	60.0
12	2449	0.457671	45.309456	0.5	323.638969	68.0
13	2519	0.476993	43.526026	0.5	310.900187	76.0
14	2156	0.381999	53.915353	0.5	385.109661	84.0
15	2388	0.441242	46.933569	0.4	268.191822	88.0
16	3608	0.860687	20.403245	0.4	116.589070	100.0
17						
18						

Basal

197
188
195 } 193

$\frac{S_{142}}{S_{-}} : \frac{316}{282} = 112.1\%$

142

281
268 } = 282

142 cm

323
310
315 } 316

APPENDIX 5A:

INSULIN SECRETION OF ISLETS AND AGGREGATES IN STATIC CULTURE

INSULIN SECRETION OF SINGLE CELLS IN FIBERS UNDER NORMAL AND LOW O2 CONDITIONS (R75)

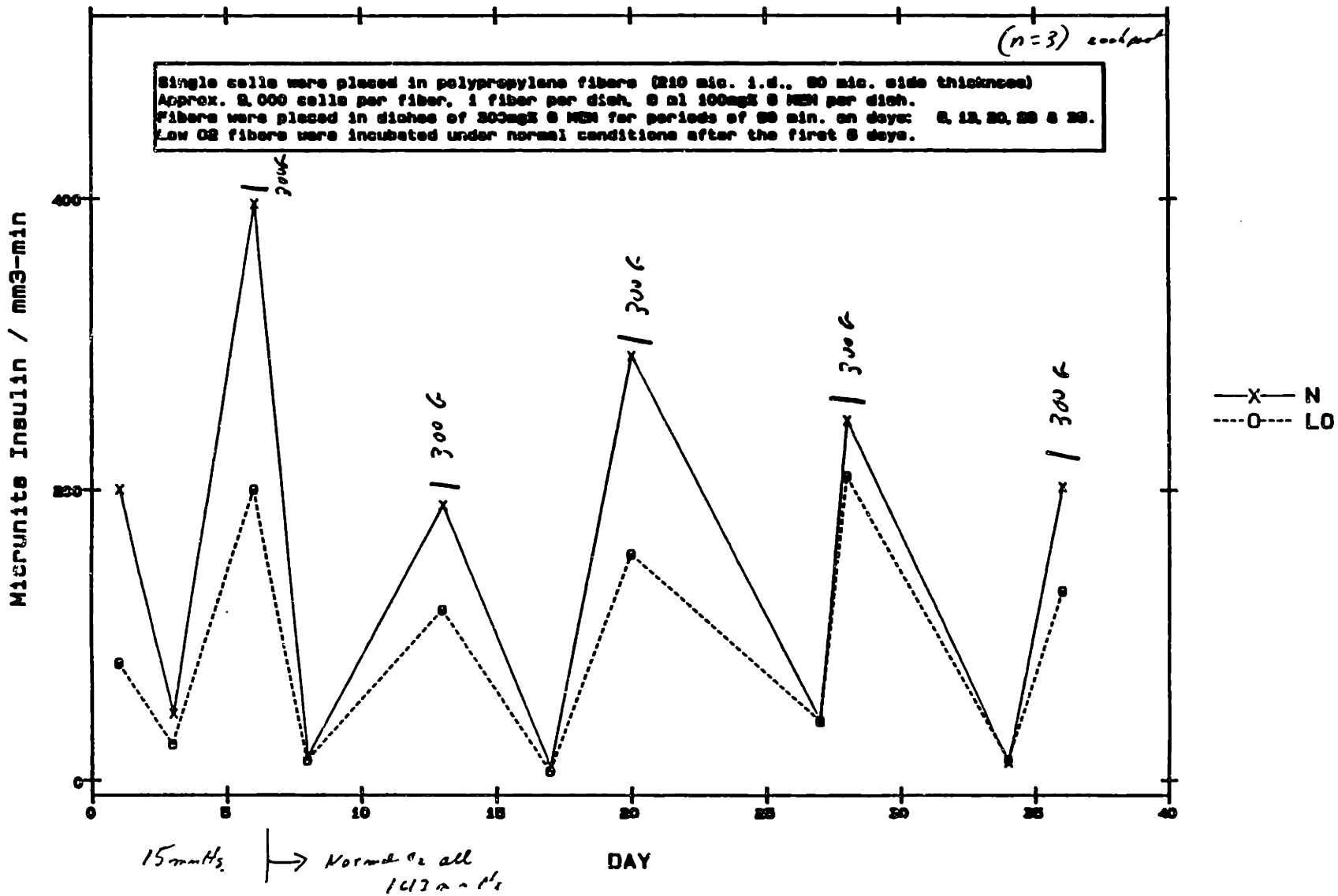

INSULIN SECRETION OF ISLETS IN FIBERS UNDER NORMAL AND LOW O2 CONDITIONS (R75)

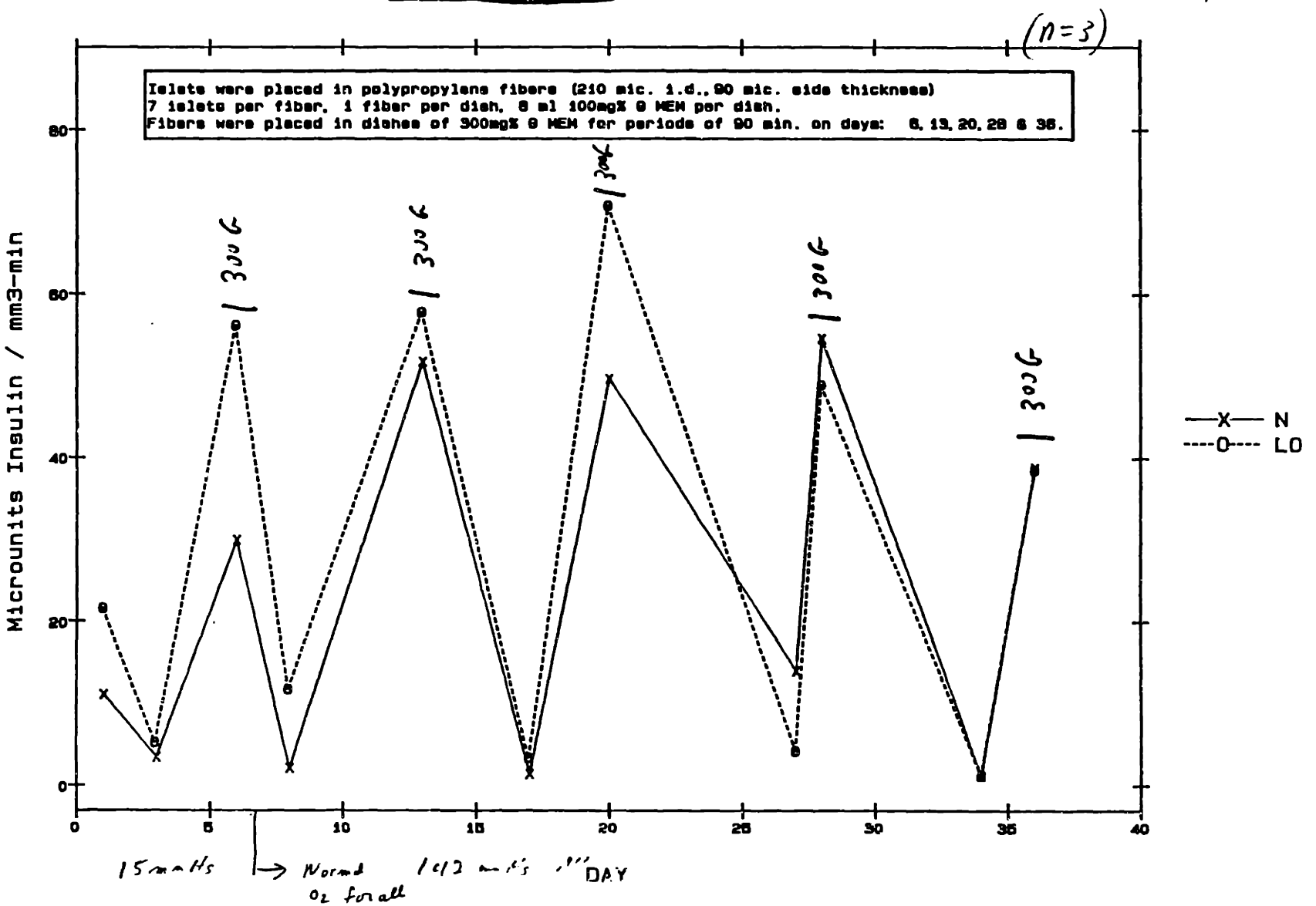

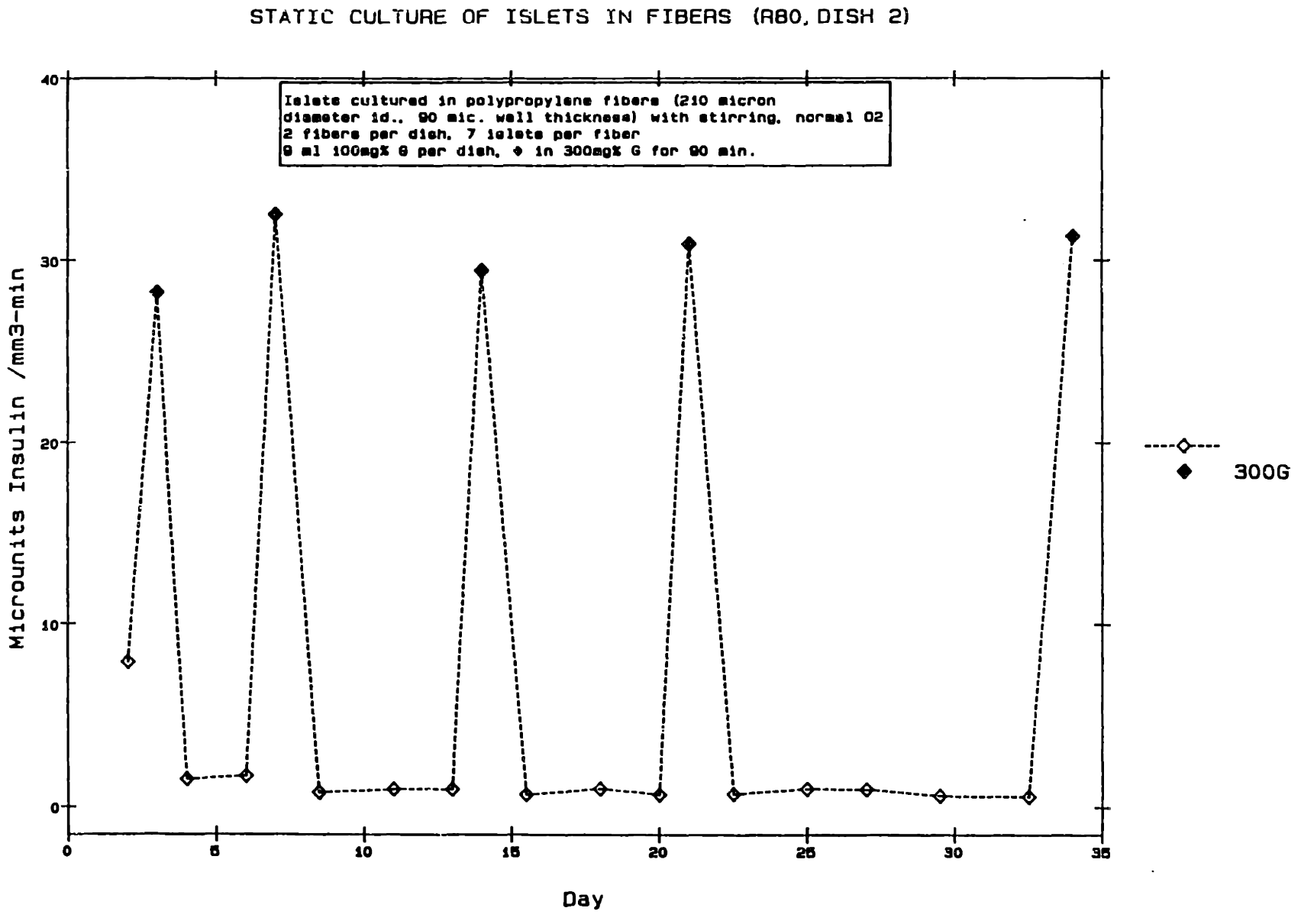
STATIC CULTURE OF ISLETS IN FIBERS (R80, DISH 2)
Islets cultured in polypropylene fibers (210 micron diameter id., 90 mic. wall thickness) with stirring, normal O2
2 fibers per dish, 7 islets per fiber
9 ml 100mg% G per dish, ◆ in 300mg% G for 90 min.
Microunits Insulin /mm3-min
Day
300G
0
10
20
30
40
0
5
10
15
20
25
30
35

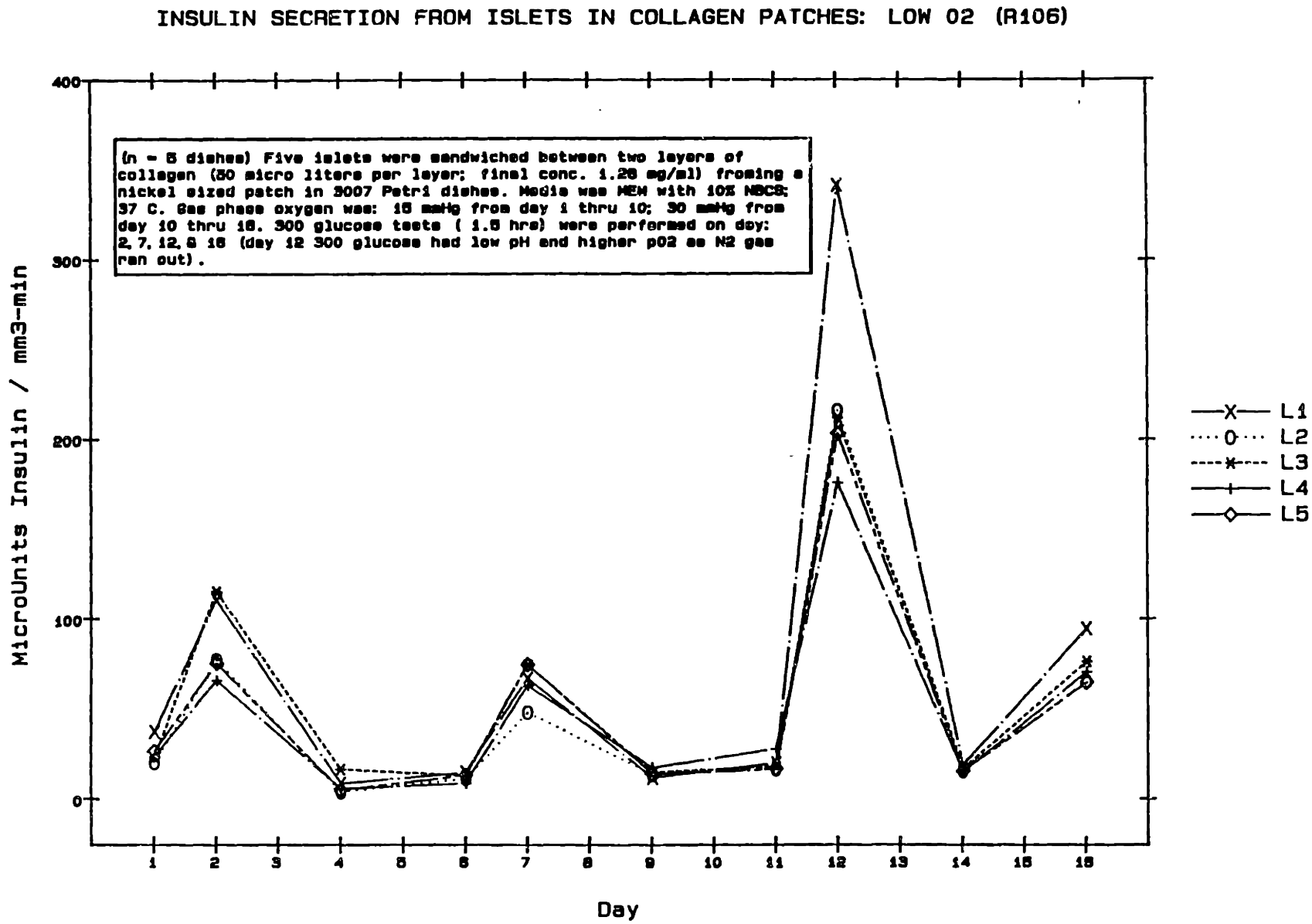
INSULIN SECRETION FROM ISLETS IN COLLAGEN PATCHES: LOW 02 (R106)
(n = 5 dishes) Five islets were sandwiched between two layers of collagen (50 micro liters per layer; final conc. 1.26 mg/ml) froming a nickel sized patch in 3007 Petri dishes. Media was MEM with 10% NBCS; 37 C. Gas phase oxygen was: 15 mmHg from day 1 thru 10; 30 mmHg from day 10 thru 16. 300 glucose tests (1.5 hrs) were performed on day: 2, 7, 12, & 16 (day 12 300 glucose had low pH and higher pO2 as N2 gas ran out).
MicroUnits Insulin / mm3-min
400
300
200
100
0
1
2
3
4
5
6
7
8
9
10
11
12
13
14
15
16
Day
L1
L2
L3
L4
L5

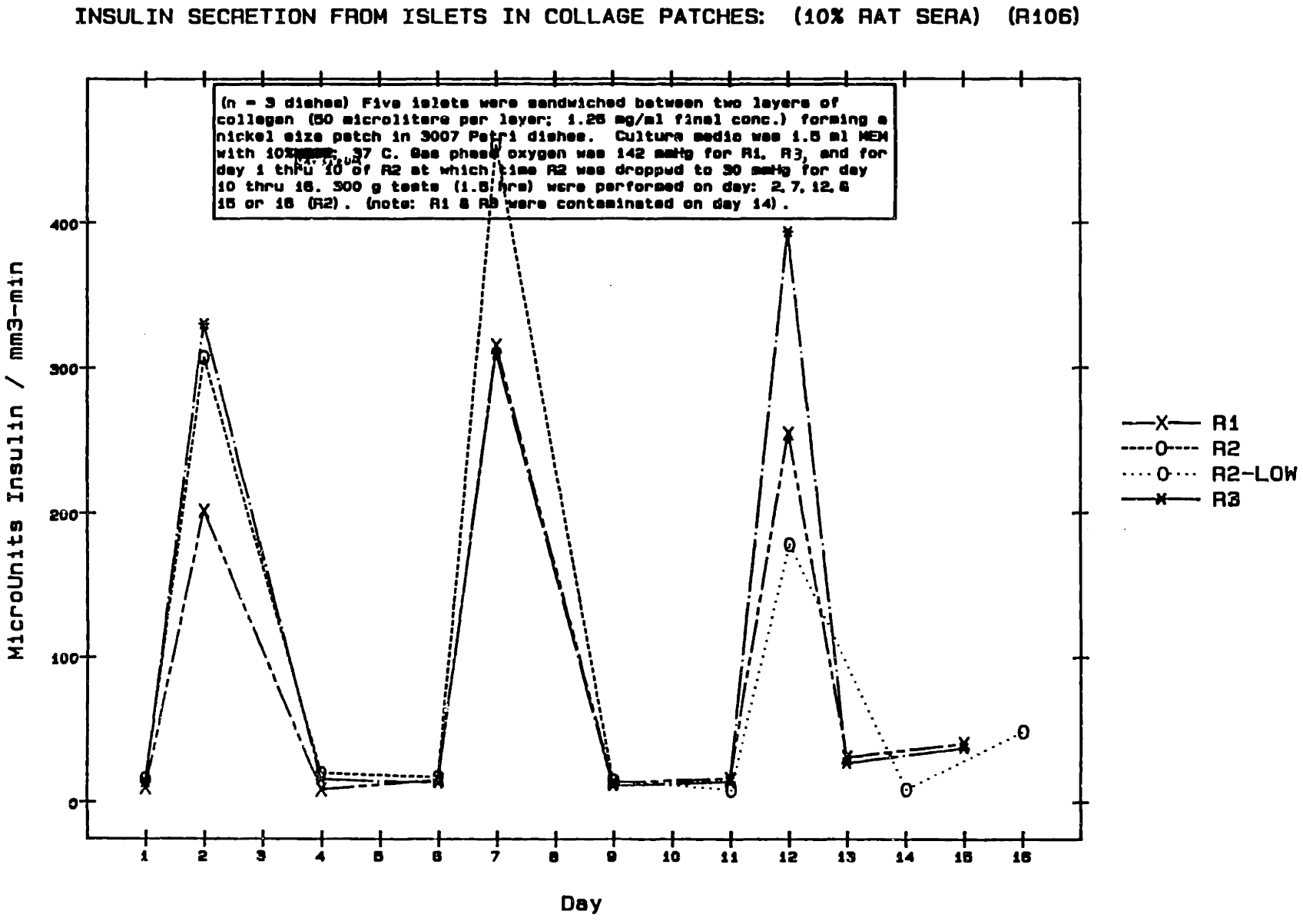
INSULIN SECRETION FROM ISLETS IN COLLAGE PATCHES: (10% RAT SERA) (R106)
(n = 3 dishes) Five islets were sandwiched between two layers of collagen (50 microliters per layer; 1.25 mg/ml final conc.) forming a nickel size patch in 3007 Petri dishes. Culture media was 1.5 ml MEM with 10% [illegible], 37 C. Gas phase oxygen was 142 mmHg for R1, R3, and for day 1 thru 10 of R2 at which time R2 was dropped to 30 mmHg for day 10 thru 16. 300 g tests (1.5 hrs) were performed on day: 2, 7, 12, & 15 or 16 (R2). (note: R1 & R3 were contaminated on day 14).
MicroUnits Insulin / mm3-min
0
100
200
300
400
1
2
3
4
5
6
7
8
9
10
11
12
13
14
15
16
Day
R1
R2
R2-LOW
R3

INSULIN SECRETION FROM ISLETS IN COLLAGEN PATCHES (R106, AVE)

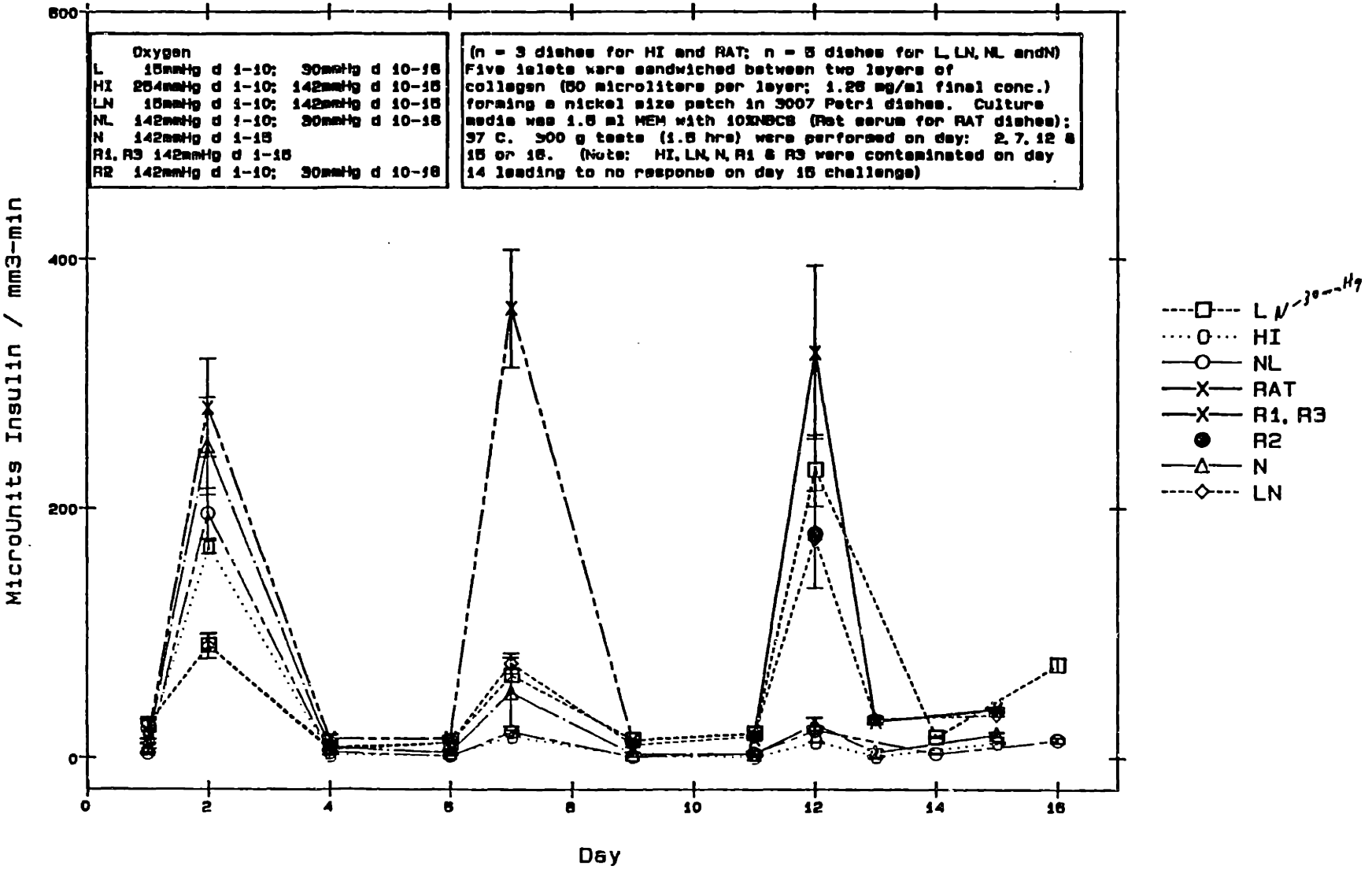

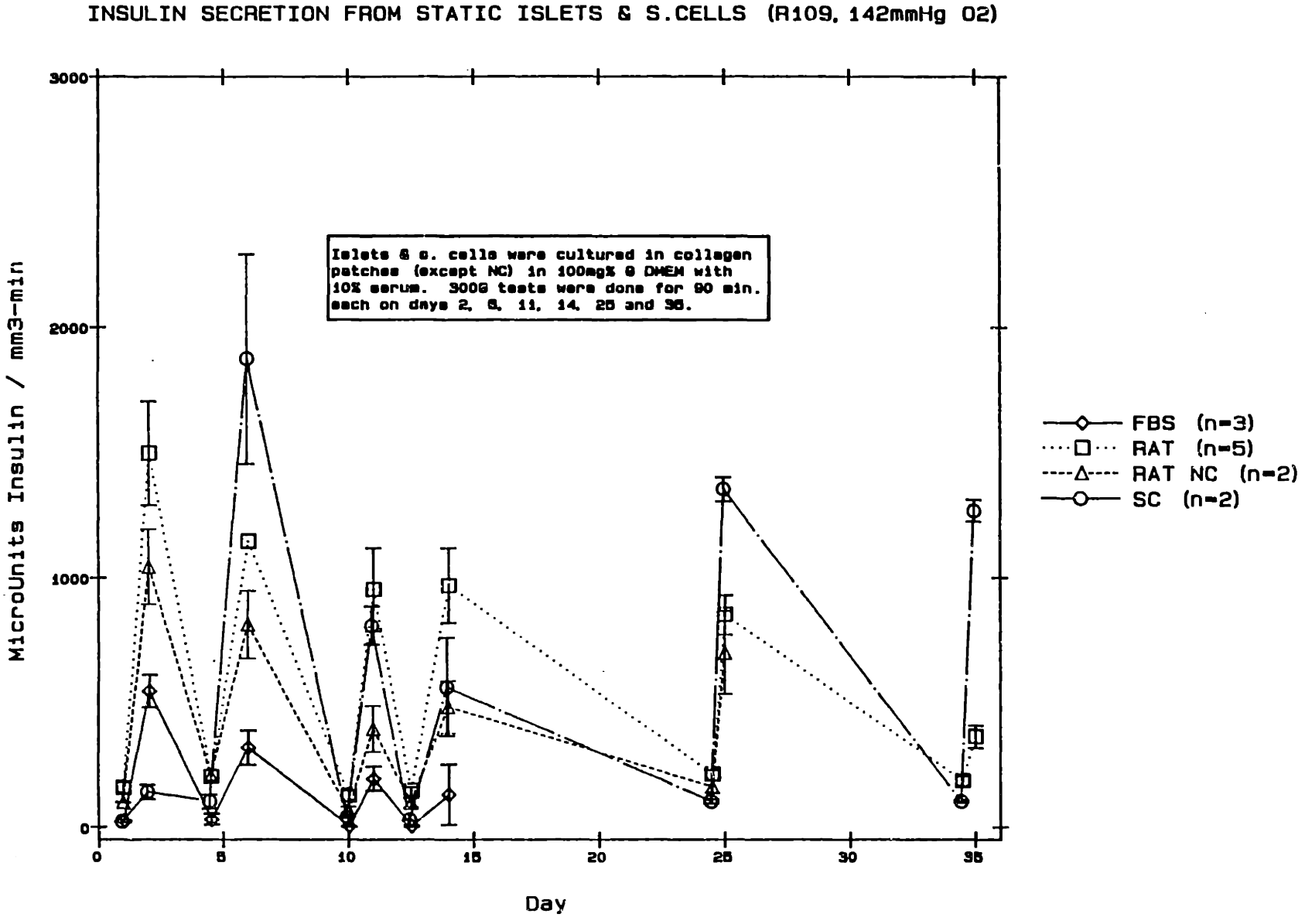
INSULIN SECRETION FROM STATIC ISLETS & S.CELLS (R109, 142mmHg O2)
Islets & s. cells were cultured in collagen patches (except NC) in 100mg% G DMEM with 10% serum. 300G tests were done for 90 min. each on days 2, 6, 11, 14, 25 and 35.
MicroUnits Insulin / mm3-min
3000
2000
1000
0
0
5
10
15
20
25
30
35
Day
FBS (n=3)
RAT (n=5)
RAT NC (n=2)
SC (n=2)

APPENDIX 6A:

COMPLETE OXGYEN UPTAKE CURVES OF INTACT ISLETS

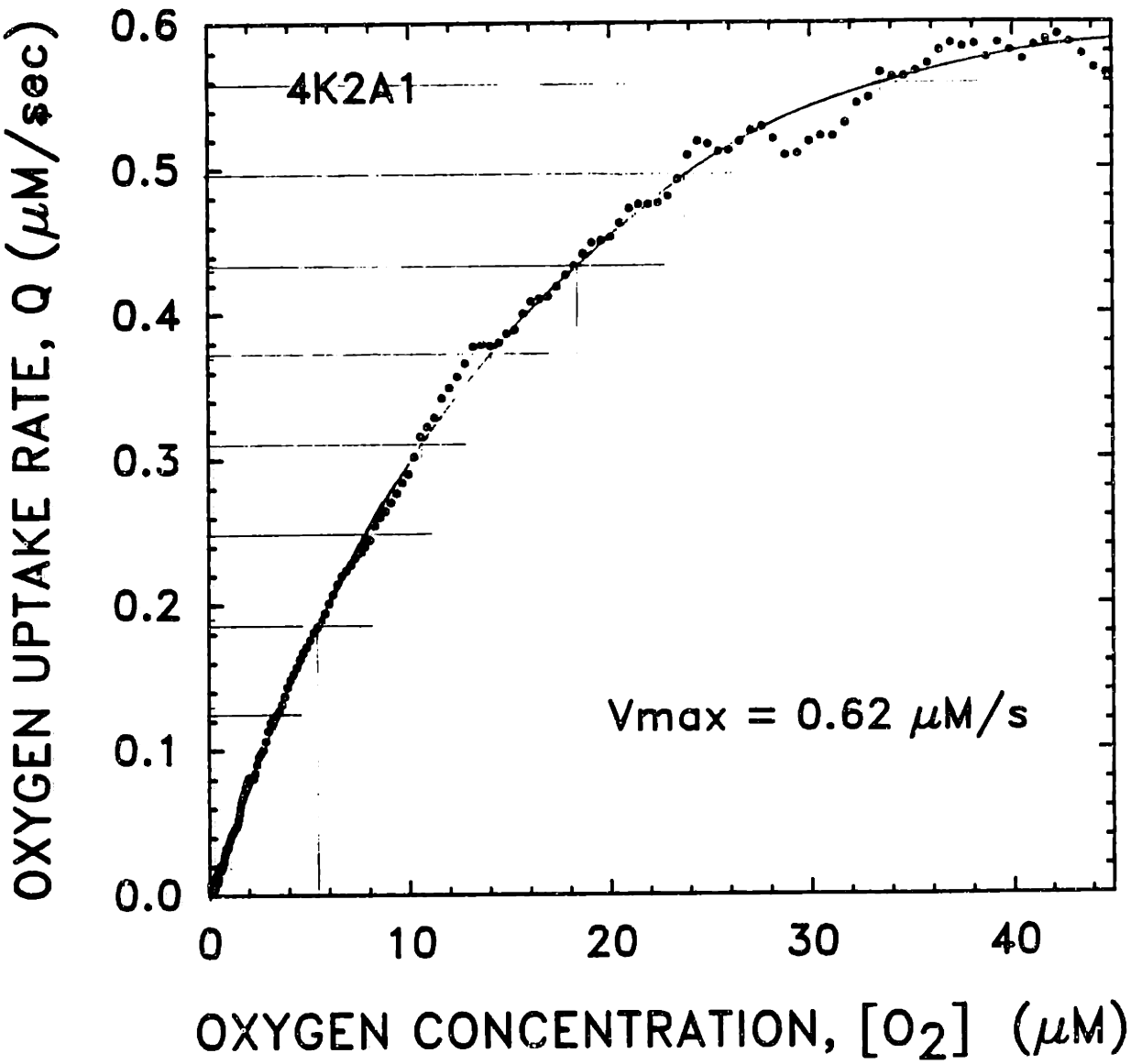

P_x	V		$[O_2]$ μM	mm-Hg
.9	.558	4.34	33.50	26.38
.8	.496	3.08	23.77	18.72
.7	.434	2.375	18.33	14.013
.6	.372	1.83	14.13	11.12
.5	.310	1.38	10.65	8.39
.4	.248	1.005	7.76	6.11
.3	.186	.700	5.40	4.25
.2	.124	.413	3.32	2.61

5.83 = 45

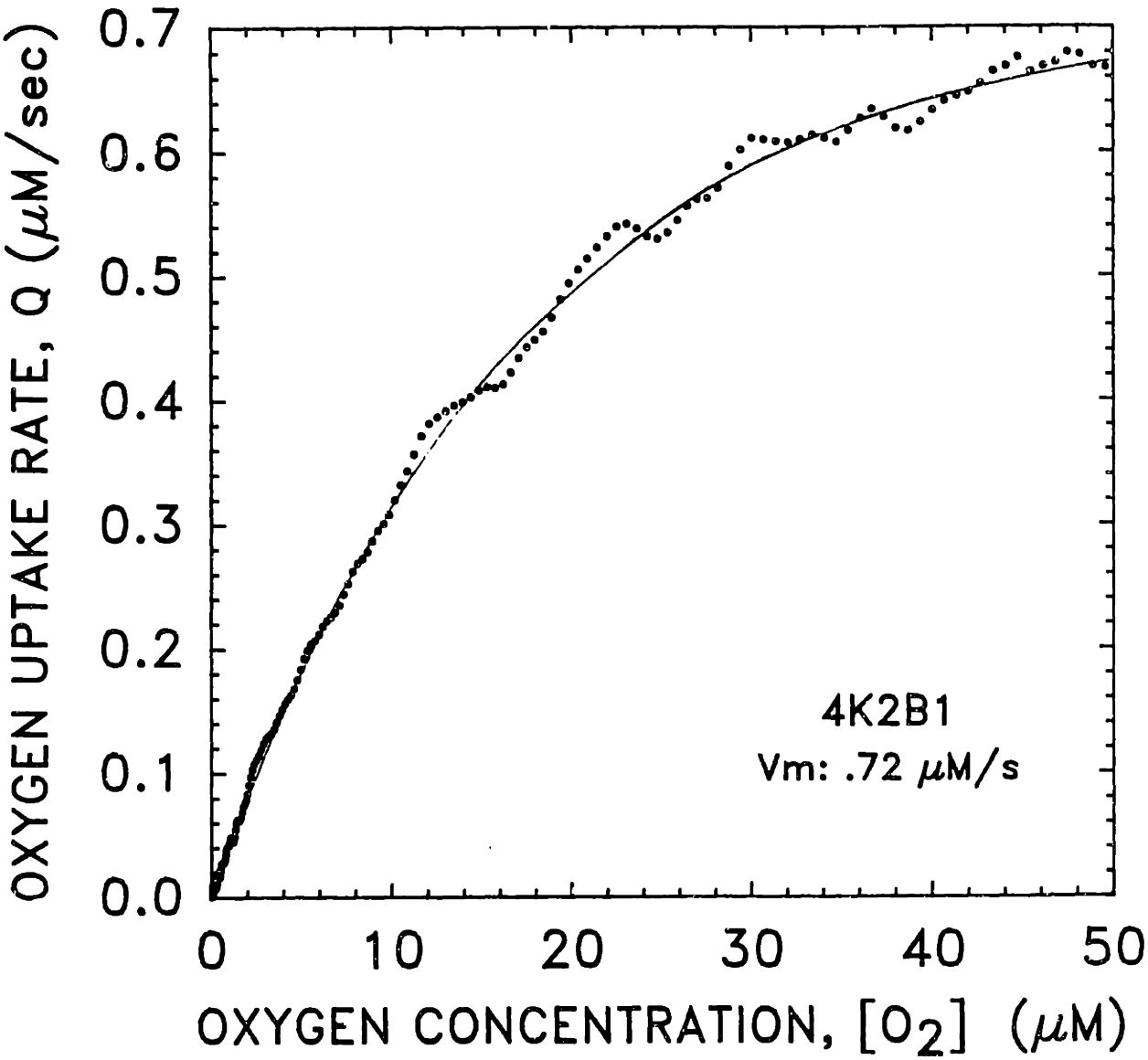
OXYGEN UPTAKE RATE, Q (μM/sec)
0.7
0.6
0.5
0.4
0.3
0.2
0.1
0.0
0
10
20
30
40
50
OXYGEN CONCENTRATION, [O2] (μM)
4K2B1
Vm: .72 μM/s

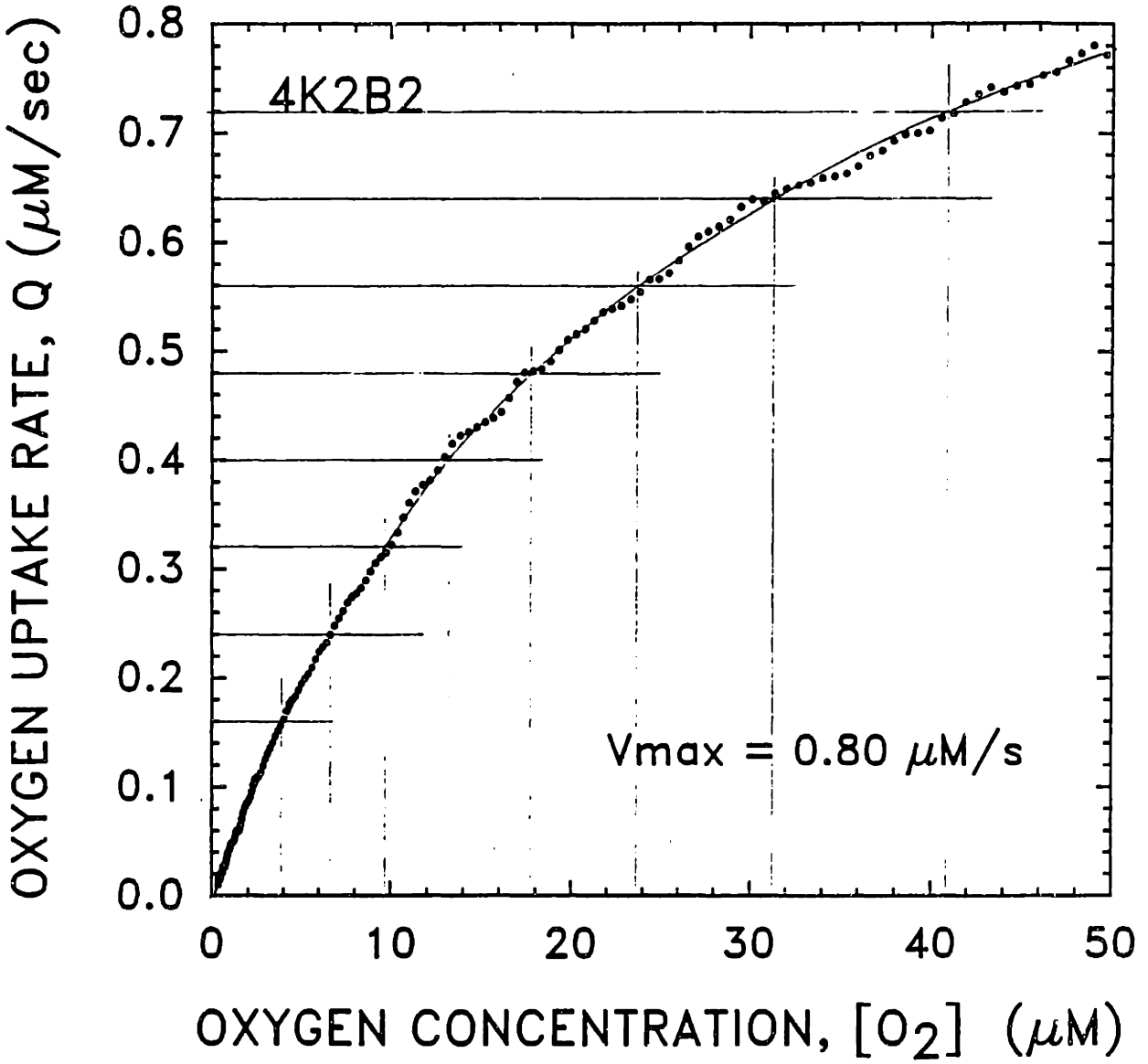

Px	V	#	$(\bar{O}_2)$ μM	mm Hg
.9	.720	4.76	40.82	32.14
.8	.640	3.64	31.22	24.58
.7	.560	2.96	23.67	18.64
.6	.480	2.065	17.71	13.94
.5	.400	1.535	13.16	10.37
.4	.320	1.12	9.61	7.56
.3	.240	.77	6.60	5.20
.2	.160	.45	3.86	3.04

50 = 5.83

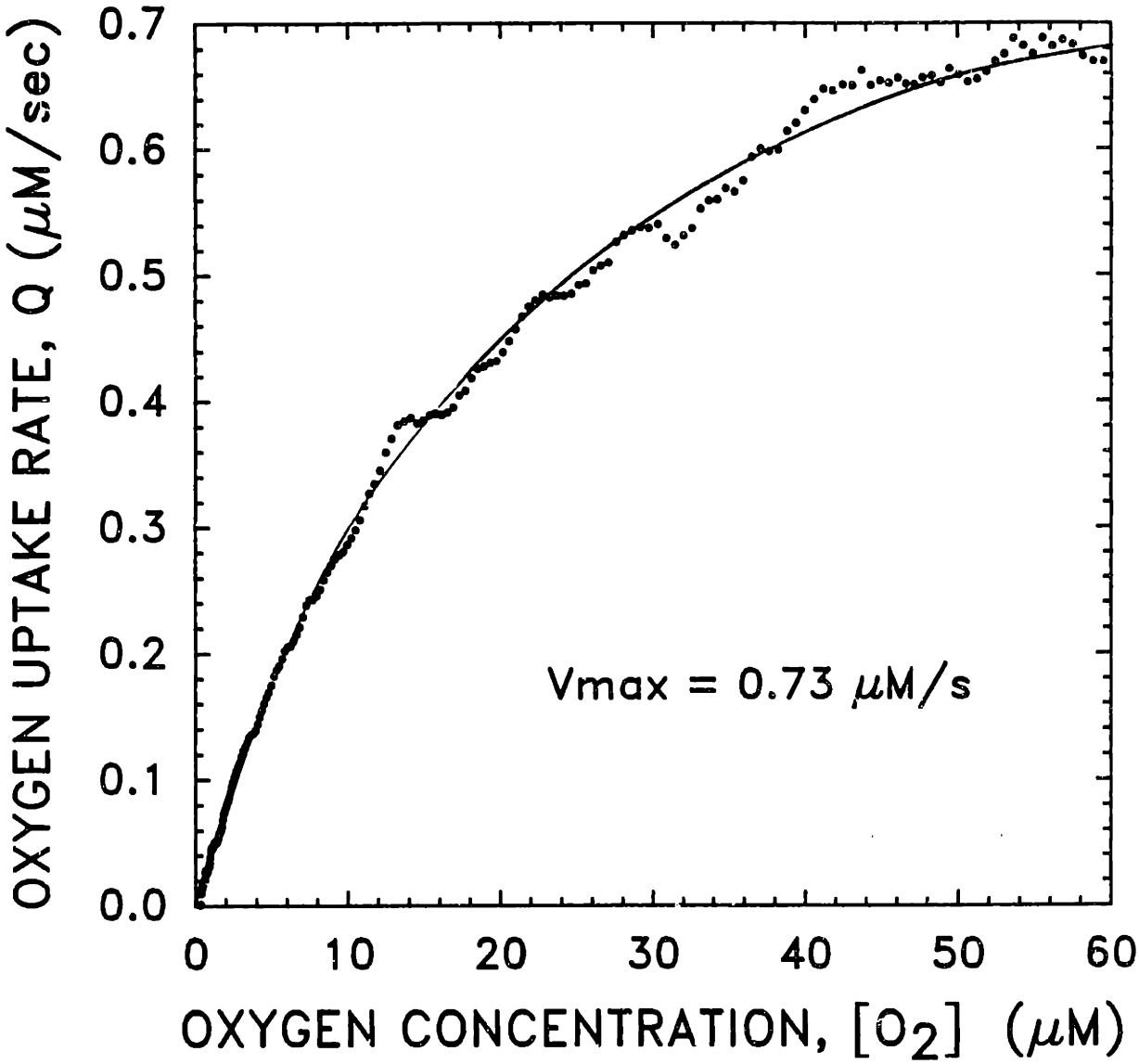
OXYGEN UPTAKE RATE, Q (μM/sec)
0.7
0.6
0.5
0.4
0.3
0.2
0.1
0.0
Vmax = 0.73 μM/s
0
10
20
30
40
50
60
OXYGEN CONCENTRATION, [O2] (μM)

$V_n = .56$

385 pt.
data not smoothed
derivative smoothed 0.2

P_1	Q		
.1	.504	35	2.7
.2	.448	26	7.0
.3	.392	19	14.6
.4	.336	41.5	11.1
.5	.280	10.8	8.3
.6	.224	8	6.15

2K4A1

Original Data – solid

Approximation – dotted

720
640
560
480
400
320
240
160
080

6.00 12 18.0 24 30.0 36 42.0 54.0

μm

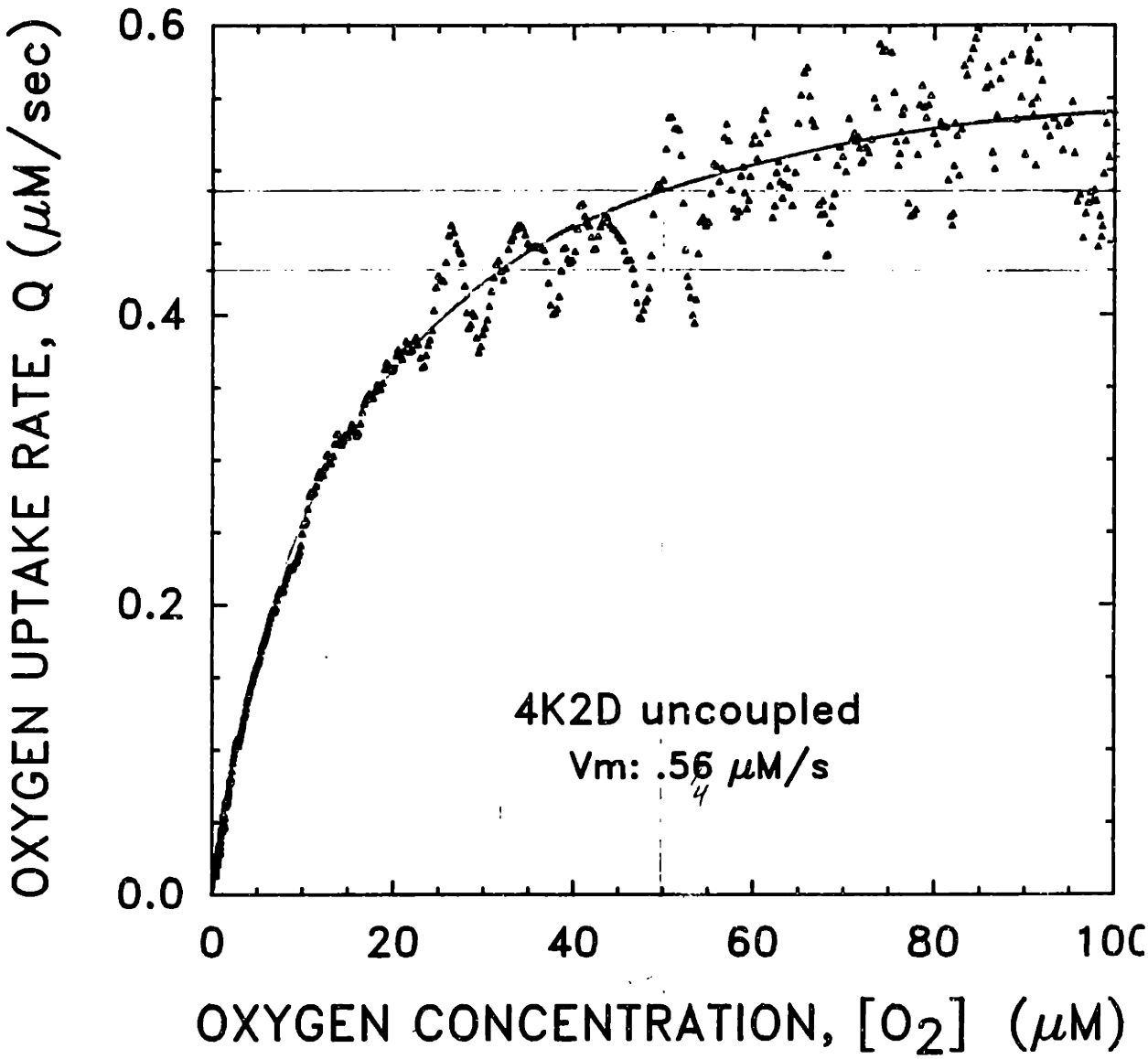

P_{O_2}	Q		
.9	.456	50	39.3
.7	.432	32	25.2
.5	.378	22	17.3
.4	.324	15.7	12.36
.3	.280	11.1	8.74
.2	.216	7.8	6.14
.1	.112	5.2	4.09
.1	.108	3.1	2.44

4k4F 550 pts

.37 / 4.2 | 32 = 2.82

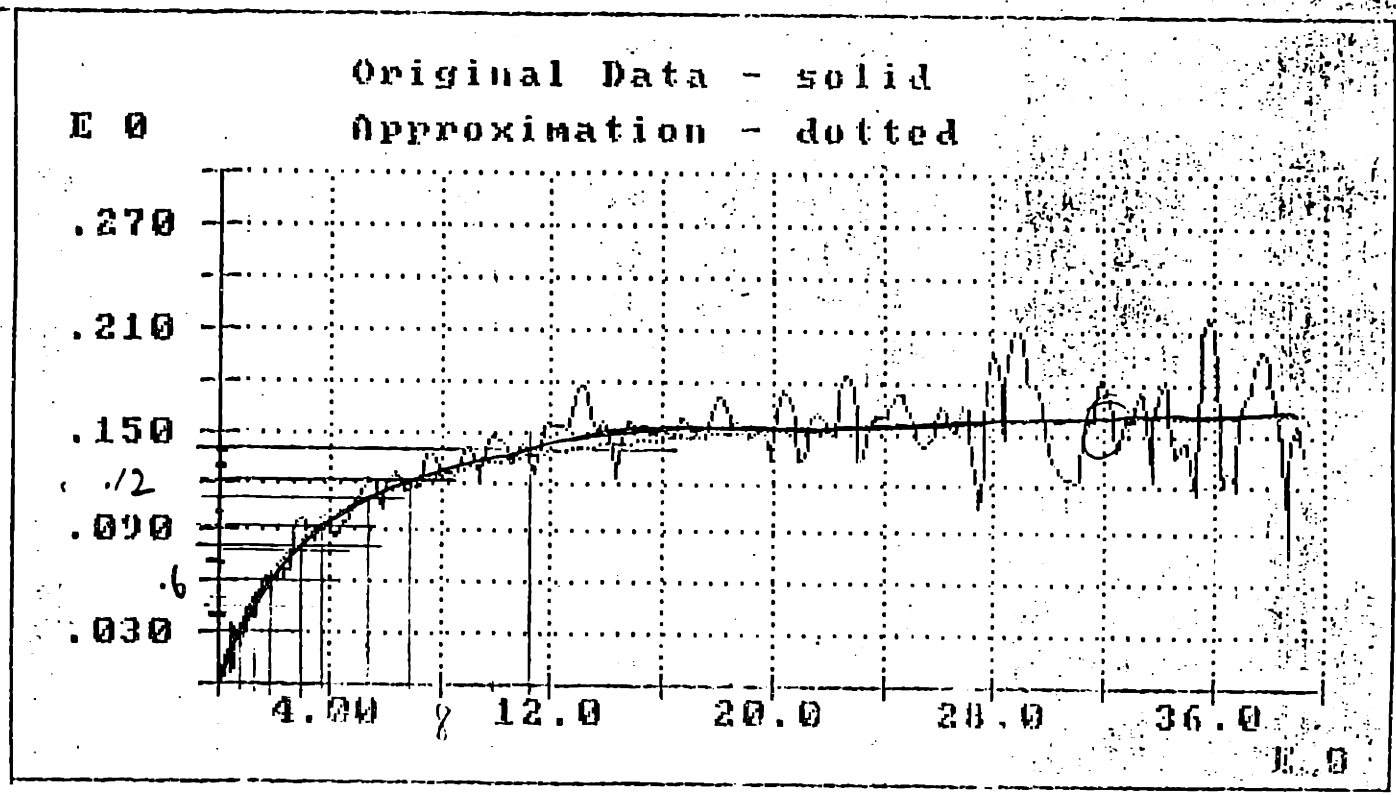

User Function

J: 75454E-1

J: 24575E0

431

APPENDIX 7A:

CALCULATION OF INTRA-TISSUE OXGYEN DIFFUSIVITY: BASIC Computer Code

```
2 REM PROGRAM: D:\KEITH\DIFFUSE2\DIFFPXM.BAS    11/28/89
5 REM New Sh # based on power number 11/28/89 KED
7 REM BATCH Program to determine DO2 of multisized spheroids given
8 REM volume fractions of spheroids, Px and Qx paired data, Vmax and
9 REM intrinsic Km of O2 uptake of cells within spheroid.
10 REM This program uses a subprogram to solve diff/rxn eq in a spheroid
11 REM with Michaelis-Menten kinetics. After non-dimensionalization,
12 REM the equation becomes:
20 REM d2P/dr2 + 2/r * dP/dr = phi*phi*P/(1+beta*P)
21 REM at r=1, P=1; at r=0, dP/dr=0; phi=(Rc2*Vm/(DO2*solI*Km))
30 REM This equation is solved numerically using a centered difference
31 REM finite difference method (Eulers method). This subprogram is a
32 REM modification of a program written by James Dunn, May, 1986.
33 REM Program modified to calculate Psurf from Pmedia at P50
34 REM using Sherwood # analogy. (March 22, 1989; KED)
35 REM Program modified to incorporate fractional O2 consumption
36 REM of each islet size range in Sh# calculation (Mar 23,1989:KED)
50 REM FNF is the non-linear kinetics
51 REM FNDFDC is the first derivative of FNF
52 REM FNR is the discretized coordinate
88  QF = .98          ' initial fractional islet uptake
89  DI = 1.301E-05     ' initial O2 diffusivity
90  IERR = 8           ' # OF ERROR LOOPS
91  ICHO = 4           ' BATCH # OF REPRESENTATIVE BATCH
92  IBAT = 7           ' # of batches in batch run
93  N=25               ' # of radial steps
94  ICAT = 7           ' # of sizes being integrated
95  IMAX = 10          ' Maximum # of diff iterations
96  DIM C(N+1), JJ(N+1,N+1), RR(N+1), DX(N+1), IPVT(N+1)
97  DIM RAD(N+1), PAVE(N), Q(ICAT), EVAR(IERR), EER$(IERR), PX(IERR)
98  DIM DIA(ICAT), NUMF(ICAT), VOL(ICAT), VOLF(ICAT), SHS(ICAT)
99  DIM QTOT(IMAX+1), QO2(IMAX+1), QFRAC(ICAT), PSURF(ICAT)
100 REM JJ is the Jacobian
101 REM RR is the residual equation
102 REM DX is the change in concentration per iteration
103 REM IPVT is the pivoting vector
104 SCREEN 2
105 DIM BAT$(IBAT), VM(IBAT), PS50(IBAT), IPEN(IBAT), DIFS(IERR)
106 FOR IP = 1 TO IBAT
107 READ BAT$(IP), VM(IP), PS50(IP), IPEN(IP)
108 NEXT IP
109 DATA "2K4A1", 3.71, 8.7, 2, "3K1A1", 3.17, 11.2, 3, "3K1A2", 4.02, 17.4, 3
110 DATA "4K2A1", 2.42, 8.3, 4, "4K2B1", 2.83, 9.4, 4, "4K2B2", 2.94, 10.3, 4
111 DATA "4K2B3", 2.87, 9.8, 4
112 DIA(1)=120: DIA(2)=150 : DIA(3)=180 : DIA(4)=210 : DIA(5)=240 : DIA(6)=270
113 DIA(7)=300
115 REM **Define Statements for Oxygen profile program**
116 DEF FNF(I)=PHI*PHI*C(I)/(1+BETA*C(I))
117 DEF FNDFDC(I)=PHI*PHI/(1+BETA*C(I))/(1+BETA*C(I))
118 DEF FNR(I)=(I-1)*H
```

```
119 FOR IT = 1 TO IERR
120 REM *****START BATCH LOOP - Initialize Parameters******
121 IMAX = 10          ' Maximum # of diff iterations
122 ITNUM = 0          ' ith iteration of diff
124 DELDI = .0000005   ' initial step size for DI
125 SOLM = 1.27E-09    ' Media Oxygen solubility
128 KM=.44            ' Michaelis-Menten coefficient
130 DO2M = .0000278    ' Media Oxygen diffusivity
131 VEL = .5           ' Root Mean Sq Mix Vel of Stirring Sys
132 SOLI = 1.02E-09    ' Oxygen tissue solubility
133 REV = 20           ' Rev/sec of stir bar
134 H=1/N
135 VMAX = VM(ICHO) * 1E-08
136 BATCH$ = BAT$(ICHO)
137 PSMEDIA = PS50(ICHO)
138 JKL = IPEN(ICHO)
139 REM **NEXT 2 LINES DEFINE THE VARIABLE ON WHICH ERROR IS RUN**
140 EVAR(1) =26.38 : EVAR(2)=18.72 : EVAR(3) = 14.43 : EVAR(4) = 11.12
141 EVAR(5) =8.390001 : EVAR(6)=6.11 : EVAR(7) = 4.25  : EVAR(8) = 2.61
142 PSMEDIA = EVAR(IT)
143 EER$(1)="PX9" : EER$(2)="PX8" : EER$(3)="PX7" : EER$(4)="PX6"
144 EER$(5)="PX5" : EER$(6)="PX4" : EER$(7)="PX3" : EER$(8)="PX2"
145 PX(1)= .9  :  PX(2)= .8  :  PX(3)=.7 : PX(4)=.6
146 PX(5)= .5  :  PX(6)= .4  :  PX(7)=.3 : PX(8)=.2
150 IF JKL <> 2 THEN GOTO 155
151 VOLF(1)=.057 : VOLF(2)=.11 : VOLF(3)=.289 : VOLF(4)=.144 : VOLF(5)=.161
152 VOLF(6)=.136 : VOLF(7)=.104
153 GOTO 165
155 IF JKL <> 3 THEN GOTO 160
156 VOLF(1)=.027 : VOLF(2)=.099 : VOLF(3)=.098 : VOLF(4)=.265 : VOLF(5)=.216
157 VOLF(6)=.145 : VOLF(7)=.149
158 GOTO 165
160 IF JKL <> 4 THEN GOTO 1431
161 VOLF(1)=.041 : VOLF(2)=.071 : VOLF(3)=.204 : VOLF(4)=.23 : VOLF(5)=.199
162 VOLF(6)=.16 : VOLF(7)=9.399999E-02
165 REM ** VOLF FRACTIONS LOADED**
177 REM  SECTION NOT NEEDED WHEN INPUTING VOLUME FRACTION
178 REM       CALCULATE VOL(i),AND VOLF(i) FOR EACH SIZE, AND TOTVOL
179 REM       TOTVOL = 0
180 REM       FOR JL = 1 TO ICAT
181 REM       VOL(JL) = (4*3.14/3)*(DIA(JL)/2)^3
182 REM       TOTVOL = TOTVOL + VOL(JL)*NUMF(JL)
183 REM       NEXT JL
187 REM       FOR KK = 1 TO ICAT
188 REM       VOLF(KK) = VOL(KK)*NUMF(KK)/TOTVOL
189 REM       NEXT KK
195 REM ***START OF LOOP FOR BIG ITERATION FOR GIVEN DO2****
196 FOR JK = 1 TO ICAT
198 REM  DEFINE RADIUS AND PHI FOR SPECIFIC SIZE CATEGORY FOR THIS DO2
200 RADIUS = DIA(JK)/2
```

```
202 PHI=RADIUS*.0001*SQR(VMAX/DI/SOLI/KM)
203 REM *Calculate Islet Surface pO2 for this diameter using Sh# at PX*
204 SHX=((.5*REV^3*.4^5*1!*(DIA(JK)*.0001)^4)/(.275*.0069^3))^.333
205 SHY = EXP(-.39347 + .3824*LOG(SHX) + .0381*(LOG(SHX))^2)
206 SH = 2! + SHY*248^.333
207 PRINT "SH # = ";SH
208 PS = PSMEDIA - ((QF*VMAX*(DIA(JK)*.0001)^2)/(6*SOLM*DO2M*SH))
209 SHS(JK) = SH
217 PRINT "DIA (MIC) = ";DIA(JK);"  PSURF (mmHg) = ";PS;"Qfrac = ";QF
218 KIT = IT
219 PRINT "ERROR PARAMETER IS ON RUN NUMBER: "; KIT
222 REM START O2 PROGRAM TO SOLVE PROFILE FOR THIS SIZE FOR THIS DO2
224 REM PROGRAM RUNS FROM LINE 222 TO LINE 1190
226 BETA=PS/KM
228 E = .00001
229 REM       PRINT "Thiele modulus = ";PHI
230 REM       PRINT "beta = ";BETA
240 FOR I=1 TO N+1
250 C(I)=1
260 NEXT I
270 REM Calculate the Jacobian and the Residual
280 JJ(1,1)=-6/H/H-FNDFDC(1)
290 JJ(1,2)=6/H/H
300 FOR I= 2 TO N
310 JJ(I,I-1)=1/H/H-1/FNR(I)/H
320 JJ(I,I+1)=1/H/H+1/FNR(I)/H
330 JJ(I,I)=-2/H/H-FNDFDC(I)
340 NEXT I
350 JJ(N+1,N+1)=1
360 RR(1)=-(6*(C(2)-C(1))/H/H-FNF(1))
370 FOR I= 2 TO N
380 RR(I)=-((C(I+1)-2*C(I)+C(I-1))/H/H+(C(I+1)-C(I-1))/H/FNR(I)-FNF(I))
390 NEXT I
400 RR(N+1)=-(C(N+1)-1)
410 REM Solving the equation JJ DX = RR
420 DET=1
430 REM LU decomposition
440 IPVT(N+1)=1
450 IF N=0 THEN GOTO 730
460 NM1=N
470 FOR K=1 TO NM1
480 KP1=K+1
490 M=K
500 FOR I=KP1 TO N+1
510 IF ABS(JJ(I,K))>ABS(JJ(M,K)) THEN M=I
520 NEXT I
530 IPVT(K)=M
540 IF M<>K THEN IPVT(N+1)=-IPVT(N+1)
550 P=JJ(M,K)
560 JJ(M,K)=JJ(K,K)
```

```
570 JJ(K,K)=P
580 REM DET=DET*P
590 IF P=0 THEN GOTO 720
600 FOR I=KP1 TO N+1
610 JJ(I,K)=-JJ(I,K)/P
620 NEXT I
630 FOR J=KP1 TO N+1
640 T=JJ(M,J)
650 JJ(M,J)=JJ(K,J)
660 JJ(K,J)=T
670 IF T=0 THEN GOTO 710
680 FOR I=KP1 TO N+1
690 JJ(I,J)=JJ(I,J)+JJ(I,K)*T
700 NEXT I
710 NEXT J
720 NEXT K
730 REM DET=DET*JJ(N+1,N+1)*IPVT(N+1)
740 REM Forward elimination
750 IF N=0 THEN GOTO 980
760 NM1=N
770 FOR K= 1 TO NM1
780 KP1=K+1
790 M=IPVT(K)
800 S=RR(M)
810 RR(M)=RR(K)
820 RR(K)=S
830 FOR I = KP1 TO N+1
840 RR(I)=RR(I)+JJ(I,K)*S
850 NEXT I
860 NEXT K
870 REM Backward substitution
880 FOR KB=1 TO NM1
890 KM1=N+1-KB
900 K=KM1+1
910 RR(K)=RR(K)/JJ(K,K)
920 S=-RR(K)
930 FOR I = 1 TO KM1
940 RR(I)=RR(I)+JJ(I,K)*S
950 NEXT I
960 NEXT KB
970 RR(1)=RR(1)/JJ(1,1)
980 FOR I=1 TO N+1
990 DX(I)=RR(I)
1000 NEXT I
1010 REM Update concentration
1020 FOR I=1 TO N+1
1030 C(I)=C(I)+DX(I)
1040 IF C(I)<0 THEN C(I)=0
1050 NEXT I
1060 REM Check convergence
```

```
1070 MAX=0
1080 SUM=0
1090 FOR I=1 TO N+1
1100 IF ABS(DX(I))>MAX THEN MAX=ABS(DX(I))
1110 SUM=SUM+DX(I)*DX(I)
1120 NEXT I
1130 SUM=SQR(SUM)
1140 REM Data output
1150 PRINT "Sum of difference vector = "; SUM
1160 REM       FOR I=1 TO N+1
1170 REM       PRINT FNR(I),C(I)
1180 REM       NEXT I
1190 IF  MAX>=E OR SUM>=E GOTO 280
1200 REM CONVERT CONVERGED PROFILE TO MMHG AND MICRONS
1202 FOR I=1 TO N+1
1204    C(I) = C(I)*PS
1206    RAD(I) = FNR(I)*RADIUS
1208    NEXT I
1209 REM NUMERICALLY INTEGRATE q(O2) FOR THIS SIZE FOR THIS DO2
1210 REM THEN SUM UP CONTRIBUTION TO OVERALL FRACTIONAL O2 UPTAKE
1211 Q(JK) = 0
1212 QLOCAL = 0
1213  FOR I = 1 TO N
1214  PAVE(I) = (C(I+1) + C(I))/2
1215  QLOCAL=(PAVE(I)/(KM + PAVE(I)))*(RAD(I+1)^3-RAD(I)^3)/RADIUS^3
1216  Q(JK) = QLOCAL + Q(JK)
1217  NEXT I
1218 REM * Compare Calculated Qislet size to QF in Sh#*
1219 IF ABS(Q(JK)-QF)<=.05 GOTO 1222
1220 QF = QF + .8*(Q(JK)-QF)
1221 GOTO 203
1222 REM Continue if QF converged, Save PS and QF for this size
1223 PSURF(JK) = PS
1224 QFRAC(JK)=Q(JK)
1225 REM Adjust QF for next larger size islet
1226 QF = QF - .04
1227 IF QF<=.01 THEN QF = .01
1228 REM ****RETURN TO DO NEXT SIZE FOR THIS DO2 *****
1229 NEXT JK
1230 REM ****END OF BIG LOOP FOR THIS DO2 ITERATION***
1232 REM ****COMPARE INTEGRATED P50 TO .5 AND UPDATE DI FOR NEXT
1233 REM     ITERATION OF O2 DIFFUSIVITY. ****
1240 QTOTAL = 0
1242 FOR J = 1 TO ICAT
1244    QTOTAL = Q(J) * VOLF(J) + QTOTAL
1245    Q(J) = 0
1246    NEXT J
1250 ITNUM = ITNUM + 1
1252 EROR = QTOTAL - PX(IT)
1254 PRINT "OXYGEN DIFFUSIVITY = "; DI
```

```
1255 PRINT "SET PX = ";PX(IT)
1256 PRINT "CALCULATED PX   = ";QTOTAL
1258 PRINT "# OF ITERATIONS = ";ITNUM
1260 QTOT(ITNUM) = QTOTAL
1262 DO2(ITNUM) = DI
1270 REM SECTION TO REDUCE DEL DI IF PASS OVER PX
1272 IF ITNUM = 1 THEN GOTO 1280
1274   IF EROR < 0 THEN IF PERR < 0 THEN GOTO 1280
1276   IF EROR > 0 THEN IF PERR > 0 THEN GOTO 1280
1278   DELDI = DELDI/3
1280 REM POP OUT OF SECTION TO REDUCE DEL DI; STORE LAST ERROR
1282 PERR = EROR
1284 REM **CHANGE DI IN APPROPRIATE DIRECTION FOR NEXT ITERATION**
1286  IF EROR > 0 THEN DI = DI - DELDI
1288  IF EROR < 0 THEN DI = DI + DELDI
1290  IF ABS(EROR) < .005 THEN GOTO 1330
1300 REM IF STATEMENT TO END PROGRAM AFTER IMAX ITERATIONS OF DO2
1305 IF ITNUM >= IMAX THEN GOTO 1330
1310 REM *****RETURN TO DO ANOTHER DI ITERATION******
1311 QF=.9
1315 GOTO 195
1330 REM ITERATIONS ARE DONE EITHER BECAUSE HAVE CONVERGED, HAVE
1331 REM PERFORMED IMAX ITERATIONS, OR BECAUSE THE PROGRAM IS FLAWED.
1370 REM Create data file
1380 OPEN EER$(IT) FOR OUTPUT AS #1
1381 PRINT #1,"batch # =";BATCH$; " Px media = ";PSMEDIA;" UPEN # = ";JKL
1382 PRINT "batch # = ";BATCH$; " P50 media = ";PSMEDIA;"  UPEN # = ";JKL
1383 PRINT #1,"CELL Km = ";KM; " Vmax =  ";VMAX;" STIR VEL = ";VEL
1384 PRINT "CELL Km = ";KM; " Vmax = ";VMAX;" STIR BAR (rev/s) = ";REV
1385 FOR I=1 TO ICAT
1386 PRINT #1,"DIA = ";DIA(I);" Ps= ";PSURF(I);" Q/Vm= ";QFRAC(I);" SH=";SHS(I)
1387 PRINT "DIA = ";DIA(I);" Psurf = ";PSURF(I);" Q/VMAX = ";QFRAC(I)
1388 NEXT I
1390 FOR I=1 TO ITNUM
1399 PRINT "CALCULATED Q/VM = "; QTOT(I);"      DO2 = "; DO2(I)
1400 PRINT #1, "CALCULATED P50 = "; QTOT(I);"     DO2 = "; DO2(I)
1410 NEXT I
1420 CLOSE
1421 DIFS(IT) = DO2(ITNUM)
1422 NEXT IT
1423 OPEN "ESAV" FOR OUTPUT AS #1
1424 FOR I = 1 TO IERR
1425 PRINT #1, "ERROR VAR = "; EER$(I); " DIFF = "; DIFS(I)
1426 NEXT I
1427 CLOSE
1430 END
1431 PRINT "*******PROGRAM COMPLETED********"
1432 PRINT  "*******DATA IS STORED*********"
1433 PRINT "THE COMPUTER IS AVAILABLE FOR USE. YOU MAY ERASE THIS SCREEN"
1434 PRINT "TYPE :  'SYSTEM'  TO EXIT  BASIC PROGRAM"
```

APPENDIX 8A:

CALCULATION OF ISLET PO_2 PROFILES: BASIC Computer Code

```
2 REM  PROGRAM:  D:\KEITH\KMI\SPHKMI.BAS      12/4/89
3 REM Program to calculate ICAT # of pO2 profiles and save them for KMI prog.
4 REM Program calculates pO2 in spheroids with laminar flow boundary layer.
5 REM Printout to file is "radius" in microns, and "pO2" in mmHg
6 REM Printout to screen is "input values", Q/Qmax, Psurf
7 REM Progra  requires Vmax, Km, diameter, fluid velocity, and solubilities.
10 REM This program uses a subprogram to solve diff/rxn eq in a spheroid
11 REM with Michaelis-Menten kinetics. After non-dimensionalization,
12 REM the equation becomes:
20 REM d2P/dr2 + 2/r * dP/dr = phi*phi*P/(1+beta*P)
21 REM at r=1, P=1; at r=0, dP/dr=0; phi=(Rc2*Vm/(DO2*soll*Km))
30 REM This equation is solved numerically using a centered difference
31 REM finite difference method (Eulers method). This subprogram is a
32 REM modification of a program written by James Dunn, May, 1986.
33 REM Program modified to calculate Psurf from Pmedia based on Qactual
34 REM using Sherwood # analogy. (March 22, 1989; KED)
50 REM FNF is the non-linear kinetics
51 REM FNDFDC is the first derivative of FNF
52 REM FNR is the discretized coordinate
90 REM N is the number of divisions
91 REM H is the step size
92 REM C is the partial pressure of oxygen
100 REM JJ is the Jacobian
101 REM RR is the residual equation
102 REM DX is the change in concentration per iteration
104 REM IPVT is the pivoting vector
106 SCREEN 2
115 REM **Define Statements for Oxygen profile program**
116 DEF FNF(I)=PHI*PHI*C(I)/(1+BETA*C(I))
117 DEF FNDFDC(I)=PHI*PHI/(1+BETA*C(I))/(1+BETA*C(I))
118 DEF FNR(I)=(I-1)*H
119 REM *****Initialize Parameters******
120 N=30                ' # of radial steps
122 ITNUM = 0            ' ith iteration of diff
123 ICAT = 9             ' # of sizes being integrated
126 VMAX = 3.14E-08      ' maximum oxygen uptake
128 KM=.44               ' Michaelis-Menten coefficient
129 QF = .98             ' initial fractional islet uptake
130 DOI = .0000153       ' islet O2 diffusivity
131 VEL = .75            ' Root Mean Sq Mix Vel of Stirring Sys
132 SOLI = 1.02E-09      ' Oxygen tissue solubility
133 DIA = 210            ' Islet diameter, microns
134 H=1/N
135 DOM = .0000278       ' Media oxygen diffusivity
136 SOLM = 1.27E-09      ' Media oxgyen solubility
140 REM **Dimension Statements**
142 DIM C(N+1), JJ(N+1,N+1), RR(N+1), DX(N+1), IPVT(N+1)
144 DIM RAD(N+1), PAVE(N), Q(ICAT)
146 DIM PM(ICAT), DUMP$(ICAT)
148 DIM QFRAC(ICAT), PSURF(ICAT)
```

```
160 REM READ IN ENSEMBLE OF MEDIA PO2S AND OUTPUT FILE NAMES.
162 FOR KG = 1 TO ICAT
164     READ PM(KG)
165     PRINT PM(KG)
166     NEXT KG
168 DATA 142, 60, 45, 35, 30, 25, 22, 15, 5
170 FOR JL = 1 TO ICAT
172     READ DUMP$(JL)
174     NEXT JL
176 DATA "S142", "S60", "S45", "S35", "S30", "S25", "S22", "S15", "S5"
196 FOR JK = 1 TO ICAT
198 REM  DEFINE Media pO2 AND PHI FOR this media pO2
199 PSMEDIA = PM(JK)
200 RADIUS = DIA/2
201 PRINT VMAX, DOI,SOLI,KM
202 PHI=RADIUS*.0001*SQR (VMAX/DOI/SOLI/KM)
210 REM *Calculate Islet Surface pO2 for this media pO2 using Sh# at QF guess
214 PSBOT = 6*SOLM*DOM^.67*VEL^.33
215 PS=PSMEDIA-((QF*VMAX*(DIA*.0001)^1.667)/PSBOT)
217 PRINT "MEDIA PO2 = ";PSMEDIA;" PSURF (mmHg) = ";PS;"Qfrac = ";QF
222 REM START O2 PROGRAM TO SOLVE PROFILE FOR THIS MEDIA PO2
224 REM PROGRAM RUNS FROM LINE 222 TO LINE 1190
226 BETA=PS/KM
228 E = .00001
229 REM       PRINT "Thiele modulus = ";PHI
230 REM       PRINT "beta = ";BETA
240 FOR I=1 TO N+1
250 C(I)=1
260 NEXT I
270 REM Calculate the Jacobian and the Residual
280 JJ(1,1)=-6/H/H-FNDFDC(1)
290 JJ(1,2)=6/H/H
300 FOR I= 2 TO N
310 JJ(I,I-1)=1/H/H-1/FNR(I)/H
320 JJ(I,I+1)=1/H/H+1/FNR(I)/H
330 JJ(I,I)=-2/H/H-FNDFDC(I)
340 NEXT I
350 JJ(N+1,N+1)=1
360 RR(1)=-(6*(C(2)-C(1))/H/H-FNF(1))
370 FOR I= 2 TO N
380 RR(I)=-((C(I+1)-2*C(I)+C(I-1))/H/H+(C(I+1)-C(I-1))/H/FNR(I)-FNF(I))
390 NEXT I
400 RR(N+1)=-(C(N+1)-1)
410 REM Solving the equation JJ DX = RR
420 DET=1
430 REM LU decomposition
440 IPVT(N+1)=1
450 IF N=0 THEN GOTO 730
460 NM1=N
470 FOR K=1 TO NM1
```

```
480 KP1=K+1
490 M=K
500 FOR I=KP1 TO N+1
510 IF ABS(JJ(I,K))>ABS(JJ(M,K)) THEN M=I
520 NEXT I
530 IPVT(K)=M
540 IF M<>K THEN IPVT(N+1)=-IPVT(N+1)
550 P=JJ(M,K)
560 JJ(M,K)=JJ(K,K)
570 JJ(K,K)=P
580 REM DET=DET*P
590 IF P=0 THEN GOTO 720
600 FOR I=KP1 TO N+1
610 JJ(I,K)=-JJ(I,K)/P
620 NEXT I
630 FOR J=KP1 TO N+1
640 T=JJ(M,J)
650 JJ(M,J)=JJ(K,J)
660 JJ(K,J)=T
670 IF T=0 THEN GOTO 710
680 FOR I=KP1 TO N+1
690 JJ(I,J)=JJ(I,J)+JJ(I,K)*T
700 NEXT I
710 NEXT J
720 NEXT K
730 REM DET=DET*JJ(N+1,N+1)*IPVT(N+1)
740 REM Forward elimination
750 IF N=0 THEN GOTO 980
760 NM1=N
770 FOR K= 1 TO NM1
780 KP1=K+1
790 M=IPVT(K)
800 S=RR(M)
810 RR(M)=RR(K)
820 RR(K)=S
830 FOR I = KP1 TO N+1
840 RR(I)=RR(I)+JJ(I,K)*S
850 NEXT I
860 NEXT K
870 REM Backward substitution
880 FOR KB=1 TO NM1
890 KM1=N+1-KB
900 K=KM1+1
910 RR(K)=RR(K)/JJ(K,K)
920 S=-RR(K)
930 FOR I = 1 TO KM1
940 RR(I)=RR(I)+JJ(I,K)*S
950 NEXT I
960 NEXT KB
970 RR(1)=RR(1)/JJ(1,1)
```

```
980 FOR I=1 TO N+1
990 DX(I)=RR(I)
1000 NEXT I
1010 REM Update concentration
1020 FOR I=1 TO N+1
1030 C(I)=C(I)+DX(I)
1040 IF C(I)<0 THEN C(I)=0
1050 NEXT I
1060 REM Check convergence
1070 MAX=0
1080 SUM=0
1090 FOR I=1 TO N+1
1100 IF ABS(DX(I))>MAX THEN MAX=ABS(DX(I))
1110 SUM=SUM+DX(I)*DX(I)
1120 NEXT I
1130 SUM=SQR(SUM)
1140 REM Data output
1150 PRINT "Sum of difference vector = "; SUM
1160 REM        FOR I=1 TO N+1
1170 REM        PRINT FNR(I),C(I)
1180 REM        NEXT I
1190 IF  MAX>=E OR SUM>=E GOTO 280
1200 REM CONVERT CONVERGED PROFILE TO MMHG AND MICRONS
1202 FOR I=1 TO N+1
1204    C(I) = C(I)*PS
1206    RAD(I) = FNR(I)*RADIUS
1208    NEXT I
1209 REM NUMERICALLY INTEGRATE q(O2) FOR THIS MEDIA PO2
1211 Q(JK) = 0
1212 QLOCAL = 0
1213  FOR I = 1 TO N
1214  PAVE(I) = (C(I+1) + C(I))/2
1215  QLOCAL=(PAVE(I)/(KM + PAVE(I)))*(RAD(I+1)^3-RAD(I)^3)/RADIUS^3
1216  Q(JK) = QLOCAL + Q(JK)
1217  NEXT I
1218 REM * Compare Calculated Q(Jk) to QF guessed in Sh#*
1219 IF ABS(Q(JK)-QF)<=.025 GOTO 1222
1220 QF = QF + .8*(Q(JK)-QF)
1221 GOTO 210
1222 REM Continue if QF converged, Save pO2 profile for this media pO2
1223 OPEN DUMP$(JK) FOR OUTPUT AS #1
1224 FOR I=1 TO N+1
1225    PRINT #1, RAD(I), C(I)
1226    NEXT I
1227 CLOSE
1228 REM ****SAVE DATA AND RETURN TO DO NEXT MEDIA PO2 *****
1230 QF = QF-.05
1231 PSURF(JK) = PS
1232 QFRAC(JK)=Q(JK)
1240 NEXT JK
```

```
1370 REM Create data file
1379 PRINT " "
1380 OPEN "QSAV" FOR OUTPUT AS #1
1381 PRINT " ######## DATA OUTPUT #########"
1382 PRINT #1, "TISSUE SOLUBILITY = "; SOLI; "MEDIA SOLUBILITY = ";SOLM
1383 PRINT #1, "TISSUE DIFFUSIVITY = ";DOI; " MEDIA DIFFUSIVITY = ";DOM
1384 PRINT #1, "CELL Km O2 = ";KM; "   Vmax =  ";VMAX;" STIR VEL = ";VEL
1385 FOR I=1 TO ICAT
1386 PRINT "Media pO2 =";PM(I); " Psurf = "; PSURF(I); " Q/Vmax =";QFRAC(I)
1389 NEXT I
1420 CLOSE
1430 END
```

APPENDIX 8B:

CALCULATION OF BEST FIT KM_I FROM ISLET PO_2 PROFILES: BASIC Computer Code

```
6 REM  PROGRAM:  D:\KEITH\KMI\KMI2OUT.BAS      11/25/89
7 REM  **********
8 REM  OCTOBER 26, 1986, UPDATE NOV 25, 1989
9 REM  PROGRAM VARIATION TO CALCULATE BEST FIT KMIN FOR MULTIPLE RUNS
10 REM  THIS PROGRAM CALCULATES THE INSULIN SECRETION FROM A SPHERICAL ISLET BY
11 REM  SUMMING THE SEGMENTAL SECRETION BASED ON THE LOCAL PO2 AND AN OVERAL
12 REM  KM FOR INSULIN SECRETION.
20 REM  INPUT INCLUDES: RADIAL POSITION, RADIAL PO2, FRACTION OF ISLET THAT IS
21 REM  THE BETA CELL CORE, KM INITIAL, FRACTION OF NORMAL INSULIN SECRETION OF
22 REM  THE ISLET UNDER REDUCED PO2,
30 REM  ISLET RADIUS, # OF STEPS, CONVERGENCE CRITERIA, AND SURFACE PO2.
40 REM  R(I) IS THE RADIAL POSITION FROM CORE (MICRONS) (INPUT IS IN MICRONS)
50 REM  P(I) IS THE RADIAL PO2 (MMHG)
60 REM  BETA IS THE VOLUME FRACTION OF BETA CELL CORE
70 REM  KM IS THE MICHAELIS MENTEN CONSTANT TO BE FIT (MMHG)
80 REM  XEXP IS THE EXPERIMENTAL Qr/Qn (FRACTION)
90 REM  RAD IS THE ISLET RADIUS (MICRONS)
100 REM N IS THE NUMBER OF RADIAL SEGMENTS (2 TO 25)
110 REM DELX IS THE CONVERGENCE CRITERIA (.02)
130 REM DIMENSION ARRAYS
139 INUM = 9            ' # OF MULTIPLE PO2 RUNS TO FIT
140 N = 30             ' # OF RADIAL SEGMENTS
141 BETA = .75          ' VOLUME FRACTON OF BETA CELL CORE
142 KM   = 5.2          ' INITIAL GUESS OF KMI
143 RAD  = 105          ' ISLET RADIUS IN MICRONS
144 DELX = .004
145 ICOUNT = 0
146 DELKMI = .1
147 ISIGN = 0
148 LSUMSQ = 0
149 SUMSQ = 0
150 DIM R(N+1),P(N+1),PAVE(N+1),VOLF(N+1),Q(N+1),QV(N+1),QO2(N+1)
160 REM INPUT "ENTER REDUCED SECRETION FRACTION, XEXP"; XEXP
170 REM INPUT "ENTER ISLET SURFACE PO2 (MMHG)"; PSURF
180 REM INPUT "ENTER NAME OF INPUT DATA FILE"; FEED$
185 REM INPUT "ENTER NAME OF OUTPUT DATA FILE"; GARBAGE$
186 REM INPUT "ENTER KMO2 (mmHg)   "; KMO2
187 FOR KK = 1 TO INUM
188 READ XMEAS(KK)
189 NEXT KK
190 DATA .021,.169,.296,.475,.619,.640,.824,.992,.999
191 PR$(1)="S5":PR$(2)="S15":PR$(3)="S22":PR$(4)="S25"
192 PR$(5)="S30":PR$(6)="S35":PR$(7)="S45":PR$(8)="S60":PR$(9)="S142"
193 FOR JJ = 1 TO INUM
194     XEXP = XMEAS(JJ)
195     OPEN PR$(JJ) FOR INPUT AS #1
200 FOR I=0 TO N
210     INPUT #1, R(I), P(I)
220     NEXT I
225 CLOSE
```

```
230 REM INITIALIZE VARIABLES
240 RS = BETA^.333 * RAD
250 ISTOP = 0
260 XSUM  = 0
265                     QO2SUM = 0
270 FOR I = 1 TO N
280     VOLF(I) = 0
290     Q(I)    = 0
295                     QO2(I) = 0
300     QV(I)   = 0
310     PAVE(I) = (P(I) + P(I-1))/2
320     NEXT I
330 REM CALCULATE VOLUME SEGMENTS OF BETA CELL CORE
340 FOR J = 1 TO N
350     IF R(J) >= RS THEN R(J) = RS : ISTOP = 1
360     VOLF(J) = (R(J)^3 - R(J-1)^3)/RS^3
365             QO2(J) =(PAVE(J) / (KMO2 + PAVE(J)))*VOLF(J)
366                     QO2SUM = QO2(J) + QO2SUM
370     IF ISTOP = 1 THEN GOTO 390
380     NEXT J
390 REM START ITERATIVE LOOP; CALCULATE Q(I),QV(I), AND XSUM
400 FOR K = 1 TO N
410     Q(K) = PAVE(K)/(KM + PAVE(K))
420     QV(K) = Q(K) * VOLF(K)
430     XSUM = XSUM + QV(K)
435     IF R(K) = RS THEN GOTO 450
440     NEXT K
450 ICOUNT = ICOUNT + 1                 ' ITERATIVE LOOP COUNTER
460 IF ABS(XSUM - XEXP) <= DELX THEN GOTO 470
470 IF ICOUNT >= 1 THEN GOTO 550
480 KM = KM + .3*(XSUM - XEXP)*KM
485 REM PRINT ICOUNT;"TH ITERATION OF KM = ";KM
490 XSUM = 0
500 GOTO 390
550     SUMSQ = SUMSQ + (XEXP - XSUM)^2
560     NEXT JJ
570     PRINT "SUMSQ =  "; SUMSQ; "KMI = "; KM
572     IF SUMSQ > LSUMSQ THEN DELKMI = -DELKMI: ISIGN = ISIGN +1
574     IF ISIGN = 3 THEN GOTO 580
576     LSUMSQ = SUMSQ
577     SUMSQ = 0
578     KM = KM + DELKMI
579     GOTO 193
580 REM CONTINUE
582     PRINT "THIS IS THE BEST FIT:  SUMSQ = "; SUMSQ; "   KMI = "; KM
584     GOTO 785
600 REM ITS TIME TO PRINT OUT THE RESULTS
610     FORM$=" ###.##    #.###^^^^    #.###^^^^       #.###^^^^ "
611     PRINT " " " " " "
620     PRINT "PSURF = "; PSURF ;"mmHg   ;";
```

```
630     PRINT "# OF ITERATIONS = "; ICOUNT
640     PRINT "XSUM = "; XSUM ;"OF NORMAL SECRETION"
650     PRINT "XEXP = "; XEXP ;"OF NORMAL SECRETION"
652     PRINT "FRACTION OF NORMAL BETA CELL O2 UPTAKE =  ";QO2SUM
655                 PRINT "KMO2 =  "; KMO2;"   mmHg oxygen"
660     PRINT "KM insulin = "; KM;"  mmHg"
661     PRINT "RADIUS OF BETA CELL CORE = ";RS;"  microns"
664     PRINT " "
665     PRINT "  RADIUS    Q (I)        QV(I)         PAVE(I)   "
666     PRINT "  ________  _______      _______       _________   "
670           FOR I = 0 TO N STEP 4
680           PRINT USING FORM$; R(I),Q(I),QV(I),PAVE(I)
690           NEXT I
750 OPEN GARBAGE$ FOR OUTPUT AS #1
751     FOR I = 0 TO N
760     PRINT #1, USING FORM$; R(I),Q(I),QV(I),PAVE(I)
770     NEXT I
780 CLOSE
785 REM
790 END
```

APPENDIX 8C:

CALCULATION OF Q/Qmax and S/Smax IN INTACT ISLETS: BASIC Computer Code

```
6 REM  PROGRAM: D:\KEITH\SPHERE\SINO2.BAS        12/4/89
7 REM Program to calculate PO2 profiles, Q/Qmax, and S/Smax in spherical
8 REM islets given:  Vmax, Km, Kmi, diameter, and perfusate velocity.
9 REM Insulin secretion is integrated only in the beta cell core.
10 REM This program uses a subprogram to solve diff/rxn eq in a spheroid
11 REM with Michaelis-Menten kinetics. After non-dimensionalization,
12 REM the equation becomes:
20 REM d2P/dr2 + 2/r * dP/dr = phi*phi*P/(1+beta*P)
21 REM at r=1, P=1; at r=0, dP/dr=0; phi=(Rc2*Vm/(DO2*solI*Km))
30 REM This equation is solved numerically using a centered difference
31 REM finite difference method (Eulers method). This subprogram is a
32 REM modification of a program written by James Dunn, May, 1986.
33 REM Program modified to calculate Psurf from Pmedia based on Qactual
34 REM using Sherwood # analogy. (March 22, 1989; KED)
35 REM Modified to calculate insulin secretion (S/Smax) in beta cell
36 REM core given KMI.  Also calculates Beta cell core O2 consumption
37 REM (May 16, 1989;  KED)
50 REM FNF is the non-linear kinetics
51 REM FNDFDC is the first derivative of FNF
52 REM FNR is the discretized coordinate
90 REM N is the number of divisions
91 REM H is the step size
92 REM C is the partial pressure of oxygen
100 REM JJ is the Jacobian
101 REM RR is the residual equation
102 REM DX is the change in concentration per iteration
104 REM IPVT is the pivoting vector
106 SCREEN 2
115 REM **Define Statements for Oxygen profile program**
116 DEF FNF(I)=PHI*PHI*C(I)/(1+BETA*C(I))
117 DEF FNDFDC(I)=PHI*PHI/(1+BETA*C(I))/(1+BETA*C(I))
118 DEF FNR(I)=(I-1)*H
119 REM ******Initialize Parameters******
120 N=30                ' # of radial steps
121 KMI = 4.2           ' Km for insulin secretion
122 ITNUM = 0           ' ith iteration of diff
123 ICAT = 1            ' # of sizes being integrated
124 BCELL = .75         ' Volume fraction of islet that is Beta cell core
126 VMAX = 3.14E-08     ' maximum oxygen uptake
128 KM=.44             ' Michaelis-Menten constant for O2 uptake
129 QF = .8            ' initial guess of fractional islet uptake
130 DI = .0000153      ' O2 diffusivity
131 VEL = .75          ' Superficial fluid velocity of perfusate
132 SOLI = 1.02E-09    ' Oxygen tissue solubility
133 QINSUM = 0         ' Initialize insulin summation counter
134 QO2BETA = 0        ' Initialize oxygen Beta cell core counter
139 H=1/N
140 REM **Dimension Statements**
142 DIM C(N+1), JJ(N+1,N+1), RR(N+1), DX(N+1), IPVT(N+1)
144 DIM RAD(N+1), PAVE(N), Q(ICAT)
```

```
146 DIM DIA(ICAT), NUMF(ICAT), VOL(ICAT), VOLF(ICAT)
148 DIM QFRAC(ICAT), PSURF(ICAT)
155 PRINT "Input media P02: ";:INPUT PSMEDIA
156 INPUT "Enter name of output file";DUMPS$
157 INPUT "Enter islet diameter";DIA(1)
158 INPUT "Enter guess of Q/Qmax O2"; QF
160 REM READ IN ENSEMBLE OF ISLET SIZES AND VOLUME FRACTIONS
162 REM        FOR KG = 1 TO ICAT
164 REM         READ DIA(KG)
165  PRINT DIA(1)
166 REM         NEXT KG
168 REM        DATA 200
170 FOR JL = 1 TO ICAT
172    READ VOLF(JL)
174    NEXT JL
176 DATA 1.0
196 FOR JK = 1 TO ICAT
198 REM  DEFINE RADIUS AND PHI FOR SPECIFIC SIZE CATEGORY
200 RADIUS = DIA(JK)/2
201 RS = BCELL^.333 * RADIUS
202 PHI=RADIUS*.0001*SQR(VMAX/DI/SOLI/KM)
210 REM *Calculate Islet Surface pO2 for this diameter using Sh# at P50*
214 PSBOT = 6*1.27E-09*.0000278^.67*VEL^.33
215 PS=PSMEDIA-((QF*VMAX*(DIA(JK)*.0001)^1.667)/PSBOT)
217 PRINT "DIA (MIC) = ";DIA(JK);"  PSURF (mmHg) = ";PS;"Qfrac = ";QF
222 REM START O2 PROGRAM TO SOLVE PROFILE FOR THIS SIZE
224 REM PROGRAM RUNS FROM LINE 222 TO LINE 1190
226 BETA=PS/KM
228 E = .00001
229 REM       PRINT "Thiele modulus = ";PHI
230 REM       PRINT "beta = ";BETA
240 FOR I=1 TO N+1
250 C(I)=1
260 NEXT I
270 REM Calculate the Jacobian and the Residual
280 JJ(1,1)=-6/H/H-FNDFDC(1)
290 JJ(1,2)=6/H/H
300 FOR I= 2 TO N
310 JJ(I,I-1)=1/H/H-1/FNR(I)/H
320 JJ(I,I+1)=1/H/H+1/FNR(I)/H
330 JJ(I,I)=-2/H/H-FNDFDC(I)
340 NEXT I
350 JJ(N+1,N+1)=1
360 RR(1)=-(6*(C(2)-C(1))/H/H-FNF(1))
370 FOR I= 2 TO N
380 RR(I)=-((C(I+1)-2*C(I)+C(I-1))/H/H+(C(I+1)-C(I-1))/H/FNR(I)-FNF(I))
390 NEXT I
400 RR(N+1)=-(C(N+1)-1)
410 REM Solving the equation JJ DX = RR
420 DET=1
```

```
430 REM LU decomposition
440 IPVT(N+1)=1
450 IF N=0 THEN GOTO 730
460 NM1=N
470 FOR K=1 TO NM1
480 KP1=K+1
490 M=K
500 FOR I=KP1 TO N+1
510 IF ABS(JJ(I,K))>ABS(JJ(M,K)) THEN M=I
520 NEXT I
530 IPVT(K)=M
540 IF M<>K THEN IPVT(N+1)=-IPVT(N+1)
550 P=JJ(M,K)
560 JJ(M,K)=JJ(K,K)
570 JJ(K,K)=P
580 REM DET=DET*P
590 IF P=0 THEN GOTO 720
600 FOR I=KP1 TO N+1
610 JJ(I,K)=-JJ(I,K)/P
620 NEXT I
630 FOR J=KP1 TO N+1
640 T=JJ(M,J)
650 JJ(M,J)=JJ(K,J)
660 JJ(K,J)=T
670 IF T=0 THEN GOTO 710
680 FOR I=KP1 TO N+1
690 JJ(I,J)=JJ(I,J)+JJ(I,K)*T
700 NEXT I
710 NEXT J
720 NEXT K
730 REM DET=DET*JJ(N+1,N+1)*IPVT(N+1)
740 REM Forward elimination
750 IF N=0 THEN GOTO 980
760 NM1=N
770 FOR K= 1 TO NM1
780 KP1=K+1
790 M=IPVT(K)
800 S=RR(M)
810 RR(M)=RR(K)
820 RR(K)=S
830 FOR I = KP1 TO N+1
840 RR(I)=RR(I)+JJ(I,K)*S
850 NEXT I
860 NEXT K
870 REM Backward substitution
880 FOR KB=1 TO NM1
890 KM1=N+1-KB
900 K=KM1+1
910 RR(K)=RR(K)/JJ(K,K)
920 S=-RR(K)
```

```
930 FOR I = 1 TO KM1
940 RR(I)=RR(I)+JJ(I,K)*S
950 NEXT I
960 NEXT KB
970 RR(1)=RR(1)/JJ(1,1)
980 FOR I=1 TO N+1
990 DX(I)=RR(I)
1000 NEXT I
1010 REM Update concentration
1020 FOR I=1 TO N+1
1030 C(I)=C(I)+DX(I)
1040 IF C(I)<0 THEN C(I)=0
1050 NEXT I
1060 REM Check convergence
1070 MAX=0
1080 SUM=0
1090 FOR I=1 TO N+1
1100 IF ABS(DX(I))>MAX THEN MAX=ABS(DX(I))
1110 SUM=SUM+DX(I)*DX(I)
1120 NEXT I
1130 SUM=SQR(SUM)
1140 REM Data output
1150 PRINT "Sum of difference vector = "; SUM
1160 REM        FOR I=1 TO N+1
1170 REM        PRINT FNR(I),C(I)
1180 REM        NEXT I
1190 IF  MAX>=E OR SUM>=E GOTO 280
1200 REM CONVERT CONVERGED PROFILE TO MMHG AND MICRONS
1202 FOR I=1 TO N+1
1204    C(I) = C(I)*PS
1206    RAD(I) = FNR(I)*RADIUS
1208    NEXT I
1209 REM NUMERICALLY INTEGRATE q(O2) FOR THIS SIZE FOR THIS DO2
1210 REM THEN SUM UP CONTRIBUTION TO OVERALL FRACTIONAL O2 UPTAKE
1211 Q(JK) = 0
1212 QLOCAL = 0
1213  FOR I = 1 TO N
1214  PAVE(I) = (C(I+1) + C(I))/2
1215  QLOCAL=(PAVE(I)/(KM + PAVE(I)))*(RAD(I+1)^3-RAD(I)^3)/RADIUS^3
1216  Q(JK) = QLOCAL + Q(JK)
1217  NEXT I
1218 REM * Compare Calculated Qislet size to QF in Sh#*
1219 IF ABS(Q(JK)-QF)<=.025 GOTO 1222
1220 QF = QF + .8*(Q(JK)-QF)
1221 GOTO 210
1222 REM Continue if QF converged, Save PS and QF for this size
1223 PSURF(JK) = PS
1224 QFRAC(JK)=Q(JK)
1228 REM ****RETURN TO DO NEXT SIZE FOR THIS DO2 *****
1229 NEXT JK
```

```
1230 REM ****END OF BIG LOOP FOR THIS DO2 ITERATION***
1232 REM ****COMPARE INTEGRATED P50 TO .5 AND UPDATE DI FOR NEXT
1233 REM     ITERATION OF O2 DIFFUSIVITY. ****
1240 QTOTAL = 0
1242 FOR J = 1 TO ICAT
1244    QTOTAL = Q(J) * VOLF(J) + QTOTAL
1245    Q(J) = 0
1246    NEXT J
1250 ITNUM = ITNUM + 1
1260 QTOT(ITNUM) = QTOTAL
1262 DO2(ITNUM) = DI
1370 REM Create data file
1380 OPEN DUMPS$ FOR OUTPUT AS #1
1382 PRINT "P02 media = ";PSMEDIA;" Insulin secretion KmI = ";KMI
1384 PRINT "CELL Km = ";KM; "   Vmax =  ";VMAX;" STIR VEL = ";VEL
1385 FOR I=1 TO ICAT
1386 PRINT "CALCULATED Q/VMAX = "; QTOT(I);"      DO2 = "; DO2(I)
1387 PRINT "DIA = ";DIA(I);" Psurf = ";PSURF(I);" Q/VMAX O2 = ";QFRAC(I)
1388 NEXT I
1390 FOR I=1 TO N+1
1400 PRINT #1, RAD(I), C(I)
1410 NEXT I
1420 CLOSE
1425 REM Calculate Insulin Secretion and O2 consumption in Beta core
1430 FOR J = 1 TO N
1432    IF RAD(J+1) >= RS THEN RAD(J+1) = RS
1435    VOLF = (RAD(J+1)^3 - RAD(J)^3)/RS^3
1440    QINSUM = QINSUM + VOLF *(PAVE(J)/(KMI + PAVE(J)))
1445    QO2BETA = QO2BETA + VOLF *(PAVE(J)/(KM + PAVE(J)))
1450    IF RAD(J+1) >= RS THEN GOTO 1470
1460    NEXT J
1470 REM **Output for beta cell core**
1474 PRINT "Beta cell core volume fraction = ";BCELL;"Beta radius =";RS
1475 PRINT "Fraction of Beta cell O2 consumption = ";QO2BETA
1480 PRINT "Fraction of Maximum insulin secretion = ";QINSUM
1485 PRINT "Name of output file is: D\KEITH\SPHERE\";DUMPS$
1490 END
```

(End)